IntechOpen

Wind Farm

Impact in Power System and Alternatives to Improve the Integration

Edited by Gastón Orlando Suvire

WIND FARM – IMPACT IN POWER SYSTEM AND ALTERNATIVES TO IMPROVE THE INTEGRATION

Edited by **Gastón Orlando Suvire**

Wind Farm - Impact in Power System and Alternatives to Improve the Integration
http://dx.doi.org/10.5772/934
Edited by Gastón Orlando Suvire

Contributors

Enrique Kremers, Jose Maria Gonzalez De Durana, Oscar Barambones, Norbert Lewald, Pablo Viejo, Ioannis Margaris, Anca Hansen, Poul Sørensen, Nicolaos Cutululis, Nikos Hatziargyriou, Jorge Blanes, Carlos Lopez, Yi Gao, Elkhatib Kamal, Abdel Wahab Aitouche, N. Senthil Kumar, Lucian Mihet-Popa, Voicu Groza, Mónica Alonso, Hortensia Amarís, Markel Zubiaga, Gonzalo Abad, Jon Andoni Barrena, Sergio Aurtenetxea, Ainhoa Cárcar, Noha Abdel-Karim, Marija Ilic, Mitch Small, Phuc Diem Nguyen Ngoc, Juan Mendez, Javier Lorenzo, Sobhy Abdelkader, Francisco Bañuelos-Ruedas, César Angeles-Camacho

Notice

First published in Croatia, 2011 by INTECH d.o.o.
eBook (PDF) Published by IN TECH d.o.o.
Place and year of publication of eBook (PDF): Rijeka, 2019.
IntechOpen is the global imprint of IN TECH d.o.o.
Printed in Croatia

Legal deposit, Croatia: National and University Library in Zagreb

Additional hard and PDF copies can be obtained from orders@intechopen.com

Wind Farm - Impact in Power System and Alternatives to Improve the Integration
Edited by Gastón Orlando Suvire

p. cm.

ISBN 978-953-307-467-2

eBook (PDF) ISBN 978-953-51-6025-0

Meet the editor

Gastón Orlando Suvire was born in San Juan, Argentina, on November 13, 1977. He graduated as an electric engineer from the National University of San Juan (UNSJ), Argentina in 2002. He received his Ph.D. from the same University in 2009, carrying out part in the COPPE Institute, in the Federal University of Rio de Janeiro in Brazil. Dr. Suvire is currently a professor of electrical engineering at the UNSJ and a researcher with CONICET. His research interests include simulation methods, power systems dynamics and control, power electronics modeling and design, and the application of wind energy and energy storage in power systems.

Contents

Preface

During the last two decades, increase in electricity demand and environmental concern resulted in fast growth of power production from renewable sources. Wind power is one of the most efficient alternatives. Due to rapid development of wind turbine technology and increasing size of wind farms, wind power plays a significant part in the power production in some countries. However, fundamental differences exist between conventional thermal, hydro, and nuclear generation and wind power, such as different generation systems and the difficulty in controlling the primary movement of a wind turbine, due to the wind and its random fluctuations. These differences are reflected in the specific interaction of wind turbines with the power system.

This book addresses a wide variety of issues regarding the integration of wind farms in power systems, from impact to modeling and simulation of wind power system. The book is the result of contributions from many researchers worldwide. I hope that the book will become a useful source of information and basis for discussion for the readers. I wish to thank all chapter authors for their efforts and the quality of the material submitted.

The book contains 14 chapters divided into three parts. The first part (Chapters 1 to 4) outlines aspects related to the impact of the wind power generation on the electric system. In the second part (Chapters 5 to 10), alternatives to mitigate problems of the wind farm integration are presented. Finally, the third part (Chapters 11 to 14) covers issues of modeling and simulation of wind power system.

In Chapter 1, wind farms impacts on power networks and on grid codes requirements are analyzed. An optimal allocation of wind farms has been selected in order to maximize the system loadability as well as to reduce any power losses of the whole network by using an optimization algorithm where reactive power capability of Double Fed Inductor Generator (DFIG) is already included in the formulation.

The focus of the Chapter 2 is on the voltage stability problem and the network capability to accommodate power from the wind systems.

In Chapter 3, the way in which power fluctuations from asynchronous fixed-speed wind turbines become voltage variations is presented. The chapter includes an

analysis of IEC 61400-21, which is the procedure for testing the wind turbines and the concept of fictitious network to determine its potential to disturb the power system.

Chapter 4 evaluates the frequency behavior of the offshore wind farms at normal operation (steady state), in function of design procedure parameters like: the cable length / characteristics, transformers connection and leakage inductance or inter-turbine grids configuration. The analysis is performed from the point of view of the wind turbines, considering them as potential harmonic sources.

Chapter 5 analyses one solution to problems of voltage deviations due to wind power generation. Variable speed operation is described for wind generators, and the use of flexible alternating-current transmission systems (FACTS) controllers is considered to improve the integration of wind generators in power systems.

Chapter 6 considers an optimal operation of wind storage system as an optimization problem that deals with primary sources, storage capacity as well as demand. The main objective is to meet the network requirements in terms of limiting the wind power fluctuations and providing possible ancillary services.

In Chapter 7, a control algorithm for wind turbines subjected to a wide range of wind variation, grid disturbance and parameter uncertainties is presented. The algorithm utilizes fuzzy systems based on "Takagi-sugeno" (TS) fuzzy models to approximate nonlinear systems.

Chapter 8 presents aspects of the control system of wind farms that need to be further developed in order to enhance their contribution in system services, e.g. primary frequency control. The chapter focuses on the impact of wind power fluctuations on power system operation through a detailed modelling approach of both conventional generation as well as of the basic commercial wind turbine configurations.

Chapter 9 contains the results of research activities in line to reduce both: the uncertainties in power forecasting and the lack in power quality for wind farms connected to public grids. The approach is a suite of studies that are focused on power forecasting for Electricity Markets and also an innovative simulation technique to evaluate the quality by using a coupled storage systems as water reservoirs, inertial systems or chemical batteries.

The objective of the Chapter 10 is to study the impact of FACTS controllers on the long term dynamic behavior of a grid connected doubly fed induction generator based wind farm. The stability of the system is studied by running time domain simulations with and without FACTS controllers.

Chapter 11 introduces wind speed models that capture variability and unpredictability in wind speed behavior. It consists of three major parts: a time series wind speed prediction model with a detailed focus on short term wind predictions, a wind power Discrete Markov Model, and a wind data decomposition model that decomposes wind speed into sub-models.

In Chapter 12, a complete simulation model of a 6 x 2 MW constant-speed wind turbines (wind farm) using cage-rotor induction generators is presented using data from a wind farm installed in Denmark. The purpose of the model is to simulate the dynamical behaviour and the electrical properties of a wind turbine existing in a wind farm.

Chapter 13 presents the application of a joint deterministic-probabilistic criterion for bulk system expansion planning in wind integrated systems. A comparison of the conventional deterministic N-1, the basic probabilistic and the joint deterministic-probabilistic criteria is illustrated for a long-term composite system planning using a wind integrated test system.

Finally, Chapter 14 concerns the wind generation module of an agent-based model for integral energy systems. The proposed model aims to represent the wind power production by modeling wind farms consisting of wind turbine units on different time scales, ranging from short (minutes) to long-term (months) simulations, taking into account fluctuating wind speeds and technical reliability.

Gastón O. Suvire
Instituto de Energía Eléctrica
Facultad de Ingeniería
Universidad Nacional de San Juan
Argentina

Part 1

Impact of Wind Power Generation on the Electric System

1

Impact of Wind Farms in Power Systems

Mónica Alonso and Hortensia Amarís
Carlos III University Madrid
Spain

1. Introduction

Beyond any doubt, we can consider century 21st as the one devoted to renewable energy. According to the International Energy Agency (IEA) (IEA, 2009) renewable sources shall provide about 35% of the European Union's (EU) electricity by 2020, and within this context, wind energy is set to contribute the most - nearly 35% - of all the power coming from renewable sources. This evolution is based on sustainability scenarios, like the BLUE one (IEA, 2008) related to the reduction of greenhouse emissions. However, the appropriate integration of such renewable energy into power system grids still presents major challenges to Power Systems Operators (PSO) and planners.

Nowadays wind energy has widely proved to be one of the most competitive and efficient renewable energy sources and, as a result, its use is indeed continuously increasing. As an example, in June 2010 total installed wind energy capacity around the world was 175,000 MW. Incorporation of wind energy units into distribution networks not only modifies power flows but also, in some situations could also result in under or over-voltage on specific points of the network (Jenkins, 2000), as well as could increase the cases of power quality problems and produce any type of alterations regarding voltage stability (Abdullah et al., 2010, Baghaee et al., 2009).

The process of high wind energy penetration requires the impact analysis of this new technology in power systems. In these terms, some countries have developed grid codes in order to establish the requirements of wind farms (WF) into power networks. Moreover, power network planning with high wind energy penetration requires the definition of several factors, such as: the best technology to be used, the optimal number of units to be connected and the optimal size to be chosen.

Currently a connected variable speed wind turbine to power systems by means of power electronics has the ability to supply reactive power to power systems. This capability allows wind turbines to participate in ancillary services as synchronous generators (Bhattacharya & Zhong, 2001), however, there are little works focusing on the participation of variable speed wind turbines in reactive power ancillary services (Amaris & Alonso, 2011; Bhattacharya & Zhong, 2001).

In this chapter, a review of wind farms impact on power networks and on Grid codes requirements are analyzed. An optimal allocation of wind farms has been selected in order to maximize the system loadability as well as to reduce active any power losses of the whole network by using an optimization algorithm where reactive power capability of Double Fed Inductor Generator (DFIG) is already included in the formulation. Finally, conclusions and future researches are shown.

2. Impact of wind energy on power systems

Incorporation of great amount of distributed resources, such as wind energy, has a significant impact on power network, which are mainly related to environmental, economical and reliability aspects.

Low wind penetration levels are usually accommodated in power networks considering that the network is passively controlled and operated.

Although there are several available tools to be used for wind power forecasting (González et al., 2004), wind energy is still considered as a non dispatchable and not centrally planned technology.

Impact of wind energy on power systems is thus focused on several issues related to security, stability, power quality and operation of power systems.

- Wind energy has several impacts on power flow that could lead to reverse power flow and, as a result, power systems operation will become more complex (Vilar, 2002). Moreover, power injection by wind farms may cause power losses in the distribution systems.
- All the utilities have to keep stable and reliable the voltage supply to the customers within specific limits of frequency and magnitude. Connection of wind farms may result in voltage changes, consequently, some countries have defined a higher short-circuit level at the connection point, normally between 20 and 25 times the wind farm capacity. There are already some examples of successful operation of power networks with a lower short circuit level (Jenkins et al., 2000).
- Power quality is related to voltage variation and harmonic distortion in the network. However, the incorporation of wind energy in power networks could affect the quality of the supplied voltage to the customers. To reduce this impact, nowadays, variable speed wind turbines equipped with power electronics are widely used in wind energy conversion. Power electronics increase power quality because they raise the harmonic distortion.
- Protection system is also affected by wind farms since the incorporation of wind power injection alters power flows; so that conventional protection systems might fail under fault situations.
- In the past, power network was passive operated and kept up stable under most circumstances. However, this statement is no longer valid if considering an increase of wind energy penetration. Recently, new requirements for wind units have been designed in order to keep power networks stable under several disturbances, such as low voltage ride through capability.

2.1 Reactive power grid code requirements

Countries with high wind energy penetration have developed grid code requirements in order to increase wind energy penetration and to improve the reliability and security of the network (Tsili & Papathanassiou, 2009). The most important aspects are related to active and reactive power regulation, power quality and low voltage ride through capability (Martínez et al., 2007) .

Nowadays, transmission systems operators (TSO) are demanding wind turbines to behave as synchronous power plants. New advances in the field of wind technologies have shown that wind generators offer regulation capabilities as conventional plants.

Some grid codes require wind farms to offer reactive power capability in order to maintain reactive power balance in power network (reactive power compensation) and to improve voltage level even in a remote node (Singh, 2009). Fig. 1 and 2 show the requirements of common grid code for power factor in terms of voltage deviations.
From country to country, there are some differences to be observed. According to German grid code (E.On, 2006), wind farms will work with leading or lagging power factor under overvoltage situations. In the case of English grid code (National Grid Electricity Transmission, 2008), wind farm must be able to supply full reactive power capacity within ±5% of nominal voltage, for voltage levels of 400kV and 275kV. English code requires an automatic voltage control at the point of connection of grid farm. Nordic grid code (Nordel, 2007) demands wind farms to have a reactive power output control in order to regulate the voltage at the point of connection.

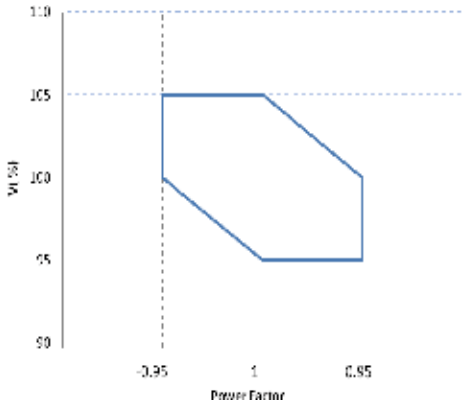

Fig. 1. Typical requirements for power factor in terms of voltage deviation

Fig. 2 shows the reactive power requirements in terms of power factor for different grid codes. According to ESB (ESB, 2007), Iris code requirements establish that wind farm must be able to work with a minimum power factor of 0.835 leading or lagging for active power outputs level around 50% of the rated one. Hydro-Quebec (Hydro Quebec, 2006) requires those wind farms with an upper rate form 10 MW to offer voltage regulation within the range of 0.95 leading or lagging power factor. Moreover, this grid code establishes that wind farms must contribute to voltage control under normal, abnormal or dynamic operation conditions. Canadian code, AESO (AESO, 2004), emphasis that voltage and reactive power regulation will be assessed at the low side of wind farm grid transformers. AESO grid code requirements are divided in two different operation conditions: for continuous operation the power factor range is set between 0.95 lagging and 0.9 leading; in the case of dynamic operation a range between 0.95 capacitive and 0.985 inductive is required. Both ranges are established in terms of power output. On the other hand, Danish grid code (Eltra, (Energinet, 2004a, 2004b)) requires wind farm to support limited reactive power by a band, which corresponds to orange line and dot-line of Fig. 2. These lines represent a power factor of 0.995. Furthermore, reactive power control can be implemented not only at each wind units but also centrally at wind farm level.
Some grid codes establish a minimum reactive power control; this requirement is related to the capability of wind units to work within a power factor range between 0.95 leading and

0.95 lagging. Modern wind units use variable speed generators connected to the grid by power electronics converters. This converters offer the possibility to control reactive power outputs of wind units by varying voltage magnitude and frequency. DFIG are the most popular employed generator in wind units, and could offer dynamic reactive power control due to the grid side converters. This converter capacity is within the range of 20% - 30% of the machine rate.

3. Voltage control and reactive power support as ancillary services

One of the main issues is the Reactive Power Management which entails the requested operation and planning actions to be implemented in order to improve the voltage profile and the voltage stability in power networks (Raoufi & Kalantar, 2009). An efficient reactive power planning could be obtained by choosing an optimum location of var sources during the planning stage, whereas efficient reactive power dispatch could be achieved by scheduling an optimum regulation of the voltage set point at the generators connection point and at the var settings during the reactive power dispatch (Hugang, 2008).
Current power systems are working close to this operational stability limit, so distribution and transmission system operators (DSO and TSO) are required to wind energy to work as a conventional power plant and contribute to ancillary service such as reactive power control. Actual wind units are considered such as a non-dispatchable energy so, in many cases, they act as a PV or PQ nodes for load flows and reactive power studies (Raoufi & Kalantar, 2009). Some wind farm technologies, such as DFIG, have the ability to supply reactive power, so it could be possible to offer this reactive power capability to TSO and DSO in order to improve voltage stability of power network.

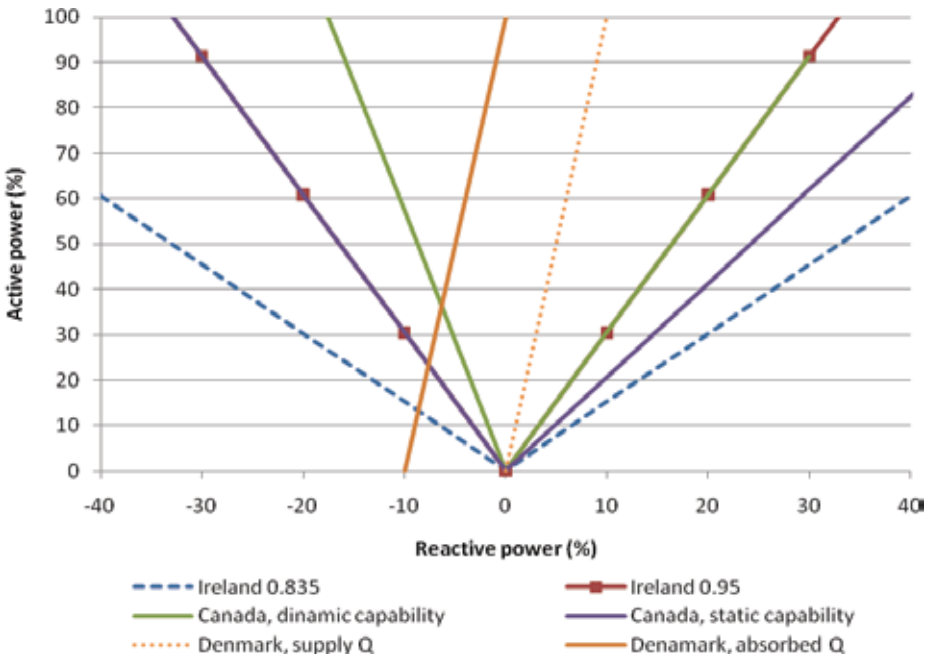

Fig. 2. Reactive power requirement for several grid codes.

3.1 Voltage stability

Voltage Stability is defined as the ability of a power system to maintain steady-state voltage at all buses in the system after being subjected to a disturbance from a given initial operating condition (Kundur, 1994). In the literature, two voltage stability problems are analysed:

- Estimation of the maximum loadability.
- Computation of the critical power system loading that could lead to voltage collapse.

Voltage stability is usually represented by P-V curve (Fig. 3). In this figure the noise point is called the point of voltage collapse (PoVC) or equilibrium point. At this point, voltage drops rapidly with an increase of the power load and subsequently, the power flow Jacobean matrix becomes singular. Classical power-flow methods fail to converge beyond this limit. This failure is considered as an indication of voltage instability and frequently associated with a saddle-node bifurcation point (Kundur, 1994).

Although voltage instability is a local phenomenon, the problem of voltage stability concerns to the whole power system, becoming essential for its operation and control. This aspect is more critical in power networks, which are heavily loaded, faulted, or with insufficient reactive power supply.

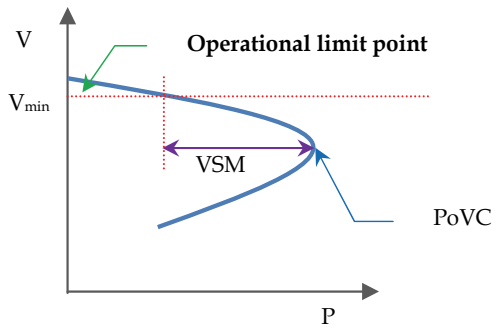

Fig. 3. P-V curve

In power networks with huge amount of wind penetration levels, the role of voltage stability is of great importance due to the lack of reactive power contribution of many wind generators as well as their integration into weak networks.

Wind farms equipped with variable speed are presented as a good alternative to alleviate problems related to voltage stability. Therefore reactive power planning in large power systems has become a particularly important point in recent years since it is necessary to develop new techniques to solve any problem that may arise.

3.2 Reactive power planning

Optimal allocation of Var sources happens to be one of the most challenging problems in power networks. The incorporation of shunt reactive power compensation devices in power networks provides voltage support, and reduces the danger of voltage instability or voltage collapse. In the past years, locations of Var sources were barely determined by estimation or by approach (Zhang et al., 2007); however, neither of both methodologies proved to be effective.

In this work, optimal locations of wind farms with reactive power capability are determined by using Genetic algorithms (GA). The methodology proposed could be successfully applied to any renewable energy resources inverted based unit offering reactive power capability (DFIG or PV).

3.3 Reactive power capability of wind units

Power systems with great amount of wind energy require a dynamic reactive power support to the network. Variable speed wind turbines, such as DFIG or full power converter technology, are connected to the grid by electronic power converters and, consequently, they have the capability to provide voltage support to the network as well as to fulfill the grid code requirements (Amaris & Alonso, 2011; Bhattacharya & Zhong, 2001).

The main drawback of this methodology is that the reactive power capability of DFIG's Power Converters is not being considered since it only incorporates reactive power capability limits of wind generators according to a maximum cos(φ) or a fixed regulation band (Vijayan, 2009)-(Sangsarawut, 2010), and so that this representation does not allow to take full advantage of the reactive power injection from the wind turbine.

In this work, a better wind turbine model is proposed that does take into account the actual available reactive power capability for each working operation point. The proposed formulation could be included indeed in any modified power flow analysis for optimum reactive power dispatch. At the same time, this methodology will enable to regulate the reactive power injection either locally, at the wind farm, or globally, in the whole network. As a result of the optimum and coordinated reactive power dispatch, the voltage stability in the power network will be significantly improved and enhanced.

3.3.1 Reactive power injection from DFIG

Double Fed Induction Generator is composed of a wound induction machine in which the stator is directly connected to the grid and the rotor is connected via slip rings to a two back-to-back converters as shown in Fig. 4. The electronic power converter allows controlling the active and the reactive power. Moreover, the Grid Side Converter (GSC) of these generators offers reactive power capability, so DFIG could work as a reactive power source injecting reactive power from the machine and from the GSC converter. According to this reactive power capacity, TSO and DSO could include in their voltage control strategies the extended reactive power capability of DFIG in order to improve the voltage stability of the whole power system.

DFIG power capability has been traditionally represented in a PQ diagram (B. Singh & S. N. Singh, 2009; Ullah & Thiringer, 2008) and it is well known that reactive power capability of DFIG is limited by:

- stator current (heating of stator coils),
- rotor current (heating of rotor coils), and
- rotor voltage (limiting the rotor speed).

The GSC could be used to control the reactive power and to improve the total reactive power capability of the wind turbine (B. Singh & S. N. Singh, 2009; Ullah & Thiringer, 2008) This potential usage represents a key aspect since it may be quite useful to system operators in order to perform a coordinated reactive power management in the whole power network. The proposed methodology could be applied in the available converter designs not being necessary to perform any physical modification to the current DFIG commercial converters.

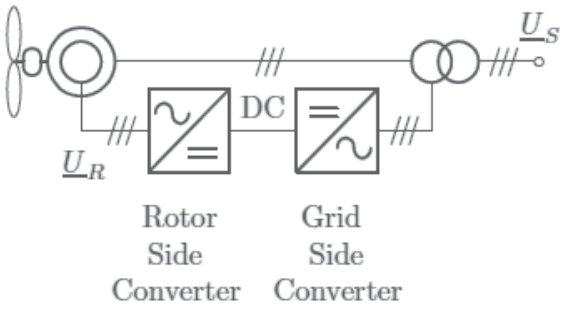

Fig. 4. DFIG Wind Turbine

Therefore, the grid side converter could be treated as a reactive power source dynamically controlled.
The total reactive power injected to the grid will be composed by the superposition of two components, the reactive power injected by the induction machine (stator) and the reactive power injection from the grid side converter (Amaris & Alonso, 2011).

$$Q = Q_S + Q_{GSC} \tag{1}$$

The reactive power capability of the GSC can be computed by:

$$Q_{GSC} = \pm\sqrt{\left(V_{GSC} I_{GSC}\right)^2 - P_R^2} = \pm\sqrt{S_{GSC}^2 - P_R^2} \tag{2}$$

Where V_{GSC} and I_{GSC} are AC side voltage and current of GSC, and P_R is the active power.
The resulting PQ capability curve is shown in (Amaris & Alonso, 2011). This extended capability would be very useful to system operators not only by performing voltage stability or contingency analysis, but also in every situation where power reactive reserves are critical factors to keep the network stable.

4. Genetics algorithm

Metaheuristic techniques have come up to be a good alternative to face the question of optimal management of reactive power, which involves operation, location and optimal size of these units. The main reason is because of their ability to reach a satisfactory solution of the problem; furthermore they are very fast and they have low computation complexity. Among all these techniques genetic algorithms stand out because of their speed of calculation and simplicity, sum up to their robustness .and the fact that they can find a global optimal solution in complex multi-dimensional search spaces (Díaz & Glove, 1996).
Genetic algorithms are a family of computational optimization models invented by Holland (1975) (Holland, 1975) and firstly implemented by Goldberg (1989) and Hopgood (2001) (Goldberg, 1981) to solve both constrained and unconstrained optimization problems. GA are based on natural evolution process, as it could be deduced from the employed operators, which are clearly inspired by these natural sequences, and from the main driver of the GA, which would be defined as a biological selection. One of the main advantages of the GA is that they work with a set of possible solutions, called population, which will be modified on each step (generation) of the algorithm according to genetic operators.

The main advantages of GA to be stressed over conventional optimization methods are:

- They do not need any prior knowledge about issues such as space limitations or any other special properties of the objective function of the problem to be optimised.
- They do not deal directly with the parameters of the problem. They work only with codes, which represent the parameters and the evaluation of the fitness function to afterwards, be able to assign a quality value to every solution produced.
- They work with a set of solutions from one generation to the next making the process likely to converge into a global minimum.

The solutions obtained are randomly based on the probability rate of the genetic operators such as mutation and crossover.

This technique is very useful for solving optimization problems such as the one proposed in this paper. The optimisation problem would be formulated as:

Min F(x)

Subject to:

$Aeq(x) = Beq$

$A(x) \leq B$

$x \in S$

where:

- F(x) is the objective function to be optimised
- Aeq is equality constraint
- A is inequality constraint
- x is the vector of variables
- S is the search space.

4.1 Representation

A population is formed by a set of individuals that correspond with a possible solution of the problem. Each individual is represented by a set of variables to be optimized and they are usually represented in a string form called chromosome.

Indeed, the method of chromosome's representation has a major impact on the performance of the GA. There are two common representation methods for numerical optimization problems: binary string or vector of integers and real numbers. Each element (bit, integer or real number) in a chromosome is called gene.

4.2 Initial population

Instead of facing a single solution each time, GA works with a group of initial solutions to start the process of optimization. This initial population could be created in two ways. The first one consists in using randomly produced solutions which have been preciously created by a random generator; this method would be preferable in those cases in which no prior knowledge existed. The second method employs a set of known solutions able to satisfy the requirements of the problem. This method does require a previous knowledge about the optimization problem and converges to an optimal solution in less time than the first one.

4.3 Fitness evaluation function

The formulation of the Fitness Function (FF) is a major aspect of the optimization problem. FF assigns a quality value to each individual of the population depending on how well the solution performs the desired functions and satisfies the given constraints. Moreover, it

allows to determinate which individuals of the population will survive for the next generation. The fitness values of individuals in a given population are employed to drive the evolution process. In the case of a GA, this calculation must be automatic and the problem lies in how to devise an effective procedure to compute the quality of the solution. These characteristics enable the GA to present excellent results even when optimizing complex, multimodal or discontinuous functions.

4.4 Genetic operators

After implementing the fitness function, three basic genetic operators are applied to the population, in order to create a new population: selection, crossover and mutation. All of these three generators are inspired by natural process, as we pointed out above; however, it is not necessary to employ all the operators in a GA simultaneously. The choice or design of the operators depends on the problem to be analyzed and the representation scheme to be employed.

4.4.1 Selection

The aim of the selection procedure is to copy individuals whose fitness values are higher than those whose fitness values are lower in the next generation. Besides this, the operator allows transmitting the best individual's genetic material in the next generations in order to drive the search towards a promising area and finding optimal solutions in a very short time.

4.4.2 Crossover

This operator is considered the most important one of GA method because it is responsible for the genetic recombination. It is used to create two new individuals (children) from two existing ones (parents), which are picked from the current population through the selection operator. There are several ways of doing this, but the most common crossover operations are: one point, two point, cycle and uniform crossovers.

4.4.3 Mutation

During this procedure all individuals of the population are checked, gene by gene, and this gene value is randomly reversed according to a specified rate. This operation introduces new information in the algorithm to force it to search new areas. Additionally, this operator helps GA to avoid premature convergence due to genetic material that has been lost during the selection operation. In addition to that already mentioned, it helps to find out a global optimal solution.

4.4.4 Control parameters

The most important control parameters of a simple GA are:
Population size: It allows a better exploration of the solution space during the search, so that the probability of convergence to the global optimal solution will be higher.
Crossover rate: It determines the frequency of the crossover operation. It is used to discover a promising area at the start of the simulation.
Mutation rate: It controls the mutation operation. In general, an increase in the mutation rate helps the GA to reach the global solution avoiding the local minimum. However, if this mutation rate parameter is too high, it could result in a wide diversity in the population and, so that the global solution will not be reached.

5. Improve management of power systems by optimal allocation of wind farms

Currently, grid code requirements of wind farms are demanding wind turbines to offer reactive power capabilities at the connection point (Energinet, 2004a; National Grid Electricity Transmission, 2008). Moreover, they must be able either to inject or to absorb reactive power according to the system operator's commands. Although there is no standard grid code yet, all national grid codes agree to include the reactive power injection from wind turbines in both normal and fault situations.
Optimal allocation and reactive power injection of wind farms equipped with DIFG unit is essential for optimal management of power systems with high wind penetration level.
In this section, a GA for optimal reactive power planning is developed. Optimal allocation and reactive power injection of wind units are determinate in order to maximize loadability of the power system and minimize real power losses of the whole network. Optimal allocation lets improve voltage stability of distribution network.

5.1 Optimization methodology for reactive power planning

5.1.1 Encoding

In the present work, value encoding of chromosomes has been used where the placement problem is modelled by using real numbers. The target is where to locate three wind farms and what is the reactive power injection of each wind farm. Each chromosome has seven genes that represent the variables of the system. The first one represents the loadability parameter of the system (λ); the other ones represent the bus number location in which wind farm could be connected and the var injection from each wind farm (Table 1).

Gen 1	Gen 2	Gen 3	Gen 4	Gen 5	Gen 6	Gen 7
λ (p.u.)	$\#WF_1$	Q_1 (Mvar)	$\#WF_2$	Q_2 (Mvar)	$\#WF_3$	Q_3 (Mvar)

Table 1. Chromosome structure

5.1.2 Fitness function

According to the objective of the work, the Fitness Function deals with the loadability of the system and the real power losses. For this purpose, a load change scenario is considered, in which P_d and Q_d can be represented as:

$$P_d = P_{d0}(1+\lambda) \tag{3}$$

$$Q_d = Q_{d0}(1+\lambda) \tag{4}$$

Where:

- P_{d0} and Q_{d0} are the original power load (base case).
- λ represents the load parameter.
  (λ =0 corresponds to the base case).

In this scenario of load change, λ_{max} corresponds to the maximum power transferred under voltage constraints.
To maximize the loadability of the system through the load parameter λ, and minimize real power losses, the FF function used is:

$$FF(x) = \tfrac{1}{2}(1-\lambda) + \tfrac{1}{2}LOSS \tag{5}$$

$$LOSS = \frac{P_{loss}}{P_{loss_{ini}}} \tag{6}$$

$$P_{loss} = \sum_{k \in N_e} g_k (V_i^2 + V_j^2 - 2V_i^2 V_j^2 \cos\theta_{ij}) \tag{7}$$

Where:

- x is a vector of variabl $Q_d = Q_{d0}(1+\lambda)$ es: load parameter, bus connection and var injection.
- λ value depends on voltage constraints violation.
- P_{loss} and $P_{lossini}$ are the real power losses for optimal allocation and var injection and for base case, respectively, calculated with eq. 7.

5.1.3 Constraints

The main constraints that are considered in the optimization process are the following:

- Voltage level at all buses should be held within established limits.
- Active and reactive power generation are limited by the generator capabilities.

5.1.4 Optimisation formulation

Tacking into account the FF objective and constraints equations, the optimization process flowchart is shown in Fig. 5 and the optimization problem can be formulated as:

$$MinF(y) = \tfrac{1}{2}(1-\lambda) + \tfrac{1}{2}LOSS \tag{8}$$

Load flow constraints:

$$\Delta P_i = P_{gi} - P_{di} - P_i \tag{9}$$

$$Q_i = V_i \sum_{i=1}^{N} V_k (G_{ik} \sin\theta_{ik} - B_{ik} \cos\theta_{ik}) \quad \Delta Q_i = Q_{gi} - Q_{di} - Q_i \tag{10}$$

Where:

$$P_i = V_i \sum_{i=1}^{N} V_k (G_{ik} \cos\theta_{ik} + B_{ik} \sin\theta_{ik}) \tag{11}$$

$$Q_i = V_i \sum_{i=1}^{N} V_k (G_{ik} \sin\theta_{ik} - B_{ik} \cos\theta_{ik}) \tag{12}$$

Voltage constraints:

$$V_{i,\min} \le V_i \le V_{i,\max} \qquad i = 1, 2, \ldots, N_B \tag{13}$$

Active and reactive power generator:

$$P_{gi,\min} \le P_{gi} \le P_{gi,\max} \qquad i = 1, 2, \ldots, N_G \tag{14}$$

$$Q_{gi,\min} \le Q_{gi} \le Q_{gi,\max} \qquad i = 1, 2, \ldots, N_G \tag{15}$$

Point of connection:

$$PC_{gi,\min} \le PC_{gi} \le PC_{gi,\max} \qquad i = 1, 2, \ldots, N_G \tag{17}$$

Limits of power flow at each branch

$$S_l \le S_{l,\max} \tag{19}$$

Reactive power capabilities constraints:
Stator side constraints:

$$I_s \le I_{s,\max} \tag{20}$$

$$V_s \le V_{s,\max} \tag{21}$$

Rotor side constraints:

$$I_R \le I_{R,\max} \tag{22}$$

$$V_R \le V_{R,\max} \tag{23}$$

Grid side converter constraints

$$S_{GSC} \le S_{GSC,nominal} \tag{24}$$

5.2 Case study

The optimization strategy has been applied to a 34 buses distribution power system Fig. 6 (Salama & Chikhani, 1993). Three wind farms equipped with DFIG have been optimal allocate and var injection is optimal management in order to maximize loadability of the systems and minimize real power losses.

Four different scenarios have been studied, the first one represents the base case without WF, the second scenery incorporate 3 WF to the distribution networks without reactive power capability, the third one incorporate reactive power capability of WF corresponds to a cosφ=0.95 leading or lagging, finally the last scenery take into account the extended reactive power capability of DFIG incorporating reactive power capability of grid side converter.

Table 2 shows the results obtained by the algorithm: column 3 and 4 are the bus number where each WF should be located and the reactive power injected by each one. Column 5 to

8 represents voltage stability parameters: the maximum loadability (λcrit.) for low limit operational voltage (0.95 p.u.), percetange of loadability increase of the power system, maximum loadability in the point of voltage collapse and increase in voltage stability margin define as the distance between the operational point and the point of voltage collapse. Finally, column 9 and 10 show the real power losses and percentage decrease of real power due to optimal allocation of WF.

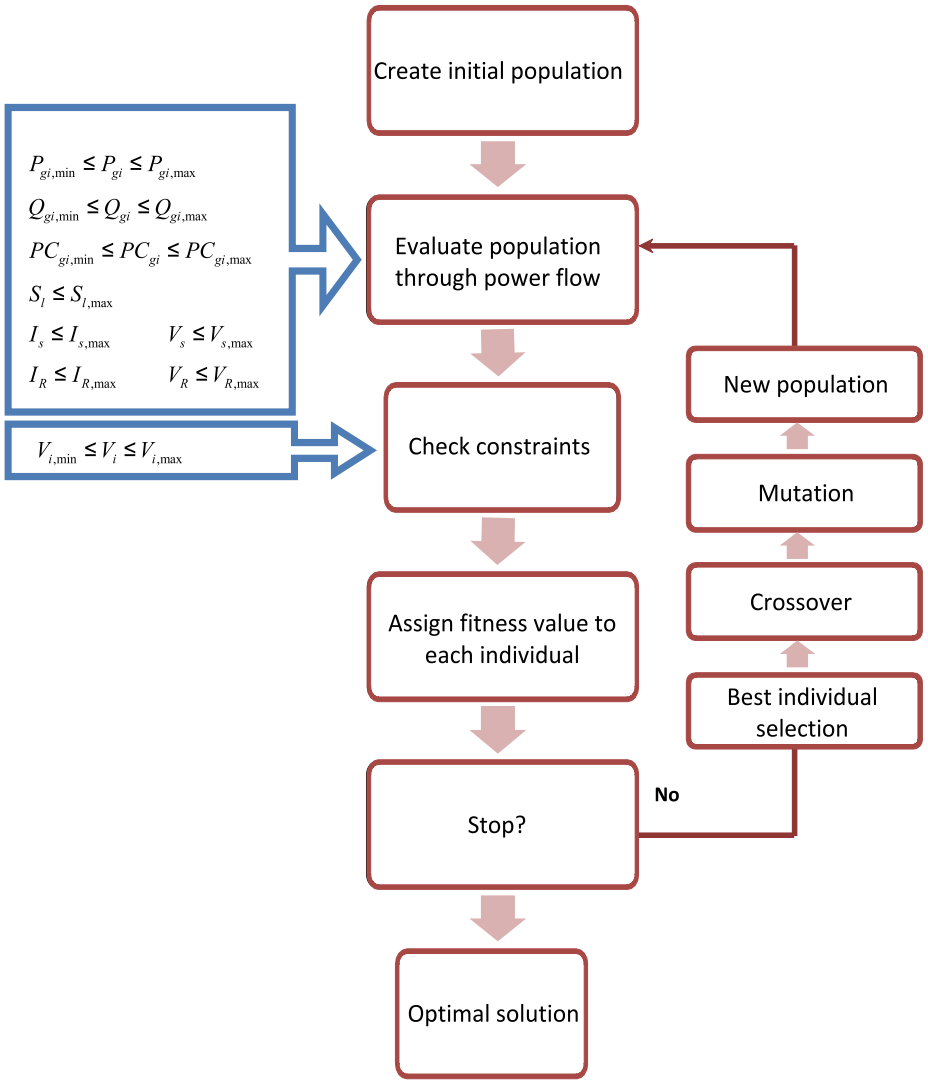

Fig. 5. Flowchart of optimization process

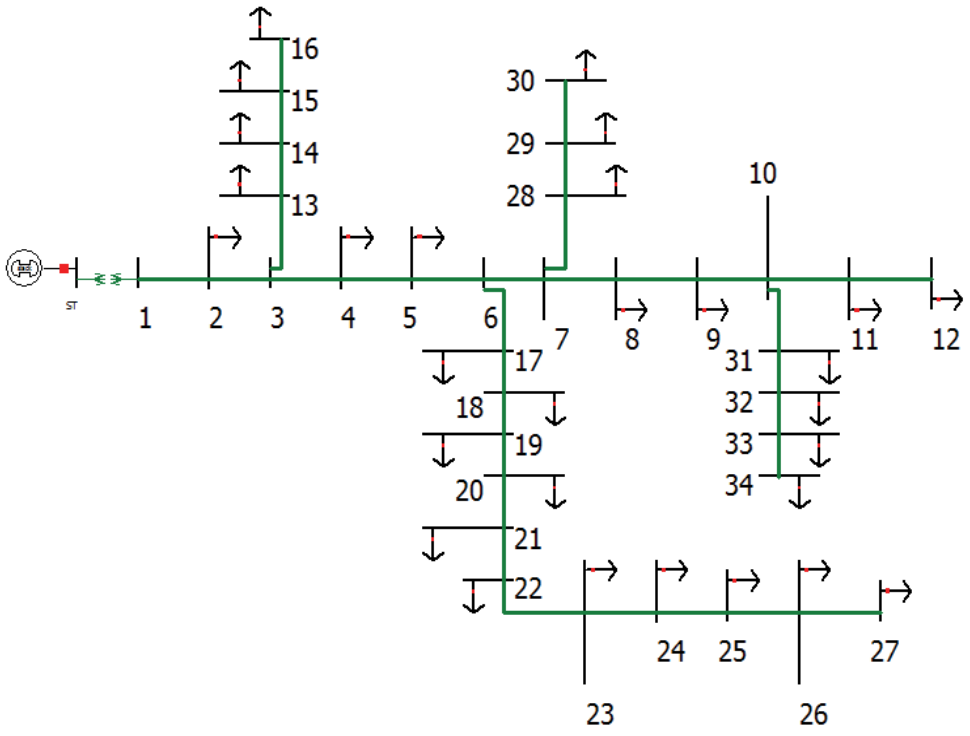

Fig. 6. Modified IEEE 34 bus system

		GA solution		Stability parameters				Losses	
		# Bus_{WF}	Q_{WFinj} (Mvar)	$\lambda_{crit.}$ (p.u.)	Δload-ability	$\lambda_{max.}$ (p.u.)	ΔVSM	P_{loss} (Mvar)	ΔP_{loss}
Scenery 0	No WF	-	-	0	-	2.8	-	0.64	-
Scenery 1	3 WF Q=0 MVar	9	0	0.26	26%	3.3	15.15%	0.44	31.25%
		25	0						
		26	0						
Scenery 2	3 WF $Q=Q_g$	24	0.059	0.285	28.5%	3.4	17.65%	0.37	42.19%
		26	0.33						
		33	0.243						
Scenery 3	3 WF $Q=Q_g+$ $+Q_{GSC}$	24	1.026	0.387	38.7%	3.5	20%	0.31	51.56%
		27	0.979						
		33	1.021						

Table 2. Results of GA

In Table 2 it must be noted that increasing in reactive power capability of WF leads to an increase in the loadability of the system, and reduce real power losses. Furthermore, as much as reactive power injection of wind farms longer the voltage collapse point.
Fig 7 shows the voltage profile at the base loadability of the case studied (λ=0), at the base case and after the application of the optimisation algorithm for the proposed scenarios. It is shown that the optimal management of wind farms in distribution networks with high wind energy enhances the voltage profile and increases the maximum loading of the system. Most specifically, if adding three wind farms with extended reactive power capability to power systems, the maximum loading of the system for operational voltage limit will increase by 38.7%, the real power losses decrease in a 51.56% and voltage stability margin is increased 20% (Fig. 8).

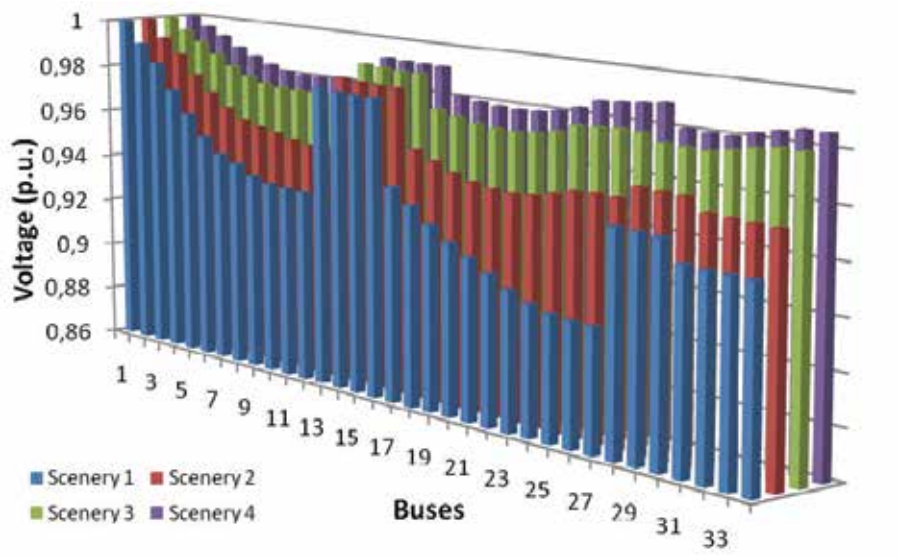

Fig. 7. Voltage profile of the modified IEEE 34 bus system

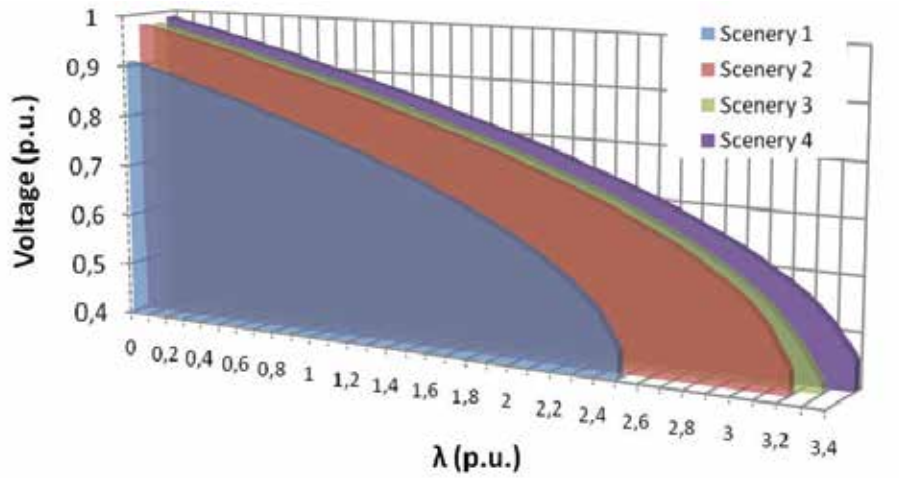

Fig. 8. Maximum loading parameter and Voltage Stability Margin

6. Conclusion

Nowadays, wind energy plays an important role in the generation mix of several countries. The major impacts resulting by the use of wind energy are related to reverse power flow, harmonics and voltage/reactive power control. At the same time, System Operator requires behaviour of wind generators similar to the conventional plant, and thus wind farms must be able to control active as well as reactive power according to the System Operator's commands. At this moment, variable speed wind turbines use electronics power converters that are capable to offer a regulation of both, active and reactive power. In this work, an optimization problem is shown in order to deal with the optimal reactive power planning of a power network with high wind energy penetration. The optimization process is based on Genetic Algorithm and is able to find out the optimal location of wind farms in order to maximize the voltage loadability and to minimize any active power losses of the whole network. The study results show that an optimal allocation of wind farms, sum up to an optimal reactive power dispatch of these ones, improve indeed voltage stability of power systems and minimize active power losses too.

7. Future researchs

The methodology proposed could be extended to work with other types of wind generators, such as full power converter. Furthermore, incorporation of fixed speed wind units in power system, equipped with FACTS devices to control reactive power, could lead a very interesting work on optimal reactive power between conventional var sources and reactive power capabilities of variable speed wind turbines.
In this work stability and economic issues are only taking into account in the optimization process. By the way, it is important to notice that wind energy, as a renewable energy, lets decrease CO2 emissions. Therefore, an interesting future research is the incorporation of reduction of CO2 emissions in the optimization problem. The optimization problem lets distributed the generation between the conventional plants and the wind farms in order to improve technical, economic and environmental issues.

8. Acknowledgment

This work has been partially supported by the Spanish Minister of Science and Innovation under contract ENE2009-13883-CO2-01.

9. References

Abdullah, N.R.H., Musirin, I. & Othman, M.M. (2010). Transmission loss minimization using evolutionary programming considering UPFC installation cost, International Review of Electrical Engineering, Vol. 5, No. 3 Part. B, (May.-Jun. 2010), pp. 1189-1203, ISSN 1827-6660.

AESO. Wind power facility technical requirements. Revision 0. Alberta Electric System Operator (AESO), Canada, November, 2004.

Amaris, H. & Alonso, M. (2011) Coordinated reactive power management in power networks with wind turbines and facts devices, Energy Conversion and Management, Vol. 52, No. 7, (Jul. 2011), pp. 2575-2586, ISSN 0196-8904.

Baghaee, H.R. , Mirsalim, M., Kashefi, A. & Gharehpetian, GB. (2009). Optimal allocation of multi-type FACTS devices to improve security and reduce the losses and fault level using multi-objective particle swarm optimization, International Review of Electrical Engineering, Vol. 4, No. 6 Part. B, (Nov.-Dec. 2009) ,pp. 1326-1335, ISSN 1827-6660.

Bhattacharya, K. & Zhong, J. (2001) Reactive power as an ancillary service, IEEE Transactions on Power Systems, Vol. 16, No. 2, (May. 2001), pp. 294–300, ISSN 0885-8950.

Díaz, A. & Glove, F. (1996). Optimización Heurística y Redes Neuronales en Dirección de Operaciones e Ingeniería, Paraninfo, ISBN 8428322694, Madrid. (in spanish).

E. On. Grid code-high and extra high voltage. E.On Netz Gmbh, Bayreuth, Germany, April 2006.

Energinet. Grid connection of wind turbines to networks with voltage above 100 kV, Regulation TF. 3.2.6. Energinet, Denmark, May 2004.

Energinet. Grid connection of wind turbines to networks with voltage above 100 kV, Regulation TF. 3.2.5. Energinet, Denmark, December 2004.

ESB. Grid code-version 3.0. ESB National Grid, Ireland, September 2007.

Goldberg, D.E. (1989) Genetic algorithms in search, optimization and machine learning, Adddison-Wesley, ISBN 0201157675, Massachusetts.

González, G. et al. (2004). Sipreólico, Wind power prediction tool for the spanish peninsular power system. Proceedings of the CIGRE 40th General Session & Exhibition, Paris, France.

Holland, J. (1975) Adaptation in Natural and Artificial Systems: An Introductory Analysis with Applications to Biology, Control, and Artificial Intelligence, Univ. of Michigan Press, ISBN 0262581116, Cambridge.

Hugang, X., Haozhong, C. & Haiyu, L. (2008) Optimal reactive power flow incorporating static voltage stability based on multi-objective adaptive immune algorithm, Energy Conversion and Management, Vol. 49, No. 5, (May. 2008), pp. 1175–1181, ISSN 0196-8904.

Hydro-Quebec. Transmission provider technical requirements for the connection of power plants to Hydro-Quebec transmission system. Hydro Quebec Transenergie, 2006.

IEA Energy Technologies Perspective 2008, OECD/IEA, March 2010, Available from: < www.iea.org/techno/etp/index.asp>

IEA Wind Energy. Annual Report 2009, March 2010, Available from: < www.ieawind.org/AnnualReports_PDF/2009.html>

Jenkins, N. et al. (2000). Embedded Generation, The Institution of Electrical Engineers, ISBN 085296 774 8, London, U.K.

Keung, P.-K., Kazachkov, Y. & Senthil, J. (2010). Generic models of wind turbines for power system stability studies, Proceedings of Conference on Advances in Power System Control, Operation and Management, London, UK, Nov. 2009.

Kundur, Prabha. (1994). Power System Stability and Control, MC-Graw-Hill, ISBN 007035958-X, California.

Martínez, I. et al. (2007). Connection requirements for wind farms: A survey on thecnical requirements and regulation. Renewable and Sustainability energy reviews, Vol. 11, No. 8, (Oct. 2007), pp. 1858-1872, ISSN 1364-0321.

National Grid Electricity Transmission. Grid code, issue 3, rev.24. National Grid Electricity Transmission plc, UK, October 2008.

Nordel. Nordic Grid Code. Nordel, January 2007.

Raoufi, H. & Kalantar, M. (2009). Reactive power rescheduling with generator ranking for voltage stability improvement, Energy Conversion and Management, Vol. 50, No. 4, (Apr. 2009), pp. 1129–1135, ISSN 0196-8904.

Salama, M.M.A. & Chikhani, A.Y. (1993). A simplified network approach to the VAR control problem for radial distribution systems. *IEEE Trans. On Power Delivery*, Vol. 8, No. 3, (Jul. 1993), pp 1529-1535, ISSN 0885-8977.

Sangsarawut, P., Oonsivila, A. & Kulworawanichpong, T. (2010). Optimal reactive power planning of doubly fed induction generators using genetic algorithms, Proceedings of the 5th IASME/WSEAS international conference on Energy; environment, ISBN 978-960-474-159-5 Cambridge, UK, Feb. 2010.

Singh, B. (2009). Wind Power interconnection into the Power System: A review of Grid Code Requirements. The electrical Journal, Vol. 22, No. 5, (Jun. 2009), pp. 54-63, ISSN 1040-6190.

Singh, B. & Singh, S. N. (2009). Reactive capability limitations of doubly-fed induction generators, Electric Power Components and Systems, Vol. 37, No. 4, (2009), pp. 427–440, ISSN 1532-5008.

Tsili, M. & Papathanassiou, S. (2009). A review of grid code technical requirements for wind farms. IET Renewable Power Generation, Vol. 3, No. 3, (2009), pp. 308-332, ISSN 1752-1416.

Ullah, N. & Thiringer, T. (2008). Improving voltage stability by utilizing reactive power injection capability of variable speed wind turbines, International Journal of Power and Energy Systems, Vol. 28 , No. 3, (2008), pp. 289–297, ISSN 1078-3466.

Vijayan, P., Sarkar, S. & Ajjarapu, V. (2009). A novel voltage stability assessment tool to incorporate wind variability, Proceedings of Power Energy Society General Meeting, ISBN 978-1-4244-4240-9, Calgary, CANADA, Jul. 2009.

Vilar, C. (2002). Fluctuaciones de tensión producidas por los aerogeneradores de velocidad fija. Ph. D. Thesis. Universidad Carlos III de Madrid. Electrical Engineering Department. 2002.

Zhang, W., Li, F. & Tolbert, L.M. (2007). Review of Reactive Power Planning: Objectives, constraints and algorithms. IEEE Trans. On Power Systems, Vol. 22, No. 4, (Nov. 2007), pp.-2177-2186, ISSN 0885-8950.

2

Wind Power Integration: Network Issues

Sobhy Mohamed Abdelkader
[1]*Queens University Belfast*
[2]*Mansoura University*
[1]*United Kingdom*
[2]*Egypt*

1. Introduction

Rise of energy prices and the growing concern about global warming have exerted big pressure on the use of fossil fuels to reduce emissions especially CO_2. Instability in some of the major oil producing countries may affect the supplies and price of oil. On the other hand the growing need for energy consumption cannot be stopped or even limited as it is directly related to the rate of development and the standard of living. Renewable energy systems offer a solution to these conflicting issues by providing a clean energy that can supply a reasonable share of the total energy requirement without contributing to air pollution. With the 20% target of the total energy consumption to be supplied by renewable energies by 2020, and the high potential of wind energy in most European countries, wind energy systems are being installed and the penetration levels of wind energy into the electrical power systems are increasing at high rates.

Concerns about integrating wind power at high penetration levels arise from the fact that the conventional network is well suited for large synchronous generators with firm capacity and fully controlled output; this network is faced with a large number of wind farms utilizing either Induction Generators (IGs) or Doubly Fed IGs (DFIGs) with small capacity spread over different voltage levels. IGs and DFIGs have no inherent voltage control capability; it is rather reactive power loads adding to the system reactive power burden and voltage control problems. Moreover, wind farms are usually installed at remote areas where strong connections to the network is are not available. The capability of the existing network to accommodate the power generated from wind becomes an important issue to investigate. The unusual power flow patterns due the injection of power at nodes at the load ends of the network require reviewing the protection system settings and may need new protection schemes based on new rules to suite the new situation.

The focus of this chapter will be on the voltage stability problem and the network capability to accommodate power from the wind. As the chapter is aimed to be a teaching tool, analysis is presented in a graphical manner using a simple two bus system.

2. Voltage stability

Voltage stability analysis methods can be categorized into either steady state or dynamic methods. The steady state methods make use of a static model such as power flow model or a linear model for the system dynamics about the steady state operating point. On the other

hand dynamic methods use a model characterized by nonlinear differential and algebraic equations which is solved by time domain simulations. Dynamic methods provide accurate replication of the actual events and their chronology leading to voltage instability; it is however very consuming in terms of computation time and the time required for analysis of the results. Moreover, it does not easily provide sensitivity information or the degree of stability. Static methods with their much less computing time requirements together with its ability to provide sensitivity information and the degree of stability are being widely used to provide much insight to voltage stability. The degree of stability is determined either by the calculation of either a physical margin (load margin, reactive power margin, etc.) or a measure related to the distance to collapse.

Most of the tests for voltage stability assessments consider the steady state stability of the power system and do not differentiate between voltage and angle stability. Only few methods such as [7] use separate tests for voltage stability and angle stability. As we are concerned with voltage stability, it is more suitable to work on the voltage plane and not on the parameter space to detect genuine voltage stability problems. For this purpose, a graphical interpretation of the problem is developed based on representation of the parameters of each load bus in the complex voltage plane. Basics of the graphical approach for the assessment of voltage stability in power systems are presented using a simple two bus power system. Despite its simplicity, the two bus system helps a lot in clar- ifying the issue because it can be handled easily by analytical methods. This helps in the acquisition of the required knowledge and concepts which can then be generalized to real power systems of any size. It is also straightforward to find a two node equivalent to a multi node power system at any of its ports. This fact makes most of the conclusions drawn from the two node system valid for a general power system.

With wind power integrated into the electrical power system at high penetration levels, the situation becomes a bit different. Power is being injected at PQ nodes. In addition to the changed power flow patterns, the characteristics of the PQ nodes, at which wind generators are connected, also changed. Wind as a stochastic source has also introduced a degree of uncertainty to the system generation.

2.1 Graphical interpretation of voltage stability limit

As mentioned above all the analysis in this chapter will be carried out for a two bus system. The system, as shown in Fig.1, has only one line of series impedance Z and no shunt admittance. The effect of the line charging can be taken into consideration by using the Thevenins equivalent of the system at the load bus. One of the two buses is considered a slack bus with constant voltage E while the other one is the load bus at which voltage stability is to be studied.

Fig. 1. Two bus system

Throughout the analysis the following symbols and conventions are adopted.
Z: impedance magnitude of the line
θ: impedance angle of the line
R: the line resistance
X: the line reactance
V: voltage magnitude at the load bus
δ: voltage angle at the load bus
P: active power injected at the load point
Q: the reactive power injected at the load.
V, **E** and any other bold variable means that it is a phasor variable
For the system of Fig.1, active power and reactive power balance equations can be written in the following forms:

$$-P = \frac{V^2}{Z}\cos(\theta) - \frac{EV}{Z}\cos(\theta+\delta) \tag{1}$$

$$-Q = \frac{V^2}{Z}\sin(\theta) - \frac{EV}{Z}\sin(\theta+\delta) \tag{2}$$

Eqns. (1) and (2) represent constraints on the load bus voltage and must be satisfied simultaneously. A11 the points in the complex voltage plane that satisfy the two constraints are possible solutions for the load bus voltage. If the system fails to satisfy these constraints simultaneously, this means that the stability limit has been exceeded and no solution will exist. These constraints will be plotted in the complex voltage plane to find the possible solutions for the voltage and also to define the voltage stability limit. Steady state analyses of power system assume constant active power, P, and constant reactive power, Q, at all load nodes and for generators reaching any of their reactive power limits. This assumption works very nicely for power flow studies and studies based on snap shot analysis. However, if the purpose is to find out the stability limit, such assumption may be misleading. In case of large wind farm connected at a relatively weak point, it will not be accurate to consider the constant P Q model. In the following sections the effect of P and Q characteristics on voltage stability limit is illustrated. Three different characteristics are examined; constant P and constant Q, quadratic voltage dependence, and induction motor/generator.

2.1.1 Constant PQ load model

Assuming a constant active and reactive power, which is the common model for PQ nodes in power flow studies and substituting for V^2 by $(V.\cos(\theta+\delta))^2+(V.\sin(\theta+\delta))^2$, Eq. (1) can be arranged and expressed as follows.

$$\left(V\cos(\theta+\delta) - \frac{E}{2\cos(\theta)}\right)^2 + (V\sin(\theta+\delta))^2 = \left(\frac{E}{2\cos(\theta)}\right)^2 - \frac{PZ}{\cos(\theta)} \tag{3}$$

Equation represents a circle in the complex voltage plane. Using the rotated axes V.cos(θ+δ) and V.sin(θ+δ) rather than real(V) and Imaginary(V) makes constructing this circle easier. On the new axes, centre of the circle is located at $(0.5E/\cos(\theta), 0)$ and its radius,

$$r_p = \sqrt{E^2/4 + RP}/\cos(\theta).$$

This circle, will be referred to as p-circle, defines the locus for constant load power in the complex voltage plane and all the points on it satisfy the active power constraint. Similarly, the reactive power balance, Eq. (2), can be rearranged and written as below.

$$\left(V\cos(\theta+\delta)\right)^2+\left(V\sin(\theta+\delta)-\frac{E}{2c\sin(\theta)}\right)^2=\left(\frac{E}{2\sin(\theta)}\right)^2-\frac{QZ}{\sin(\theta)} \tag{4}$$

Again, Eq.(4) represents a circle in the complex voltage plane. A11 points on this circle satisfy the reactive power balance constraint and it will be referred to as the q−circle. On the same axes as in the case of p-circle, centre of the q-circle is located at $(0, 0.5E/\sin(\theta))$ and its radius

$$rq=\sqrt{E^2/4+QX}/\sin(\theta)\,.$$

Fig.2. shows the complex voltage plane with circles for different values of P and Q. The values used to produce this figure are: E= 1 pu, Z=0.7 pu and θ=60°. In this figure, P0 =0, P1 =0.3, P2 = 0.48, Q0 =0 and Q1 =0.23 (all in pu). The following points can be observed from the figure:

1. Centre locations of the two circles, CP and CQ, are determined by E, Z, and θ only. This means that the distance between the two centres remains constant as long as there is no change in E or the line impedance whatever the values of P and Q are.
2. Both of r_p and r_q are load dependant. As the load (P and/or Q) gets larger, r_p and/or r_q gets smaller. This is clear on Fig. 2 where $r_{p0} > r_{p1} > r_{p2}$ & $r_{q0} > r_{q1}$.
3. As long as r_p+r_q is greater than the distance between the two centres, the two circles intersect each other in two points and hence there will be two possible voltage solutions for the load bus. The voltage solution with higher magnitude will be called the higher voltage, V_H, while the other will be called the lower voltage, V_L.
4. At light loads r_p+r_q is much greater than the distance between the centres, this causes a large difference between the points of intersection (the voltage solutions). This difference gets smaller as the load increases due to the reduction in r_p+r_q.
5. If the load is increased until r_p+r_q becomes just equal to the distance between the centres, the two solutions coincide with each other and there will be only one solution. Any further increase in either P or Q will cause even this single solution to cease to exist.
6. The circles P0 and Q0 intersect at V=1 =E, and at V=0. These are the two possible solutions at no load. Increasing P to P1 while keeping Q at 0, the new voltage solutions are those defined by the two arrows. When Q increases to Q1, the two circles P1 and Q1 are tangential and the voltage solutions coalesce into one solution. Any further increase in either P or Q will cause this one solution to disappear. The circles P2 and Q0 are tangential, having one voltage solution, revealing that the loading condition (P2,Q0) is a voltage stability limit. As the figure shows, as the system approaches the stability limit the voltage solutions become closer until they coalesce in one solution. The end point of the voltage vector at the stability limit always lies on the line V.cos(δ) = 0.5*E. Each point on this line defines a voltage stability limit for a different combination of P and Q. It is easy to prove the singularity of the load flow Jacobian at each point of this line. Each other known criterion for voltage the stability limit, such as maximum Q, maximum P, refers to a subset of the conditions defined by this line.

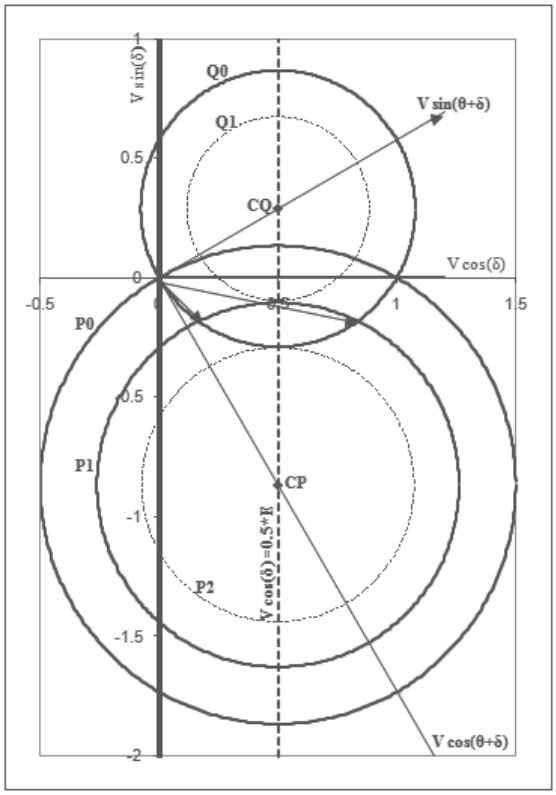

Fig. 2. Loci for active and reactive power balance constraints in the complex voltage plane

2.1.2 Constant impedance load

If the load is considered to have constant impedance, then both P and Q can be expressed as functions of voltage as follows:

$$P = G.V^2 \tag{5}$$

$$Q = B.V^2 \tag{6}$$

Substituting for P from (5) into (1) the active power equation can be arranged in the following form:

$$V = \frac{E}{G.Z + \cos(\theta)}.\cos(\delta + \theta) \tag{7}$$

Eq.(7) represents a circle in the complex voltage plane with its centre lying on the *V cos(θ+δ)* axis at *V cos (θ+δ) = 0.5 E./(G. Z+cos (θ))* and its radius equal to *0.5 E./(G. Z+cos (θ))*. Similarly the Q equation can be re—written as*:*

$$V = \frac{E}{BZ + \sin(\theta)}.\sin(\delta + \theta) \tag{8}$$

which again is a circle in the complex voltage plane with its centre lying on the V sin*(θ+δ)* axis at *V sin(θ+δ) = 0.5 E/(BZ+Sin(θ))* and its radius equal to *0.5 E/(BZ+Sin(θ))*. Fig. 3 shows these two circles on the complex voltage plane. Inspection of the graph and the circle parameters leads to the following observations:

1. The locations of the centres of the circles are load dependant and so are the radii.
2. The two circles always have two intersection points one of which is V= 0.0. The other one depends on the load impedance. So, there is only one feasible solution. However, this solution always exists as long as the load impedance is greater than zero.
3. The nonzero voltage magnitude can be calculated from (7) and (8) as:

$$V = \frac{E}{\sqrt{1 + Z^2\left(G^2 + B^2\right) + 2BZ\sin(\theta) + 2GZ\cos(\theta)}} \tag{9}$$

   It is easy to find out that this voltage decreases as G and/or B increases. This means that this voltage solution is always stable. So, for constant impedance load, there is only one possible solution and it is stable for the whole range of load impedance.
4. Active and reactive powers can be derived by substituting for V from (9) into (5) and (6) respectively yielding:

$$P = \frac{GE^2}{1 + Z^2\left(G^2 + B^2\right) + 2BZ\sin(\theta) + 2GZ\cos(\theta)} \tag{10}$$

$$Q = \frac{BE^2}{1 + Z^2\left(G^2 + B^2\right) + 2BZ\sin(\theta) + 2GZ\cos(\theta)} \tag{11}$$

   But, in all cases the voltage is stable and the voltage of a system with such load can not collapse like in the case of constant power load.
5. The condition for maximum power transfer to the load bus can be derived by equating the determinant of the Jacobian matrix of P and Q w.r.t G and B to zero. This can be found to be:

$$G^2 + B^2 = \frac{1}{Z^2} \tag{12}$$

A11 of the points satisfying this condition are lying on the border line defined in the case of constant power load (*V cos (θ+δ) = 0.5 E)*. However, in this case this line is not the border between stability and instability area, but it is the border between two areas with different sensitivities for load power to changes in G and B. In the area to the right hand side, load has positive sensitivity to changes in G and B, whereas in the area to the left hand side if G and/or B is increased beyond this limit, the load power will decrease, but in the two areas voltage always decreases as G and/or B increases and vice versa.

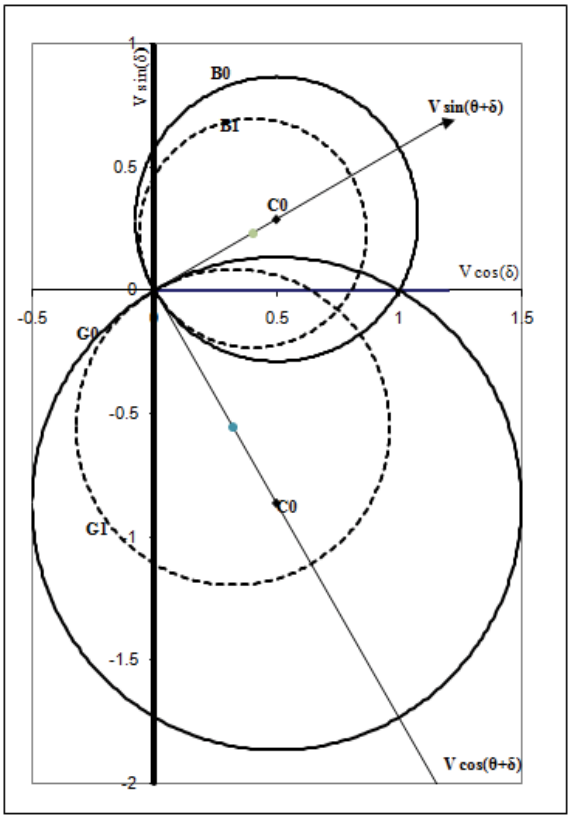

Fig. 3. Loci for constant load admittance parameters in the complex voltage plan

2.1.3 Constant current load

In this case, both P and Q are proportional to the load voltage magnitude i.e;

$$P = \alpha.V \tag{13}$$

$$Q = \beta.V \tag{14}$$

With the load voltage taken reference, the load current, I, will be:

$$I = \alpha - j\beta = \sqrt{\alpha^2 + \beta^2}\angle - \tan^{-1}(\beta / \alpha) \tag{15}$$

As seen from (15), the current magnitude is constant while its direction is dependent on the voltage angle. So, the voltage drop on the line will have a constant defined magnitude while its angle is unknown until the voltage direction is determined. This can be represented in the voltage plane as a circle with its radius equal to *I.Z* and its centre located at the end of the E vector which is on the real axis.

Since α and β are constants, then the load power factor is also constant. The locus for a constant power factor in the voltage plane can be found (by dividing (1) by (2), equating the result with tan(φ), expanding *cos (θ+δ)* & *sin (θ+δ)* terms, and rearranging) to be a circle with its equation is:

$$\left(V\cos(\delta)-\frac{E}{2}\right)^2+\left(V\sin(\delta)-\frac{E}{2}\tan(\frac{\pi}{2}-\theta+\phi)\right)^2=\left(\frac{E}{2\cos(\frac{\pi}{2}-\theta+\phi)}\right)^2 \quad (16)$$

This circle can be constructed in the voltage plane as follows:

- The centre is defined by the intersection of the line making an angle = arctan (ß/a) with the *V sin (θ+δ)* axis (counter clockwise for lagging power factor and clockwise for leading power factor) and the line *Vcos (δ)*= 0.5 E.
- The radius is the distance between the centre and the origin.

Fig (4) shows these circles on the voltage plane for different values of load current, and different power factors. There are always two points of intersection. However, one of these points corresponds to a load condition while the other to a power injection i.e. generation. So, for load of constant current behaviour, there is always one voltage solution and this solution is totally stable according to the criterion stated before. The limiting factor in this case will not voltage stability, it would rather be the thermal limit of the lines or the voltage regulation.

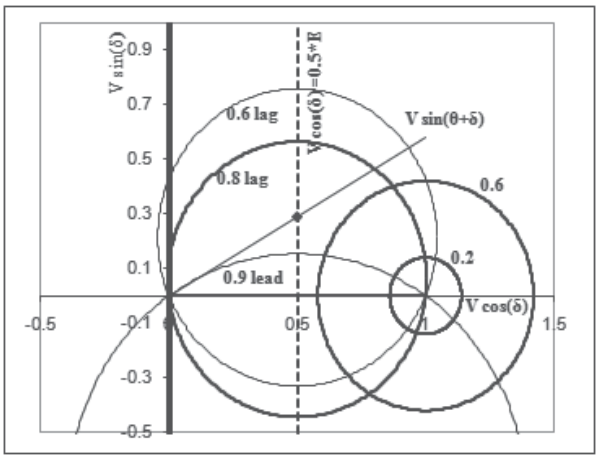

Fig. 4. Constant current and constant power factor circles in the complex voltage plane

For further comparison between the three type of loads, Fig. 5.a shows the voltage against the load parameter, i.e P for constant power load, G for constant impedance load, and α for constant current load. A11 loads are assumed to have the same power factor of 0.8 lagging. The rest of the system parameters are E=1.0 pu, Z=0.7 pu, and θ=60°. This figure confirms what has been observed from Figs. 2 - 4 regarding the voltage magnitude. Fig. 5.b shows the P-V curve, which is found to be the same for all types of loads. Fig.5.c shows the maximum loading limits in the P-Q plane, and also it found to be the same for all the three cases. It is to be noted that the mapping of this limit into the voltage plane is the line which we called the border line (BL). Although the constant impedance and constant current can have a stable equilibrium point on the lower part of the P-v curve, they are not allowed to reach this part. This is because if such loads are operated in this part and it was required to shed some load, disconnecting part of these loads will increase their power demand instead of reducing it as it is desired. Also, reaching this part of the curve means that the voltage is very low.

Now, if these loads are allowed only to be operated in the upper part of the P-v curve, the stability limit will be the same for all of the three load types. Bearing in mind that the locus of the stability limit in the voltage plane is the BL defined above, therefore if the voltage solution lies on that line, the voltage stability limit is reached. This means that the voltage solution at the stability limit is determined by the intersection point of the P- locus, the Q locus and the BL. In other words, if the intersection point of the P-locus with the BL and the intersection point of the Q-locus with the border line coincide with each other, the voltage stability limit is reached.

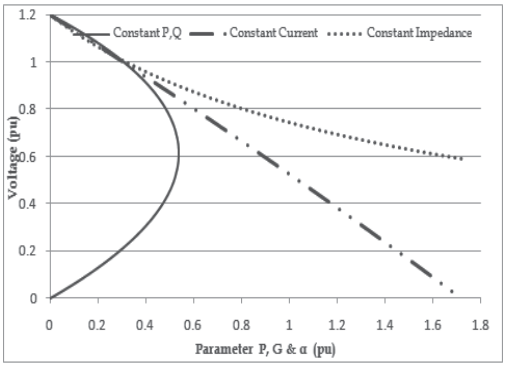

a. Voltage/Load parameters

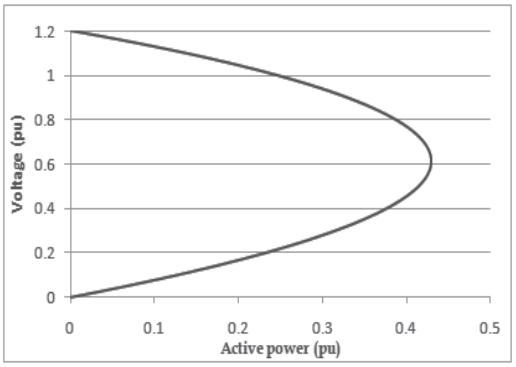

b. Voltage/Active power

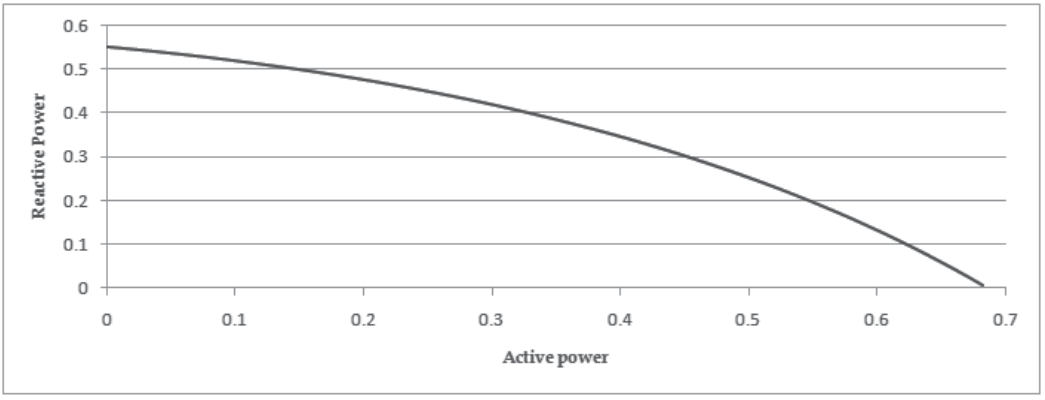

c. Voltage stability limit in the complex power plane

Fig. 5. Comparison of the behaviour of different types of loads regarding voltage stability

The fact that the border line between voltage stability and voltage instability region is the same, in terms of active power and reactive power, makes almost all voltage stability assessment methods use one of the features of this border line as a voltage stability measure or indicator. $Vcos(\delta) = 0.5\ E$, which is the border line equation in the voltage plane, is one form of the indicator introduced by Kessel P. & Glavitch, H. (1986). At any point on the BL, the voltage is equal in magnitude to the impedance drop; this implies that the load impedance is equal in magnitude to the system impedance, which was used as another indicator by Abdelkader, S. (1995) and Elkateb, M. et al (1997) have presented mathematical proofs for the indicators introduced by Chebbo, A. et al (1992)., Semlyn, A. et al (1991),

Tamura, Y et al (1983) and Kessel P. & Glavitch, H. (1986) are all different characteristics or features of the border line.

If a wind farm employing IGs or DFIGs is connected to the network at a node where it represents the major component of the power injected at that node, the models described above will not be suitable to represent the wind generators for assessing voltage stability. Moreover, the voltage stability limit will be different than the border line defined above. Abdelkader, S. & Fox, B. (2009) have presented a graphical presentation of the voltage stability problem in systems with large wind farms. The following section describes how voltage stability in case of large penetration levels of wind power is different than the case of constant or voltage dependant loads.

2.2 Voltage stability of wind generators

It is assumed here that IG is employed as a wind turbine generator. If an IG is connected at load node of the two node system, the equivalent circuit of the system will be as shown in Fig. 6.

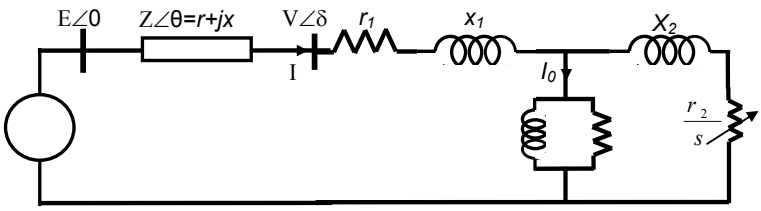

Fig. 6. Equivalent circuit of the two bus system with IG

Neglecting the no load current, I_0, the current delivered by the induction generator to the system can be calculated as

$$I = \frac{E}{(r + r_1 + \frac{r_2}{s}) + j(x + x_1 + x_2)} \tag{17}$$

Voltage at the end of the transmission line can be calculated as follows.

$$V\angle\delta = E\angle 0 - \frac{E}{(r + r_1 + \frac{r_2}{s}) + j(x + x_1 + x_2)}.Z\angle\theta \tag{18}$$

With s as a parameter, the voltage vector locus in the voltage plane can be obtained through some manipulations of (18). It is found to be as follows.

$$\left(V\cos(\delta) - (E - \frac{E.x}{2(x + x_1 + x_2)})\right)^2 + \left(V\sin(\delta) - \frac{E.r}{2(x + x_1 + x_2)}\right)^2 = \left(\frac{E.Z}{2(x + x_1 + x_2)}\right)^2 \tag{19}$$

Equation (19) represents a circle in the complex voltage plane. The coordinates of its centre, CG, and its radius are clearly defined in (19). Fig. 7 shows the complex voltage plane with the IG circle diagram. System data are same as for Fig.2. IG data used to produce this figure are x1= x2=0.2 pu and r1=r2=.05 pu. The figure displays the locus of the IG voltage, the

circle cantered at CG, the loci for Q=0 and P=0. The figure shows clearly that even with the magnetizing current neglected the IG cannot deliver any power at Q=0 as the IG circle has no intersection points with Q=0 except at P=0. When reactive power consumed at the point of connection increases, radius of the Q circle gets smaller and there will be two intersection points where the IG can deliver power.

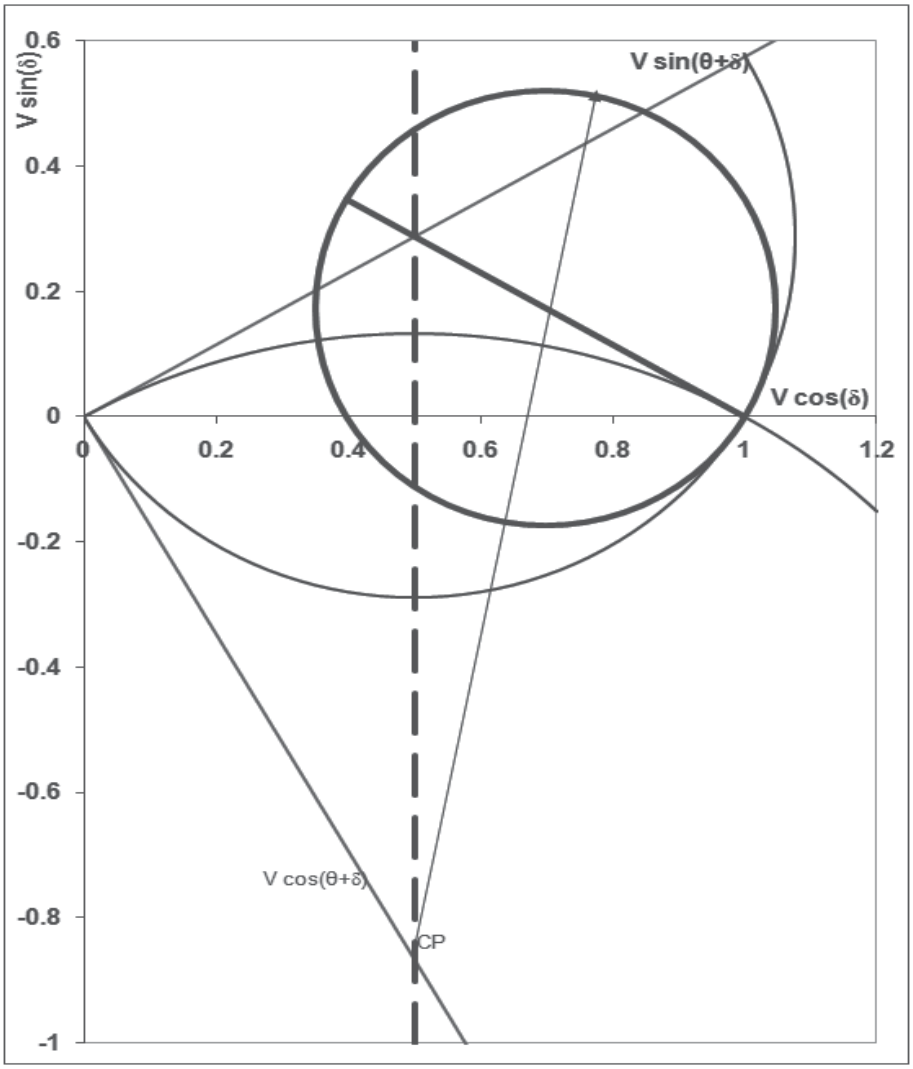

Fig. 7. Complex voltage plane for the case of IG

As the power delivered by the IG increases, the P-circle radius increases until a value is reached where the P circle becomes tangent to the IG circle at the point Pm in Fig. &. This is the maximum limit of the IG power. No equilibrium point exists if P is increased beyond this limit. The point of maximum power, or the steady state stability limit, Pm, is determined by connecting the centres of the IG and the P circles with a line and extending it until it intersects the IG circle in Pm. The most important thing to note is that the stability

limit is no longer the same for the case of constant PQ load, the dashed line on Fig. 7. Therefore, all the indicators based on the PQ load model might be misleading if used for the case of IG. In other words, voltage stability in case of a WF employing IGs is not determined by only the terminal conditions of the IG, P and Q injections, but also by the IG characteristics. It is also clear that at each active power output from the IG there is a specific value of reactive power that has to be consumed by the IG. Nothing new about that, but the new thing the graph offers is that the reactive power support required at each active power output can be determined. Moreover, other limits of voltage magnitude, maximum and minimum, as well as the thermal capacity of the line connecting the farm to the system can all be represented graphically in the complex voltage plane. This enables to determine which of these limits are approached or violated. Mapping these into the complex power plane helps fast determination of a quick local remedial action.

2.2.1 Application to multi node power system

To apply the graphical method to assess the voltage stability of IG, the power system is to be reduced to its Thevenin equivalent at the node where the IG is installed. A method for finding the Thevenin equivalent using multiple load flow solutions is described by Abdelkader, S & Flynn, D. (2009) and is used in this paper. Thévenin's equivalent is determined using two voltage solutions for the node of concern as well as the load at the same node. The first voltage solution is obtained from the operable power flow solution while the second is obtained from the corresponding lower voltage solution. The voltage for the operable solution is already available within data available from the EMS and hence it will be required to solve for the lower voltage solution. The Thévenin's equivalent can be estimated using the two voltage solutions as follows.

$$E_{TH} = \frac{\left|\bar{V}_H\right|^2 - \left|\bar{V}_L\right|^2}{\left|\bar{V}_H - \bar{V}_L\right|} \tag{20}$$

$$\left|\bar{Z}_{TH}\right| = \frac{\left|\bar{V}_H\right|.\left|\bar{V}_L\right|}{\sqrt{P^2+Q^2}} \quad , \qquad \Theta_{TH} = \Phi \; - \delta_H - \delta_L \tag{21}$$

Where V_H and V_L are the complex values for the higher and lower voltages of the load node, P is the active power, Q is the reactive power, θ_{TH} is the angle of Z_{TH}, Φ = atan(Q/P), and δ_H, δ_L are the angles of the high- and low-voltage solutions respectively. A graph for a multi-node power system having a WF connected at one of its nodes is developed as follows.

1. An IG equivalent to the WF is to be determined. Assuming that all generators of the WF are identical, the equivalent IG rating will be MVAeq = MVA.n, and Zeq=Z/n. MVA is the rating of one IG, n is the number of IGs in the farm, and Z stands for all impedance parameters of one IG.
2. A Thevenin equivalent is determined at the WF terminal using (20), (21).
3. The system graph with the IG in the complex voltage plane is drawn as described above.

4. The graph can be mapped into the complex power plane bearing in mind that any a point (x,y) in the voltage plane maps to a point (p,q) in the complex power plan, where p, q are related to x,y by the following equations.

$$p = \frac{x.E-(x^2+y^2)}{Z}\cos(\theta)-\frac{E.y}{Z}.\sin(\theta) \quad (22)$$

$$q = \frac{x.E-(x^2+y^2)}{Z}.\sin(\theta)+\frac{E.y}{Z}.\cos(\theta) \quad (23)$$

2.3 Test case

The IEEE 30 bus system with the standard data is used as a test system. A WF is connected at bus 30. The DIgSilent power factory is used for power flow solution of the detailed system model with the WF installed. The WF consists of 50 IG 900 kW each. The IG is rated at 6.6 kV with X=0.1715581 pu, and R/X=0.1. The magnetizing current Im is assumed to be 0.1pu.

The higher voltage solution of bus 30 for the standard case data is V_H =1.0056∠-12.63^o pu, and the corresponding lower voltage solution is V_L =0.0782∠-65.65^o pu. Parameters of the Thevenin equivalent for bus 30 are E_{TH}=1.0463 pu and Z_{TH} =0.7302∠70.64^o pu.

Fig. 8 shows the complex voltage plane with the graphs of bus 30 and the equivalent IG. The figure also shows the voltage limits constraints, V_{min} = 0.95 pu and V_{max}=1.05 pu. The thermal capacity of the line connecting the WF to bus 30 is assumed 0.6 pu and is also represented in Fig. 8. The magnetizing current of the IGs is taken into consideration as it can be noticed by shifting the IG circle along the line A-GC by Im.Z_{TH}/(X_{th}+X), X_{th}=Z_{TH}.sin(θ) and X is the IG reactance.

It can be noticed that maximum power point of the IG is not the PQ voltage stability line as discussed earlier. The voltage stability limit will not V cos (δ) = 0.5 E_{TH} as in the case of PQ load, but it will be the max power line on Fig 8. The stable operating range of the IG is thus the part of the circle starting at point A passing through points B, C, D, E, and ending at Pm, the maximum power point.

Fig 9 shows the system loci and limits mapped to the power plane and it reveals important information. First, the range of power output from the WF extends from point A up to point Pm. The value of Pm for this case is found to be - 64.8 MW. This is verified through running the detailed power flow analysis of the system on DIgSilent software. The WF power, P, is increased until the power flow diverges. The maximum value P at which the power converges is found to be the same as that obtained from the graph. That is Pm = 64.7 MW. The graphical method is also verified by running the detailed power flow solution with WF power values corresponding to points B, C, D, and E. The results were in perfect agreement with that obtained from the graph.

It is interesting to note that along A-B, the WF delivers its output with all constraints satisfied. Between B and C, the maximum voltage constraint is violated. From C to D, all constraints are satisfied again. Between B (P=13.7 MW) and C (P=38.6 MW), more reactive power will need to be consumed to get the voltage back below the maximum voltage limit. This can be obtained from the graph by the vertical difference between the IG line and the

maximum voltage limit line. At D, the thermal capacity of the line connecting the WF to the system is reached. From D to E, only the thermal capacity limit is violated. The graph shows that a reactive power equal to the vertical difference between the IG line and the thermal limit line will relief the overload. This can be done as long as no other constraint is violated. So, many indications about the system state and also corrective measures can be obtained using this simple graph. Most of these are tested using the detailed power flow analysis.

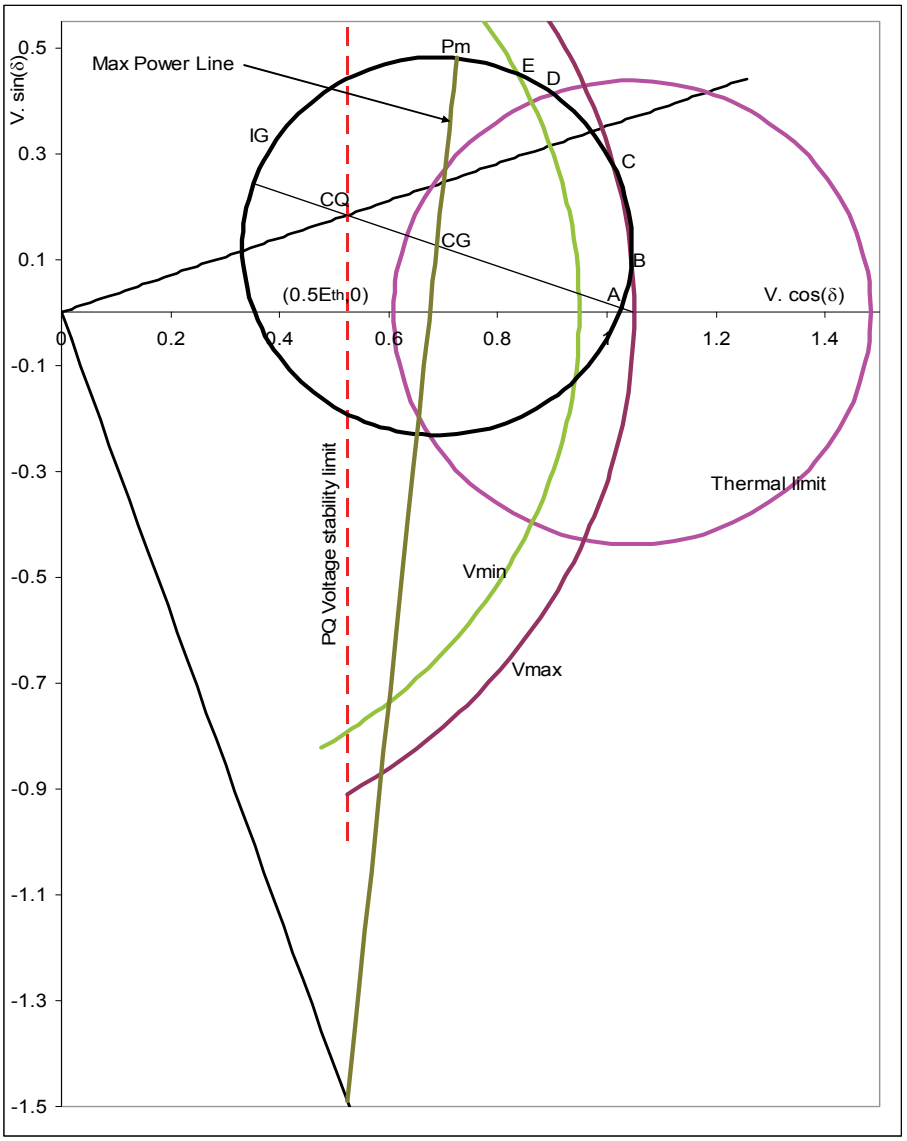

Fig. 8. Complex voltage plane for bus 30 of the IEEE 30 bus system with IG

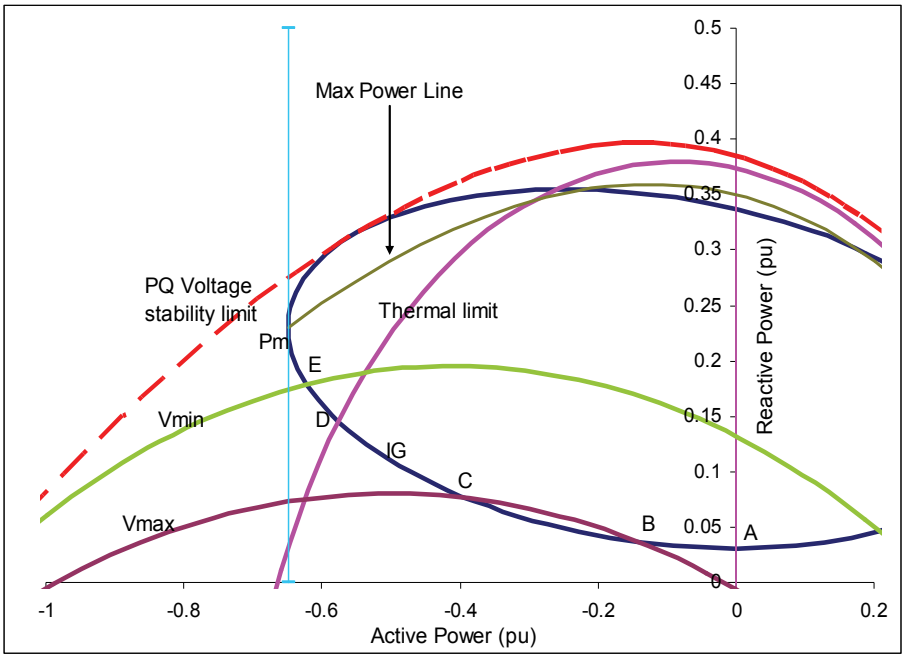

Fig. 9. Power plane graph for bus 30 of the IEEE 30 bus system with IG

3. Capability chart

This section presents a graphical method for determining network limits for wind power integration. For each candidate node, where a wind farm is planned, a capability chart is constructed defining the allowable domain of power injection where all operating and security constraints are satisfied. Like what has been done is sec. 2, operating and security constraints are graphically constructed in the complex voltage plane and then mapped to the complex power plane defining the allowable operating region of wind generator/farm.

3.1 Graphical representation of operation and security constraints

The available generation limits both active and reactive power, thermal limits of the transmission line, upper and lower voltage limits and voltage stability limit at the node where the WF is connected are all considered. As has been done in section 2, all the analysis is carried out on the simple two bus system of Fig.1. Application to a multimode power system will be done using Thevenin equivalent in the same manner described above. The reader is advised to refer to Abdelkader, S. & Flynn D (2009) for detailed analysis and applications. In this chapter, the idea is introduced in a simple manner that makes it suitable for teaching.

3.1.1 Generator power limits

The active power of the generator of the simple system of Fig. 1 can be determined as:

$$P_G = \frac{E^2}{Z}\cos(\theta) - \frac{E.V}{Z}\cos(\theta - \delta) \tag{24}$$

which can be rearranged as follows:

$$V.\cos(\theta-\delta) = E.\cos(\theta) - \frac{P_G.Z}{E} \tag{25}$$

Eqn. 25 represents a straight line in the complex voltage plane, and although it is easy to draw such a relation on the reference (V.cos(δ) & V.sin(δ)) axes, it is much easier to do so on the rotated V.cos(θ-δ) axis shown in Fig. 10, where a particular value of P_G correspond to a line perpendicular to this axis. Figure 2 shows the line AB representing P_G=0 which is drawn from the point A(E,0) on the V.cos(δ) axis perpendicular to the V.cos(θ-δ) axis. Other values of P_G can be represented by lines parallel to the line AB, but shifted by a distance representing (P_G.Z/E). The maximum P_G line is thus a line parallel to AB and shifted from it by a distance of (P_{Gmax}.Z/E), line P-P in Fig. 10. The minimum limit on P_G is also represented by the line marked P_{Gmin}.
The reactive power of the generator, given by (26), can also be rearranged in the form of (27) below.

$$Q_G = \frac{E^2}{Z}.\sin(\theta) - \frac{E.V}{Z}.\sin(\theta-\delta) \tag{26}$$

$$V.\sin(\theta-\delta) = E.\sin(\theta) - \frac{Q_G.Z}{E} \tag{27}$$

Similar to the case for active power, it is clear that (27) represents a straight line in the complex voltage plane. Examining the geometry of Fig. 10 confirms that the line AC perpendicular to the V.sin(θ-δ) axis and passing through the point A represents the zero reactive power line. The maximum reactive power line is Q-Q which is parallel to AC and shifted by ($Q_{G\,max}$.Z/E) from AC, while the minimum reactive power limit is represented by the line marked Q_{Gmin}. Hence, the shaded area bordered by the active and reactive power constraints represents the area of feasible generator. Upper and lower active power limits of the generator are both positive, while the lower reactive power limit is assumed negative. These is common for synchronous generators. However, in this work negative lower limit for active power of the slack bus will be expected in the case of representing the equivalent of a multi node power system. Negative lower limit of active power generation means that the active power injected at the PQ node will have a capacity credit so that the schedueled conventional generation in the system is less than the total load.

3.1.2 Transmission line thermal limit

Thermal limit of the transmission line is defined by the maximum allowable current. Representing a constant current in the complex voltage plane is discussed in section 2.1.3 and the graphical representation is shown in Fig. 4 above.

3.1.3 Voltage stability limit

As discussed above, voltage stability limit in case of static loads (constant power, constant current, and constant impedance) is the line *Vcos (δ) = 0.5 E* and it is drawn and marked on figs 2, 3. The voltage stability limit in case of IG is different, but in this chapter voltage stability is considered the same as for static loads. This is to keep presentation of the capability chart as simple as possible.

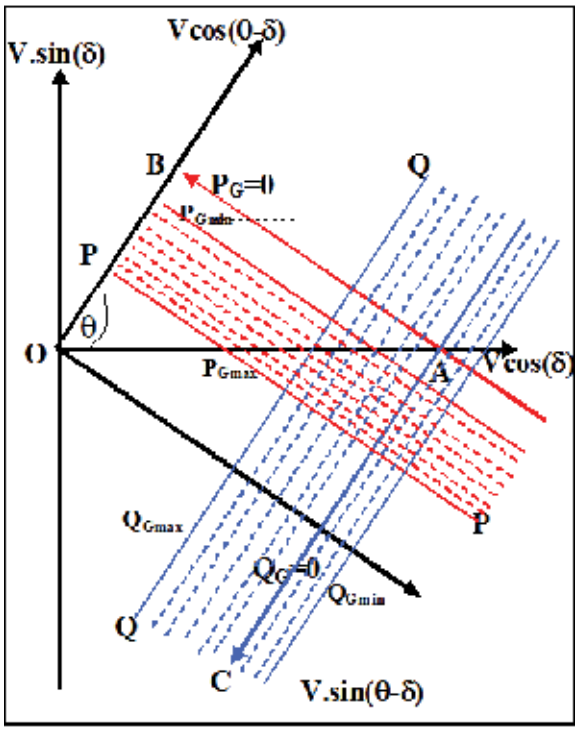

Fig. 10. Generator capability limits in the complex voltage plane of the load node

3.1.4 Maximum and minimum voltage limits at the WF terminals

Voltage at the WF terminals, and actually at all system nodes, is required to be kept above a lower limit, V_{min}, and below a high limit, V_{max}. This can be expressed as:

$$V_{\min} \leq |V| \leq V_{\max} \tag{28}$$

In the voltage plane, the inequality defined by (28) represents the area enclosed between two circles both centred at the origin, the inner, smaller, circle has radius V_{min} whereas the larger circle has a radius V_{max}. Minimum and maximum voltage constraints are now drawn along with the previous constraints in the voltage plane as shown in Fig. 11 with the shaded area representing the domain of allowable PQ bus voltage. It can be seen that the feasible operating area, for the present case, is limited by P_{Gmax} at the bottom, then by Q_{Gmin}, by V_{max} at the right hand side, by P_{Gmin}, line capability and Q_{Gmax} at the top, and by V_{min} on the left hand side. For a particular system the above limits may well change, and will also be influenced by changes in the operating conditions of the same system.

It is clear now that the feasible operating region of a power system node can be determined graphically in the complex voltage plane. Having the feasible operating region defined in the complex voltage plane, it can be easily mapped to the complex power plane to get the capability chart of the node at which the WF is connected. Mapping from complex voltage plane to complex power plane is done using the method described in sec. 2.2.1 and equations (22) and (23). Fig. 12 shows mapping of the constraints of fig. 11 into the complex power plane. The shaded area in Fig. 12 is the capability chart for the PQ node.

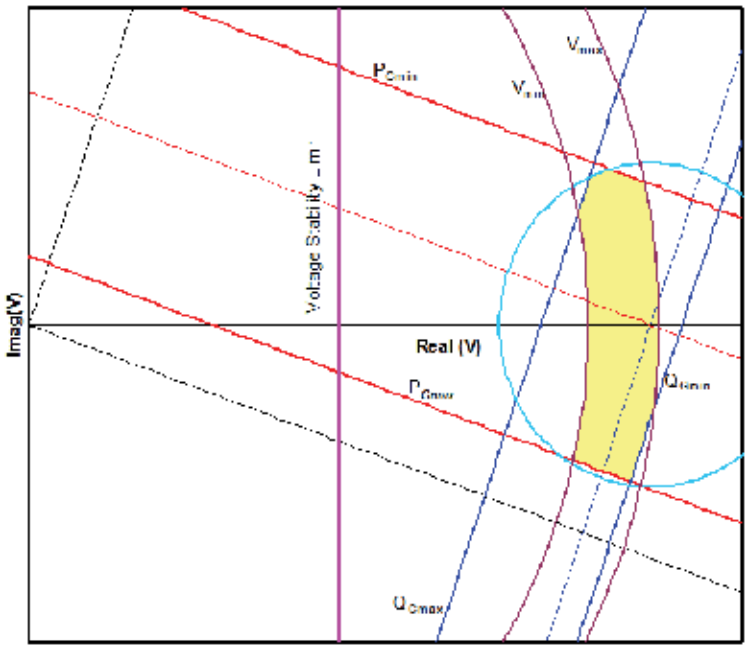

Fig. 11. The complex voltage plane with all of the constraints on the PQ node voltage

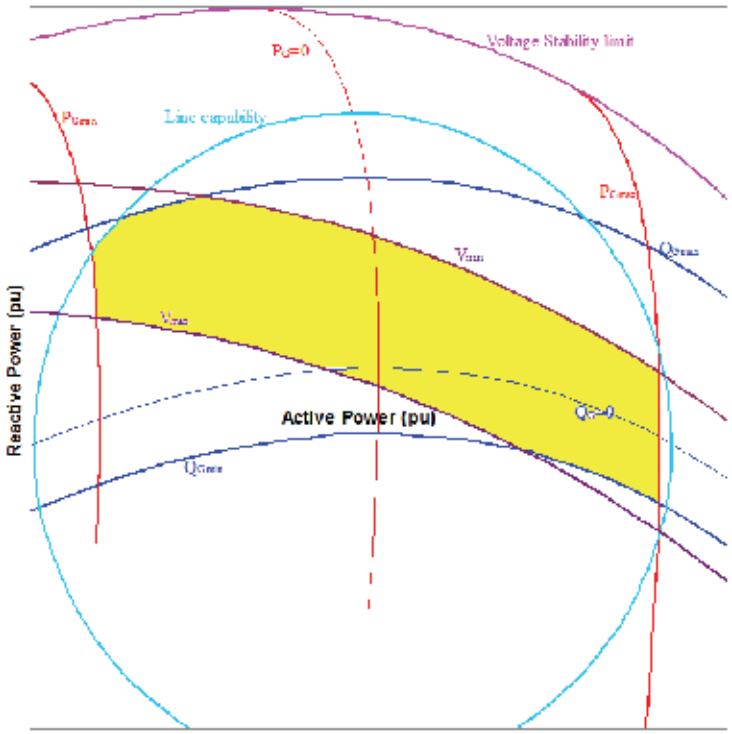

Fig. 12. Operating and stability constraints in the P-Q plane

3.2 Test case

IEEE 30 bus system is used as a test system for the voltage stability analysis and it will be the test system for this section as well. Bus 30 is chosen for application of the proposed method because it is the weakest bus of this system and WFs are usually connected at remote areas where the network is weak. The method can, however, be applied at any other bus. At the base case, active power load at bus 30 is 10.6 MW (0.106 pu) and the reactive power is 1.9 MVAr (0.019 pu). The higher voltage solution V_H, V_L and Thevenin equivalent are the same as in sec. 2.3. A capability chart is drawn, Fig. 13, with the load at node 30 marked by a diamond. The load point lies well within the allowable area with all the constraints satisfied.

The accuracy of the capability chart can be further tested in many different ways. A second way is to evaluate the corners of the feasible region, points A, B, C, D, E, F and G of Fig. 13. Each corner is the intersection of two constraints that are about to be violated. The active and reactive power coordinates of the corner points are used as P and Q injections at bus 30 and a detailed load flow study is carried out using DIgSILENT Power Factory software. The results are listed in Table 1, which identifies the corner points, the corresponding power injections, the limiting constraints, and the values obtained from load flow calculations for the voltage and current at bus 30. Threshold values for the constraints are shown within brackets following the first incident of each constraint. Examining the first row of the table, for corner point A, the voltage at node 30 is 1.061 pu exceeding the maximum allowable voltage; PG is -0.3326 pu which is less than P_{Gmin}; I and QG are both within limits. The same validation can be observed for all other corner points with an error less than 2%.

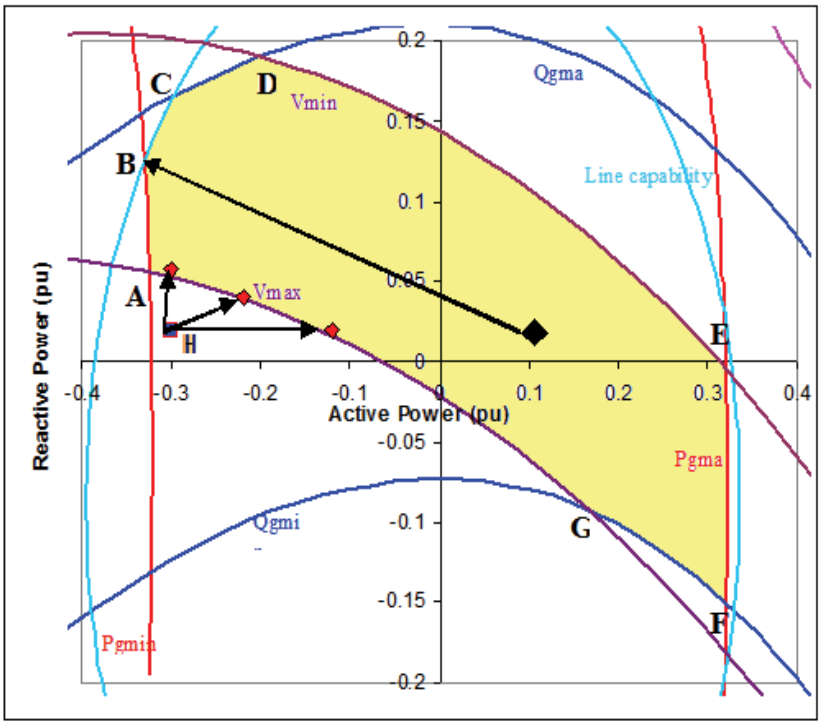

Fig. 13. The capability charts for bus 30 of the IEEE 30 bus system

As one further approach to confirm the benefits of the proposed capability chart, consider point H on Fig 13, where excessive wind generation causes an over voltage at bus 30. The three arrows emanating from H suggest three different ways to correct the situation. The first option is to maintain wind power at 30 MW and increase the reactive power consumption at bus 30 from 2 MVAr to 5.8 MVAr. A second option is to curtail 8 MW of wind power and add 2.1 MVAR load. Finally, a third option is to leave reactive power unchanged and reduce the output of the wind farm to 12 MW. These corrective actions are applied to the detailed system model, one at a time, and a load flow calculation is carried out. The voltage at bus 30 is found to be 1.06∠3.85° pu, 1.06∠0.54° pu, and 1.06∠-3.58° pu for each of the three cases respectively, which is again in complete agreement with the chart.

	Power injections		Constraints Violated		Load Flow Calculated Values			
	P MW	Q MVAR			V (pu)	I (pu)	P_G^* (pu)	Q_G^* (pu)
A	-32.35	6.20	V_{max}(1.06)	P_{Gmin}(-0.3)	1.061	0.311	-0.3326	0.0817
B	-33	13	I_m(0.35)	P_{Gmin}	1.015	0.354	-0.3402	0.1676
C	-29	17	I_m	Q_{Gmax}(0.25)	0.979	0.344	-0.2989	0.2154
D	-20	19.5	V_{min}(0.94)	Q_{Gmax}	0.946	0.295	-0.2057	0.2452
E	32	-0.18	V_{min}	P_{Gmax}	0.935	0.342	0.3321	-0.0016
F	32	-14.4	Q_{Gmin}(-0.07)	P_{Gmax}	1.032	0.339	0.3319	-0.1276
G	16.5	-9.7	V_{max}(1.06)	Q_{Gmin}	1.061	0.180	0.1696	-0.1230

Table 1. Voltage collapse indicators for bus 30 for load shedding in different directions

4. Conclusion

In this chapter, a graphical method for analysis of some network issues arising from integration of wind power at high penetration level is presented. Voltage stability for the case static power injections at a node is analysed graphically followed by analysis of the effect of a WF with large IGs connected to a system. The graphical method proved its accuracy in indicating the system state and in quick estimation of an effective remedial action.

It has been shown graphically and verified through numerical simulations that the voltage stability indicators, based on the PQ model, are not suitable for the case of a WF with IG. It has been also shown that the reactive power control of a WF does not only change quantitatively with variations in the WF output, but also qualitatively as the direction of reactive power support may be required to change. The graphical method is simple but rich in its indication and usage. Its simplicity makes it suitable for online monitoring of the WF. Also, it can be a useful educational tool helping to gain insight of WF interaction with power systems.

This chapter also presents a graphical method for determining network limits for wind power integration. For each candidate node, where a wind farm is planned, a capability

chart is constructed defining the allowable domain of power injection where all operating and security constraints are satisfied. The capability chart gives a clear indication about the allowable size of the wind farm. In case the planned wind farm size exceeds the allowable limits the chart determines the active limits and provides a quick assessment of the potential solutions.

The capability chart is fast to construct, versatile in indication, and simple to use. Therefore, it can also be a useful tool for on-line monitoring and control of power system containing wind farms or any other renewable energy resource. Relying on the information and indicators provided by the chart the operator can make decisions about local corrective actions at the node where the wind farm is connected. The accuracy of the proposed chart is validated through comparing the information obtained from the chart with those obtained from the detailed load flow calculation using the IEEE 30-bus test system, which are found to be in nearly perfect agreement with each other.

5. Acknowledgment

This work was supported by The Charles Parsons Energy Research Awards, which were created in September 2006 by the Minister for Communications, Marine & National Resources of Ireland and Science Foundation Ireland under the Strategy for Science, Technology and Innovation.

6. References

Abdelkader, S.(1995). *Power system security assessments with particular reference to voltage instability,* PhD Thesis, Faculty of engineering, Mansoura University *Egypt.*

Abdelkader, S.& Fox, B. (2009). Voltage Stability Assessment For Systems With Large Wind Power Generation, *Proceedings of UPEC 2009, 44th International Universities Power Engineering Conference*, pp. 14-17, ISBN 842-6508-23-3, Glasgow, Scotland, UK, September 1-4, 2009

Abdelkader, S. & Flynn, D. (2009). Graphical determination of network limits for wind power integration. *IET Generation, transmission & Distribution,* Vol.3, No.9, (September 2009), pp. 841-849, ISSN 1751-8687

Chebbo, A. ; Irving, M. & Sterling, M. (1992). Voltage collapse proximity indicator: behavior and implications, *IEE Generation, transmission & Distribution,* Vol.144, No.3, (May 1992), pp. 241-252, ISSN 1350-2360

Elkateb, M.; Abdelkader, S. & Kandil, M. (1997). Linear indicator for voltage collapse in power systems. *IEE Generation, transmission & Distribution,* Vol.139, No.2, (March 1997), pp. 139-146, ISSN 1350-2360

Kessel, P., & Glavitch, H., (1986). Estimating the voltage stability, *IEEE Trans. on Power Delivery,* Vol.1, No.3, pp. 346-354

Semlyen. A.. Gao. B.. & Janischewskyj. W (1991). Calcnlation of the extreme loading condition of a power system for the assessment of voltage stability, *IEEE Trans. on Power Systems,* Vol. 6, No.1, (Jan 1991), pp. 307-312.

Tamura, Y; Mori, H. & Iwamoto, S (1983). Relationship between voltage instability and multiple load flow solutions in electric power systems, *IEEE Trans. on Power Apparatus and Systems,* Vol.PAS-102, No.3, (May 1983), pp. 1115-1123.

3

Voltage Fluctuations Produced by the Fixed-Speed Wind Turbines during Continuous Operation - European Perspective

Carlos López and Jorge Blanes
Universidad de León
Spain

1. Introduction

Since wind energy begun to have importance in some countries, several authors from different countries have presented in international publications the influence of such injection of energy over the power quality in the electrical power system. Since the concept of wind turbine employed at that time was mostly the asynchronous generator directly connected to the grid, the problems originated by the fluctuations in the power output of these generators (and therefore in the voltage, resposible of the *flicker* phenomenon) began to be a matter of concern for the scientific community.
In Europe the Agencies and Universities in the Northern countries have pioneered the study of power quality of wind turbines and the problems of their integration into the grid. The collaboration between these agencies and universities has enabled their joint participation in the project funded by the Fourth Framework Program of the European Union "European Wind Turbine Testing Procedure Developments", completed in 2001 (Sorensen et al., 1999). This project provided cover for the then emerging standard IEC 61400-21.

2. Mechanical power fluctuations

It is well known that a wind turbine produces, in general, a variable mechanical power, eventually resulting in a delivered electrical power which is also variable, causing voltage variations in the network. The variations of the wind speed (mainly of stochastic nature) together with the aerodynamic effects of the turbine, of periodic regular basis, are the main responsible for this behavior.
The wind speed is usually characterized by its average value at intervals of 10 minutes (estimated bymeans of the *Weibull*[1] *distribution*), that overlaps the variable component or "turbulent", heavily dependent on the exact location of the turbine. The frequency spectrum of the resulting power of the wind on the surface swept by the rotor reveals (Pierik et al., 2004) that, for diameters larger than 20 m, the components above 0.3 Hz are practically non-

[1] The function of the Weibull distribution is: $F(V_0) = P(V_0 < V) = e^{-\left(\frac{V_0}{C}\right)^k}$, being C an scaling factor and, usually, $1{,}5 < k < 3$. For the value $k = 2$ it is known as Rayleigh distribution.

existent. This effect added to the great inertia of the rotor makes impossible to follow the rapid changes in the wind speed (Papathanassiou & Papadopoulus, 1999)].

It is unanimously accepted that the causes of the periodic fluctuations of the power are the stratification of the wind speed (wind gradient) and, to a greater extent, the *tower shadow* effect (Thiringer, 1996), both illustrated in figure 1. The first of these phenomena is due to the fact that the speed of the incident wind on the turbine increases with the height (Thiringer & Dahlberg, 2001). The growth law depends on factors such as the roughness of the terrain, the type of atmosphere, etc. This means that, even assuming a constant wind speed, the torque transmitted by each blade on different parts of its pathway is not constant. Instead, it has a periodic component of frequency $3p$, being p the frequency of the rotor rotation.

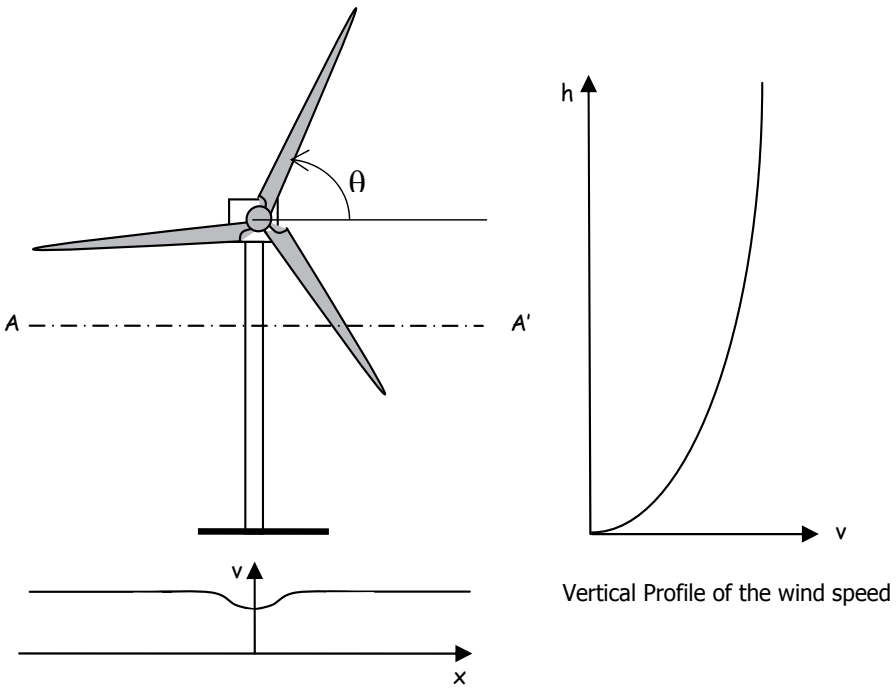

Fig. 1. Effect *shadow of tower* and stratification of the wind speed with the height

The *tower shadow* effect is caused by the local wind speed decrease in the vicinity of the tower, which causes the decline of the instantaneous torque each time one of the blades passes through its lowest position. The frequency of torque oscillations induced by this effect is, again, $3p$. Each time one of the blades is faced with the tower (minimum torque), none of them is at the highest position (maximum torque), resulting in an addition of both effects (Larson, 1996).

Wind turbines equipped with variable speed generators can mitigate, at least in part, the variations in the mechanical power by increasing or decreasing its stored kinetic energy. On the other side, turbines equipped with fixed speed generators deliver the fluctuations of the mechanical power to the power system, instantly and barely mitigated. Therefore, this type

of turbine, equipped with an asynchronous generator and usually known as the "Danish concept", is the potential source of voltage fluctuations causing flicker. In the course of this paper we refer to this type of wind turbine.
In virtually all the studies published in this field (Papathanassiou & Papadopoulus, 1999; Thiringer & Dahlberg, 2001), the maximum amplitude of the periodic power fluctuations produced by the asynchronous fixed speed is quantified as 20% of the average power, and takes place when the turbine operates with a high wind speed. When this speed is low, the oscillations are lower in relative value. The frequency of the oscillations of the three blade fixed-speed commercial turbines varies between 0.7 and 2.2 Hz (Takata et al. 2005). In the case of the turbine Neg Micon 52/900 the rotation speed is 22.4 r.p.m., so that the 3*p* frequency corresponds to:

$$f_{3p} = \frac{22.4 \times 3}{60} = 1.12\,Hz$$

Figure 2 shows, as an example, the spectral analysis of the electric power supplied by a 500 kW fixed speed generator (NTK 500/41)[2], located in the Risoe Campus in Roskilde (Denmark) and the wind speed cubed, which is proportional to the power of the wind.
Note the presence of 3p frequency components and some of its multiples in the power generated, but not in the wind power, this implies that these components are introduced by the turbine itself.

3. Voltage variations

Once accepted that the electrical power output of a wind generator is not constant, the problem that arises is to calculate how these changes affect the voltage at the point of common connection (PCC) and, therefore, the flicker emitted.

3.1 Theoretical analysis on the P-Q generator model

The classical way to analyze the impact of a generator (or load given the case) of a certain power, over the voltage of the grid is to represent this last by its Thevenin equivalent at the connection point and consider the active and reactive power flows between the generator and the grid (see fig. 3).
This model is considered valid for analysis of stationary voltage variations (including *flicker*) (Larson, 1996). In case of transient analysis, dynamic models should be used for the generators (Cidrás & Feijóo, 2002).
The baseline data for the calculation of the variation in supply voltage at a certain point of the network are the active and reactive power exchanged between the generator and the network (after taking into account the compensation by the capacitor), the equivalent impedance of the network at the connection point, $\vec{Z} = R + jX$, and the voltage U_0 (which is taken as constant).

[2] Analysis carried out from time series data of ten minutes provided by the DTU, courtesy of Kurt Hansen. The sampling period is 0.028 s, which corresponds to a sampling frequency of 35.714 s^{-1}. The series was analyzed in 1024 data windows, this is, of 28.672 seconds wide.

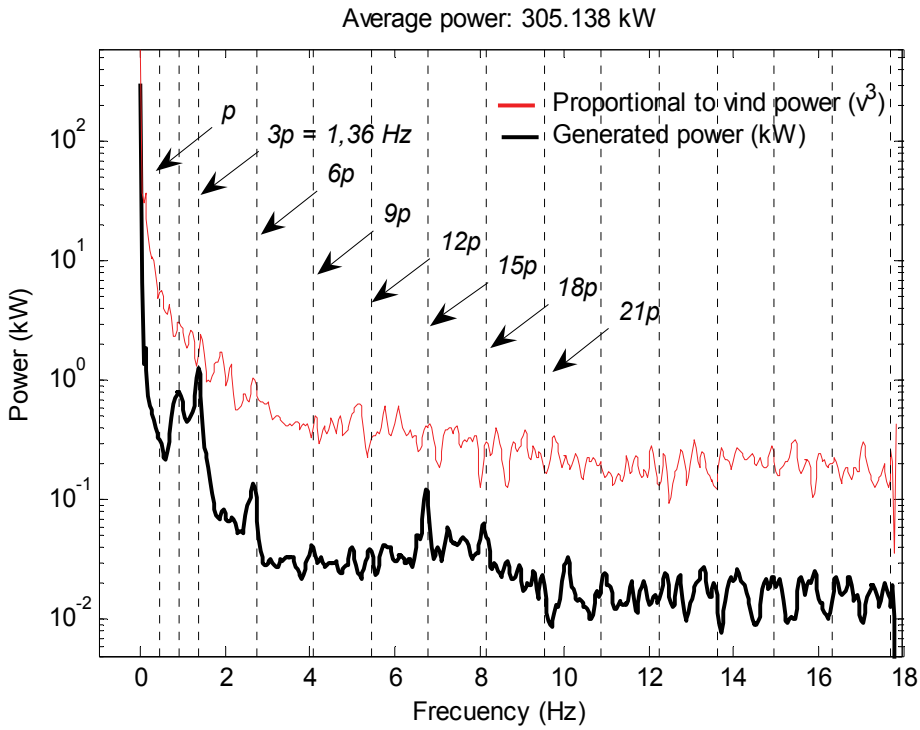

Fig. 2. Spectral analysis of the electric power supplied by a 500 kW fixed speed generator and the power of the wind.

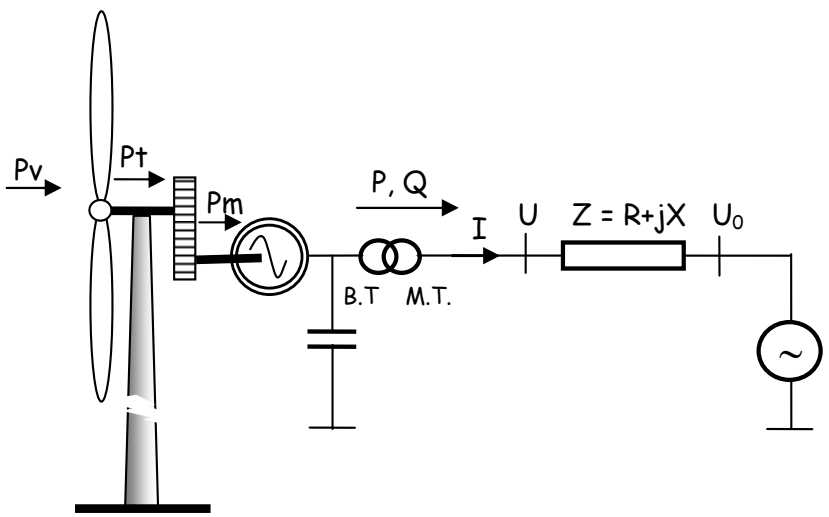

Fig. 3. Model of a generator directly connected to the grid

The active power *P* corresponds to that produced by the electric generator as a result of the mechanical power *Pm* provided by the set turbine-multiplier, converted from the wind power *Pv*. If the instantaneous power of the wind is constant, active power also would be. In practice, this ideal situation never shows up, either by variations in wind speed, of stochastic nature, or aerodynamic effects discussed in the previous section. As a result, the electric power will show, with a specific mitigation, such variations.

Regarding the reactive power, in an asynchronous machine it is related to the active power and the applied voltage. Assuming that the voltage is almost constant, the reactive power depends only on the active power. Typically, a capacitor compensates, at least, the reactive power consumed in an open circuit operation. However, nowadays it is usual to install capacitor banks that, automatically adjust the power factor at the turbine output to values close to one. When changes in power are important, the control system of the capacitor bank acts for an optimal reactive power compensation. Otherwise, if the variations are small, the capacitors remains at a fixed value. The switching in the battery should not be too frequent to limit the transients due to these operations (Thiringer et al., 2004).

In Spain, the Royal Decree 2818/1998 established that wind farms should operate with a power factor as close to unity as possible. Later, the operating procedure 7.4 (Ministerio de Industria y Energía de España, 2000) extended the band of operation of wind farms operating outside conventional generators, from 0.989 inductive to 0.989 capacitive. In this sense, there has been a shift in countries with high penetration of wind power, which has begun to require them to cooperate in the regulation of the supply voltage by an adequate flow of reactive power. This is achieved in the wind farms based on fixed speed asynchronous generators, through the installation of multi-stage capacitors at the substation. In the variable speed generators the regulation of reactive power is done by the control system of each turbine.

The impact of a wind farm on the voltage at the connection point can be studied from two viewpoints: the slow voltage variations and the fast variations.

a. Slow voltage variations

These are changes in the rms voltage expressed, typically, as average values in intervals of ten minutes. The injection of significant amounts of active and reactive power in the network causes local changes in the voltage that can affect other nearby users.

To predict the magnitude of the voltage variations attributable to the wind farm, two extreme situations should be considered: maximum (nominal) and minimum (zero) energy production, with the corresponding reactive power values. A more accurate calculation should include the other users and also requires to perform a load flow analysis (Tande, 2002). In this case, the extreme situations to be taken into account are the turbine maximum power generation and minimum power consumption (by other of users), and minimum wind power and maximum power consumed.

The limit of the permissible voltage variation at a particular node of the grid is fixed by the competent authorities in each area or, in other cases, by the power companies. In Spain, the Transport System Operator (TSO), REE, has fixed limits from 0.93 to 1.07 pu in the transmission grid.

In Sweden and Denmark the voltage variation in the distribution lines should not exceed 2.5%. This margin is extended to 5% (Larson, 1999) if wind turbines are the only elements connected.

Some authors (Larson, 1996) set the limit of the allowable percentage change in the LV networks in 3%, interpreting the curve provided by the IEC 868: *Flickermeter – Functional and*

design specifications, of 1986 [3] (fig. 4). Based on this philosophy, but using the IEC 07/03/1000 (IEC, 1996)[4], the curve to consider would be the one shown in fig. 5, obtained from the data included in this Standard for voltages of 230 V. In that document the fixed limits for compatibility are $P_{st} = 1$ and $P_{lt} = 0.8$ for LV and MV networks, and the emission limits $P_{st} = 0.9$ (0.8) and $P_{lt} = 0.7$ (0.6) for MV and HV grids.

The emission level of a fluctuating load is the level of *flicker* that occurs in the power system if there were no other fluctuating loads. We assume here that this definition is valid for generators.

The first value represented in the graph in figure 5 corresponds to a frequency of 0.1 changes per minute ($8.33 \cdot 10^{-4}$ Hz), this means a change every ten minutes, and corresponds to a relative variation of the voltage of 7.364% . Taking into account the emission limit in MV we can conclude that every ten minutes the variation in voltage should not exceed $0.9 \cdot 7{,}364 = 6.628\%$.

Finally, according to EN 50160 (EN, 1999), applicable to MV and LV public distribution networks, in the period of a week, the permissible range for the variations of the rms voltage (averaged during 10 min) is ± 10% (percentile 95) and +10%/-15% to all the periods of 10 min.

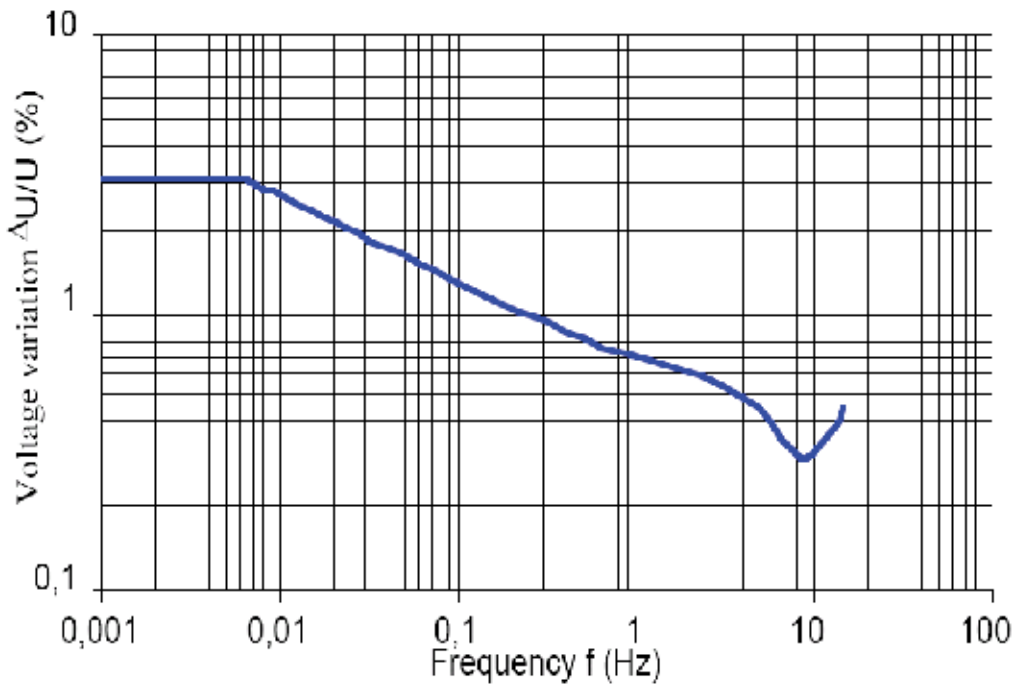

Fig. 4. Allowable limit of *flicker* according to IEC 868

[3] In Spain the UNE-EN 60868 was adopted in October 1995 [14].

[4] The values and graphics supplied by IEC 1000-3-7 reproduce, in turn, those of the IEC 1000-2-2 (EMC) - *Electromagnetic environment for low-frecuency conduced disturbances and signalling in public power supply systems*- CEI 1990.

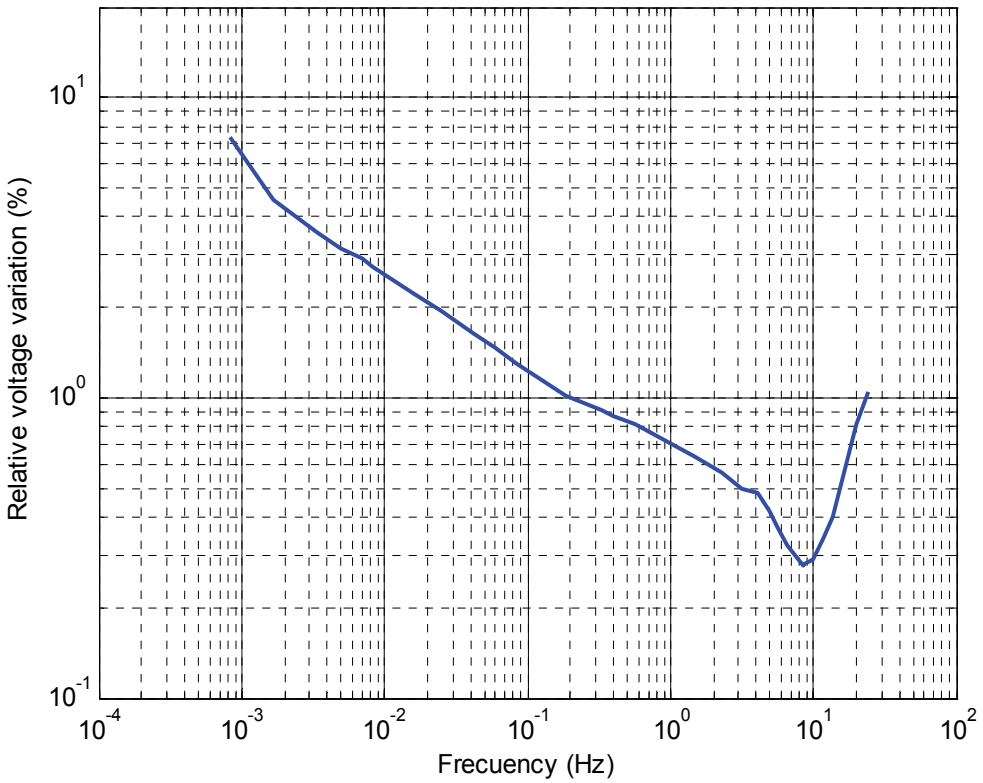

Fig. 5. Curve of P_{st} = 1 for rectangular voltage variations in 230 V networks according to IEC 1000-3-7

b. Fast voltage variations (flicker)

When the voltage variations are faster, in the order of a few hertz, the problem that arises is the *flicker* phenomenon. Now the cause is not a variation of the average wind speed, but the gusts and turbulences of the wind, including those due to the effect of tower shadow and wind stratification seen before. The permissible limits are now narrower and more dependent on the frequency of the variations. The worst are those between 8.5 and 10 Hz, for which a rectangular voltage changes close to 0.3% would produce a P_{st} of value 1 and would, therefore, potentially produce discomfort to users (fig. 5). However, it seems more realistic to consider that the fast voltage variations are sinusoidal rather than rectangular. In this case the P_{st} unit curve would be as shown in figure 6.

Now the frequencies of interest are those corresponding to the blade passing (*3p*).Thus, for a frequency of 1 Hz the allowable voltage variation would be of 2%, to 1.51% of 1.5 Hz, and to 2 Hz of 1.24%. These values are well above those obtained from the IEC 1000-3-7 (IEC, 1996), which for frequencies similar to those establishes: 0.725% to 0.92 Hz, 0.64% to 1.47 Hz and 0.56% to 2.27 Hz. The difference is due, as mentioned above, to the fact that this standard considers rectangular fluctuations, which are more disturbing than the sinusoidal ones.

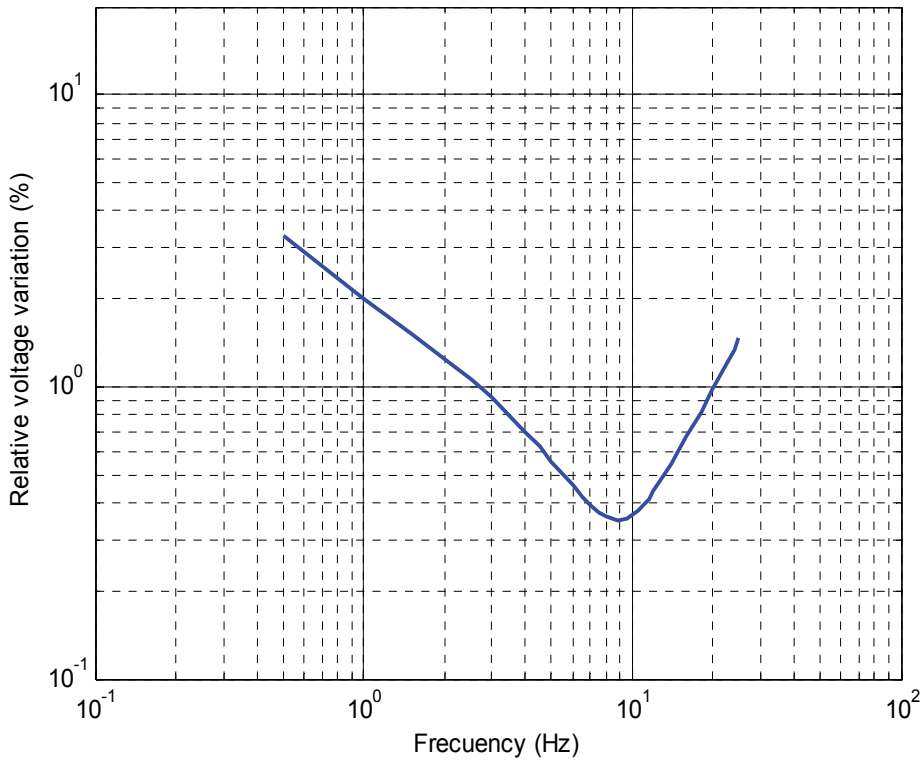

Fig. 6. Curve of P_{st} = 1 for sinusoidal oscillations (according to IEC 61000-4-15)

3.2 Calculation of the slow voltage variations

According to the figure 3, the voltage drop through the equivalent impedance of the network (Z_0) is responsible of the voltage variation al the connection point. The relative voltage drop thus is:

$$\Delta U = \frac{U - U_0}{U_0}$$

being U and U_0 the rms phase voltages. The phase values of the active and reactive power generated by the wind farm are:

$$P = U \cdot I \cdot \cos\varphi; \quad Q = U \cdot I \cdot sen\,\varphi \tag{1}$$

being φ the angle difference between the voltage and current. Figure 7 shows a phasor diagram illustrating the situation for a grid impedance of argument ψ = 45 °, this is, with equal real and imaginary parts ($X/R = 1$).

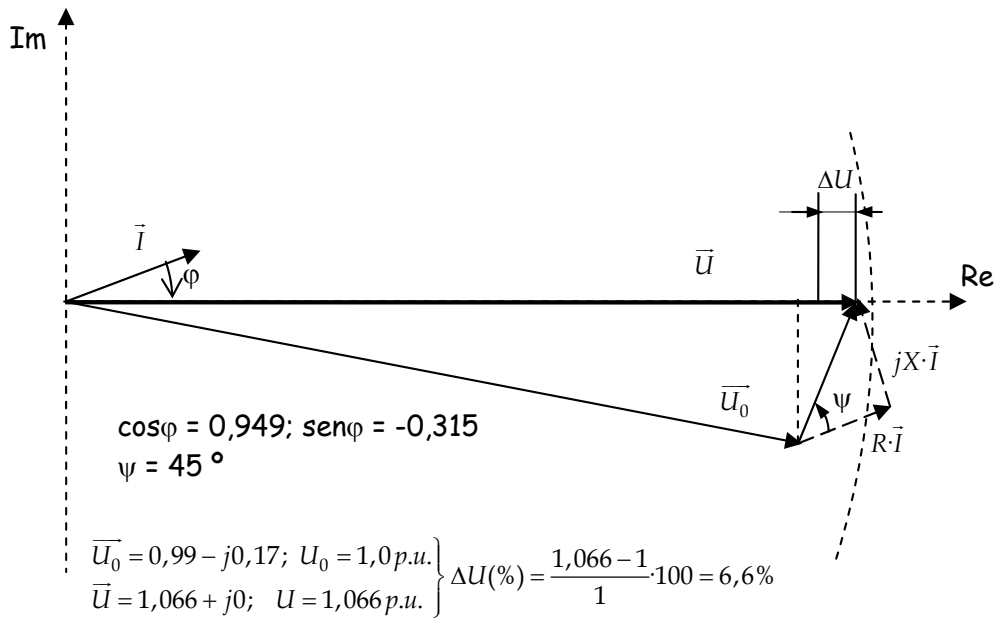

Fig. 7. Example of voltage drop for cos φ = 0,949 and ψ = 45 º

In this example the generator is supplying active power and consuming reactive power, in similar proportions to those that would occur in an asynchronous generator with insufficient reactive compensation, resulting in a power factor of 0.95.
The geometrical figure formed by the points corresponding to the voltage of an infinite power network will be an arc of radius the rms voltage, in this case with a value of 1 pu. From the above circuit and diagram follows:

$$\vec{U} = \vec{U}_0 + R\cdot\vec{I} + jX\cdot\vec{I} = \vec{U}_0 + R\left(I\cos\varphi - jI\cdot sen\varphi\right) + jX\left(I\cos\varphi - jI\cdot sen\varphi\right)$$

$$\vec{U}_0 = U_{0R} + jU_{0X}$$

being U_{0R} and U_{0X}, the real and imaginary components of the phasor $\vec{U}_0$. Separating the complex voltage in the generator $\vec{U}$ in its real and imaginary parts, and taking into account that the latter is zero, we obtain:

$$U = R\cdot I\cos\varphi + X\cdot I\cdot sen\varphi + U_{0R}$$

$$0 = -R\cdot I\cdot sen\varphi + X\cdot I\cos\varphi + U_{0X}$$

Solving for P and Q given in (1) and substituting in the previous,

$$I\cdot\cos\varphi=\frac{P}{U};\quad I\cdot sen\varphi=\frac{Q}{U};\quad\Rightarrow\quad\begin{cases}U=\dfrac{R\cdot P+X\cdot Q}{U}+U_{0R}\quad(4.2)\\ \dfrac{R\cdot Q-X\cdot P}{U}=U_{0X}\end{cases}\tag{2}$$

Bearing in mind that

$$U_0=\sqrt{U_{0R}^2+U_{0X}^2}\Rightarrow U_{0R}=\sqrt{U_0^2-\left(\frac{R\cdot Q-X\cdot P}{U}\right)^2}$$

On the other hand, as expression (2) may be written as:

$$U-\frac{R\cdot P+X\cdot Q}{U}=\sqrt{U_0^2-\left(\frac{R\cdot Q-X\cdot P}{U}\right)^2}$$

from here:

$$U^2+\left(\frac{R\cdot P+X\cdot Q}{U}\right)^2-2\left(R\cdot P+X\cdot Q\right)=U_0^2-\left(\frac{R\cdot Q-X\cdot P}{U}\right)^2$$

finally:

$$U^4-\left[2\left(R\cdot P+X\cdot Q\right)+U_o^2\right]U^2+\left(R\cdot P+X\cdot Q\right)^2+\left(R\cdot Q-X\cdot P\right)^2=0$$

Calling:

$$\begin{aligned}a&=U_0^2\big/_2+\left(R\cdot P+X\cdot Q\right)\\ b&=\left(R\cdot P+X\cdot Q\right)^2+\left(R\cdot Q-X\cdot P\right)^2=Z^2\left(P^2+Q^2\right)\end{aligned}\tag{3}$$

and taking into account that for $Z = 0$, which means $b = 0$, the voltages U and U_0 must be equals, the rms voltage at the connection point (U) results:

$$\begin{aligned}U&=\sqrt{a+\sqrt{a^2-b}}\\ \Delta U(p.u.)&=\frac{U-U_0}{U_0}\end{aligned}\tag{4}$$

The former expressions, as accurate as the assumptions adopted, are not useful for a physical or intuitive interpretation of the voltage variation. For this doing is more interesting to have an equation where it is evident the influence of each quantity over the relative variation of voltage. From expression (2) and approaching $U_{0R}\approx U_0$ and $U_{0R}\cdot U\approx U_0^2$ it results for the relative voltage variation:

$$\Delta U(p.u.) = \frac{U - U_0}{U_0} \approx \frac{U - U_{0R}}{U_0} = \frac{R \cdot P + X \cdot Q}{U_0 \cdot U} \approx \frac{R \cdot P + X \cdot Q}{U_0^2} \tag{5}$$

The above expression is commonly used to estimate the change in voltage produced by a facility that provides an active (P) and reactive (Q) powers, on an equivalent impedance grid $\vec{Z} = R + jX$ of rated voltage U_0 (Larson, 1999). As shown, the values of both powers, as the composition of the grid impedance have influence on this value.
The expression (5) shows that the active power voltage variation occurs in the resistive component of the network and the reactive power in the reactive component. Thus, in weak grids, predominantly resistive, as is the case of the typical MV distribution networks, the active power is the magnitude of greatest influence on the voltage variation. By contrast, in grids with high X/R ratios the reactive power is more important than the active.
Figure 8 shows the voltage variations obtained for different compositions of the equivalent grid impedance. For this doing, it has been considered an asynchronous generator connected to a grid whose short-circuit power is only ten times that of the generator.

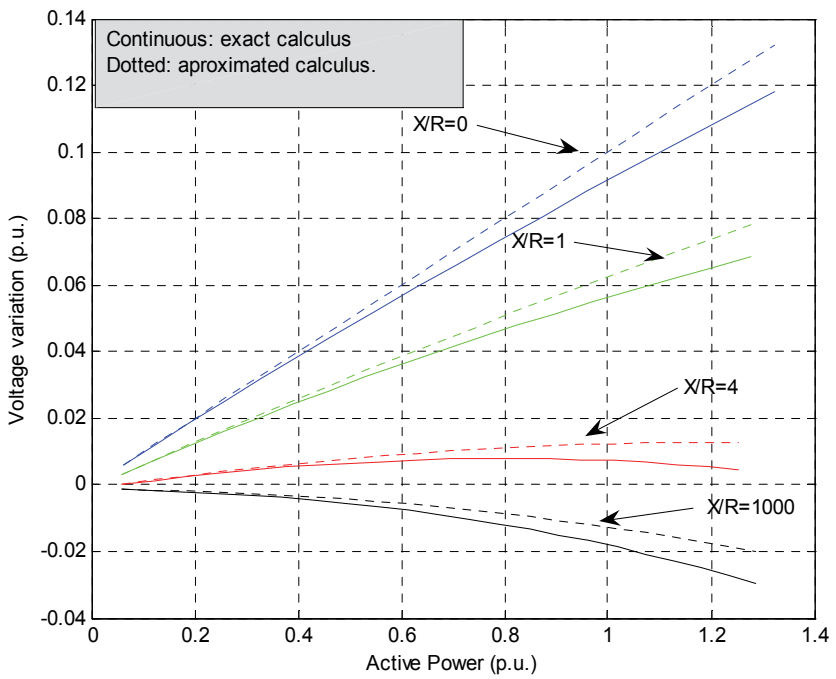

Fig. 8. Voltage variation for different X/R ratios according to the exact and aproximated expressions

In the same figure it can be seen that the estimated values given by (5) (dotted lines), always gives voltage variations greater than the exact calculation (4).
At first glance, it looks that the estimation provides a certain margin of safety. However, this is not true because what is of relevance is the absolute value of the voltage variation, regardless of its sign. These curves were obtained with a generator whose P-Q characteristic,

for the different cases studied, is shown in fig. 9. Since the voltage changes in different ways depending on the *X/R* ratio, so does the slope of the generator *P-Q* characteristic.
As figure 9 shows, in a resistive grid, where the voltage rises further, the increase of reactive power demanded by the generator is partially compensated by the capacitor, while the grids in which the voltage rises less, the current increases more and so does the consumption of reactive by the leakage reactances of the windings.

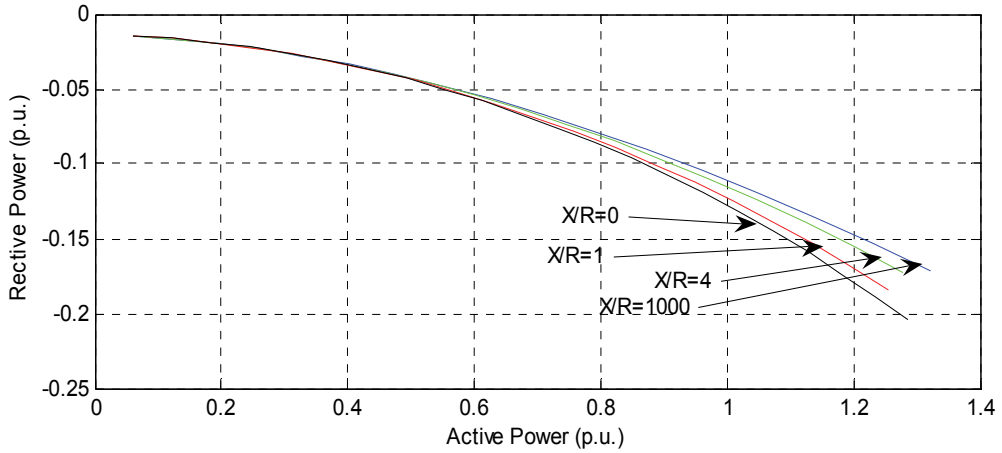

Fig. 9. Reactive power supplied versus active power (note that the scales are different)

Figure 10 shows the different phasor diagrams for the same values of *X/R* of the previous figures for the case of maximum power supplied by the generator.

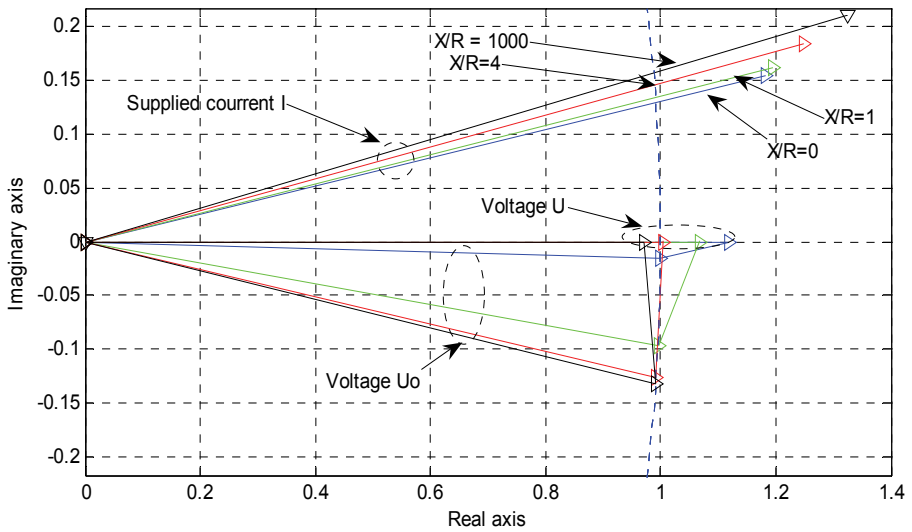

Fig. 10. Complex voltages and currents for maximum power values in fig 8 (note that the scales are different)

These graphics show clearly the reason for the greater increase of the voltage in resistive networks: the voltage drop in the impedance of the network has the smallest angular difference with the voltage. In contrast, in the example given, for *X/R = 4* the voltage in the impedance is almost perpendicular to that of the connection point $\vec{U}_0$, so it produces just a small voltage variation.

Different *P-Q* curves of the set generator–capacitor bank, would give different families of voltage variation graphs similar to that of figure 8. One advantage of the approximate expression (5) is that it allows an immediate estimation not only on the relative changes in voltage but also in reactive power that, for a given active power and a certain equivalent impedance it produces a specific voltage variation (for example zero).

It also allows to calculate the *X/R* ratio which, for a given active and reactive power, produces a specific voltage variation. For example, in figure 9 it can be deduced that the machine consumes 0.12 pu of reactive power and 1 pu of active power. The zero voltage drop will occur when:

$$X / R = -P / Q = 8.33$$

As discussed below, this result is far from that obtained by more precise calculations. Indeed, comparing the voltage drops (in absolute value) obtained for a particular relationship between the short circuit power of the grid, *Scc* and the active power supplied by the generator, *P* for different values of the ratio *X/R* of the grid impedance, using the exact expression (4) and the approximate (5), there are significant differences.

Figure 11 shows the absolute values of the voltage drops corresponding to a power ratio *Scc/P* = 10. The dotted line corresponds to a quasi-exact expression, which is obtained before the last approximation of expression (5), evaluating the voltage *U* by using (2) and assuming $U_0 \approx U_{0R}$. The graphs show clearly the difference between the results obtained by each method. In addition, no voltage drop occurs, according to the approximate calculation for *X/R* = 8.33 as previously obtained, but far from the value 5.8 obtained by the exact calculation method.

In view of all the above, it seems advisable to use the approximate expression (5) with some reservations. Some authors (Bossanyi et al., 1998) evaluate the error when using approximate methods for prediction of P_{st} up to 20%, so it is recommended to use the exact method, according to equation (4).

3.3 Fast voltage variations

So far it has been taken into account the maximum active power, with the corresponding reactive power put into play by a wind turbine to estimate the voltage variation in the worst case, this is, comparing the voltage at the PCC without power generated with the maximum production from wind turbines. In order to estimate the fast voltage variations, although its origin is also the variation of the power supplied by the wind turbines, the approach is slightly different.

First, the relationship between the active and reactive power depends on the area of operation of the machine, since the slope of the *P-Q* characteristics is not constant (see fig. 9). Second, since the power fluctuation is essentially a local phenomenon of each turbine, it is necessary to determine how to add each other to assess the overall impact of an installation with several wind turbines.

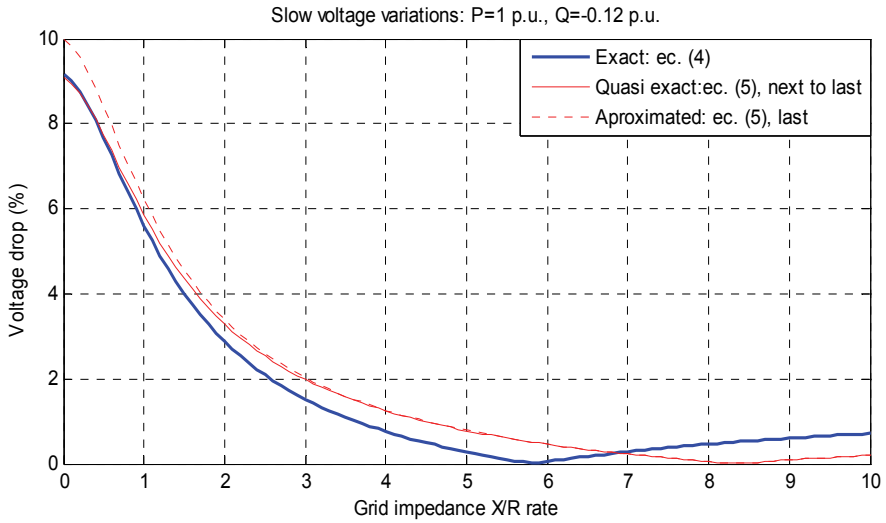

Fig. 11. Comparative calculation of the slow voltage variations

To calculate the voltage variation due to a generator whose output fluctuates around a mean value P_0, from the expression (2), eliminating the denominator and approaching U_{0R} by U_0, gives:

$$U^2 = R \cdot P + X \cdot Q + U \cdot U_0$$

from here:

$$2U \cdot dU = R \cdot dP + X \cdot dQ + U_0 \cdot dU$$

Since the initial data is the variation of the active power, it is of interest to express the variation of reactive power according to that:

$$dQ = \left(\frac{\partial Q}{\partial P} \right)_{Po} \cdot dP = \alpha \cdot dP$$

being α the slope of the P-Q characteristic in the operating point of the generator. Substituting this last expression in the above equation and solving for the voltage variation:

$$dU = \frac{R \cdot dP + X \cdot dQ}{2U - U_0} \Rightarrow \frac{\Delta U}{U_0} \approx \frac{(R + \alpha \cdot X) \cdot \Delta P}{U_0^2} (p.u.) \tag{6}$$

This expression coincides with that obtained directly from (5) which assumes, once again, that the voltage at the connection point (U) and that of the infinite power grid U_0 are very close.

For a value more adjusted to reality, although somewhat more complex to obtain, squaring and differentiating (4), it results:

$$2U \cdot dU = da + \frac{1}{2}\left(a^2 - b\right)^{-1/2}\left(2a \cdot da - db\right)$$

$$\frac{dU}{U_0} = \frac{2 \cdot da + \left(a^2 - b\right)^{-1/2}\left(2a \cdot da - db\right)}{4U \cdot U_0} \tag{7}$$

being *da* and *db* the differentials of the expressions a and b defined in (3):

$$da = R \cdot dP + X \cdot dQ = \left(R + \alpha \cdot X\right) dP$$

$$db = Z^2\left(2P \cdot dP + 2Q \cdot dQ\right) = 2Z^2\left(P + \alpha \cdot Q\right) dP$$

Similar to what was done in the slow voltage variations, it is interesting to compare the results obtained by calculating the fast variations of each method, assuming that the connected machine is the same as that used above (fig. 12). In this case we have taken active power variations of ±10% compared to the nominal machine (20% of total variation). The slope of the *P*-*Q* curve in *P* = 1 p.u. is α = -0.2, as seen in figure 9. The exact calculation is obtained by using (7) and the approximated calculation by using the expression (6) in a similar way as (5) was used for the slow variations.

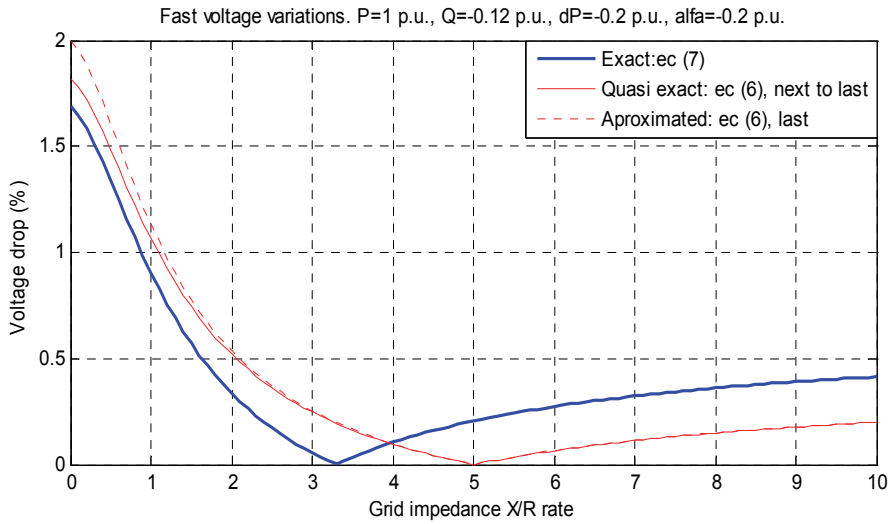

Fig. 12. Comparative calculation of the phase voltage variations

Again, significant differences arise between the two methods, so the conclusion is also the same: the estimation is simple but not very accurate, so it would not be recommend its use for estimating the *flicker*. The *X/R* ratio of the grid for which the voltage variation is zero is found to be 3.3 according to the exact calculation and 5 with the approximate one. From these values, the respective voltage drops, after passing through zero, change their sign, although the graphic merely shows the absolute value.

3.4 Power limit on a gird due to voltage drops

Until now we have evaluated separately the slow voltage variations, due to the injection of all the power of a generator in the grid, and the fast voltage variations, due to the stationary variation in the power with respect to a reference, such as the rated value.

To determine whether a generator can be connected to a particular grid, it should be taken into account both circumstances, considering the percentages of allowable voltage variation in both cases. Thus, knowing the *P-Q* characteristic of a machine, supposing a certain amplitude and frequency of the power fluctuations and assuming certain allowable limits for the slow and fast voltage variations, it can be determined, for each value of the *X/R* ratio, the minimum short-circuit power of the grid not to exceed those limits.

As discussed above, the usual limits are 0.7% for fast variations at 1 Hz and 3% for the slow ones. Some authors (Larson, 1996) represent the curves of constant voltage variation equal to those limits and, therefore, delimit the areas where the variation of the voltage is higher or lower than those mentioned above.

Figure 13 shows separately the limit curves for slow and fast changes calculated by the different methods of the previous section (methods 2 and 3) and a third procedure consisting on solving the equations of the equivalent circuit of the machine in steady state, in order to validate the results obtained with the previous methods. It can be appreciated the coincidence between the exact and the one that uses the machine model, together with the mismatch of both with respect to the approximate method.

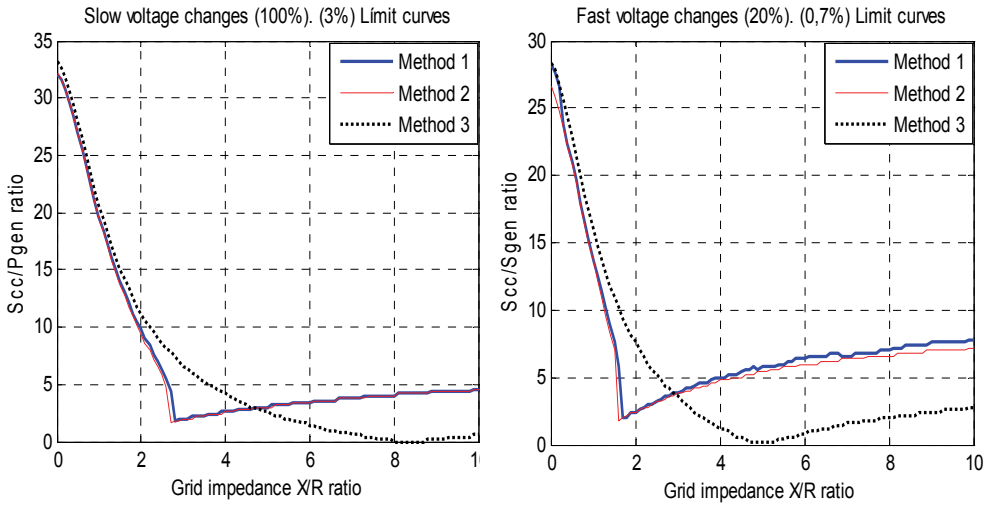

Fig. 13. Comparison of the limit curves obtained for different methods: Method 1: machine model, Method 2: exact analytical calculation, Method 3: approximate calculation.

Figure 14 shows together the two limit curves, very similar to those reported in previous studies (Larson, 1996). The area above the two curves is free of disturbances, since the fast and slow variations will be lower than the limits. Until the value of *X/R* = 2.7 the slow voltage variations are responsible for limiting the minimum short-circuit power of the grid. For higher values of the *X/R* ratio, the responsible are the fast variations, this means the *flicker*. Logically, a change in the limits of the permissible voltage or in the *P-Q* characteristic gives different curves.

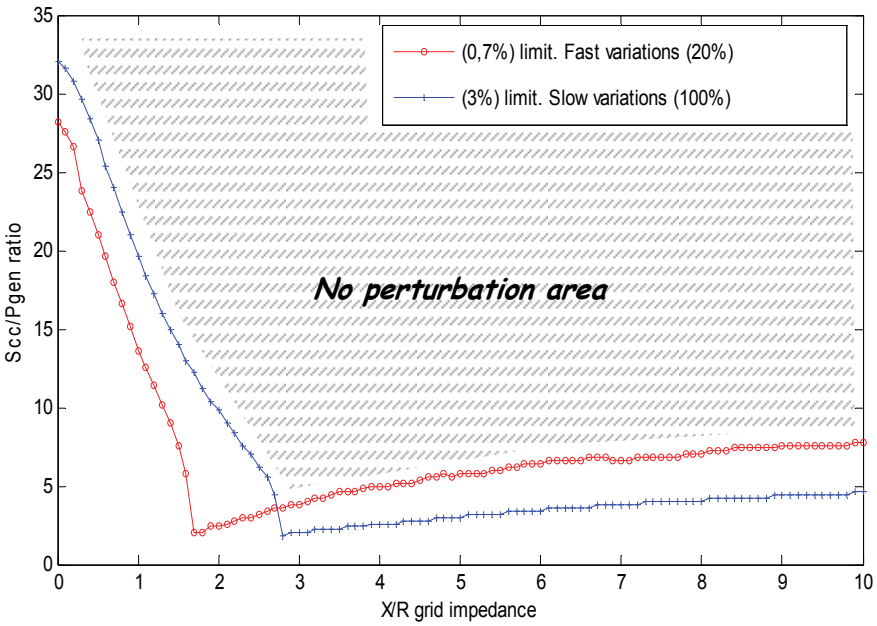

Fig. 14. Definition of areas of potential disturbance due to voltage variations

It should be noted that sometimes, the generator-grid model as that of figure 3 will be difficult to implement due to the ignorance of the exact parameters of the grid or because they vary along the time, for example, due to the presence of other users at the same PCC. In these cases it would be desirable a load flow analysis to determine the variation margins of the voltage (Tande et al. 2002). In this reference an example is given where the voltage variation, estimated by expression (5) is 68% and it is confirmed that, in practice, the variation is acceptable.

Other authors found no such discrepancy if not the opposite. Larson showed the match between the slow voltage variations measured and calculated in a real turbine (Larson, 1996) and also compared the results reached using the exact analytical calculation (4) and the load flow (Larson, 2000).

Figure 14 shows that one way to avoid significant voltage changes would be to impose, as a condition for the connection of a wind farm, that the short-circuit power of the grid at the connection point must be several times greater than the rated power of the wind farm. In Spain this approach is adopted since 1985 (Ministerio de Industria y Energía de España, 1985). For the authorization of a new wind farm, consisting of both synchronous and asynchronous generators, its rated power cannot exceed 1/20 of the short circuit power at the PCC.

3.5 Combined effect of several generators

Until now, we have considered the effect of a single generator connected to the grid. It is usual, in practice, to group a few dozen of wind turbines forming an installation which is called wind farm. As the distances to cover are usually a few kilometers, each generator (or

small group of them) has a transformer to raise the LV generated by the wind turbine (typically 690 V) to the value of the MV grid.
To estimate the total voltage distortion of a wind farm due to slow voltage variations, the effects of all generators may be taken into account on the basis of their active and reactive rated power. In other words, the wind farm could be considered as a single generator which power is equal to the sum of the powers of the single units.
Concerning the fast voltage variations, the question is not as simple because it is not realistic to assume that the power fluctuations are coincident in time (even assuming that they have the same magnitude in all the generators), neither that they may cancel each other. The practice is to follow the recommendation of the IEC1000-3-7 standard (IEC, 1996) considering that each turbine is responsible of a certain value of flicker, P_{sti} and, the combined effect of all the turbines can be taken into account by:

$$P_{st} = \sqrt[m]{\sum P_{sti}^{m}} \tag{8}$$

The value of m depends on the characteristics of the main sources of the fluctuations and can take values from 1 to 4. Value 4 is set for the cases in which the fluctuations should not be coincident and 1 for those other cases in which the probability of occurrence is very high. Value 2 is used in cases in which the coincidence is just as likely as that of random noise. That means that the fluctuations are not correlated. This is the most appropriate value to wind farms since, in principle, the disturbance of each turbine is independent of the others. This means that, in the usual case all the turbines are identical and all cause an individual disturbance P_{sti} which is equal for all of them; the global disturbance for N turbines will be:

$$P_{stN} = \sqrt{N \cdot P_{sti}^{2}} = \sqrt{N} \cdot P_{sti} \tag{9}$$

By the above expression, if the disturbance caused by a generator is proportional to its power, a single generator which power is equal to the sum of the powers of N generators will produce in the grid a disturbance $N \cdot P_{sti}$, clearly higher than the disturbance produced by N generators given by (9). This is due to the partial cancellation of the disturbances that occurs when the number of elements increases.

4. Measurement and evaluation of the voltage fluctuations caused by wind turbines (CEI 61400-21)

According to the previous sections, the estimation of voltage variations that would produce a particular turbine or an entire wind farm into the grid would be conditioned by the use of one or another expression. It would also depend on the availability of the P-Q characteristics of the generators (or in the overall substation) and the presumption of a certain fluctuation of the power supplied by the turbines. There is no doubt that there are too many uncertainties that would lead to results far from reality. For the sake of all the agents involved in the wind power sector it is necessary to clarify and to unify all the aspects related to the quality of power supplied by the wind turbines.
The UNE-EN 61400-21 2003 (EN, 2003) is the Spanish version of the European Standard of February 2002, which adopts the International Standard IEC 61400-21:2001. Its purpose is to provide a uniform methodology to ensure consistency and accuracy in measurement and evaluation of the quality of power supplied by the wind turbines connected to the grid.

Different reports describe briefly (Sorensen at al., 1999) or more extensively (Sorensen at al., 2001), the work, both experimental and theoretical, conducted as part of the project "*European Wind Turbine Testing Procedure Developments*" (Fourth Framework Program of the EU). This project is carried out by several EU States and it is coordinated by the Risø National Laboratory in Denmark. The aim of this project is to make recommendations for the new standard of measurement and testing of the power quality supplied by the wind turbines.

The works on the quality standards of the power supplied by the wind turbines began in 1995 by the IEC. At the end of 1998 there was already a draft of the IEC 61400-21. According to this standard, there are three parameters to evaluate the quality of supply:

- Steady voltage.
- Voltage fluctuations (in continuous operation and in switching operations).
- Harmonics.

4.1 Measuring and testing. Fictitious network

For testing purposes, the turbine must be connected to the network through a MV standardized transformer and in a PCC with a short circuit power at least 50 times the maximum permissible power of the turbine.

Moreover, some requirements must be fulfilled. These requirements deal with the quality of the voltage at the PCC (rms value, frequency, unbalance and distortion) and the wind turbulence, which must be between 8% and 16%. The precision class required for the measurement equipment is 1.

Since the MV grid used in the test will have, in general, other loads, it is necessary to provide some mechanism to exclude any disturbances not attributable to the turbine itself. For this reason the standard specifies a method based on collecting temporal series of voltages and currents at the turbine terminals and the use of a circuit model, called *fictitious network* to determine, by calculation, the voltage fluctuations caused exclusively by the wind turbine.

The fictitious network (fig. 15) consists of an ideal voltage source $u_0(t)$ in series with the grid resistance (R_{fic}) and inductance (L_{fic}). The wind turbine is represented as an ideal current source $i_m(t)$ whose instantaneous value corresponds to the phase current measurements in the turbine during the test. The instantaneous value of $u_{fic}(t)$ is given by equation (10).

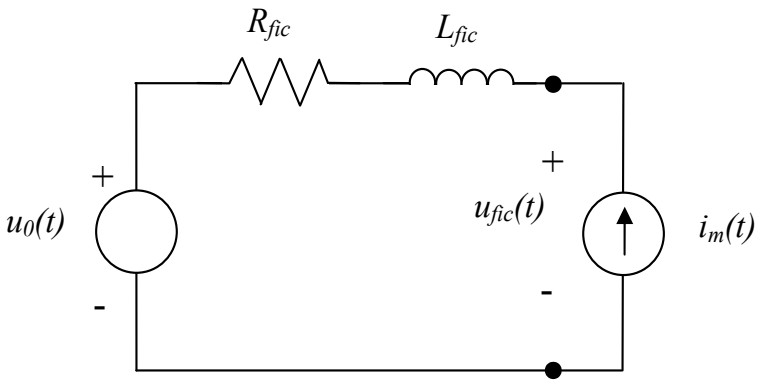

Fig. 15. Fictitious network according to UNE-EN 61400-21

$$u_{fic}(t) = u_0(t) + R_{fic} \cdot i_m(t) + L_{fic} \cdot \frac{di_m(t)}{dt} \tag{10}$$

Concerning the ideal voltage source, two properties must be fulfilled:

- the ideal voltage should contain no fluctuation, this is, the flicker on the voltage should be zero.
- $u_0(t)$ must have the same electrical angle, $\alpha_m(t)$, than the fundamental component of the measured voltage. This ensures that the phase angle between $u_{fic}(t)$ and $i_m(t)$ is correct, provided that $|u_{fic}(t) - u_0(t)| << |u_0(t)|$.

To comply with the conditions imposed in the standard $u_0(t)$ and $\alpha_m(t)$ are defined as:

$$\left.\begin{aligned} \alpha_m &= 2 \cdot \pi \cdot \int_0^t f(t)dt + \alpha_0 \\ u_0(t) &= \sqrt{\frac{2}{3}} \cdot U_n \cdot sen(\alpha_m(t)) \end{aligned}\right\} \tag{11}$$

where $f(t)$ is the frequency, α_0 is the electrical angle at $t = 0$ and U_n the rms value of the rated grid voltage. The values of R_{fic} and L_{fic} are chosen to get grid angles (ψ_k) of 30º, 50º, 70º and 85º (X_{fic}/R_{fic}=0.577; 1.19; 2.75; 11.43) and a short-circuit power which, *as a guide, it is suggested to be 50 times higher than the rated power of the turbine*.

The instantaneous voltage $u_{fic}(t)$ obtained by expression (10) is introduced into an algorithm that meets IEC specifications for the flickermeter (according to IEC 61000-4-15) to obtain the value of $P_{st,fic}$. From it the flicker coefficient is obtained by:

$$c(\psi_k) = P_{st,fic} \cdot \frac{S_{k,fic}}{S_n} \tag{12}$$

Where S_n is the rated power of the wind turbine and $S_{k,fic}$ is the short circuit power of the fictitious grid.

Continuing with the standard, for the test of the turbine, the temporal series of voltage and current measurements should be obtained for steps of wind speed of 1 m/s, between the speed of onset and 15 m/s. It is commonly accepted, and so is assumed in the standard, that the annual distribution of wind speed (integrated in values each 10 minutes) in a particular location is often adapted to the *Rayleigh Law*, the function of cumulative probability distribution is given by:

$$F(v) = 1 - e^{-\frac{\pi}{4} \cdot \left(\frac{v}{v_a}\right)2}$$

being v the wind speed and v_a its annual average. If the flicker coefficients, $c(\psi_k)$, obtained for each wind speed are multiplied by a weighting factor that takes into account the probability of occurrence of that speed for a given annual average of the wind speed, another flicker coefficients can be obtained $c(\psi_k, v_a)$, which are a function of the angle of the grid impedance and the annual average wind speed, v_a (the average speeds to consider are: 6 m/s, 7.5 m/s and 8.5 m/s).

The standard details the calculation procedure to obtain these coefficients, which represent the 99th percentile of each distribution. The test result, concerning the continuous operation, will be a table of flicker coefficients $c(\psi_k, v_a)$ (included in the standard). From the table of coefficients, the emission of flicker (99th percentile) of a wind turbine during continuous operation should be estimated by the expression:

$$P_{st} = P_{lt} = c(\psi_k, v_a) \cdot \frac{S_n}{S_k} \tag{13}$$

being S_n/S_k the relationship between the rated power of the turbine and the network short circuit power at the point of connection. Since the grid angle ψ_k and the annual wind speed v_a, in a particular site will, generally, not match those in the table, the flicker coefficient $c(\psi_k, v_a)$ should be obtained by interpolation of those.
The standard also specifies that in cases where several turbines are connected, the emission of flicker can be estimated by:

$$P_{st\Sigma} = P_{lt\Sigma} = \frac{1}{S_k} \cdot \sqrt{\sum_{i=1}^{N_{wt}} (c_i(\psi_k, v_a) \cdot S_{n,i})^2} \tag{14}$$

being i each of the N_{wt} turbines. This expression is equivalent to (8), proposed in the IEC 1000-3-7.

5. Conclusions

In this chapter it is studied the way in which power fluctuations from asynchronous fixed-speed wind turbines become voltage variations. Although it might seem rather obvious, the need to use as variables of analysis the active and reactive power involves either the use of simple but approximate expressions, or complex and more accurate. Moreover it must be added that it is an asynchronous machine which acts as a power source, according to its P-Q characteristic. The issue has been addressed theoretically, obtaining the more or less approximate expressions that appear in the references concerning the subject. The results by using the above expressions have been compared by computer simulations. It has been shown that some widely used expressions may yield in inaccurate results.
Following the pattern of other researchers, the influence of the grid parameters where the generator is connected have been taken into account for the evaluation of slow and fast voltage variations. The relationship between the resistive and reactive components of the network impedance is shown as a crucial factor in the magnitude of the resulting voltage fluctuations. Therefore it is essential in deciding whether a grid supports the injection of a given power limitations based on the slow or fast voltage variations produced.

6. References

Bossanyi, E.; Saad-Saoud, Z & Jenkins, N. (1998). *Prediction of flicker produced by wind turbines*. Wind Energy, 1, pp. 35-51.

Cidrás J. & Feijóo A., (2002). *A Linear Dynamic Model for Asynchronous Wind Turbines With Mechanical Fluctuations*. IEEE Trans. On Power Systems, Vol. 17, Nº 3.

EN (1997). UNE-EN 60868: *Medidor de Flicker. Parte 0: Especificaciones funcionales y de diseño.* AENOR.

EN (1999). UNE-EN 50160: *Características de la tensión suministrada por las redes generales de distribución*. AENOR.

EN 61400-21: *Medida y evaluación de las características de la calidad de suministro de las turbinas eólicas conectadas a la red*. AENOR 2003

IEC (1996). EC 1000-3-7: (EMC): *Assessments of emission limits for fluctuating loads in MV and HV power systems*.

Larson A. (1996). *Flicker and Slow Voltage Variations from Wind Turbines*. Proc. of the 7th International Conference on Harmonics and Quality of Power (ICHQP'96), Las Vegas, USA, pp. 270-275. October 1996.

Larson A. (1999), *Guidelines for Grid Connection of Wind Turbines*. 15th International Conference on Electricity Distribution (CIRED'99). Niza, France, June 1999.

Larson A., (2000) *The Power Quality of Wind Turbines*. Ph.D. Thesis. Chalmers University of Technology, Goteborg, Sweden 2000.

Ministerio de Industria y Energía de España (1985). Orden Ministerial de 5 de septiembre de 1985: *Normas Administrativas y Técnicas para el Funcionamiento y Conexión a las Redes Eléctricas de Centrales Hidroeléctricas de hasta 5.000 KVA y Centrales de Autogeneración Eléctrica*. B.O.E., 12 September 1985.

Ministerio de Industria y Energía de España (2000). *Resolución de 10 de marzo de 2000, de la Secretaría de Estado de Industria y Energía, por la que se aprueba el procedimiento de operación del sistema (P.O. – 7.4) "Servicio complementario de la tensión de la re de transporte"*. BOE nº. 67, 18 Mars 2000.

Papathanassiou, S.A. & Papadopoulus, M.P. (1999). *Dynamic Behavior of Variable Speed Wind Turbines under Stochastic Wind*. IEEE Transactions on Energy Conversion, Vol. 14, No. 4.

Pierik, J.T.G.; Morren, J.; Wiggelinkhuizen, E.J.; de Haan, S.W.H.; van Engelen, T.G. & Bozelie, J. (2004). *Electrical and Control Aspects of Offshore Wind Farms II (Erao II). Volume 1: Dynamic models of wind farms*. ECN. TUDelft (Holland).

Sorensen P.; Gerdes G.; Klosse R.; Santier F.; Robertson N.; Davy W.; Koulouvary M.K.; Morfiadakis E. & Larson A. (1999), *Standards for Measurements and Testing of Wind Turbine Power Quality*. European Wind Energy Conference (EWEC'99). Niza, France, Mars 1999.

Sorensen P.; Pedersen T.F.; Gerdes G.; Klosse R.; Santier F.; Robertson N.; Davy W.; Koulouvary M.K.; Morfiadakis E. & Larson A. (2001). *European Wind Turbine Testing Procedure Developments. Task 2: Power Quality*. Riso-R-1093(EN). Riso National Laboratory, Denmark.

Takata G.; Katayama N.; Miyaku M. & Nanahara T. (2005). *Study on Power Fluctuation Characteristics of Wind Energy Converters with Fluctuating Turbine Torque*. Electrical Engineering in Japan, vol. 153, Nº 4.

Tande, J. O. (2002). *Applying Power Quality Characteristics of Wind Turbines for Assessing Impact on Voltage Quality*. Wind Energy, 5:37-52.

Thiringer T. (1996). *Power Quality Measurements Performed on a Low-Voltage Grid Equipped With Two Wind Turbines.* IEEE Trans. on Energy Conversion, Vol. 11, Nº 3, pp.601-606.

Thiringer T. & Dahlberg J-A. (2001). *Periodic Pulsations from a Three-Bladed Wind Turbine*. IEEE Trans. on Energy Conversion, Vol. 16, Nº 2, pp. 128-133.

Thiringer T.; Petru T. & Lundberg S. (2004). *Flicker Contribution From Wind Turbine Installations*. IEEE Trans. on Energy Conversion, Vvol. 19, Nº 1, pp. 157-163.

4

Evaluation of the Frequency Response of AC Transmission Based Offshore Wind Farms

M. Zubiaga[1], G. Abad[1], J. A. Barrena[1], S. Aurtenetxea[2] and A. Cárcar[2]
[1]*University of Mondragon,*
[2]*Ingeteam Corporation*
Spain

1. Introduction

Nowadays, the state of the distribution grids is significantly different in comparison with the state of two decades ago. One important reason for that is the existence of non-lineal loads. These non-lineal loads can provoke disturbances, like a high level harmonics in current and voltages (Pigazo, 2004).
In the same way, there is consolidating a distributed generation system for the distribution grids. This kind of grids contain a combination of many types of generation plants, like cogeneration, combined cycle, wind farms, photovoltaic…Thus, if the distribution grid is made up with many small and medium generation plants, the waveform of the voltage may be distorted.
In conclusion, the electric transmission and distribution system is evolving to a scenario with multiple harmonic sources. So, the frequency analysis of the electric grids is becoming an important tool, because can help to improve their efficiency reducing the power associated to these disturbances.
As regards to AC offshore wind farms, the interaction between the offshore installations and the onshore grid can cause harmonic amplifications. This aspect is not trivial, because as a result of this harmonic amplification, the harmonic level in the point of common coupling of the wind farm can be unacceptable for the grid code requirements.
Offshore wind farms are connected through a widespread medium voltage submarine cable network and connected to the transmission system by long high voltage cables. Submarine power cables, unlike underground land cables need to be heavily armored and are consequently complicated structures. So, in particular this type of power cables have a relatively larger shunt capacitance compared to overhead lines which make them able to participate more in resonant scenarios (Kocewiak et al., 2010).
The present chapter evaluates the frequency behavior of the offshore wind farms at normal operation (steady state), in function of design procedure parameters like: the cable length / characteristics, transformers connection and leakage inductance or inter-turbine grids configuration. The analysis is performed from the point of view of the wind turbines, considering them as potential harmonic sources. Thus, the knowledge of the frequency behavior of the offshore wind farm can help to avoid as much a possible the harmonic amplification, at the design stage of the wind farm. This presents new challenges in relation to understanding the nature, propagation and effects of the harmonics.

2. Power transmission lines

2.1 Power transmission cables

The purpose of a power cable is to carry electricity safely from the power source to different loads. In order to accomplish this goal, the cable is made up with some components or parts. Fig. 1 shows a description of the cable's components, which are:

Conductor

The conductor is referred to the part or parts of the cable which carry the electric power. Electric cables can be made up by one conductor (mono-phase cables), three (three-phase cables), four, etc.

Insulation

Dielectric material layer with the purpose of provide insulation between conductors of different phases or between phases and ground.

Shield

metal coating, which covers the entire length of the cable. It is used to confine the electric field inside the cable and distribute uniformly this field.

Armor or sheath

Layer of heavy duty material used to protect the components of the cable from the external environment.

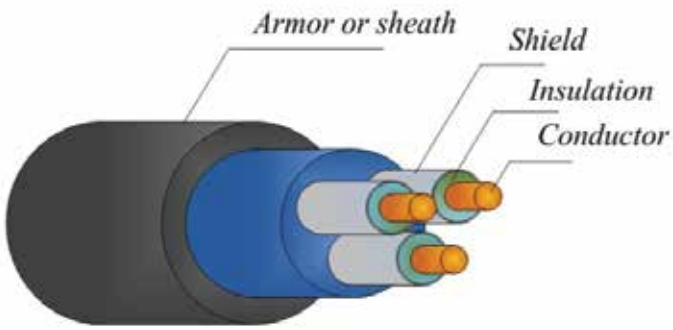

Fig. 1. Generic representation of an electric power cable

The electric behavior of the power transmission cable can be represented by several electromagnetic phenomena, yielding to behavioral characteristics such as; the conductor of the cable presents small resistivity or when an electric current flow through a conductor generates a magnetic field around it. Another effect is caused by the voltage difference from the conductor to ground, which provokes the storage of electric charge in the conductor. Finally, there is a leakage current to ground. The dielectric is a material with low conductivity, but not zero.

Thus, through the years, many authors have agreed that a transmission cable can be represented electrically for each differential length with distributed *RLCG* parameters, (Jiang, 2005; Sánchez, 2003; Weedy & Cory, 1998). Where:

- The distributed resistance *R* of the conductors is represented by a series resistor (expressed in ohms per unit length).

- The distributed inductance *L* (due to the magnetic field around the wires, self-inductance, etc.) is represented by a series inductor (henries per unit length).
- The capacitance *C* between the two conductors is represented by a shunt capacitor *C* (farads per unit length).
- The conductance *G* of the dielectric material separating the two conductors is represented by a conductance *G* shunted between the signal wire and the return wire (Siemens per unit length).

In DC circuits, the current density is similar in all the cross section of the conductor, but in AC circuits, the current density is greater near the outer surface of the conductor. This effect is known as the skin effect.

Due to this phenomenon, AC resistance of the conductor is greater than DC resistance. Near to the center of the conductor there are more lines of magnetic force than near the rim. This causes an increment in the inductance toward the center and the current tends to crowd toward the outer surface. So at higher frequencies the effective cross section area of the conductor decreases and AC resistance increases.

In short, the skin effect causes a variation in the parameters of the cable, due to the non uniform distribution of the current through the cross section of the cable. This variation is in function of the frequency, producing that the *RGLC* parameters are frequency dependent. If this effect is taken into account the electric representation of the cable for each differential length yields as shown in Fig. 2.

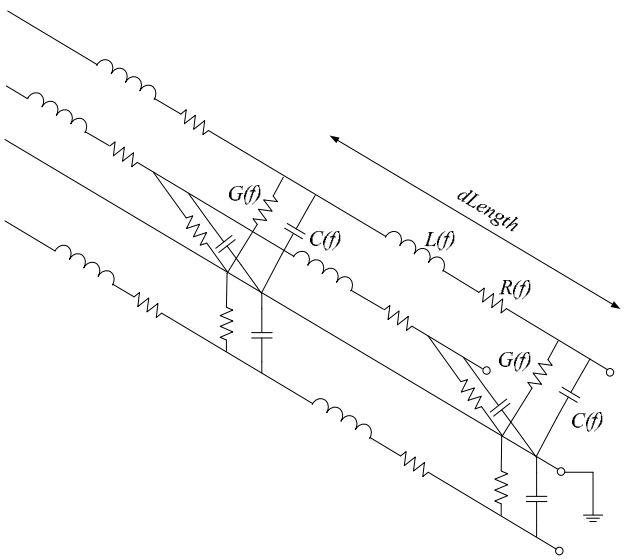

Fig. 2. Electrical representation of the cable per differential length with frequency dependent parameters

2.2 Modeling options of the power transmission cable

Based on the electric representation of the cables and depending on the cable model requirements, it is possible to perform more or less simplifications, in order to maintain the accuracy of the model and reduce its complexity. Thus, there are several ways for modeling a cable; these models can be classified as follows (Restrepo et al., 2008).

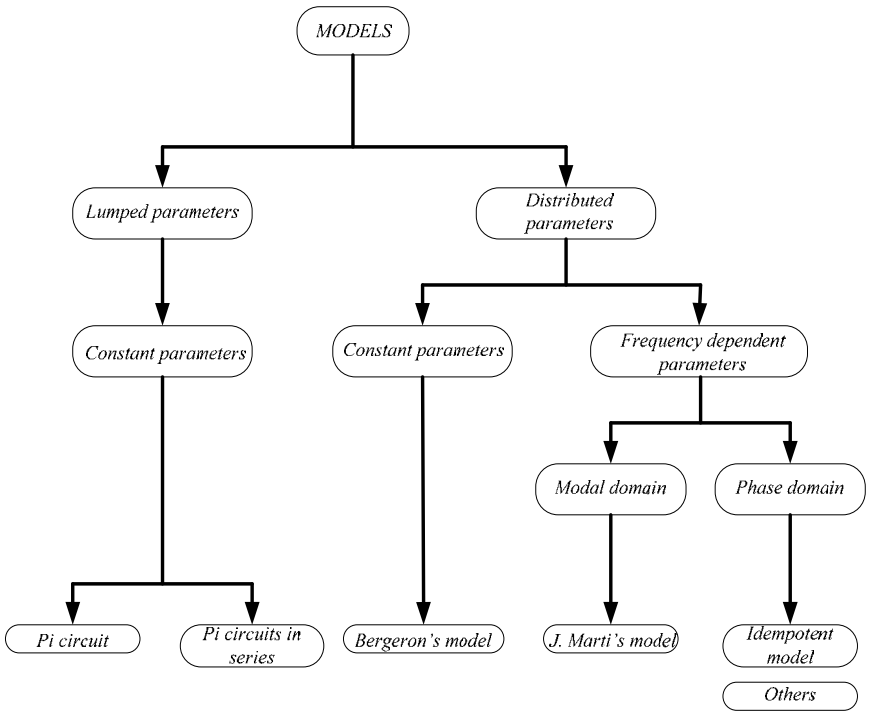

Fig. 3. Classification of the different types of cable models

2.2.1 Frequency dependent model in phase domain (Idempotent model)

The selected model to carry out the evaluation of the frequency response of the offshore wind farm, is the PSCAD's frequency dependent phase model based on the idempotent model. The reason to select the most complex and accurate model is because the cable model has to represent a wide frequency range.

The Idempotent model is analyzed in (Castellanos et al., 1997; Marcano, 1996; Restrepo et al., 2008).

The idempotent model with some changes / improvements detailed in (Gustavsen et al., 1999) is used in PSCAD as the most accurate model. Moreover, the PSCAD user's guide guaranties that its cable model, frequency dependent in phase domain is very accurate (Power System Computer Aided Design [PSCAD], 2003). This model used by PSCAD also has been successfully validated experimentally in (Nian, 2009; Meier, 2009).

2.3 Cable parameter adaptation to PSCAD

Based on the physical characteristics of one specific cable as served in Table 1 (Courtesy of General Cable), PSCAD solves / estimates the equivalent impedances (*RLGC* parameters) for the electric representation of the cable shown in, Fig. 2. In this way, for complex models, where many parameters and detailed electric specifications are required, the definition of the cable is simpler.

PSCAD provides a template to fill into it the data of the cable. Nevertheless, for complex cables it is not possible to represent the whole cable. The template has concentric, circular and homogeneous layers to introduce the data of the cable. Even though there are subsea

cables made up with other physic characteristics like: semiconductor layers, conductors made up with crown of strands or the fill between conductors.
Due to the impossibility to fill in directly the data of the cable to the PSCAD software, the physic parameters have to be modified / corrected. The purpose of this correction is to achieve the same value of the equivalent impedances for PSCAD estimation and the cable manufacturers. The modified parameters are those ones related to the conductor, shield and insulation.

Parameter	Value
Rated voltage	87 / 150*kV*
Rated current	1088*A*
Conductors cross section	1.200mm^2
Separation between conductors	97.839996*mm*
Buried depth	1*m*
Shields cross section	30mm^2
Shield type	Metallic strip
Armor type	Strands crown
Diameter of conductor	43,5*mm*
Insulation thickness	20*mm*
Diameter upon the insulation	88,5*mm*
Diameter down the sheath	215,6*mm*
Diameter down the armor	226,7*mm*
Sheath thickness	8,9*mm*
External diameter	244,5*mm*
Relative dielectric constant	2,50
Resistivity of the conductor d.c. at 20°C	0,0151*Ohm/km*
Resistivity of the conductor a.c.	0,0205*Ohm/km*
Resistivity of the shield d.c. at 20°C	0,6264*Ohm/km*
Rated capacitance of the cable	0,233$\mu F/km$
Inductance of the cable	0,352*mH/km*

Table 1. Cable characteristics provided by General Cable

2.3.1 Conductor

Looking at Table 1, the conductor has a 43.5mm diameter and also an effective cross section of 1200mm². If the conductor is considered as a solid core, homogenous and circular (as the template of PSCAD does), the cross section for this diameter (equation (1)) is not the same.

$$A = \pi \cdot r^2 = \pi \cdot 21.75^2 = 1486.17 mm^2 \quad (1)$$

Therefore, to solve this difference it is necessary to correct the resistivity of the conductor ρ. To this end, at the first step the real resistivity of the conductor is calculated (based on the data of the cable given by the manufacturer), equations (2) -(3).

$$R_{DC} = \frac{\rho_c \cdot l}{A_c} = 0.0151 \ ohm/Km \quad (2)$$

$$\rho_c = \frac{R_{DC} \cdot A_c}{l} = 1.812 \cdot 10^{-8} \quad (3)$$

Where: ρ_c is the resistivity, l is the length of the cable and A_c is the effective cross section of the conductor (1200 mm²).
At the second step, the resistivity of the conductor's material is modified in order to maintain the same absolute resistance of the conductor, (Nian, 2009). Based on the conductor radius given by the manufacturer, in function of the effective cross section and the real cross section, is corrected the resistivity:

$$\rho_c' = \rho_c \frac{\pi \cdot r^2}{A_c} = 2.24412 \cdot 10^{-8} \quad (4)$$

To verify this estimation, the absolute resistance of the conductor at 50 Hz is calculated with equation (5). From this equation, it is possible to achieve practically the same results in comparison with the characteristics of the manufacturer.

$$R_{a.c.}(50) = \frac{\rho_c}{\delta_{50}} \cdot \frac{l}{\pi\left(D - \delta_{50}\right)} = 0.0204 \ \ ohm / Km \quad (5)$$

$$\delta_{50} = \sqrt{\frac{2 \cdot \rho_c}{\omega \cdot \mu}} = 0.010662 \quad (6)$$

Where: l is the length of the cable, D is the diameter of the conductor, ρ_c is the resistivity, ω is the angular speed of the current ($2\pi f$), μ is the absolute magnetic permeability of the conductor ($\mu_0\,\mu_r$), μ_0 is the magnetic constant or the permeability of the free space ($4\pi \times 10^{-7}$ N/A²) and μ_r is the relative magnetic permeability.

2.3.2 Shield

The next parameters that must be modified are the size of the diameter of the insulation and its relative permeability, in order to maintain the shield with 30mm² and the same capacitive component.
Assuming that the outer diameter of the shield's conductor layer is 88.5mm, it is possible to obtain the inner diameter, equations (7) - (9).

$$A_s = R_s^2 - r_s^2 \quad (7)$$

$$30mm2 = 44.45^2 - r_s^2 \quad (8)$$

$$r_s = \sqrt{44.25^2 - 30} = 43.9mm \quad (9)$$

2.3.3 Insulation

To correct the area of the shield the radius of the insulation is modified. As a result, the value of the capacitive component using the radius calculated in equation (9) is slightly different in comparison with the characteristic provided by the manufactures.
Therefore, to represent correctly the submarine cable, the dielectric constant is corrected in order to represent in PSCAD the same the capacitive component of the manufacturer's data sheet, equations (10) - (11).

$$\varepsilon_r = 0.233 \cdot 17.97 \cdot \ln\left({}^{43.9}\!/_{21.75}\right) = 2.94 \tag{10}$$

$$C = \frac{\varepsilon_r}{17.97 \cdot \ln\left({}^{b}\!/_{a}\right)} = \frac{2.94}{17.97 \cdot \ln\left({}^{43.9}\!/_{21.75}\right)} = 0.233 \quad \mu F / Km \tag{11}$$

2.3.4 Measure with PSCAD the adapted parameters

To validate the modification of parameters carried out in the preceding sections, a submarine cable in PSCAD (Fig. 4) is defined, based on the physic data of the cable shown in Table 1 with these modifications. Then, using PSCAD software, its internal *RLCG* parameters are obtained, Table 2.

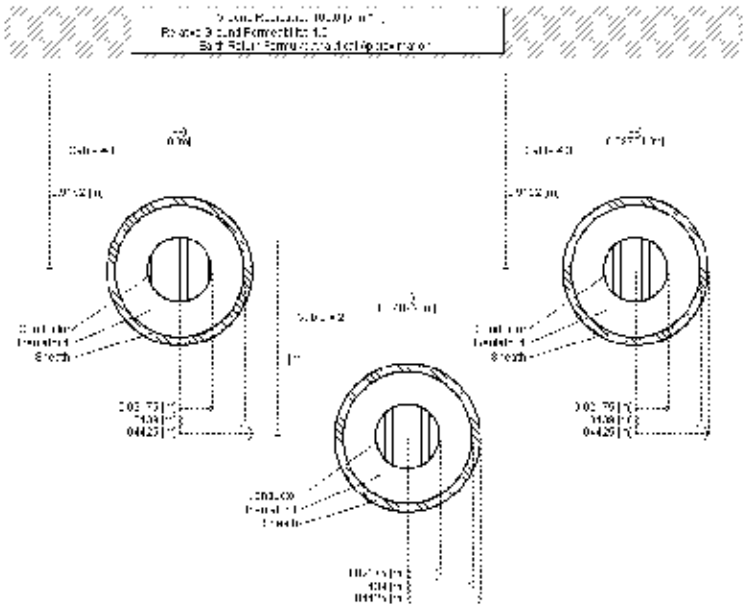

Fig. 4. Graphic representation in PSCAD of the three-phase cable

	Resistivity	Inductivity	Capacitance
Electric parameters (50*Hz*)	0.0311***Ohm/km*	0.334*mH/km*	0.233*μF/km*

*Resistivity without taking into account the shield, conductor 0.0190*Ohm/km*

Table 2. *RGLC* electrical parameters calculated by PSCAD in function of the physic dimensions and characteristics

From the results displayed in Table 2, it is possible to see that the electrical parameters calculated by PSCAD are substantially similar to the parameters specified by the manufacturer.

3. Frequency response of the transmission system via PSCAD simulation

3.1 Frequency response of the basic transmission system via PSCAD simulation

The transmission system is the part of the offshore wind farm which makes possible the energy transmission from the collector point (offshore) to the point of common coupling (onshore), in other words, the physic medium to transfer the energy from the wind farm to the main grid and all the support devices.

The transmission system is made up by the step-up transformer, the submarine cable, reactive power compensation elements (if required), and the support devices to integrate the energy in the main grid (if required).

The knowledge of the frequency response of the transmission system and the influence of each component upon this frequency response can help to avoid undesired resonances and harmonics. For that purpose, firstly, in this section the simplest lay-out for the transmission system (transformer, cable and grid, Fig. 5) is considered, i.e. the necessary elements to perform the energy transmission, without the support devices to improve the transmission.

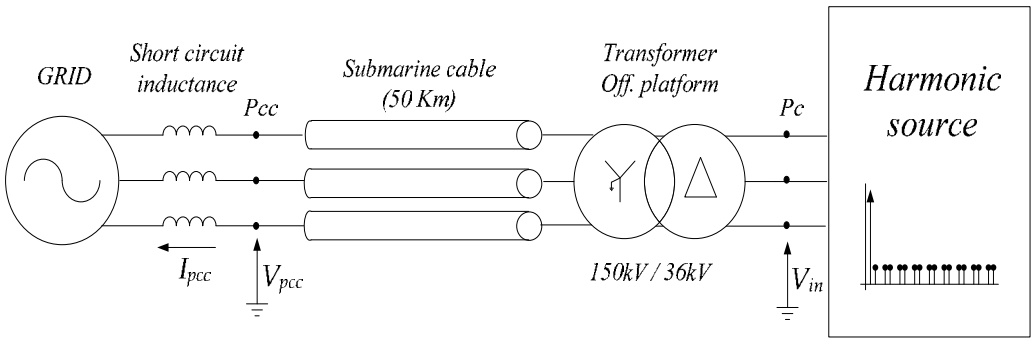

Fig. 5. Simulation scenario of the simplest lay-out of the transmission system: the step-up transformer, the submarine cables and the distribution grid

To calculate the impedance of the transmission system in function of the frequency, a harmonic voltage source is used. The harmonic train of input voltage (V_{in}), is composed by sinusoidal components in the range of frequencies: 50-5000Hz. The amplitude of these harmonic voltages is 10% of the fundamental (50Hz-150kV). Starting from the 50Hz, the harmonic train has voltage components separated 10Hz one from other, as illustrated in Fig. 6. These input harmonics in a simplified way can represent the effect of the harmonics generated by the wind turbines, when they are generating energy from the wind.

Measuring the current at the PCC (I_{pcc}) and performing the FFT (Fast Fourier Transform) of the signal, it is possible to obtain the impedance of the transmission system for each one of the excited frequencies, i.e. it is possible to obtain the evolution of the impedance in function of the frequency.

To model the grid in a simple manner, a voltage source and short circuit impedance is used. Its characteristics are summarized in Table 3. The transformer's connection is Δ- gY, while its characteristics are shown in Table 4. Finally, the cable characteristics and cable model are the same of the section 2.

The frequency response of the described transmission system layout is depicted in Fig. 7.

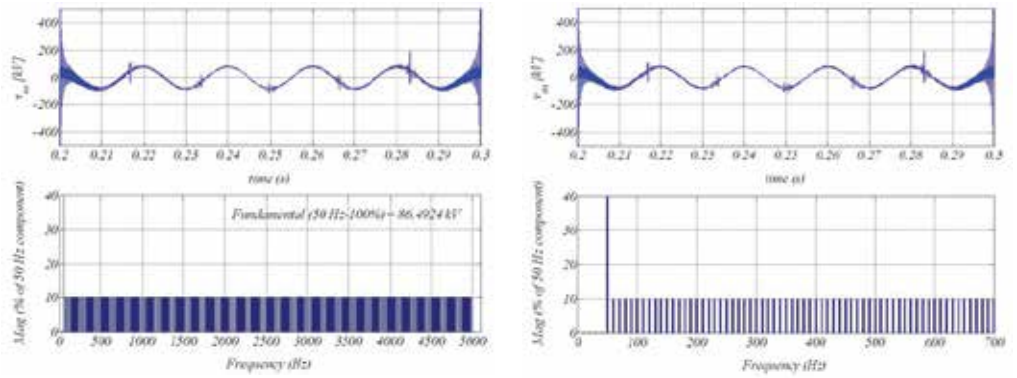

(a) (b)

Fig. 6. Harmonic voltage train applied to the submarine cable model (resolution 10 Hz)

Parameter	Value
Nominal power (Pn)	150*MW*
Nominal voltage (Vn)	150*kV*
Short circuit inductance	5%

Table 3. Characteristics of the main grid

Parameter	Value
Rated power	150*MVA*
Primary voltage	33*kV*
Secondary voltage	150*kV*
Connection	Δ- gY
Transformers leakage resistance	1%
Transformers leakage inductance	6%
No load losses	1,78%

Table 4. Characteristics of the step-up transformer

Looking at Fig. 7, it is possible to observe that all the multiples of the 3rd order harmonics generated in the wind turbines, cannot trespass to the PCC. This occurs because between these points is placed a transformer with star (grounded)-delta connection.

The transmission system is composed with several inductive components, like the transformer or the short circuit impedance of the main grid. This inductive impedances provokes a significant attenuation of the high frequencies, as can be seen in Fig. 7 (c), thus, the high frequency harmonic voltages do not affect to the current of the PCC. In fact, in the present analysis, the harmonics higher than 700Hz almost do not affect to the current at PCC.

However, the interaction of the inductive component of the transmission system with the capacitive component of the submarine cable provokes a resonance at 400Hz, becoming these frequencies which are around the 400Hz potentially problematic.

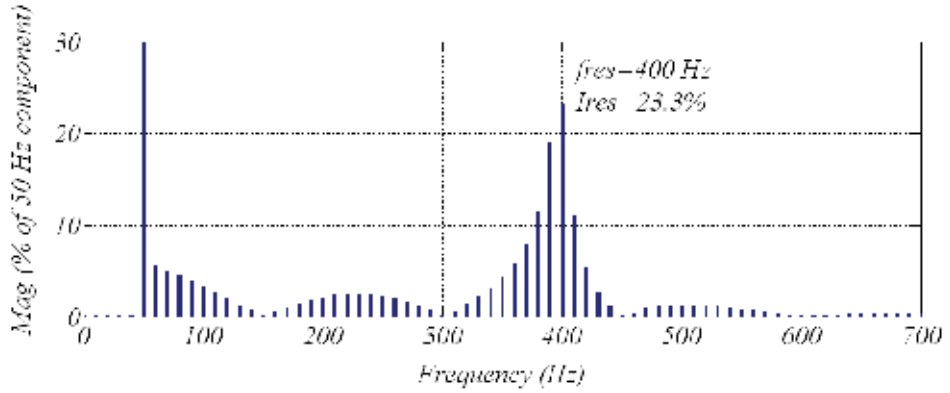

(a)

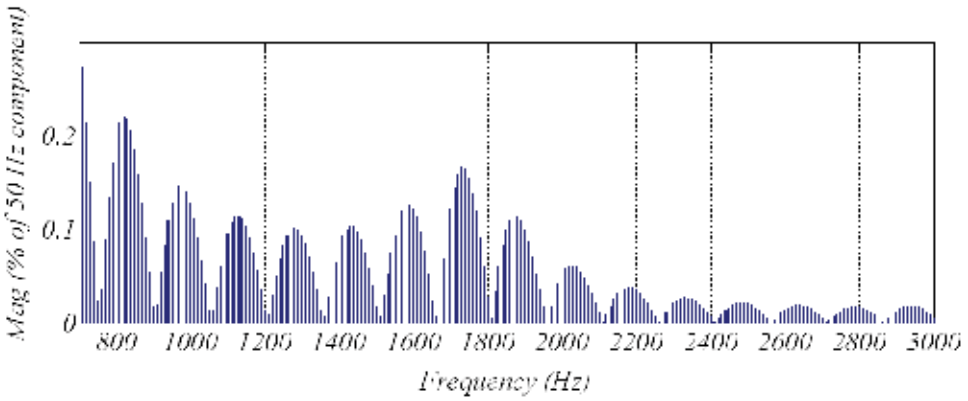

(b)

Fig. 7. Frequency response of the transmission system with only: grid impedance, step-up transformer and submarine cable (50 Km). FFT of the current at PCC: (a) detail in the neighborhood of the main resonance and (b) detail in high frequencies

3.2 The effect of the different parts of the transmission system in its frequency response

The analysis of how affects each one of the elements of the transmission system in its frequency response is the first step to avoid undesired resonances and optimize the transmission system design.

Therefore, this section analyses the frequency response of the transmission system varying the characteristics (impedance) of its three main components:

- The leakage impedance of the step-up transformer.
- The impedance of the submarine transmission line (variation of the cable length).
- The short circuit impedance of the main grid.

Firstly the influence of the step-up transformer is evaluated. Based on the same scenario of the Fig. 5 and applying the same harmonic train (Fig. 6), the frequency responses of the transmission system are obtained. In this first case, the transformer's leakage inductance has a variation from 3% to 12%, the results are depicted in Fig. 8.

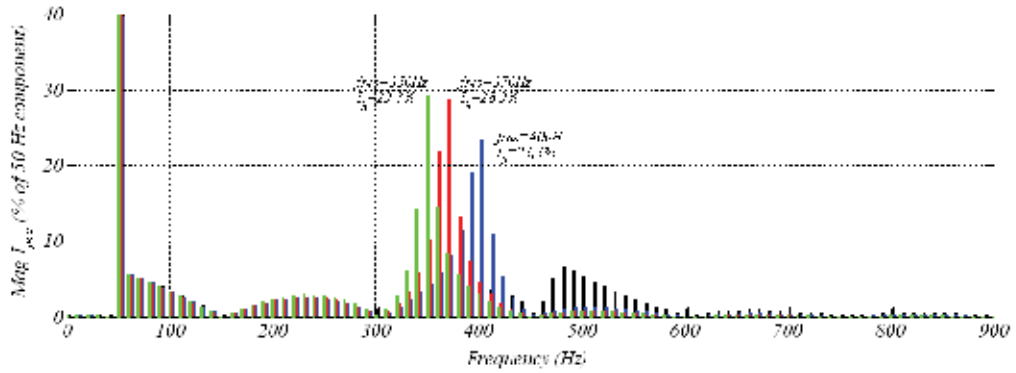

Fig. 8. Frequency response of the transmission system varying the leakage inductance of the step-up transformer from: 3% (black), 6% (blue), 9% (red) and 12% (green)

As is shown in Fig. 8, as the leakage inductance of the step-up transformer increases, the frequency of the resonance decreases (from 450Hz to 350Hz).
For the specific case where the leakage inductance is 3%, it is possible to see how the transformer connection does not allows to cross to the PCC the harmonics close to the resonance, Fig. 9. The resonance is still there (450Hz), but, there are not harmonics to be amplified.

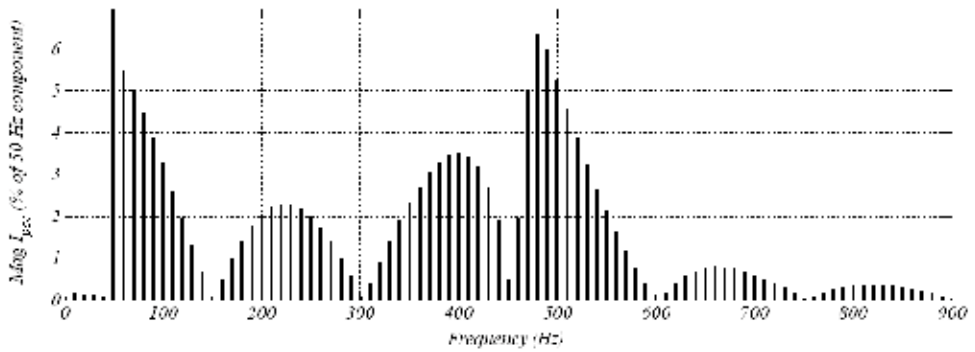

Fig. 9. Frequency response of the transmission system with a leakage inductance of 3% of the step-up transformer

The harmonic train used for this analysis has components into de 50-5000Hz range, but not continuously in all this range, the harmonic source generates harmonic voltages in steps of 10 Hz. Thus, using the harmonic train is possible to determinate the resonance with 10 Hz accuracy, i.e. the system has a 10 Hz accuracy
With regards to the amplitude of the resonance, this varies very quickly in few Hz close to the resonance frequency. As a consequence, if the harmonic resonance matches up with the exact resonance frequency, the measured amplitude in the simulation will be bigger than in cases where the harmonics in the train are close to the exact frequency of the resonance. Thus, this analysis can measure accurately the frequency of the resonance, but not the amplitude, the amplitude is only an approximated value.

In the next step of the analysis, the influence of the cable length in the range of 20Km to 110Km is evaluated. The frequency response of the considered transmission system with this variation is shown in Fig. 10.

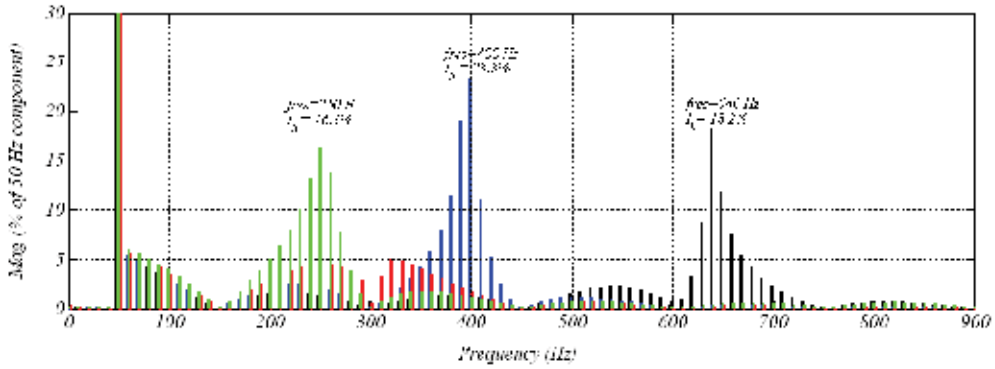

Fig. 10. Frequency response of the transmission system varying the cable length from: 20Km (black), 50Km (blue), 80Km (green) and 110Km (red)

In this case, as the submarine cable length increases, the resonance frequency decreases. Note that the resonance of the transmission system with 80Km cable disappears, because in this case also all the multiples of the 3rd order harmonics cannot trespass the transformer.
In the third and last case there are considered different values for the short circuit impedance. This variation is from the 2 % to 11 %, the simulation results are depicted in Fig. 11

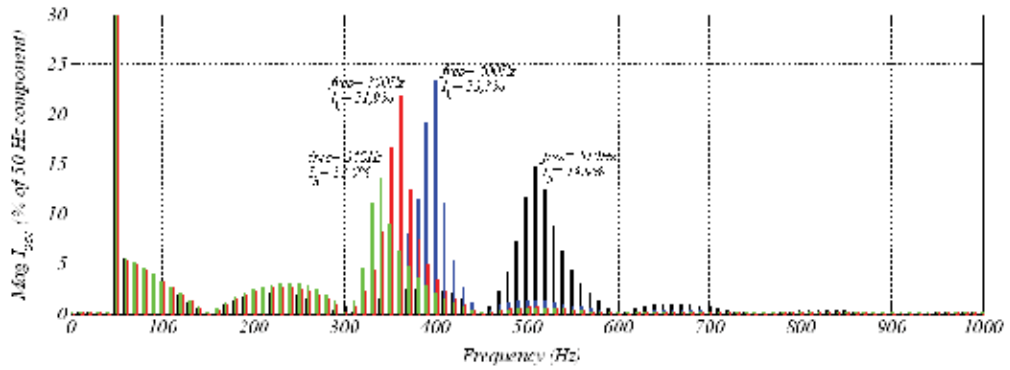

Fig. 11. Frequency response of the transmission system varying the short circuit impedance from: 2 % (black), 5 % (blue), 8 % (green) and 11 % (red)

In this last case, increasing the short circuit impedance decreases the resonance frequency, i.e. as in the two previous cases, increasing the inductive impedance or the capacitive impedance the frequency of the resonance decreases. In the analyzed cases, the biggest variation is between 640Hz-250Hz, caused varying the cable length from 20Km to 110Km. However, in most of the cases the resonance is between 450Hz and 250Hz. In concordance with these results, in (Breuer & Christl, 2006) is highlighted that AC transmission systems in conjunction with step-up transformer of the offshore substation, present the risk to amplify harmonics at low frequencies (inherently 3rd, 5th and 7th order harmonics).

3.3 Frequency response of the transmission system via analytic calculus

The objective of this section is to estimate the main resonance frequency in a simple and accurate way, alternatively to the method described in the previous section. Thus this section studies the calculation of the first resonance frequency of the transmission system, which is the main characteristic of the frequency response, using two different analytic ways.

To characterize in an easy way the main resonance frequency, with a potential risk of harmonic amplification, in (Plotkin et al., 2008) is presented a simple method. This approximation only takes into account the capacitive component of the submarine cable, neglecting the resistive and inductive components. In this way, it is possible to simplify the whole transmission system as an equivalent *RLC* circuit. Then, the resonance frequency of this simplified *RLC* circuit serves to approximate the resonance of the transmission system.

The second method uses state-space equations to estimate the resonance frequency of the transmission system. These equations take into account all the components of the cable and the short circuit impedance of the main grid, with the advantage that is not too more complicated than the first method.

Finally, to validate these two methods, the results obtained via analytic calculus are compared with the results obtained in simulation with PSCAD as described in section 3.2.

3.3.1 State-space equations for the transmission system modeled with a unique "π" circuit

At first, in order to explain with an example the method of the state-space equations, the simplest case is analyzed. The step-up transformer is considered as an equivalent inductance and the main grid as an ideal voltage source with short circuit impedance.

With regards to the submarine cable, this is modeled using several "π" circuits in series, (Khatir et al., 2008). This model has a frequency limit to represent the cable, i.e. the cable model has a valid range in frequency, out of this frequency range the cable model and in consequence the state-space equations cannot be used, since the error becomes too high. For the simplest case, the present case, the cable is modeled as a unique "π" circuit (N=1).

Once the equivalent circuit of the circuit in impedances is determined, it is possible to obtain the frequency response applying the state-space equations, the procedure is as follows:

In the first step, the names and the directions for all the currents of all the branches of the circuit are established as illustrated in, Fig. 12.

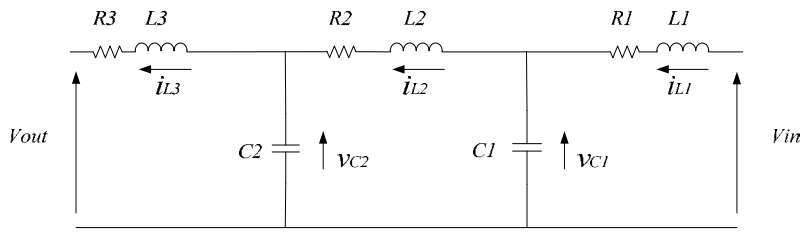

Fig. 12. Mono-phase representation of the transmission system with the submarine cable modeled as a unique "π" circuit

Where: *L1* represents the equivalent inductance of the step-up transformer, *R1* represents the equivalent resistance of the step-up transformer, *R2* represents the resistive part of the

submarine cable, *L2* represents the inductive part of the submarine cable, (*C1*=*C2*) represent the capacitive part of the submarine cable and (*L3* and *R3*) represent *Lsc* and *Rsc* respectively, short circuit impedances.
In the second step, the differential equations are obtained, (12) -(16).

$$\frac{di_{L1}}{dt} = \frac{1}{L1} \cdot \left(Vin - v_{C1} - i_{L1} \cdot R1 \right) \tag{12}$$

$$\frac{dv_{C1}}{dt} = \frac{1}{C1} \cdot \left(i_{L1} - i_{L2} \right) \tag{13}$$

$$\frac{di_{L2}}{dt} = \frac{1}{L2} \cdot \left(v_{C1} - v_{C2} - i_{L2} \cdot R2 \right) \tag{14}$$

$$\frac{dv_{C2}}{dt} = \frac{1}{C2} \cdot \left(i_{L2} - i_{L3} \right) \tag{15}$$

$$\frac{di_{L3}}{dt} = \frac{1}{L3} \cdot \left(v_{C2} - Vout - i_{L3} \cdot R3 \right) \tag{16}$$

Looking at equations (12) - (16), the variables of the differential equations i_{LX} and v_{CX} are independent. In the same way, these variables represent independent physical elements, so, those variables are state variables. Thus, if these equations are written in matrix notation (equation (17)), the state-space matrix is obtained as follows:

$$d\,/\,dt\ [x] = [A] \cdot [x] + [B] \tag{17}$$

$$d\,/\,dt \cdot \begin{bmatrix} i_{L1} \\ v_{C1} \\ i_{L2} \\ v_{C2} \\ i_{L3} \end{bmatrix} = \begin{bmatrix} -R1/L1 & -1/L1 & 0 & 0 & 0 \\ 1/C1 & 0 & -1/C1 & 0 & 0 \\ 0 & 1/L2 & -R2/L2 & -1/L2 & 0 \\ 0 & 0 & 1/C2 & 0 & -1/C2 \\ 0 & 0 & 0 & 1/L3 & -R3/L3 \end{bmatrix} \cdot \begin{bmatrix} i_{L1} \\ v_{C1} \\ i_{L2} \\ v_{C2} \\ i_{L3} \end{bmatrix} + \begin{bmatrix} 1/L1 & 0 \\ 0 & 0 \\ 0 & 0 \\ 0 & 0 \\ 0 & -1/L3 \end{bmatrix} \cdot \begin{bmatrix} Vin \\ Vout \end{bmatrix} \tag{18}$$

Finally, the poles or eigenvals of the system are calculated (from *A* matrix), to determine its resonance frequency.

3.3.2 State-space equations of the transmission system modeled with N "π" circuits

In the next step forward, the procedure explained in the previous section (3.3.1.), is applied to a generic case where the transmission system has a cable modeled with N "π" circuits, Fig. 13.

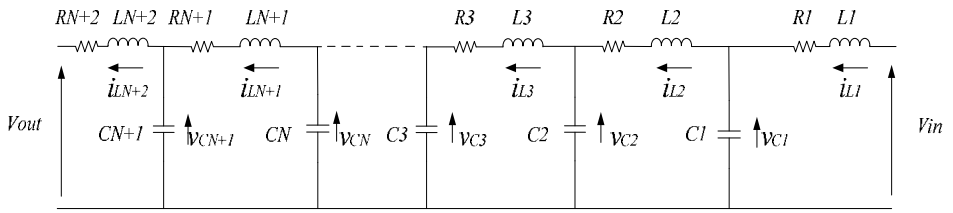

Fig. 13. Mono-phase representation of the transmission system with the submarine cable modeled as N "π" circuits

Where: *L1* represents the equivalent inductance of the step-up transformer, (*R2=R3=RN+1*) represent the resistive part of the submarine cable, (*L2=L3=LN+1*) represent the inductive part of the submarine cable, (*C1* to *CN+1*) represent the capacitive part of the submarine cable and (*LN+2* and *RN+2*) represent *Lsc* and *Rsc* respectively, short circuit impedances.
For the generic transmission system, following the procedure explained in the previous section, the state-space variables are defined and the estate-space equations are obtained. These state-space equations in matrix notation are displayed in equation (19). The reader can find the similarities of the matrix structure in expressions (18) and (19).

$$d/dt\cdot\begin{bmatrix} i_{L1} \\ v_{C1} \\ i_{L2} \\ .... \\ i_{LN+1} \\ v_{CN+1} \\ i_{LN+2} \end{bmatrix} = \begin{bmatrix} -R1/L1 & -1/L1 & 0 & .... & 0 & 0 & 0 \\ 1/C1 & 0 & -1/C1 & .... & 0 & 0 & 0 \\ 0 & 1/L2 & -R2/L2 & .... & 0 & 0 & 0 \\ .... & .... & .... & .... & .... & .... & .... \\ 0 & 0 & 0 & .... & -RN+1/LN+1 & -1/LN+1 & 0 \\ 0 & 0 & 0 & .... & 1/CN+1 & 0 & -1/CN+1 \\ 0 & 0 & 0 & .... & 0 & 1/LN+2 & -RN+2/LN+2 \end{bmatrix} \cdot \begin{bmatrix} i_{L1} \\ v_{C1} \\ i_{L2} \\ .... \\ i_{LN+1} \\ v_{CN+1} \\ i_{LN+2} \end{bmatrix} + \begin{bmatrix} 1/L1 & 0 \\ 0 & 0 \\ 0 & 0 \\ .... & .... \\ 0 & 0 \\ 0 & 0 \\ 0 & -1/LN+2 \end{bmatrix} \cdot \begin{bmatrix} Vin \\ Vout \end{bmatrix} \quad (19)$$

3.3.3 Frequency response of the transmission system via state-space equations

Finally, the frequency response of the transmission system with the submarine cable, the step-up transformer and the main grid of the previous section (Table 1, Table 3 and Table 4) via state-space equations is obtained.
For the submarine cable model, 10 "π" circuits in series are considered. In this way, the cable model is composed by sufficient "π" circuits to make possible the representation of the submarine cable in the correct frequency range, i.e. sufficient to represent correctly the cable until the resonance. In more detail, with 10 "π" circuits it is possible to represent the

submarine cable in a valid range for all the resonances analyzed in the previous section (Khatir et al., 2008), by means of equation (20).

$$f_{\max} = \frac{Nv}{8 \cdot l} = \frac{N}{8 \cdot l \cdot \sqrt{LC}} = 1250Hz \Rightarrow 7884rad / s \tag{20}$$

If the resonance frequency estimated in this way is out of the cable model valid range, it is not valid and the analysis must be repeated with a valid cable model.
Finally, applying the developed generic equation (19), to the considered transmission system, the frequency response depicted in Fig. 14 is obtained.

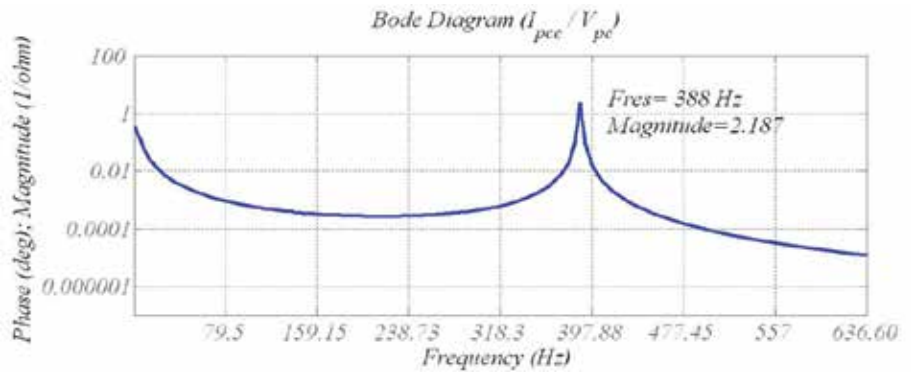

Fig. 14. Frequency response of the transmission system with the cable modeled as 10 "π" circuits in series using state equations

As can be observed in Fig. 14, the first resonance of the system is located at 388 Hz, very close to the 400 Hz estimated via PSCAD simulation. With regards to the amplitude of the resonance, in this case also is an approximation, due to the fact that the calculus is based on a model with lumped parameters, not in a model with distributed parameters which is more accurate.

3.3.4 Frequency response of the transmission system via *RLC* simplification

The other method used to compare with the state-space equations is the simplified *RLC* method, described in (Plotkin et al., 2008). Thus, a comparative is performed comparing the resonance frequency estimated with these three methods for different transmission system. Similarly as done in section 3.2, but in this case, the analysis only varies the cable length and the equivalent inductance of the step-up transformer. The short circuit impedance of the main grid is not taken into account because the simplified *RLC* method does not consider it.
The resonance frequency for the simplified *RLC* method of (Plotkin et al., 2008) is estimated with the following equation (21).

$$f_{\mathrm{Re}sonance} = \frac{1}{2 \cdot \pi \cdot \sqrt{\left(L_{Transfomer} + L_{Cable}\right) \cdot C_{Cable}}} \tag{21}$$

3.3.5 Comparison and validation of the frequency response via analytic calculus

The objective of this section is to validate the state-space equations based method to estimate the first resonance. For that purpose, a comparative of three different methods is carried out.

The method based on PSCAD simulation with the validated cable is considered as the most accurate method.
Hence, Table 5, summarizes the obtained resonance frequencies varying the equivalent inductance of the step-up transformer for the considered three methods. The variation of the equivalent inductance is the same of the section 3.2. (3% to 12%).

Transformers L	3 %	6 %	9 %	12 %
PSCAD simulation	470	400	370	360
State equations	453,6	388,3	356,5	339
Simplified RLC	264,75	218	190,9	171,4

Table 5. Comparative of the resonance frequencies (Hz) obtained varying the equivalent inductance of the step-up transformer

To verify the state-space equations method at different conditions, a second comparative is carried out. In this second case, the cable length is varied, yielding the resonances depicted in Table 6.

Cable length (Km)	*20*	*50*	*80*	*110*
PSCAD simulation	640	400	310	255
State equations	631,8	388,3	297,6	246,6
Simplified RLC	392	218	156,67	124,8

Table 6. Comparative of the resonance frequencies (Hz) obtained varying the cable length

Looking at Table 5 and Table 6, it can be concluded that the state-space equation method is a good approximation for estimating the resonance frequency, even under different transmission conditions options.
On the other hand, the simplified *RLC* method does not provide as accurate results as expected to characterize the resonance frequency. However it could be useful to obtain a very simplified and first approximated value.

4. Frequency response of the offshore wind farm

In the present work, the electric infrastructure of the offshore wind farm's connection is divided into two parts: The transmission system and the inter-turbine grid. The frequency response of the transmission system has been already characterized in previous section, therefore, the next step consist on characterizing the frequency response of the entire electric infrastructure, including the inter-turbine grids. Thus, this second part of the analysis is mainly focused on the inter-turbine grid and its characteristics.
The equivalent impedance of an offshore wind farm varies with changes in the configuration of the inter-turbine grid. As a result, the frequency response of the system varies as well. Consequently, based on the transmission system evaluated in section 3.1, the analysis performed in this section is focused on the effect of different aspects of the wind farm, like: number of feeders (or radials) in the inter-turbine grid or the location of each wind turbine. The analysis is made from the viewpoint of the wind turbine, which is considered the potential harmonic source in normal operation.

Without the appropriate models is not possible to estimate the resonances of the system. In consequence, a scenario is defined in order to base the analysis of the resonances on it.
The considered scenario presents a radial design for the inter-turbine grid, where each one of those radials is composed by 6 wind turbines of 5MW. The voltage level of the inter-turbine grid is medium voltage, 33kV. As regards to the spatial disposition of the wind turbines, there is considered as a rectangle (Hopewell et al., 2006). In short, the simulation scenario has similar features of Nysted, (Fig. 15).

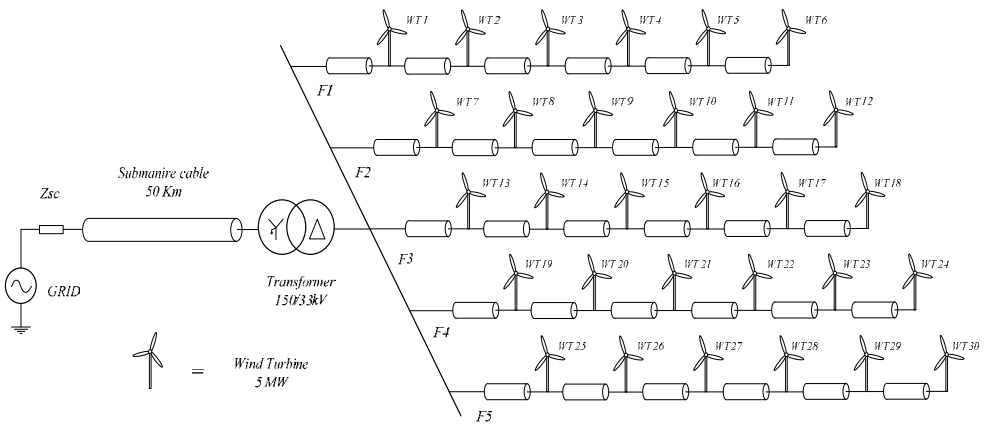

Fig. 15. The lay-out of the offshore wind farm, which is the base of the resonances analysis

Considering that the transmission system is equal to the characterized in section 3.1, the last feature to define the whole offshore wind farm is the inter-turbine submarine cable. Hence, as inter-turbine submarine cable an ABB XLPE cable (Asea Brown Boveri [ABB], 2005) with the adequate nominal voltage and power is chosen. The characteristics of this cable are shown in Table 7.

Parameter	Value
Rated voltage	$30kV$ ($36kV$)
Rated current	765 (65^oC) – 930 (90^oC) A
Cross section of conductor	$800mm^2$
Separation between conductors	$123.65mm$
Buried depth	$1m$
Shields cross section	$35mm^2$
Diameter of conductor	$33.7mm$
Insulation thickness	$8mm$
Diameter upon the insulation	$51.9mm$
Relative dielectric constant	2,30
Resistivity of the conductor d.c. at 20°C	$0{,}02265Ohm/km$
Resistivity of the conductor a.c.	$0{,}024959Ohm/km$
Rated capacitance of the cable	$0{,}38\mu F/km$
Rated inductivity of the cable	$0{,}31mH/km$

Table 7. Characteristics of the inter-turbine submarine cable (ABB, 2005).

These characteristics are filled into the PSCAD template, for the model explained in section 2 with the corrections exposed in section 2.3.
The aim of this evaluation is to calculate the frequency response of the entire electric connection infrastructure. Thus, the wind turbine model is not considered as a key issue. Therefore, the wind turbines are considered as an ideal controlled voltage source with a *LCL* filter, Table 8. The filter is used to connect the wind turbine to the local inter turbine grid, Fig. 16.

LCL values	*Fres*
0.8 mH-175uF-0.4mH	*550Hz*

Table 8. Characteristics of the LCL filter.

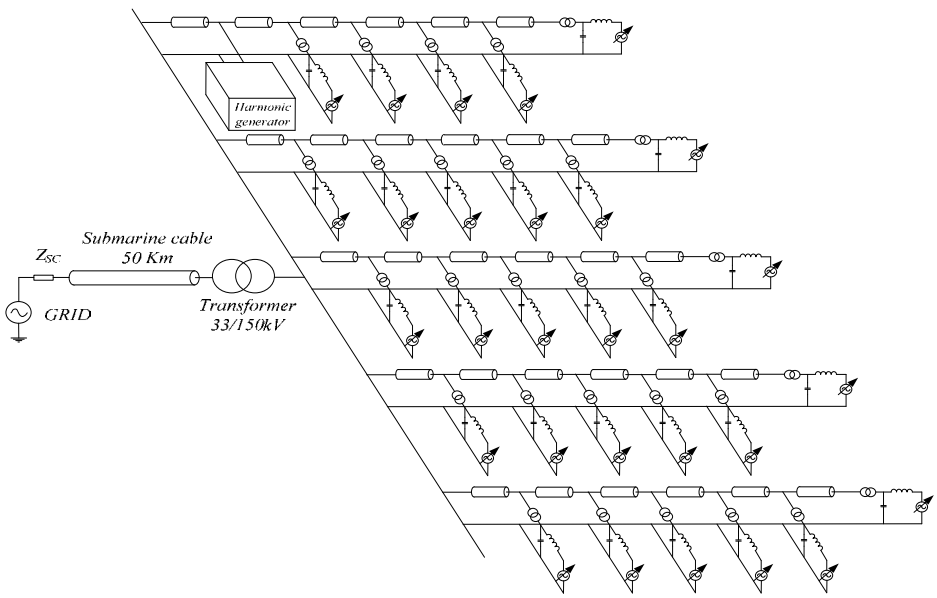

Fig. 16. Simulation scenario of the offshore wind farm, which is the base for the frequency response analysis

Taking the scenario depicted in Fig. 16 as base to estimate the frequency response, the same procedure of section 3.1 is used. In this way, to know the frequency response for a specific wind turbine, it is substituted by a harmonic voltage generator (Fig. 16), which generates a harmonic train in the frequency range of 50Hz-5000Hz, Fig. 6.

4.1 Frequency response of a wind turbine in function of its position in the inter-turbine network

Looking at Fig. 15, it is possible to observe how from the viewpoint of each wind turbine, the equivalent impedance seen is different in function of its location in the inter-turbine grid, i.e. there is not the same equivalent impedance at the output of the 25th wind turbine and at the output of the 30th wind turbine.

To quantify the variation of the frequency responses of each wind turbine, in this section the frequency responses for all the wind turbines of a feeder are estimated. To perform this evaluation, the harmonic voltage source is placed in different positions of the feeder (or radial) and for each position the signals at the PCC are measured. Then, applying the FFT to the signals of the PCC, it is possible to estimate the frequency response for each individual wind turbine.
In the first evaluation, the frequency response of each wind turbine is obtained from the 25th to the 30th. The results for the harmonic currents are depicted in Fig. 17 and the results for harmonic voltages are depicted in Fig. 18.

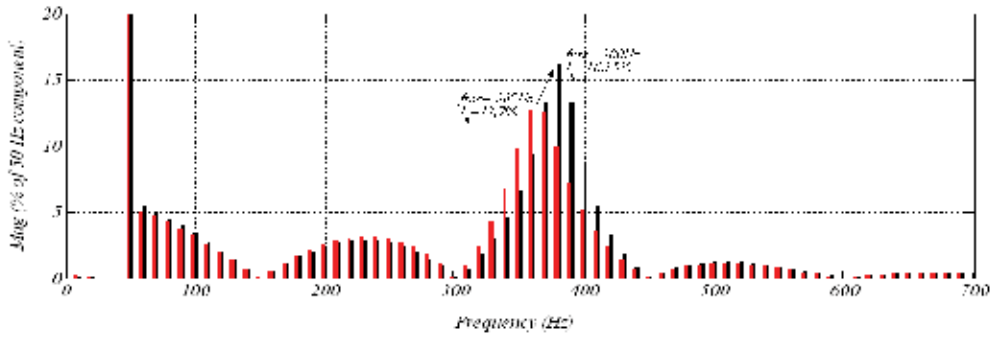

Fig. 17. Harmonic currents at the PCC in function of the location of the harmonic voltage source within the inter turbine grid. For the 30th wind turbine (red) and for the 25th wind turbine (black)

The frequency response of the whole system is similar to the frequency response of the transmission system only. However, the resonance frequency has a short variation. The transmission system presents the resonance at 400 Hz (section 3.1, Fig. 7), but as can be seen from the Fig. 17, the frequency response from the wind turbine viewpoint depends on each wind turbine and is located in the range of 360-380 Hz, close to the 400Hz but not the same.
As seen in section 3.2, the step-up transformer does not allow to transmit 3rd order harmonics and multiples. Looking to the results for the 30th wind turbine, the harmonics located at 360Hz and 370Hz have similar amplitudes in both cases (current and voltage), probably the resonance is between them. This fact, can explain the notorious amplitude reduction.
Applying the FFT to the voltage at PCC (Fig. 18), it is possible to see other two more "small resonances" (attenuated frequencies, but less than the rest), besides the transmission system's resonance.
The first one of these two frequency groups less attenuated than the rest is located between the 1500Hz and 2000Hz. This small resonance has not variations, i.e. is independent to the location of the wind turbine. However, the second group of these frequencies less attenuated is in function of the location of the wind turbine. Thus, in function of the location of the wind turbine, the "small resonance" can be around 2500Hz or 3500Hz. The closer is placed the wind turbine to the offshore substation (shorter cable length to the collector point, and less impedance), bigger is the frequency of the resonance.
Note that these two "small resonances" have significantly smaller amplitude than the main resonance at (360Hz-380Hz).

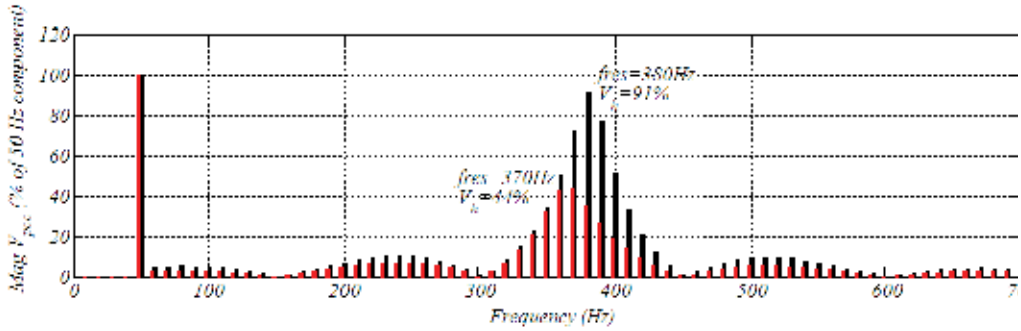

(a)

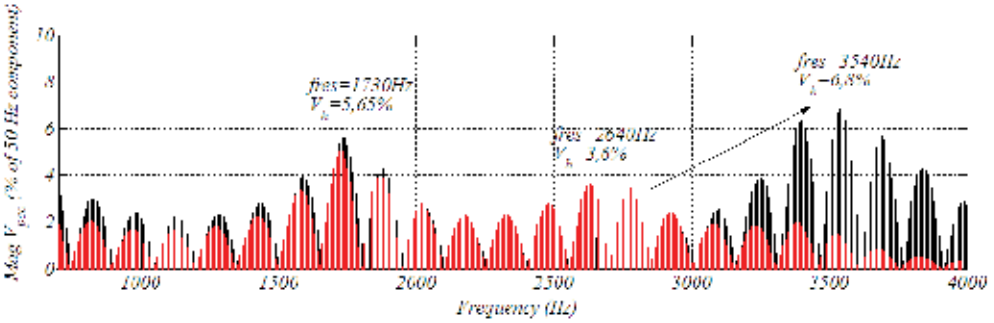

(b)

Fig. 18. Harmonic voltages at the PCC in function of the location of the harmonic voltage source inside the inter turbine grid. For the 25th wind turbine (black) and for the 30th wind turbine (red): (a) more detail in the main resonance and (b) more detail in high frequencies

4.2 Frequency response of the offshore wind farm in function of the feeders in its inter-turbine network

In the first scenario described in section 4, 5 feeders (F1-F5) of 6 wind turbines each one are considered, Fig. 15. However, the internal impedance of the wind farm can have variations with configuration changes, like changes in the number of feeders.

Thus, in this section the frequency response is evaluated for different inter-turbine grid configurations. Inter turbine grids with 2 feeders (F1 and F2) to 5 feeders (F1-F5), Fig. 15 are considered, maintaining the same number of wind turbines for each radial, not the total number of wind turbines of the wind farm.

In this case, the harmonic voltage source is placed at the first wind turbine of each feeder (7, 13, 19 or 25, Fig. 15), because at this point, the second "small resonance" is closer to the fundamental frequency than in any other location of the feeder, Fig. 18 (b). The simulation results (FFT of the current and voltage at the PCC) for the considered configurations are depicted in Fig. 19 and Fig. 20.

From the evaluation of the results of Fig. 19, it is possible to determine that the first and main resonance of the system have not big variations for different configurations of the local inter-turbine grid. However, the second of the "small resonances" (frequency groups less

attenuated) varies with these configuration changes. If there are fewer feeders, the second "small resonance" occurs at higher frequencies.

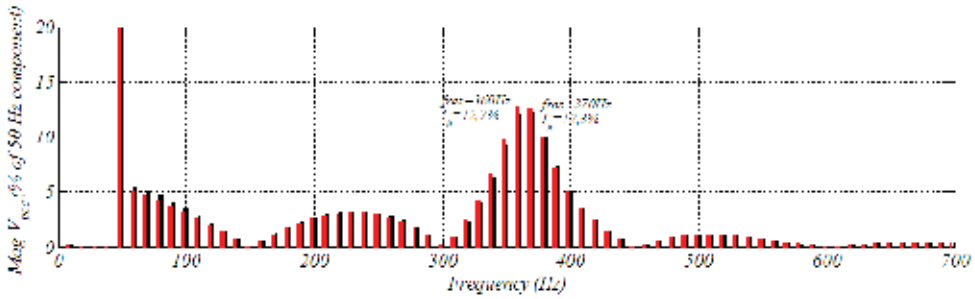

Fig. 19. Harmonic currents at the PCC in function of the number of feeders in the inter-turbine grid: With 2 feeders F1-F2 (black) and with 5 feeders F1-F5 (red)

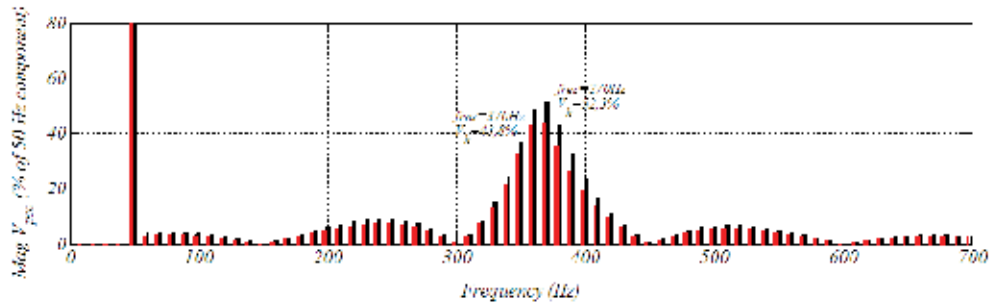

(a)

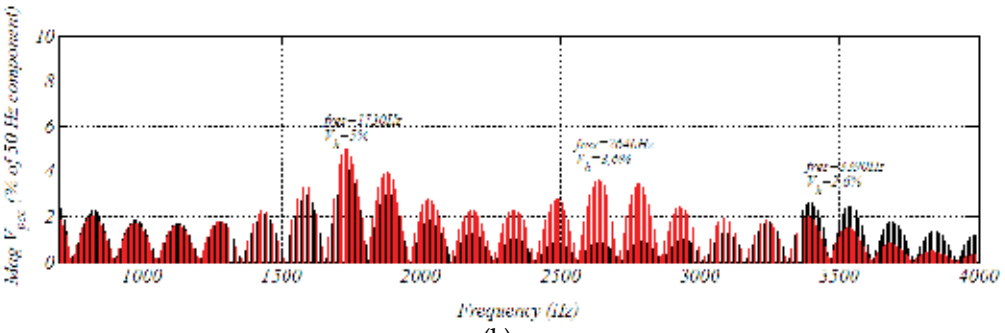

(b)

Fig. 20. Harmonic voltages at the PCC in function of the number of feeders in the inter-turbine grid: With 2 feeders F1-F2 (black) and with 5 feeders F1-F5 (red)

4.3 Frequency response of the offshore wind farm in function of the number of feeders for each step-up transformer's primary

In order to take into account cases where the offshore wind farm have a step-up transformer in the offshore substation with more primary windings than one, the present section

analyzes an inter-turbine network configuration with two primary windings, as depicted in Fig. 21.
The purpose of the analysis is to know how affects this extra primary winding to the frequency response of the offshore wind farm.

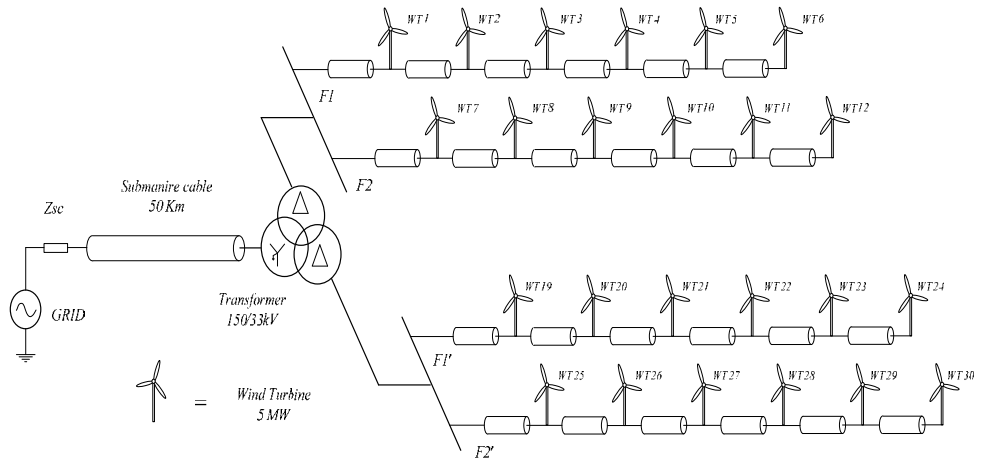

Fig. 21. Simplified scheme of the simulation scenario of the offshore wind farm with two primary windings

To know the influence of the extra winding, the results of the configuration depicted in Fig. 21 and the configuration depicted in Fig. 15 with only two feeders, are compared. The comparison these frequency responses are served Fig. 22 and Fig. 23.

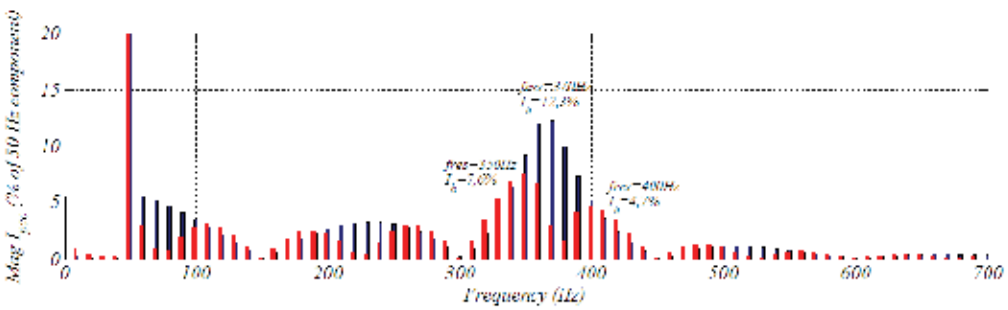

Fig. 22. Harmonic currents at the PCC: With 2 feeders F1-F2 (red) and with 2 feeders on each primary winding F1-F2 and F1'-F2' (black)

Looking at the results in Fig. 22, it is possible to see that the use of two windings connected as delta-star(grounded)-delta, where the secondary windings have delta connection, does not allow to transmit multiples of 3rd order divided by two harmonics (multiples of 150Hz/2, 75 Hz) to the PCC. As a result, the frequency response of the system from the viewpoint of the wind turbine presents less harmonic components.
However, as can be seen in Fig. 23 (b), for the voltage harmonics, there is a new group of frequencies less attenuated at 2520 Hz.

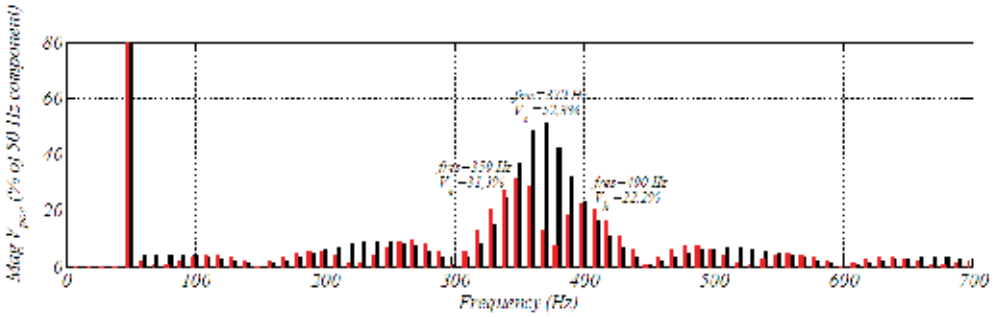

(a)

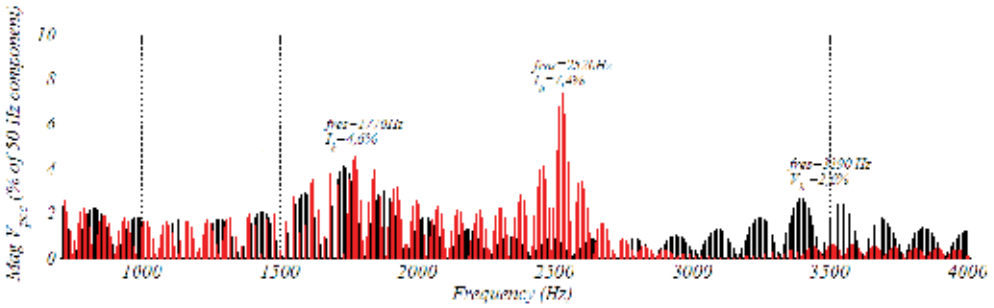

(b)

Fig. 23. Harmonic voltages at the PCC: With 2 feeders F1-F2 (black) and with 2 feeders on each primary winding F1-F2 and F1'-F2' (red)

5. Conclusions

The study presented in this chapter is focused on the evaluation of the frequency response of the offshore wind farm. This frequency response depends on design parameters such as: the cable length and characteristics, transformers connection and leakage inductance or inter-turbine grid's configuration. The analysis carried out estimates the potential risks on the voltage and current harmonic amplifications.

For that purpose, the state equations are a good approximation in order to estimate in an easy way the frequency response and main resonances of the system. The results obtained with this method are very similar to the simulation results in PSCAD.

As regards to the harmonic risk of the AC offshore wind farms, this kind of wind farms have the potential to amplify low order harmonics due to the iteration between the capacitive component of the submarine cable and the leakage inductance of the step-up transformer. The bigger are the impedances of those two elements, lower is the frequency of the resonance. From the results of this study, it is possible to observe, that the resonance frequency is mainly in function of the characteristics of the submarine cable (its capacitive component).

The main resonance of the AC offshore wind farm from the viewpoint of the wind turbines is the same of the transmission systems resonance. The inter turbine grid, does not cause big variations in the frequency response and for different positions in the inter turbine grid, the

frequency response is similar. However, the inter turbine grid causes "small resonances", which varies with the wind turbines position in the inter-turbine grid. This little resonance has less potential to amplify harmonic components, but, grid codes (like IEEE-519 standard) are more restrictive with the high order harmonics.
To avoid as far as possible the harmonic amplification in normal operation due to the resonance of the transmission system, one good option seems to choose a configuration which the resonance frequency of the transmission system coincides with one of the frequencies that the step up transformer does not allow to transmit, Fig. 9.

6. References

ABB, (2005). XLPE cable systems, user's guide, rev 2.

Breuer, W. & Christl, N. (2006). Grid Access Solutions Interconnecting Large Bulk Power On- / Offshore Wind Park Installations to the Power Grid, *GWREF.*

Castellanos, F., Marti, J.R. & Marcano, F. (1997). Phase-domain multiphase transmission line models, *International Journal of Electrical Power & Energy Systems, Elsevier Science Ltd. vol. 19, No. 4, pp. 241-248.*

Gustavsen, B., Irwin, G., Mangelrod, R., Brandt, D. & Kent, K. (1999). Transmission line models for the simulation of interaction phenomena between parallel AC and DC overhead lines, *IPST 99 Procedings, pp. 61-67.*

Hopewell, P.D., Castro-Sayas, F. & Bailey, D.I. (2006). Optimising the Design of Offshore Wind Farm Collection Networks, *Universities Power Engineering Conference, UPEC '06. Proceedings of the 41st International, 2006, pp. 84-88.*

Jiang, Y.L. (2005), mathematical modelling on RLCG transmission lines, *Nonlinear Analysis Modelling and Control*, Vol. 10, Nº 2, 137-149, Xi'an Jiantong University, China.

Khatir, M., Zidi, S., Hadjeri, S. & Fellah, M.K. (2008). of HVDC line models in PSB/SIMULINK based on steady-state and transients considerations, *Acta Electrotechnica et Informatica Vol. 8, No 2.*

Kocewiak, L.H., Bak, C.L. & Hjerrild, J (2010). Harmonic aspects of offshore wind farms, *Proceedings of the Danish PhD Seminar on Detailed Modelling and Validation of Electrical Componentes and Systems*, Aalborg.

Marcano, F. (1996). Modeling of transmission lines using idempotent decomposition, *M. Sc. Thesis, Department of Electrical Engineering, The University of British Columbia, Vancouver, Canada.*

Meier, S. (2009). System Aspects and Modulation Strategies of an HVDC-based Converter System for Wind Farms, *Ph. D. thesis, KTH Stockholm, ISBN 978–91–7415–292–0.*

Nian, L (2009). *Transients in the collector Grid of a novel Wind Farm topology*, Msc Thesis KTH, Stockholm.

Pigazo, A. (2004). *Método de control de filtros activos de potencia paralelo tolerante a perturbaciones de la tensión de red*, thesis, universidad de Cantabria.

Plotkin, J., Schaefer, U. & Hanitsch, R.E. (2008). Resonance in the AC Connected Offshore Wind Farms, *WECS.*

PSCAD, (2003). User's guide.

Restrepo, L.H., Caicedo, G. & Castro-Aranda, F (2008). Modelos de línea de transmisión para transitorios electromagnéticos en sistemas de potencia, *Revista Energía y computación Vol 16 No 1 p.21-32.*

Sánchez, M.C.M. (2003). *Medida de párametros de ruido de dispositivos activos, basadoa en fuente adaptada*, Thesis, UPC.

Weedy, B.M. & Cory, B.J. (1998). *Electric power systems*, (4th ed.) Wiley, ISBN 0-471-97677-6, Great Britain.

Part 2

Alternatives to Mitigate Problems of the Wind Power Integration

5

FACTS: Its Role in the Connection of Wind Power to Power Networks

C. Angeles-Camacho[1] and F. Bañuelos-Ruedas[2]
[1]*Universidad Nacional Autónoma de México, UNAM*
[2]*Universidad Autónoma de Zacatecas, UAZ, Zacatecas*
México

1. Introduction

Environmental and political worries for a sustainable development have encouraged the growth of electrical generation from renewable energies. Wind power generation of electricity is seen as one of the most practical options and with better relation cost-benefit inside the energetic matrix nowadays (Angeles-Camacho & Bañuelos-Ruedas, 2011). Nevertheless, given that some renewable resources like the speed of wind or the solar radiation are variable, so is generated electricity. Without an adequate compensation, the voltage in the point of connection and the neighboring nodes will fluctuate in function to variations of the renewable primary power resource used. This phenomenon can affect the stability of the system and compromise quality of the energy of the neighboring loads (Gallardo, 2009). Nowadays, the generation with renewable resources integrated to electrical systems covers a small part of the total demand of power. The major generation comes from other sources such as the hydraulics, nuclear and fossil fuels. If the wind penetration system is small, the synchronous conventional generation will determine dynamic behaviour of the system, for example nodal voltages are maintained inside its limits of operation for this centralized generation (Ackerman, 2005). Nevertheless, with the increase in capacity and the number of power plants that use renewable resources added to the electrical systems, these will replace power from conventional sources, in such a way that the contribution of these cannot be ignored and the control of the nodal voltages will not be possible using the traditional methods.

The modelling of the dynamic interaction between the wind farms and the electrical systems can provide valuable information. The analysis of dynamic power flows allows the study in the time domain frame of reference with steady-state models and dynamic models. The simulation of the power network will allow analyzing the effects of the plants proposed depending on the time. The evaluation of the parameters of the network in the time will make it possible to see the complete range of his parameters with any injection of active power of the wind power station. Because of the need to deliver low energy parameters regulated by country, in recent years power electronics devices (FACTS) have been developed, which allow interconnection of different energy sources, including those of random behaviour such as wind turbines, on the same network supply (Angeles-Camacho, 2005).

2. Why power electronics?

Power electronics deals with the processing of electrical energy. Power electronics is an enabling technology, providing the need for interface between the electrical source and the electrical load. The electrical source and the electrical load can, and often do, differ in frequency, voltage amplitudes and the number of phases. Power electronics involves the interaction of three elements: copper, which conducts electric current; iron, which conducts magnetic flux; and, in prime position, silicon (Mohan et al., 2003).
The field is one of growing importance: it is estimated that over half the electrical energy generated is processed by power electronics before its final consumption, a proportion that is likely to reach 90% during the next decades.

2.1 Benefits

- To convert electrical energy from one form to another, facilitating its regulation and control
- To achieve high conversion efficiency and therefore low loss
- To minimize the mass of power converters and the equipment (such as motors) that they drive.
- Intelligent use of power electronics will allow consumption of electricity to be reduced

Two kinds of emerging power electronics applications in power systems are already well defined:

a. Bulk active and reactive power control
b. Power quality improvement (Angeles-Camacho, 2005)

The first application area is known as FACTS, where the latest power electronic devices and methods are used to electronically control high-voltage side of the network (Anderson & Fouad, 1994). The second application area is custom power, which focuses on low voltage distribution and is a technology created in response to reports of poor power quality and reliability of supply, affecting factories, offices and homes. It is expected that when widespread deployment of the power electronics technology takes place, the end-user will see tighter voltage regulation, minimum power interruptions, low harmonic voltages, and acceptance of rapidly fluctuating and other non-linear loads in the vicinity (Conseil International des Grands Réseaux Électriques [CIGRE], 2000).
Power electronics is a ubiquitous technology which has affected every aspect of electrical power networks, not just transmission but also generation, distribution and utilization. Deregulated markets are imposing further demands on generating plants, increasing their wear and tear and the likelihood of generator instabilities of various kinds. To help to alleviate such problems, power electronic controllers have been developed to enable generators to operate more reliably in the new market place.
Power electronics circuits using conventional thyristors have been widely used in power transmission applications since the early seventies (IEEE Power Engineering Society [IEEE-PES], 1196). More recently, fast acting series compensators using thyristors have been used to vary the electrical length of key transmission lines, with almost no delay, instead of classical series capacitors, which are mechanically controlled.

This work was supported in part by DGAPA-UNAM under project IN111510
C. Angeles-Camacho and F. Bañuelos-Ruedas are with the Instituto de Ingeniería, Universidad Nacional Autónoma de México, México, D. F. 04512

3. Flexible alternating-current transmission systems

Power electronics form the basics of one devices family called FACTS, which offers a faster response times and lower maintenance costs compared to conventional electromechanical technology (Hingorani & Gyugyi, 2000). The FACTS concept is based on the incorporation of power electronic devices and methods into the high-voltage side of the network, to make it electronically controllable. FACTS controllers build on many advances achieved in high-current, high-power semiconductor device technology, control and signals conditioning (Acha et al., 2004). The power networks have limits that define the maximum electrical power that can be transmitted. Angular stability, voltage magnitude, thermal limits, transient stability, and dynamic stability are some of these limits (Song & Johns, 1999), and any violations of these limits can cause damage to transmission lines and/or electric equipment. These limits have been relieved traditionally by the addition of new transmission and generations facilities, but FACTS controllers can enable the same objective to be met without major changes to the system layout. Figure 1 illustrates the active power compensation achieved by different kinds of FACTS devices.

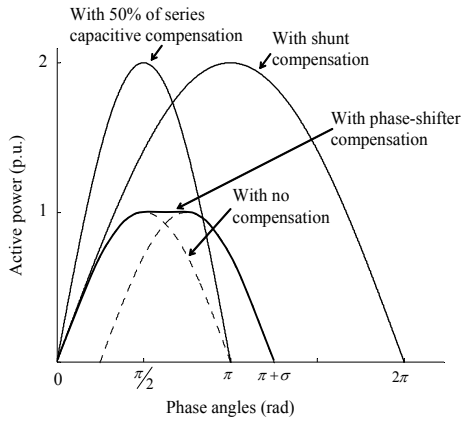

Fig. 1. Active power transmission characteristic for different types of compensation

The new reality of making the power network electronically controllable, has began to alter the thinking and procedures that go into the planning and operation of transmission and distribution networks in the world.

From the operational point of view FACTS introduces additional degrees of freedom to control power flow over desired transmission routes, enabling secure loadings of transmission lines up to their thermal capacities. They also provide a more effective utilization of available generation and prevent outages from spreading to wider areas. A three-bus network is employed to illustrate the use of FACTS to active power flow control.

The new reality of making the power network electronically controllable, has began to alter the thinking and procedures that go into the planning and operation of transmission and distribution networks in many parts of the world. The potential benefits brought about by FACTS controllers include reduction of operation and transmission investment cost, increased system security and reliability, increase power transfer capabilities, an over enhancement of the quality of the electric energy delivered to customers, and environmental benefits gained by increased asset utilization, Figure 2 shows active and reactive compensation achieved by different kinds of FACTS controllers (CIGRE, 2000).

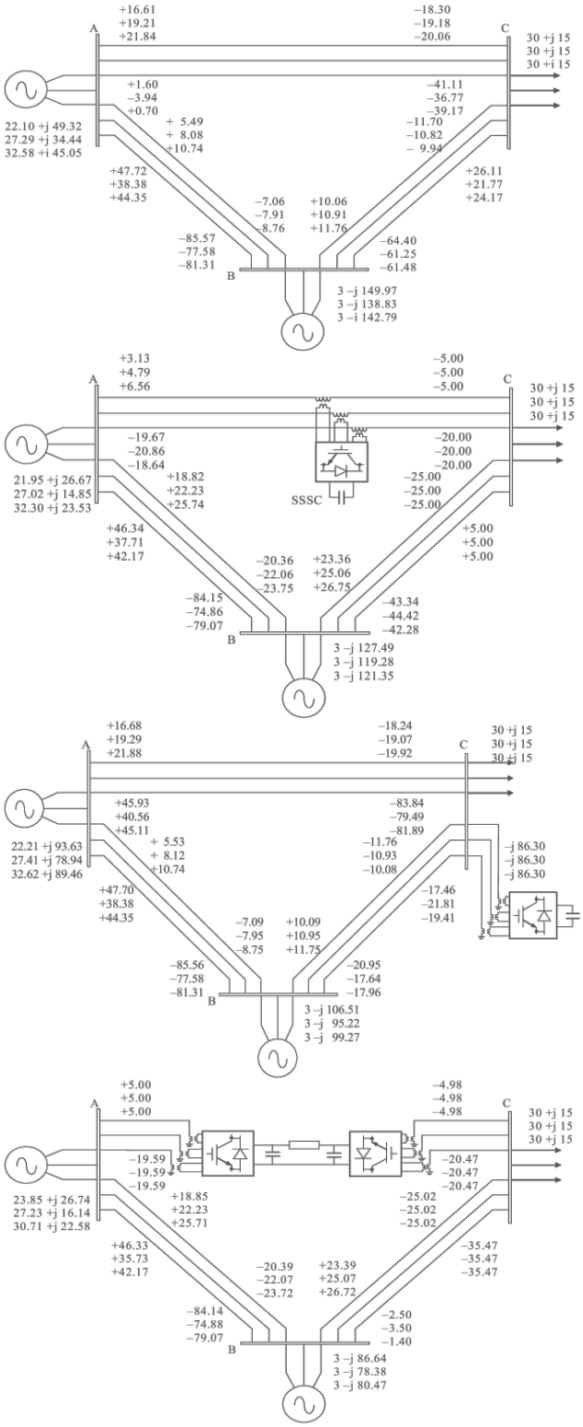

Fig. 2. Active and reactive power flows for different kind of power control: a) without compensation, b) phase shift control, c)shunt compensation, d) DC link.

Since FACTS devices are able to respond quickly to voltage fluctuations and provide dynamic reactive power compensation, there is mounting evidence that they would be very successful when considering the effects of a varying source of energy, such as wind generation, on a network.

4. Wind generation

An interconnected power system is a complex enterprise that may be subdivided into four main components: generation, transmission, distribution and utilization. The source of the mechanical power, commonly known as the prime mover, may be hydraulic turbines, steam turbines whose energy comes from the burning of coal, gas and nuclear fuel, gas turbines, or occasionally internal combustion engines burning oil.

Interest in renewable energy started in earnest in the early 1980s following the oil crises of the 1970s, when issues of security and diversity of energy supply and, to a lesser extent, long-term sustainability became apparent. Wind power generation became one of the most cost-effective and now is commercially competitive with new coal and gas power plants.

The wind resource is often best in remote locations, making it difficult to connect wind farms to the high-voltage transmission systems. Instead, connection is often made to the distribution system. The inclusion of a fluctuating power source like wind energy distributed throughout an electrical grid affects the control of the grid and the delivery of the stable power. The introduction of large amounts of wind power into the grid increases the short-term variability of the load as seen by the traditional generator, thus increasing the need for spinning reserve. It also changes the long-term means load as winds change, disrupting the planning for bringing generation on lines (Song & Johns, 1999).

Wind power grid penetration is defined as the ratio of the installed power to the maximum grid-connected load. Presently, Denmark has the highest grid penetration of wind at 19%. It has been suggested that with additional technology, 50% grid penetration will be feasible. For instance, in the morning hours of 8 November 2009, wind energy produced covered more than half the electricity demand in Spain, setting a new record, and without problems for the network (Manwell et al, 2002).

Induction generators are often used in wind turbines applications, since they are robust, reliable and efficient. They are also cost-effective due to the fact that they can be mass-produced. In the case of large wind turbines or weak grids, compensation capacitors are often added to generate the induction generator magnetizing current. Furthermore, extra compensation (such as a power electronic system) is added to compensate for the demand of the induction generator for reactive power. Some typical configurations of wind turbines connections are shown in Figure 3.

5. Grid integration technical problems

There exist a number of barriers which slow down the wind power exploitation. As the interconnection of wind power involves a number of technical problems different challenges need to be addressed. The assessment of the technical impacts of an installation must be accomplished, including,

- Transient Stability
- Voltage Control
- Frequency control

- Short Circuit Currents
- Power Quality Issues

The impact and consequently the level of penetration for power system network is an important issue. Methodologies and tools to overcome the technical problems need to be addressing the issue for increasing the wind power connection large–scale power system (Diaz-Guerra, 2007).

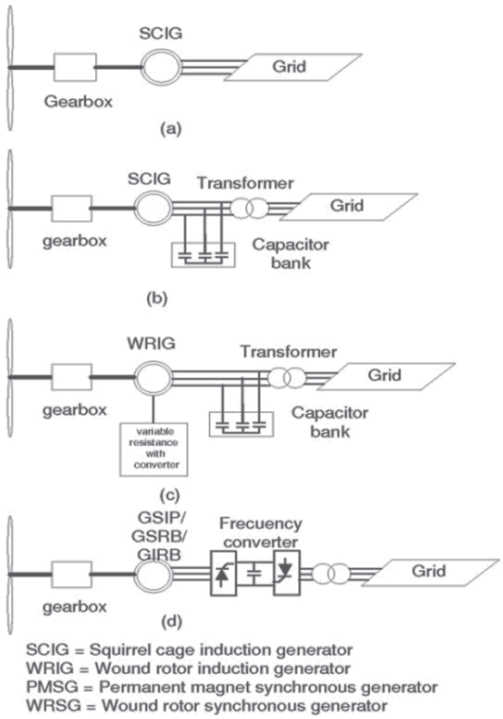

Fig. 3. Typical wind turbines connections.

Transient Stability, traditional generators attempt to follow the fluctuating load in order to minimize voltage and frequency fluctuations. During fault (voltage depression) generators accelerates due to the imbalance between mechanical and electrical powers. When the fault is cleared they absorb reactive power depressing the network voltage, if not enough reactive power is supplied a voltage collapse is eminent. Synchronous generator exciters increase reactive power output during low voltages and thus support voltage recovery, In contrast induction generators tend to impede voltage recovery. If the penetration of wind generation is high and they disconnect at small voltage reductions it can lead to a large generation deficit, to prevent this wind parks are required to have adequate compensation (Fault Ride Through Capability).

Voltage Control, Nodal voltages in power systems are normally allowed to fluctuate from ±5% to up to ±7%. Synchronous generator and other compensator devices regulate nodal voltage by supplying or absorbing reactive power. In contrast induction generators absorb reactive power and have no direct control over reactive power flows. Even variable-speed wind turbines may not be able to control the voltage at the point of connection, because the wind farm network is predominantly capacitive.

Frequency control, Frequency in large electric grids is maintained at ±0.1% of the desired value, in order to have frequency control, generator power must increase or decrease. Wind generators respond to frequency changes by adjusting either, in fixed-speed the pitch angle or in variable-speed by operating it away from the maximum power extraction curve. In any case, thus leaving a margin for frequency control in wind generation.
Short-Circuits Currents, The induction wind generators, contribute to the short-circuit current only in the instant of appearance of the fault. In contrast, during voltage depression a large short-current is needed, synchronous generators contribute "many times" their nominal current. With high penetration levels the risk of disconnections by voltage depression will increase.
Power Quality Issues, voltage harmonic distortion and flicker are the principal quality effects of wind power generation. The injection of harmonics into the power system is the main drawback associated with variable speed turbines because these contain power electronics. Voltages fluctuations (flicker) are produced by the variability of the power generated in fixed-speed wind turbines.

6. Wind farm model

One of the tools most used in the electric systems planning and design is the analysis of power flows; a variant of this tool is the analysis of Dynamic Power Flows. Investors and companies execute the necessary preliminary studies.
The analysis will allow us to evaluate the effects of the plant proposed over the network to be incorporate. However, models to perform the power flow analysis and understand the dynamic interaction between the wind farms and the electric systems must be developed.
A basic model of a wind farm consists of four parts, the simulator of wind speed, the wind turbine with the gear box, the generator with its individual (optional) compensation and the electrical network to which it will be interconnected (Diaz-Guerra, 2007). In the case of not having compensation it will deliver the active power and will take of the network the reactive power, (Figure 3a), where there appears a wind generator of induction connected directly to the electrical.
The present work makes use of a wind farm model based on several wind generators as the scheme presented in the Figure 4, where an induction generator is connected to the network and compensation is supplied in order to supply the requirements of the generator´s reactive power. The bank of capacitor provides an affixed amount of reactive power locally, so that it does not have to be imported from other parts of the grid. It is assumed that the site being considered for a wind farm is comprised of 12 wind turbines rated 2500 kW each.
The goal of the model is to calculate the active power provided by the wind generator, given the measured values of wind speed and his direction (Feijoo & Cidras, 2001), as well as the reactive power, which depend on the active power and the voltage of connection. The active power produced by a turbine can be expressed by the following equation:

$$P = 1/2 \rho A v^3 C_p \quad (1)$$

where P is the real power in Watts, ρ is air density in kg/m^3, A is the rotor area in m^2, and C_p is the power coefficient.

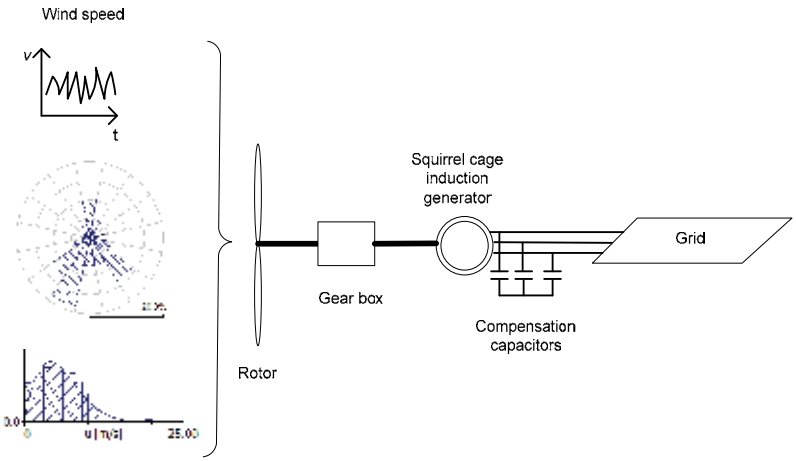

Fig. 4. Grid coupled wind generator.

6.1 Active power

To show the relation between the active power produced and the wind speed, one month of 28 days (February 2008) real data for a specific site in the Mexican state of Zacatecas is used for the wind model; data points for speed are at 10 minutes interval (4,032 points). The data points are connected to get a wind speed curve, seen in the upper plot of Figure 5. The real power produced by each wind turbine is calculated using equation 1. The contributions of the twelve individual turbines are summed at each 10 minute intervals to derive the total real power curve for the wind farm. Figure 5 shows the wind speed (top) and the real power (bottom) produced by a wind farm.

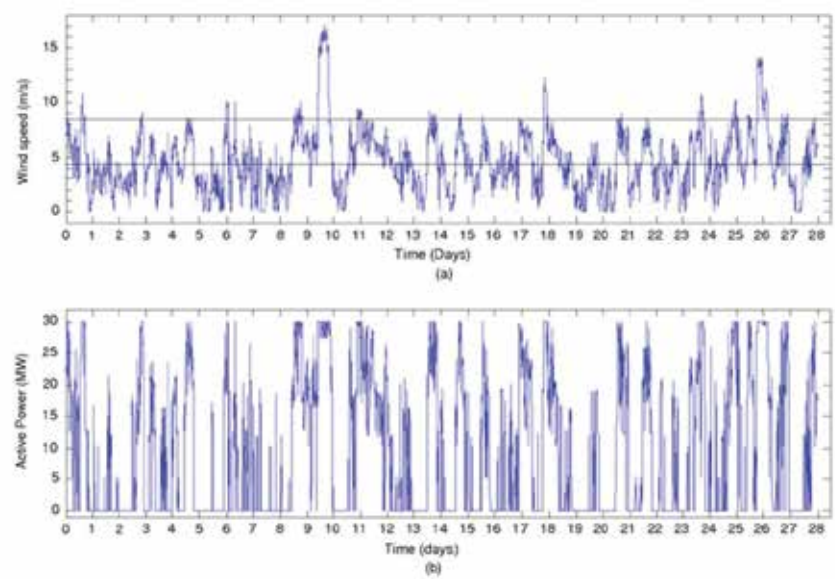

Fig. 5. Wind speed (a) and the real power produced (b) by a wind farm.

The cut-in speed is a conventional one of 4.5 m/s, it cab observed as producing no real power below it. Rated wind speed is 8.5 m/s, when it is surpassed; the active power curve flattens out at 30 MW. The cut-out wind speed of 24 m/s is not reached in this time period.

6.2 Reactive power

Reactive power can be calculated using the steady-state model of the induction machine and applying the Boucherot´s theorem (Feijoo & Cidras, 2001),

$$Q = \frac{V^2\left(X_c - X_m\right)}{X_c X_m} + \frac{X\left(V^2 - 2RP\right) - X\left[\left(V^2 - 2RP\right)^2 - 4P^2\left(R^2 + X^2\right)\right]^{\frac{1}{2}}}{2R^2 + 2X^2} \tag{2}$$

where V is the voltage, P is the real power, X is the sum of the stator and rotor reactances, X_c is the reactance of the capacitor bank, X_m is the magnetizing reactance, and R is the sum of the stator an rotor resistances. Both active and reactive powers are knows and the generator can be modeled as a PQ bus for power flow analyses and dynamic power flow analysis. The generator requires proportionally more reactive power at higher real power outputs. Figure 6 shows the relationship between active power production and reactive power absorption (top) and the respective reactive power absorption for the PQ model. The wind farm is modeled as being situated in Zacatecas, México. Wind speed actual data for the month of February 2008 is used.

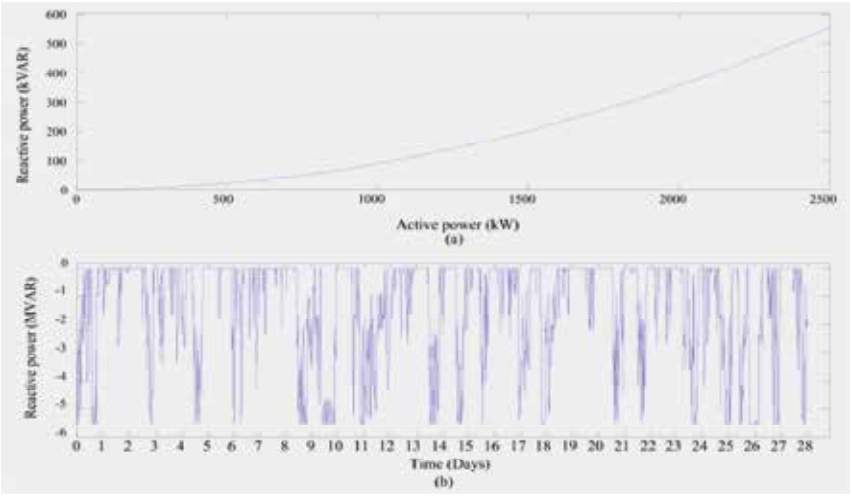

Fig. 6. Relationship between active and reactive power (a) and reactive power generated in function of wind speed and nodal voltage (b).

7. Wind integration study case: FACTS role

Digital software for analysis and control of large-scale power networks under both balanced or unbalanced conditions was developed. The software was written in Visual C++ with the philosophy "Object Oriented Programming (OOP)". The three-phase OOP power flow program has been applied to the analysis of a large number of multi phase power networks, of

different sizes and complexity. Power flow solutions converge in five iterations or less to a tolerance of $1e^{-12}$, starting from a flat voltage profile. The accuracies of the solution have been tested again with commercial software and single-phase program (Angeles – Camacho, 2005).

7.1 Power flow case study

A small traditional network (Acha et al, 2005) shown in Figure 7 is used as the basis for illustrating how the PQ wind farm model works for two kinds of power analysis tools, firstly a power flow analysis is performed and secondly a dynamic power flow analysis is carried out. This is a five-bus network containing two generator, four loads and seven transmission lines. Figure 7, shows the test network used in the study with two particular solutions, (a) with zero wind power and (b) with maximum wind power (30 MW) which represents 15% of wind penetration. The Newton-Raphson power flow program takes a maximum of six iterations to reach convergence at each of the 4,032 data points.

Nodal voltages	Wind power	Nodes at network					
		North	South	Lake	Main	Elm	Wind
Magnitude (p.u.)	Without	1.06	1.0	0.987	0.984	0.972	0.979
	Maximum	1.06	1.0	0.989	0.986	0.973	0.982
Phase Angle (degrees)	Whitout	0	-2.06	-4.64	-4.96	-5.77	-5.39
	Maximum	0	-1.25	-3.42	-3.51	-3.97	-2.60

Table 1. Voltage of five-node network for zero and maximum wind power generation

It can be observed from the results presented in Figure 7 and Table 1 that all nodal voltages are within accepted voltage magnitude limits, i.e. 100 ± 6% in the UK in both cases, minimum and maximum wind power injections. At minimum wind power the largest power flow takes place in the transmission line connecting the two generator buses: 89.3 MW leave North. This is also the transmission line that incurs higher active power loss, i.e. 2.5 MW. The active power system loss is 6.12 MW per phase, this represents the 3.57 % of the active power generation. In maximum wind power injection the line is unloaded to 66.5 MW in general must lines are unloaded and losses are reduced to 4.66 MW. However, lines connecting Main-Wind changes the flow direction of power to wind-main. The new transmission line Main-Wind will reverse the active power flowing from Main towards Wind originally at 6.60 MW to a new flow towards Main at 10 .72 MW. Whereas the transmission line connecting Wind to Elm increases the active power flow from 6.58 MW to 19.28 MW, it means an increase of almost two hundred percent.

7.2 Dynamic power flows

A general dynamic power flow algorithm using an implicit trapezoidal integration method with Newton-Raphson iterative method has been developed and used (Burden & Fires, 2000). The algorithm takes advantage of the power flow used in the previous section. Ordinary differential equations describing the active power plant components and the algebraic equations corresponding to the active and reactive nodal power injections are now solved, simultaneously. There are 4,032 data points, for each data the software take five iterations to reach converge.

As expected, the nodal voltage magnitudes of all of the loads buses are affected by the variability condition of the primary source of power, the wind. They have high fluctuations.

Only bus slack (North) and PV bus (South) are not affected. They remain constant at 1.06 and 1.0 pu. The wind farm was modeled with a source of reactive power that is equal to 70% of the reactive power consumed by the generator at nominal voltage and its correspond active power produced by the wind speed data. Figure 8 shows the impact of the wind power produced in the voltage magnitude profile of nodal voltages of five-node network.

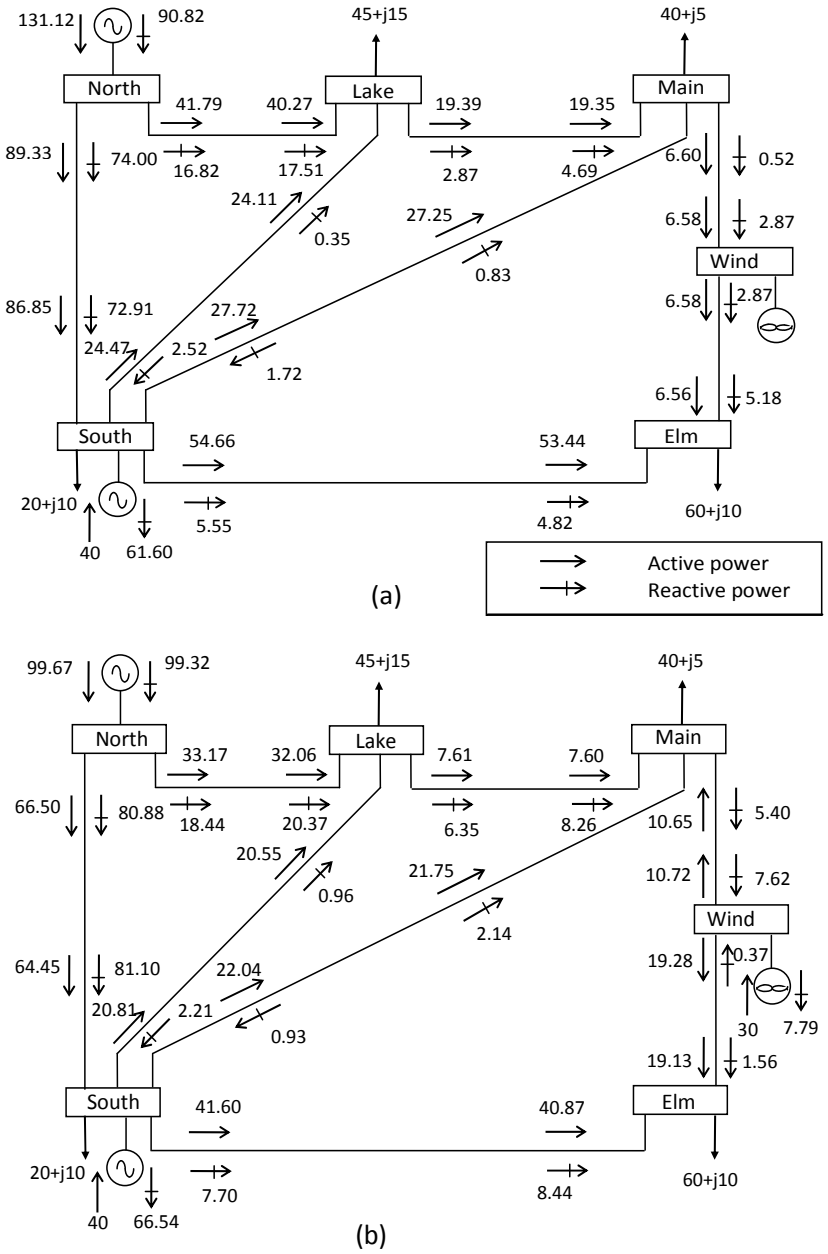

Fig. 7. Five-bus test network, (a) with zero, and (b) within maximum wind generation.

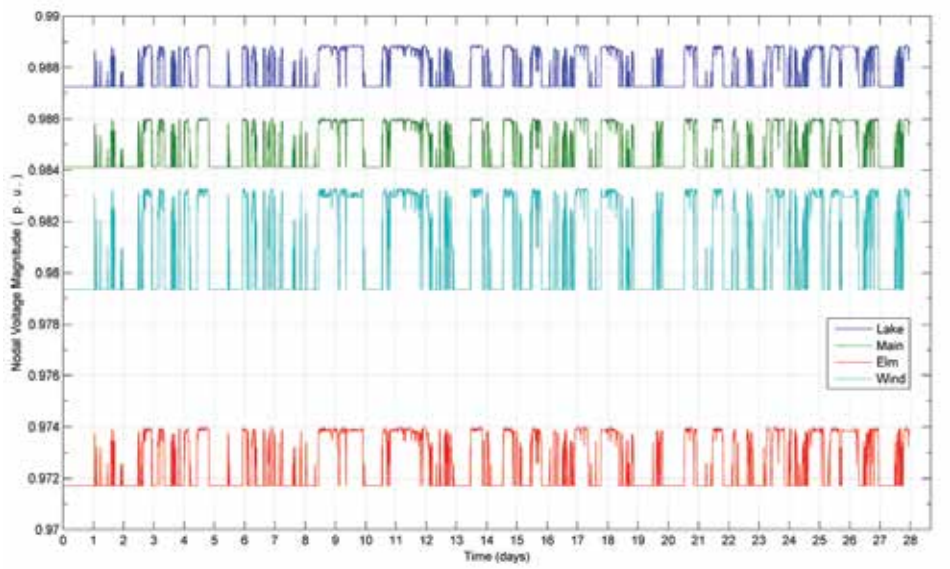

Fig. 8. Nodal voltages profile of five-node network with wind power generation.

Due to the high fluctuations of active and reactive power injection, transmission lines are under stress for short times. On the other hand transmission lines are now unloaded due to the fact that now active power is supplied locally rather than transmitted long distances. Figure 9 shows the transmission line active power flows. It is noticed that apart from flow reduction and flow fluctuation which do not seem to be significant, the transmission line connecting Main to Wind is under several reverse active power flows in short times, in power systems it is not a problem at all, however, at distribution levels, transmission lines trip can arise.

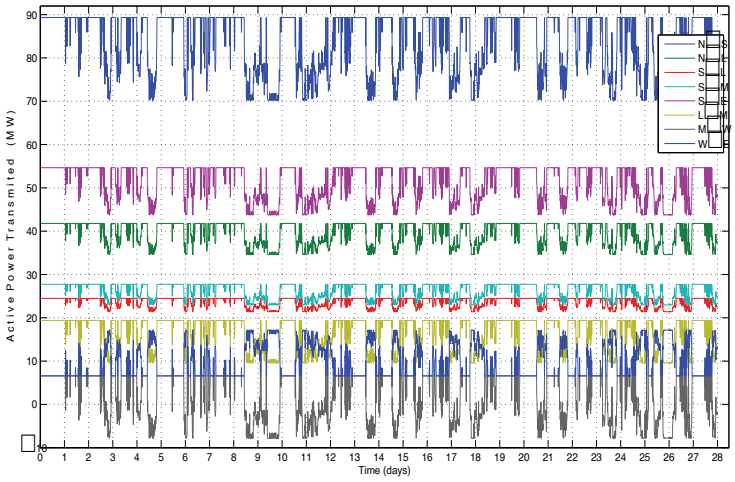

Fig. 9. Active power transmited over transmision lines.

8. Incorporation of FACTS into the dynamic power flow

As can be seen in the previous figures, power generation using wind resources creates voltages fluctuations in the networks due to the varying injection of real power and varying absorption of reactive power, exposing the network to voltage deviations. Dynamic reactive power compensation with FACTS controllers can potentially stabilize the voltage fluctuations associated with the wind farms and provide seamless grid interconnection. Also, the sensibility of the wind turbines to voltage trips can be improved. Dynamic reactive power compensation locally can allow the wind farm to remain operational during faulty conditions, this would avoid power unbalances or even systems collapse. FACTS technology offers an attractive option when considering the effects of a varying source of energy, such as wind and solar generation.

The static compensator (STATCOM) is a power system controller VSC based suitable to provide dynamic compensation to transmission system. Its speed of response enables increased transient stability margins, voltage support enhancements, and damping of low frequency oscillation. The voltage generated by the STATCOM is adjusted with little delay by virtue of semiconductor valves switching. The STATCOM can be seen as a ideal voltage regulator for long-term dynamic power flows. In other words magnitude voltage at the point connection is maintained at the set value in the face of voltage variations.

The five-bus network used is modified to include the STATCOM model (Angeles-Camacho & Barrios-Martinez, 2009). Using the software developed, a power flow analysis was carried out for the 4,032 data points. It is used to control voltage magnitude at Lake at one per unit. The objective of this simulation is to assess the capability of the controller to keep a constant voltage magnitude at the connecting bus. The power flow results indicate that the STATCOM generates 20.45 MVAR, in order to achieve the voltage magnitude target at minimums wind power injection. Nodal voltages profiles of five-node network with wind power generation and within the STATCOM embed are shown in Figure 9.

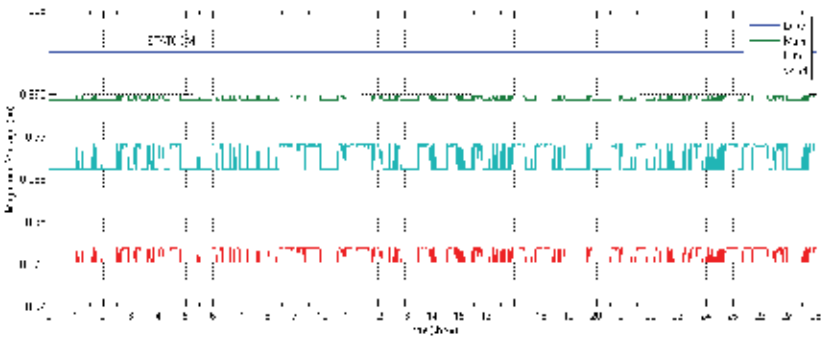

Fig. 10. Nodal voltages profiles of five-node network with wind power generation and within the STATCOM embed.

Analyses of Figure 9 show that significant changes occur in nodal voltage magnitudes when the STATCOM is present in the network compared with the case study where no STATCOM is included. For one the voltage magnitude in the STATCOM bus boosted by the STATCOM is maintained at its set value of one per unit. Keeping the voltage magnitude at the STATCOM bus at one per unit also flatted the remains nodal voltages.

8.1 Dynamic power flow case of study FACTS embedded

The dynamic power flow enables the study of different kinds of disturbances, which may occur at any point in time during simulation time. Among these are load increments/decrements, switching in and out of transmission lines, short-circuits faults, and loss of generation.

The five-bus network was used for testing the dynamic power flow algorithm. For the purpose of this test case, both generators were selected to be steam power plants. Gains and time constants were adjusted to maximize dynamic effects. Generating plants were assumed to be equipped with AVR, governor and a three-stage steam turbine. The dynamic response of the network was assessed by simulating major disturbance events and less severe events causing only voltage step changes of different magnitudes.

Using the software developed, a dynamic power flow analysis was carried out. This case study is a sudden reduction of three-phase power system load followed by a restoration to its normal level. The per phase load connected to bus Elm is disconnected and restored minutes later. It becomes apparent that any step load perturbations in power network loads have an effect on the outputs of all generating plants in the interconnected system. Power generation is altered by the regulatory action of the speed governor and turbine; hence, frequency and nodal voltages are deviated from schedule values. The remaining variables at each generator are also altered.

The objective of this simulation is to assess the capability of the controller to improve transient stability and avoid the wind generation being disconnected by voltage, frequency or load angle reduction after disturbs in the power network. If wind generation is disconnected can lead a large generation deficit. Figures 10 and 11 show the response of the generating plants to a step load disturbance for both cases (a) without compensation and (b) compensated.

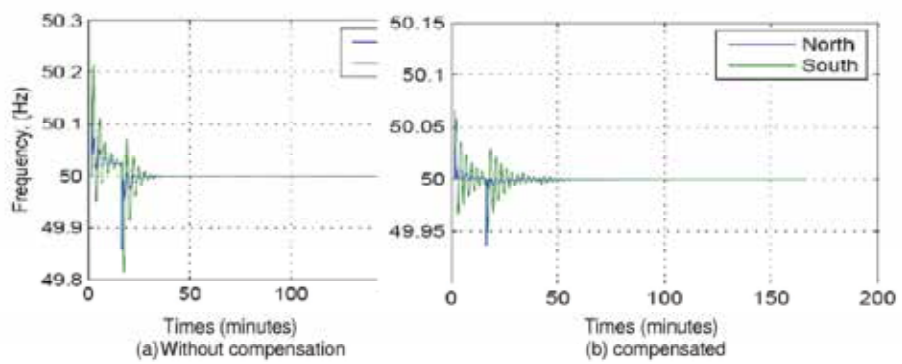

Fig. 11. Frequency generating plant response of the system; (a) without and (b) with STATCOM.

9. Conclusions

Today there is an increasing demand for planning the connection of renewable generation in details seen from the perspective of the electricity grid.

A large-scale penetration of renewable requires improvements in the infrastructure of the transmission network, both within a national electrical system and in the interconnections

between countries, to balance variable power output and demand across regions and to transmit the renewable energy generated by non-conventional Renewable energies (NCRE) power stations.

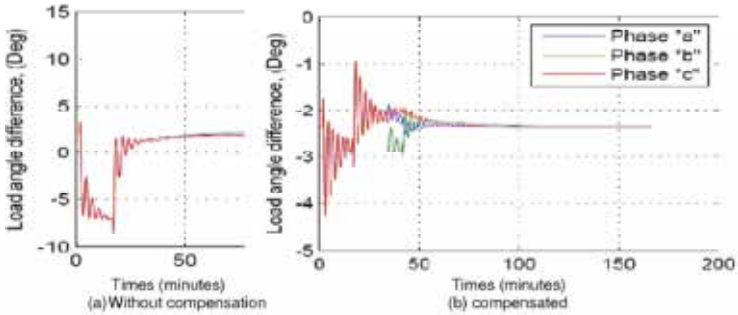

Fig. 12. Load angle generating plant response of the system; (a) without and (b) with STATCOM.

These are typical questions that have to be considered by the system operator before commissioning a power plant using renewable energies. Is there a risk of low voltage gradients due to changes of the renewable resource?; How would a black out of a wind farm affect the stability of the grid?; Can the wind farm run through a 3-phase-fault on the grid?. Load flow analyses and dynamic studies have to be made in advance to analyze how the decentralized power production from renewable energies would affect the load flow conditions in the grids. This chapter focuses on using a wind farm model suitable for incorporation in both power flow analysis and dynamic power flow analysis. The chapter presents a set of case studies to illustrate the benefits that FACTS technologies bring to facilitate the connection of wind power to power systems.

10. Acknowledgment

Dr. Angeles-Camacho wishes to convey his gratitude for the support provided by DGAPA-UNAM under the project IN11510-2. Dr. Bañuelos-Ruedas wishes to express his gratitude to ''Programa de Mejoramiento del Profesorado (PROMEP)'' and to the UAZ for their support while this work was being compiled.

11. References

Acha, E., Fuerte-Esquivel, C.R., Ambriz-Perez, H., & Angeles-Camacho, C. (2004). *FACTS: Modeling and Simulation in Power Networks*, John Wiley & Sons, ISBN: 978-0-470-85271-2, Chichester, UK.

Ackerman T. (Ed.). (2005). *Wind Power in Power Systems,* John Wiley and Sons, 0-470-85508-8, Chicester, UK.

Anderson, P. M. & Fouad, A. A. (1994). *Power System Stability and Control* (Revised Printing), The Institute of Electrical and Electronics Engineers Press, Inc. ISBN: 0-471-23862-7, New York, USA.

Angeles-Camacho, C. & Bañuelos-Ruedas, F. (2011), Incorporation of a Wind Generator Model into a Dynamic Power Flow Analysis, (in Spanish), *Ingeniería. Investigación y*

tecnología. Revista de la Facultad de Ingeniería de la Universidad Nacional Autónoma de México. ISSN 1405-7743.

Angeles-Camacho, C. & Barrios-Martinez, E. (2009). Dynamic Phase-domain Modelling and Simulation of STATCOM in Large-scale Power Systems, Proceedings of IEEE Bucharest PowerTech, Bucharest, Rumania, Julio 2009.

Angeles-Camacho, C. (2005). *Phase domain modeling and simulation of large-scale power systems with VSC-based FACTS equipment*". A thesis submitted to the Dep. of Elec. & Elec. Eng. of the University of Glasgow for the degree of Doctor of Philosophy, Glasgow, Uk.

CIGRE, (2000). FACTS Technology for open access, JWG 14/37/38/39-24. Final draft report, Augost 2000.

Diaz-Guerra B. (2007). Integración de la generación eólica en el sistema eléctrico español Experiencia del Operador del Sistema, (in Spanish). Seminario Internacional Santiago, Chile, October 2007

Feijoo A.E, & Cidras J. (2001). Modeling of wind farms in the load flow analysis, *IEEE Trans. on Power Systems*,Vol. 15, No. 1, Feb. 2001, pp. 110-115. ISSN: 0885-8950.

Gallardo Q.F. (2009). *Estabilidad y Amortiguamiento de Oscilaciones en Sistemas Eléctricos con Alta Penetración Eólica*, (in Spanish). Tesis Doctoral, Departamento de Ingeniería Eléctrica, Electrónica y Automática, Universidad Carlos III de Madrid. 2009.

Hingorani, N.G. & Gyugyi, L. (2000). *Understanding FACTS: Concepts and Technology of Flexible AC Transmission Systems*, The Institute of Electrical and Electronics Engineers Press, Inc. ISBN: 0-7803-3455-8, New York, USA.

IEEE Power Engineering Society (1996). FACTS Applications, IEEE *Service Center*, Special Issue, 96TP116-0, Piscataway, N.J., USA.

Manwell, J. F., McGowan, J.G. & Rogers, A.L. (2002). *Wind Energy Explained,* John Wiley & Sons, ISBN 0-471-49972-2, Chichester, UK.

Mohan, N., Undeland, T. M. & Robbins, W. P. (2003). *Power Electronics: Converter Applications and Design*, (3rd Edition), John Wiley & Sons, ISBN 0-471-22693-9, USA.

Song, Y.H. & Johns, A.T. (Eds.) (1999). *Flexible AC Transmission Systems (FACTS)*", Institution of Electrical Engineers, 0-85296-771-3, London, UK.

6

Optimal Management of Wind Intermittency in Constrained Electrical Network

Phuc Diem Nguyen Ngoc[1], Thi Thu Ha Pham[2],
Seddik Bacha[1] and Daniel Roye[1]
[1]*Grenoble Electrical Engineering Laboratory (G2ELAB), Saint Martin d'Hères*
[2]*Projects & Engineering Center (PEC) - Schneider Electric*
France

1. Introduction

Wind electricity has known a spectacular increase since 1990, essentially due to governments' voluntarist policy. At present, this renewable energy is considered as the best economic profitability.

The success is accompanied by difficulties in short and medium terms and deep questionings in long term. Thus, coupling problem between wind generator and network perturbation, usually resulted by untimely decoupling, has to be studied. In medium term, the question will be around the general ancillary services problem such as voltage and frequency regulation. In long term, numerous questionings concerning the network capacity of wind power integration (e.g.: in Germany, 50 GW is planned by 2020) and the unsatisfying current premier reserves will be purposed. Therefore, new production infrastructures have to be built, especially with improved management plan which will link these new productions to stocks and load pilot.

Moreover, because of the continuously increasing penetration rate of wind power in power system, the management of wind power intermittency become more and more important.

In fact, network driver will meet a serial of difficulties that cannot be solved without actions directly on the flux of wind energy or indirectly by economical incitements (penalty/bonus) to wind producers.

An interesting schema for the wind energy management can be a coupling of wind generators and storages. Naturally, there are multiple varieties of wind generator and storage systems.

However, for the power level that can influence the grid, the most adapted systems of storage is turbine/pump ones.

In order to optimize the operation of wind and storage system, particular attention in existent research is given to maximizing economic benefit. Such an economical approach, suitable in the short-time frame for encouraging the wind development, assesses the wind intermittency as a technical-economic problem with network operating limit conditions. With large-scale of wind integration, the intermittency will have great impact on power system operation (fluctuations, stability, reserve capacity…). Network needs to apply more and more constraints on power quality delivery by wind system. In this context, the current

work considers optimal operation of wind storage system as an optimization problem that deals with primary sources, storage capacity as well as demand. The main objective is to meet grid requirements in term of limiting the fluctuations and providing possible ancillary services. The intermittency management will be assessed into two steps: anticipation phase and reactivity phase. The first one, which will generally be done at Month-1, Week-1 or Day-1, consists in using forecast information (weather, network demand …) to define the optimal operation schedule for wind – storage system. On real time operation, the system has to deal with possible vagaries and take the right adjustment control with actual capacity. The problem is complex with numerous discrete control variables and continuous ones. A mixed-integer linear programming (MILP) is used to efficiency solve the problem. An example is given to illustrate the proposed method. Results indicate that wind power with storage can meet the network requirements while best ensure its profits. Results also show that the proposed optimal operation strategy which limits considerably the fluctuations on power system will facilitate the integration of more wind power.
In this chapter, we deal with a wind system combined with a hydraulic storage (we name the system W+S since now) where the input is the network demand power and the output is the provided wind power. This system has to response to the management requirements in taking into account the wind vagaries, the storage and de-storage capacity, the energetic cost of the flux transfer and highlighting economical efficiency.

2. Introduction of corrective measures in order to face the intermittencies of wind energy

Because of the fluctuations of wind energy, some corrective measures have been proposed to face the intermittencies.

- The choice of location for a wind power plant building

The choice of an optimal geographic location is one of the first criteria to be considered and analyzed in order to plan a significantly and stabilized production. Many geographic areas seem to be appropriate to the wind energy development: a uniform wind speed with few or no weather anomalies (storms and cyclones) guarantees a controlled production of energy.
For example, in France, the priority fields of wind energy development are determined by the following parameters:

- A high wind potential with three distinct wind patterns: north, west, south;
- The possibility to be connected to a national electrical network;
- The preservation of the land-use sites, that is to say, the guarantee of a low impact on landscape, environment, fauna, historic edifices and all other protected areas.
- Avoid proximity with military areas, airports, radar detections…

The priority regions for the wind energy development are (in France) Lorraine, Bretagne, Languedoc-Roussillon, Picardie, Champagne-Ardenne, Rhône-Alpes, Midi Pyrénées,…

- The improvement of the wind forecast accuracy (speed and direction)

Forecasting is a main factor giving the entry parameters of all the operational decisions related to the operation of the electrical systems in general, of the wind energy plants in particular. However, due to the continuous variation of the weather conditions, the wind speed forecast accuracy and to a lesser extent wind direction, is a main topic.

- Energy storage

Energy storage is the key of all kind of integration of intermittency primary sources. Nevertheless, all the existing mature technologies are little or no adapted to the wind energy power scales (MW). Except for the three following ones:

- Big sized hydraulics or gravity-fed systems in general;
- Compressed air;
- Flywheels;

Each system is characterized by its power or its mass or energy volume, its efficiency and its cost; these parameters will be relevant ones for the choice of a technology than another.
And in this party, the use of wind power combined with storage means (mainly, pumped hydro storage system) is often proposed and chosen to limit the impact of the variability of wind power [SOM-03], [ANA-07].

3. Problem description of operation of a wind power plant with an hydraulic storage within the electrical network

3.1 An economic problem (old policy: only economic constraints taken into account)

Beforehand, the energy policies emphasized the wind energy producers by introducing advantages on their produced energy purchase price and by neglecting the ancillary services criteria for this kind of energy. Indeed, the producers supplied energy without being concerned by:

- Voltage regulation;
- Frequency regulation and power regulation required by the grid;
- Adaptation of supplied energy in case of variable situations (dramatic wind speed fluctuations or network voltage drop).

With the growth of renewable energies in general and that of wind energy particularly, these advantages gradually decreased:

- The evolution of energy policy: subventions dedicated to renewable energies decrease;
- In prospect: increase of participation rate of renewable energies in the electrical network (20% attempted in 2020);
- Increasing of imposed technical constraints.

Thus, optimization of (W+S) system operation is needed in order to better integrate the wind energy into the electrical system according to the new requirements of the grid.

3.2 A technical-economic problem (real time or reactive management)

Wind power plant management is the adaptation to the wind intermittencies in order to satisfy the electrical network requests. This is a global exercise where all elements must be carefully analyzed. Then, study of sources (location, weather and installed capacity), the prevision of the operation mode (seasonal forecasts, month, week, day and hour) and on the real time, optimal driving strategy must be considered.
Management of wind energy intermittencies can be separated in two phases: anticipation phase based on forecasting data (static management) and reactive phase on the real time (dynamic management).

- Anticipation management

Concerning this kind of management, the optimal operate diagram of a day is established thanks to previous day data. The drawback is that the performances depend on the accuracy of forecast data. The difference between the forecast data and the real data can generate

technical errors and economic losses. To overcome this problem, a real time management can be proposed and anticipation plan for the optimal operation of system will be forecasted for tomorrow.

- Real time or reactive management

The aim is to obtain adapted optimal operate strategy and dynamic on the real time in case of unpredictable variations concerning wind speed or required grid power for example. The method is based on a continuous daily update as soon as entry data are not conformed to expected ones. As a result, a new optimal operate strategy is determined.

Thanks to the combination of the two management phases, the wind energy system with a hydraulic storage (W+S) is fully controlled. First, the forecast data is used. Then, they are compared to the real ones and the deviations, if there is one, is adapted in order to obtain a new optimal operate plan.

4. Problem characterization

4.1 W+S system characterization

The energy flux of the W+S system is presented as the following figure. This system principal characterization is discussed in the next paragraphs of this part.

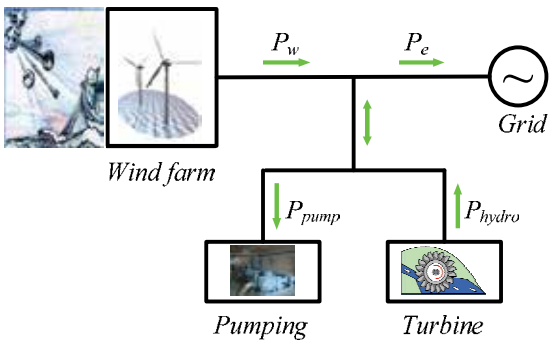

Fig. 1. Connection of the W+S system to electric grids

a. Continuous, discreet and intermittent nature

- The wind power is an intermittent source

The variability of wind energy is due to the intermittent nature of wind and the process of converting wind energy into electrical energy.

The wind speed is constantly changing. This is a climatic phenomenon, which depends on several variables that are very difficult to predict with accuracy. Normally we use statistical tools to describe this phenomenon: the variation of wind is given by (1) using a Weibull distribution function and is illustrated in Figure 5. The statistical model is characterized by the scale factor C (m/s) and the shape factor k (dimensionless).

$$f(V) = \left(\frac{k}{C}\right) \cdot \left(\frac{V}{C}\right)^{k-1} \cdot \exp\left[-\left(\frac{V}{C}\right)\right] \quad (1)$$

The C and k factors are estimated by using historical data of wind on the site considered for a long period. A description of wind conditions at many sites in Europe shows that in

general, the value of C factor is between 2 and 8 and the k factor takes a value between 1.5 and 2, [BUR-01], [GAR-06], [GEN-05], [DWIA].

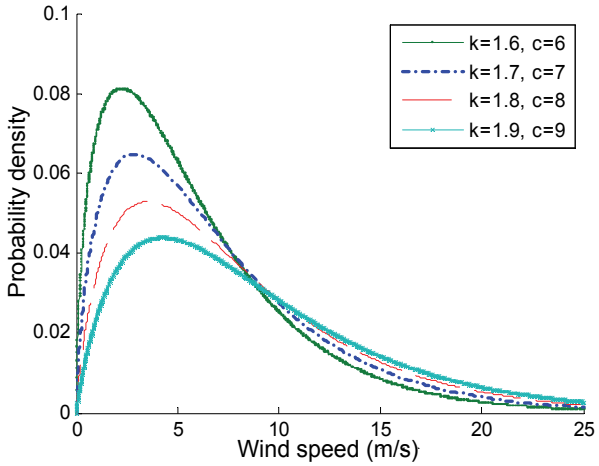

Fig. 2. Probability density

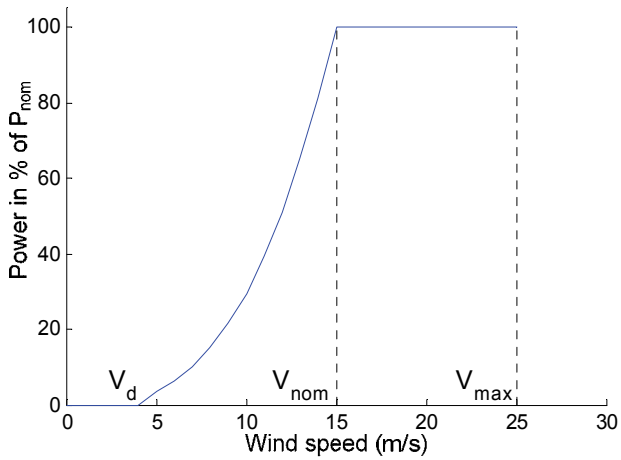

Fig. 3. Characteristic of the wind power according to the wind

In the wind turbines, electricity generation is directly related to the wind speed. The turbines convert wind energy into mechanical energy, which is then used by the electrical generator. The conversion process of a wind turbine is described by a power curve given by Betz expression:

$$P = \frac{1}{2} \cdot C_p \cdot \rho \cdot \pi \cdot \left(\frac{D}{2} \right)^2 \cdot V^3 \tag{2}$$

Where:
ρ: density-dependent temperature
P : power generated by wind turbine
Cp: drag coefficient of power (specific to the wind farm)
V: wind speed
D: diameter of the blades
This expression is quite similar for different manufacturers and turbine types. The power is null if the wind speed is less than a starting speed (cut – in speed) (Vd = 2 to 4 m/s), this power is also proportional to the wind speed rise between cut – in speed and the rated speed (about Vnom = 12 to 16 m/s). At the rate speed the power is near its nominal value. Power is constant between the rated speed and cut - out speed (Vmax = 25 to 30 m/s). Beyond the cut-off speed, the turbine is stopped for safety reasons.
By observing Figure 5 we see that the winds are more frequently at low and average speed than at strong velocity. Otherwise the (2) shows that the average wind power supplied by the turbine varies strongly with the cube of the average wind speed. Thus, a doubling of wind speed corresponds to an increase in its capacity energy 2^3 = 8 times.
Consequently, the variability of the wind and the process of energy conversion makes the wind generation an intermittent nature.

- The electric grid is considered as an intermittent source

The electric grid is a complex multi-actor system consisting of many uncertain factors like technical, human and natural factors. The uncertainty is present at several levels.

- Stochastic variation of demands (usually considered as the prediction error) has important effects on anticipating and on managing the real-time system. It is due to some related climates and consumer behaviours.
- Several types of uncertainty exist in electricity generation where the generating units cannot reach their production plans or where the production unit cannot start as expected or is stopped suddenly by natural or technical causes.
- Operation limits of the transportation and distribution systems have to be taken into account. The risk of disruption is high if one of these limits is violated, usually when the capacity of power transmission exceeds its limit or there are some technical restrictions on the use of lines. We called them congestion problems. They are unpredictable and normally occur following any incidents (errors of operations) or external aggressions (a tree branch falling on a line, overload, lightning or discharge on some lines...).

The combination of these uncertainties and the physic nature of the system, in plus with the difficulty of predicting the behavior of all factors increase the uncertainty on the system. Therefore the electric grid is considered as an intermittent source.

- Hydraulic storage system is a cumulative resource

In this storage system, water is stored in high basin in the form of potential energy. It is removed from storage into turbines to produce electricity when needed. Providing hydraulic pumping increases the storage energy while the discharge by the turbine reduces the volume of the basin. It is the characteristic of "storability" which leads us to consider not only the operation flexibility but also gives us un opportunity to produce energy at better valuated times. Thus, the main characteristic quantities of the storage system are:

- storage volume (in m3) and storage capacity (in watt-hours (Wh));
- different altitude between the two basins (upper and lower) (m);
- installed power and performance of hydroelectric turbines and pumping station.

The storage state at any time is determined by the accumulation of volume available in the past and the provided and discharged volume at the time.

- Turbine and pump are the two alternate functions

The storage system, which operates with two closed basins, is considered as a closed circuit. In case of overproduction wind, water can be pumped into the upper to accumulate potential energy. The hydroelectric turbines use this water to produce electricity during high load demand. Therefore, both turbine and pumping are alternated functions. Moreover, the W+S arms to maximize the value of wind energy. The hydroelectric storage plays the supported role. It is a non-permanent status (discrete). It is also important to note that for economic reasons, it is undesirable or even impossible to run two functions simultaneously, especially in the case where the system has only one forced operating system - type II.

b. Dynamics

The W+S is a dynamic system. The time horizon considered for the W+S system can be viewed at different time scales where the amplitude variation has not same values.

First, wind generation is intermittent but it sometimes shows a certain periodicity. In different seasons, we see that wind generation is more favourable in winter in the Nordic countries with a low pressure weather, or better in summer in the Mediterranean region thanks to the summer breezes [GAR-06], [PET-97].

The annual consumption of the electrical system also has a regular trend and is periodic. The power consumption increases year-by-year following the country development. The growth rate depends on development degree: low in industrialized countries and very strong in developing countries. In a year, season-by-season, energy demand is much higher in winter than in summer in cold countries and inverted trend in hot countries [GAR-06], [PET-97].

A example of annual win energy statistic is given in the following figures. Figure 7 gives potential wind energy between 2003 and 2008 on a site in Montpellier (southern France). Figure 8 shows of the monthly power consumption in France between 2003 and 2008.

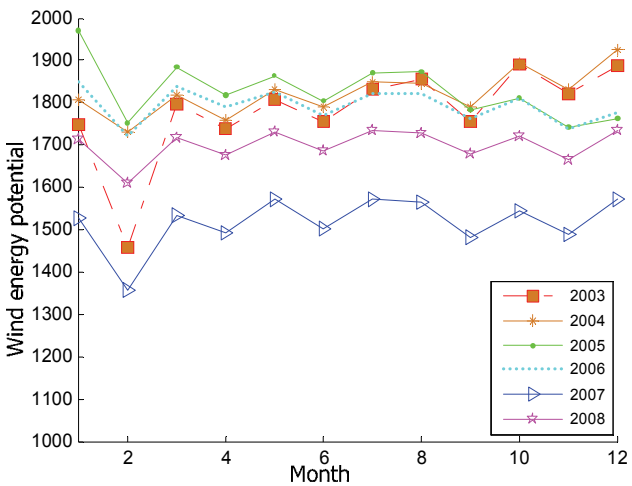

Fig. 4. Potential wind energy

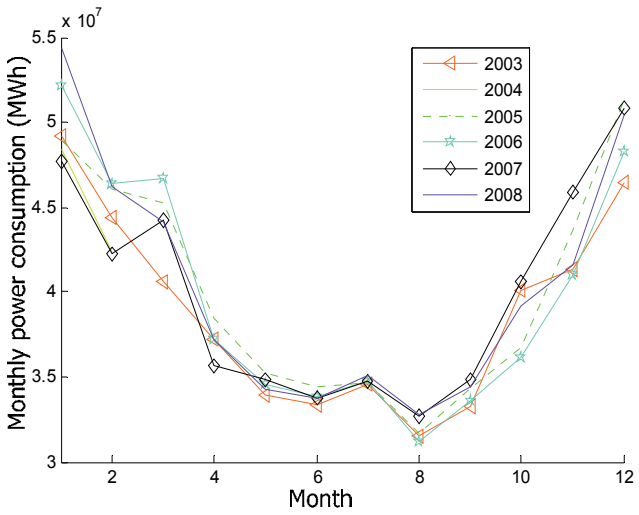

Fig. 5. Monthly power consumption

Thus, at this time scale, the forecast is based on the past history and on the modeling of climate effects or others recurring effects (festivals, big events ...).
We also note that diurnal cycles are mainly due to the effect of temperature for both wind generation and power consumption.
In reduced time scales (order of a minute) it is difficult to predict exactly the average wind speed and its level of fluctuation. Consumption also fluctuates unpredictably for the reasons cited in the above paragraph. However, we note that changes in short-term consumption are rather "continuous" or "progressive".

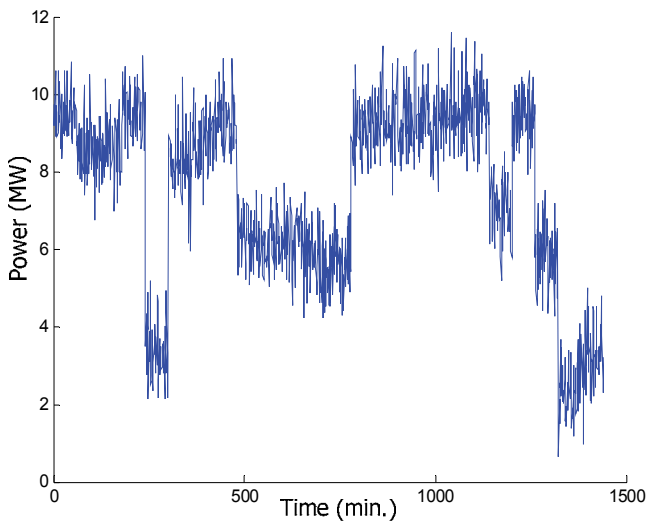

Fig. 6. Wind generation

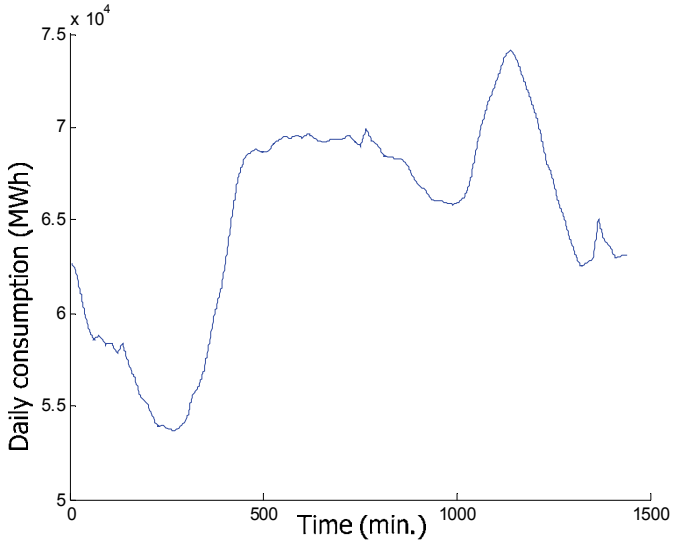

Fig. 7. Daily consumption

The following analyses show us some observations:

- in medium term (week, month, season, year): variability is rather slow and periodic;
- in short term (day): the variations are large and associated with large uncertainties;
- in very short term (some minutes): fluctuations are very fast with amplitudes rather unpredictable.

Every time horizon type of variability and its impact on the operation of different system. Therefore, it is important to take into account this dynamic characteristic of the W + S in the developed approaches which arms to optimize the intermittency management.

c. System benefits

The economic and financial needs have to meet the profitability of the system. Because, despite technological and techniques progress in recent decades, the economic incitements and the trend of wind energy integration into electrical system, the price of energy produced by this source is still higher than conventional sources. The economic criteria are still among the top regardless of adopted management strategy.

4.2 Towards an optimized management

The presented characteristics of the W + S system have highlighted a need to develop a optimized and appropriate management approach. It arms to determine the schedules of on- off operation and the quantity of energy of all components in the system (wind - hydro - pumping), which meets the technical and / or economic criteria. The coordination of components operation in the system should be part of an overall vision and be composed of several levels of control for the different time scales.

How do we define an optimal strategy of operation management? The answer depends on the conditions of wind integration in the electrical system.

Nowaday, the development of wind power in several European countries (Germany, Spain, Denmark...) is explained by the support policy adopted by its governments. These include not only regulation policy (required purchase, quotas) applied to electricity distributors but

also an attractive remuneration per kWh generated by wind power (investment subsidies, guaranteed purchase price). This policy, known mechanism of integration, is obviously intended to increase wind energy generation to maximize its profitability. Fluctuations are less disadvantageous and are even negligible for wind power producers. The operational and financial responsibility of the intermittent management refers to different actors of the electrical system. The quality of results and the effectiveness of this policy are proven by the substantial growing of wind turbines installation over worldwide during recent years. Thus, for wind energy producers, the best management approach arms to maximize the profit from selling wind generation by maximizing win energy penetration into the grid, at the best price [HAL-01], [GER-02], [CAS-03], [MAG-03], [CAS-04a], [CAS-04b], [CAS-04c], [KAL-07], [BEN-08], [NGU-09], [EWE-09].

A management strategy is supported when wind generation is still a marginal source among available sources. The impact caused by the intermittent operation of the system is less visible and often merged by the consumption vagary. So if we investigate for medium term, wind power should continue to grow. The management of vagary involved in wind energy would be of not only a technical challenge - because the dependability of the system depends, but also an economic issue - for the management of the vagary has a cost (disturbances need increase operating margins...). The question supposed to the electrical system is that will be the acceptable level of fluctuation? Should we accept these risks or consider eventually wind power as an independent producer in order to meet specific technical constraints and electricity market rules. The management of the wind system in upcoming years would inevitably focus on the answer to this question.

We focus on this context and are going to set up an optimized management approach of the W+S system.

5. Optimized management method for W+S systems

5.1 Architect of the management system

To initialize an optimized management method for W+S systems, we base on two levels of control: the anticipation of the operation system and the dynamic and responsive management in real time.

a. Anticipation of the operation system

In general, the anticipation is the most important step in the operation system. The objectives here are to define the plan of operation of all components in the system in subjecting to meet all the technical constraints in order to achieve the target during a period. Therefore, the anticipation is an optimization problem.

The principle of anticipation is based on predictions such as: weather forecast (wind data, temperature...) and the network demand (power, energy and / or curve of electricity prices), the actual generation capacity of each component (condition, planned maintenance...) ... etc. The anticipation is purely theoretical (no physical control). It permits us to prepare the set values to be applied to each component in the in situ operation. The instructions are determined because they are calculated as a reference in the physical exchange with the network and thus provide an opportunity to address the risks due to uncertainties or vagaries. The calculations are performed using the average values over a time horizon, which is the duration of the operation plan to be determined. Depending on the length of this horizon, the goal may be different.

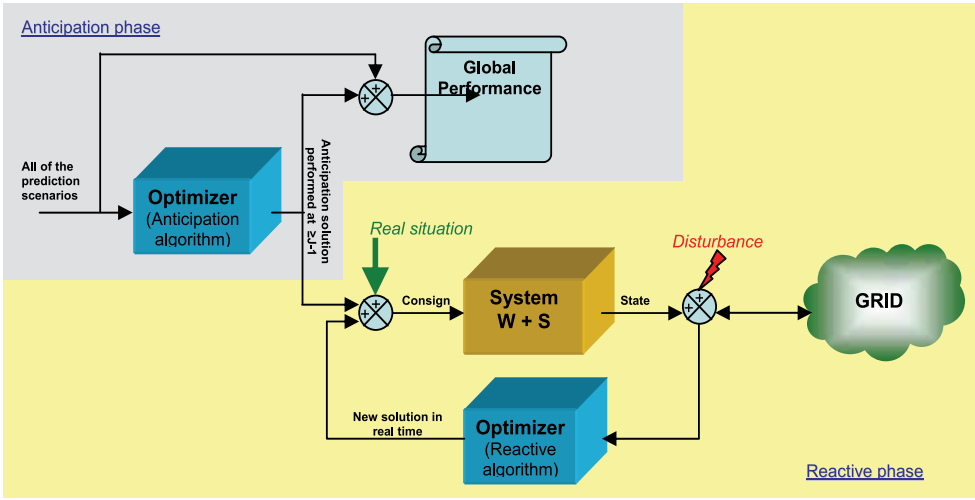

Fig. 8. Architect of the management system

In order to know the operation anticipation of the system W + S, we distinguish two levels of anticipation:

- Anticipation of the hydro storage operation: it consists in defining the macro level of the operation plan of the W + S system, especially is the use of storage capacity in order to better adapt to wind availability. It seeks to determine the maximum and minimum storage basins at specific times.
  The horizon of anticipation to be considered has to suit the storage capacity, the wind power capacity and the quality of forecasts. It is possible to plan the operation rather medium-term (days, weeks, month or season). It can be called the anticipation plan at the horizon of the day ahead D-1. The more storage capacity has, the longer anticipation horizon is. This allows us to anticipate a global view of operations and system performance over time. However, the longer horizon to consider is, the worse forecast is and so we has the risk of predicting values which are averages, shrouded uncertainty. Moreover, by considering the system over a long period, the calculation sample must be carefully chosen because the size and complexity of the optimization problem and the solution time depends on it. Typically, the sample varies from 1:00 to 3:00.
- Anticipation of the exchange between wind energy and the network: whatever the type of centralized power system (vertically integrated) or decentralized (managed by the electricity markets), the anticipation at the day ahead for the next day is an obligation for each participant. The challenge of this step is important because it provides the network manager the information needed to ensure proper coordination between the production and the consumption of system participants. For the W + S system, the anticipation arms to define an operating plan that allows us:
  - to propose its best offer of production to maximize the benefit of wind power production;
  - to anticipate risks and to predict the operating margin to minimize the impact of the intermittent nature of production and thus limit the these impacts on the network.

  The horizon to be considered is therefore 24 hours (from midnight to midnight), also called anticipation on the horizon of the day ahead D-1. Sampling computation depends on that used by the system, typically it is 15, 30 minutes or 1 hour.

Thanks to optimal computations of operation plan, estimated costs and benefits are calculated. Moreover, beyond a simple prediction of operation, anticipating on the horizon of the day ahead D-1 must be able to "secure" the achievement of the target. The notion of "secure" is indeed to provide in terms of control a certain level of flexibility and tolerance face to the disturbances. This could be achieved by further analysis on sensitivity of obtained solutions in function of input parameters variability.

b. Dynamic and reactive management in real time

The purpose of the dynamic and reactive pilotage in real time is the intermittent and dynamic characteristic of the system W + S. Indeed, at first, it is simply to ensure that it functions correctly according to the plan of operation in anticipation. Subsequently, face to the problem appears with the disturbances up to the day ahead, the problem is a proactive and dynamic management, which permits us to found the best compromise to minimize the damage. The consequences of decisions taken at a given time should be reassessed continuously and, if necessary, modified. Then, new actions should be taken. For these reasons, the process is considered reactive management based on two levels:

- Reactive "spontaneous" management: the adjustment is within the capacity of internal regulation of each component of the system (wind, hydroelectric and pump);
- Predictive management at the slipped horizon: it arms to call the optimizer, each time when the difference between the measured value and the prediction value exceeds a certain acceptable threshold (at instant H in Fig 1), review or redefine the operating plan for the period called the prediction horizon slipped between H+1 and T (the end of the expected prediction horizon). Following this reassessment in function of new available data the new instructions are recalculated. The illustration of the predictive management process in real time is presented in Fig 12.

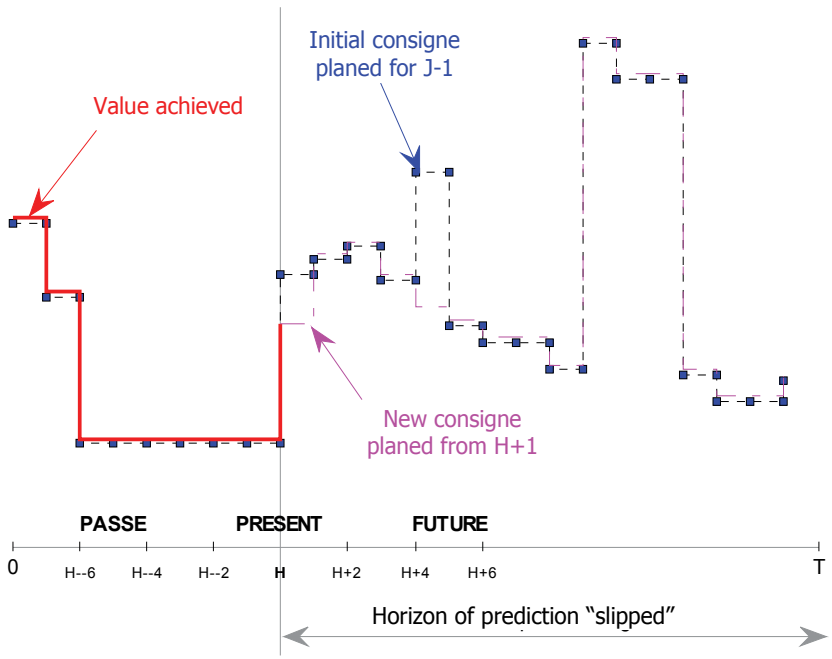

Fig. 9. Nesting time in the reactive management

In this section, we proposed the architecture of the optimized management system. The following sections are specifically devoted to the optimization module with: the structure of input and output data, the mathematical modeling of the problem and the choice for method resolution.

5.2 Hypotheses and data structuring

a. Prediction of wind power

As already mentioned in the above paragraph, the wind power is a variable and intermittent energy source. To develop a method for managing the wind energy, a good forecast of wind production associated with the estimation of uncertainty is primarily important input data.
The purpose of the wind generation prediction is to provide an estimate power generation at a given time in the future. The "peak" prediction is the most common model: for each time step in the future, a single value is provided. The forecast is given in power because it uses the characteristic curve that directly converts the wind speed in power. It is defined by several time horizons:

- a few days a week: this forecast could facilitate the anticipation of the use of storage;
- a few hours in the range from 24 to 72 hours: This prediction is essential for managing the electricity system in general and the wind system in particular. We'll use this prediction for the anticipation of our system operation;
- a few minutes of one hour: it is the very short term forecast - even in real time, which can be used for active control of the turbines.

Naturally, the quality of the prediction increases as the prediction horizon is reduced.
Knowing that the forecast still contains certain of error what is defined as the difference between the measured and estimated (predicted) value, theoretically, several research exist to take into account the uncertainties such as:

- a stochastic model: we assume that these uncertainties are random variables following the probability law;
- interval model: we assume it is possible to determine an interval of plausible values that bound the actual values;
- scenario model: one defines a number of scenarios of possible uncertainties based on the study of histories, trends ...

In this article, we use the combination of two models: intervals and scenarios by determining 3 values for each point of prediction (minimum, average and maximum).

b. Operation of the W + S system in the electrical system

The electrical system in which the W + S participates, presents a deregulated organization. The coordination of production and consumption bases on a sequence of two modules at medium action and horizon distinct actions (cf. [SAG-07]).

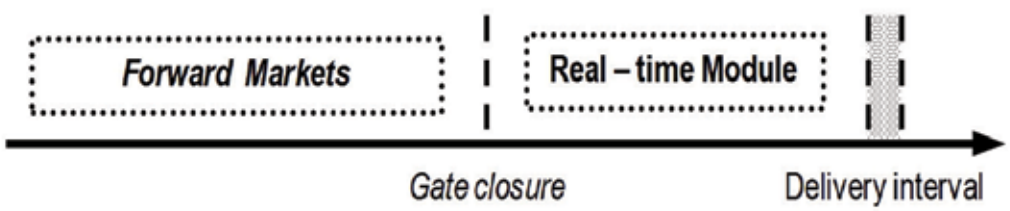

Fig. 10. Principle of the organization of electricity markets

The first module of electricity markets permits its participants to prepare a decentralized mode and forecast their energy exchanges in real time. These markets, called "forward", are composed of several levels:

- market before the day ahead D-1 arms to prepare long scale trade (week, month, year);
- market of the day ahead D-1 arms to prepare the coordination of production and consumption the next day;
- market of infra hours arms to coordinate the operation for the next few hours, so as to exploit all opportunities to better manage the vagaries.

The participant producers in forward markets respect the following common rule: based on forecasts (weather, consumption...); producers anticipate their operation to identify offer production, i.e. a quantity of energy exchanged with the network for each delivery interval. The choice of the length of this interval depends on the considered system.

This step is purely financial and trade deals are permitted until a time called the gate closure. At the time of gate closure, the market therefore has all the information needed to define, based on production offers and demand loads, the best compromise towards the power demand and the amount of energy to be delivered. This is to minimize the total operating costs while ensuring the safe operation of the system. Thus, the electricity price for each delivery interval is determined.

In France one day is from midnight to midnight, composed of 48 intervals of 30 minutes. The gate closure is 16 pm the previous day for the markets forward. The market of infra hours is 45 minutes before physical delivery. The price used is the weighted average price (PMP: Prix Moyen Pondéré in French).

The second module, in which the actual time starts from the gate closure, performs the centralized coordination of production programs with the overall consumption and the management of physical constraints of the system. Any variation between the proposal at forward markets and the physical delivery will require the network manager to use the necessary actions to ensure system balance. For this reason this module is called an adjustment mechanism. It consists of two stages:

- *Stage 1:* Set frequency - power (primary and secondary) automatically by the responsible groups of the balance (with a specific contract with the network manager) within a very short time (less than 10 minutes);
- *Stage 2:* optimization of load distribution and return operating margins. This setting is available through modifying operation demands of the other actors in the system. All producers or consumers are eligible for this adjustment phase.

The adjustment mechanism is expressed by the rule of difference at unique or a double price. In France, the adjustment is at double price, Table 1. This is to encourage favorable ranges and to penalize unfavorable ranges in the system. In the first case, the ranges are generally favorable for PMP defined by the market of the day ahead D-1. In the second case, the unfavorable range is penalized for PMP price revised at a multiplicative factor [SAG-07], [TEN]

For example, at time t, the tendency of the network is increasing. It means that the system is in energy deficit. A producer provides an amount of energy:

- either less than the offer made at D-1, that will aggravate the situation. There will be penalized for each kWh not supplied at a price of: $PMP \cdot (k+1)$;
- or greater than the offer made at D-1, which goes in the right direction to relieve the system. It will be paid for each additional kWh at a cost of: PMP .

	Trend of adjustment mechanism		
	upward	downward	null
Positive difference	PMP	$\frac{PMP}{(k+1)}$	PMP
Negative difference	$PMP \cdot (k+1)$	PMP	PMP

Note : In France since 2005, k = 0.12

Table 1. Price of regulation of ranges in the adjustment mechanism

It is the network manager who will make the selection to offer and activate the change order from the operation program of selected producers.
Thus, in the context of this thesis, we consider that the W + S system works in electricity market following the same rule as other producers as described above. Nevertheless, by its intermittent nature, we assume that the W + S system does not intervene at the first stage of the adjustment mechanism. That is to say, it does not offer the reserve primary and secondary frequency.

6. Problem formulation

The problem of optimal management of the W + S system described in the preceding paragraphs has all characteristics of an optimization problem where we use limited resources to achieve optimal goals. This can be solved by techniques optimization.
Optimization techniques are algebraic and numerical approaches based on mathematical programming. An optimization technique based on a class of decision variables and arms to prove the existence of a scenario that is the best of all possible scenarios. This scenario is known as optimal solution. Two large families of optimization methods exist:

- exact methods;
- heuristic methods.

Early approaches, such as their name suggests, are accurate and effective. The optimality of obtain results is mathematically proven. However, these methods require knowledge of mathematical programming in order to build adequate and appropriate models. Problem formulation (objective function and constraints) in mathematical form is sometimes laborious especially when the complexity of the problem increases. The cost of calculation time and informatics resources is also a weak point which demotivates to choose these methods if there are problems of very large size. In the area related to resource allocation, linear programming and its extensions such as integer programming or mixed linear programming and dynamic programming are mathematical techniques commonly used for solving such problems.
The latter approaches are methods of solving complex problems and mathematically less robust but based on good significations. They do not guarantee obtaining the optimal solution but a solution whose performance is generally quite good and similar to those of the first approaches, we speak of sub-optimal solutions. These reduced robust approaches can save time and computational cost for complex and large problems.
To address the problem of optimal management of the W + S system, we choose a method belonging to the family of exact methods: linear programming. It is an effective and realistic

method. It has the advantage of flexibility modeling which allows us easily introduce extensions (including consideration of new variables or constraints).
In addition, the combination of increased computing power with specialized software strides such as the CPLEX solver, the solver JLPK or one integrated in MATLAB (MPT ...) makes a possibility of solving very large linear programs in a reasonable time [MOM-01].

6.1 Linear Programming (PL)

The implementation of the linear programming technique can be divided into several stages:

- identifying the problem as being solvable by linear programming. This identification is the contribution of deep knowledge of the physical phenomena and to the mathematical modeling of the problem;
- formulating the problem with using a linear mathematical model (equation formulation of variables, objective function and constraints);
- solving the theoretical problem using techniques algorithmic;
- determining a real solution from the theoretical (mathematical) solution;
- verification and validating the solution.

a. Mathematical model

The term "linear programming (LP) implies that solutions must be found to be represented by real variables. The objective function and constraints are represented in linear form.
When the problem consists of continuous and discrete variables (integer or binary), Linear Programming extends to the Mixed Linear Programming (MLP) or Integer Linear Programming (ILP). In the following, we use the name "PML".
The general expression of the PML is:

Minimize: $F(x)$

Subject to constraints: $A \cdot x \le b$

$lb \le x \le ub$

Where:
x : vector of variables (continuous, discrete)
lb, ub : lower and upper bounds of x
A, b : constraint matrices
F : expression of the objective function
All types of objective functions or constraints can be written in standard form.
For an objective function to maximize:

Maximize $P(x)$ is equivalent to Minimize $-P(x)$

For an equality constraint: $a(x) = b$ is equivalent to $a(x) + \delta \ge b$

$-a(x) - \delta \le -b$

with $\delta \ge 0$

For an upper inequality constraint: $a(x) \ge b$ is equivalent to $-a(x) \le -b$

Example :

Maximize: $P(x) = 8x_1 + 5x_2 + 6x_3$

Constraints: $2x_1 + 3x_2 + 2x_3 \leq 85$

$$x_1 + 2x_2 + 1x_3 \leq 81$$

$$4x_1 + 3x_2 + 1x_3 \leq 120$$

$$x_i \geq 0, i = [1 \ldots 3]$$

The presentation of the problem in standard form is as follows:

Minimize: $F(x) = -8x_1 - 5x_2 - 6x_3$

Therefore, we have:

$$x = \begin{bmatrix} x_1 \\ x_2 \\ x_3 \end{bmatrix},\ lb = \begin{bmatrix} 0 \\ 0 \\ 0 \end{bmatrix},\ ub = \begin{bmatrix} +\infty \\ +\infty \\ +\infty \end{bmatrix},\ F = \begin{bmatrix} -8 \\ -5 \\ -6 \end{bmatrix},\ A = \begin{bmatrix} 2 & 3 & 2 \\ 1 & 2 & 1 \\ 4 & 3 & 1 \end{bmatrix},\ b = \begin{bmatrix} 85 \\ 81 \\ 120 \end{bmatrix}$$

b. Solution approach

- Algorithm for solving Linear Programming (PL)

Considering the constraints and limits imposed on the variables, we can determine the trust region. This region collects all the feasible solutions. If we fail to build a region where all constraints are verified, the problem is considered infeasible.

There is a solution in this region, which corresponds to a minimum of the objective function (the problem is presented in its standard form, so the objective function to minimize). This solution is called the optimal solution.

Moreover, it is possible to have one or more optimal solutions that give the same optimum.

Many methods have been developed to solve the LP problem whose variables are strictly continuous. The most frequently used techniques are known as the graphical method, simplex method and its variants.

- *Graphical method:* a feature of the PL is that the optimal solution, if it exists, is one of the highlights point of the "polytope" formed by the constraints and bounds of variables. Therefore, after building the region of feasible solutions, it suffices to inspect the vertices and find the solution that gives the minimum value of the objective function. The illustration of the graphical method is given in Fig. 11.

This method is very illustrative but is difficult to apply to large problems.

- *Simplex method:* developed by Dantzig in 1947, this method and its variants are widely used in solving the PL. This method based on the matrix approach is much more efficient for computer-assisted calculations.

The idea is to transform inequality constraints into equality constraints by adding slack variables / artificial δ. The problem becomes:

Minimize: $F(x)$

Subject to: $A \cdot x \leq b$ which is transformed into $A \cdot x + \delta = b$

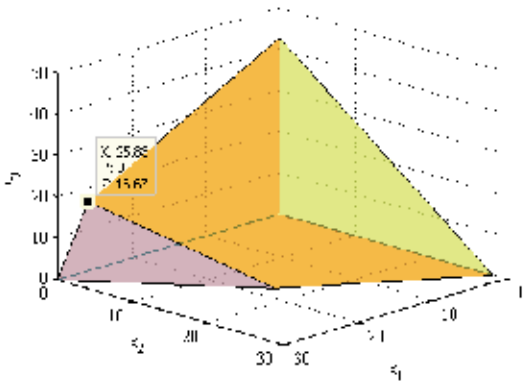

$$x = \begin{bmatrix} 25.83 \\ 5.67 \cdot 10^{-8} \\ 16.67 \end{bmatrix}$$

$$F_{\min} = -306.67$$

$$P_{\max} = 306.67$$

Fig. 11. Feasible region and optimal solution of the presented example

- Then, by solving the equation $A \cdot x + \delta = b$ we can obtain some cases:

- no solution : the problem is considered infeasible;
- a unique solution: the optimal solution;
- infinity of solutions forming a feasible region: the region obtained by examining the highlight points in order to find a solution that minimizes the objective function

- Solving Algorithm the Mixed Linear Programming (PML)

By nature of our problem, the variables are of continuous type on one hand and binary decision on the other. The PML problem is a difficult problem. The most common method for this kind of problem is the "Branch and Bound". Its principle is to:

- First, divide the problem into several linear sub problems which are numbered in a logical sequence (separation process) in order to obtain solutions containing only continuous variables;
- Then evaluate each of these sub problems in order to find the optimal solution using the resolution algorithm of the PL (procedure) in making each "tree node";
- Finally, choose the best tree constructed.

In this way, the problem is finding an optimal solution from a combination of NM solutions; with N being the number of integer variables and M is the range of values of considered variables.

For the presented example, if we add a constraint considering that all variables are integers, the optimal solution is:

$$x = \begin{bmatrix} 26 \\ 0 \\ 16 \end{bmatrix} \text{ and } F_{\min} = -304 \text{ , } P_{\max} = 304$$

c. Sensitivity of the optimal solution to parameter variations

Once the optimal solution is obtained, we investigate the sensitivity of input parameters. Knowing that the W + S input parameters tainted by uncertainty, analysis of the optimal solution is particularly important goal, which is to propose a management method for W+S systems.

How is the optimal solution if the parameters of the objective function or those relating to constraints vary? In which condition the optimal solution changes or in a worse case where the solution is no longer feasible?
This sensitivity analysis of post-optimization will allow us to answer these questions and to secure the optimal solution to face the intermittent input parameters.
We analyze in this paragraph, two types of uncertainty: first the parameters of the objective function and second the second member of the constraints.

- Uncertainty about the parameters of the objective function f_i

Continuing the example presented in previous paragraphs, we suppose it has an uncertainty on the parameter of the objective function:

$$F = \begin{bmatrix} -8 \\ -5 \\ -6+\delta \end{bmatrix}, \text{ with } -\infty \le \delta \le +\infty$$

We can draw its graph based on the coefficient of variation (see Fig. 12)

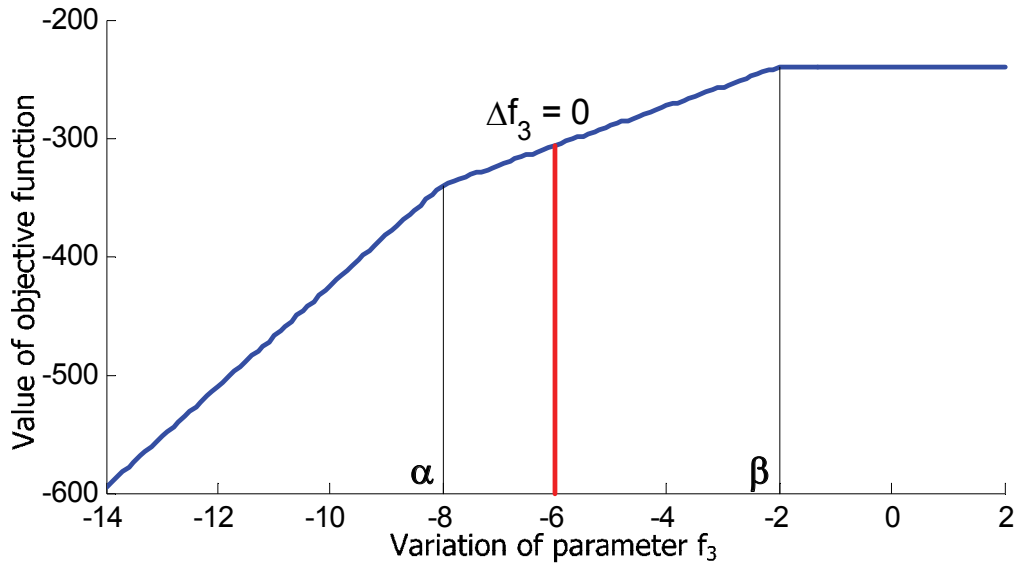

Fig. 12. Sensitivity of the objective function to parameter variation f_i

With $\delta = 0$, the optimal solution is that initially obtained.
It is found that the value of δ can have two specific values α and β :

- With :

$$f_3 = -6 + \delta \le \alpha \quad \leftrightarrow \quad \delta \le \alpha + 6$$

Note that the objective function responds linearly to a linear change of the coefficient f3. The more δ decreases the more objective function decreases, then is minimized, and vice versa.

- With :

$$\begin{cases} f_3 = -6 + \delta \geq \alpha & \leftrightarrow \quad \delta \geq \alpha + 6 \\ f_3 = -6 + \delta \leq \beta & \leftrightarrow \quad \delta \leq \beta + 6 \end{cases} \rightarrow \quad \alpha + 6 \leq \delta \leq \beta + 6$$

The optimal solution is feasible but the value of the objective function only varies flexibly from the change δ.

- With :

$$f_3 = -6 + \delta \geq \beta \quad \leftrightarrow \quad \delta \geq \beta + 6$$

The variable x3 is too expensive and the optimal solution is no longer feasible. We say that x3 has more influence on the objective function, which becomes "flat" compared to f_3 .

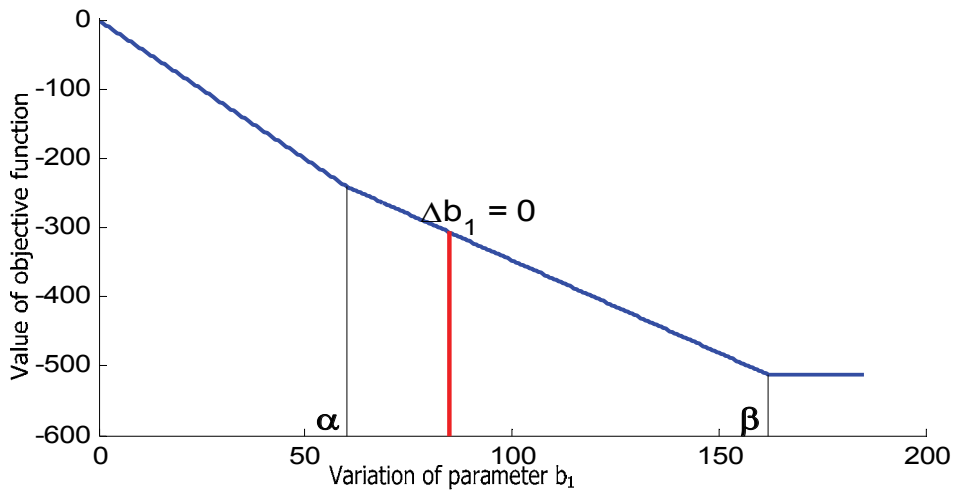

Fig. 13. Sensitivity of the objective function to parameter variation bi

- Uncertainty of the parameters b_j

We continuing the presented example and suppose it has an uncertainty on the parameter constraint b_1 :

$$b = \begin{bmatrix} 85 + \delta \\ 81 \\ 120 \end{bmatrix} \text{ avec } -\infty \leq \delta \leq +\infty$$

We can draw its graph according to the variation of this coefficient (see Fig. 13).
With $\Delta b_1 = 0$, the optimal solution is that obtained originally.
We see that there are also two specific values of δ : α and β

- With :

$$b_1 = 85 + \delta \geq \beta \quad \leftrightarrow \quad \delta \geq \beta - 85$$

The constraint on b_1 is always satisfied with all x and δ. It is said that this constraint is unnecessary or redundant. She hasn't influence on both the area of feasible solutions and objective function value.

- With :

$$\begin{cases} b_1 = 85 + \delta \geq \alpha & \leftrightarrow \quad \delta \geq \alpha - 85 \\ b_1 = 85 + \delta \leq \beta & \leftrightarrow \quad \delta \leq \beta - 85 \end{cases} \rightarrow \quad \alpha - 85 \leq \delta \leq \beta - 85$$

The optimal solution is feasible and the value of the objective function varies linearly with the inverse of the variation of δ. The more δ increases, the more the objective function decreases then is minimized.

- With :

$$b_1 = 85 + \delta \leq \alpha \quad \leftrightarrow \quad \delta \leq \alpha - 85$$

Note that the objective function increases more strongly compared to the previous area because this constrain has become increasingly difficult to verify.

7. Optimized management of the W+S system by PLM

In this section we describe our problem in mathematic expressions. Firstly we use some nomenclatures.

Glossary	Symbole
System parameters	
Optimization period	T
Time step	Δt
Nominal power of wind generator	$P_w{}^{nom}$
Nominal power of hydroelectric turbine	$P_{hydro}{}^{nom}$
Nominal power of pump system	$P_{pump}{}^{nom}$
Maximal/Minimal power of wind generator	$P_w{}^{max} / P_w{}^{min}$
Minimal power of hydroelectric turbine	$P_{hydro}{}^{min}$
Minimal power of pump system	$P_{pump}{}^{min}$
Efficiency of energy accumulation system (hydraulic turbine and water driving network)	η_{hydro}
Efficiency of energy accumulation system (pump system and generator and water driving network)	η_{pump}
Functioning cost of pump system per kWh	C_{pump}
Maximal capacity of upper/lower storage basins	$S_{\sup}^{\max}$, $S_{\inf}^{\max}$
Minimal limitation of upper/lower storage basins	$S_{\sup}^{\min}$, $S_{\inf}^{\min}$
Initial state of of upper/lower storage basins	$S_{\sup}^{init}$, $S_{\inf}^{init}$
Final state of of upper/lower storage basins at the end of optimization period	$S_{\sup}^{fin}$, $S_{\inf}^{finit}$

Glossary	Symbole
Signs	
Upper sign for variables in anticipation calculation	a
Upper sign for anticipation variables in reactive calculation	r
Inputs	
Projected power of wind generator	$P_w(t)$
Projected electricity cost	$SP_e(t)$
Projected cost for power gap	C_p (t)
Instant of a possible disturbance	tP
Real cost for power gap	$PMP(t)$
Results	
Required power for hydraulic turbine	$P_{hydro}(t)$
Required power for pump system	$P_{pump}(t)$
Required exchanged power to network	$P_e(t)$
Power gap between required and real exchanged power to network	$\Delta P_e(t)$
Total benefit during period T	BT
Intern working cost of W+S system during period T	CT

Table 2. Parameters and variables used in this section

7.1 Objective functions

a. Anticipation of system operation W+S

We recall that the anticipation the system W + S aims to maximize the profit from the sale of wind energy. In this way the objective function is expressed by the difference between the sale of energy and the cost of internal work:

$$FO^a = BT - CT = \sum_{t=1}^{T} SP_e(t) \cdot P_e^a(t) - \sum_{t=1}^{T} C_{pump}(t) \cdot P_{pump}^a(t) \quad (3)$$

b. Reactive optimized management

There is no mathematical optimization to be done to manage "spontaneous" reactive in real time. At the moment where the injection system meets the anticipation plan, the W + S system components work with calculated instructions. Ether wind turbine generator or hydroelectric, if it is functioning, supports the operation in the limit of its capacity.

The problem is complicated with possible disruptions because they can probably change the system state and thus affect the final result. For example with an increase of wind speed, the power injected to the network is more important.

- If this power difference is paid, that is to say that the network trend is upward, it is not necessary to review the operating plan of the W + S because this event enhances the benefit of system.
- On the other side, if the power difference is penalized, that is to say that the trend of the network is downward, would it be wiser to recalculate the level of the W + S system in changing the starting or stopping of the hydro-electric generator or theirs of the pumping station to compensate for this loss of profit or simply make better use of the excess energy?

Here's another example: we suppose the network is lack of power (problem of congestion, defects, consumer vagaries...). So the price of regulation of power deviation is very high, that is to say, each piece of extra supplied energy to the network at that time will be very well paid and each kWh of shortfall from the expected plan will be much penalized.

- If the system W + S is consistent with the anticipatory plan, there will be no impact on the final result.
- Otherwise, using the optimization, the W + S system is able to provide more energy to relieve the network while is maintaining or even is improving the final outcome.

Each time, we call the optimization calculation engine to calculate a new operating plan. This plan covers the period from tP (the appearance of the disturbance) at the end of the anticipation period (T = 24) taking into account new data on the situation following the actual disturbance.

To maximize the overall operation of the system, the objective is to minimize the negative impact of the disturbance according to the best level of function defined in the offer. Thus, the objective function is expressed by an estimate of the penalty due to all kWh gap to minimize:

$$FO^r = \sum_{t=tP+1}^{T} C_p(t) \cdot \left| P_e^r(t) - P_e^a(t) \right| \tag{4}$$

Two remarks are identified by considering l'(4).

- The first is the value of the cost penalty. As the price of regulation of power deviation is only known in real-time, penalty cost introduced by CP values were estimated (based on analysis of historical and current trends of actual network). They are used to better manage the different injected power to the grid.
- The second point concerns the equation formulation of this objective function. An absolute value is considered nonlinear. It requires a mathematical transformation to write the standard form of PML.

By adding a new variable nonnegative $\Delta P_e(t)$:

$$\Delta P_e(t) \geq \left| P_e^r(t) - P_e^a(t) \right| \tag{5}$$

The constraint described in (3) is equivalent to the following two constraints:

$$P_e^r(t) - \Delta P_e(t) \leq P_e^a(t) \tag{6}$$

$$-P_e^r(t) - \Delta P_e(t) \leq P_e^a(t) \tag{7}$$

The objective function of (2) is written so well in a linear form as following:

$$FO^r = \sum_{t=tP+1}^{T} C_p(t) \cdot \Delta P_e(t) \tag{8}$$

7.2 System constraints

System constraints W + S can be divided into two types: static and dynamic. The first type is in fact specific technical limitations at each component. The second type represents the time

interdependence of various values during operation. Constraints described below are applicable to the proactive and reactive phase.

a. Static constraints

The components of the system are supervised by their maximum and minimum.

- Wind turbine:

$$P_w^{\min} \le P_w(t) \le P_w^{\max} \tag{9}$$

- Hydroelectric generator:

$$P_{hydro}^{\min} \le P_{hydro}(t) \le P_{hydro}^{\max} \tag{10}$$

- Pumping station:

$$P_{pompe}^{\min} \le P_{pompe}(t) \le P_{pompe}^{\max} \tag{11}$$

- Basin capacity:

$$S^{\min} \le S(t) \le S^{\max} \tag{12}$$

- The exchange with the network is considered without technical limitations assuming that the network is sufficiently large to receive the maximum power that can be delivered by the system W+S.

b. Dynamic constraints

- The energy produced by the W + S system will be injected to the network.

At any moment we have:

$$P_w(t) + P_{hydro}(t) - P_{pompe}(t) - P_e(t) \ge 0 \tag{13}$$

- It is preferable not to operate the turbine and pumping in parallel:

$$P_{hydro}(t).P_{pump}(t) = 0 \tag{14}$$

In linear programming, variables are only defined by linear relationships. To get to express this constraint we see the need to introduce a binary decision variable $\alpha(t)$ by referring to [HA-06], so that:

$$\begin{cases} P_{hydro}^{\min} \le P_{hydro}(t) \le \alpha(t)\, P_{hydro}^{\max} \\ -P_{pump}^{\max} \cdot (1 - \alpha(t)) \le -P_{pump}(t) \le 0 \end{cases} \tag{15}$$

Demonstration:

$$\text{Si } \alpha(t) = 1 \rightarrow \begin{cases} P_{hydro}^{\min} \le P_{hydro}(t) \le P_{hydro}^{\max} \\ P_{pump}(t) = 0 \end{cases}$$

→ Only the function of turbine is activated

$$\text{Si } \alpha(t)=0 \quad \rightarrow \begin{cases} P_{hydro}(t)=0 \\ -P_{pump}^{\max} \le -P_{pump}(t) \le 0 \end{cases}$$

$$\rightarrow \begin{cases} P_{hydro}(t)=0 \\ 0 \le P_{pump}(t) \le P_{pump}^{\max} \end{cases}$$

→ Only the pumping function is activated

- The power supplied by hydro-electric generator at each time step is limited by the available energy stored in the upper basin and the storage capacity of the lower basin:

$$\frac{P_{hydro}(t)\cdot\Delta t}{\eta_{hydro}} \le \min\left\{\left(S_{\sup}(t)-S_{\sup}^{\min}\right),\left(S_{\inf}^{\max}-S_{\inf}(t)\right)\right\} \tag{16}$$

- The energy storable in the upper basin at each time step is limited by the available storage capacity of the upper basin and the storage capacity available in the lower basin:

$$P_{pump}(t)\cdot\eta_{hpump}\cdot\Delta t \le \min\left\{\left(S_{\sup}^{\max}-S_{\sup}(t)\right),\left(S_{\inf}(t)-S_{\inf}^{\min}\right)\right\} \tag{17}$$

- The stock state of the basin at the beginning and at the end of the day must respect the limits of maximum and minimum filling of the reservoir defined in the macro-plan of operation (advance phase of the storage)

$$S_{\sup}(t=0)=S_{\sup}^{init} \tag{18}$$

$$S_{\sup}(t=T)=S_{\sup}^{fin} \tag{19}$$

$$S_{\inf}(t=0)=S_{\inf}^{init} \tag{20}$$

$$S_{\inf}(t=T)=S_{\inf}^{fin} \tag{21}$$

- The temporal evolution of the state of available storage is calculated by examining the input and output powers of the basins:

$$S_{\sup}(t+1)=S_{\sup}(t)-\frac{P_{hydro}(t)\cdot\Delta t}{\eta_{hydro}}+\eta_{pump}\cdot P_{pump}(t)\cdot\Delta t \tag{22}$$

$$S_{\inf}(t+1)=S_{\inf}(t)-\eta_{pump}\cdot P_{pump}(t)\cdot\Delta t+\frac{P_{hydro}(t)\cdot\Delta t}{\eta_{hydro}} \tag{23}$$

7.3 Sensitivity of the optimal solution to the data

For the W + S system, the uncertain parameters are: wind power forecasting and stochastic nature of the grid, which are realized as a change in the cost of penalty (the price of

regulation of power deviation) when there is no correlation between demanded power and supplying power. We will consider changes in the form of a tree of scenarios.

$$P_{w,S}(t) = P_w(t) + \delta_w(t) \text{ with } \delta_{w\min} \le \delta_w(t) \le \delta_{w\max} \quad (24)$$

$$SP_e(t) = SP_e(t) + \delta_{SPe}(t) \text{ with } \delta_{SPe\,\min} \le \delta_{SPe}(t) \le \delta_{SPe\,\max} \quad (25)$$

8. Study case

A representative study case of a wind power plant in Montpellier is chosen. All the parameters for the system sizing problem are recapitulated in the Table 3.
Without loss of generality, it is considered that the two storage basins have the same capacity.

Parameters	Variable	Value	Unit
Nominal power of wind generator	P_w^{nom}	10	(MW)
Maximal power of wind generator	P_w^{max}	10	(MW)
Minimal power of wind generator	P_w^{min}	0	(MW)
Nominal power of hydroelectric turbine	P_{hydro}^{nom}	3	(MW)
Nominal power of pump system	P_{pump}^{nom}	3	(MW)
Minimal power of hydroelectric turbine	P_{hydro}^{min}	0	(MW)
Minimal power of pump system	P_{pump}^{min}	0	(MW)
Efficiency of energy accumulation system (hydraulic turbine and water driving network)	η_{hydro}	0.8671	-
Efficiency of energy accumulation system (pump system and water driving network)	η_{pump}	0.865	-
Storage maximal capacity	S^{max}	24	(MWh)
Minimal limitation of storage basin	S^{min}	1	(MWh)

Table 3. Parameters of W+S system

We consider the system of this study case with the same management process as presented in previous sections.

9. Results and discussion

9.1 Anticipation plan of system function at J- 1

a. Anticipation plan of storage use

As mentioned in the section 6, the main objective of the anticipation plan for the storage use is to define a system macro function plan in order to adapt to the wind availability.
An anticipation calculation of the wind speed and the electricity price for the next 7 days is given on the Fig. 14

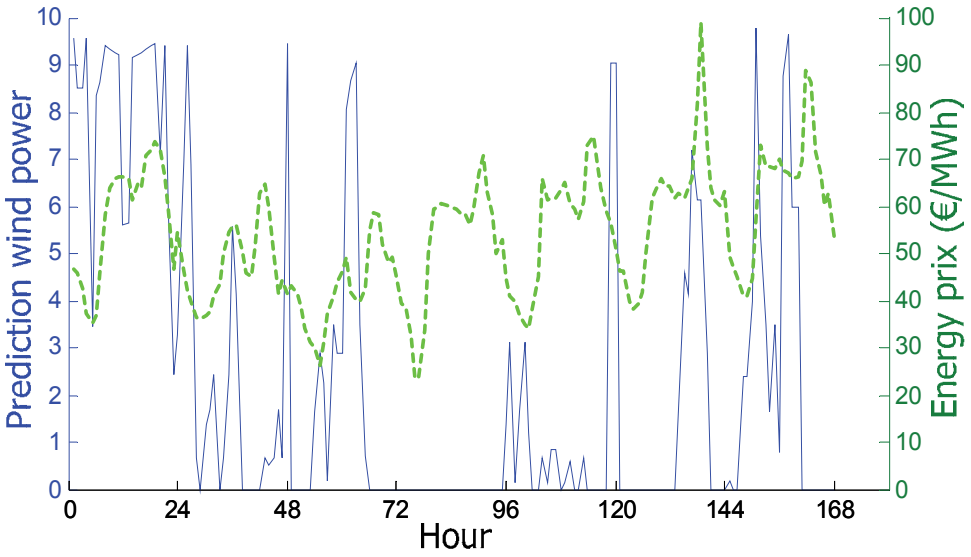

Fig. 14. Forecast date for the next 7 days

It can be observed in this example that a non-homogenous repartition of the wind energy potential capacity during these 7 days, while the electricity price evolution is rather cyclic. The wind potential estimation is summed up in this following table:

Day	Forecasted produced power (MWh)	Observation
1	188.96	Strong potential
2	55.86	Middle potential
3	57.75	Middle potential
4	31.266	Low potential
5	46.27	Low potential
6	56.46	Middle potential
7	63.876	Middle potential

Table 4. Forecast wind energy

There are different ways to proceed toward the anticipation plan of the storage use. Two of them will be compared: the first based on "1 day optimization", the second on "7 days optimization".

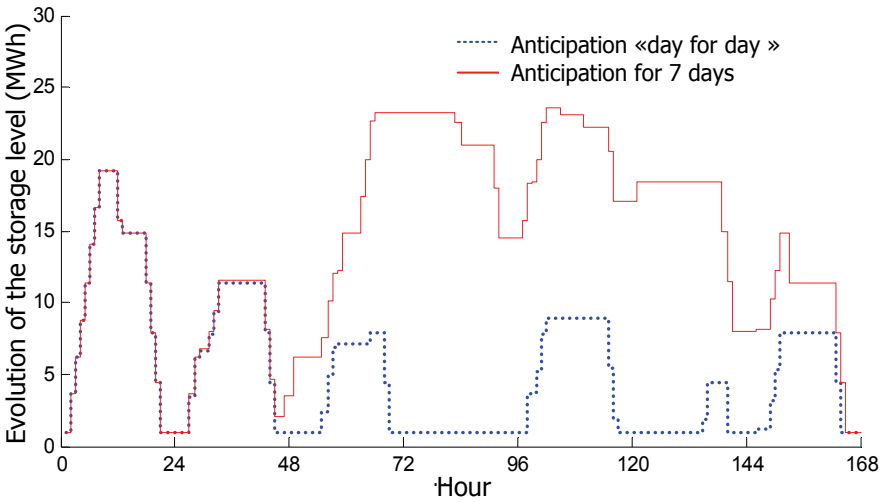

Fig. 15. Different strategies of storage management

We notice clearly two ways to manage the hydroelectric storage. In the first case (illustrated by the dotted line on the Fig. 15), the system management aims to best exploit the storage day by day. In order to optimize economical objective, the system destocks completely at the end of the day. The second case is illustrated by the full-filled line on the Fig. 15. As the objective consist to optimize the system benefit on 7 days period, the system stocks energy during the strong production potential days in order to ensure a better energy development. In both cases, the use rate of the wind energy is maximized: 95.4% in the first case and 96.3% in the second. In this example, the longer term optimization (7 days) makes a better use the energy sale to the network. The economical result of the second case is 1.32% higher than the first.

However, this difference is sensitive to the forecast wind power repartition and to the considered time scale. It is interesting for the W+S operator to compare cases in order to find out the best adapted strategy to the wind availability.

b. Anticipation plan of system function at D-1

At D-1, the system has a more precise forecast. This stage is very important as it can help to define energy production offer to the market Day D. In using the data of Day 1 (Fig. 14 and Table 4), the instructions are to be applied to the hydroelectric turbine (Fig. 16, full-filled line) and to the pump system (Fig. 16, dotted line).The energy exchanged with the network at Day D can be forecasted as in Fig. 17

c. Sensitivity to incertitude of anticipation plan

This exploitation program is the one engaged with the network. It has to be respected in spite of the forecast incertitude and the wind intermittency. In this section, we analyse this program's sensitivity to the wind production variation in order to predict the margin of operation and the actions in disturbance cases. This analysis is carried out based on the sensitivity analyse method previously presented in the section §6.1.c.

We suppose that the precision of the forecast of the average wind speed is ± 30% (cf.Fig. 18). The aim is to manage the system function in such a way that minimizes the power gap between the real exchanged power to the network and the forecasted one.

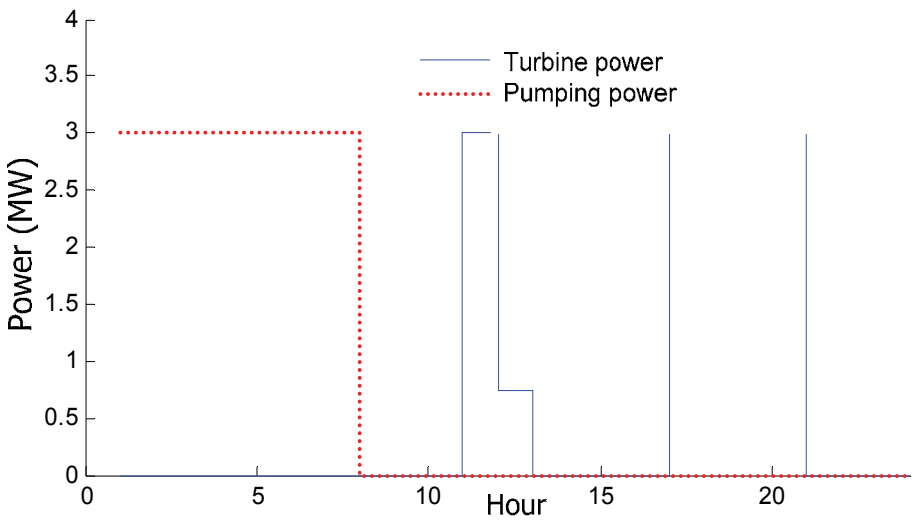

Fig. 16. Power thresholds for hydroelectric turbine and pump Day D

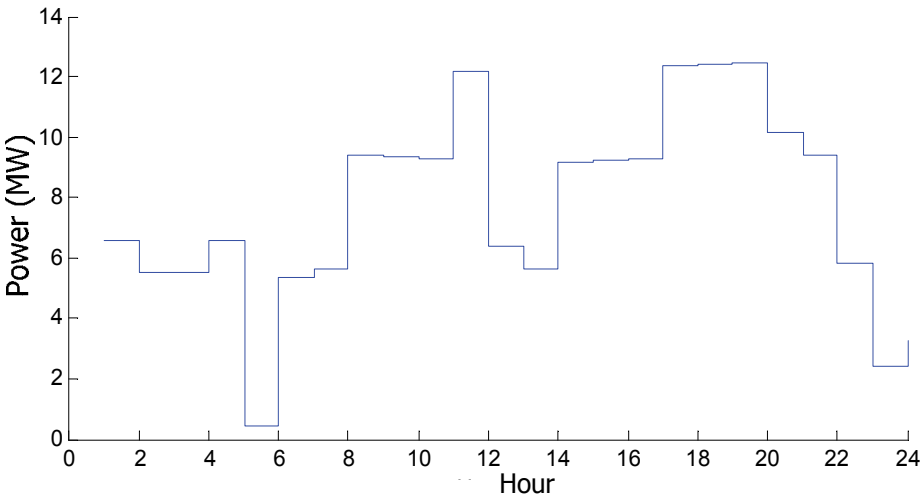

Fig. 17. Forecast of exchanged power to network at Day D

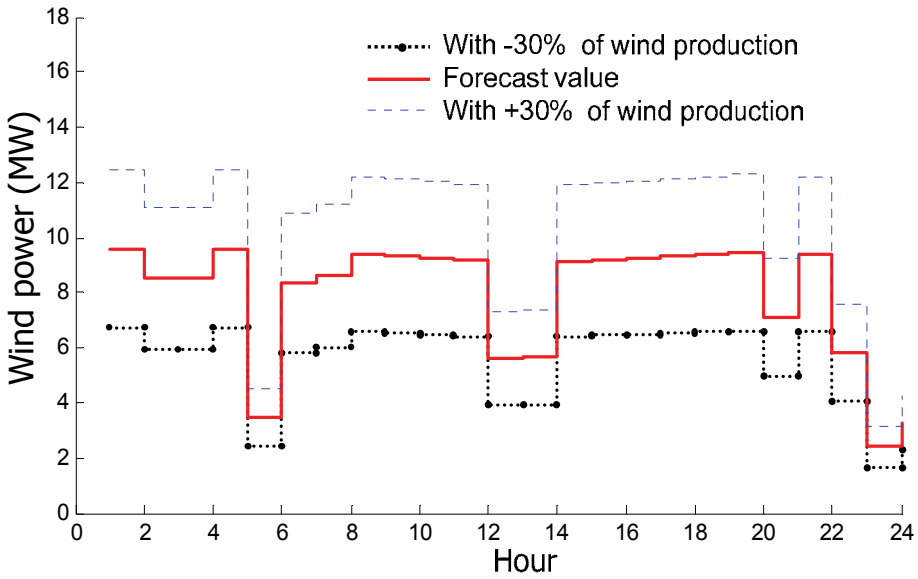

Fig. 18. Scenarios for wind power variation

When the produced wind power is lower than the forecasted one (Fig. 19, dotted line with mark "."), it is recommended to adjust the storage volume and the destocking plan. In order to best reduce the gap between the real and the projected exchanged power, more the wind production tends to decrease, more the storage volume for the day is big.

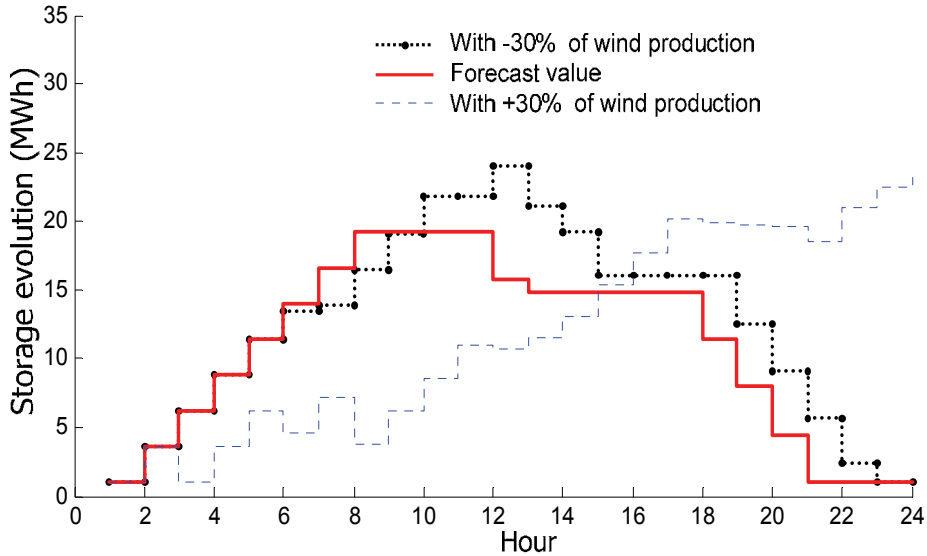

Fig. 19. Storage evolution in relation to produced wind power incertitude

When the wind production tends to increase, the wind generator can ensure the projected exchange power to the network. Note that the storage need is lower. At the end of the day, the storage level may be not equal to the initially expected level (Fig. 19, dotted line). In this way, the storage use plan for the next days is challenged. It is the responsibility of the wind power manager to decide whether the function plan has to be reviewed. The decision may be made in function of forecast data and the difference between the projected and real storage levels.

The injected power plans of the wind generator to the network are given in the Fig. 20 in 3 cases of wind production scenarios: with initially expected plan (Fig. 20, fulfilled line), with 30% more than expected (dotted line mark ".") and with 30% than expected (dotted line). The difference with the initial plan creates penalties.

The objective function's variation is showed in the as the difference between the energy sale benefit (paid by the network) and the penalties. The results are given in percentage compared to the expected power. It is interesting to see that with incertitude of about ±30% on the wind production, the objective function would vary only about 6%. That proves the interest of the proposed optimal management method.

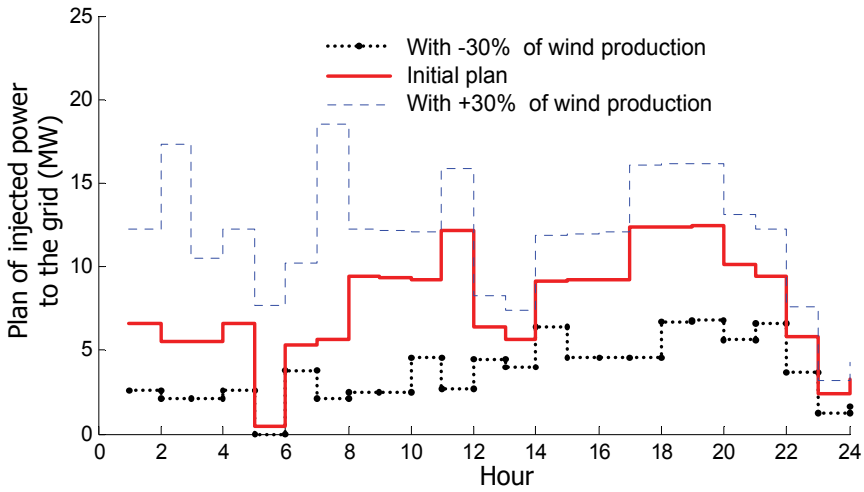

Fig. 20. Plan of injected power to the grid

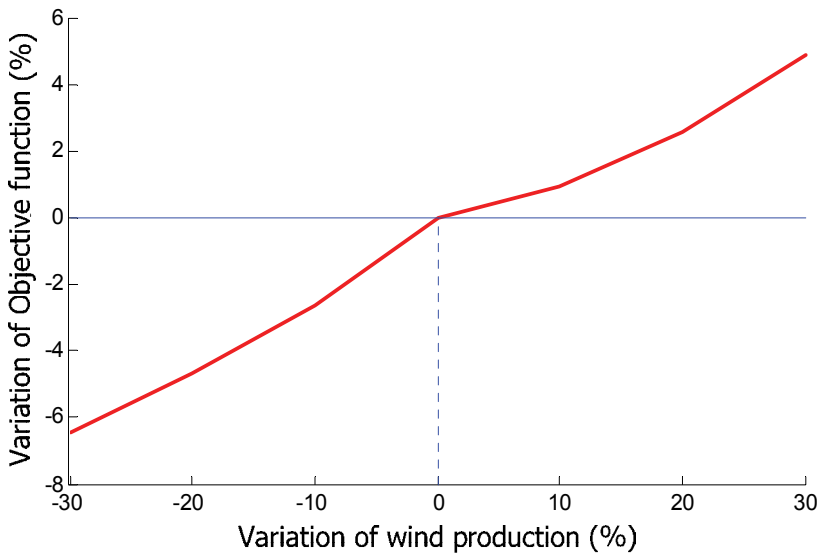

Fig. 21. Objective function's variation in relation to the produced wind power difference (with the expected value)

9.2 Reactive management in real-time

We are now J-Day and suppose that some disturbances occur during this day.

- At 5 a.m, a lack of power can be translated by an increasing penalty price for each MW that the W+S system does not provided to the network (from 26.51 €/MWh to 76.51 €/MWh).
- At 10 a.m, the wind production increases from 9.26 MW to 11.26 MW.
- At 3 p.m, to response to the network need to reduce injected power, the W+S system has to decrease its provided power from 9.84 MW to 7.84 MW.

The following graphics show the W+S system's behaviour under these conditions and the impact of these disturbances on the global result.

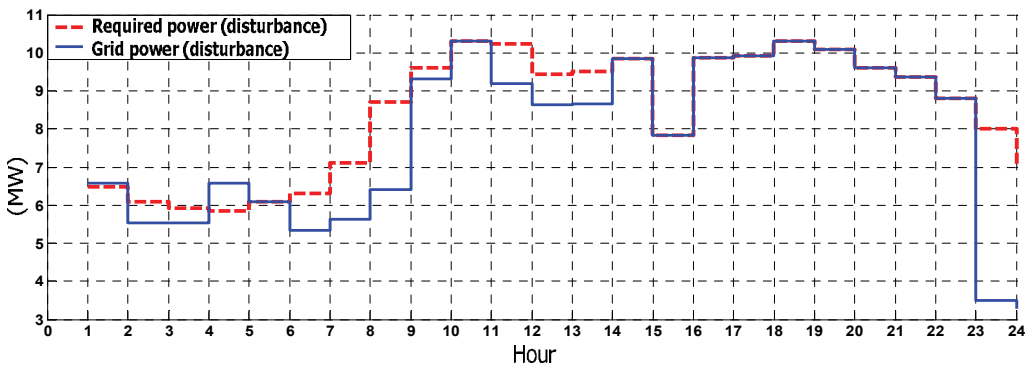

Fig. 22. Final required and exchanged power plan during disturbances

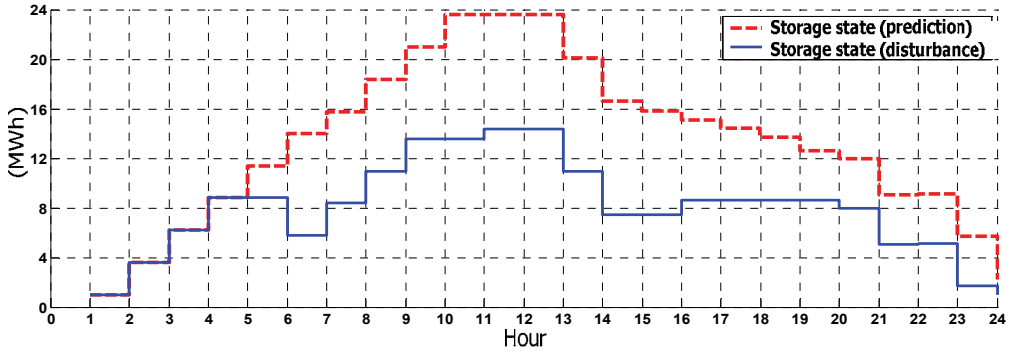

Fig. 23. Evolution of storage state

In order to face these events, new optimal operate plans are computed each time disturbances occurred.
A suitable response is proposed in order to manage several unpredicted events disturbing the system and the electrical network. The optimization response most suits in function of unpredictable constraints occurring. Concretely, the actual total penalty cost is equal to 1020 € per day instead of 2363 € per day without disturbances (cf. Table 5).

	Case I Maximal economic gains (in the case forecast - anticipation)	Case II Minimal power deviations (in the case disturbance – reactive management)
Total profits [€/day] (1)	5614	5352
Total penalty cost [€/day] (2)	2363	1020
Total net profit [€/day] (3) = (1) – (2)	3251	4332

Table 5. Simulations of profit and penalty cost considering two kinds of forecast and disturbances

The benefits of case II is lower than that of case I. But the penalty cost of case II represents only 43.17% of case I. But the net profit is higher in case II. In conclusion, it is more efficient to manage the reactive management of minimal power gaps is more efficient than the management by anticipation of maximal economic gains.

10. Conclusions

The development of an optimized management method of W+S systems was the main topic of this chapter. First, a thorough analysis of the W+S system parameters (intermittencies, dynamic, cost efficiency) has been implemented.
Then, bibliography on management methods of W+S systems has been carried on. The differences between the methods are mainly due to the applied conditions concerning the wind energy implementation. With support mechanisms, the objective is to maximize the benefits of the wind energy selling to the electrical network. This strategy allowed a

significant growth of the wind energy during the last years. But, with the increasing of wind energy growth rate a new management method of intermittencies is needed. Its objective is to minimize the impact of intermittencies on the power system.
The purpose of the management method dedicated to the optimal operation of a wind farm coupled to a storage system (W+S) which has been proposed in this chapter is its adaptation to the specific characteristics of the system in the new context of the wind energy implementation within the electrical network. The optimal management of the W+S exploitation reduces the impacts of intermittencies impacts and better controls the dynamic. Moreover, the economical rentability is preserved. The energy flow optimisation technique allows the supply of a power adapted to the electrical network requirements (network system services). This method is efficient with several disturbance sources such as wind speed intermittency, variable network requirements, penalty cost variability. This system is characterized by the intermittency of the primary source, and by the unpredictable behaviour of the electrical network. The proposed systems of control enable an efficiently operate system management with and without disturbances. In other words, the architecture of the management system is based on two driving levels: anticipative management and real time reactive management. Anticipation is a main step. Operate plan and W+S system involvement are determined by anticipation. The mathematic description which has been detailed is based on MLP algorithm which is used for optimisation problem and is seem to be adapted to such problem complexity being highly flexible and fast. Concerning the real time reactive management, its main role is to manage variation and intermittency impacts in real operating time. The optimisation management requires a robust and efficient algorithm. Also, a method of sensitivity analysis has been presented. This analysis gave us a methodological framework to evaluate the impacts of disturbances on the optimal operate system. By this way, the wind energy intermittency is treated on several time scales. Obtained results are based on a feasibility study case. This gives a global view of how operates the system.

11. References

[ANA-07] Anagnostopoulos J. S., Dimitris E. Papantonis, "*Pumping station design for a pumped-storage wind-hydro power plant*", School of Mechanical Engineering, National Technical University of Athens, Heroon Polytechniou 9, 15780 Zografou, Athens, Greece Available online 27 August 2007

[BEN-08] Benitez L. E., Benitez P. C., Cornelis V. K. G., "*The Economics of Wind Power with Energy Storage*", Energy Economics, Volume 30, Issue 4, July 2008, pp. 1973-1989.

[BUR-01] Burton T., Sharpe D., Jenkins N., Bossanyi E. (2001) "*Wind Energy Handbook*", John Wiley & Sons, Ltd/Inc., Chichester.

[CAS-03] Castronuovo E.D., Peças L. J. A., "Wind and small-hydro generation: An optimisation approach for daily integrated operation", Proceedings of the 2003 EWEC (European Wind Energy Conference). June 16–19, 2003, Madrid, Spain.

[CAS-04a] Castronuovo E.D., Peças L. J. A., "On the optimization of the daily operation of a wind-hydro power plant", IEEE Transactions on Power Systems, Volume 19, Issue 3, Aug. 2004, pp. 1599 – 1606

[CAS-04b] Castronuovo E.D., Peças L. J. A., "Bounding active power generation of a wind-hydro power plant", Proceedings of the PMAPS-2004 (8th. International Conference on Probabilistic Methods Applied to Power Systems). September 13-16, 2004, Ames, Iowa, USA.

[CAS-04c] Castronuovo E.D., Peças L. J. A., "Optimal operation and hydro storage sizing of a wind–hydro power plant", International Journal of Electrical Power & Energy Systems, Volume 26, Issue 10, December 2004, pp. 771-778.

[DWIA] Danish Wind Industry Association, http://guidedtour.windpower.org/fr/tour/wres/weibull.htm

[EC2007a] EU renewable energy policy, http://www.euractiv.com/en/energy/eu-renewable-energy-policy-linksdossier-188269

[EWE-09] European Wind Energy Association, "*The Economics of Wind Energy*", www.ewea.org, mars 2009

[GAR-06] Gary L. J. (2006), "*Wind Energy Systems*", Manhattan, KS

[GEN-05] Genc A., Erisoglu M., Pekgor A., Oturanc G., Hepbasli A., Ulgen K., "*Estimation of Wind Power Potential Using Weibull Distribution*", Energy Sources, Part A: Recovery, Utilization, and Environmental Effects, Volume 27, Issue 9 July 2005, pages 809 – 822

[GER-02] Gergaud O., "Modélisation énergétique et optimisation économique d'un système de production éolien et photovoltaïque couplé au réseau et associé à un accumulateur", Thèse de doctorat de l'Ecole Normale Supérieure de Cachan, Décembre 2002.

[HAL-01] Halldorsson K., Stenzel J. "*A scheduling strategy for a renewable power marketer*", Power Tech Proceedings, 2001 IEEE Porto Volume 1, 10-13 Sept. 2001, vol.1, pp. 6 pages.

[KAL-07] Kaldellis J.K., Zafirakis D.,"Optimum energy storage techniques for the improvement of renewable energy sources-based electricity generation economic efficiency", Energy Volume 32, Issue 12, December 2007, Pages 2295-2305

[MAG-03] Magnus K., Holen A. T., Hildrum R., "*Operation and sizing of energy storage for wind power plants in a market system*", International Journal of Electrical Power & Energy Systems, vol. 25, Issue 8, October 2003, pp. 599-606.

[MOM-01] Momoh J. A., "*Electric Power System Applications of Optimization*", CRC Press; 1 edition (January 15, 2001), 478 pages

[NGU-09] Nguyen Ngoc P.D., Pham T.T.H; Bacha S., Roye D. "*Optimal operation for a wind-hydro power plant to participate to ancillary services*", Industrial Technology, 2009. ICIT 2009. IEEE International Conference on Digital Object Identifier: 10.1109/ICIT.2009.4939699, Publication Year: 2009, pp. 5 pages

[RTE] Réseau de Transport d'Électricité, http://clients.rte-france.com/

[RTE-08] RTE2008: http://www.rte-france.com/fr/nous-connaitre/espace-esse/dossiers - de-presse/le-bilan-electrique-francais - 2008

[SAG-07] Saguan M., "L'analyse economique des architectures de marches electrique. Application au market design du "temps reel", Thèse de Doctorat de l' Université Paris-Sud 11, Avril 2007.

[SOM-03] Somaraki M., "*A Feasibility Study of a Combined Wind - Hydro Power Station in Greece*", a thesis submitted for the degree of Master in Science in "Energy Systems and the Environment", University of Strathclyde, Department of Mechanical Engineering, October 2003 - Glasgow

7

Intelligent Control of Wind Energy Conversion Systems

Abdel Aitouche[1] and Elkhatib Kamal[2]
[1]*Hautes Etudes d'Ingenieur, University Lille Nord*
[2]*Polytech-Lille, University Lille Nord*
France

1. Introduction

Wind turbines form complex nonlinear mechanical systems exposed to uncontrolled wind profiles. This makes turbine controller design a challenging task (Athanasius & Zhu, 2009). As such, control of wind energy conversion systems (WECS) is difficult due to the lack of systematic methods to identify requisite robust and sufficiently stable conditions, to guarantee performance. The problem becomes more complex when plant parameters become uncertain. Fuzzy control is one of the techniques which deal with this class of systems. The stability of fuzzy systems formed by a fuzzy plant model and a fuzzy controller has recently been investigated. Various stability conditions have been obtained through the employment of Lyapunov stability theory (Schegner & La Seta, 2004; Tripathy, 1997), fuzzy gain- scheduling controllers (Billy, 2011a, 2011b; Iescher et al., 2005), switching controllers (Lescher *et al.*, 2006) and by other methods (Chen & Hu, 2003; Kamal *et al.*, 2008; Muljadi & Edward, 2002). Nonlinear controllers (Boukhezzar & Siguerdidjane, 2009; Chedid *et al.*, 2000; Hee-Sang *et al.*, 2008) have also been proposed for the control of WECS represented by fuzzy models.

In addition to stability, robustness is also an important requirement to be considered in the study of uncertain nonlinear WECS control systems. Robustness in fuzzy-model-based control has been extensively studied, such as stability robustness versus modelling errors and other various control techniques for Takagi–Sugeno (TS) fuzzy models (Kamal *et al.*, 2010; Uhlen *et al.*, 1994).

In order to overcome nonlinearity and uncertainties, various schemes have been developed in the past two decades (Battista & Mantz, 2004; Boukhezzar & Siguerdidjane, 2010; Prats *et al.*, 2000; Sloth *et al.*, 2009). (Battista & Mantz, 2004) addressing problems of output power regulation in fixed-pitch variable-speed wind energy conversion systems with parameter uncertainties. The design of LMI-based robust controllers to control variable-speed, variable-pitch wind turbines, while taking into account parametric uncertainties in the aerodynamic model has been presented (Sloth *et al.*, 2009). (Boukhezzar & Siguerdidjane, 2010) comparing several linear and nonlinear control strategies, with the aim of improving wind energy conversion systems. (Prats *et al.*, 2000) have also investigated fuzzy logic controls to reduce uncertainties faced by classical control methods.

Furthermore, although the problem of control in the maximization of power generation in variable-speed wind energy conversion systems (VS-WECS) has been greatly studied, such

control still remains an active research area (Abo-Khalil & Dong-Choon, 2008; Aggarwal *et al.*, 2010; Barakati *et al.*, 2009; Camblong et al., 2006; Datta & Ranganathan, 2003; Galdi *et al.*, 2009; Hussien *et al.*, 2009; Iyasere et al., 2008; Koutroulis & Kalaitzakis, 2006; Mohamed et al., 2001; Prats *et al.*, 2002; Whei-Min. & Chih-Ming, 2010). (Abo-Khalil & Dong-Choon, 2008; Aggarwal *et al.*, 2010; Camblong *et al.*, 2006; Datta & Ranganathan, 2003; Whei-Min. & Chih-Ming, 2010) maximum power point tracking (MPPT) algorithms for wind turbine systems have been presented (Galdi *et al.*, 2009) as well as design methodology for TS fuzzy models. This design methodology is based on fuzzy clustering methods for partitioning the input-output space, combined with genetic algorithms (GA), and recursive least-squares (LS) optimization methods for model parameter adaptation. A maximum power tracking algorithm for wind turbine systems, including a matrix converter (MC) has been presented (Barakati *et al.*, 2009). A wind-generator (WG) maximum-power-point tracking (MPPT) system has also been presented (Koutroulis & Kalaitzakis, 2006), consisting of a high efficiency buck-type dc/dc converter and a microcontroller-based control unit running the MPPT function. An advanced maximum power-tracking controller of WECS (Mohamed *et al.*, 2001), achieved though the implementation of fuzzy logic control techniques, also appears promising. The input to the controller consists in the difference between the maximum output power from the WES and the output power from the asynchronous link and, the derivative of this difference. The output of the controller is thus the firing angle of the line-commutated inverter, which transfers the maximum tracked power to the utility grid. Fuzzy controllers also permit the increase of captured wind energy under low and high wind speeds (Prats *et al.*, 2002; Hussien *et al.*, 2009). The fuzzy controller is employed to regulate, indirectly, the power flow in the grid connected WECS by regulating the DC current flows in the interconnected DC link. Sufficiently stable conditions are expressed in terms of Linear Matrix inequalities (LMI). (Iyasere *et al.*, 2008) to maximize the energy captured by the wind turbine under low to medium wind speeds by tracking the desired pitch angle and rotor speed, when the wind turbine system nonlinearities structurally uncertain.

Concerning other studies, due to the strong requirements of the Wind Energy Field, fault tolerant control of variable speed wind turbine systems has received significant attention in recent years (Bennouna *et al.*, 2009; Gaillard *et al.*, 2007; Odgaard *et al.*, 2009; Ribrant, 2006; Wang *et al.*, 2010; Wei *et al.*, 2010). To maintain the function of closed-loop control during faults and system changes, it is necessary to generate information about changes in a supervision scheme. Therefore, the objective of Fault Tolerant Control (FTC) is to maintain current performances close to desirable performances and preserve stability conditions in the presence of component and/or instrument faults. FTC systems must have the ability to adjust off-nominal behaviour, which might occur during sensor, actuator, or other component faults. A residual based scheme has been presented (Wei *et al.*, 2010) to detect and accommodate faults in wind turbines. An observer based scheme (Odgaard *et al.*, 2009) has been proposed to detect and isolate sensor faults in wind turbine drive trains. A study of fault tolerant power converter topology (Gaillard *et al.*, 2007) and fault identification and compensation for a WECS with doubly fed induction generator (DFIG), has also been done. In addition, a survey on failures of wind turbine systems in Sweden, Finland and Germany (Ribrant, 2006), has been carried out, where the data are from real maintenance records over the last two decades. Robust fault tolerant controllers based on the two-frequency loop have also been designed (Wang *et al.*, 2010). The low-frequency-loop adopts a PI steady-state optimization control strategy, and the high-frequency-loop adopts a robust fault tolerant

control approach, thus ensuring the actuator part of the system during failure in normal operation. Fault signature analysis to detect errors in the DFIG of a wind turbine has again been presented (Bennouna *et al.*, 2009).

It is well known that observer based design is a very important problem in control systems. Since in many practical nonlinear control systems, state variables are often unavailable, output feedback or observer-based control is necessary and these aspects have received much interest. (Khedher *et al.*,2009, 2010; Odgaard *et al.*, 2009; Tong & Han-Hiong, 2002; Tong *et al.*, 2009 ; Wang *et al.*, 2008; Yong-Qi, 2009; Zhang *et al.*, 2009) fuzzy observer designs for TS fuzzy control systems have been studied, and prove that a state feedback controller and observer always result in a stabilizing output feedback controller, provided that the stabilizing property of the control and asymptotic convergence of the observer are guaranteed through the Lyapunov method. However, in the above output feedback fuzzy controllers, the parametric uncertainties for TS fuzzy control systems have not been considered. As such robustness of the closed-loop system may not be guaranteed.

In this chapter, a Robust Fuzzy Fault Tolerant control (RFFTC) algorithm is proposed for hybrid wind-diesel storage systems (HWDSS) with time-varying parameter uncertainties, sensor faults and state variable unavailability, and measurements based on the Takagi-Sugeno (TS) fuzzy model. Sufficient conditions are derived for robust stabilization in the sense of Lyapunov asymptotic stability and are formulated in the form of Linear Matrix Inequalities (LMIs). The proposed algorithm combines the advantages of:

- The capability of dealing with non-linear systems with parametric uncertainties and sensor faults;
- The powerful Linear Matrix Inequalities (LMIs) approach to obtain fuzzy fault tolerant controller gains and observer gains;
- The maximization of the power coefficient for variable pitch variable-speed wind energy conversion systems;
- In addition, reduction of voltage ripple and stabilization of the system over a wide range of sensor faults and parameter uncertainties is achieved.

Also in this chapter, a Fuzzy Proportional Integral Observer (FPIO) design is proposed to achieve fault estimation in TS fuzzy models with sensor faults and parameter uncertainties. Furthermore, based on the information of online fault estimation, an observer-based robust fuzzy fault tolerant controller is designed to compensate for the effects of faults and parameter uncertainties, by stabilizing the closed-loop system. Based on the aforementioned studies, the contributions of this chapter are manifold:

- A new algorithm for the estimation of time-varying process faults and parameter uncertainties in a class of WECS;
- And a composite fault tolerant controller to compensate for the effects of the faults, by stabilizing the closed-loop system in the presence of bounded time-varying sensor faults and parameter uncertainties.

This chapter is organized as follows. In section 2, the dynamic modelling of WECS and system descriptions is introduced. Section 3 describes the fuzzy plant model, the fuzzy observer and the reference model. In section 4, robust fuzzy fault tolerant algorithms are proposed, to close the feedback loop and the stability and robustness conditions for WECS are derived and formulated into nonlinear matrix inequality (general case) and linear matrix inequality (special case) problems. Section 5 presents the TS Fuzzy Description and Control structure for HWDSS. Section 6 summarizes the procedures for finding the robust fuzzy fault tolerant controller and fuzzy observer. In section 7 simulation results illustrate the

effectiveness of the proposed control methods for wind systems. In section 8, a conclusion is drawn.

2. WECS model and systems descriptions

2.1 The wind turbine characteristics

Variable Speed wind turbine has three main regions of operation as shown in Fig.1. (Galdi et al., 2009). The use of modern control strategies are not usually critical in region I, where the monitoring of the wind speed is performed to determine whether it lies within the specifications for turbine operation and if so, the routines necessary to start up the turbine are performed. Region II is the operational mode in which the goal is to capture as much power as possible from the wind. Region III is called rated wind speed. The control objectives on the full load area are based on the idea that the control system has to maintain the output power value to the nominal value of the generator. The torque at the turbine shaft neglecting losses in the drive train is given by (Iyasere *et al.*, 2008):

$$T_G = 0.5\pi C_t(\lambda,\beta) R^3 \rho v^2 \tag{1}$$

where T_G is the turbine mechanical torque, Where ρ is the air density (kg /m^3), R is the turbine radius (m),v is the wind velocity (m/s), and $C_t(\lambda,\beta)$ is the turbine torque coefficient. The power extracted from the wind can be expressed as (Galdi *et al.*, 2009) :

$$P_a = \omega_t T_G = 0.5 C_p(\lambda,\beta)\rho\pi R^2 v^3 \tag{2}$$

where $C_p(\lambda,\beta)$ is the rotor power coefficient defined by the following relation,

$$C_p(\lambda,\beta) = \lambda C_t(\lambda,\beta)$$

$$C_p(\lambda,\beta) = (0.44 - 0.0167\beta)\sin[\pi(\lambda-3)/15 - 0.3\beta] - 0.00184(\lambda-3)\beta \tag{3}$$

β is the pitch angle of rotor blades (rad) (β is constant for fixed pitch wind turbines), λ is the tip speed ratio (TSR) and is given by:

$$\lambda = R\omega_t / v \tag{4}$$

where ω_t is the rotor speed (rad/sec). It is seen that if the rotor speed is kept constant, then any change in the wind speed will change the tip-speed ratio, leading to the change of power coefficient C_p as well as the generated power out of the wind turbine. If, however, the rotor speed is adjusted according to the wind speed variation, then the tip-speed ratio can be maintained at an optimal point, which could yield maximum power output from the system. Referring to (3) optimal TSR λ_{opt} can be obtained as follow:

$$\lambda_{opt} = \left(\frac{15 - 0.3\beta}{\pi}\right)\cos^{-1}\left[\frac{0.00184\beta(15-0.3\beta)}{\pi(0.44-0.167\beta)}\right] + 3 \tag{5}$$

From (5) it is clear that λ_{opt} depends on β. The relationship of C_p versus λ, for different values of the pitch angle β, are shown in Fig 2. The maximum value of C_p ($C_{p(max)}$= 0.48) is achieved for β = 0º and for λ= 8. This particular value of λ is defined as the optimal value of TSR (λ_{opt}).Thus the maximum power captured from the wind is given by:

$$P_{a(\max)} = 0.5 C_{p(\max)}(\lambda_{opt}, \beta)\rho \pi R^2 v^3 \tag{6}$$

Normally, a variable speed wind turbine follows the $C_{p(max)}$ to capture the maximum power up to the rated speed by varying the rotor speed at ω_{opt} to keep the TSR at λ_{opt} .

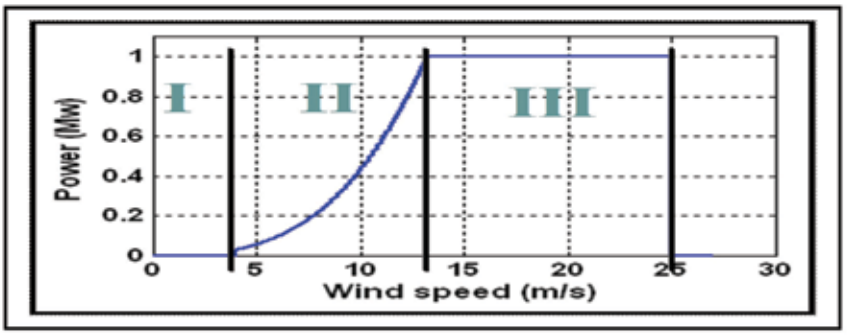

Fig. 1. Power-wind speed characteristics

2.2 WECS system description

A wind-battery hybrid system consists of a wind turbine coupled with a synchronous generator (SG),), a diesel-induction generator (IG) and a battery connected with a three-phase thyristor-bridge controlled current source converter. In the given system, the wind turbine drives the synchronous generator that operates in parallel with the storage battery system. When the wind-generator alone provides sufficient power for the load, the diesel engine is disconnected from the induction generator. The Power Electronic Interface (PEI) connecting the load to the main bus is used to fit the frequency of the power supplying the load as well as the voltage. Fig. 3 shows the overall structure of wind-battery system: E_{fd} is the excitation field voltage, f is the frequency, V_b is the bus voltage, C_a is the capacitor bank, V_c is the AC side voltage of the converter, and I_{ref} is the direct-current set point of the converter.

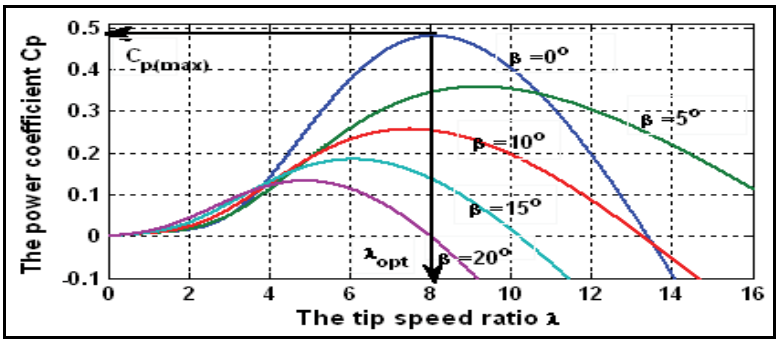

Fig. 2. Power coefficient C_p versus TSR λ

The dynamics of the system can be characterized by the following equations (Kamal et al., 2010):

$$\dot{x} = Ax(t) + Bu(t), \quad y = Cx(t) \quad , \tag{7}$$

where

$$x(\mathrm{t}) = [\mathrm{V_b} \quad \omega_s]^{\mathrm{T}}, \quad u(\mathrm{t}) = [\mathrm{E_{fd}} \quad I_{\mathrm{ref}}]^{\mathrm{T}},$$

$$A = \begin{bmatrix} 1 & 1 \\ 0 & 1 \end{bmatrix} \begin{bmatrix} \dfrac{L_f}{\tau' \omega_s L_{md}} & \dfrac{L_f}{\tau' \omega_s L_{md}}(L_d i_{sd} - \dfrac{r_a i_{sq}}{\omega_s}) \\ \dfrac{P_{ind} - P_{load}}{J_s \omega_s V_b} & -\dfrac{D_s}{J_s} \end{bmatrix} \quad B = \begin{bmatrix} 1 & -\dfrac{V_c}{\omega_s J_s} \\ 0 & -\dfrac{V_c}{\omega_s J_s} \end{bmatrix}, C = \begin{bmatrix} 1 & 0 \\ 0 & 1 \end{bmatrix}$$

where ω_s is the bus frequency (or angular speed of SG) J_s, D_s are the inertia and frictional damping of SG, i_{sd}, i_{sq} are the direct and quadrature current component of SG, L_d, L_f are the stator d-axis and rotor inductance of SG, L_{md} is the d-axis field mutual inductance, τ`is the transient open circuit time constant, r_a is the rotor resistance of SG, P_{ind} is the power of the induction generator, P_{load} is the power of the load. Equation (7) indicates that the matrices A and B are not fixed, but change as functions of state variables, thus making the model nonlinear. Also, this model is only used as a tool for controller design purposes.

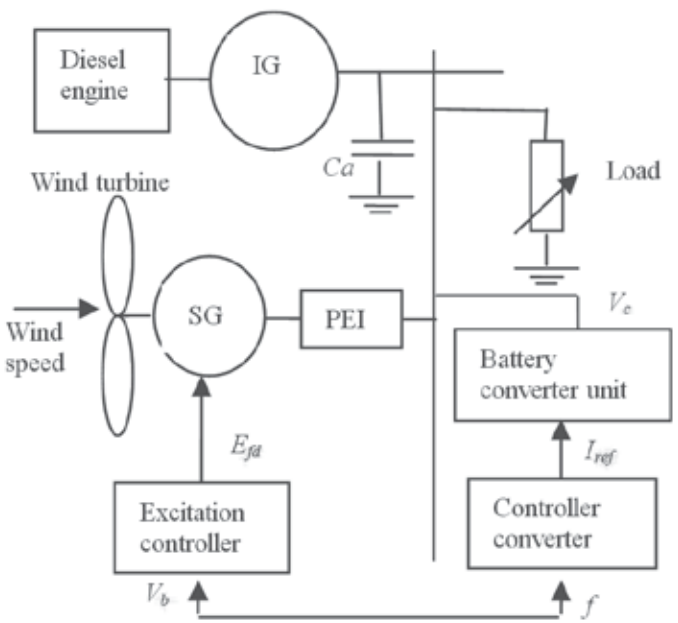

Fig. 3. Structural diagram of hybrid wind-diesel storage system

The used system parameters are shown in Table 1 (Chedid *et al.*, 2000; Kamal *et al.*, 2010).

Rated power	1 [MW]
Blade radius	37.38 [m]
Air density	0.55 [kg /m^3]
Rated wind speed	12.35 [m/s]
Blade pitch angle	0^o
Rated line ac voltage	230 [V]
AC rated current	138 [A]
DC rated current	239 [A]
Rated Load power	40 [kW]
The inertia of SG	1.11 [kg m^2]
Rated power of IG	55 [kW]
The inertia of the IG	1.40 [kg m^2]
Torsional damping	0.557 [Nm/ rad]
Rotor resistance of SG	0.96 [Ω]
Stator d-axis inductance of SG	2.03 [mH]
Rotor inductance of SG	2.07 [mH]
d-axis field mutual inductance	1.704 [mH]
The transient open circuit time constant	2.16 [ms]

Table 1. System parameters

3. Reference model, TS fuzzy plant model and fuzzy proportional-integral observer

3.1 Reference model

A reference model is a stable linear system without faults given by (Khedher et al., 2009, 2010),

$$\dot{\bar{x}}(t) = \mathrm{A}_r\,\bar{\mathrm{x}}(\mathrm{t}) + \mathrm{B}_r\mathrm{r}(\mathrm{t})\ ,\ \bar{y}(t) = C_r\bar{x}(t) \tag{8}$$

where $\bar{\mathrm{x}}(t) \in \kappa^{\mathrm{nx1}}$ is the state vector of reference model, $\mathrm{r}(t) \in \kappa^{\mathrm{nx1}}$ is the bounded reference input, $A_r \in \kappa^{\mathrm{nxn}}$ is the constant stable system matrix, $B_r \in \kappa^{\mathrm{nxn}}$ is the constant input matrix, $C_r \in \kappa^{\mathrm{gxn}}$ is the constant output matrix. $\bar{\mathrm{y}}(t) \in \kappa^{\mathrm{gx1}}$ is the reference output.

3.2 TS fuzzy plant model with parameter uncertainties and sensor faults

The continuous fuzzy dynamic model, proposed by TS, is described by fuzzy IF-THEN rules, which represent local linear input-output relations of nonlinear systems. Consider an uncertain nonlinear system that can be described by the following TS fuzzy model with parametric uncertainties and sensor faults (Khedher *et al.*, 2009, 2010; Tong & Han-Hiong, 2002). The i-th rule of this fuzzy model is given by:

Plant Rule *i*: $q_1(t)$ is N^i_1 AND … AND $q_\psi(t)$ is N^i_ψ
Then

$$\dot{x}(t) = (\mathrm{A_i} + \Delta\mathrm{A_i})\,\mathrm{x(t)} + \mathrm{B_i u(t)}\ ,$$

$$y(t) = C_i x(t) + \mathrm{E_i f(t)} \tag{9}$$

where N^i_Ω is a fuzzy set of rule *i*, $\Omega = 1,2,\ldots,\psi$, $i=1,2,\ldots,p$, $\mathrm{x}(t) \in \kappa^{\mathrm{nx1}}$ is the state vector, $\mathrm{u}(t) \in \kappa^{\mathrm{nx1}}$ is the input vector, $\mathrm{y}(t) \in \kappa^{\mathrm{gx1}}$ is the output vector, $\mathrm{f}(t) \in \kappa^{\mathrm{mx1}}$ represents the fault which is assumed to be bounded, $A_i \in \kappa^{\mathrm{nxn}}$ and $B_i \in \kappa^{\mathrm{nxn}}$, $C_i \in \kappa^{\mathrm{gxn}}$, $\mathrm{E_i}$ are system matrix, input matrix, output matrix and fault matrix, respectively, which are assumed to be known, $\Delta A_i \in \kappa^{\mathrm{nxn}}$ is the parameter uncertainties of A_i within known. It is supposed that the matrix E_i is of full column rank, i.e. rank(E_i)= *r*. It is assumed that the derivative of *f(t)* with respect to time is norm bounded, i.e. $\left\|\dot{\mathrm{f}}(t)\right\| \le f_1$ and $0 \le f_1 < \infty$ (Zhang *et al.*, 2009), *p* is the number of IF-THEN rules, and $q_1(t),\ldots, q_\psi(t)$ are the premise variables assumed measurable variables and do not depend on the sensor faults. The defuzzified output of (9) subject to sensor faults and parameter uncertainty is represented as follows (Khedher *et al.*, 2009, 2010; Tong & Han-Hiong, 2002):

$$\dot{x}(t) = \sum_{\mathrm{i=1}}^{\mathrm{p}} \mu_i(\mathrm{q(t)})[(\mathrm{A_i} + \Delta\mathrm{A_i})\mathrm{x(t)} + B_i \mathrm{U(t)}]\ ,$$

$$y(t) = \sum_{\mathrm{i=1}}^{\mathrm{p}} \mu_i(\mathrm{q(t)})[C_i \mathrm{x(t)} + \mathrm{E_i f(t)}] \tag{10}$$

where

$$h_i(q(t)) = \prod_{\alpha=1}^{\psi} N^i_\alpha(q(t))\ ,\ \mu_i(\mathrm{q(t)}) = h_i(q(t)) / \sum_{i=1}^{p} h_i(q(t))$$

Some basic properties of

$$h_i(q(t)) \ \text{ are } h_i(q(t)) \ge 0\ ,\ \sum_{\mathrm{i=1}}^{\mathrm{p}} h_i(q(t)) \ge 0$$

$$0 \le \mu_i(\mathrm{q(t)}) \le 1, \qquad \sum_{\mathrm{i=1}}^{\mathrm{p}} \mu_i(\mathrm{q(t)}) = 1 \quad \forall \mathrm{i} = 1,2,\ldots,\mathrm{p} \tag{11}$$

3.3 TS Fuzzy Proportional Integral Observer (FPIO)

Definition 1: If the pairs (A_i,C_i), $i=1, 2,\ldots,p$, are observable, the fuzzy system (10) is called locally observable (Xiao-Jun et al., 1998).
For the fuzzy observer design, it is assumed that the fuzzy system (10) is locally observable. First, the local state observers are designed as follows, based on the triplets (A_i,B_i,,C_i). In order to detect and estimate faults, the following fault estimation observer is constructed (Khedher *et al.*, 2009, 2010; Tong & Han-Hiong, 2002).

Observer Rule *i*: $q_1(t)$ is N^i_1 AND … AND $q_\psi(t)$ is N^i_ψ
Then

$$\dot{\hat{x}}(t) = A_i \hat{x}(t) + B_i u(t) + K_i (y(t) - \hat{y}(t)) ,$$

$$\dot{\hat{f}}(t) = L_i (y - \hat{y}) = L_i \tilde{y}$$

$$\hat{y}(t) = C_i \hat{x}(t) + E_i \hat{f}(t) \quad i=1, 2,\ldots,p \tag{12}$$

where K_i is the proportional observer gain for the i-th observer rule and L_i are their integral gains to be determined, $y(t)$ and $\hat{y}(t)$ are the final output of the fuzzy system and the fuzzy observer respectively. The defuzzified output of (12) subject to sensor faults is represented as follows:

$$\dot{\hat{x}}(t) = \sum_{i=1}^{p} \mu_i (q(t))[A_i \hat{x}(t) + B_i U(t) + K_i (y(t) - \hat{y}(t))]$$

$$\dot{\hat{f}}(t) = \sum_{i=1}^{p} \mu_i L_i (y - \hat{y}) = \sum_{i=1}^{p} \mu_i L_i \tilde{y}$$

$$\hat{y}(t) = \sum_{i=1}^{p} \mu_i (q(t))[C_i \hat{x}(t) + E_i \hat{f}(t)] \tag{13}$$

4. Proposed fuzzy fault tolerant algorithm and stability conditions

The goal is to design the control law $u(t)$ such that the system state $x(t)$ will follow those of a stable reference model of (8) in the presence of parametric uncertainties and sensor faults.

4.1 PDC technique

The concept of PDC in (Wang et al., 1996) is utilized to design fuzzy controllers to stabilize fuzzy system (10). For each rule, we can use linear control design techniques. The resulting overall fuzzy controller, which is nonlinear in general, is a fuzzy blending of each individual linear controller. The fuzzy controller shares the same fuzzy sets with the fuzzy system (10).

4.2 Proposed RFFTC controller

Definition 2: If the pairs (A_i, B_i), $i= 1, 2,\ldots, p$, are controllable, the fuzzy system (10) is called locally controllable (Xiao-Jun *et al.*, 1998).
For the fuzzy controller design, it is assumed that the fuzzy system (10) is locally controllable. First, the local state feedback controllers are designed as follows, based on the pairs (A_i,B_i). Using PDC the i-th rule of the fuzzy controller is of the following format:
Controller Rule i: $q_1(t)$ is N^i_1 AND … AND $q_\psi(t)$ is N^i_ψ

Then

$$u(t)=u_i(t) \tag{14}$$

where $u_i(t) \in \kappa^{nx1}$ is the output of the i-th rule controller that will be defined in the next sub-section. The global output of the fuzzy controller is given by

$$U(t) = \sum_{i=1}^{p} \mu_i(q(t))u_i(t) \tag{15}$$

From (10), (11) and (15), writing $\mu_i(q(t))$ as μ_i, we obtain

$$\dot{x}(t) = \sum_{i=1}^{p} \mu_i (A_i + \Delta A_i)\, x(t) + Bu_i]$$

$$y(t) = \sum_{i=1}^{p} \mu_i [C_i x(t) + Ef(t)] \tag{16}$$

where

$$B = \sum_{i=1}^{p} \mu_i B_i \text{ and } E = \sum_{i=1}^{p} \mu_i E_i \tag{17}$$

Note that B and E are known. Also from (11), (12) and (15), we have

$$\dot{\hat{x}}(t) = \sum_{i=1}^{p} \mu_i [A_i \hat{x}(t) + Bu_i(t) + K_i (y(t) - \hat{y}(t))]$$

$$\dot{\hat{f}}(t) = \sum_{i=1}^{p} \mu_i L_i (y - \hat{y}) = \sum_{i=1}^{p} \mu_i L_i \tilde{y}$$

$$\hat{y}(t) = \sum_{i=1}^{p} \mu_i [C_i \hat{x}(t) + E\hat{f}(t)] \tag{18}$$

4.3 Stability and robustness analyses for the proposed algorithm

We derived the stability and robustness conditions for a generalized class of WECS with sensor faults and parameter uncertainties described by (16).The main result is summarized in the following lemma 1 and theorem.

Lemma 1: The fuzzy control system of (16) subject to plant sensors faults and parameter uncertainties is guaranteed to be asymptotically stable, and its states will follow those of a stable reference model of (8) in the presence of bounded sensor faults and parameter uncertainties, if the following two conditions satisfy;

- Z is nonsingular. One sufficient condition to guarantee the nonsingularity of Z is that there exists P such that,

$$Z_i^T P + P Z_i < 0 \qquad \forall i \tag{19}$$

- The control laws of fuzzy controller of (15) are designed as, If $e_1(t) \neq 0$; When B is an invertible square matrix, the control law is given by

$$u_i(t) = Z^{-1} Z_{ui} \tag{20}$$

When B is not a square matrix, the control law is given by

$$u_i(t) = B^T Z^{-1} Z_{ui} \tag{21}$$

Where Z_{ui} is given by

$$Z_{ui} = \left\{ [\mathrm{He}_1(t) + \mathrm{A}_r \bar{\mathrm{x}}(t) + \mathrm{B}_r \mathrm{r}(t) - \frac{\mathrm{e}_1(t) \left\| \mathrm{e}_1(t) \right\| \left\| P_1 \right\| \left\| \Delta \mathrm{A}_i \right\|_{\max} \left\| \mathrm{x}(t) \right\|}{\mathrm{e}_1(t)^T P_1 \mathrm{e}_1(t)} \right.$$

$$\left. - \frac{\mathrm{e}_1(t) \left\| \mathrm{x}(t) \right\| \left\| D \right\|_{\max} \left\| \mathrm{x}(t) \right\|}{\mathrm{e}_1(t)^T P_1 \mathrm{e}_1(t)} - \mathrm{A}_i \mathrm{x}(t) - \frac{1}{2} \frac{\mathrm{e}_1(t) \left\| \hat{\mathrm{f}}(t) \right\| \left\| S_{\mathrm{E}} \right\|_{\max} \left\| \hat{\mathrm{f}}(t) \right\|}{\mathrm{e}_1(t)^T P_1 \mathrm{e}_1(t)} + \mathrm{S}\hat{\mathrm{f}}(t) \right\} \tag{22}$$

If $\mathrm{e}_1(t) = 0$

$$u_i(t) = Z^{-1} \left\{ \mathrm{A}_r \bar{\mathrm{x}}(t) + \mathrm{B}_r \mathrm{r}(t) - \mathrm{A}_i \mathrm{x}(t) + \mathrm{S}\hat{\mathrm{f}}(t) \right\} \; ; \; u_i(t) = B^T Z^{-1} \left\{ \mathrm{A}_r \bar{\mathrm{x}}(t) + \mathrm{B}_r \mathrm{r}(t) - \mathrm{A}_i \mathrm{x}(t) + \mathrm{S}\hat{\mathrm{f}}(t) \right\} \tag{23}$$

where $Z = B$ if B is an invertible square matrix or $Z = BB^T$ if B is not a square matrix, $\left\| \cdot \right\|$ denotes the l_2 norm for vectors and l_2 induced norm for matrices, $\left\| S_{\mathrm{E}} \right\| \le \left\| S_{\mathrm{E}} \right\|_{\max}$, $\left\| \Delta \mathrm{A}_i \right\| \le \left\| \Delta \mathrm{A}_i \right\|_{\max}$ and $\left\| D \right\| \le \left\| D \right\|_{\max}$, $H \in \kappa^{\mathrm{nxn}}$ is a stable matrix to be designed and choosing S so that $S = E$ and $S_{\mathrm{E}} = S^T S$, $\mathrm{D} = \mathrm{B}_{\mathrm{ai}}^{\mathrm{T}} \mathrm{B}_{\mathrm{ai}}$.

Theorem: If there exist symmetric and positive definite matrices P_{11}, P_{22}, some matrices K_i and L_i ,and matrices X_i , Y_i, such that the following LMIs are satisfied, then the TS fuzzy system (16) is asymptotically stabilizable via the TS fuzzy model based output-feedback controller (15) ,(20) and(21)

$$A_i^T \mathrm{P}_{11} + \mathrm{P}_{11} A_i - (Y_i C_i)^T - Y_i C_i + \mathrm{P}_{11} \mathrm{P}_{11} < -\delta I \tag{24}$$

$$(\mathrm{X}_{\mathrm{i}} E)^{T} + \mathrm{X}_{\mathrm{i}} E + P_{22} P_{22} < -\delta I \tag{25}$$

Proof. Before proceeding, we recall the following matrix inequality, which will be needed throughout the proof.

Lemma 2(Xie, 1996): Given constant matrices W and O appropriate dimensions for $\forall \varepsilon > 0$, the following inequality holds:

$$\mathrm{W}^{\mathrm{T}}\mathrm{O} + O^{T} W \le \varepsilon W^{T} W + \varepsilon^{-1} O^{T} O$$

Let

$$\mathrm{e}_{1}(\mathrm{t}) = \mathrm{x}(\mathrm{t}) - \bar{\mathrm{x}}(\mathrm{t}) \tag{26}$$

$$\mathrm{e}_{2}(\mathrm{t}) = \mathrm{x}(\mathrm{t}) - \hat{\mathrm{x}}(\mathrm{t}) \quad , \quad \tilde{\mathrm{f}}(\mathrm{t}) = \mathrm{f}(\mathrm{t}) - \hat{\mathrm{f}}(\mathrm{t}) \tag{27}$$

The dynamic of $e_1(t)$ is given by $\dot{\mathrm{e}}_{1}(\mathrm{t}) = \dot{\mathrm{x}}(\mathrm{t}) - \dot{\bar{\mathrm{x}}}(\mathrm{t})$

$$\dot{\mathrm{e}}_{1}(\mathrm{t}) = \sum_{\mathrm{i}=1}^{\mathrm{p}} \mu_{i}[(\mathrm{A}_{\mathrm{i}} + \Delta\mathrm{A}_{\mathrm{i}})\,\mathrm{x}(\mathrm{t}) + B\,u_{i}(\mathrm{t}) - \mathrm{A}_{\mathrm{r}}\,\bar{\mathrm{x}}(\mathrm{t}) - \mathrm{B}_{\mathrm{r}}\mathrm{r}(\mathrm{t})] \tag{28}$$

The dynamic of $e_2(t)$ is expressed as follow:

$$\dot{e}_{2}(t) = \sum_{i=1}^{p} \mu_{i}[(\mathrm{A}_{\mathrm{i}} - \mathrm{K}_{\mathrm{i}}\mathrm{C}_{\mathrm{i}})\mathrm{e}_{2}(\mathrm{t}) - \mathrm{K}_{\mathrm{i}}\mathrm{E}\tilde{\mathrm{f}}(\mathrm{t}) + \Delta\mathrm{A}_{\mathrm{i}}\,\mathrm{x}(\mathrm{t})] \tag{29}$$

The dynamics of the fault error estimation can be written: $\dot{\tilde{\mathrm{f}}}(\mathrm{t}) = \dot{\mathrm{f}}(\mathrm{t}) - \dot{\hat{\mathrm{f}}}(\mathrm{t})$. The assumption that the fault signal is constant over the time is restrictive, but in many practical situations where the faults are time-varying signals. So, we consider time-varying faults rather than constants faults; then the derivative of $\tilde{\mathrm{f}}(\mathrm{t})$ with respect to time is

$$\dot{\tilde{\mathrm{f}}}(\mathrm{t}) = \dot{\mathrm{f}}(\mathrm{t}) - \dot{\hat{\mathrm{f}}}(\mathrm{t}) = \dot{\mathrm{f}}(\mathrm{t}) - \sum_{i=1}^{p} \mu_{i}[\mathrm{L}_{\mathrm{i}}\mathrm{C}_{\mathrm{i}}\mathrm{e}_{2}(\mathrm{t}) + \mathrm{L}_{\mathrm{i}}\mathrm{E}\tilde{\mathrm{f}}(\mathrm{t})] \tag{30}$$

From (29) and (30), one can obtain:

$$\dot{\phi} = \mathrm{A}_{o}\phi + B_{o}\dot{\mathrm{f}}(\mathrm{t}) + \mathrm{B}_{\mathrm{a}}\,x(t) \tag{31}$$

$$\text{with } \phi = \begin{bmatrix} e_{2}(t) \\ \tilde{\mathrm{f}}(\mathrm{t}) \end{bmatrix}, B_{o} = \begin{bmatrix} 0 \\ \mathrm{I} \end{bmatrix}, A_{o} = \sum_{i=1}^{p} \mu_{i} A_{oi}, B_{a} = \sum_{i=1}^{p} \mu_{i} B_{ai}, \text{where}$$

$$\mathrm{A}_{\mathrm{oi}} = \begin{bmatrix} A_{i} - K_{i}C_{i} & -K_{i}E \\ -L_{i}C_{i} & -L_{i}E \end{bmatrix}, \mathrm{B}_{\mathrm{ai}} = \begin{bmatrix} \Delta A_{i} \\ 0 \end{bmatrix}$$

Consider the Lyapunov function candidate

$$V(e_1(t),\phi(t)) = \frac{1}{2} e_1(t)^T P_1 e_1(t) + \frac{1}{2}\phi(t)^T P_2 \phi(t) \tag{32}$$

where P_1 and P_2 are time-invariant, symmetric and positive definite matrices. Let

$$V_1(e_1) = \frac{1}{2} e_1(t)^T P_1 e_1(t) \ , \ V_2(\phi) = \frac{1}{2}\phi(t)^T P_2 \phi(t) \tag{33}$$

The time derivative of $V_1(e_1(t))$is

$$\dot{V}_1(e_1(t)) = \frac{1}{2}\dot{e}_1(t)^T P_1 e_1(t) + \frac{1}{2} e_1(t)^T P_1 \dot{e}_1(t) \tag{34}$$

By substituting (28) into (34) yields

$$\dot{V}_1 = \frac{1}{2}\left\{ \sum_{i=1}^{p} \mu_i [(A_i + \Delta A_i)x(t) + B u_i(t) - A_r \bar{x}(t) - B_r r(t)] \right\}^T P_1 e_1(t)$$

$$+ \frac{1}{2} e_1(t)^T P_1 \left\{ \sum_{i=1}^{p} \mu_i [(A_i + \Delta A_i)x(t) + B u_i(t) - A_r \bar{x}(t) - B_r r(t)] \right\} \tag{35}$$

we design $u_i(t)$, $i=1,2,\ldots,p$ as follows,

- When B is an invertible square matrix, the control law is given by

$$u_i(t) = Z^{-1} Z_{ui} \tag{36}$$

- When B is not a square matrix, the control law is given by

$$u_i(t) = B^T Z^{-1} Z_{ui} \tag{37}$$

where Z_{ui} is given from (22). A block diagram of the closed-loop system is shown in Fig.4. It is assumed that Z^{-1} exists (Z is nonsingular). In the latter part of this section, we shall provide a way to check if the assumption is valid. From (35), (36) or (37) and assuming that $e_1(t) \neq 0$ and using Lemma 2, one obtain

$$\dot{V}_1 = \frac{1}{2} e_1(t)^T (H^T P_1 + P_1 H + P_1 P_1) e_1(t) + \frac{1}{2}\sum_{i=1}^{p} \mu_i \left\| e_1(t) \right\| \left\| P_1 \right\| (\left\| \Delta A_i \right\| - \left\| \Delta A_i \right\|_{\max}) \left\| x(t) \right\|$$

$$+ \frac{1}{2} (\left\| \hat{f}(t) \right\| (\left\| S_E \right\| - \left\| S_E \right\|_{\max}) \left\| \hat{f}(t) \right\| - \left\| x(t) \right\| \left\| D \right\|_{\max} \left\| x(t) \right\|) \tag{38}$$

The time derivative of $V_2(\phi(t))$ is

$$\dot{V}_2(\phi(t)) = \frac{1}{2}\dot{\phi}(t)^{\mathrm{T}} P_2 \phi(t) + \frac{1}{2}\phi(t)^{\mathrm{T}} P_2 \dot{\phi}(t) \tag{39}$$

By substituting (31) into (39) yields

$$\dot{V}_2(\phi(t)) = \frac{1}{2}\sum_{i=1}^{p}\mu_i \phi(t)^{\mathrm{T}}(A_{oi}^T P_2 + P_2 A_{oi})\phi(t) + \frac{1}{2}\sum_{i=1}^{p}\mu_i[\dot{f}(t)^{\mathrm{T}} B_o^{\mathrm{T}} P_2 \phi(t) + \phi(t)^{\mathrm{T}} P_2 B_o \dot{f}(t)]$$

$$+ \frac{1}{2}\sum_{i=1}^{p}\mu_i[x(t)^{\mathrm{T}} B_{ai}^T P_2 \phi(t) + \phi(t)^{\mathrm{T}} P_2 B_{ai} x(t)] \tag{40}$$

Using Lemma 2 and the definition (Billy, E. (2011)) $\dot{f}(t)^{\mathrm{T}} B_o^{\mathrm{T}} B\dot{f}(t) = f_1^2 \lambda_{\max}(B_o^{\mathrm{T}} B_o)$, one obtain

$$\dot{V}_2(\phi(t)) = \frac{1}{2}\sum_{i=1}^{p}\mu_i \phi(t)^{\mathrm{T}}(A_{oi}^T P_2 + P_2 A_{oi} + P_2 P_2)\phi(t) + \frac{1}{2} f_1^2 \lambda_{\max}(B_o^{\mathrm{T}} B_o) + \frac{1}{2} x(t)^{\mathrm{T}} D x(t) \tag{41}$$

where $\lambda_{\max}(\bullet)$ denotes the largest eigen value. Combining (38) with (41), the time derivative of V can be expressed as

$$\dot{V}(e_1(t), \phi(t)) \le -\frac{1}{2} e_1(t)^{\mathrm{T}} Q_1 e_1(t) - \phi(t)^{\mathrm{T}} Q_2 \phi(t) + \frac{1}{2}\left\|\hat{f}(t)\right\|\left(\left\|S_{\mathrm{E}}\right\| - \left\|S_{\mathrm{E}}\right\|_{\max}\right)\left\|\hat{f}(t)\right\|$$

$$+ \sum_{i=1}^{p}\mu_i \left\|e_1(t)\right\|\left\|P_1\right\|\left(\left\|\Delta A_i\right\| - \left\|\Delta A_i\right\|_{\max}\right)\left\|x(t)\right\| + \left\|x(t)\right\|\left(\left\|D\right\| - \left\|D\right\|_{\max}\right)\left\|x(t)\right\| \tag{42}$$

where $Q_2 = -(A_{oi}^T P_2 + P_2 A_{oi} + P_2 P_2 + \delta)$, $Q_1 = -(H^{\mathrm{T}} P_1 + P_1 H + P_1 P_1)$ are a symmetric positive definite matrix, where $\delta = 0.5 f_1^2 \lambda_{\max}(B_o^{\mathrm{T}} B_o)$, as $\left\|S_E\right\| - \left\|S_E\right\|_{\max} \le 0$, $\left\|\Delta A_i\right\| \le \left\|\Delta A_i\right\|_{\max}$, $\left\|D\right\| \le \left\|D\right\|_{\max}$, from (42), we have

$$\dot{V}(e_1(t), \phi(t)) \le -\frac{1}{2} e_1(t)^{\mathrm{T}} Q_1 e_1(t) - \phi(t)^{\mathrm{T}} Q_2 \phi(t) \tag{43}$$

e_1 and ϕ converges to zero if $\dot{V} < 0$. $\dot{V} < 0$ if there exists a common positive definite matrix P_1 and P_2 such that

$$H^{\mathrm{T}} P_1 + P_1 H + P_1 P_1 < 0 \tag{44}$$

$$A_{oi}^{\mathrm{T}} P_2 + P_2 A_{oi} + P_2 P_2 < -\delta I \qquad i=1,2,\ldots,p \tag{45}$$

From (43) , (44) and (45)

$$\dot{V} \le -\frac{1}{2} e_1(\mathrm{t})^{\mathrm{T}} Q_1 e_1(\mathrm{t}) - \phi(\mathrm{t})^{\mathrm{T}} Q_2 \phi(\mathrm{t}) \le 0 \tag{46}$$

If the time derivative of (32) is negative uniformly for all $e_1(t), \phi(t)$ and for all $t \ge 0$ except at $e_1(t) = 0, \phi(t) = 0$ then the controlled fuzzy system (16) is asymptotically stable about its zero equilibrium. Since each sum of the equation in (46) is negative definite, respectively, then the controlled TS fuzzy system is asymptotically stable. According to the (45), the most important step in designing the fuzzy observer based fuzzy controller is the solution of (45) for a common $P_2 = P_2^T$, a suitable set of observer gains K_i and L_i ($i = 1,2,\ldots,p$). Equation (45) forms a set of bilinear matrix inequalities (BMI's). The BMI in (45) should be transformed into pure LMI as follows:

1. For the convenience of design, assume $P_2 = diag(P_{11}, P_{22})$
2. This choice is suitable for simplifying the design of fuzzy observer. Define M as in (47) and apply congruence transformation (i.e. multiply both side of inequality (45) by M (Tuan et al., 2001).

$$M = \begin{bmatrix} M_{11} & 0 \\ 0 & I \end{bmatrix} = \begin{bmatrix} P_{11}^{-1} & 0 \\ 0 & I \end{bmatrix} \tag{47}$$

   where $M_{11} = P_{11}^{-1}$
3. With $Y_i = P_{11} K_i$ and $X_i = -P_{22} L_i$, apply the change of variables. Since four parameters P_{11}, P_{22}, K_i and L_i should be determined from (45) after applying the above mentioned procedures which results in the LMI's conditions (24) and (25).

The inequalities in (24) and (25) are linear matrix inequality feasibility problems (LMIP's) in P_{11}, P_{22}, Y_j and X_i which can be solved very efficiently by the convex optimization technique such as interior point algorithm (Boyd et al., 1994). Software packages such as LMI optimization toolbox in Matlab (Gahinet et al., 1995) have been developed for this purpose and can be employed to easily solve the LMIP. By solving (24) and (25) the observer gain (K_i and L_i) can be easily determined.

In the following, we shall derive a sufficient condition to check the existence of Z^{-1}. From (17), and considering the following dynamics system,

$$\dot{\theta}(t) = Z\theta(t) = \sum_{i=1}^{p} \mu_i Z_i \theta(t) \tag{48}$$

Consider the following Lyapunov function

$$V_z = \theta(\mathrm{t})^{\mathrm{T}} \mathrm{P} \theta(\mathrm{t}) \tag{49}$$

where $P \in \kappa^{nxn}$ is a symmetric positive definite matrix. The time derivative of V_z is

$$\dot{V}_z = \dot{\theta}(t)^T P\theta(t) + \theta(t)^T P\dot{\theta}(t) \tag{50}$$

By substituting (48) into (50) yields

$$\dot{V} = -\sum_{i=1}^{p} \mu_i \theta(t)^T Q_{zi} \theta(t) \tag{51}$$

where $Q_{zi} = -(Z_i^T P + PZ_i)$. If $Z_i^T P + PZ_i < 0 \ \forall i$, then from (51), we have,

$$\dot{V}_z = -\frac{1}{2}\sum_{i=1}^{p} \mu_i \theta(t)^T Q_{zi} \theta(t) \le 0 \tag{52}$$

From (52), the nonlinear system of (48) is then asymptotically stable and Z^{-1} exists if there exist $Z_i^T P + PZ_i < 0 \ \forall i$

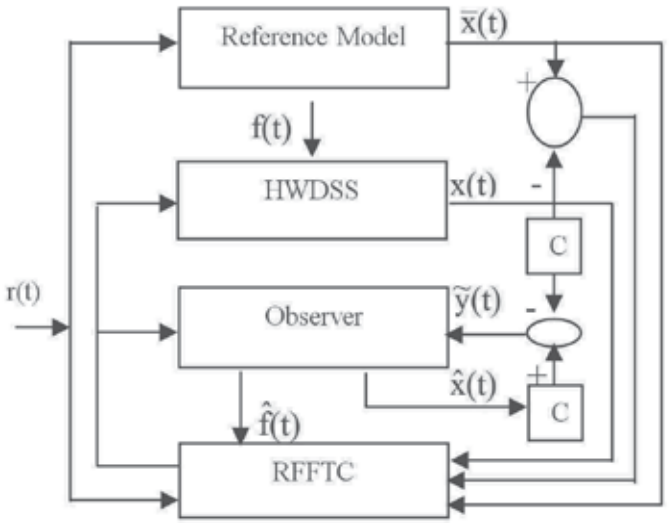

Fig. 4. Block diagram of RFFTC scheme

5. TS Fuzzy description and control structure

5.1 Control structure

Fig. 5 depicts the input and output relationship of the wind-battery system from the control point of view. The control inputs are the excitation field voltage (E_{fd}) of the SG and the direct-current set point (I_{ref}) of the converter. The measurements are the voltage amplitude (V_b) and the frequency (f) of the AC bus. The wind speed (v) and the load (v_1) are considered

to be disturbances. The wind turbine generator and the battery-converter unit run in parallel, serving the load. From the control point of view, this is a coupled 2×2 multi-input-multi-output nonlinear system.

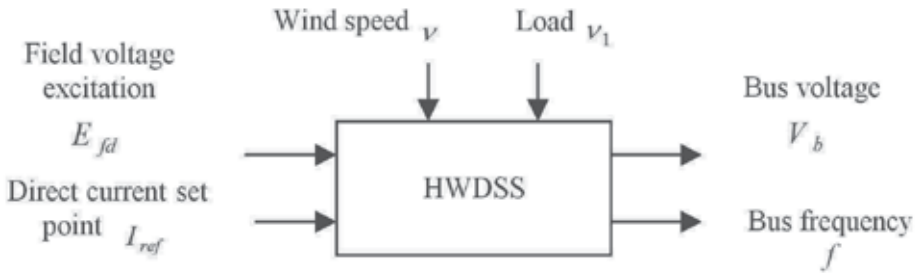

Fig. 5. The HWDSS control system

5.2 TS Fuzzy WECS description

To design the fuzzy fault tolerant controller and the fuzzy observer, we must have a fuzzy model that represents the dynamics of the nonlinear plant. The TS fuzzy model that approximates the dynamics of the nonlinear HWDSS plant (7) can be represented by the following four-rule fuzzy model. Referring to (10) the fuzzy plant model given by:

$$\dot{x}(t) = \sum_{i=1}^{4} h_i [(A_i + \Delta A_i)\, x(t) + B_i\, u(t)]$$

$$y(t) = \sum_{i=1}^{4} \mu_i [C_i x(t) + E_i f(t)] \tag{53}$$

where $x(t) \in \kappa^{2x1}$, $u(t) \in \kappa^{2x1}$ are the state vectors and the control input, respectively. For each sub-space, different model $(i = 1,2,3,4)$ and $(p = 4)$ is applied. The degree of membership function for states V_b and ω_s is depicted in Fig.6. Where

$$A_g = \begin{bmatrix} -0.006 & 1.213 \\ 0 & -0.002 \end{bmatrix}, \quad A_j = \begin{bmatrix} -0.0063 & 1.207 \\ 0 & -0.002 \end{bmatrix}, \quad B_g = \begin{bmatrix} 1 & -0.5808 \\ 0 & -0.5808 \end{bmatrix},$$

$$B_j = \begin{bmatrix} 1 & -0.5979 \\ 0 & -0.5979 \end{bmatrix}, \quad E_g = E_j = E = \begin{bmatrix} 10 & 1 \\ 0.1 & 0.01 \end{bmatrix} \qquad g=1,2 \text{ and } j=3,4$$

ΔA_i represent the system parameters uncertainties but bounded, the elements of ΔA_i randomly achieve the values within 40% of their nominal values corresponding to A_i, $\Delta B_i = 0$ (i=1,2,3,4), and the faults $f(t)$ are modeled as follow:

$$f_1(t) = \begin{cases} 0 & t < 20.75 \sec \\ 5.9 \sin(\pi t) & t \geq 20.75 \sec \end{cases}, \quad f_2(t) = \begin{cases} 0 & t \leq 20.75 \sec \\ 1 & t \geq 20.75 \sec \end{cases} \tag{54}$$

where $f_1(t)$ is the bus voltage sensor fault and $f_2(t)$ is the generator speed sensor fault.

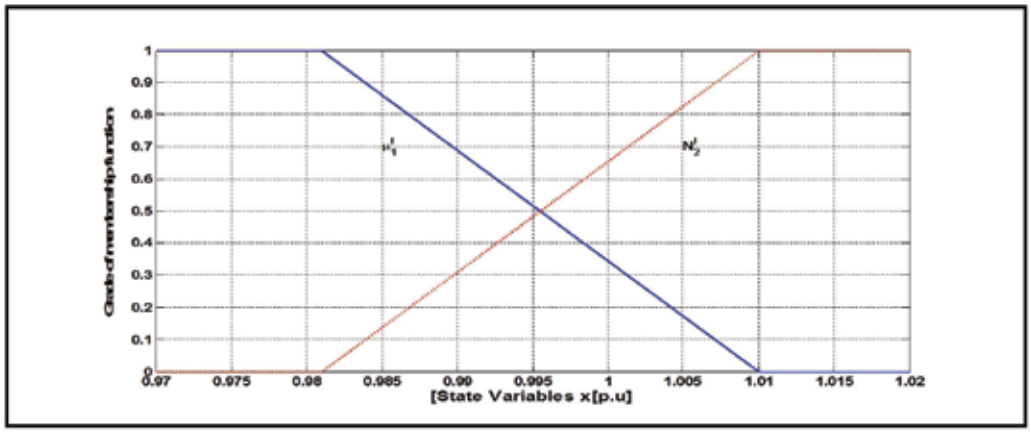

Fig. 6. Membership functions of states ω_s and V_b

6. Procedures for finding the robust fuzzy fault tolerant controller and fuzzy observer

According to the analysis above, the procedure for finding the proposed fuzzy fault tolerant controller and the fuzzy observer summarized as follows.

1. Obtain the mathematical model of the HWDSS to be controlled.
2. Obtain the fuzzy plant model for the system stated in step (1) by means of a fuzzy modeling method.
3. Check if there exists Z^{-1} by finding P according to Lemma 1. If P cannot be found, the design fails. P can be found by using some existing LMI tools.
4. Choose a stable reference model.
5. Solve LMIs (24) and (25) to obtain X_i , Y_i , P_{11}, P_{22}, K_i and L_i thus ($K_i = P_{11}^{-1} Yi$ and $L_i = -P_{22}^{-1} X_i$).
6. Construct fuzzy observer (12) according to the theorem and fuzzy controller (14) controller according to the Lemma 1.

7. Simulation studies

The simulations are performed on a simulation model of hybrid wind-diesel storage system (7). The proposed Fuzzy Fault Tolerant controller for the HWDSS is tested for two cases. The proposed controller is tested for random variation of wind speed signal as shown in Fig.7 to prove the effectiveness of the proposed algorithm. The reference input ($r(t)=\omega_{t(opt)}=v\lambda_{opt}/R$) is applied to the reference model and the controller to obtain the maximum power coefficient from the wind energy.

7.1 System responses of the fuzzy control system without and with parameter uncertainties

Fig. 8 shows the HWDSS responses of the fuzzy control system without (solid lines) and with parameter uncertainties (dash lines), and the reference model (dotted lines) under $r(t)$.

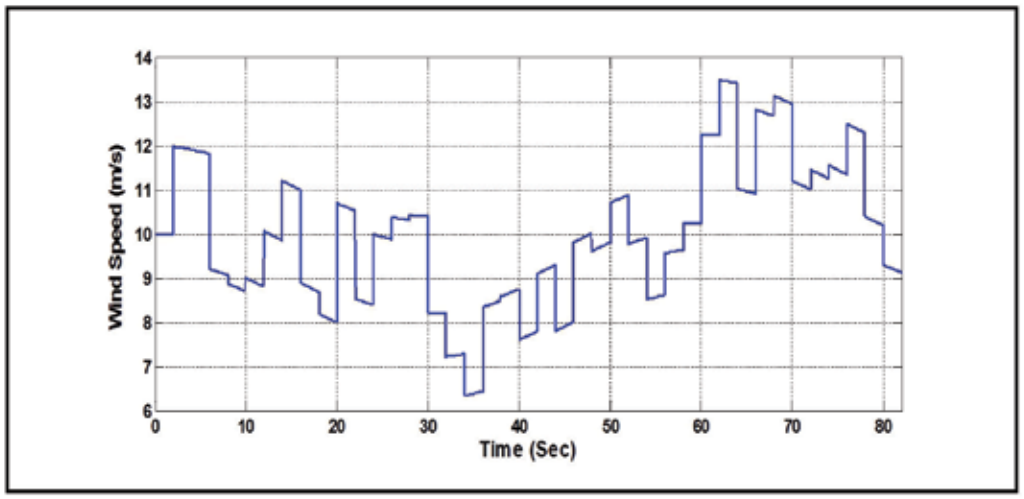

Fig. 7. Wind speed

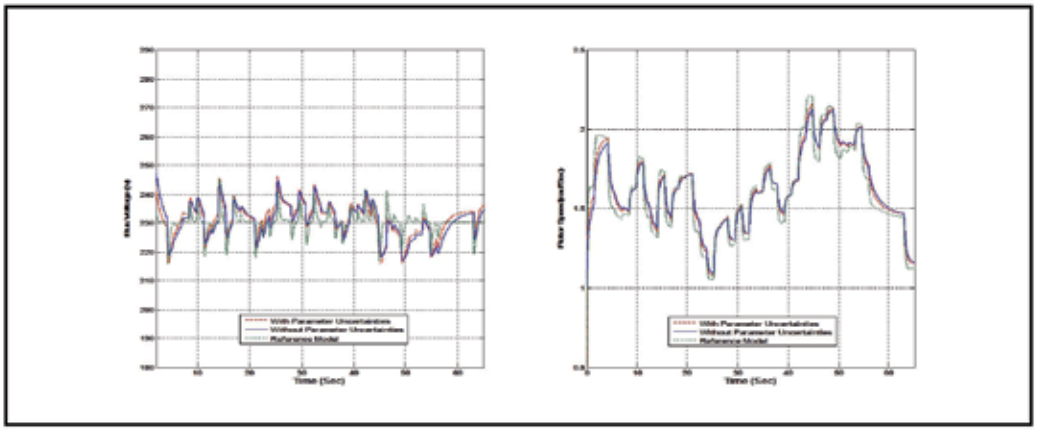

Fig. 8. Responses of bus voltage (V_b) and rotor speed (ω_s) of the fuzzy control system without (solid line) and with parameter uncertainties (dash line), and the reference model (dotted line) under *r(t)*

7.2 System responses of the fuzzy control system with sensor faults and with parameter uncertainties

The Fig.9 (top) shows the time evolution of the sensor fault f(t) (solid lines) and its estimate $\hat{f}(t)$ (dash lines) based on (54) while the bottom part shows the fault estimation errors $\tilde{f}(t)$. The response of the HWDSS states (solid lines), the states of the observer (dash lines) and reference model states (dotted lines) are given in Fig.10. The state estimation errors ($V_b - \hat{V}_b, \omega_S - \hat{\omega}_s$) are shown in the top of Fig.11, while the bottom part shows the state tracking errors($V_b - \overline{V}_b, \omega_s - \overline{\omega}_s$). As the wind speed varying as the random variation, the produced power curve takes almost the wind speed curve as shown in Fig. 12, but there is only spike when the fault is detected at 20.75 sec.

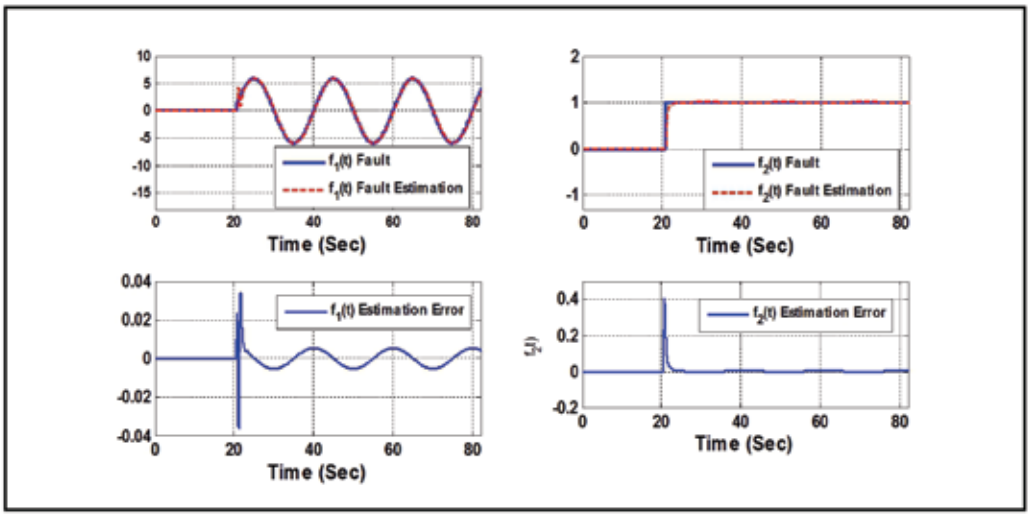

Fig. 9. Faults and their estimations (bus voltage sensor fault $f_1(t)$ and its estimate and generator speed sensor fault $f_2(t)$ and its estimate)(top) Fault estimation errors (bottom)

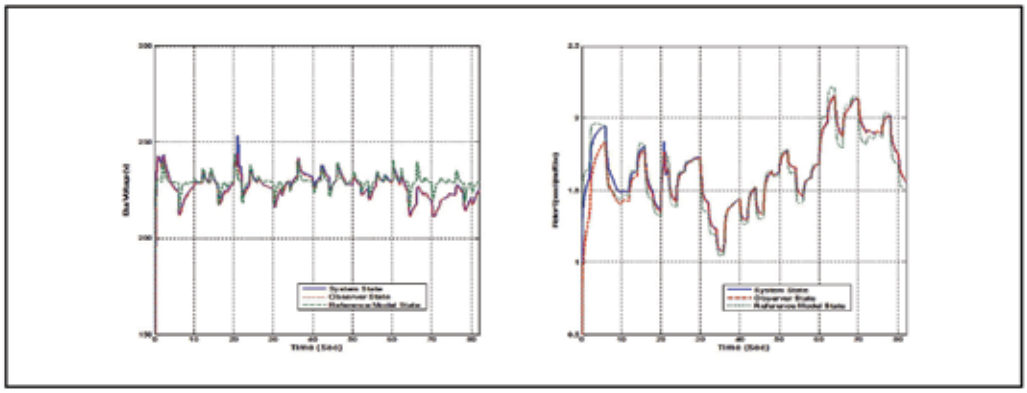

Fig. 10. Responses of bus voltage (V_b) and rotor speed (ω_s) of the fuzzy control system (solid line) , observer (dash line) and the refence model (dotted line) with parameter uncertainties and sensor faults based on (54) under the same refence input $r(t)$

It can be seen from the simulation results that the states of the HWDSS system follow those of the reference model in the presence bounded parametric uncertainties and sensor faults. Fig. 8 shows that the responses of the fuzzy control system with parameter uncertainties are better than that of the fuzzy control system without parameter uncertainties. This is because an additional control signals, i.e., $\frac{e_1(t)\|e_1(t)\|\|P_1\|\|\Delta A_i\|_{max}\|x(t)\|}{e_1(t)^T P_1 e_1(t)}, \frac{e_1(t)\|x(t)\|\|D\|_{max}\|x(t)\|}{e_1(t)^T P_1 e_1(t)}$ are used, the reason can also be seen from (42), i.e., $\sum_{i=1}^{p}\mu_i\|e_1(t)\|\|P_1\|(\|\Delta A_i\| - \|\Delta A_i\|_{max})\|x(t)\| + \|x(t)\|(\|D\| - \|D\|_{max})\|x(t)\|$ makes error e(t) approach

zero at a faster rate. Figs. 10 shows there is spike when the fault is detected at 20.75 sec and then the HWDSS trajectory follows the trajectory of the reference model, this is because an additional control signals, $\mathrm{e}_1(t)\left\|\hat{\mathrm{f}}(\mathrm{t})\right\|\left\|S_{\mathrm{E}}\right\|_{\max}\left\|\hat{\mathrm{f}}(\mathrm{t})\right\| / \mathrm{e}_1(t)^T P_1 \mathrm{e}_1(t)$.

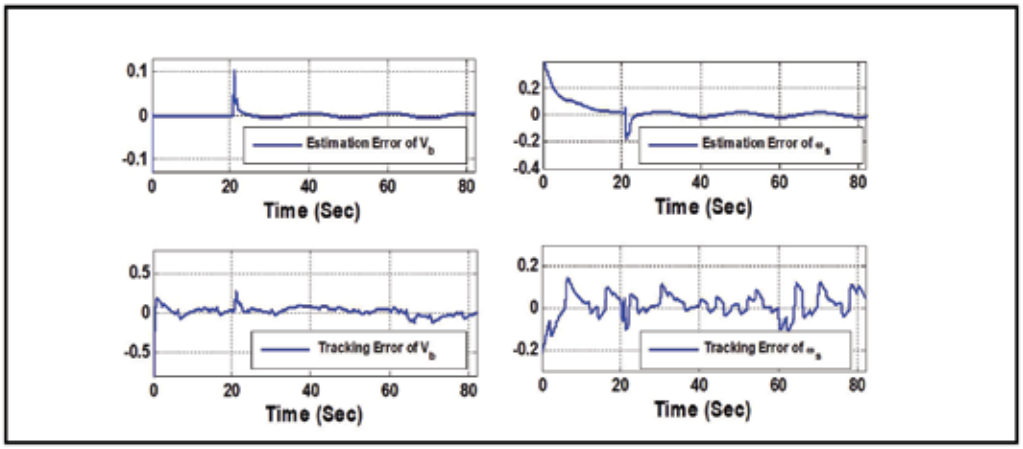

Fig. 11. State estimation errors ($V_b - \hat{V}_b$, $\omega_S - \hat{\omega}_s$)(top) State tracking errors ($V_b - \overline{V}_b$, $\omega_s - \overline{\omega}_s$) (bottom)

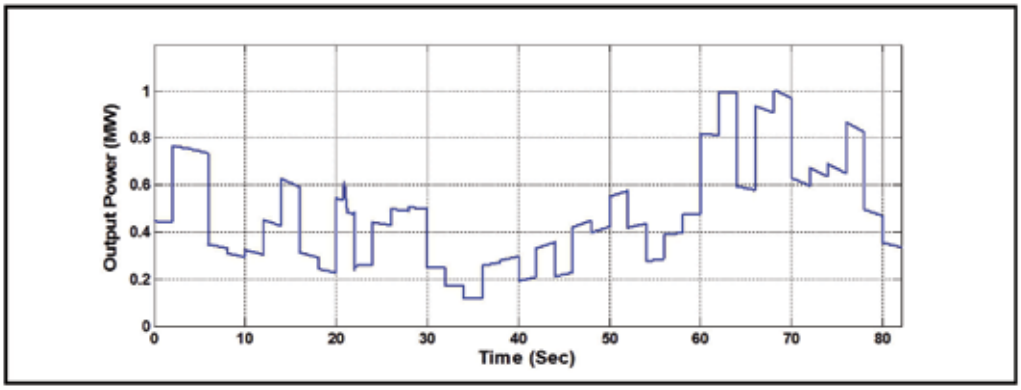

Fig. 12. Per unit wind turbine produced power

In summery results, we can be seen that the system trajectory follows the trajectory of the reference model which represents the trajectory of the HWDSS in the fault free situation. Thus, the TS fuzzy model based controller through fuzzy observer is robust against norm-bounded parametric uncertainties and sensor faults. Comparing the results of the proposed algorithm, with that given in the previous algorithms, we can be seen that the proposed controller has the following advantages:

1. It can control the plant well over a wide range of sensor faults compared with (Wei *et al.*, 2010 ; Odgaard *et al.*, 2009; Gaillard *et al.*, 2007).

2. Is stable over a wide range of uncertainty up to 40% compared with (Uhlen *et al.*, 1994).
3. The generated power is increased up to 45% compared with (Chen & Hu, 2003; Kamal *et al.*, 2010).
4. The algorithm is more robust in the presence of high nonlinearity.
5. Bus voltage is nearly constant and voltage ripple is reduced to 25% compared with (Chedid *et al.*, 2000; Kamal *et al.*, 2010).

8. Chapter conclusion

The stability analysis and design of nonlinear HWDSS control systems have been discussed. An improved stability criterion has been derived. In this chapter, we have developed a new robust fuzzy fault tolerant controller to control a HWDSS, while taking into account sensor fault(s) and parametric uncertainties in the aerodynamic model under the conditions that the state variables are unavailable for measurement as well as enabling the system to capture as much wind power as possible. A reference model is used and the proposed control is then designed for guaranteeing the convergence of the states of the HWDSS to the states of a reference model even if sensor fault(s) occurs and with parametric uncertainties. The basic approach is based on the rigorous Lyapunov stability theory and the basic tool is LMI. Some sufficient conditions for robust stabilization of the TS fuzzy model are formulated in the LMIs format. The closed-loop system will behave like a user-defined reference model in the presence of bounded sensor faults and parameter uncertainties. A simulation on HWDSS has been given to show the design procedure and the merits of the proposed fuzzy fault tolerant controller.

9. References

Abo-Khalil, A.G. & Dong-Choon, L. (2008). MPPT Control of Wind Generation Systems Based on Estimated Wind Speed Using SVR. IEEE Trans. on Industrial Electronics, vol.55, no.3, 2008, pp.1489-1490.

Aggarwal, V.; Patidar, R.K. & Patki, P. (2010) A Novel Scheme for Rapid Tracking of Maximum Power Point in Wind Energy Generation Systems", IEEE Trans. on Energy Conversion, vol.25, no.1), 2010 pp. 228-236.

Athanasius, G.X. & Zhu, J.G. (2009). Design of Robust Controller for Wind Turbines. 2nd International Conference on Emerging Trends in Engineering and Technology (ICETET), pp.7-12, 2009.

Barakati, J.D.; Kazerani, & M. Aplevich (2009). Maximum Power Tracking Control for a Wind Turbine System Including a Matrix Converter. IEEE Trans. on Energy Conversion, vol.24, no.3, 2009, pp.705-713.

Battista, H. & Mantz, R. J. (2004). Dynamical Variable Structure Controller for Power Regulation of Wind Energy Conversion Systems. IEEE Trans. on Energy Conversion, vol.19, no.4, 2004, pp.756-763.

Bennouna, O.; Hèraud, N.; Camblong, H.; Rodriguez, M. & Kahyeh, M. (2009). Diagnosis and Fault Signature Analysis of a Wind Turbine at a Variable Speed. Proc. I. Mech , vol. 223, 2009, pp.41-50.

Billy Muhando, E.; Senjyu, T.; Uehara, A. & Funabashi, T.(2011). Gain-Scheduled H∞ Control for WECS via LMI Techniques and Parametrically Dependent Feedback Part I: Model Development Fundamentals," IEEE Trans. On Industrial Electronics, vol.58, no.1, 2011, pp.48-56.

Billy Muhando, E.; Senjyu, T.; Uehara, A. & Funabashi, T. (2011). Gain-Scheduled H∞ Control for WECS via LMI Techniques and Parametrically Dependent Feedback Part II: Controller Design and Implementation. IEEE Trans. On Industrial Electronics, vol.58, no.1, 2011, pp.57-65.

Boukhezzar , B. & Siguerdidjane, H. (2009). Nonlinear control with wind estimation of a DFIG variable speed wind turbine for power capture optimization. Energy Conversion and Management , vol. 50, 2009, pp.885–892.

Boukhezzar, B. & Siguerdidjane, H. (2010). Comparison between linear and nonlinear control strategies for variable speed wind turbines. Control Engineering Practice, vol.18, 2010, pp.1357-1368.

Boyd , S.; Ghaoui, L. El; Feron, E. & Balakrishnan, V. (1994). Linear matrix inequalities in systems and control theory. SIAM., PA: Philadelphia, 1994.

Camblong, H.; Martinez de Alegria, I.; Rodriguez, M. & Abad, G.(2006). Experimental evaluation of wind turbines maximum power point tracking controllers. Energy Convers. Manage., vol.47, no.18-19, November 2006, pp.2846-2858.

Chedid, R. B.; Karaki, S.H. & El-Chamali, C. (2000). Adaptive Fuzzy Control for Wind Diesel Weak Power Systems. Transactions on Energy Conversion, vol. 15, no. 1 , 2000, pp. 71-78.

Chen, Z. & Hu, Y.(2003). A Hybrid Generation System Using Variable Speed Wind Turbines and Diesel Units. IEEE Transactions on Energy Conversion, 2003, pp. 2729-2734.

Datta, R. & Ranganathan, V.T. (2003). A method of tracking the peak power points for a variable speed wind energy conversion system", IEEE Trans. on Energy Conversion, vol.18 no.1, 2003, pp.163-168.

Gahinet, P.; Nemirovski, A.; Laub, A. J. & Chilali, M.(1995). LMI Control Toolbox. Natick, MA: The Math Works 1995.

Gaillard, A.; Karimi, S.; Poure, P.; Saadate, S. & Gholipour, E.(2007).A fault tolerant converter topology for wind energy conversion system with doubly fed induction generator. Power Electronics and Application,2007 European Conference, pp.1-6, 2007.

Galdi, V.; Piccolo, A. & Siano, P. (2009). Exploiting maximum energy from variable speed wind power generation system by using an adaptive Takagi-Sugeno-kang fuzzy model. Energy Conversion and Management, vol.50, 2009, pp.413-420.

Hee-Sang, K.; Lee, K. Y.; Kang, M. & Kim, H.(2008).Power quality control of an autonomous wind_diesel power system based on hybrid intelligent controller. Neural Networks, vol. 21, 2008, pp.1439-1446.

Hussien Besheer, A.; M. Emara, H. & Abdel-Aziz, M. M.(2009). Wind energy conversion system regulation via LMI fuzzy pole cluster approach. Electric power Systems research, vol.79, 2009, pp. 531-538.

Iescher,F; Zhao,J.Y; Borne,P.(2005). Robust Gain Scheduling Controller for Pitch Regulated Variable Speed Wind Turbine. Studies in Informatics and Control , vol. 14,no. 4, 2005, pp 299-315.

Iyasere, E.; Salah, M.; Dawson, D. & Wagner, J.(2008). Nonlinear robust control to maximize energy capture in a variable speed wind turbine. American Control Conference, pp. 1824-1829, 2008.

Kamal, E.; Koutb, M.; Sobaih, A. A. & Kaddah, S. (2008). Maximum power control of hybrid wind-diesel-storage system. Advances in Fuzzy Systems ,vol. 8, 8 2008, pp.1-9

Kamal, E.; Koutb, M.; Sobaih, A. A. & Abozalam, B.(2010). An Intelligent Maximum Power Extraction Algorithm for Hybrid Wind-Diesel-Storage System. International Journal of Electrical Power & Energy Systems ,vol. 32, no.3, 2010, pp.170-177.

Khedher, A.; Ben Othman, K.; Maquin, D. & Benrejeb, M.(2009). State and Sensor Faults Estimation via a Proportional Integral Observer. International Multi-Conference on Systems, Signals and Devices, 2009.

Khedher, A.; Ben Othman, K.; Maquin, D. & Benrejeb, M.(2010). Design of an adaptive faults tolerant control: case of sensor faults. WSEAS Transactions on Systems, vol.9, no.7, 2010, pp. 794-803.

Koutroulis, E . & Kalaitzakis, K.(2006). Design of a maximum power tracking system for wind-energy-conversion applications. IEEE Trans. on Industrial Electronics, vol.53,no.2, 2006, pp.486-494.

Lescher, F.; Zhao, J. & Borne, P. (2006). Switching LPV Controllers for a Variable Speed Pitch Regulated Wind Turbine. International Journal of Computers, Communications & Control, vol. 1, no.4, 2006, pp.73-84.

Mohamed, A. Z.; Eskander, M. N. & Ghali, F. A.(2001). Fuzzy logic control based maximum power tracking of a wind energy system. Renew. Energy, vol.23, no.2, 2001, pp. 235-245.

Muljadi, E. & Edward McKenna, H. (2002). Power Quality Issues in a Hybrid Power System. IEEE Transactions on industry applications, vol.38, no.3, 2002, pp.803-809.

Odgaard, P. F.; Stoustrup, J.; Nielsen, R. & Damgaard, C.(2009). Observer based detection of sensor faults in wind turbines. In Proceedings of European Wind Energy Conference 2009, Marseille, France, March 2009.

Prats, M. M.; Carrasco, J.; Galvan, E.; Sanchez, J.; Franquelo, L. & Batista, C. (2000). Improving transition between power optimization and power limitation of variable speed, variable pitch wind turbines using fuzzy control techniques. Proc. IECON 2000, Nagoya, Japan, vol.3, 2000, pp.1497-1502.

Prats, M. M.; Carrasco, J.M.; Galvan, E.; Sanchez, J.A. & Franquelo L.G.(2002). A new fuzzy logic controller to improve the captured wind energy in a real 800 kW variable speed-variable pitch wind turbine. IEEE 33th Annual power Electronics Specialists Conference, vol.1, pp.101-105, 2002.

Ribrant, P J. (2006). Reliability Performance and Maintainance: A Survey of Failure in Wind Power Systems. KTH school of Electrical Engineering, KTH: Sweden, 2006.

Schegner, P. & La Seta, P. (2004). Stability of Asynchronous Wind Generators Using Lyapunov's Direct Method. Bulk Power System Dynamics and Control - VI, pp.144-150, 2004.

Sloth, C.; Esbensen, T.; Niss Michae, O.K.; Stoustrup, J. & Odgaard, P. F. (2009). Robust LMI-Based Control of Wind Turbines with Parametric Uncertainties",18th IEEE International Conference on Control Applications Part of 2009 IEEE Multi-conference on Systems and Control Saint Petersburg, pp.776-781, 2009.

Tong, S. & Han-Hiong, L. (2002). Observer-based robust fuzzy control of nonlinear systems with parametric uncertainties. Fuzzy Sets and Systems, vol. 131, 2002 , pp.165-184.

Tong, S.; Wang, T. & Wang, T.(2009). Observer Based Fault-Tolerant Control for Fuzzy Systems with Sensor and Actuator Failures. Int. J. of Innovative Computing, Information and Control, vol.5, no.10, 2009, pp. 3275-3286.

Tripathy, S. C. (1997). Dynamic simulation of hybrid wind-diesel power generation system with superconducting magnetic energy storage. Energy Convers Mgmr, vol.38, no. 9, 1997, pp. 919-930.

Tuan, H. D.; Apkarian, P.; NariKiyo, T. & Yamamoto, Y.(2001). Parameterized linear matrix inequality techniques in fuzzy system design. IEEE Trans. Fuzzy Syst., vol. 9, no.2, 2001, pp. 324-332.

Uhlen, K.; Foss, B. A. & Gjosaeter, O. B.(1994). Robust control and analysis of a wind-Diesel hybrid power plant. IEEE Trans. on Energy Conversion, vol. 9, no.4, 1994, pp.701-708.

Wang, H. O.; Tanaka, K. & Griffin, M. F. (1996). An approach to fuzzy control of nonlinear systems: Stability and design issues. IEEE Trans. Fuzzy Syst., vol. 4, 1996, pp. 14-23.

Wang, X.; Wang, Y.; Zhicheng, J. & Dinghui, W. (2010). Design of Two-Frequency-Loop Robust Fault Tolerant Controller for Wind Energy Conversion Systems. 5th IEEE Conference on Industrial Electronics and Applicationsis, pp. 718-723, 2010.

Wang, Y.; Zhou, D.; Joe Qin, S. & Wang, H.(2008).Active Fault-Tolerant Control for a Class of Nonlinear systems with Sensor faults. International Journal of Control, Automation, and System, vol.6, no. 3, 2008, pp. 339-350.

Wei, X.; Verhaegen, M. & van Engelen, T. (2010).Sensor fault detection and isolation for wind turbines based on subspace identification and Kalman filter techniques . Int. J. Adapt. Control Signal Process, vol. 24, 2010 ,pp. 687-707.

Whei-Min, L. & Chih-Ming, H. (2010). Intelligent approach to maximum power point tracking control strategy for variable-speed wind turbine generation system. Energy, vol.35 no.6, 2010, pp.2440-2447.

Xiao-Jun, M.; Zeng-Qi, S. & Yan-Yan, H. (1998). Analysis and Design of Fuzzy Controller and Fuzzy Observer. IEEE Trans on Fuzzy Systems, vol. 6, no.1, 1998, pp.41-51.

Xie, L.(1996). Output Feedback H∞ Control of Systems With Parameter Uncertainties. international journal of control, vol.63, no.4, 1996, pp. 741-750.

Yong-Qi , C. (2009). Design and application of fault observer for variable speed wind turbine system. Computer Engineering and Applications, vol. 45, no. 14, 2009, pp. 223-227.

Zhang, K.; Jiang, B. & Shi, P.(2009). A New Approach to Observer-Based Fault-Tolerant Controller Design for Takagi-Sugeno Fuzzy Systems with State Delay. Circuits Syst Signal Process , vol. 28, 2009, pp. 679-697.

8

Operation and Control of Wind Farms in Non-Interconnected Power Systems

Ioannis D. Margaris[1,2], Anca D. Hansen[2], Nicolaos A. Cutululis[2], Poul Sørensen[2] and Nikos D. Hatziargyriou[1,3]
[1]*National Technical University of Athens (NTUA),*
[2]*Risø DTU National Laboratory for Sustainable Energy,*
[3]*Public Power Corporation (PPC) S.A.,*
[1,3]*Greece*
[2]*Denmark*

1. Introduction

Autonomous power systems are characterized by the absence of interconnections with neighbouring systems due to geographical, economic and political reasons. These systems face particular problems associated with safety and reliability during the design and operation procedure associated with safety and reliability. Typical problems include large variations in frequency because of the low inertia and the large fluctuations voltage due to the low short circuit ratio. The quality of the provided electricity to consumers is threatened. At the same time, special features of non interconnected systems, such as concentration of production in a limited number of power stations, the large size of the units in relation to the load, the need for larger spinning reserve due to the absence of interconnections, and the small stability margins raise the impact on safety and cost of operation.

Under these conditions, the effective handling of transient phenomena arising due to serious disorders is particularly critical. The systems should respond adequately to dynamic events and ensure static and dynamic safety. The most common faults that may cause undesired events are the loss of transmission lines, the sudden loss of load, and short circuits – especially three phase errors – and loss of production units. Based on collected operational data, incidents of loss of unit during operation are quite common and cause serious problems, therefore require special treatment. In several cases, such events have led in the past in smaller or even general black-outs.

These problems are becoming more intense due to the increasing penetration of wind power in the last decade. Since renewable energy sources and particularly wind energy have stochastic behaviour, the power output is not guaranteed. This is the main factor that imposes restrictions on the expansion because in general, distributed energy sources do not contribute to the control and regulation of the system in the same way as conventional units. Another important point, which differentiates the turbines compared with conventional synchronous generators used in electric systems, is associated with the technology of converting mechanical energy into electrical. The wind turbines are in large proportion

equipped with asynchronous generators (possibly in conjunction with electronic power converters) and therefore have substantial differences in the dynamic response over conventional units. For these reasons, limits are always imposed in the instantaneous penetration of wind power. These limits vary across the power systems, depending on the specific circumstances prevailing in each autonomous system, both in terms of conventional units (e.g. production technology, control capabilities, etc.) and wind farms (size and technology of the wind turbines, dispersion of wind turbines on the island, etc.). It is often the case that the limit set by the system operator for the instantaneous penetration of wind power is around 30% -40% of the load. In order to allow both the evaluation of the dynamic behaviour of autonomous systems after severe disturbances (e.g. ability of the system to restore frequency back to the desired limits after a major disturbance, such as loss of production and / or lines) as well as the definition of safe penetration limits, it is essential to conduct numerous studies. These include transient stability, load - frequency regulation, etc. The development of appropriate models for dynamic simulations in non interconnected systems is critical.

2. Power system model

2.1 Thermal power plant models

The conventional generating capacity comprises usually diesel, gas and steam plants with different ratings and control attributes. Each thermal plant contains several control blocks, which are essential for power system of dynamic simulations, e.g. voltage controller, primary controller (governor), primary mover unit and the synchronous generator. In many cases, due to lack of accurate data, simplified models for the conventional units are used in simulations. In this study, the exact models for each unit were used to ensure optimal representation of the interaction between wind farms and the power system.

The following three different models, already existing as built-in standard models in PowerFactory, (DIGSILENT, 2006), are used for the governors: GAST2A model for the gas turbines, DEGOV1 model for the diesel generators and IEEEG1 general model for the steam plants. A detailed description of the GAST2A built-in model in PSS/E for the governor used in the gas plant is described in (Mantzaris et al., 2008), while details on the corresponding standard IEEEG1 model for the governor in the steam plant can be found in (DIGSILENT, 2006). The parameters of these models, validated both in Matlab and PSS/E software packages, are presented in (Mantzaris et al., 2008). For the Automatic Voltage Regulators (AVR), the built-in SEXS model of PowerFactory is used with adjusted parameters for each unit.

2.2 Dynamic load models

The electrical loads of the systems include typically various kinds of electrical devices. An appropriate approach for the dynamic modeling of the loads connected to Medium Voltage (MV) feeders is to assume constant impedance of the loads during dynamic simulations, (Cutsem & Vournas, 1998):

$$P = P_0(V / V_0)^2 \tag{2.1}$$

$$Q = Q_0 (V / V_0)^2 \tag{2.2}$$

where P, P_0 and Q, Q_0 are the active and reactive power consumed by the load for voltage equal to reference voltage V, V_0 respectively.

2.3 Protection system

The protection system was also modeled in the simulation platform. The settings for both under/over voltage and under/over frequency protection system are crucial for the operation and dynamic response of the system during transient instances. As mentioned in the Introduction, non interconnected system, like the one used in this report as a study case, face the problem of significant variations in voltage and frequency. The relays, which act on either the production (protection of the conventional units or protection of the wind turbines), or the demand side (relays attached on the Medium Voltage feeders) decide the disconnection of equipment or loads, when the limits set by the system operator (or the production unit user) are violated. Regarding the loads, this leads to the so called load shedding, which often determines also the dynamic security margins for the system. It is often the case, in isolated systems, with low inertia, that during frequency variations, large proportion of the load is disconnected to avoid further frequency drop and possible frequency instability, i.e. due to sudden loss of a production unit.

The voltage and frequency protection system was modeled specifying the lower (or upper) limit of the value and the time duration, during which the variable measured, is out of the accepted range. One kind of under/over frequency protection operating in modern power systems is the so called ROCOF protection (Rate of Change of Frequency). The relays controlled by this system, open when the frequency changes at a rate faster than the specified one for a specific time. Thus, a part of the substation loads is disconnected. However, in many non-interconnected systems, especially those designed many decades ago, the under/over frequency protection system controlling the relays at substation loads measures the actual frequency and not the rate of change. Thus, if the frequency drops lower than a specified limit for specific time duration, the relay is ordered to open.

As a case study the small size island system of Rhodes is used. Rhodes power system for the reference year 2012 includes a 150 kV transmission system, two power plants, distributed in the north and in the south, as shown in Figure 1, and five wind farms. A significant proportion of the generation comes from wind turbines and diesel units. In 2012, the total installed wind power capacity and the maximum annual power demand are assumed to be about 48 MW and 233 MW, respectively (see Table 1).

The present Rhodes power system model is based on dynamic models of conventional generating units, loads and wind turbines. In order to be able to perform power system simulation studies for 2012, the present system model has to be modified with additional generating units and wind farms, which are expected to be online by the year of study, 2012, (Margaris et al. 2009). The protection system, mainly under/over frequency and voltage protection relay is also included in the dynamic power system model. In the reference year study 2012, five wind farms with different technologies will be connected online in Rhodes power system. Table 2 depicts the wind turbine technology and the size of each wind farm.

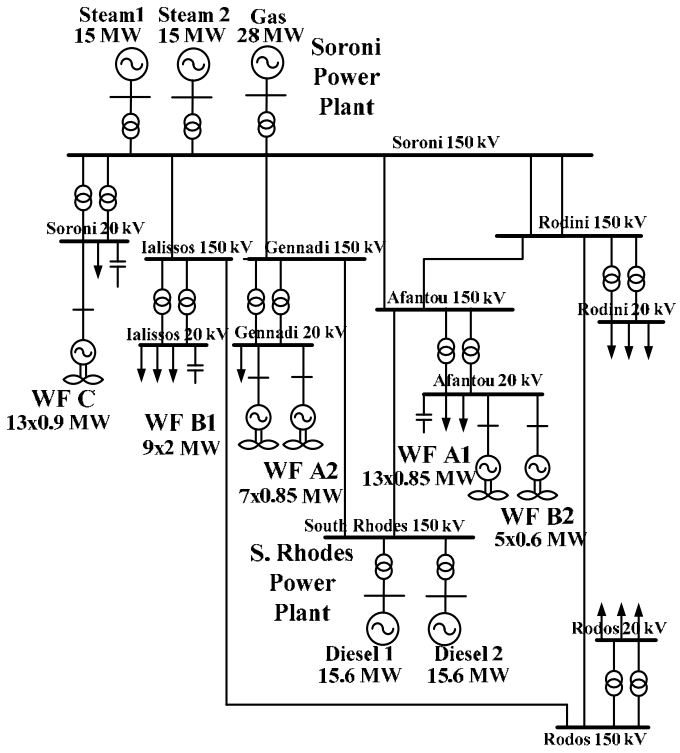

Fig. 1. Rhodes power system

The basic characteristics of Rhodes power system in 2012 are summarized in Table 1:

Rhodes power system	
Max Power Demand (MW)	233.1
Rated Thermal Power (MW)	322.9
Rated Wind Power Generation (MW)	48.8

Table 1. Basic Characteristics of Rhodes Power System (2012)

	Wind Turbine Technology	**Installed Capacity (MW)**
Wind Farm A1	DFIG	11.05
Wind Farm A2	DFIG	5.95
Wind Farm B1	PMSG	18
Wind Farm B2	PMSG	3
Wind Farm C	ASIG	11.7

Table 2. Wind Farms in Rhodes Power System (2012)

2.4 Load scenarios

Regarding the first step of the approach, the operating scenarios have to be carefully defined. These scenarios are based on collected operational data of the power system and correspond to the possible severe condition of operation. In this way, it is ensured that their analysis covers the intermediate modes of operation in terms of security. Three reference scenarios were defined as follows:

- The Peak Load Demand scenario – SCENa
- The Maximum Wind Power Production scenario (in absolute values of power) – SCENb
- The Maximum Wind Power Penetration scenario (in percentage of the load demand) – SCENc

The first scenario is the base case scenario and is used to evaluate the operational mode of the system in terms of security without significant wind power production, because annual peak load occurs in a hot summer day with typically very low wind. The second scenario is used to investigate security with large wind power production levels. In this case the levels of wind penetration are quite high going beyond 20% of the total load demand. The third scenario examines a penetration level above the 30% margin, which has been used until now for wind energy as a rule of thumb in autonomous island systems.

2.5 Static security analysis

Under the different scenarios, the secure operation of the system for steady operation has to be ensured, based on the N and N-1 criteria. Among the security requirements which have to be fulfilled by the power system are the following:

- The loading of the transmission lines should be within the accepted limits
- Bus voltages should be in the range of ±5% around the nominal voltage for normal operation (N)
- Bus voltages should be in the range of ±10% around the nominal voltage for emergency operation (N-1)

3. Wind power fluctuations

This part addresses different grid integration issues of large wind farms in non-interconnected power systems with respect to secure operation during variable wind and load profiles. Today, the power systems all over the world need a dramatic and continuous restructuring, as different renewable energy technologies are going to replace some of conventional units in the near future. This means, that there is urgent need for accurate modeling of various different generation technologies and novel wind turbine control strategies to fulfill requirements set by the TSOs, in order to ensure the dynamic security of such power systems.

Especially referring to wind power, the fluctuating nature of wind power imposes serious challenges to system operators. Power system inertia, protection relays settings, voltage and frequency stability in autonomous power systems have to be carefully and thoroughly analyzed before the penetration margin levels are expanded.

In most of the cases, operation experience defines the accepted penetration levels keeping the margin at 25-30% of peak annual load. However, higher or lower values can actually be accepted depending on the combination of power generator technologies online, (Margaris et al. 2009) – as it is the case of the specific power system under study here.

Modeling considerations of the power system under study are presented, especially speed governors and automatic voltage regulators of the conventional units. Defining accurate models of these system components is of vital importance for the overall system performance. Modeling and control issues for three different wind turbine technologies are described. The study case of Rhodes island is presented through simulations for various load and wind scenarios. The frequency fluctuations are calculated using wind time series based on measured and validated results, (Sørensen et al., 2007).

3.1 Wind farms modelling

Modern power systems include a variety of wind turbine technologies. The different response of each kind in dynamic phenomena requires separate and detailed modeling of each one. Three wind turbine technologies are considered here, namely Doubly Fed Induction Generator (DFIG), Permanent Magnet Synchronous Generator (PMSG) and Active Stall Induction Generator (ASIG) based wind turbines.

In order to investigate the interaction between these large wind farms and the power system, an aggregated method for modeling the wind farms is used, (Akhmatov et al., 2003; Poeller & Achilles, 2003). Such modeling approach is commonly used for power system studies, as it reduces substantially both the complexity of the system and the computation time, without compromising the accuracy of the simulation results.

Models for all these different wind turbine technologies are implemented, including the main components of each wind turbine configuration:

- Drive train and aerodynamics
- Pitch angle control system
- Control system
- Protection system

The system configuration, as well as some modeling and control issues for each wind turbine technology are described in the following section.

3.1.1 System configuration of variable speed DFIG wind turbine

The DFIG wind turbine configuration stands nowadays as the mainstream configuration for large wind turbines, (A.D. Hansen & L.H. Hansen, 2007). To ensure a realistic response of a DFIG wind turbine, the main electrical components as well as the mechanical parts and the controllers have to be considered in the model. The model used in this study for the wind farms with DFIG wind turbines is described in detail in (A.D. Hansen et al., 2006). The DFIG system is essentially a wound rotor induction generator with slip rings, with the stator directly connected to the grid and with the rotor interfaced through a back-to-back partial-scale power converter (A.D. Hansen & G. Michalke, 2007). The converter consists of two conventional voltage source converters (rotor-side converter RSC and grid-side converter GSC), and a DC-bus, as illustrated in Figure 2.

A two-mass model is used to represent the drive train to illustrate the dynamic impact of wind turbines on the grid properly. A large mass for the wind turbine rotor and a small mass for the generator are thus connected by a flexible shaft characterized by stiffness and damping for the low-speed shaft. A simplified aerodynamic model, based on a two-dimensional aerodynamic torque coefficient Cq table, (A.D. Hansen & G. Michalke, 2007), is typically sufficient for such studies.

The control system consists of a pitch control system and an electrical control system of the converters. The pitch control system is realized by a PI controller with antiwind-up, using a servomechanism model with limitation of both the pitch angle and its rate-of-change. As the pitch angle controls directly the generator speed to its reference signal, this control is able to prevent over-speeding both in normal operations and during grid faults, by limiting the mechanical power extracted from the wind and thus restoring the balance between electrical and mechanical power.
The efficiency of the pitch control system is crucial for studies like in this work, where the response of the wind farms under variable and extreme wind conditions is vital from the power system perspective.
The electrical control system, depicted in Figure 2, is essential for a good behavior of a DFIG wind turbine during both normal and grid fault operations. Decoupled control of active and reactive power is applied through vector control techniques, (A.D. Hansen & G. Michalke, 2007), allowing for changes in the active and reactive power in the range of milliseconds. The RSC controls mainly the active and reactive power delivered to the grid, while the GSC ensures nominal voltage at the common DC-bus at unity power factor operation of the converter. As illustrated in Figure 2 and described in details in (Gail et al., 2006; M.H. Hansen et al., 2005), the control of the converters is based on cascade control loops: a very fast inner current controller regulates the currents to the reference values that are specified by the outer slower power controller.

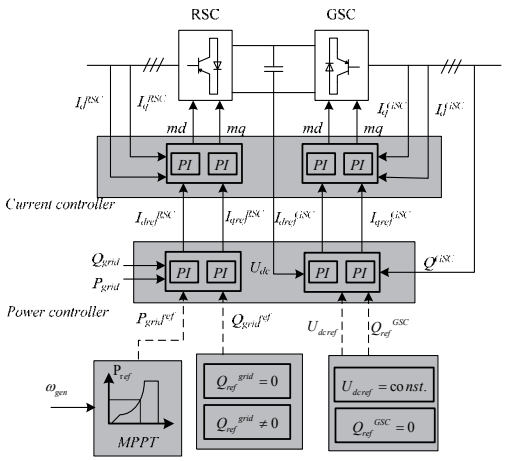

Fig. 2. Electrical control scheme for the DFIG wind turbine

3.1.2 System configuration of variable speed PMSG wind turbine

Similar to the DFIG wind turbine configuration, the PMSG model consists both of a wind turbine mechanical level (i.e. aerodynamics, gearless drive-train and pitch angle control) and a wind turbine electrical level (i.e. multi-pole PMSG with a full-scale frequency converter and its control).
The synchronous generator is connected to the grid through a full-scale frequency converter system that controls the speed of the generator and the power flow to the grid. The full-scale frequency converter system consists of a back-to-back voltage source converter (generator-side converter and the grid-side converter connected through a DC link), controlled by IGBT

switches. The rating of the converter system in this topology corresponds to the rated power of the generator plus losses. The presence of such a converter enables the PMSG to keep its terminal voltage on a desired level and to adjust its electric frequency according to the optimized mechanical frequency of the aerodynamic rotor, independently of the fixed electric frequency and the voltage of the AC grid.
The wind turbine mechanical level of PMSG (aerodynamics, drive train and the pitch control) is modelled similarly to that for the DFIG wind turbine. The generic control strategy of the frequency converter for the PMSG wind turbine, as illustrated in Figure 3, is described in details in (A.D. Hansen & G. Michalke, 2008).

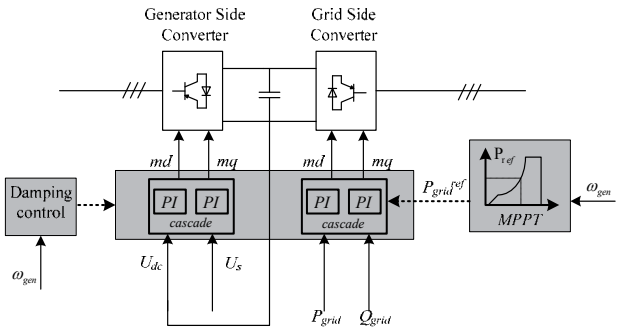

Fig. 3. Power converter control strategy for the variable speed wind turbine with multi-pole PMSG

The damping controller ensures stable operation for the wind turbine, by damping the torsional oscillations excited in the drive-train and reflected in the generator speed ω_{gen}. The generator-side converter controller keeps DC-bus voltage U_{dc} constant and controls the generator stator voltage U_s to its rated value in the stator voltage reference frame. The advantage of controlling the generator stator voltage U_s to its rated value is that the generator and the power converter always operate at the rated voltage, for which they are designed and optimized. The grid-side converter controller controls independently the active P_{grid} and the reactive Q_{grid} power to the grid in the grid voltage reference frame. The controllers of the converter are also based on control loops in cascade, similarly to the DFIG control scheme.

3.1.3 System configuration of fixed speed ASIG wind turbine

The sub-models for aerodynamics, mechanical components and the squirrel cage induction generator in the ASIG wind turbine configuration are as described in (A.D. Hansen et al., 2003). The drive train is again represented by a two-mass model, similar to the other configurations. The turbine's power is controlled directly by the pitch controller through the pitch angle. The operation of the wind turbine is based on two control modes:

- Power limitation - where the turbines power is limited to the rated power above rated wind speed. The stall effect is thus controlled by adjusting accordingly the pitch angle.
- Power optimization - where the aerodynamic efficiency and thus the power output is maximized for wind speeds below rated wind speed. The pitch angle as function of the wind speed is shown in Figure 4.

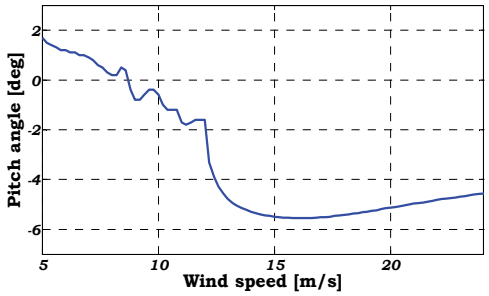

Fig. 4. Pitch angle as a function of the wind speed

Notice that all three wind turbine configurations are using a gain scheduling procedure, (Ackermann, 2005), in their pitch control system in order to compensate for the existing non-linear aerodynamic characteristics. The fundamental principle of the gain scheduling feature is that the proportional controller of the pitch angle controller is varied so that the total gain of the system remains unchanged for all the operating points of the wind turbine.

3.2 Simulation results

In the following, the emphasis is made on the secure operation of the system under variable load and wind profiles. The goal of these simulations is to illustrate and evaluate the interaction between the five wind farms with Rhodes power system during different load scenarios and winds. The first set of simulations focuses on the dynamic response of the three types of wind farms configurations, considered in this article and on the impact on the system during deterministic wind speed steps. The second set of simulations is carried out in order to illustrate and evaluate the fluctuations that occur in the generator speed and the power of wind turbines in the presence of a turbulent wind. The attention is also drawn to the impact of these fluctuations on the power system of Rhodes and to the wind farm controller capability to ensure safe operation of the wind farms during different variable load and wind profiles.

3.2.1 Turbulent wind speed in wind farms

In the following, simulations with turbulent wind speed time series are presented and discussed. The goal of these simulations is to evaluate the fluctuations in the system frequency due to wind speed fluctuations during different load scenarios. It is assumed that all five farms are running with turbulent wind speed.

The wind turbine time series, which are inputs to the wind farms, are generated based on the wind speed fluctuation model developed by Sorensen et. al., (Sørensen et al., 2007). This wind speed fluctuation model has been validated against wind speed measurements from large wind farms.

For each wind farm site and each wind and load scenario, different wind time series are generated for 10 minutes. The correlation between the wind speeds of the wind turbines in a wind farm is taken into account in the wind speed fluctuation model. The correlation aspect is even more important for such isolated power system as it is the case of Rhodes island. As the distances between the wind farms are quite small, the wind speeds seen by the wind farms can be highly correlated.

Figure illustrates the wind time series, which has been applied to the wind farms, during the load scenario with maximum load demand, i.e. SCENa. Notice, that all wind farms are running in power optimization mode, as their wind speeds are below the rated wind speed.
In this scenario, the wind farms produce in total 7.5 MW, accounting only for 3% of the total demand. The system frequency fluctuations due to the wind speed fluctuations are negligible, as illustrated in Figure 6, thus the wind power impact on the power system is in this case very small. As expected, although visible, the fluctuations are of quite small magnitude and they are therefore not leading to problems in the system security.

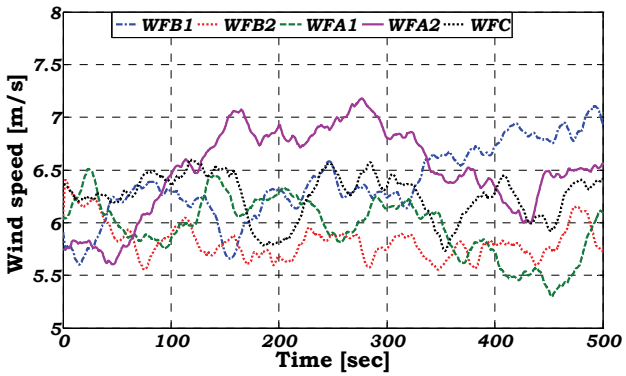

Fig. 5. Wind time series applied to the wind farms – SCENa

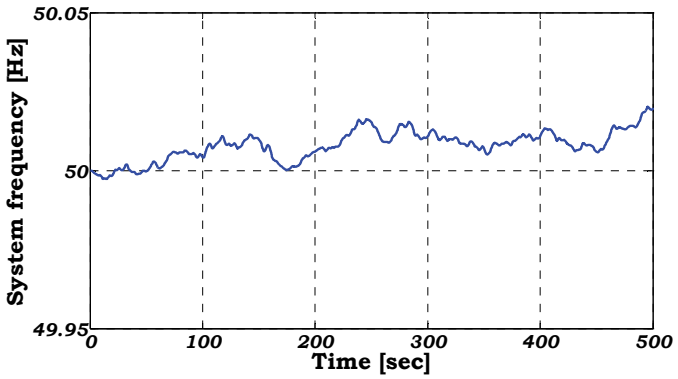

Fig. 6. System frequency for wind time series - SCENa

Figure 7 illustrates the wind time series, which has been applied to the wind farms, during the load scenario with maximum wind power production, i.e. SCENb.
Notice that in this SCENb, the wind turbines operate in a narrow range around their rated capacity and it can thus be presumed that the wind power fluctuations' impact on the Rhodes power system to be more significant compared to the SCENa.
Due to the highly correlated the wind speeds, the form that frequency fluctuations appear to have in Figure 8, is not directly related to a specific wind time series, but rather to the combination of the active power fluctuations delivered by all five wind farms.

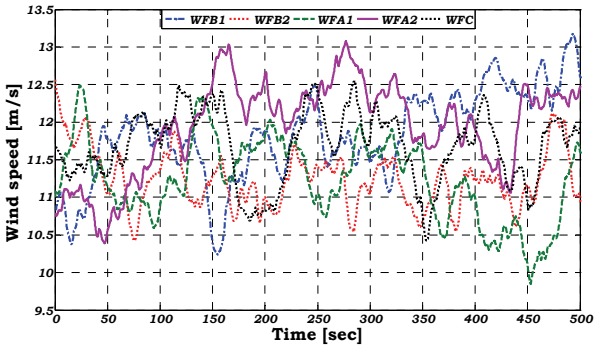

Fig. 7. Wind time series applied to the wind farms - SCENb

In this scenario, the wind farms produce in total 45.2 MW, which corresponds to 26% of the total demand. Notice that the system frequency, illustrated in Figure 8, has very fast dynamic deviations in the range 49.96 Hz – 50.1 Hz, which is considered safe from the power system security point.

Even though the wind power penetration is significant in SCENb, the frequency fluctuations are not considered large enough to impose security questions. The high correlation among the wind in all the wind farms is ensuring that the system frequency is not strongly dependent on a sudden drop or increase of the wind in only one wind farms. One of the most important factors influencing the frequency deviations – besides the parameters of the conventional units and their emergency rate of power undertake – is of course the size of each wind farm and the type of generator used.

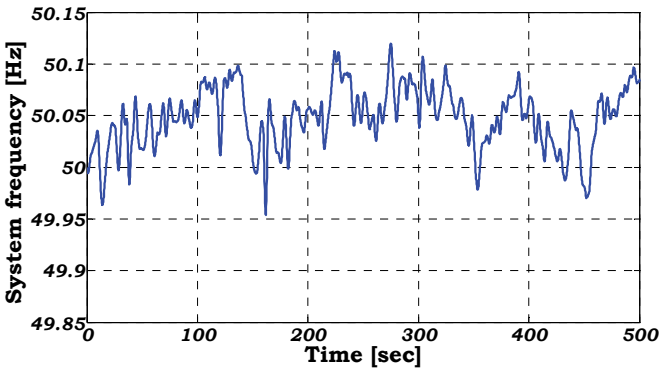

Fig. 8. System frequency for wind time series - SCENb

The following graphs show the performance during the scenario SCENb of two wind turbine technologies, i.e. ASIG wind turbine and PMSG wind turbine, which are picked-up to illustrate the behavior of a generic fixed and variable speed wind turbine, respectively. Beside the wind speed, typical quantities, as generated power to the grid, generator speed and the pitch angle are illustrated.

Figure 9 illustrates the wind speed time series applied as input to an ASIG wind turbine inside wind farm WFC. Notice that the wind turbine is simulated at an average wind speed

of about 11.5 m/s. This operational point corresponds to a transition operational regime for the wind turbine, between power optimization and power limitation regime.
The strong correlation between the wind speed fluctuations, active power output and generator speed is obvious in Figures 9 -11. As expected for a ASIG wind turbine, the 3p fluctuation in the wind is visible both in the active power output and the generator speed. It should be noticed that, in this scenario SCENb, the ASIG wind farm produces around 6 % of the total demand.

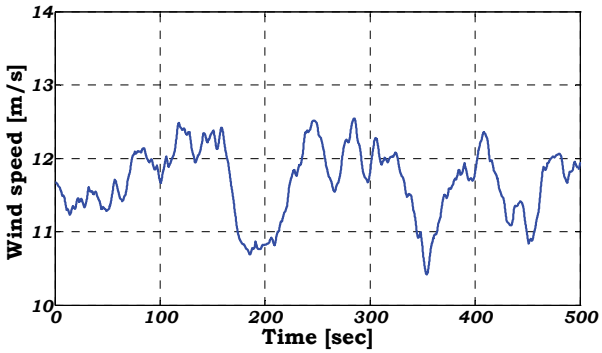

Fig. 9. Wind time series in ASIG wind farm WFC - SCENb

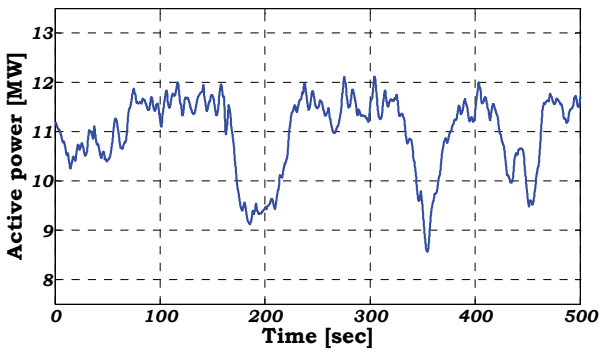

Fig. 10. Wind farm active power output for ASIG wind farm WFC - SCENb

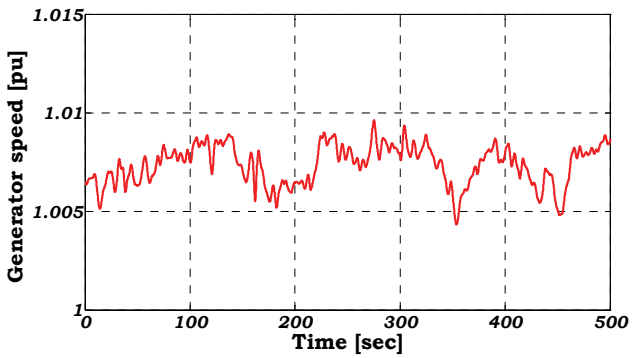

Fig. 11. Generator speed for ASIG wind turbine in wind farm WFC - SCENb

Figure 12 shows the pitch angle of ASIG wind turbine during SCENb. When the wind speed is less than the rated wind, the wind turbine produces maximum possible power. In this case, the pitch angle is equal with its optimal value, i.e. -1.7 deg. When the wind speed is above rated wind speed value, the pitch angle corresponds to the values which keep the turbine power to the rated power. Notice that the pitch system responds with delay due to the pitch rate limiter existing in the actuator. Despite the very fast wind speed deviations, the pitch control system manages to ensure smooth transition between the optimization and limitation range whenever the wind speed crosses the rated value.

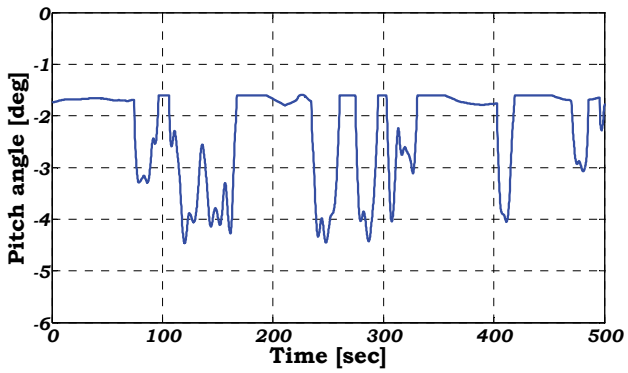

Fig. 12. Pitch angle for ASIG wind turbine in wind farm WFC - SCENb

Figures 13-16 illustrate how the wind farm WFB2 equipped with PMSG wind turbines behaves during the scenario SCENb. Figure shows the wind speed time series, which has been applied as input to a PMSG wind turbine inside wind farm WFB2.

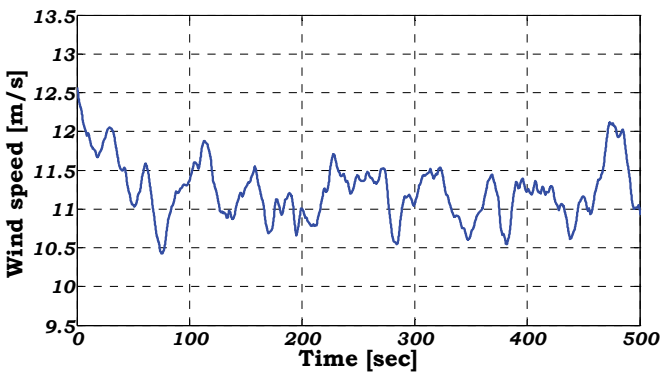

Fig. 13. Wind time series in PMSG wind farm WFB2 - SCENb

Similar to the ASIG wind turbine, discussed previously, the operation point of the PMSG wind turbine corresponds again to a transition operational regime for the wind turbine, between power optimization and power limitation regime.
This wind farm has rated capacity 3 MW, which stands for 1% of the total demand. As illustrated in Figure14, whenever the wind speed goes above the rated value, the pitch control manages to keep the active power output constant and equal to nominal power.

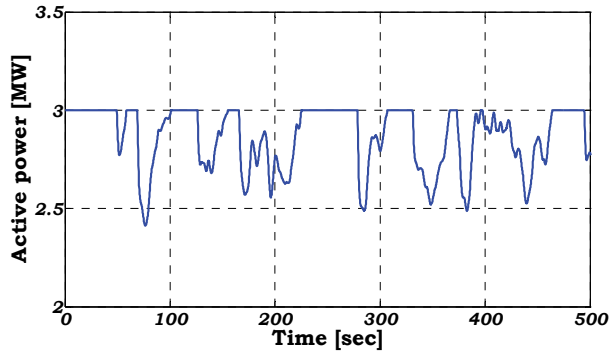

Fig. 14. Wind farm active power output for PMSG wind farm WFB2 - SCENb

Notice that the generator speed of the PMSG wind turbine is tracking the slow variation in the wind speed each time the turbine is running in the operation mode, while in power limitation mode, the speed controller tries to control the generator speed to its rated value.

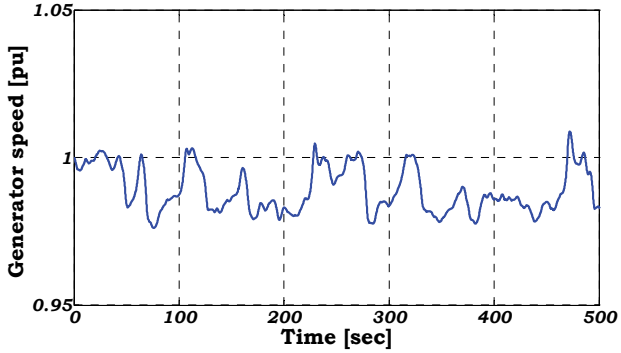

Fig. 15. Generator speed for PMSG wind turbine in wind farm WFB2 – SCENb

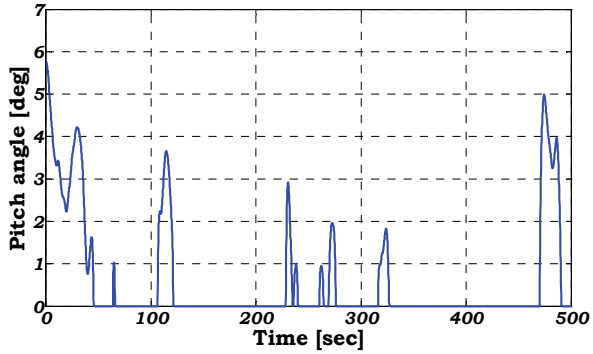

Fig. 16. Pitch angle for PMSG wind turbine in wind farm WFB2 – SCENb

The damping controller manages to damp the torsional oscillations in the drive train and ensures safe operation of the wind turbine. Compared to the results from the ASIG wind farm above, the fast deviations in the wind are filtered out from the electrical power. The

generator is decoupled from the grid through the converter at its terminal and any rapid fluctuations in the wind are not influencing the power delivered to the grid. Figure 16 gives the pitch angle, which is increased from its optimal value each time the turbine is running in power limitation mode.

In this scenario, the wind power penetration is maximum, reaching 32% of the total demand. The wind farms however are not producing as much as in SCENb. This scenario is considered the worst case scenario, as the fluctuations in the wind may have serious impact on the power system operation.

Figure 17 illustrates the wind time series, which has been applied to the wind farms, during the load scenario with maximum wind power penetration, i.e. SCENc.

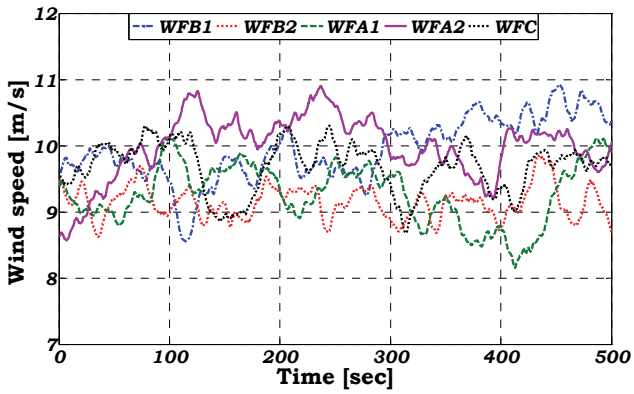

Fig. 17. Wind time series applied to the wind farms - SCENc

The range of operation for the wind turbines in this case covers the optimization area, where the control of the wind turbine has to ensure optimum power output.

As illustrated in Figure 18 , due to the wind fluctuations, the system frequency varies between 50 Hz and 50.25 Hz, which is considered safe for the system operation. Although the wind speeds in each wind farm may have sudden changes, as it is illustrated in Figure 17, the overall response of the system is satisfactory, and the power outputs from the wind

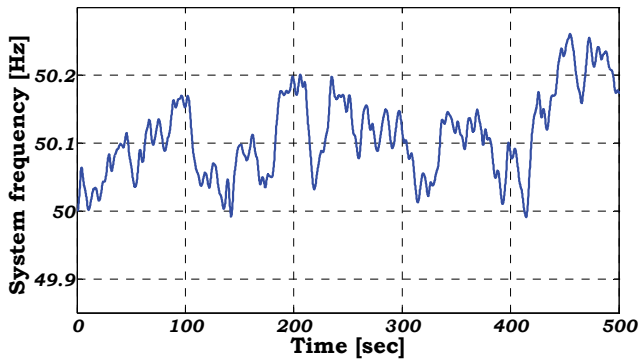

Fig. 18. System frequency for wind time series – SCENc

farms seem to counteract each other in the frequency impact. The system frequency deviates more in this case than in SCENb (see Figure 8), which is due to the increased wind power

penetration levels in this scenario. Nevertheless, the emergency rate of power undertaken by the conventional units is sufficient to overcome the rapid active power fluctuations produced by the wind farms on the island.
In the following, the attention is directed in details towards the performance of two wind turbine technologies during SCENc, this time on a ASIG wind turbine and a DFIG wind turbine. Again typical quantities, as generated power to the grid, generator speed and the pitch angle are illustrated.
Figure 19 illustrates the wind speed time series, which has been applied as input to the ASIG wind farm WFC. In scenario SCENc, this wind farm produces around 7 MW i.e. 8 % of the total demand.

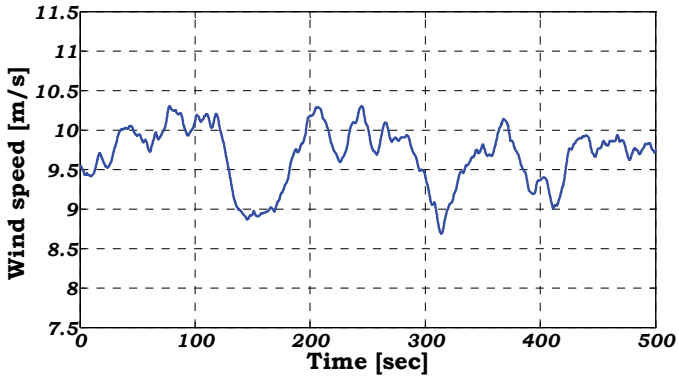

Fig. 19. Wind time series in ASIG wind farm WFC - SCENc

Notice in Figures 19-21 that the fluctuations in wind speed, active power output, generator speed are strongly correlated in this case, and the fast dynamic deviations are also here significant. Figure 22 shows the pitch angle, which is reduced accordingly although restricted by the pitch rate limiter when the wind speed changes at very high rate.

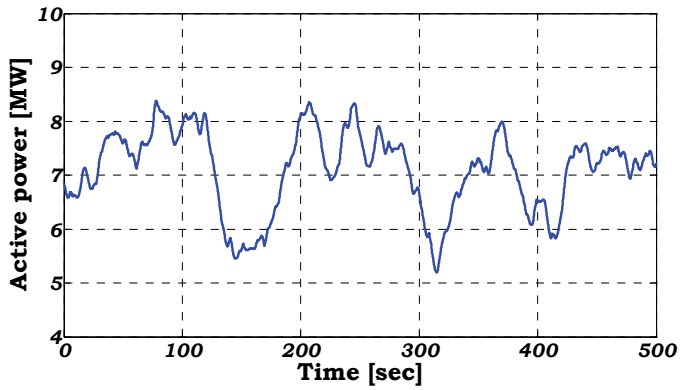

Fig. 20. Wind farm active power output for ASIG wind farm WFC – SCENc

The dynamic performance of the DFIG wind farm WFA1 during SCENc is in the following addressed in order to illustrate the efficiency of the designed models. This farm produces

almost 6.5 MW i.e. 7.5% of the total demand. Figure 23 shows the wind speed time series, which has been applied as input to the DFIG wind farm during SCENc.

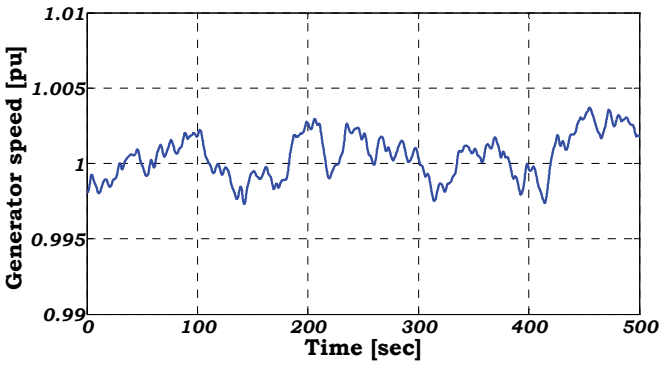

Fig. 21. Generator speed for ASIG wind turbine in wind farm WFC - SCENc

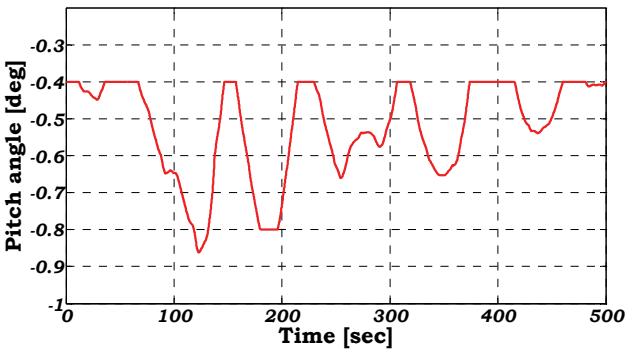

Fig. 22. Pitch angle for ASIG wind turbine in wind farm WFC - SCENc

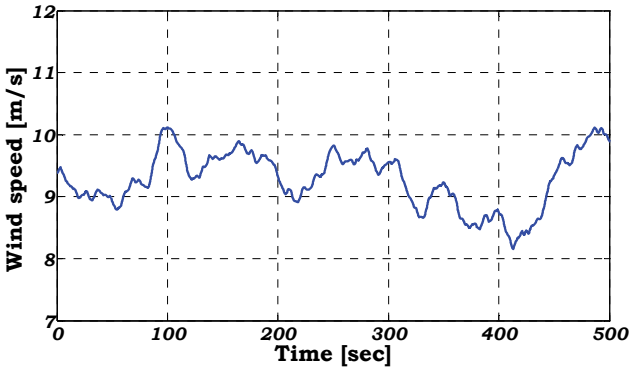

Fig. 23. Wind time series in DFIG wind farm WFA1 - SCENc

The Maximum Power Tracking (MPT) strategy, implemented in the RSC (rotor-side converter) of the DFIG system ensures optimum operation of the wind turbine maximizing the aerodynamic coefficient Cp in every wind speed. In this operational area for the DFIG

wind turbines, small changes in the rotor speed result in significant changes in the active power output of the system. This is due to the fact, that the designed MPT characteristic is very stiff in this area.
Notice that, contrary to an ASWT wind farm, where the correlation between the system frequency and the wind turbine response is very strong, in the case of DFIG configuration the generator is partially decoupled from the system frequency, as seen in Figure 18s 18, 21 and 25.

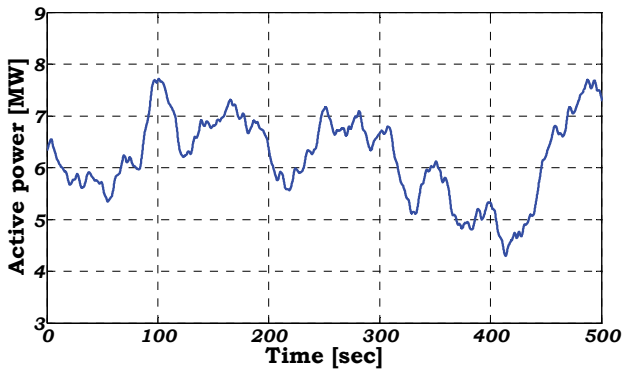

Fig. 24. Wind farm active power output for DFIG wind farm WFA1 - SCENc

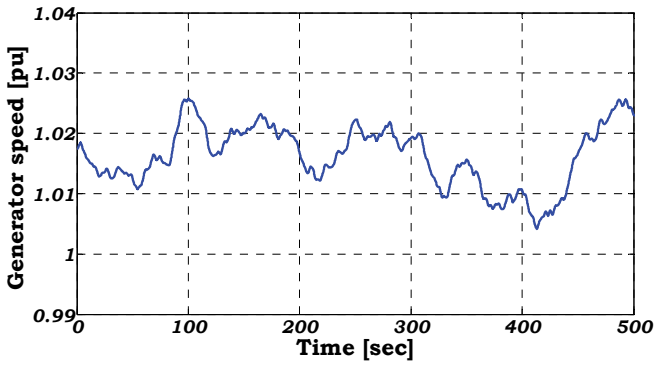

Fig. 25. Generator speed for DFIG wind turbine in wind farm WFA1 - SCENc

The generator speed is continuously adapted to the wind speed in order to extract maximum power out of wind. As wind farm is running in optimization mode, the pitch angle is passive, being kept constant to its optimal value.

4. Frequency control of wind power

Increasing wind power penetration especially in non-interconnected systems is changing gradually the way grid frequency control is achieved. The technical requirements set by the networks operators include various aspects, such as fault ride-through of wind turbines during faults, voltage-reactive power control and overall control of the wind farms as conventional power plants. A key aspect of the operation of wind farms in autonomous power systems is the frequency control. This session presents the results from a study on the

Rhodes power system already presented above, focusing on frequency control. The Rhodes power system has been used to address all the main issues related to system secure operation under different system conditions. The response of the wind farms in frequency disturbances is analyzed and the different characteristics of each wind turbine type related to frequency are described. Three different wind turbine configurations have been used – Active Stall Induction generator (ASIG), Doubly Fed Induction generator (DFIG) and Permanent Magnet Synchronous generator (PMSG). An auxiliary control has been designed for the DFIG type to enhance the capability to support the frequency control. The load shedding following severe frequency disturbances is calculated and the under/over-frequency protection relay settings are discussed under the novel system conditions. Results for different system conditions and control methods are presented and discussed focusing on the ability of modern wind turbine technologies to assist in frequency control in isolated power systems during severe disturbances in the production-consumption balance.

As wind power penetration increases in modern power systems, a variety of technical and regulatory issues regarding the interaction between large wind farms and power system is under constant discussion. The system operators are setting onerous requirements that that wind farms have to fulfill. Among these, voltage and frequency control play an important role. Frequency control has started to appear as emerging need under increasing wind power penetration conditions and due to the extended replacement of conventional generators by large wind farms in power supply. The impact of wind farms in frequency phenomena is even more vital in non-interconnected power systems, where the power system inertia is limited.

It is often the case, that when auxiliary services of wind turbines, like frequency control, are investigated, simple models are used for either the power system or the wind turbines. In this article, detailed model for all different components of the system were used to evaluate the system response in serious events with maximum accuracy. The dynamic security of power systems has to be carefully examined, before wind power penetration limits are expanded. The response of conventional units, the load dependency on frequency and voltage and the wind turbines' response during events that affect system frequency are some of the key aspects that have to be modeled in detail for this kind of investigations.

In this article the main issues of frequency control in isolated power systems, with high wind power penetration are investigated. Rhodes power system, includes three different types of conventional generators – namely gas, diesel and steam units – and three different types of wind turbines – Active Stall Induction generator (ASIG), Doubly Fed Induction generator (DFIG) and Permanent Magnet Synchronous generator (PMSG) wind turbines. This variety of components gives the chance for a wide range investigation of frequency issues for modern power systems.

Definitions regarding the frequency control in autonomous power systems are given and the protection relay system settings related to under/over frequency deviations are discussed. The response of different wind turbine technologies during frequency events is explained. Three different primary frequency control schemes implemented in the developed model are analyzed. Finally, the basic characteristics of the power system are given followed by a brief description of the available wind turbine technologies available on line in the system for the reference year 2012. Results from various simulations are discussed

and the capability of modern wind farms to provide auxiliary frequency control is demonstrated.

Frequency definitions and protection system

In this section, some basic definitions on frequency are given to introduce the main issues regarding frequency control with emphasis on isolated power systems.

In the power system, frequency is the variable indicating balance or imbalance between production and consumption. During normal operation, the frequency should be around the nominal value. The deadband which is considered as safe operation in most European grid codes is the zone 50 ± 0.1 Hz, although the limits vary between the different system operators in Europe, mainly due to the different characteristics of each grid. The range $49 \div 50.3$ Hz is in general the dynamic security zone that in most of the cases is not allowed to be violated at any means, (Lalor et al., 2005). However, these safety margins for frequency deviations are often expanded in autonomous power systems, where system inertia is low, to avoid constant load shedding whenever the balance between production and consumption is lost.

In case of sudden generation loss or large load connection, the frequency of the frequency starts to drop. The two main system functions that ensure return of an unbalanced system to nominal frequency are:

- Primary Control: During the first 30-40 sec after the event leading to frequency deviation, the rotational energy stored in large synchronous machines is utilized to keep he balance between production and consumption through deceleration of the rotors. The generation of these units (often referred to as primary control units) is thus increased until the power balance is restored and the frequency is stabilized.
- Secondary control: After the primary response of the generators, a slow supplementary control function is activated in order to bring frequency back to its nominal value. The generators connected to the system are ordered to change their production accordingly either through an Automatic Generation Control scheme, either through manual request by the system operator – which is often the case in isolated systems like Rhodes.

These two main frequency control functions are illustrated in Figure 26 for a sudden drop in system frequency.

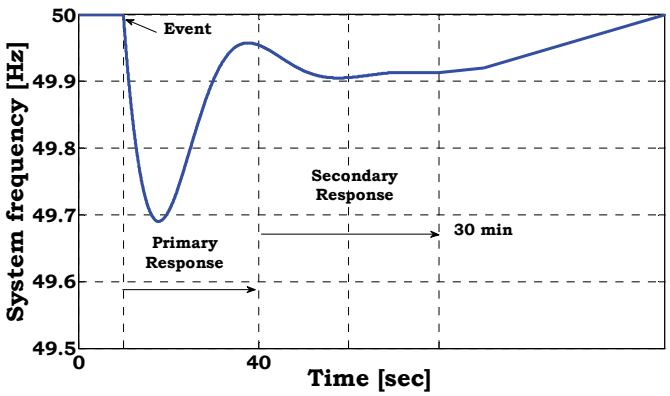

Fig. 26. Definitions of frequency control in power systems

The rate, at which the frequency changes following an event i.e. drops in Figure 34, is depending on the so called inertia of the system thus the total angular momentum of the system which is the sum of the angular momenta of the rotating masses in the system i.e. generators and spinning loads. The frequency control implemented in this study tries to improve the system response in terms of initial Rate of Change of Frequency and minimum frequency (frequency nadir). Therefore, the discussion and also the results will emphasize the capability of wind farms to provide with primary frequency support in the first seconds after the event which causes the frequency deviation.

4.1 Response of wind turbines to frequency events

The replacement of conventional synchronous generators by wind farms in modern power systems with increased wind power penetration, changes the way traditional frequency control was treated in power systems. Wind turbines connected to the grid, depending on their configuration, have a different response to frequency deviations. In this Session, the relation between each wind turbine configuration and its response during frequency deviations is discussed and explained.

4.1.1 Response of ASIG wind turbines in frequency events

One of the most common wind turbine configurations in modern power systems is the standard fixed speed wind turbine based on induction generator connected to the rotor through a transmission shaft and a gearbox. The Active Stall Induction Generator wind turbine model developed to simulate the fixed speed wind turbines in this study is described in previous sections.

As described in (Morren et al., 2006), the induction machine based wind turbine inertia response is slower and lower than the conventional synchronous generator's response. This difference is mainly because of the reduced coupling of the rotational speed of the WT and the system frequency and of the lower inertia constant of the WT compared to a standard conventional generator connected to the grid.

However, in the case of a frequency drop, like the one illustrated in Figure 34, the inertia response of the ASIG wind turbine is not negligible due to usual low nominal slips. The rotor of the ASIG is decelerating following the system frequency drop. The kinetic energy which was accumulated in the rotating mass is transformed into electrical energy delivered to the grid. The amount of the available kinetic energy is determined from the total angular momentum of the WT – thus the sum of the angular momenta of the electrical generator, the rotating blades and the gearbox – and the rotational speed. There are some studies estimating this available energy (Ullah et al., 2008; Ramtharan et al., 2007) through rough estimations.

A comparison between the inertia response provided by the three different wind turbine configurations studied in this article is given in Figure 27 for loss of the largest infeed in the system of Rhodes. When the frequency starts to drop, the ASIG provides with significant active power surge to the grid, thus, reducing the initial rate of change of frequency. The response of the DFIG and PMSG wind turbine types is explained further below. It is obvious that, fixed speed wind turbines have an intrinsic behavior that provides auxiliary service to the system during frequency imbalances, although they can not contribute to other services, i.e. voltage – reactive power control, in the same way the variable speed wind turbines can.

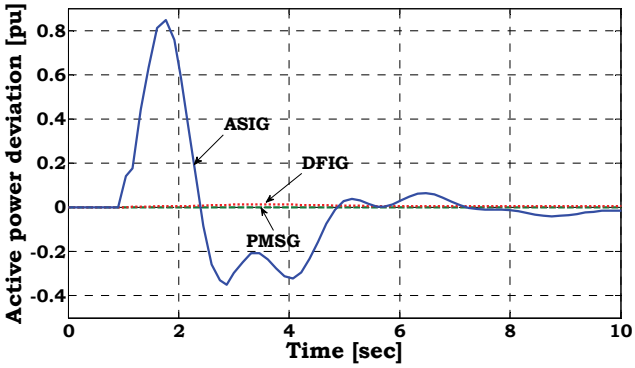

Fig. 27. Change in active power production during a frequency drop for the three main wind turbine configurations

4.1.2 Response of DFIG wind turbines in frequency events

The DFIG wind turbine configuration, which is the most common configuration for large wind turbines, is mainly based on an induction generator and a frequency converter connected to the rotor circuit via slip rings. Details on the model developed in this study, including control aspects, can be found in section 3.1.1.

As described in (Ullah et al., 2008), the response of a DFIG wind turbine is slightly different than the one described above for synchronous and induction generators. The inertial response of the DFIG type is mostly based on the applied control scheme acting on the converter connecting the rotor to the grid (Morren et al., 2006). The overall response can be explained as the result of two opposite torques acting on the rotor during a frequency change, i.e. a frequency drop: a decelerating torque, proportional to the rate of change of the rotor speed $\frac{d\omega}{dt}$ and therefore to the frequency $\frac{df}{dt}$, which makes the rotor speed follow the frequency drop – an accelerating torque, which is produced by the difference in the electromagnetic torque, controlled by the speed controller of the machine, and the aerodynamic torque acting on the rotor of the turbine. This last component tends to cancel the decreasing effect that would eventually make the DFIG have a similar response to a simple induction generator connected to the grid, (Ekanayake et al., 2003).

4.1.3 Response of PMSG wind turbines in frequency events

A multi-pole PMSG wind turbine is connected via a full-scale frequency converter to the grid. The converter decouples the generator from the grid; the generator and the turbine system are not directly subjected to grid faults in contrast to the direct grid connected wind turbine generators. Therefore, the power output from the WTG does not change and no inertial response is obtained during a frequency event. The rotor speed of the multi-pole synchronous generator is not connected with system frequency at any means.

Large wind turbines nowadays substitute conventional generators in modern power systems under increasing wind power penetration conditions. The effect on the power system inertia and the availability of inertia response from wind turbines have become key issues for the secure integration of wind energy into the electrical grids, especially in autonomous power systems like Rhodes. In power systems, like the one studied in this

article, regular load shedding occurs due to large frequency deviations. Although sufficient spinning reserve is ensured to overcome any frequency problems, increasing wind power penetration is challenging the system security.

Supplementary control attributes have been proposed in the literature in order to achieve active frequency control by the wind turbines, (Morren et al., 2006; Ullah et al., 2008; Ekanayake et al., 2003; Ekanayake & Jenkins, 2004; Holdsworth et al., 2004; Suwannarat et al., 2007). In most of these publications, simple models for either the power system or the wind turbines are used based mainly on the assumption that the aerodynamic torque acting on the rotor during the frequency event does not vary significantly. In this section, the three different frequency control methods, which were applied in the DFIG wind turbine models used in the Rhodes power system model, are described:

- Inertia Control
- Droop Control
- Combined Control

Results from frequency events in the Rhodes power system when these control methods are used in the wind farms equipped with DFIG wind turbines are given in Section VI. The general control scheme is illustrated in Figure 28.

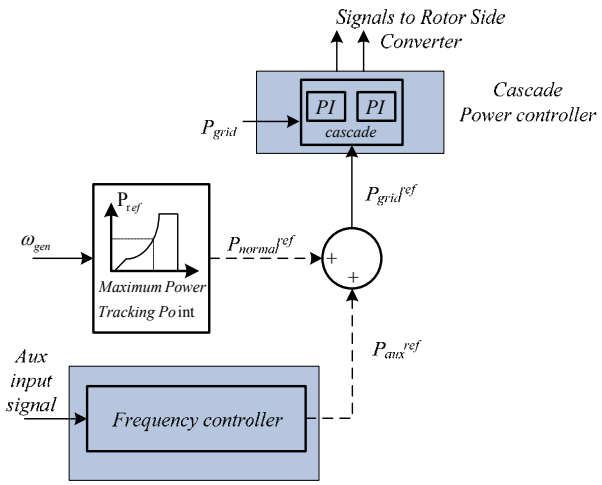

Fig. 28. General frequency control scheme for DFIG wind turbines

In the first method, the inertial response of the DFIG is restored through an additional loop in the power reference block providing the active power reference signal to the Rotor Side Converter. Details for the basic control structure of the DFIG model designed in this study for normal operation can be found in section 3.1.1. Figure29 shows the inertia control loop.

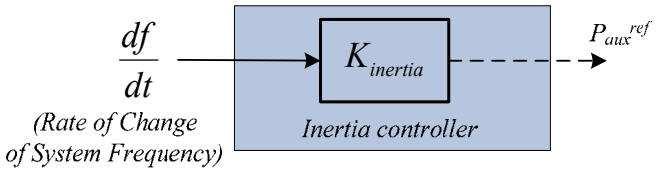

Fig. 29. Inertia controller for DFIG wind turbine

This feature is often referred to as "virtual inertia" effect, thus the control aim is to control the DFIG wind turbine to adjust its power output when subjected to frequency deviations. The rate of change of frequency defines the additional power reference signal, which is added to the normal power reference provided by the Maximum Power Tracking Controller. This auxiliary signal introduces a term proportional to $2H\frac{df}{dt}$, where H is the total inertia constant of the wind turbine, (Suwannarat et al., 2007). This inertia constant is expressed in seconds and represents the time that the wind turbine is able to provide with rated active power when decelerating the rotor from the nominal speed down to zero using only the available kinetic energy in the rotor mass, (Ullah et al., 2008). Thus, in physical terms the values of the proportional parameter $K_{inertia}$ shown in Figure 29 are restricted by this amount of energy. However, the wind turbine could be ordered to provide with even more active power, given that the stability of the system is ensured.
The second control method applied in the DFIG models is the Droop control, illustrated in Figure 30.

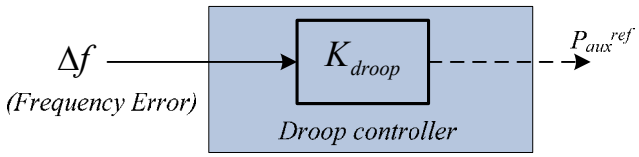

Fig. 30. Droop controller for DFIG wind turbine

In this case, the additional reference signal is equal to:

$$P_{aux}^{ref} = K_{droop}\left(f - f_o\right) \tag{6.1}$$

where f_o is the nominal system frequency, 50 Hz for the Rhodes power system. This control method is based on the primary frequency control applied to conventional generators. Typical values for the droop parameter of large conventional units are 3%-5%, depending on the type of unit.
This control loop aims to decrease the accelerating torque acting on the generator rotor during a frequency drop, as described above for DFIG wind turbines, (Ekanayake et al., 2003). The droop control can be assumed to be implemented in the wind farm controller level instead of individual wind turbine controller. This means that the overall wind farm controller provides the auxiliary signal P_{aux}^{ref} which is distributed to the individual wind turbine controllers. In that case, the communication delays should be taken into consideration, as the rate at which the wind farm changes its output during the first milliseconds following the frequency event is crucial for the overall system response. Results from both control levels, thus Droop controller on individual wind turbine controller and Droop controller on wind farm controller, are shown and compared.
The last method tested in this study, is actually a combination of the two first control methods. Based on the analysis made in (Ekanayake et al., 2003) and referred in section 2.2 for DFIG wind turbines, the sum of Droop and Inertia control should manage to counteract

the opposite torques acting on the generator rotor during frequency phenomena. The Combined control scheme is given in Figure 31.
As a first approach, this last method of Combined Control seems to be optimum for the DFIG wind turbines. In most of the publications available, Droop Controller and Inertia controller have been treated independently. Discussion on the results from each control method proposed here is made in section 4.2.

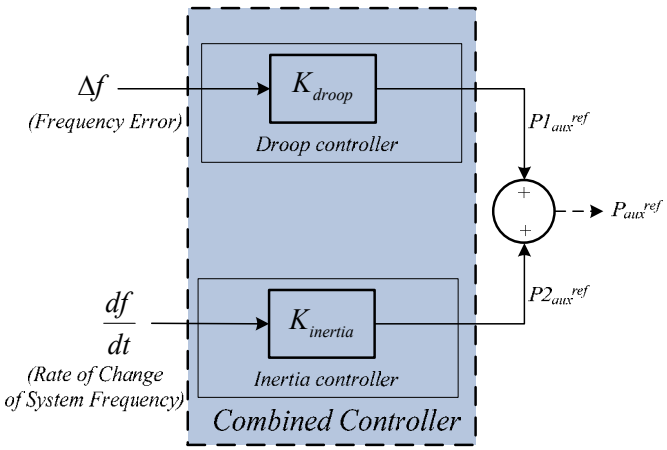

Fig. 31. Combined controller for DFIG wind turbine

4.2 Results

In this section, results from the Rhodes power system are presented. The frequency control capability of DFIG wind turbines is investigated for the load scenarios defined above. The standard event often used to check the dynamic security of power systems, thus the loss of the largest conventional generator, is simulated and the frequency response of the system under the different frequency control methods is illustrated. The emphasis on these results is given on the first seconds of the primary control operation of the system and the load shedding following the event is computed, based on the action of the under-frequency protection relay settings.
In SCENb, the wind farms online produce close or equal to their rated capacity. The total wind power production is 45.21 MW which stands for 27% of the total demand. The wind speeds in both wind farms equipped with auxiliary frequency control capability the wind is considered constant during the event studied, close to 11.5 m/s. The largest conventional unit produces 20.1 MW when ordered to trip, leading to loss of 11% of the total production. Figure 32 shows the response of three wind farms during this fault, when no auxiliary control is activated in the wind turbines. The wind farm with ASIG wind turbines increases its active power output during the first seconds following the frequency drop, contributing to the system inertia. On the other hand, the wind farm with DFIG wind turbines has almost negligible power contribution, while the PMSG wind farm does not change its active power output during the frequency drop. These results confirm the analysis made in Section III

regarding the natural response of each wind turbine type. The change in active power output for each wind farm in Figure 32 is given in p.u. of the rated capacity of each wind farm.

Figure 33 shows the frequency response for all different control methods for frequency control in the wind farms with DFIG wind turbines described in Section IV. In SCENb, these two wind farms produce in total 15 MW – 9% of the total demand. In the same figure, the results for Droop control implemented in the wind farm level or the wind turbine level are included.

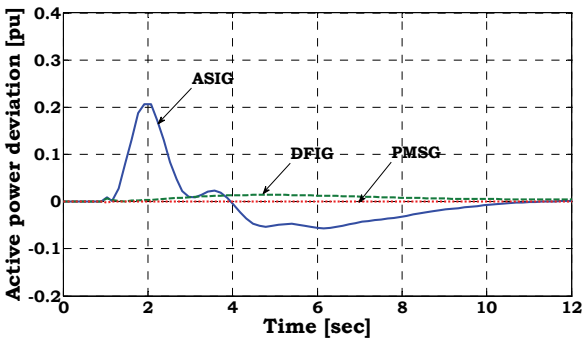

Fig. 32. Change in power in different wind turbine configurations during frequency drop - SCENb

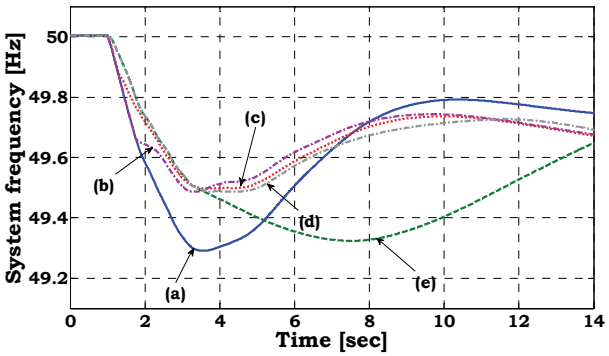

Fig. 33. System frequency for largest unit loss when frequency control is applied by DFIGs – (a) No auxiliary control, (b) Droop control on WF level, (c) Droop control on WT level, (d) Combined control, (e) Inertia control - SCENb

When no aux control (case (a)) is used in the DFIG wind farms, the frequency reaches its minimum (see also Table 2 below) with the highest initial rate of change of frequency. In this scenario, even in the case with no auxiliary control provided from wind farms there is no load shedding as the system inertia is high enough to ensure moderate frequency drops. The Droop control implemented in the wind farm control level (case (b)) does not manage to improve the maximum rate of change of frequency, although the minimum frequency is higher compared to the case (a). The best case, in terms of minimum frequency, is as expected case (c), where Droop control is implemented in the wind turbine control level. On the other hand, the Inertia control (case (e)) achieves the slowest rate of change of frequency

although the frequency minimum is the lowest among the different frequency control methods proposed here. The optimum performance seems to be achieved through the Combined control scheme (d) where both minimum frequency and maximum rate of change of frequency are improved. This last control method seems to combine the pos from the Droop and Inertia control schemes. The droop control implemented in the wind turbine control level (case (c)) has slightly higher minimum frequency but the difference is negligible (0.01 Hz).
Figure 34 shows frequency drop during the first 2 seconds after the loss of the conventional unit to clarify the effect of each control method on the initial rate of change of frequency.

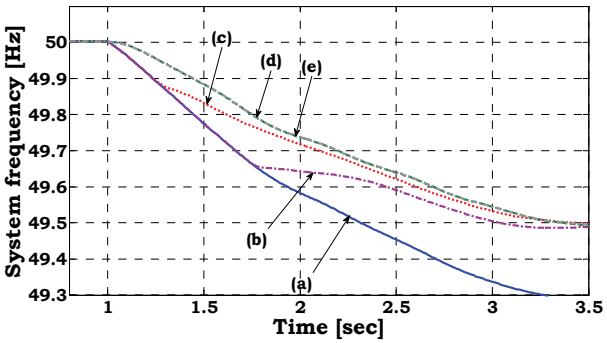

Fig. 34. System frequency for largest unit loss when frequency control is applied by DFIGs – Zoom in the first seconds after the event (a) No auxiliary control, (b) Droop control on WF level, (c) Droop control on WT level, (d) Combined control, (e) Inertia control - SCENb

The results for this scenario are summarized in Table 3, where the minimum frequency, the maximum rate of change of frequency and the load shedding are computed for all the cases demonstrated above.

Frequency Control Scheme		Minimum Frequency (Hz)	Maximum Rate of change of frequency (Hz/sec)	Load Shedding (MW)
(a)	**No auxiliary control**	49.29	-0.48	0
(b)	**Droop control on WF level**	49.49	-0.48	0
(c)	**Droop control on WT level**	49.41	-0.48	0
(d)	**Combined control**	49.49	-0.36	0
(e)	**Inertia control**	49.32	-0.36	0

Table 3. Results for SCENb– loss of largest infeed

The contribution of the wind farms during the frequency drop is obvious from the results presented above. From the wind turbine side now, the results for the rotor speed and the active power output of wind farm A1 (see Table 2) equipped with DFIG wind turbines are illustrated here for all the cases of frequency control.
As already discussed in section 2.2, the rotor speed of the DFIG wind turbines is not affected if no auxiliary frequency control is applied. Therefore, the inertia response of the DFIG is negligible (see Figure 35). In all the other cases, the rotor decelerates while the system frequency drops. Thus, the kinetic energy accumulated in the rotor mass is converted to electrical energy and delivered to the grid – giving the power surge during the primary frequency control period shown in Figure 36.
When Inertia control is used (case (e)), the rotor speed goes back to its pre fault value, as the auxiliary power reference signal is calculated based on the derivative of the frequency $\frac{df}{dt}$.
When the frequency stabilizes after the primary frequency control period, although not nominal yet as the secondary control has not been activated in this time frame, the derivative goes to zero and the auxiliary power reference signal goes also to zero. However, in the rest of the frequency control schemes, when droop control is used, the rotor speed is decreasing reaching another steady state value, as the difference from the nominal value remains even after the stabilization of the frequency. This means, that the wind turbine is no longer operating in the maximum power tracking curve as the normal control demands, (Ekanayake & Jenkins, 2004). The tertiary response which re-establishes the rotor speed of the wind turbine may take place several seconds after the event, when the power system has overcome the imbalance and the stress to stabilize the frequency. This procedure could also be implemented as part of an Automatic Generation controller operating in the whole power system, including the wind farms as active components, (Margaris et al., 2010).

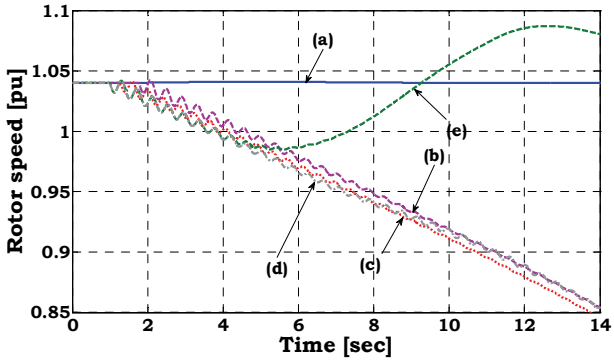

Fig. 35. Rotor speed deviations after largest unit loss for different frequency control methods applied in DFIGs - (a) No auxiliary control, (b) Droop control on WF level, (c) Droop control on WT level, (d) Combined control, (e) Inertia control - SCENb

The active power output of the wind farm A1 is given in Figure 36. In cases (d) and (e), where Inertia control and Combined control are used respectively, the wind farm increases its active power at a high rate, thus leading to lower rate of change of frequency as described in Table 3 above. In case (a) of course, when no auxiliary control is provided the active power change is negligible. In cased (b), where the Droop controller is assumed to work in the wind farm control level, the power surge is delayed compared to case (a).

In SCENc, the wind power penetration is maximum. The total wind power production is 28.2 MW in total 83 MW of demand (34 %). Although, the wind farms produce less than in the Maximum Wind Power Production scenario (SCENb) studied above, the impact of wind power in the power system operation is considered far more significant. The system inertia is decreased in this case, making the frequency control task in the system more complex. The wind speeds in this scenario is almost 9.3 m/s for the wind farms A1 and A2 (see Table 2).

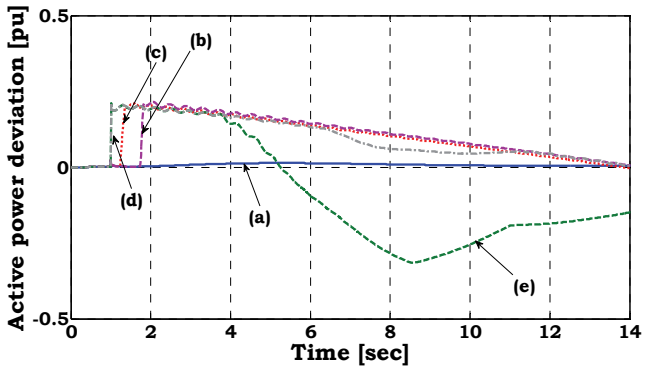

Fig. 36. Change in active power output after largest unit loss for different frequency control methods applied in DFIGs - (a) No auxiliary control, (b) Droop control on WF level, (c) Droop control on WT level, (d) Combined control, (e) Inertia control - SCENb

The largest conventional unit in the system produces 21 MW before the protection system acts to take it out of operation – this means production loss equal to 25 % of the total demand. The fault is severe and the power system stability is checked for all the frequency control schemes designed in this study.

Figure 37 illustrates the response of the three different wind turbine configurations available in the Rhodes power system, during the event, when no auxiliary control is activated in the DFIG wind farms. The comments made in section 2.2 are confirmed by the results (see also

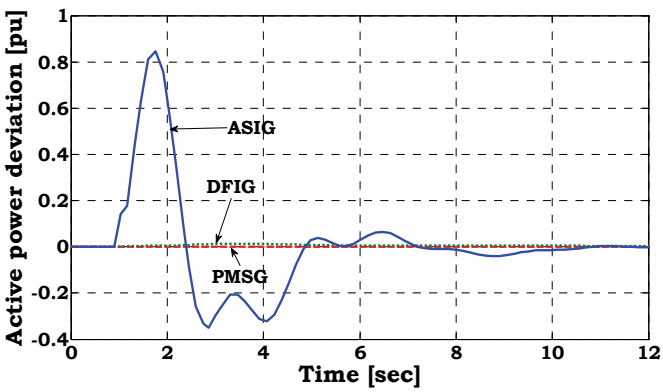

Fig. 37. Change in power in different wind turbine configurations during frequency drop – SCENc

Figure 32). Comparing to Figure 32, which demonstrates the response for SCENb, the contribution of the ASIG in SCENc is higher. The change in the active power production of the wind farm with ASIG wind turbines is higher than 0.8 pu compared to almost 0.2 p.u. in SCENb. This can be explained comparing the frequency response in both cases. In SCENb (see Figure 33 – case (a)), the frequency does not decrease as much as in SCENc (see Figure 38 – case (b)), therefore, the rotor of the ASIG wind turbines decelerates more in the first scenario, leading to higher active power contribution. In Figure 37 the response of wind farms equipped with DFIG or PMSG wind turbines is almost negligible, as explained in section 2.2.

In Figures 38 and 39 the system frequency for all the different frequency control schemes implemented in the wind farms A1 and A2 (see Table 2) is shown. In this scenario, the minimum frequency following the event is very low compared to SCENb, whereas the maximum rate of change of frequency is significantly higher.

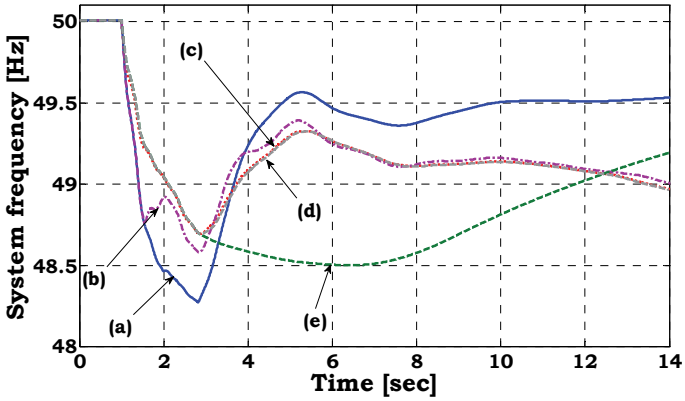

Fig. 38. System frequency for largest unit loss when frequency control is applied by DFIGs – (a) No auxiliary control, (b) Droop control on WF level, (c) Droop control on WT level, (d) Combined control, (e) Inertia control - SCENc

In case (a), when the wind farms do not have auxiliary frequency control, the frequency drops below 48.5 Hz which is the upper zone of the under-frequency protection relay settings acting on the loads. This drop leads to disconnection of 15.1 MW of load – 18 % of the total demand. This load shedding is not considered accepted in terms of dynamic security terms, (Margaris et al. 2009). However, in all the other cases, where the frequency control is activated in the DFIG wind farms, the load shedding is avoided totally. The maximum frequency drop appears in case (e), where the inertia controller is used. The optimum frequency drop in terms of minimum frequency is achieved in cases (c) and (d), thus when either Droop control is implemented on the wind turbine control level (case (c)) or when the Combined control is used (case (d)).

In this scenario, the effect of auxiliary frequency control on the maximum rate of change of frequency is very crucial. As illustrated in Figure 39, where the initial drop of the frequency for all cases is zoomed in, and as summarized also in Table 4, this rate is very high compared to SCENb (see also Table 3). The inertia of the system in this case is lower because the number of the conventional generators connected to the system in SCENc, and which are the ones determining the system inertia in large percentage, are reduced.

The rate of change of frequency is close to 2.8 Hz/sec (in absolute value) in cases (a) and (b), although in the last case the minimum frequency does not drop below 48.5 Hz. Inertia control manages to reduce the rate to less than 1.8 Hz/sec, which is the highest rate among all the cases. Here also, as explained for SCENb above, the Combined control seems to be the best compromise in terms of minimum frequency and maximum rate of change.

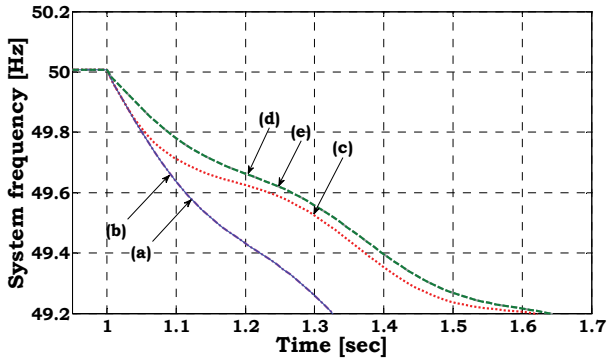

Fig. 39. System frequency for largest unit loss when frequency control is applied by DFIGs – Zoom in the first seconds after the event (a) No auxiliary control, (b) Droop control on WF level, (c) Droop control on WT level, (d) Combined control, (e) Inertia control - SCENc

Frequency Control Scheme		Minimum Frequency (Hz)	Maximum Rate of change of frequency (Hz/sec)	Load Shedding (MW)
(a)	**No auxiliary control**	48.28	-5	15.1
(b)	**Droop control on WF level**	48.58	-5	0
(c)	**Droop control on WT level**	48.69	-5	0
(d)	**Combined control**	48.69	-3.8	0
(e)	**Inertia control**	48.50	-3.8	0

Table 4. Results for SCENc – loss of largest infeed

Figure 40 and Figure 41 show respectively the rotor speed deviation and the change in active power output for wind farm A1, during the frequency drop. The comments made in SCENb are also valid here, regarding the differences among the various frequency control schemes. However, looking at the active power produced by the wind farm A1 in SCENc the contribution of the wind farms is more significant during the primary frequency response. The rotor deceleration is higher, thus more kinetic energy from the rotor mass is delivered to the grid as active power.

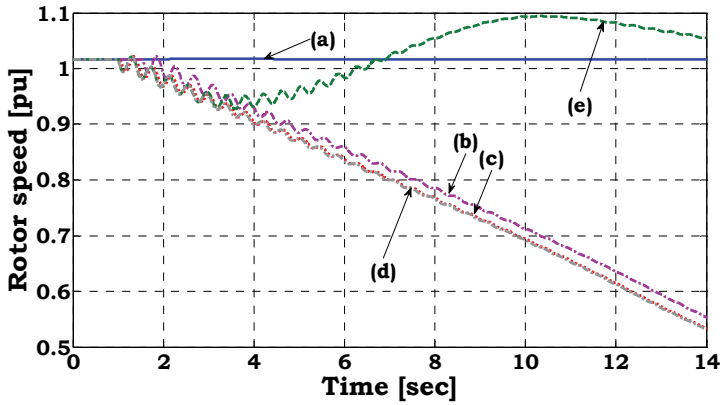

Fig. 40. Rotor speed deviations after largest unit loss for different frequency control methods applied in DFIGs - (a) No auxiliary control, (b) Droop control on WF level, (c) Droop control on WT level, (d) Combined control, (e) Inertia control – SCENc

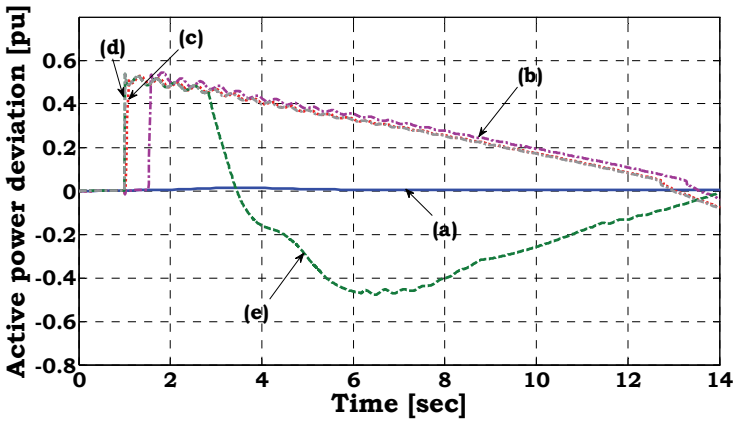

Fig. 41. Change in active power output after largest unit loss for different frequency control methods applied in DFIGs - (a) No auxiliary control, (b) Droop control on WF level, (c) Droop control on WT level, (d) Combined control, (e) Inertia control - SCENc

In the last part of the results section, comparative results will be shown for SCENb between the cases, where Combined frequency control is implemented only in one wind farm and the later, where the control is incorporated in both wind farms with DFIG wind turbines. All

the results presented previously are extracted when both wind farms A1 and A2 have this frequency control capability.
As shown in Figure 42 and also summarized in Table 5 below, in case (d1) only wind farm A1 provides auxiliary frequency control leading to bigger frequency drop and higher rate of

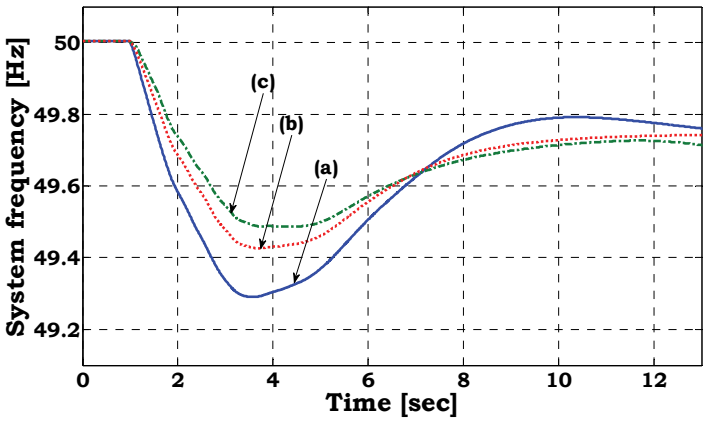

Fig. 42. System frequency for largest unit loss for different frequency control methods applied in DFIGs - (a) No auxiliary control, (b) Combined control provided by only one wind farm (c) Combined control provided by two wind farms

Frequency Control Scheme		Minimum Frequency (Hz)	Maximum Rate of change of frequency (Hz/sec)	Load Shedding (MW)
(a)	**No auxiliary control**	49.29	-0.48	0
(b)	**Combined control through one wind farm**	49.43	-0.4	0
(c)	**Combined control through two wind famrs**	49.49	-0.36	0

Table 5. Results for SCENb – loss of largest infeed

change of frequency compared to case (d2) where also wind farm A2 is equipped with this control capability. Thus, the inertia of the system, including the "virtual" inertia provided by the DFIG wind turbines, is obviously reduced when the proportion of the wind turbines providing auxiliary control is smaller. It is noted here, that in this comparison the Combined control method was chosen, as it is concluded by the previous results that this scheme achieves the best performance among the other proposed ones.
The conclusions from all the results presented in this section will be summarized in the next session, where also discussion on the expansion of the maximum allowed penetration in autonomous systems, like Rhodes, is made.

5. Conclusions

This chapter presented a detailed investigation of Rhodes power system dynamic security in the case of reference year 2012, when large wind farms are expected to be connected to the island. The conventional units, including Automatic Voltage Regulators and Speed Governors, were modeled in detail. The response of the governors during dynamic phenomena in the system is essential for the overall response. Especially the emergency rate of power undertake by the all different kinds of units i.e. steam, gas and diesel plants, is a major factor defining the overall system operation. The presented models includes also the models of the five wind farms which are connected in the system, comprising detailed models for three different wind turbine technologies – namely Doubly Fed Induction Generator (DFIG), Permanent Magnet Synchronous Generator (PMSG) and Active Stall Induction Generator (ASIG) based wind turbines.
Different load scenarios, relevant for the island operation, are analyzed, such as maximum wind power penetration scenario, maximum wind power production scenario and maximum load demand scenario.
In many non-interconnected systems the penetration of wind power has started to reach the boundaries of 30%. Serious concerns are expressed by the operators of these systems and wind fluctuations are one of the aspects that has to be evaluated before expanding the penetration levels, (Margaris et al., 2011). From the results, it is concluded that even in the worst case scenario, the Maximum Wind Power Penetration, the frequency fluctuations resulting from the wind speed fluctuations are not considered to pose security questions for the power system. However, the impact of wind variations is obvious in the system frequency and the correlation between wind speeds and system frequency has to be always investigated before reviewing the penetration levels.
Increased wind power penetration does not only limit the ability of thermal plants to undertake power, but also limits inertia. Systems inertia in cases of increased wind penetration is crucial for system stability as it defines the rate of frequency drop. The designed models for the conventional units in Rhodes power system, were sufficient to undertake power despite the rapid wind changes and the resulting active power fluctuations delivered by the wind farms. This study has proven that, when it comes to wind power fluctuations, the penetration levels of wind power can be expanded beyond 30% of the load.
Another issue, which should be remarked, is that the increased wind power penetration does not only limit the ability of thermal plants to undertake power, but also the inertia of

the system. Systems inertia in cases with increased wind penetration is crucial for system stability, as it defines the rate of frequency drop.

The second part of the investigations provided a survey on frequency control issues of the autonomous power system with high wind power penetration, (Margaris et al., 2011). Frequency response during severe faults, i.e. the sudden loss of the biggest conventional generator, was simulated for two different load scenarios. These scenarios correspond to different system inertia but also to different operating points of the wind turbines. The wind turbines have different response when the system frequency varies, depending on the specific electrical configuration characteristics. Although the fixed speed ones contribute to the system inertia during frequency phenomena, this is not the case for DFIG and PMSG wind turbines, where the rotor is partially or totally detached form the system frequency respectively. The under-frequency protection system acting on the loads connected to MV substations can measure either the rate of change of frequency or the actual frequency to act on the relays. Modeling the protection system in the power system provides more accurate results regarding the load shedding, a variable that defines the dynamic security level of a system. As wind power penetration is increasing in modern power systems, the wind turbines have to contribute to the frequency stability of the system, acting similar to conventional power plants. In this article, three different frequency control schemes were investigated to enhance the primary frequency support of DFIG wind turbines. Simulation ended up to the following conclusions:

Non interconnected systems face the problem of decreased system inertia, especially when wind farms tend to substitute conventional units under increasing wind power penetration conditions. The DFIG wind turbines can be equipped with auxiliary Inertia control, providing with valuable inertia response during the first seconds following the frequency event. This control, reestablishes in the DFIG wind turbines the intrinsic characteristic of the fixed speed ASIG wind turbines, thus, using the kinetic energy accumulated in the rotor mass to support the grid during frequency variations.

Additional control methods can also be used in DFIG wind turbines, like Droop control used in conventional generators providing primary frequency support. The case, where the Droop control is implemented in the wind farm control level, instead of the turbine level, was also investigated to check the effect of communication delay in the response of the wind farm. Although when the Inertia control is used, the rate of change of frequency is significantly reduced, the Droop control seems to benefit more power system when looking at the minimum frequency after the event.

A Combined control, where both Inertia and Droop control schemes are used, was incorporated in the model. This last method manages to combine the positive effects of both methods, improving not only the initial rate of change of frequency after the fault but also ensuring lower frequency drop.

In some cases, when wind power production is higher than 30 % of the total demand, the auxiliary frequency control implemented in two wind farms in the Rhodes power system, manages to avoid load shedding totally. Therefore, the rule of thumb of 30 % penetration, which is often used in autonomous power systems, can be further expanded as long as auxiliary frequency control is provided by wind farms.

The benefits of the primary frequency support from modern wind turbines increase as the number of the turbines with this capability rises. This means that, if all new wind farms

installed in autonomous power systems are equipped with primary frequency control capability, the frequency stability can be ensured even for penetration levels that today are hard to consider.

From the wind turbine side, in some cases the turbine may be forced to operate away from the maximum power-tracking curve, which means economic cost for the wind farm. So, before the system operators set any requirements for frequency control, the economic costs of frequency control for the wind turbine owner should be addressed.

The review of the frequency protection system settings can be done, as long as the frequency stability of the system is ensured. In many cases, the protection settings are quite sensitive and large amounts of load are cut off. The review of the protection system in modern power systems has to follow the progress made in the wind farms' capability to support the grid during disturbances.

Although, technology such as flywheels can support system inertia in autonomous power systems, advanced frequency control implemented in wind turbines will make it possible to achieve the penetration levels for wind power that today seem hard to reach.

There are some measures that can further enhance the dynamic security of systems like Rhodes:

The review of the frequency protection system settings can be done, if the dynamic security is ensured through FRT capability of wind farms online. The protection settings are quite sensitive and large amounts of load can be cut off just after the fault incident.

Systems like SVC or STATCOM for fast voltage control systems can guaranty the uninterrupted operation of wind parks, especially those consisting of fixed speed wind turbines. For instance, the substation, where most of these wind parks are connected, could be considered as the most appropriate for this installation. Under these conditions, wind power penetration could increase beyond 30% of the load, keeping the dynamic security of the system in the acceptable levels.

6. References

Ackermann, T. (Ed.) (2005). *Wind Power in Power Systems*, John Wiley and Sons, ISBN: 9780470855089.

Akhmatov V. (2003). *Analysis of dynamic behavior of electric power systems with large amount of wind power*, PhD thesis, 2003, Ørsted DTU.

Cutsem, T.V., Vournas C. (1998). *Voltage Stability of Electric Power Systems*, Springer, ISBN: 9780792381396 .

DIgSILENT (2006). *DIgSILENT technical documentation – PowerFactory*.

Ekanayake J., Holdsworth L., and Jenkins, N. (2003). Control of DFIG wind turbines. *Power Engineer*, Vol. 17, No. 1, (2003), pp. 28–32.

Ekanayake J, and Jenkins N. (2004). Comparison of the response of doubly fed and fixed-speed induction generator wind turbines to changes in network frequency. *IEEE Trans. Energy Conversion*, Vol. 19, No. 4, (2004), pp. 800–802.

Gail G., Hansen A.D., and Hartkopf T. (2006). Controller design and analysis of a variable speed wind turbine with doubly-fed induction generator, *EWEC*, Athens, 2006.

Hansen A.D., Jauch C., Sørensen P., Iov F., and Blaabjerg F. (2003). Dynamic wind turbine models in power system simulation tool DIgSILENT. *Risø-R-1400(EN)*, 2003.

Hansen A.D., Sørensen P., Iov F., Blaabjerg F. (2006). Centralised power control of wind farm with doubly-fed induction generators. *Renewable Energy*, Vol. 31, (2006), pp. 935-951.

Hansen A.D., and Hansen L.H. (2007). Market penetration of different wind turbine concepts over the years, EWEC, Milano, 2007.

Hansen A.D., and Michalke G. (2007). Fault ride-through capability of DFIG wind turbines. *Renewable Energy*, Vol. 32, (2007), pp 1594-1610.

Hansen A.D., and Michalke G. (2008). Modelling and control of variable speed multi-pole PMSG wind turbine. *Wind Energy*, Vol. 11, No. 5, (2008), pp 537-554.

Hansen M.H., Hansen A.D., Larsen T.J., Øye S., and Sørensen P. (2005). Control design for a pitch-regulated variable speed wind turbine, *Risø-R-1500 (EN)*, 2005.

Holdsworth L., Ekanayake J.B., and Jenkins N. (2004). Power system frequency response from fixed speed and doubly fed induction generator-based wind turbines. *Wind Energy*, Vol. 7, DOI:10.1002/we.105, pp. 21-35.

Jauch C., Hansen A.D., Sørensen P., and Blaabjerg F. (2004). Simulation Model of an Active-stall Fixed-speed Wind Turbine Controller. *Wind Engineering*, Vol. 28, No. 2, (2004), pp. 177-195.

Lalor G., Mullane A., and O'Malley M.J. (2005). Frequency Control and Wind Turbine Technologies. *IEEE Transactions on Power Systems*, Vol. 20, No. 4, (2005).

Mantzaris J, Karystianos M., and Vournas C. (2008). Comparison of Gas Turbine and Combined Cycle Models for System Stability Studies, *6th Mediterranean. Conf. MedPower*, Thessaloniki, Greece, 2008.

Margaris I.D., Mantzaris J.C., Karystianos M.E., Tsouchnikas A.I., Vournas C.D., Hatziargyriou N.D., and Vitellas I.C. (2009). Methods for evaluating penetration levels of wind generation in autonomous systems, *IEEE PowerTech Conf.*, Bucharest, June 2009.

Margaris I.D., Hansen A.D., Cutululis N.A., Sørensen P., and Hatziargyriou N. (2010). Impact of wind power in autonomous power systems – Power fluctuations – Modeling and Control issues. *Wind Energy*, online: DOI: 10.1002/we.417. 2010.

Margaris I.D., Papathanassiou S.A., Hatziargyriou N., Hansen A.D. and Sørensen P. (2011). Frequency control in autonomous power systems with high wind power penetration. under review in IEEE Transactions.

Morren J., Pierik J., and de Haan S.W.H. (2006). Inertial response of variable wind turbines. *Electric Power Systems Research*. Elsevier, Vol. 76, (2006), pp. 980-987.

Poeller M., and Achilles S. (2003). Aggregated wind park models for analyzing power system dynamics, *Fourth international workshop on large-scale integration of wind power and transmission networks*, Billund, Denmark, October 2003.

Ramtharan G., Ekanayake J.B., and Jenkins N. (2007). Frequency support from doubly fed induction generator wind turbines. *IET Renew. Power Gener.*, Vol. 1, No. 1, (2007), pp. 3–9.

Sørensen P., Cutululis N.A., Vigueras-Rodríguez A., Madsen H., Pinson P. , Jensen L.E., Hjerrild J. and Donovan M. (2007). Modelling of power fluctuations from large offshore wind farms. *Wind Energy*, Vol. 11, (2007), pp. 29–43.

Suwannarat A., Bak-Jensen B., Chen Z., Nielsen H., Hjerrild J., Sørensen P., and Hansen A.D., (2007). Power system operation with large scale wind power integration, *PowerTech 2007*, Lausanne Switzerland, July 2007.

Ullah N.R., Thiringer T., and Karlsson T. (2008). Temporary Primary Frequency Control Support by Variable Speed Wind Turbines – Potential and Applications. *IEEE Transactions on Power Systems*, Vol. 23, No. 2, (2008).

9

Short-Term Advanced Forecasting and Storage-Based Power Quality Regulation in Wind Farms

Juan Mendez and Javier Lorenzo
Universidad de Las Palmas de Gran Canaria
Spain

1. Introduction

This Chapter contains the results of our research activities in the line to reduce both: the uncertainties in power forecasting and the lack in power quality for Wind Farms connected to public grids. Our approach is a suite of studies that are focused on power forecasting for Electricity Markets and also an innovative simulation technique to evaluate the quality by using a coupled storage systems as water reservoirs, inertial systems or chemical batteries.
The use of renewable energy sources (RES) in electricity generation has many economical and environmental advantages, but has a downside in the instability and unpredictability introduced into the public electric systems. The more important renewable sources, wind and solar power, are mainly related to the weather in a local geographic area. However, the weather is a chaotic system with limited predictability. Many countries follow two trends in the development and planning of their public electric systems; the first is the increase in the generation power from RES and the second one is the transition to open electricity markets. These two trends have a common impact on the public grids, because they both increase the number of agents in the system and the level of uncertainty in the balance between generation and load.
The access of more and bigger RES electricity producers can increase the risk of fail and decrease the service quality. That risk can be reduced by increasing the power reserve based on high response gradient systems. These, e.g. diesel or hydraulic, have a high speed of change in their generated power, that is suitable to balance the frequent sudden and unpredictable changes of RES-based electricity production. Therefore, the positive impact of the use of RES on the cost of fuel consumption would have a negative impact on the global cost of electricity systems.
The control and planning of public electric systems covers a widespread set of levels, ranging from the hundred millisecond domain associated to the frequency and voltage controlErlich et al. (2006), to the yearly planning domain. Precise regulations for these levels are the concern of the national Electricity Authorities of each country as well as to supranational agencies. The EC Project STORIESPanteri (2008) provides an overview of existing regulations and the respective legislative framework related to RES implementation at a European level. In each national system, the Transmission System Operator(TSO) deals with the management of the electric system in the different control and planning levels. With the increasing penetration

of RES systems, the TSO becomes concerned with the impact on system stabilityEriksen et al. (2005).
The forecasting of RES power production is a basic tool in the reduction of these high operative reserve, which must be ready to be used. According to the practical experiences of E.ON, the largest German electric company, wind power is only as reliable as the weather forecastingE.ON-Netz (2004). If the wind power forecast differs from the actual infeed, the TSO must cover the difference by using the reserves, which must amount to 50-60% of the installed wind power. According to E.ON, the expected maximum forecast deviation is more important that the mean forecast error. This is because even if the actual infeed deviates from the forecast level on only a few days of the year, the TSO must also be prepared for this improbable eventuality and have sufficient capacity available, *spinning reserve*, for a reliable supply to still guaranteed and the correct balance between generation and load to be restored.
The Electric Authorities of many different countries have included the power forecasting in its Regulatory Norms in order to preserve the quality of the electricity supply. The planning of an Electric System requires several levels related to different time scales and whether forecasting requires also different levels. Very close short-term forecasting, or nowcasting, is the immediate prediction in a time scale ranging from some minutes to several hours. Short-term forecasting address a time scale that ranges from one to three days, while medium-term forecasting covers from four days to several weeks.
The statistical approach for short-term wind prediction has been used due to the system complexity of whether and the chaotic fluctuations of wind speed. The statistical models such as ARMA, ARX and Box-Jenkins methods have been used historically for short-term wind forecasting up to few hours ahead Landberg et al. (2003); Nielsen & Madsen (1996); Nielsen et al. (2006). Giebel Giebel (2003) reports some of the statistical state of the art models and methods for wind power forecasting which have been developed and used, such as time series models for up to a few hours by means of statistical approaches and neural networks, as well as models based on Numerical Weather Prediction(NWP).
The simplest time scale in power predictions is the nowcasting, which can be carried out by using the time series analysis. The short-term scale requires the cooperation between statistical and NWP tools, in regional and mesoscale weather models and cooperating with predictive systems as HIRLAN and MM5. The power forecasting for RES in Spanish Regulations is related to hourly periods of planning of the electricity market. All the power supplies and demands of the energy agents must be related to these hourly periods. The regulations for the short-term Spanish Electricity Market comprise two steps:

Short-term Forecasting. The RES producers, solar and wind farms, with power greater than 10 MW must provide 30 hours ahead the power forecasting for every hourly period of a full range of 24 hours.

Nowcasting. One hour ahead of each hourly period, corrections to the previous values can be sent to the Electricity Authority.

This means that in the nowcasting time scale, the computation of the predicted value must be carried out for the period covering two hours ahead. The second step can be carried out by using time series approaches, but the first requires the cooperation with NWP tools.
Artificial Neural Networks (ANN)Haykin (1999) have been widely used for modeling and predictions in the field of renewable energy systems Kalogirou (2001); Li et al. (1997) because they are able to handle noisy, incomplete data and non-linear problems to perform predictions and classifications Alexiadis et al. (1998); Kandil et al. (2006); Zhang et al. (1998). Hippert et

al Hippert et al. (2005) have addressed the construction, and evaluation, of their performance of very large ANNs in electric systems to forecast the load profile. Recurrent ANN Mandic & Chambers (2001) have been used as generalizations of predictive systems as ARMA. Also, they can be used to generalize linear predictive systems as Kalman filter Haykin (2001). Recurrent and recurrence in each layer, called multilayer recurrent, architectures have been also used in wind power predictionLi (2003).

Many studies about the use of ANN in wind power have been preformed, but the criteria to evaluate their performance have been mainly based on error parameters. Based on more modern standard protocol for forecastingMadsen (2004), the published results will provide improvement criteria over the persistence or references models of its same place. Persistence forecasting is a simple model that is intrinsic to the data, that is, it is a no algorithm approach. Any new proposed algorithm is so good or bad as how much is able to overtake the persistence. The use of ANN can provide a suitable procedure to beat it and other reference model based on the Wiener predictive filter. An application is presented applying the standard protocols with Feed Forward(FNN) and Recurrent Neural Networks(RNN) architectures in the background of the requirements for Open Electricity Markets.

The prediction in the time scale of nowcasting can be carried out by using the time series analysis approach. The short-term scale requires the cooperation between statistical and NWP tools, in regional and mesoscale weather models. In many countries the power forecasting for RES is related to hourly periods of planning of the electricity market. All the power supplies and demands of the energy agents must be related to these hourly periods. For example, as has been presented, the regulations for the short-term Spanish Electricity Market comprise two steps. In the step 1 in short-term time scale, the RES producers must provide the power forecasting for every hourly period of a full range of 24 hours 30 hours in advance. In step 2 in the nowcasting time scale, one hour ahead of each hourly period, corrections to the previous values can be sent to the Electricity Authority. This means that at the end of the hour h, the RES producer must send the corrections for the expected value of the average power, $\widehat{P}_{h+2}$, for hour $h+2$.

The prediction based on persistence is the simplest model and is based on the assumption of a high inertia in the subjacent physical model. If $y(t)$ is the value at time t of a time series, in persistence model the predicted value for k time ahead is: $\widehat{y}(t+k) = y(t)$. The simple persistence model can be overtaken by other. more advanced, models that involve persistence-like information. A reference model to compare different forecasting models has been proposed Madsen (2004); Nielsen et al. (1998). It includes very short-term information, such as persistence, and long-term information. This proposed reference model is an extension of the pure persistence defined by the linear expression: $\widehat{y}(t+k) = b + ay(t)$.

In an Electricity Market applications we have two kinds of power values, the spot power $P(t)$ and its hourly average P_h. For the TSO, the spot power is very important to ensure the system stability at any time, but in the Electricity Market the hourly average is that required to RSE agents. The reference model for wind power forecasting proposed by Madsen Madsen (2004) can be applied for hourly average power such as that required in the Spanish regulation as: $\widehat{P}_{h+2} = A_0 P_h + (1 - A_0)\overline{P}$, where A_0 and $\overline{P}$ are parameters computed from large-term training information. It is difficult to beat this reference model because is based on the shortest-term information, P_h, and in the longest-term information, $\overline{P}$.

Even if the forecasting techniques for RES power were perfect, the problems that its high penetration introduce in grids would not be avoided. Figure 1 shows a power series $P(t)$ in time steps of one minute, and their hourly average P_h. That last one is the best prediction

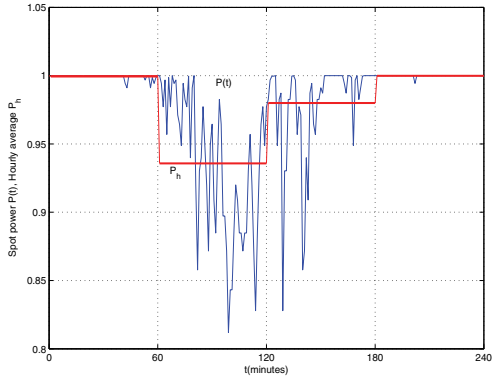

Fig. 1. Spot power and its hourly average for a wind power generator. Even though we can have the perfect hourly prediction, the lack of quality in spot power can be significative

that we can achieve. Even using this ideal case, the difference between the spot power $P(t)$ and the best estimated planed power $\widehat{P}_h = P_h$ is significant. The lack of quality in the electricity production based on RES, such as wind power, must require of higher power spinning reserves that entail additional costs. If the penetration of RES based power increases significantly, those costs will be billed to the RES producer by means of penalties. These are, or will be, imposed by the Electricity Authorities associated with the lack of quality in the fed energy.

The variance shown in every hourly period can be avoided by using short-term storage systems that reduce the impact of the chaotic behavior of the local weather in the public grids. Short-term storage systems can be implemented by using different technologies such as electric batteries, hydraulic reservoirs or inertial systems. Lazarewicz and Rojas Lazarewicz & Rojas (2004) identify some of the basic problems involved in frequency regulation and their solution by using large batteries of inertial systems. Drouilhet Drouilhet (1999) presents a wind power system with a diesel generator and a short-term energy storage using electric batteries. This system focuses on the power flow management, frequency and voltage control for high penetration of wind sources, mainly in isolated rural electrical systems. Its conclusion is that in conventional power generation systems, the short-term load variations are usually small and the main power source can supply the demand, but in the high penetration wind power systems the power feed to the system is stochastic in nature and highly variable. EdsingerEdsinger et al. (1978) focuses on the evaluating of the economic feasibility as well as on the general performance of wind energy systems with energy storage options.

An application where the use of storage energy systems have been used extensively is in space applications where the supply of solar power changes along the orbit. The use of hybrid system of batteries and flywheels has been proposed and simulated Beaman & Rao (1998). To avoid the inertial problems, two or more counter-rotating wheels are used to produce null angular momenta. The design of such systems requires the definition of the battery and flywheel charging control schemes and the solar array regulation. The main advantages of inertial storage systems that have been proposed for satellite and space oriented applications is its reduce mass Fausz & Richie (2000); Wilson et al. (2005). The simulation of these systems was conducted using the power model for the Flywheel Attitude Control,

Energy Transmission, and Storage (FACETS), which is constructed by using blocks provided in the Matlab and Simulink packages.
Our approach is to study the energy and power management rather than the modeling and simulation associated with any specific technology, device or technical solution. We agree that a first level of a simulation can be a general one based on the power and energy flows and transfer, while a more detailed simulation of a defined solution, which must use defined models for wind farmsTande et al. (2007) and grid interactionHansen et al. (2002), can be achieved after the analysis of the results obtained in the power and energy oriented simulation. For example, a general simulation can provide the total amount of energy storage needed for an RES system based on its logged power data. At this stage, it does not matter which kind of technology is used in a more detailed forward modeling. This paper includes a mathematical model of power and energy transfer between the RES source, the energy storage and the public grid.

2. Power forecasting by using ANN

Persistence is the simplest model for forecasting. It is based on the assumption of a high inertia in the subjacent physical model. If $y(t)$ is the value at time t of a time series, in persistence model the predicted value for k times ahead is: $\widehat{y}(t+k) = y(t)$. This kind of forecasting is really simple but can be very useful in practical, because it can be used as reference model to compare different theoretical and practical applications. Any proposal of a new model or approach that requires some computational resource is required to have at least a better performance that this simple one. The level of improvement over this reference model must be a level of utility of the additional formal and computational cost. A high value in an error parameter, as MAE or RMSE, in a hardly predictable site can be a better result that a small value in a easily predictable site. However there are not a parameter to define what site has a hardly or easily predictable wind. A option is the use the own persistence as the reference to which compare the performance of proposed algorithms.
The pure persistence model can be overtaken by other model that involve persistence-like information. A reference model to compare different forecasting models has been proposed Madsen (2004); Nielsen et al. (1998). It is more advanced because it includes very short-term information, as persistence, and long-term information. This proposed reference model is an extension of the pure persistence as a linear expression: $\widehat{y}(t+k) = b + ay(t)$. A detailed analysis allows to show that is really the first order case of a more general linear predictive filter, as the Wiener filter with general expression:

$$\widehat{y}(t+k) = B + \sum_{i=0}^{m} A_i y(t-i) \tag{1}$$

where coefficients A_i and B can be computed from the matrix containing the cross correlation between $y(t+k)$ and $y(t-i)$. The constant parameter is $B = (1 - \sum_{i=0}^{m} A_i)\overline{y}$, where $\overline{y}$ is the large-term average value of $y(t)$. For the simplest case of first order filter: $\widehat{y}(t+k) = B + A_0 y(t)$, the value of the coefficient is:

$$A_0 = \frac{\int [y(t+k) - \overline{y}][y(t) - \overline{y}]dt}{\int [y(t) - \overline{y}]^2 dt} \tag{2}$$

In an Electricity Market we have two kind of power values, the spot power $P(t)$ and its hourly average P_h. For the TSO, the spot power is very important to assure the system stability at

any time, but in the Electricity Market the hourly average is the required to RSE agents. The proposed reference model for wind power forecasting by Madsen Madsen (2004), is applied for hourly average power in nowcasting as the required in the Spanish regulation as:

$$\widehat{P}_{h+2} = A_0 P_h + (1 - A_0)\overline{P} \tag{3}$$

where A_0 and $\overline{P}$ are parameters computed from large-term training information. This reference model, which we can call as improved persistence or Wiener persistence, is harder to beat because is based in the shortest-term information, P_h, and in the longest-term information, $\overline{P}$.

The basic theory for using ANN in prediction, its architectures and algorithms are in the area of adaptive and predictive linear filterMandic & Chambers (2001). The use of ANN has generated generalizations that has introduced improvements in the original linear models by allowing the construction of nonlinear predictive systems. The relationship between ANN, in special recurrent architectures, with linear predictive systems as ARMA allows nonlinear generalizations of previous statistical linear approaches. A generalization of recurrent ANN is the multilayer recurrentLi (2003); Mandic & Chambers (2001). In the wind power forecasting the problem can be formulated by using Feed Forward(FNN), without feedback, or Recurrent(RNN) ones:

$$\widehat{P}_{h+2} = F\left[V_h, \ldots, V_{h-n+1}, P_h, \ldots, P_{h-m+1}\right] \tag{4}$$

The used training procedure was the Bayesian regularization Foresee & Hagan (1997); MacKay (1992) which updates the weight and bias values according to the Levenberg-Marquardt Levenberg (1944); Marquardt (1963) optimization procedure. It uses as goal function a combination of squared errors and weights, and then determines the correct combination so as to produce a network that generalizes well. The Bayesian regularization implementation that has been used is the implemented in the training function *trainbr* of the Neural Networks Toolbox of MATLABDemuth et al. (2008). The NARX architecture have been used for RNN with the same window size for input data, the wind speed, and feedback data, the wind power.

2.1 Results in power forecasting

We have used a wind data series acquired in Gran Canaria Island(Spain). The wind speed series comprise about 33 days data from a meteorological tower in time steps of one minute. Wind power series are obtained from the wind speed at 40 meters high and from a power transfer function with 5 and 12.5 m/sec cut-off values. Relative values about the nominal values, $P(t)/P_n$, are used in the power series. The data set was split in two subset, the train and test. The train data is 2/3 of the global data. The standard protocol for performance evaluation suggested by MadsenMadsen (2004) was used. It includes the definition of the Evaluation Criteria(EC) BIAS, MAE, RMSE and SDE, and also the improvement over the reference model which are computed in percent value as:

$$Imp_{ref,EC}(\%) = 100\frac{EC_{ref} - EC}{EC_{ref}} \tag{5}$$

Many training procedures of ANN use optimization procedures that run from initial random states. The optimization tries to reach a minimum value of some goal function, but the reached value and the trained network depend on the initial random state. In the practice, that means that the performance of a trained ANN has some random degree. To reduce the uncertainty

	Pers. Ref.	RNN1	RNN2	RNN3	RNN4	RNN5
Delay		(2:3)2	(2:5)4	(2:7)6	(2:7)6	(2:7)6
Hidden Nodes		80	40	10	40	60
BIAS	0.6 0.9	0.5 ± 0.1	0.3 ± 0.1	0.1 ± 0.3	0.3 ± 0.4	0.3 ± 0.1
MAE	14.5 15.3	15.5 ± 0.2	15.3 ± 0.1	15.7 ± 0.5	15.3 ± 0.2	$15.3 \pm 0,1$
RMSE	23.7 22.3	22.3 ± 0.3	21.6 ± 0.1	22.5 ± 1.2	21.5 ± 0.1	21.6 ± 0.1
SDE	23.7 22.3	22.4 ± 0.3	21.6 ± 0.1	22.5 ± 1.2	21.6 ± 0.1	21.6 ± 0.1
Imp_MAE		$-0.4\pm, 1.2$	1.1 ± 0.5	-2.5 ± 3.3	0.6 ± 1.0	0.4 ± 0.9
Imp_RMSE		0.0 ± 1.2	3.3 ± 0.3	-1.0 ± 5.3	3.3 ± 0.6	3.2 ± 0.6
Imp_SDE		-0.1 ± 1.2	3.2 ± 0.3	$-1.1\pm, 5.3$	3.2 ± 0.6	3.1 ± 0.6

Table 1. Comparative results for two hours ahead prediction by using several RNN configurations trained with Bayesian regularization. All Evaluation Criterion and their improvements over the reference model are in percent(%) normalize to the nominal power. The mean and standard deviation, $\mu \pm \sigma$, values are provided for 25 training trials

	FNN1	FNN2	FNN3	FNN4	FNN5	FNN6
Delay	(2:4)3	(2:4)3	(2:6)5	(2:6)5	(2:11)10	(2:11)10
Hidden Nodes	3	6	5	10	10	20
BIAS	3.0 ± 1.8	4.0 ± 2.5	1.4 ± 0.3	1.4 ± 0.9	2.4 ± 2.4	3.2 ± 3.1
MAE	16.2 ± 1.0	16.8 ± 1.2	15.7 ± 0.4	16.0 ± 0.7	16.7 ± 1.3	17.4 ± 1.7
RMSE	22.7 ± 0.4	22.9 ± 0.6	22.2 ± 0.4	22.4 ± 0.5	22.6 ± 0.8	23.4 ± 1.3
SDE	22.5 ± 0.2	22.5 ± 0.3	22.2 ± 0.3	22.4 ± 0.5	22.5 ± 0.6	22.0 ± 1.1
Imp_MAE	$-4.8\pm, 6.5$	-8.6 ± 8.0	-1.3 ± 2.7	-3.1 ± 4.8	-7.4 ± 8.0	-12.3 ± 10.7
Imp_RMSE	-2.1 ± 2.0	-2.9 ± 3.0	2.7 ± 1.6	-0.6 ± 2.3	-1.5 ± 3.4	-4.7 ± 5.8
Imp_SDE	-1.0 ± 0.9	-0.8 ± 1.2	$0.4\pm, 1.5$	-0.4 ± 2.1	-0.5 ± 2.5	-2.9 ± 5.0

Table 2. Comparative results by using several FNN networks configurations. Additional data are the same as in Table 1

in the results, we provide the mean and the standard deviation obtained from 25 training trials as: $\mu \pm \sigma$. Following the suggestion of ZangZhang et al. (2001) that users should pay more attention to selecting the number of input nodes, we have cross correlated the power with itself and correlated it with the wind speed and concluded that the highest values are for offsets until the range of 4-6 hours back. It means that the size of the more useful data window must be around this range.

Tables 1 and 2 contain the results for several configurations of RNN and FNN respectively. Table 1 contains also the error values for the persistence and reference model. The computation of the reference model data was performed by using the train set, its parameters are: $A_0 = 0.82$ and $\overline{P} = 0.68$. The reported results are related to architectures including one hidden layer. The experiments have shown that more layers increases the computational cost and have no better performance. In both tables, the delays are taken in relation to the prediction time; they are represented as: $(h_1 : h_2)w$, where $w = h_2 - h_1 + 1$ is size of the time window. In all cases $h_1 = 2$ to met the regulations. Remark that the values of BIAS and MAE are related to the first moment of the error, therefore they are related to the generated power, but the values of RMSE and SDE are related to the second order moment and the variance of the error.

All the tested RNN architectures perform better on BIAS values, such as significatively reduce the level in relation to the reference model and the persistence. It means that the feedback of RNN architectures systematically corrects the biased offset in the prediction. The FNN architectures without such feedback are systematically biased. The inclusion of innovation filters can be needed for the FNN case but is no necessary for the RNN one. However, in

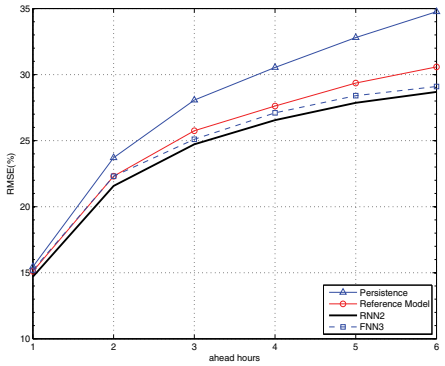

Fig. 2. Comparative RMSE of several models in the very short-term prediction

MAE criterium the persistence value is not beaten neither reference nor any tested ANN architecture. The variance of the error provided by RMSE and SDE criteria are outperformed by some RNN architectures in relation to persistence, reference model and FNN. The range of parameters that provide better results are around values 4 and 6 for windows size, and around 40 for hidden nodes. The use of narrow windows or lower number of hidden nodes performs worse. There are not tradeoff between reducing the window size and increasing the hidden nodes as shows on the RNN1 case. The increasing of hidden nodes does not performs much better as is shown in RNN6 case. The FNN architectures are more unstable, eg. the FNN3 have a good improvement of 2.7 in mean value in the RMSE criterium, but has a big standard deviation value of 1.6. It is unstable if compared with the RNN2 case with 3.3 value in mean and 0.3 value in standard deviation.
Figure 2 shows the comparative performance in several hours ahead for the RMSE criterium. The included models are the persistence, the reference model the RNN2 and the FNN3 cases. It is shown that the reference model performs much better that the persistence and both ANN cases outperform the reference model. Also it is shown that the relative efficiency of the predictive models of ANN in relation to persistence increases when increases the ahead hours.

3. Mathematical model of power quality

The outline of the generic model of a RES producer coupled to a energy storage and connected to a public grid is shown in Figure 3. The RES provides a power $P(t)$ that varies according the wind speed or sun radiation. The power planned to be sent to the grid in the hourly period is P', its value had been computed by means of some forecasting procedure before being sent to the TSO. The power that the system is effectively sending to the grid is $P_o(t)$. The difference $P_o(t) - P'$ is the deviation between the planned and the fed power; this difference is logged by the measurement systems of the TSO and the control system. These values will provide some quality parameters that will reduce the economic billing of the RES producer. This paper focuses only on the technical problem of the energy flows and on the measurement of the quality parameters and does not address the economic downside that is strongly dependent on the National Regulations of each country.
If no storage system is used, $P_o(t) = P(t)$, the penalties are related to the chaotic evolution of the local weather and some basic freedom degrees of the wind power system, eg. the pitch regulation of the blades. Precise forecasting procedures can reduce such impact but only

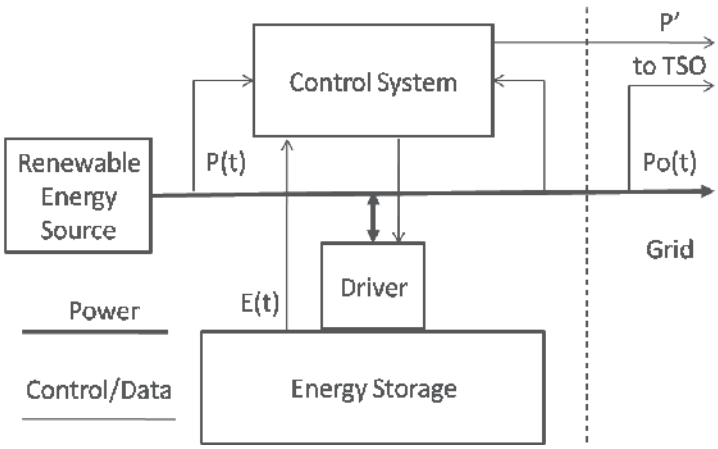

Fig. 3. The Storage and Energy Management System

partially, because most of the Electricity Markets are related to hourly periods, and one hour is too long a time period to have constant wind speed.
The National Regulations of some countries with high RES penetration have defined some quality constraints for the divergences and its economical downsides. In this paper, we adopt a simplified model: the energy sent to the grid must meet some quality constraints if penalties are to be avoided. It must be in an offset band such as $P' - \Delta \leq P_o(t) \leq P' + \Delta$. The Δ value is defined by the Grid Regulations and it can be defined as a fraction, δ, of the nominal power: $\Delta = \delta P_n$.
We define two logical conditions, the *into band* one when the output power is within the offset band, $P_o(t) \in P' \pm \Delta$, and the converse *out band* condition when the output power is outside this offset band $P_o(t) \notin P' \pm \Delta$. We can introduce some measures of energy amount and quality. The raw energy provided by the RES generator E_{res} and the energy feed in the grid E_{grid} are defined as follows:

$$E_{\text{res}} = \int P(t)dt \qquad E_{\text{grid}} = \int P_o(t)dt \tag{6}$$

If no storage system is used, both values are the same. The planned energy, E_{planne} and the energy feed into the grid outside of the quality band are expressed as:

$$E_{\text{planned}} = \int P'dt \qquad E_{\text{out}} = \int_{P_o(t) \notin P' \pm \Delta} P_o(t)dt \tag{7}$$

Moreover, we can introduce the excess or deficiency of energy feed when the system is out band as:

$$E_{\text{deviation}} = \int_{P_o(t) \notin P' \pm \Delta} |P_o(t) - P'|dt \tag{8}$$

3.1 Modeling the storage subsystem

A simplified model of the storage subsystem is composed of two parts: the energy storage itself and the driver or set of physical devices(electronic, electrical and mechanical) that allows the storage and recovery processes. The driver subsystem is an abstract wrapper of a complex

system involving very different technologies. The energy storage can be implemented by electric batteries or hydraulic reservoir, while the driver can be a system of power electronics or water turbines and pumps. We will suppose that the energy amount is an observable variable by mean of some suitable sensors. Let $E(t)$ and $E_{\max}$ be the stored energy and the maximum energy capacity of the storage subsystem, verifying: $0 \leq E(t) \leq E_{\max}$. The main issue in the modeling is the energy conservation equation. However, a detailed model is required to take account of the efficiency in the storage/recovery processes. The changes in the stored energy are defined as:

$$\frac{dE}{dt} = \dot{E}_{\text{in}} - \dot{E}_{\text{out}} - \dot{E}_{\text{loss}} \tag{9}$$

where $\dot{E}_{\text{in}}$ is the input rate in the storage phase, $\dot{E}_{\text{out}}$ is the rate in the energy recovery phase and $\dot{E}_{\text{loss}}$ is the rate of energy lost in the storage itself. The increase in the stored energy is the following when $E < E_{\max}$:

$$\dot{E}_{\text{in}} = \begin{cases} \eta_s[P(t) - P'] & P(t) > P' + \delta_1 \\ 0 & \text{otherwise} \end{cases} \tag{10}$$

where η_s is the efficiency of the driver in the storage phase, and $\delta_1 \leq \Delta$. The decrease of energy in the recovery phase is the following when $E > 0$:

$$\dot{E}_{\text{out}} = \begin{cases} \frac{1}{\eta_r}[P' - P(t)] & P(t) < P' - \delta_2 \\ 0 & \text{otherwise} \end{cases} \tag{11}$$

where η_r is the efficiency of the recovery phase and $\delta_2 \leq \Delta$. It is possible to model some losses as a ratio of the stored energy:

$$\dot{E}_{\text{loss}} = -\lambda E \tag{12}$$

where λ is a decay factor. The efficiency factors η_s and η_r in a hydraulic system are the efficiency of the pump in storage phase and the turbine in the recover one respectively. The output power that is sent to the grid, $P_o(t)$, is:

$$P_o(t) = \begin{cases} P' & P(t) > P' + \delta_1 \wedge E < E_{\max} \\ P' & P(t) < P' - \delta_2 \wedge E > 0 \\ P(t) & \text{otherwise} \end{cases} \tag{13}$$

One additional constraint can be introduced by defining an upper value for the maximum gradient for energy change, $|dE/dt| < D\text{max}$, which is the maximum power of the driver system.

We have designed a basic object to simulate storage related problems with limited upper and lower capacities. This basic object is related to the following differential equation involving $x(t)$ as the data, which is the rate of change of the stored value, and $y(t)$ which is the stored value itself:

$$\frac{dy}{dt} + \lambda y = \eta\, x(t) \qquad y(t) \in [0, y_{\max}] \qquad \left|\frac{dy}{dt}\right| \leq d_{\max} \tag{14}$$

where the efficiency depends on the direction of the storage/recovery process.

$$\eta = \begin{cases} \eta_s & x(t) \geq 0 \\ \frac{1}{\eta_r} & x(t) < 0 \end{cases} \tag{15}$$

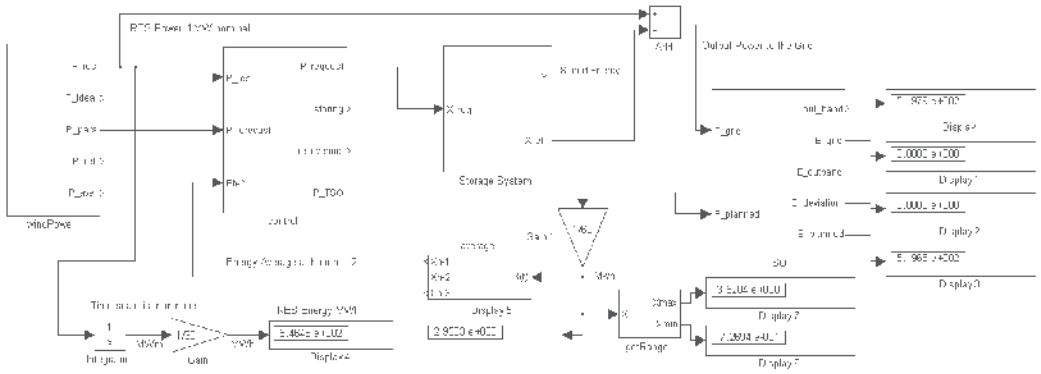

Fig. 4. Blocks in the modeling and simulation

Figure 4 shows the blocks of the modeling and simulation systems. The block Storage implements the defined model of a generic storage system focused on the power and energy management. The data source of the system is provided by the block windPower, which provides the spot power and some model of basic forecasting. It is implemented as a wrapper of a MATLAB file containing the power series in time steps of one minute and the whole series comprises 33 days. These data are obtained from wind speed series and a transfer function for a pitch regulated wind generator with values of 4 m/sec and 13 m/sec for cut-off and saturation respectively. The power is constant at the nominal value to the 25 m/sec limit, which is never reached in the series. The block windPower also provides some values of three basic forecasting models for hourly periods. The simplest model is the persistence model, which provides the predicted value: $\widehat{P}_{h+2} = P_h$. The second forecasting model is that suggested as the reference model Madsen (2004); Nielsen et al. (1998), which provides the predicted values: $\widehat{P}_{h+2} = a_2 P_h + (1 - a_2)\overline{P}$, where $\overline{P}$ is a long-term average of the available data of source power and a_2 is the correlation coefficient between P_h and P_{h+2}. These values in our case are: $a_2 = 0.82$ and $\overline{P} = 0.68$. The last forecasting model is not actually a forecasting, we called it the ideal forecasting because is the best, and unreal, prediction that can be achieved: $\widehat{P}_{h+2} = P_{h+2}$. It is included only for testing purposes, because this ideal and unreal forecasting does not solve the problems concerning the lack of quality in the power fed to the grid.

By simulating the systems we have experienced that the storage system becomes systematically empty or full depending on the configuration parameters. In those states the system can neither store nor recover energy to regulate the output power, because it runs into its non-linear zones. To avoid that the energy storage systematically becoming full or empty, a factor of innovation can be introduced in the planned power k hours ahead as:

$$\widehat{P}^{(inv)}_{h+k} = \widehat{P}_{h+k} + k_1(E_h - E_{\text{obj}}) \tag{16}$$

where E_h is the average stored energy in the h hour, k_1 is a small constant parameter and E_{obj} is some objective level of storage. This strategy corrects the systematically biases and non linear states. The Control block implements the storage strategy. An additional parameter has been added to avoid feeding power to the grid at power lower than a defined minimum value. This $P_{\min}$ value and the lower threshold δ_2 in Equation (13) mean that no power is fed to the grid lower than the $P_{\min} - \delta_2$ value. It computes the planned power for each two hours ahead period and sends it to the TSO block. At every simulation step it computes the power balance

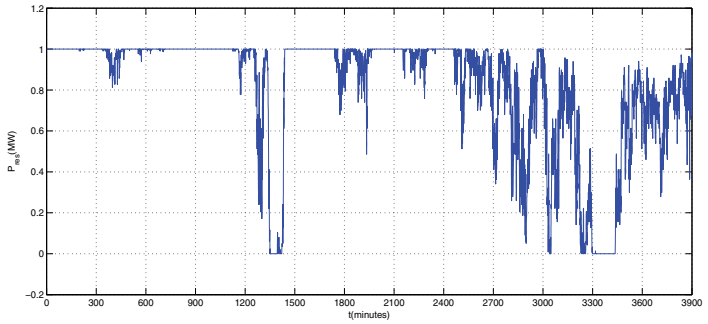

Fig. 5. Power feed to grid by an unregulated wind generator

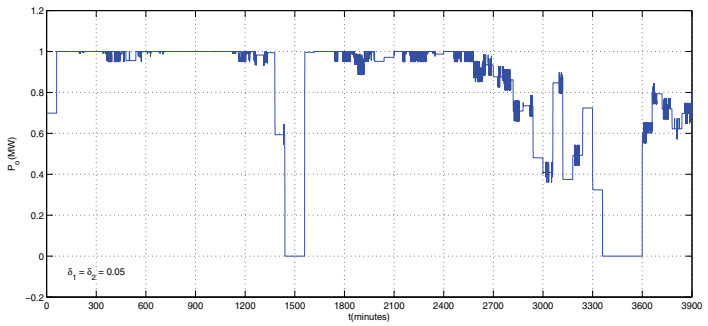

Fig. 6. Simulation results of the regulated system. In each hourly period the power feed to the grid can change at most $\pm 5\%$ of the nominal power.

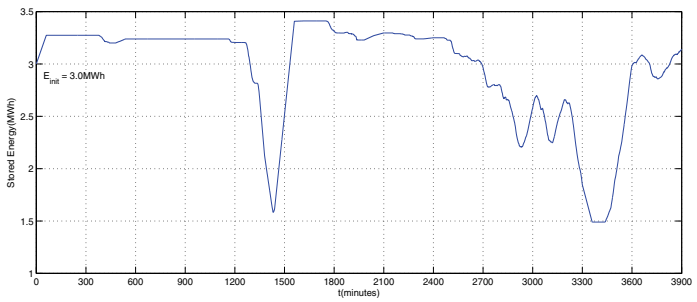

Fig. 7. Simulation results of the regulated system. The stored energy.

and sends the requested power to the storage system to be stored or recovered. It uses the data provided by the Average block that implements the feedback innovation term to correct the states of bias.

The TSO block is mainly a logger of the power feed to the grid. It detects the *in band* and *out band* states according to the Δ parameter, which is defined in the Regulatory Norms of the Electricity Authority, and the planned power for each Market period. The energy feed in the different states is computed by integrating the power.

Energy(MWh)	P(NS)	R(NS)	I(NS)	P	R	I	P(In)	R(In)	I(In)
E_{grid}	546.48	546.48	546.48	526.89	521.56	540.14	519.76	519.73	536.46
E_{out}	270.05	471.36	174.41	7.88	1.25	4.37	0.00	0.00	0.00
$E_{\text{deviation}}$	110.90	132.80	41.84	14.20	5.00	1.58	0.00	0.00	0.00
E_{planned}	546.51	546.63	546.48	540.93	525.81	540.90	519.68	518.67	534.78
E_{init}	-	-	-	3.00	3.00	3.00	3.00	3.00	3.00
E_{end}	-	-	-	0.43	2.11	0.01	2.95	3.32	2.86
E_{max}	-	-	-	3.00	5.00	3.42	3.52	3.59	3.48
E_{min}	-	-	-	0.00	0.00	0.00	0.73	0.92	2.45

P: Persistence, R: Reference Model, I: Ideal Forecasting, NS: No Storage, In: Innovation

Table 3. Quality Parameters

3.2 Results in energy storage

The first test performed on the system was the computation of the results of the TSO block without any storage system. This test provided the raw quality factors corresponding to the RES generator. The test was based on a time series of 791 hours. The first three columns on Table 3, with the label no storage(NS), contain the energy values for the three forecasting strategies, P(Persistence), R(Reference Model) and I(Ideal). An unexpected conclusion that can be obtained is that the Reference Model introduced by NielsenNielsen et al. (1998) and MadsenMadsen (2004) has the worst quality values. It has been claimed that it has less error in wind power forecasting than the Persistence Model but it performs worse in terms of the quality of the energy supplied to the grid.

When the storage system is used, the energy provided by the RES generator is managed by the control system. It is stored and recovered according to the defined strategy. It means that some energy amount will be lost due to the efficiency of the storage driver. The use of the storage system provides more quality in the power fed to the grid, at the cost of lower amount of feed energy. The more quality, the less energy is an approach that will be economically feasible depending on the structure of prices, penalties and subsidies of each country.

Figure 5 shows 3900 minutes of the power provided by the RES generator. Figure 6 shows the power feed to the grid with a storage system. The parameters for the control block are: $\delta_1 = \delta_2 = 0.05$, $k_1 = 0.1$, $E_{obj} = 3\,\text{MWh}$ and $P_{\text{min}} = 0.25\,\text{MW}$. The last of those means that no energy is fed with a power lower than $P_{\text{min}} - \delta_2 = 0.2\,\text{MW}$. The parameters of the storage system are $E_{\text{int}} = 3\,\text{MWh}$, $E_{\text{max}} = 5\,\text{MWh}$, $\lambda = 0$ $\eta_r = \eta_s = 0.9$ and no constraint is imposed in the maximum allowable gradient. Figure 6 shows how the power holes of the RES generator are time-delayed in relation to the fed power. This allows the TSO to have the planned power two hours in advance, thus avoiding uncertainty in the planning od the public electricity system.

Table 3 contains the results for a large simulation, the same parameter previously considered with a lower efficiency: $\eta_r = \eta_s = 0.8$, which means a global efficiency of $\eta_s\eta_r = 0.64$. The columns without the label innovation(in) do not use the innovation factor, which means: $k_1 = 0.0$. Other included data are the values of the initial and final energy, as well as the maximum and minimum energy values.

In the columns without the innovation term, the Reference Model performs better than the other forecasting. It has the lowest values in out band and deviation energy. However, it was the more unstable because the storage became full and empty in the simulation. The last three columns have the best performance in quality. The storage was neither full nor empty, and also the final storage capacity was also close to the initial one. This means that the storage was always in the linear zone and the out band and deviation energies were null. However, the

energy amount fed to the grid was lower in the three cases than in the same strategies in the previously considered groups.
In the performed experiment, which concern to 1 MW of power, the storage of 5 MWh in capacity was sufficient except in the case of the Reference Model without innovation, where there is an overflows. These results are consistent with the analysis by ButlerButler (1994) that evaluated the storage needed for several tasks in the electric system. For spinning reserves between 10-100 MW that author estimated about one half hour; for local frequency regulation related to 1 MW one hour and for a renewable application of 1 MW, 1-4 hours, equivalent to 1-4 MWh in line with the simulated results.

4. Conclusions

The short-term forecasting of wind power for Electricity Markets requires two kind of time scales prediction. The first requires detailed prediction for 1-2 days ahead, which needs the cooperation of some tools of NWP. The second is for the time scale of few hours ahead, which can be carried out by using time series analysis. In this time scale, ANN can be applied successfully for wind power forecasting useful in Open Electricity Markets.
This study has used the standard protocols to evaluate the performance of forecasting procedures that some authors have introduced. We have compared the results according these protocol. We have shown that the new reference model, based on the first order Wiener filter, perform better in variance criteria as RMSE and SDE, but it is worse in first order moment as BIAS and MAE. Some ANN architectures, as Recurrent and Feed Forward, have been tested. The main conclusion is that Recurrent architectures have better performance in first and second order statistical moments and can beat the reference model in the range of nowcasting useful in the Electricity Market.
The higher penetration of the RES in the future will introduce high disturbance into the electric systems by increasing the risk of instability. This risk can be avoided by increasing the spinning reserves; that is, by increasing the cost of the public electricity systems. The Electricity Regulations would move toward increasing the effects of the quality parameters in the system of prices and penalties. In addressing those problems, we have defined a mathematical model for energy storage based on general parameterized systems and also constructed a simulator focused on the management of the power and energy. This model can be used as a first level approach to simulate storage systems. With this approach, we avoid the device dependent details to obtain general conclusions about strategies, storage capacity, quality and efficiency. The simulator provides precise data about the increase in quality parameters and the corresponding decreasing in the amount of energy fed to the grid.

5. References

Alexiadis, M., Dokopoulos, P., H.S.Sahsamanoglou & Manousaridis, I. (1998). Short-term forecasting of wind speed and related electric power, *Solar Energy* 63(1): 61–68.

Beaman, B. G. & Rao, G. M. (1998). Hybrid battery and flywheel energy storage system for leospacecraft, *The Thirteenth Annual Battery Conference on Applications and Advances*, pp. 113 – 116.

Butler, P. C. (1994). Battery storage for utility applications: Phase I - oportunities analysis, *Technical Report SAND94-2605*, Sandia National Laboratories.

Demuth, H., Beale, M. & Hagan, M. (2008). *Neural Network Toolbox 6, User's Guide*, The MathWorks, Inc.

Drouilhet, S. (1999). Power flow management in a high penetration wind-diesel hybrid power system with short-term energy storage, *Technical Report CP-500-26827*, NREL.

Edsinger, A. W., Warren, A. W., Gordon, L. H. & C.Chang, G. (1978). SIMWEST - a simulation model for wind energy storage systems, *Proceedings 13th Intersociety Energy Conversion Engineering Conference*, pp. 2108 – 2114.

E.ON-Netz (2004). Wind Report 2004, *Technical report*, EON.

Eriksen, P. B., Ackermann, T., H. Abildgaard, H., P.Smith, Wintera, W. & Garcia, J. M. R. (2005). System operation with high wind penetration, *IEEE Power and Energy Magazine* 3(6): 65–74.

Erlich, I., Winter, W. & Dittrich, A. (2006). Advanced grid requirements for the integration of wind turbines into the German transmission system, *IEEE Power Engineering Society General Meeting*, pp. 7–13.

Fausz, J. L. & Richie, D. J. (2000). Flywheel simultaneous attitude control and energy storage using a VSCMG configuration, *Proceedings IEEE International Conference on Control Applications*, pp. 991 – 995.

Foresee, F. D. & Hagan, M. (1997). Gauss-newton approximation to Bayesian regularization, *Proceedings of the 1997 International Joint Conference on Neural Networks*, pp. 1930Ű–1935.

Giebel, G. (2003). EC Project ANEMOS: The state-of-the-art in short-term prediction of wind power. a literature overview, *Technical report*, Risø National Laboratory.

Hansen, A. D., Sørensen, P., Blaabjerg, F. & Becho, J. (2002). Dynamic modelling of wind farm grid interaction, *Wind Engineering* 26(4): 191–208.

Haykin, S. (1999). *Neural Networs*, Prentice Hall.

Haykin, S. (2001). *Kalman Filtering and Neural Networks*, John Wiley and Sons, Inc.

Hippert, H. S., Bunn, D. W. & Souza, R. C. (2005). Large neural netwoks for electricity load forecasting: Are they overfitted?, *Int. Journal of Forecasting* 21: 425–434.

Kalogirou, S. A. (2001). Artificial neural networks in renewable energy systems applications: a review, *Renewable and Sustainable Energy Reviews* 5: 373–401.

Kandil, N., Wamkeue, R., Saad, M. & George, S. (2006). An efficient approach for short term load forecasting using artificial neural networks, *Electrical Power and Energy Systems* 28: 525–530.

Landberg, L., Giebel, G., Nielsen, H. A., Nielsen, T. & Madsen, H. (2003). Short-term prediction – an overview, *Wind Energy* 6: 273–280.

Lazarewicz, M. L. & Rojas, A. (2004). Grid frecuency regulation by recycling electrical energy in flywheels, *IEEE Power Engineering Society General Meeting*, Vol. 2, pp. 2038–2042.

Levenberg, K. (1944). A method for the solution of certain non-linear problems in least squares, *The Quartely of Applied Mathematics* 2: 164–168.

Li, S. (2003). Wind power prediction using recurrent multilayer perceptron neural network, *IEEE Power Engineering Society General Meeting* 4: 225–230.

Li, S., Wunsch, D. C., OHair, E. & Giesselmann, M. G. (1997). Neural network for wind power generation with compressing function, *IEEE International Conference on Neural Network*, Vol. 1, pp. 115–120.

MacKay, D. J. C. (1992). A practical framework for backpropagation networks, *Neural Computation* 4(3): 448–472.

Madsen, H. (2004). EC Project ANEMOS: A protocol for standardizing the performance evaluation of short-term wind power prediction models, *Technical report*, Technical University of Denmark.

Mandic, D. P. & Chambers, J. A. (2001). *Recurrent Neural Networks for Prediction*, John Wiley and Sons Ltd.

Marquardt, D. (1963). An algorithm for least-squares estimation of nonlinear parameters, *SIAM Journal on Applied Mathematics* 11: 431–441.

Nielsen, H. A. & Madsen, H. (1996). Wind power prediction using arx models and neural networks, *Proceedings of the Fifteenth IASTED International Conference on Modelling, Identification and Control*, p. 310–313.

Nielsen, T. S., Joensen, A., Madsen, H., Landberg, L. & Giebel, G. (1998). A new reference model for wind power forecasting, *Wind Energy* 1: 29–34.

Nielsen, T. S., Madsen, H., Nielsen, H. A., Pinson, P., Kariniotakis, G., Siebert, N., Marti, I., Lange, M., Focken, U., von Bremen, L., Louka, P., Kallos, G. & Galanis, G. (2006). Short-term wind power forecasting using advanced statistical methods, *European Wind Energy Conference & Exhibition 2006*.

Panteri, E. (2008). EC Project STORIES. Set of the existing regulations and legislative framework related to RES implementation, http://wwww.storieproject.eu.

Tande, J. O. G., Muljadi, E., Carlson, O., Pierik, J., Estanqueiro, A., Sørensen, P., OŠMalley, M., Mullane, A., Anaya-Lara, O. & Lemstrom, B. (2007). Dynamic models of wind farms for power system studies. IEA wind annex XXI, *Technical report*, IEA.

Wilson, B. C., Babuska, B., Potter, C. & Fausz, J. L. (2005). Power system design for a spacecraft simulator using energy storage flywheels, *3rd International Energy Conversion Engineering Conference*.

Zhang, G. P., Patuwo, B. E. & Hu, M. Y. (2001). A simulation study of artificial neural networks for nonlinear time-series forecasting, *Computers & Operations Research* 28: 381–396.

Zhang, G., Patuwo, B. E. & Hu, M. Y. (1998). Forecasting with artificial neural networks: The state of the art, *Int. Jorunal of Forecasting* 14: 35–62.

10

Dynamic Simulation of Power Systems with Grid Connected Windfarms

N. Senthil Kumar
Electrical and Electronics Engineering
RMK Engineering College, Tiruvallur District, Tamilnadu, India

1. Introduction

Wind energy development is consumer and environment friendly, it requires shorter construction time compared to thermal, nuclear generation and is cost competitive. It becomes one of the most competitive sources of renewable energy. However, wind power has some disadvantages. For example, wind power is considered an intermittent power supply because wind does not blow 100% of the time. Besides, the superior wind sites are usually located in remote areas; therefore, it may require substantial infrastructure improvement to deliver the wind- generated power to the load center. There are four major types of wind generators, which are used very widely. (i) Squirrel cage induction generators (ii) Doubly fed induction generators. (iii) Direct driven synchronous generator (iv) Permanent magnet synchronous generator.

2. Literature review

The dynamic stability of a single wind turbine generator supplying an infinite bus through a transmission line was studied by developing the linearized model of the power system under different loading conditions (Abdel magid, 1987).
The effect of wind turbines on the transient fault behavior of the Nordic power system was investigated for different faults (Clemens Jauch, 2004). A novel error driven dynamic controller for the static synchronous compensator (STATCOM) FACTS device was designed to stabilize both a stand-alone wind energy conversion system as well as a hybrid system of wind turbine with Hydro Generators(Mohamed S.Elmoursi, Adel M.Sharaf,2007) . A new definition on rotor speed stability of asynchronous generators is proposed (Olof Samuelsson and Sture Lindahl,2005). A control structure for DFIG based turbines under unbalanced conditions is proposed. (Istvan Erlich.2007). The application of VSC based transmission controllers for Wind energy conversion systems is discussed in (Varma R.K. and Tejbir S.Sidhu, 2006). The dynamic behavior of the power system is analyzed with high wind power penetration is analyzed in (Vladislav Akhmatov, 2003). The impact of FACTS controllers on the rotor speed /rotor angle stability of power systems connected with wind farms is discussed in (N.Senthil Kumar and M.Abdullah Khan, 2008).
The objective of the present chapter is to study the impact of FACTS controllers on the dynamic behavior of a grid connected doubly fed induction generator based wind farm with

and without FACTS controllers. The stability of the system is studied by running time domain simulations without and with FACTS controllers. The following FACTS controllers are considered for the analysis.

i. Static Var Compensator (SVC)
ii. Static Compensator (STATCOM)
iii. Thyristor Controlled Series Capacitor (TCSC)
iv. Unified Power Flow Controller (UPFC).

This chapter is organized as follows. Section 3 presents the modeling of power system and DFIG along with FACTS controllers. Section 4 presents the dynamic simulation results obtained on the system with and without FACTS controllers. Section 5 presents discussion on the simulation results and conclusion.

3. Doubly Fed Induction Generator

The DFIG is the most commonly used machine for wind power generation. In an induction machine, the rotor is symmetrical, i.e. there is no preferred direction of magnetization. This is in contrast with a salient-pole synchronous machine. Speed of the rotor in an induction machine is not fixed. It varies with load. It impacts selection of the pair of orthogonal axes in which the voltage equations will be written down. Unlike in a synchronous machine, there is no dc excitation supplied to the induction machine rotor. Currents are induced in the rotor windings, idealized or actual depending upon the construction, due to relative speed between the rotor and rotating magnetic field produced by the stator currents. The currents induced are ac with a frequency equal to the slip between the two speeds. They produce magnetic field with the same number of poles as produced by stator currents.

3.1 Modelling of wind energy conversion system

Normally a wind turbine creates mechanical torque on a rotating shaft, while an electrical generator on the same rotating shaft is controlled to produce an opposing electromagnetic torque. The power and torque equations for the wind turbine are as follows. The rotor terminals are fed with a symmetrical three-phase voltage of variable frequency and amplitude. This voltage is supplied by a voltage source converter usually equipped with IGBT –based power electronics circuitry. The basic structure of the DFIG based wind energy conversion scheme is shown in fig. 1.

$$P = \frac{1}{2} C_p . \rho . A V^3 \tag{1}$$

$$T = \frac{P}{\omega} \tag{2}$$

where P-output power of the turbine (W), T- Mechanical torque (N.m.),
ω -Rotor speed of wind turbine (rad/s), ρ - Density of air (=1.22 kg/m^3),
A - Swept area of the blade (m^2), C_p -Performance Co-efficient, Wind speed (m/s)
The wind farm is represented as an aggregated model of 10 wind turbines of each 2MW. Identical torque input is used for all the wind turbine models.

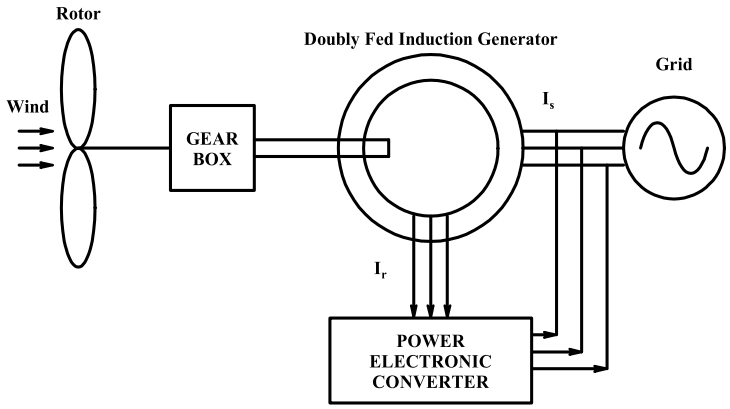

Fig. 1. DFIG Wind Energy Conversion Scheme

The wind energy conversion scheme used for simulation consists of a doubly- fed Induction Generator (Rotor Circuit connected to the grid through power electronic converter). The power electronic converter consists of two-voltage source converters connected through a capacitor.If shaft, turbine and generator damping are neglected, the two-mass model is described by the following equations. (Fig.2) .(Haizea Gaztanaga,2005)

$$T_t = J_t \frac{d\omega_t}{dt} + K_s\theta_s \tag{3}$$

$$T_e = J_g \frac{d\omega_r}{dt} - K_s\theta_s \tag{4}$$

$$\frac{d\theta}{dt} = \omega_t - \omega_r \tag{5}$$

Where T_t is the mechanical torque referred to the generator side [Nm], T_e is the electromagnetic torque [N.m], J_t is the equivalent turbine –blade inertia referred to the generator side [kg m^2], ω_t is the turbine's rotational speed (rad/s), ω_r is the generator's rotational speed (rad/s), K_s is the shaft stiffness [N.m/rad] and θ_s is the angular displacement between the ends of the shaft [rad]. Fig 2 gives the two mass representation of the wind turbine

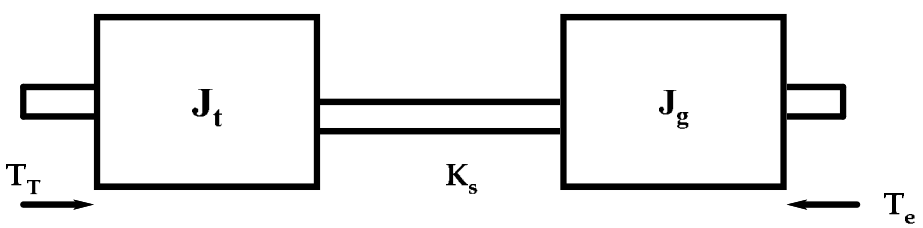

Fig. 2. Two Mass representation of the wind turbine

3.1.1 Doubly fed induction generator model

Equations (6) - (10) represent the complete set of mathematical relationships that describe the dynamic behavior of the machine. The per unit system is adopted as a unit of measurement for all quantities, and the sign convention is chosen in such a way that consumed inductive reactive powers are positive.

Voltage Equations:

$$\frac{d\psi_S}{dt} = r_S I_S + j\omega \psi_S - V_S \tag{6}$$

$$\frac{d\psi_r}{dt} = r_r I_r + j(\omega - \omega_r).\psi_r - V_r \tag{7}$$

Flux Linkages:

$$\psi_s = l_s I_S + l_m I_r \tag{8}$$

$$\psi_r = l_m I_S + l_r I_r \tag{9}$$

Equations of motion:

$$\frac{d\omega_r}{dt} = \frac{1}{\theta_s}(\psi_{sd} i_{sq} - \psi_{sq} i_{sd} + t_m) \tag{10}$$

where

I_s, Ir: stator and rotor currents, V_s, V_r- stator and rotor terminal voltages

ψ_s, ψ_r- stator and rotor flux linkages, L_m-mutual inductance (in per unit it is equal to X_m) r_s, r_r- Stator and Rotor resistances

ω_r, ω- rotor angular speed, synchronous speed

d,q- direct, quadrature axis component

t_m – Mechanical torque

The DFIG model used is a 3rd order model (Equations 6, 7 and 10) the state variables being stator and rotor flux components and rotor speed. Independent control of real and reactive power can be achieved through rotor current control.

From the basic equations of DFIG, setting all derivatives to zero (steady state) and with stator resistance r_s=0 we get

$$V_r = r_r i_r + js\left(x_m \frac{(v_S - jx_m i_r)}{jx_S} + x_r i_r \right) \tag{11}$$

Considering a coordinate system where the d – axis is located along V_s it follows that

$$V_{rd} = r_r i_{rd} + s(\frac{x_m}{x_s}(V_s) - i_{rq}\, \sigma\, x_r) \tag{12}$$

$$V_{rq} = r_r i_{rq} + s\, i_{rd} \sigma\, x_r \tag{13}$$

Where leakage coefficient $\sigma = \left(1 - \frac{x_m^2}{x_r x_s}\right)$ is introduced. s is the operating slip of the generator. The voltage drops over the rotor resistance in (13) and (14) can be interpreted as auxiliary signals, which are outputs of the intended rotor current controller. PI controllers are introduced to control the rotor voltages and hence rotor currents.

$$V_{rd} = r_r i_{rd} = K_I\left(1 + \frac{1}{pT_1}\right)\left(i_{rd\text{-}ref} - i_{rd}\right) \tag{14}$$

and

$$V_{rq} = r_r i_{rq} = K_I\left(1 + \frac{1}{pT_1}\right)\left(i_{rq\text{-}ref} - i_{rq}\right) \tag{15}$$

The corresponding block diagram of the rotor current controller is shown in Fig.3.
PI controllers are introduced to control the rotor voltages and hence rotor currents.
The rotor current controller is modeled using the model editor menu of EUROSTAG.

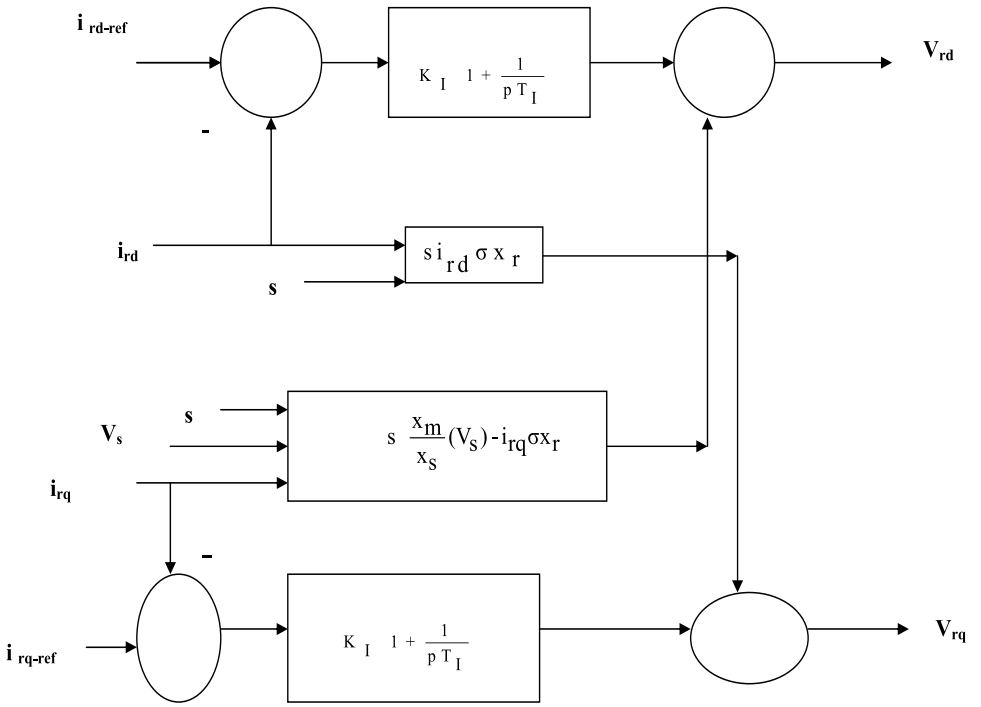

Fig. 3. Rotor Current Controller

3.2 Synchronous generators

The synchronous machine model used for this dynamic analysis is the two axis model with four state variables. (E_d', E_q',δ,ω).

3.3 Static Var Compensators (SVC)

A SVC is basically a shunt connected Static Var Generator /Absorber whose output is adjusted to exchange capacitive or inductive current so as to maintain or control specific power system variables. Typically, the controlled variable is the SVC bus voltage. It is modeled as a variable susceptance controller as shown in Fig. 4 for the execution of the dynamic simulation program. (Nadarajah Mithulananthan, et al.2003)

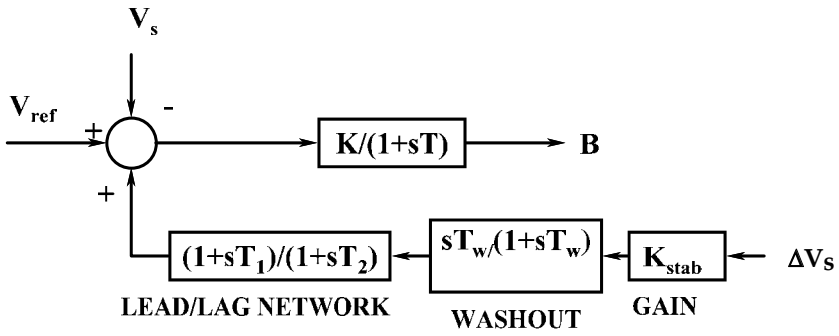

Fig. 4. Dynamic model of Static Var Compensator

3.4 Statcom

The basic electronic block of a STATCOM is the voltage source converter (VSC) which in general converts an input dc voltage into a three-phase output voltage at fundamental frequency, with rapidly controllable amplitude and phase. α is the phase shift between the controller VSC ac voltage and its bus Voltage V_s. V_{ref} is the reference voltage setting.(Claudio Canizares etal ,2003).A phase control strategy is assumed for control of the STATCOM bus voltage, and additional control block and signals are added for oscillation damping as shown in figure 5.

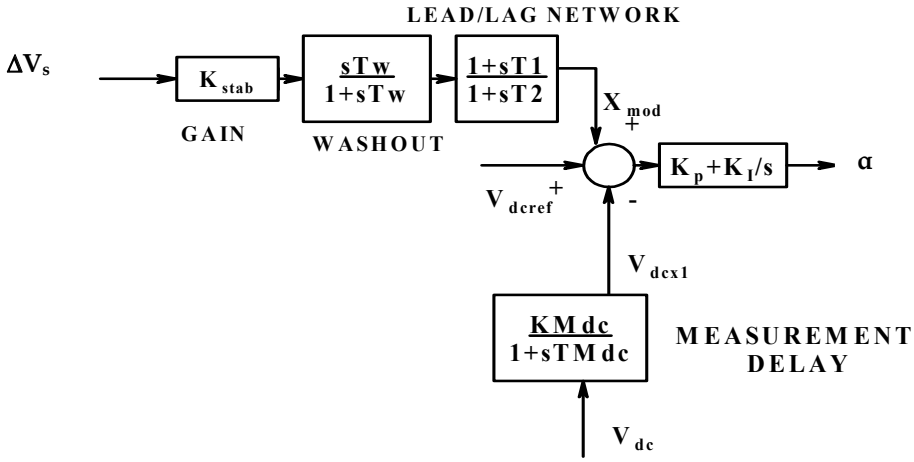

Fig. 5. Dynamic Model of STATCOM

3.5 Thyristor Controlled Series Capacitors (TCSC)

Thyristor controlled series Capacitor schemes typically use a thyristor-controlled reactor in parallel with a capacitor to vary the effective compensating reactance. The variable reactance model of TCSC used for dynamic simulation is shown in Fig.6. (R.Mohan Mathur and Rajiv K.Verma, 2003).

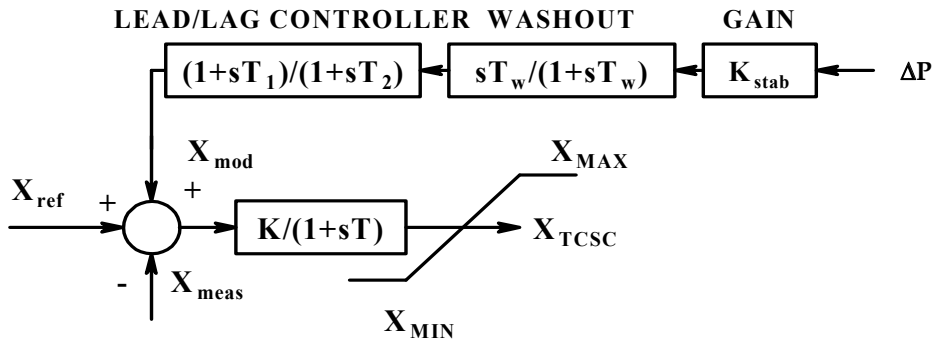

Fig. 6. Dynamic Model of TCSC

3.6 Unified power flow controllers

The UPFC is the most versatile FACTS controller developed so far, with all encompassing capabilities of voltage regulation, series compensation, and phase shifting. It comprises two Voltage Source Converters coupled through a common dc link.

The UPFC is modeled in the power flow program using the power injection model with two real and reactive power injections at two nodes of the system. The power injections at both the nodes are selected such that the base case power flow with doubly fed induction generator is maintained. The active and reactive power flow control loops of the UPFC are shown in fig.7 and 8.

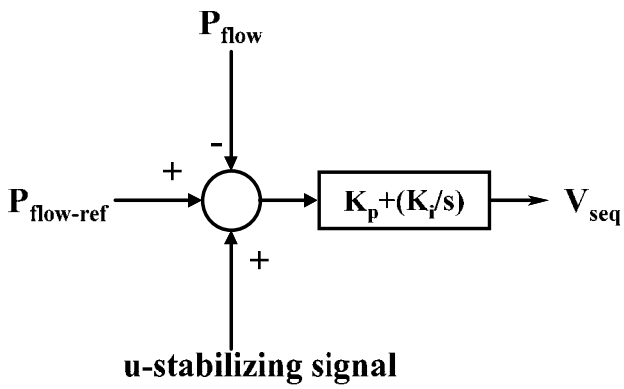

Fig. 7. Active Power Control Loop

V_{seq} is the component of series injected voltage in quadrature with the line current.

Q_{ref} from Fig.8 is the reference value of reactive power flow in the UPFC controller. V_{sep} is the component of A.C. voltage injected in phase with the line current.

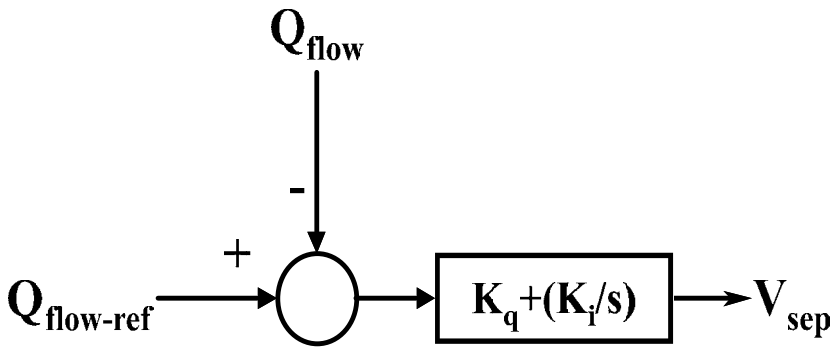

Fig. 8. Reactive Power Control Loop

3.6.1 Parameter tuning

The gains of the FACTS controllers in the forward path of the transfer function are tuned by using an optimization algorithm which minimizes the voltage oscillations of the induction generator bus. The tuning is posed as an optimization problem with the objective as minimizing the oscillations of Point of Common Coupling (PCC) voltage from the desired value and is given by,
Minimize:

$$PI = \sum_{k}\left[(V_{ref} - V_k)^2 + (\omega_{ref} - \omega_k)^2\right] \tag{16}$$

$$K_{min} \le K \le K_{max}$$

where V_{ref} = 1.0 per-unit and PI is the sum squared deviation index of the PCC voltage. For the test system chosen ST is the point of common coupling (Fig. 9.The optimization problem is solved using sequential quadratic programming. The optimization problem is solved iteratively with pre selected initial guess of gain.

4. Dynamic simulation results and stability investigation

The single line diagram of the test system with the doubly fed induction generator connected is shown in Fig 9. The test system consists of a 7 bus system with two synchronous generators G1 and G2.The doubly fed induction generator (DFIG) is connected to the grid through a three winding transformer. IG denotes the stator of the doubly -fed induction generator. At Node ST the stator of induction generator is connected and at node RT the rotor of the doubly fed induction generator is connected. At bus 5 the load is represented as a combination of Impedance and voltage frequency dependant load in the dynamic simulation. . The shunt connected FACTS controllers (SVC and STATCOM)are located at bus 3 and the series connected FACTS controllers are located in one of the lines in grid wind farm line (2-3). The total MW loads on the two load buses 5 and 4 of the test system are 500 MW and 5000 MW respectively.The steady state active power generated by generator G1 is 800 MW and that of G2 is 5000 MW.The wind genertor (DFIG) supplies 2.5. MW in the steady state.

This specific test system is chosen for the dynamic simulation study as this system has two synchronous machines which is good enough for conducting a stability investigation on a wind farm. The doubly fed induction generator is modelled as two active power injections in the load flow program of EUROSTAG at nodes ST and RT.The FACTS controllers are modelled as power injections in the load flow program. The SVC is modelled as a shunt reactive current in the load flow program.The TCSC and UPFC are modelled with two power injections between buses 2 –3 .

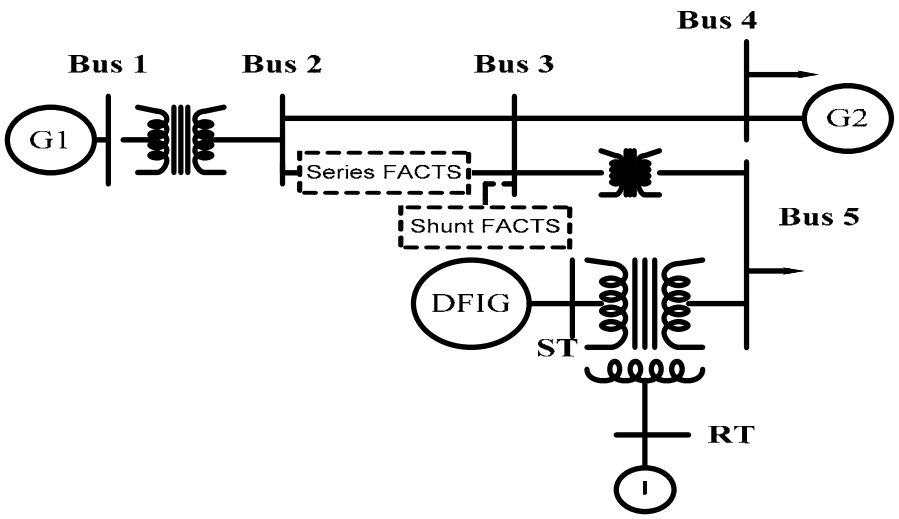

Fig. 9. Single Line Diagram of the power system with Wind Turbine stator connected to Node ST and Rotor Connected to Node RT.

4.1 Rotor angle deviations of synchronous generators without wind farm, with wind farm and with FACTS controllers

Fig.10 shows the rotor angle response of the synchronous generators without the wind farm in the network. From the figure it can be observed that after the fault the generator rotor angle of G1 deviates slightly but after the fault clearance the system returns to a new post equilibrium rotor angle value. Generator G2, which supplies a local load, lies far away from the transient fault and hence is left unperturbed. Fig.11 shows the rotor angle response of the synchronous generators with wind farm included in the network.

From Fig. 11 it can be observed that the rotor angle of synchronous generator G1 oscillates indefinitely. This leads to dynamic instability (sustained oscillations of rotor angle) in the system.Fig.12 and 13 show the rotor angle response of synchronous generators with shunt and series controllers included in the transmission line network. The controller parameters of the static var compensator/STATCOM are tuned to stabilize the oscillations as given by the objective function of equation (16).

From Fig. 12 it can be observed that rotor angle oscillations settle down after 4 seconds with the SVC controller included in the network. The oscillations settle down in 2 seconds with STATCOM. This may be attributed due to the fact that STATCOM (A voltage source converter based FACTS controller) has a faster transient response compared to Static Var compensator (a passive thyristor switched reactor/capacitor).

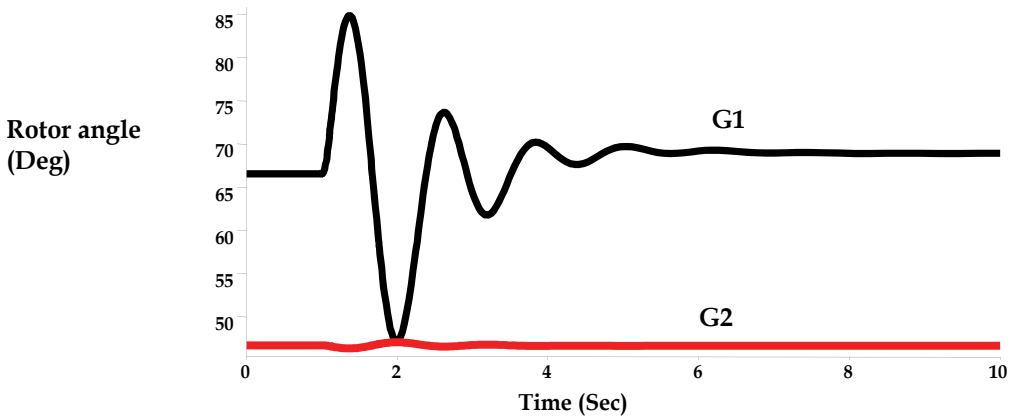

Fig. 10. Rotor angle response without Wind farm

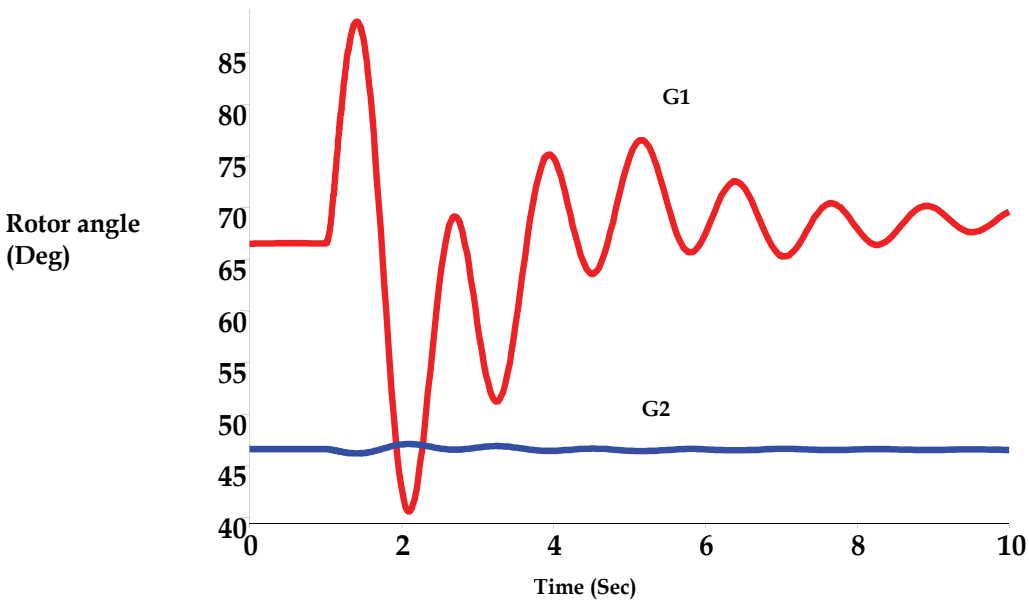

Fig. 11. Rotor angle response with Wind Farm- without FACTS controllers in the network

From fig. 13 it can be observed that there are no oscillations in the rotor angles of synchronous generator with UPFC in the network.

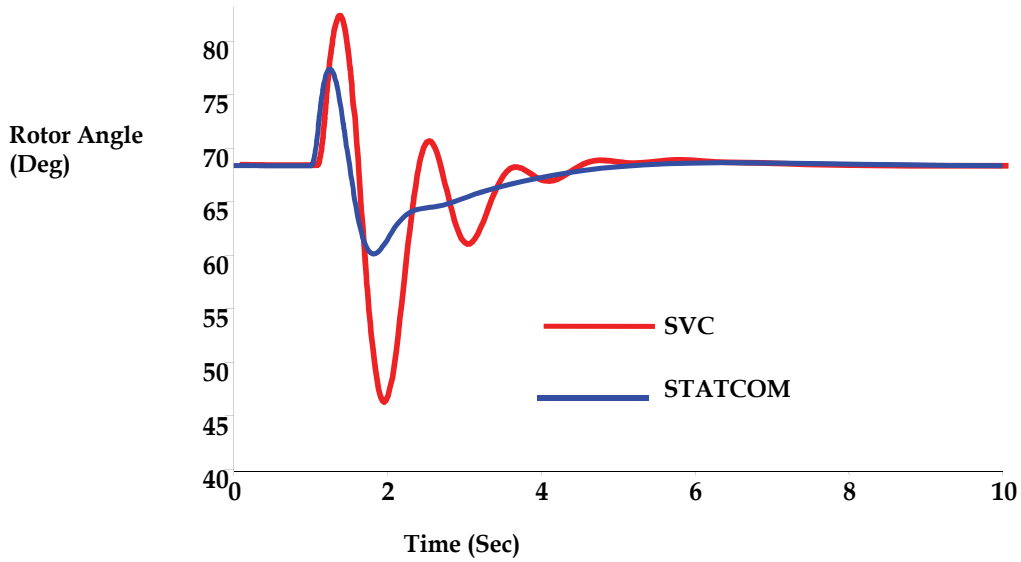

Fig. 12. Rotor angle response of synchronous machine G1 with windfarm – Effect of SVC and STATCOM

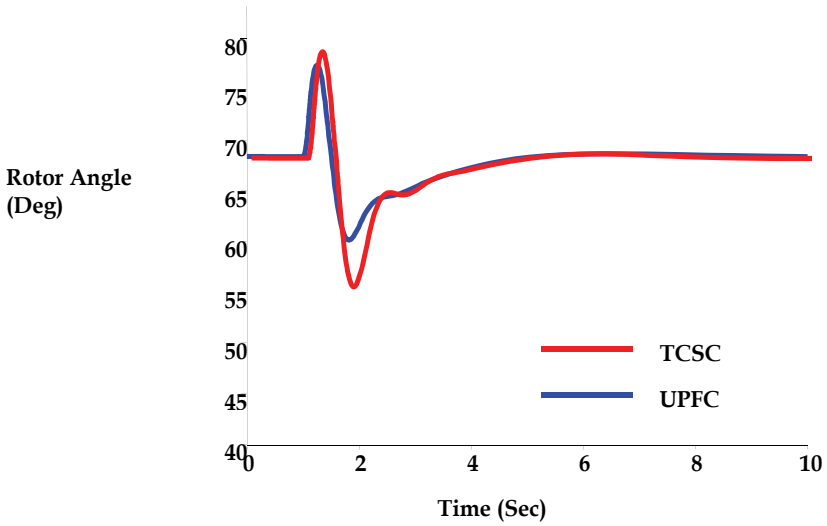

Fig. 13. Rotor angle response of Synchronous Machine G1 with Windfarm–Effect of TCSC and UPFC

4.2 Rotor speed deviation of DFIG- Effect of FACTS controllers

Fig. 14 demonstrates the effect of FACTS devices on the rotor speed response of DFIG after the disturbance**.** The speed of the induction generator tends to increase towards its maximum value set (1.22 per unit) in the dynamic simulation without FACTS controllers in the network After the clearance of the fault it is observed that the speed of the wind turbine does not reach its prefault steady state value of 1.1 p.u.This post fault rotor speed deviation of the asynchronous generator causes rotor speed instability.

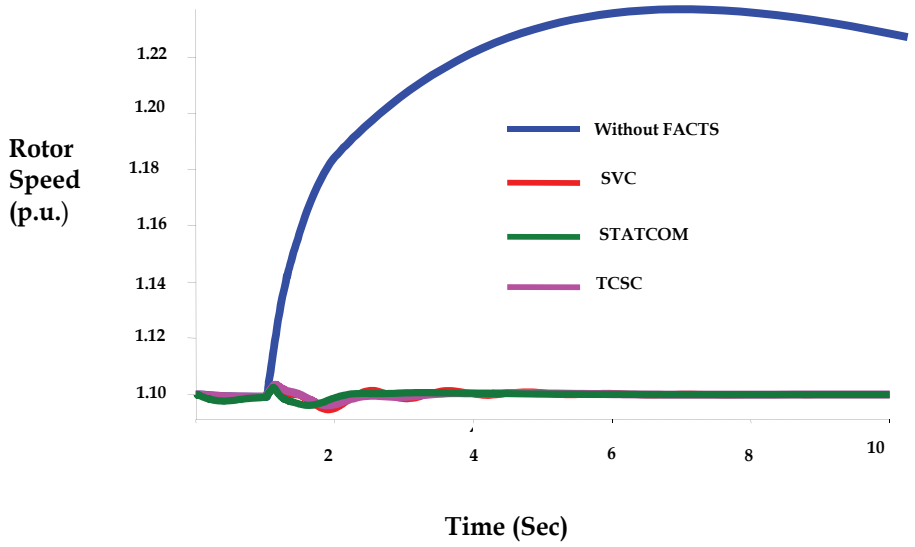

Fig. 14. Rotor Speed Deviation – Effect of FACTS devices

The rotor speed response of DFIG with SVC /STATCOM is displayed in Fig.15. It can be noticed that due to the additional dynamic reactive power support of SVC and the damping signal provided suppresses the rotor speed oscillations of the asynchrnous generaotors. From Fig 16 it can be inferred that there are no appreciable rotor speed deviations with UPFC controller in the network. This is due to the effectivenss of UPFC damping controller attached with its power flow controller and also due to the shunt reactive support provided by the UPFC.Hence it can be concluded that UPFC damps out rotor speed /rotor angle oscillations of asynchronous and synchrous generators more effectively.

4.3 Active power injected by the DFIG –effect of FACTS controllers

Fig. 17 shows the active power injected by the wind turbine into the grid folloiwng the three phase fault carried on one of the lines near bus 3.The stator protection system associated with the induction generator disconnects the stator from the grid if the terminal voltage of the induction generator is less than 0.75 p.u. for a period of 0.08 seconds, hence the stator active power delivered comes down to zero after the fault. The active power injected comes down to zero from its initial value of 5.5. Megawatts specified in the load flow.

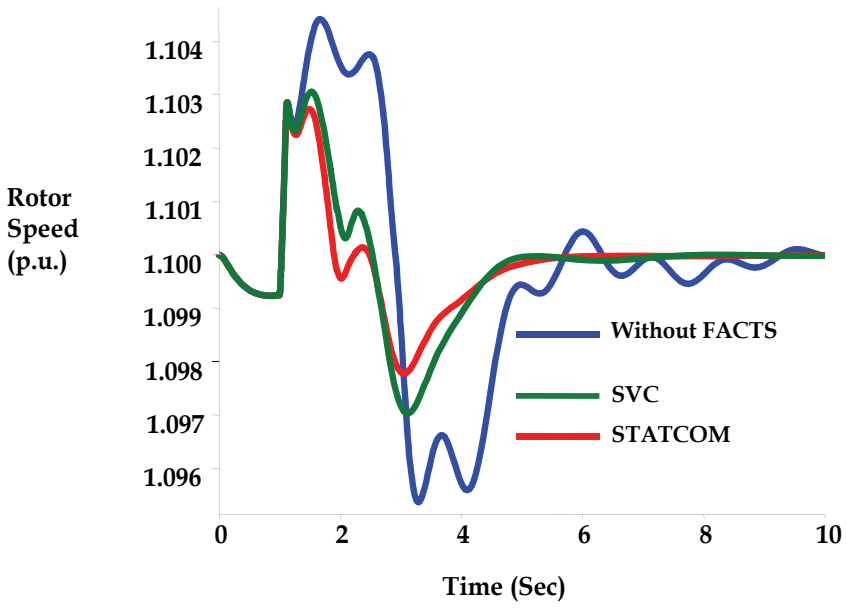

Fig. 15. Rotor Speed Deviation – Effect of Shunt FACTS devices –

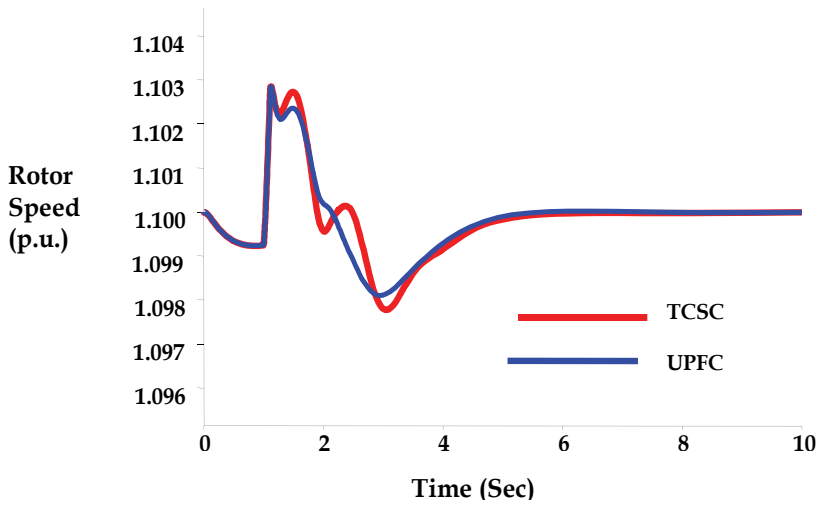

Fig. 16. Rotor Speed Deviation – Effect of Series FACTS devices – TCSC & UPFC

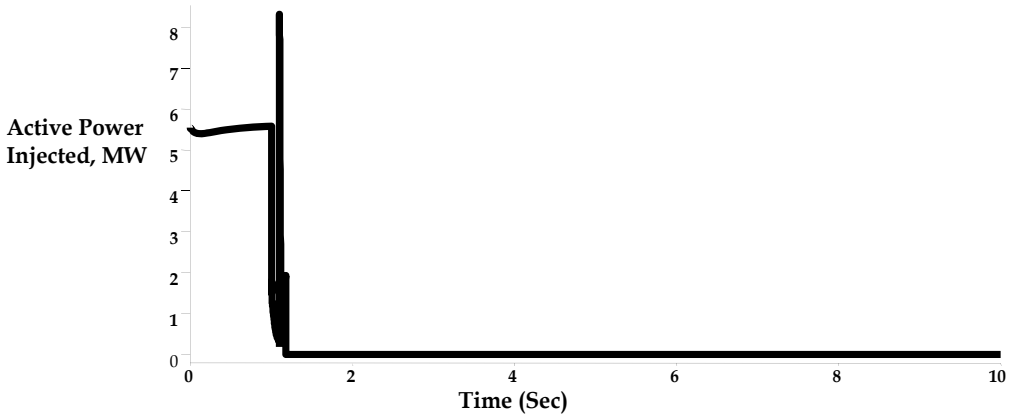

Fig. 17. Active Power Injected by the wind farm without FACTS

The power calculation according to equation (1) is based on a single wind speed. However, in reality, the wind speed may differ slightly in direction and intensity across the area traversed by the blades. To consider this effect, the wind speed is supplied through a lag block to the power conversion equation. This creates a slight change in the active power delivered to the grid before the disturbance at 1 second.

4.4 Induction generator terminal voltage –effect of FACTS controllers

The response in induction generator terminal voltage following the transient fault is shown in Fig. 18, without FACTS controllers in the network. The under voltage protection system associated with the wind turbine disconnects the stator from the network if the voltage at its stator terminals is less than 0.75 p.u. for a period of 0.08 seconds.

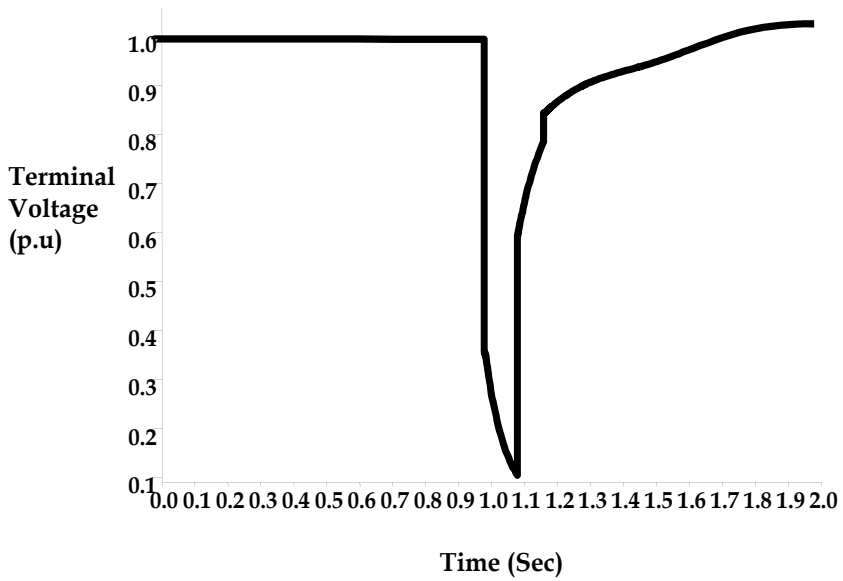

Fig. 18. Induction Generator Terminal Voltage without FACTS

Fig. 19 and 20 show the response of the induction generator terminal voltage with SVC/TCSC and STATCOM. /UPFC.
It can be concluded that terminal voltage of the DFIG is above 0.75 p.u. after 0.1 seconds. Comparing Fig. 18, 19 and 20 it can be concluded that the UPFC improves the fault ride through capability of the DFIG very effectively.

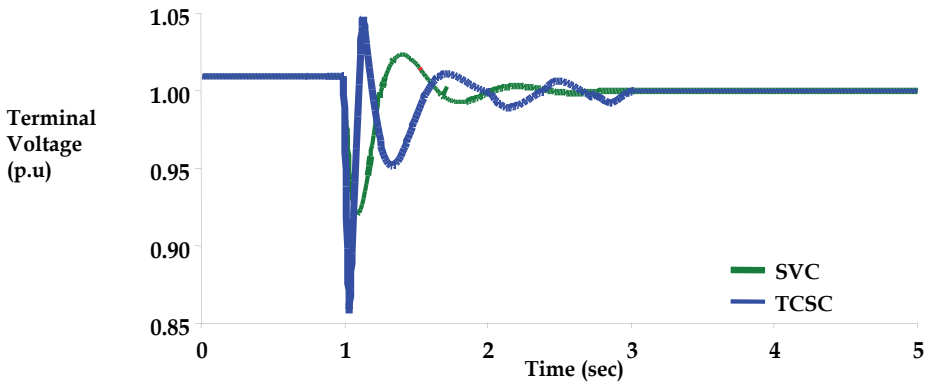

Fig. 19. Induction Generator Terminal Voltage – Effect of SVC and TCSC

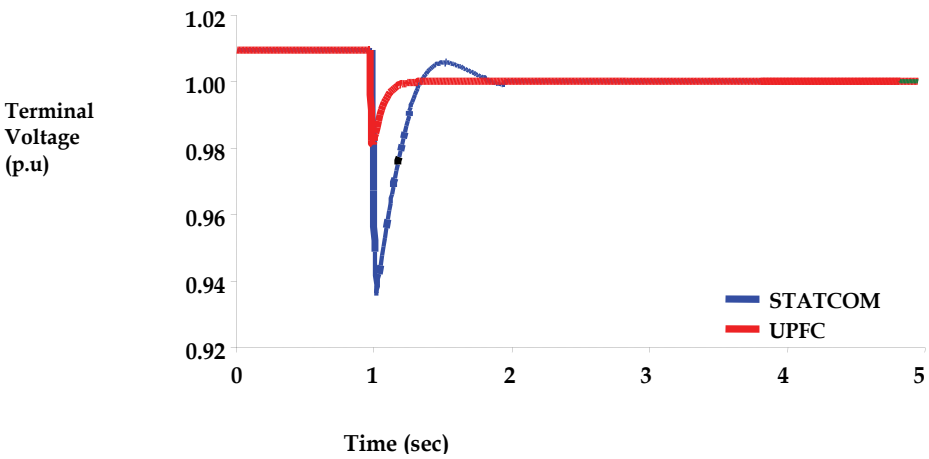

Fig. 20. Induction Generator Terminal Voltage – Effect of STATCOM and UPFC

4.5 Effect of wind speed variations

The dynamic performance of the FACTS controllers with doubly fed induction generator (DFIG) based wind farm is investigated using the wind speed model shown in Fig. 21.[7]

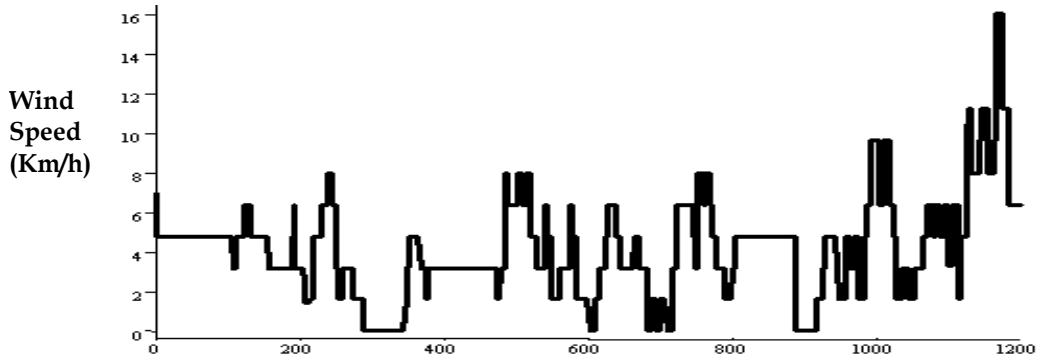

Fig. 21. Wind speed Model considered for long term dynamic simulation

The average wind speed is around 5 Km/h approximately. The wind speed data are obtained by measuring the wind speed changes over an hour from the regional meteorological website.

It can be observed that during the time period from 0- 1000 sec the wind speed fluctuates around an average wind speed of 5 Km/h. But the wind speed reaches 16 Km/h around 1,200 seconds. The corresponding rotor speed variation by the induction generator is shown in Fig 22. It can be observed that the rotor speed changes from its initial value to 1.25 p.u. following wind speed increase at 1200 seconds.

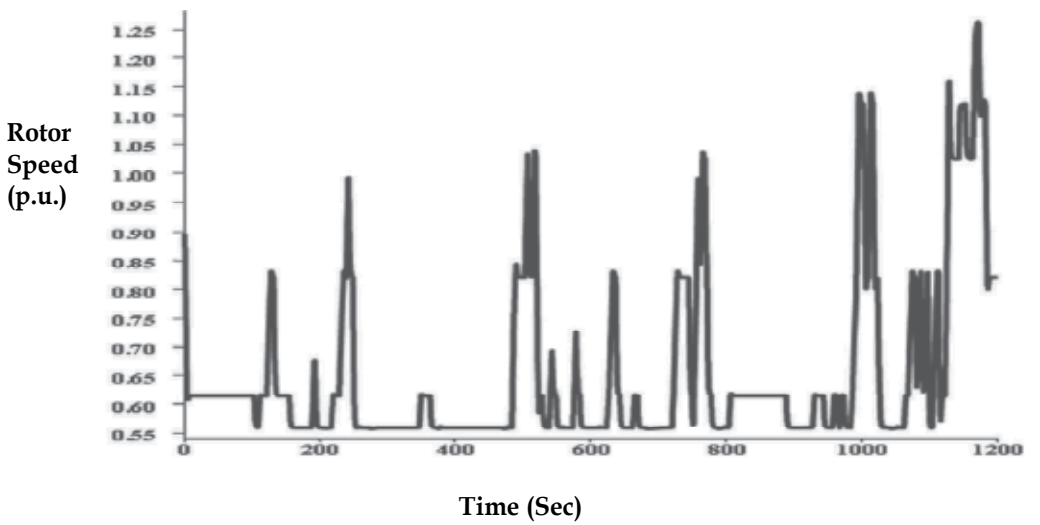

Fig. 22. Rotor Speed response of DFIG

The corresponding active power variations are shown in Fig.23.

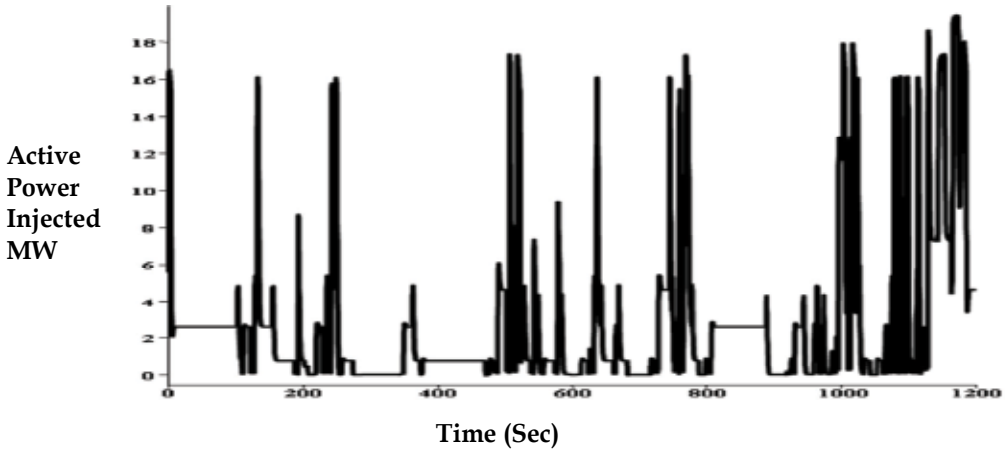

Fig. 23. Active Power Injected by the wind farm

The active power variations following the wind speed changes are highly fluctuating from the steady state load flow level to the grid. The performance coefficient C_p of the wind turbine is kept as 0.48 in the algebraic equation $P = \frac{1}{2} C_p . \rho . A V^3$. Fig. 24 shows the impact of an SVC/STATCOM controller on the rotor speed response of the DFIG.

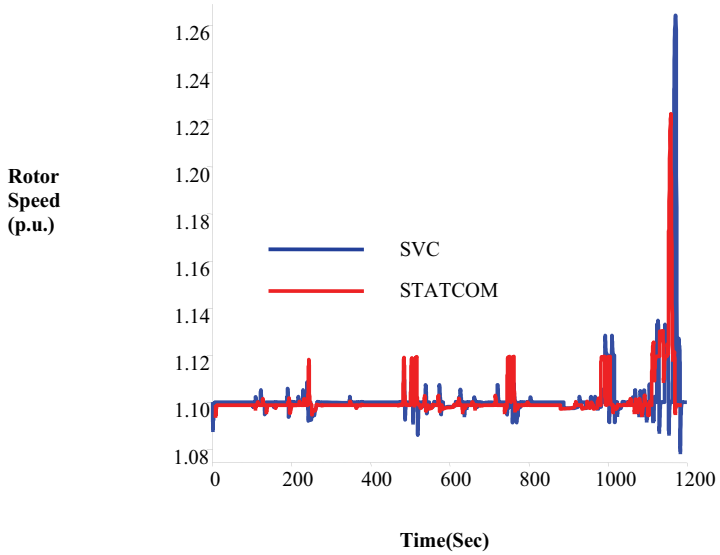

Fig. 24. Rotor Speed Response of induction Generator with SVC/STATCOM

There are no significant rotor speed oscillations in the rotor speed of the induction generator with SVC in the network; however the rotor speed increases to 1.26 p.u. with SVC in the network following wind speed increase of 16 Km/h near 1200 seconds. The rotor speed response of induction generator with TCSC/UPFC is shown in Fig 25.

It can be noticed that the rotor speed oscillations are damped effectively with UPFC in the network.

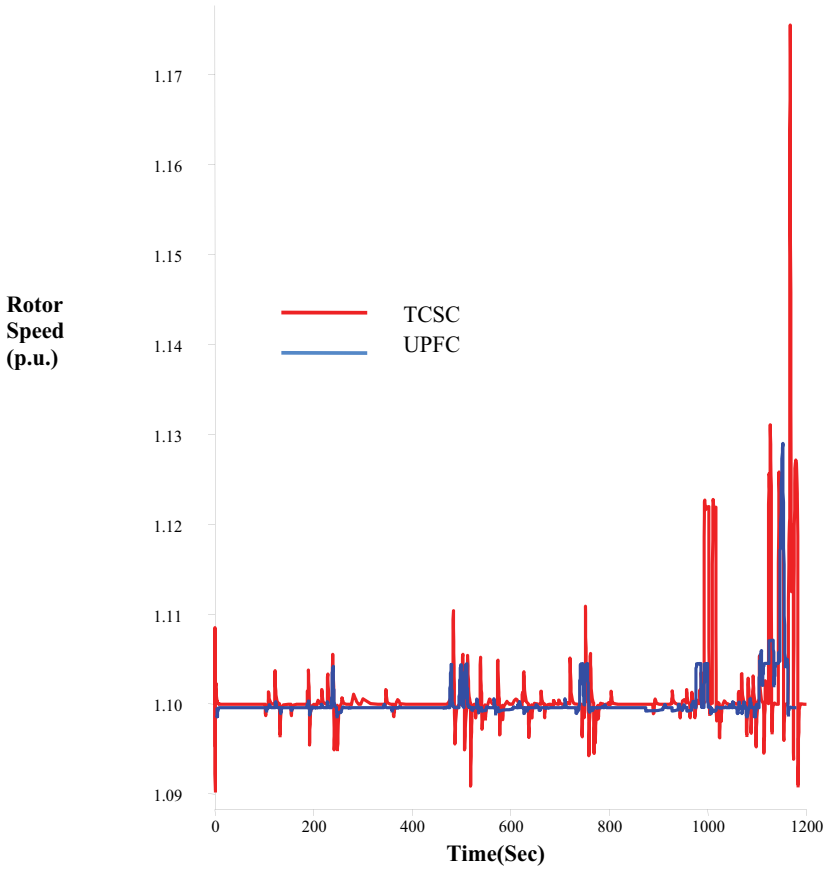

Fig. 25. Rotor speed Response of Induction generator with TCSC/UPFC.

5. Conclusion

For the simulation study the gains and time constants of the FACTS controllers are tuned using a conventional optimization program, which minimizes the voltage /rotor speed oscillations of the induction generator. Among series connected FACTS controllers the UPFC damps both rotor angle oscillations of synchronous generators and rotor speed oscillations of induction generator very effectively when compared with TCSC. This is due to the reactive support provided by the shunt branch of the UPFC following the disturbance. However the reactive power rating of UPFC is very high compared to that of the TCSC .It is suggested that a STATCOM of suitable rating may be installed at the point of common coupling (PCC) with or without a capacitor may be used for stabilizing rotor speed oscillations associated with doubly fed variable speed induction generators following transient faults and disturbances.

The development of wind turbine and wind farm models is vital because as the level of wind penetration increases it poses dynamic stability problems in the power system. For the

present work we have taken a taken a doubly fed induction generator model and illustrated the presence of sustained oscillations with wind farms. Suitable Flexible A.C.Transmission Systems controllers are modeled using the non-linear simulation models and the transient ratings of the FACTS controller are obtained to stabilize the rotor speed/rotor angle oscillations in a DFIG based wind energy conversion scheme. The rotor speed stability of the DFIG based system following a generator outage is studied. It can be observed that the effect of low voltage ride through (LVRT) is very minimum following the contingency and the presence of a FACTS device like the SVC improves the rotor speed stability.

This chapter also presented the results of a long term dynamic simulation of a grid connected wind energy conversion system which simulated wind speed changes. From the results it is observed that STATCOM and UPFC are effective candidates for damping the rotor speed oscillations of the induction generator.

6. Appendix

a. Parameters

Base values for the per unit system conversion.

Base Power: 100 MVA, Base Voltage: 0.69 KV for low voltage bus bar, 150 KV for high voltage busbar.

b. Doubly- Fed Induction Generator

Rated apparent power MVA: 2 MVA, Rotor inertia: 3.527 MW s/MVA

R_s (p.u.) = 0.0693,X_s (p.u.) = 0.080823,R_r (p.u.) =0.00906,X_r (p.u)= 0.09935,

X_m (p.u) = 3.29, Minimum Rotor Speed: 0.56 p.u., Maximum Rotor Speed: 1.122 p.u.

c. Transformers

Three winding transformer (150 KV: 0. 69 KV), Primary rated apparent power=25 MVA, Secondary rated apparent power = 25MVA,Tertiary rated apparent power = 6 MVA.

7. Acknowledgement

The author sincerely thanks **Dr.M.Abdullah Khan**, Professor of Eminence/EEE, B.S.Abdur Rahman University (Formerly B.S.A.Crescent Engineering College) for his invaluable guidance for completing the research work. The author sincerely thanks his father Mr.**S.K.Natarajan** & wife Mrs. **Bhuvana** for the moral support extended to him, at times of pressure during the research work.

The author also wishes to place on record his sincere gratitude to **Mr.R.M.Kishore** Vice Chairman, RMK Engineering College and **Prof.Geetha Ramadas**, Head of the Department, Electrical and Electronics Engineering, RMK Engineering College, Tiruvallur District, Tamilnadu, India.

8. References

Abdel – Magid Y.L. and El-Amin I.M., (1987)"Dynamic Stability of wind –turbine generators under widely varying load conditions", *Electrical Power and Energy Systems*, Vol.9, No.3, pp.180-188,1987.

Chai Chompoo-inwai, Wei-Jen Lee, Pradit Fuangfoo, Mitch Williams and James. R.Liao, (2005), "System Impact study for the interconnection of wind generation and utility system", *IEEE Transactions on Industry Applications*, Vol.41, No.1, pp.163- 168..

Claudio A. Canizares, Massimo Pozzi, Sandro Corsi, Edvina Uzunovic,(2003), "STATCOM modelling for voltage and angle stability studies", *Electrical Power and Energy Systems*, Vol.25,pp.431-441.

Clemens Jauch, Poul Sorensen, Ian Norheim, Carsten Rasmussen, (2007) "Simulation of the Impact of Wind power on the transient fault behavior of the Nordic Power System", *Electric Power System Research*, Vol. 77, pp.135-144.

Haizea Gaztanaga, Ion Etxeberria-Ottadui, Dan Ocnasu,(2007) "Real time analysis of the transient response improvement of wind farms by using a reduced scale STATCOM prototype", *IEEE Transactions on power systems*, Vol.22, No.2, pp.658-666.

http://www.kea.metsite.com-online website for wind speed data.

Istvan Erlich, Jorg Kretschmann, Jens Fortmann, Stephan Mueller-Engelhardt and Holger Wrede, (2007),"Modeling of Wind Turbines Based on Doubly-Fed Induction Generators for Power System Stability Studies", *IEEE Transactions on Power Systems*, Vol.22, No.3, 2007, pp.909-919, 2007.

Kundur.P,(1994), "*Power System Stability and Control*", McGraw hill.

Lie Xiu, Yi Wang,(2007), "Dynamic Modeling and Control of DFIG based Wind Turbines under Unbalanced Network Conditions*, IEEE Transactions on Power Systems*, Vol.22, No.1, pp. 314-323..

Mohamed S.Elmoursi, Adel M.Sharaf,(2006), "Novel STATCOM controllers for voltage stabilization of standalone Hybrid schemes", *International Journal of Emerging Electric Power Systems*, Vol.7, Issue 3, Art 5,pp. 1-27.

Mohan Mathur R, Rajiv .K Varma, (2002),*Thyristor – Based FACTS controllers for electrical transmission systems*, IEEE press, Wiley and Sons Publications..

Nadarajah Mithulananthan, Claudio A. Canizares, Graham J.Rogers ,(2003), "Comparison of PSS, SVC and STATCOM controllers for Damping Power System Oscillations", *IEEE Transactions on Power Systems*, Vol.8, No.2, pp.786-792.

Olof Samuelsson and Sture Lindahl, (2005),"On Speed Stability", *IEEE Transactions on Power Systems*, Vol.20, No.2,pp. 1179-1180.

Senthil Kumar.N. , Abdullah Khan.M., (2008) ,"Impact of FACTS controllers on the dynamic stability of power systems connected with Wind Farms", *Wind Engineering*, Vol.32, No.2, pp.115-132.

Varma R.K. and Tejbir S.Sidhu, (2006)"Bibliographic Review of FACTS and HVDC applications in Wind Power Systems", International Journal of Emerging Electric Power Systems, Vol.7, No. 3, pp. 1-16..

Vladislav Akhmatov, (2003),"Analysis of dynamic behavior of electric power systems with large amount of wind power", Ph.D thesis, Technical University of Denmark..

Dr.N.SENTHIL KUMAR is presently working as Professor in the department of Electrical and Electronics Engineering, RMK Engineering College, Chennai. His area of research includes modeling of FACTS devices for power system studies, modeling of wind energy conversion systems for power system stability analysis. Email: nsksai@rediffmail.com

Part 3

Modelling and Simulation of Wind Power System

11

Modeling Wind Speed for Power System Applications

Noha Abdel-Karim, Marija Ilic and Mitch J. Small
Carnegie Mellon University
USA

1. Introduction

The intermittent nature of wind power presents special challenges for utility system operators when performing system economic dispatch, unit commitment, and deciding on system energy reserve capacity. Also, participation of wind power in future electricity markets requires more systematic modeling of wind power. It is expected that the installed energy capacities from wind sources in the United States will increase by up to 20% by the year 2020. New York Independent System Operator (NYISO), General Electric (GE), and Automatic Weather Stations Inc., (AWS) conducted a project for the future of wind energy integration in the United States. They stated that NY State has 101 potential wind energy sites and it should be able to integrate wind generation up to at least 10% of system peak load without further expansion (GE report 2005). In order to integrate wind power systematically, it is necessary to solve the technical challenges as well as policy regulation designs. Some of these polices have been updated to allow increased intermittent renewable energy by settling imbalances in generation rulemakings and portfolio standards, where the most commonly used one at this time is the production tax credit portfolios.
Due to intermittent nature of wind power, forecasting methods become a powerful tool and of great importance to many power system applications that include uncertainties in generation outputs. The recent work has discussed several methods to develop wind power forecasting algorithms to anticipate the degrees of uncertainty and variability of wind generation. (C. Lindsay & Judith, 2008) use an auto-regressive moving average model to estimate the next ten-minute ahead production level for a hypothetical wind farm and investigate the possibility of pairing wind output with responsive demand to reduce the variability in the net wind output. In (Kittipong M. et al., 2007), the authors develop an Artificial Neural Network (ANN) model to forecast wind generation power with 10-min resolution. Current and previous wind speed and wind power generation are used as input parameters to the network where the output from the ANN is the wind generation power. (M. S. Miranda & R. W. Dunn, 2006) predicted one-hour-ahead of wind speed using both an auto-regressive model and Bayesian approach. (D. Hawkins & M. Rothleder, 2006), discuss operational concerns with increased amount of wind energy in the Day-ahead- and Hour-ahead-Market for CAISO in California. They emphasize the importance of forecasting accuracy for unit commitment and ancillary services and the implications of load following or supplemental energy dispatch to rebalance the system every five minutes. In (Alberto F. at el., 2005), the authors propose a probabilistic method to estimate the forecasting error for

a Spanish Electricity System. They propose cost assessment with wind energy prediction error. The assessment is developed to estimate the cost associated with any energy deviation they cause. (Dale L. Osborn, 2006) discusses the impact of wind on the LMP market for Midwest MISO at different wind penetrations level. His LMP calculations decrease with the increase of wind energy penetration for the Midwest area. The authors of (Cameron W. Potter at el., 2005) describe very short-term wind prediction for power generation, utilizing a case study from Tasmania, Australia. They introduce an Adaptive Neural Fuzzy Inference System (ANFIS) for short-term forecasting of a wind time series in vector form that contains both wind speed and wind direction.

We next describe our modeling approach to derive a family wind models ranging from short through and long term models. Using the same data, we illustrate achievable accuracy of this model. This chapter presents three major parts in sections 2, 3 and 4. First, section 2 presents a short term wind speed linear prediction model in state space representation using linear predictive coding (LPC), FIR and IRR filters. 10-minute, one-hour, 12-hour, and 24-hour wind speed predictions are evaluated in least square error sense and the prediction coefficients are then used in the state space stochastic formula representing past and future predicted values. One year wind speed data in 10 minute resolution are first fitted by two Weibull distribution parameters and then transformation to normal distribution is done for prediction calculation purposes.

Second, section 3 of the chapter models wind speed patterns by decomposing it in different time scales / frequency bands using the Fourier Transform. The decomposition ranges from hourly (high frequency) up to yearly (low frequency), and are important in many power grid applications. Short, medium and long-term wind speed trends require data analysis that deals with changing frequencies of each pattern. By applying Fourier analysis to wind speed signal, we aim to decompose it into three components of different frequencies, 1) Low Frequency range: for economic development such as long term policies adaptation and generation investment (time horizon: many years), 2) Medium Frequency range: for seasonal weather variations and annual generation maintenance (time horizon: weeks but not beyond a year), 3) High frequency range: for Intra-day and Intra-week variations for regular generation dispatches and generation forced outage (time horizon: hours but within a week). Each decomposed signal is presented in a lognormal distribution model and a Discrete Markov process and the aggregated complete wind speed signal is also applied.

Third, section 4 presents the prediction results using past histories of wind data, which support validity of Markov model. These independencies have been modeled as linear state space discrete Markov process. A uniform quantization process is carried to discretize the wind speed data using an optimum quantization step between different state levels for both wind speed distributions used. Also state and transition probability matrices are evaluated from the actual representation of wind speed data. Transition probabilities show smooth transitions between consecutive states manifested by the clustering of transition probabilities around the matrix diagonal.

2. Wind speed prediction model

2.1 Wind data distribution models

This prediction model uses more than 50 thousands samples of one-year wind speed data in 10-minute resolution. The data are used to determine the best fitted parameters of the

Weibull distribution model. Wind speed data are obtained from National weather station in NYISO zonal areas by approximate longitudes and latitudes station's allocation (National weather station, Available online). The empirical cumulative distribution function (CDF) for the wind speed random variable (RV) X has been evaluated using n samples based on the statistical Weibull formula as (Noha Abdel-Karim at el., 2009):

$$\hat{F}_X(x) = \frac{Rank(x)}{n+1} \tag{1}$$

α	Slope β	Standard Error (intercept)	Standard error (slope)	R-square
0.0356	1.77	1.4×10^{-3}	8×10^{-4}	99.4%

Table I. Linear regression defines Weibull distribution parameters

Where a random variable X (R.V) represents wind speed, and "n" is the total sample size. Knowing ahead that the wind speed RV is best characterized by the Weibull distribution model:

$$\begin{aligned} f_X(x) &= \alpha\beta x^{\beta-1} e^{-\alpha x^{\beta}} \\ &= \frac{\beta}{a}\left(\frac{x}{a}\right)^{\beta-1} e^{-\left(x/a\right)^{\beta}} \end{aligned} \tag{2}$$

$$\begin{aligned} F_X(x) &= 1 - e^{-\alpha x^{\beta}} \\ &= 1 - e^{-\left(x/a\right)^{\beta}} \end{aligned} \tag{3}$$

Where in equation (2) or (3), we mention two alternate, yet equivalent forms of Weibull PDF and CDF related by $a = \alpha^{(-1/\beta)}$. Linear regression is performed between $X = \ln(x)$, where x is the data plotted on the horizontal axis, versus the following CDF metric on the vertical axis:

$$Y = \ln\left(-\ln(1-\hat{F}_X(x))\right) \tag{4}$$

It is known that the PDF parameters are related to the linear regression slope m and Y-intercept C, as follows:

$$\begin{aligned} &\beta = slope = m \\ &\alpha = \exp(C) \;\Leftrightarrow a = \exp\left(-C/\beta\right) \end{aligned} \tag{5}$$

The regression results are shown in table I and both empirical and Weibull cumulative distributions are plotted in figure 1.

Figure 1 presents a best Weibull distribution fit with the empirical CDF to wind speed data. The next step is the transformation to normal distribution with mean zero and variance one.

This transformation is used in both the fitting and prediction processes. The histograms of wind speed signals in both Weibull and Normal distributions are shown in Figures 2 and 3, respectively. By looking to Figure 3, the shape of the actual signal is shifted down with the exact pattern due to the normalization process, (Noha Abdel-Karim at el., 2009).

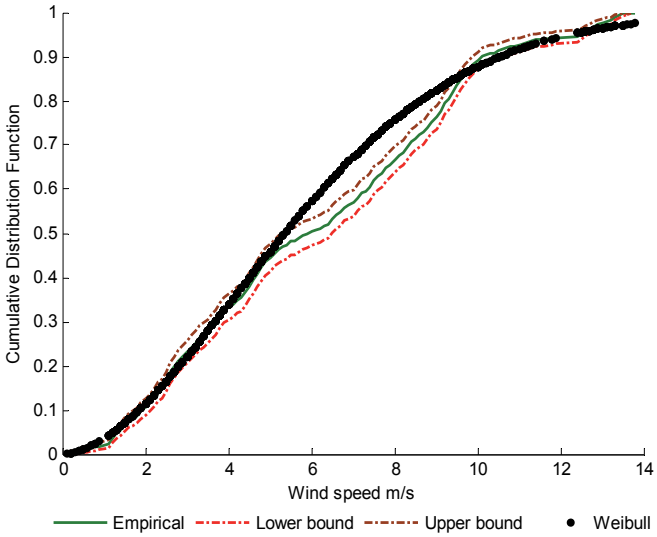

Fig. 1. Empirical and Weibull Cumulative Distribution Functions.

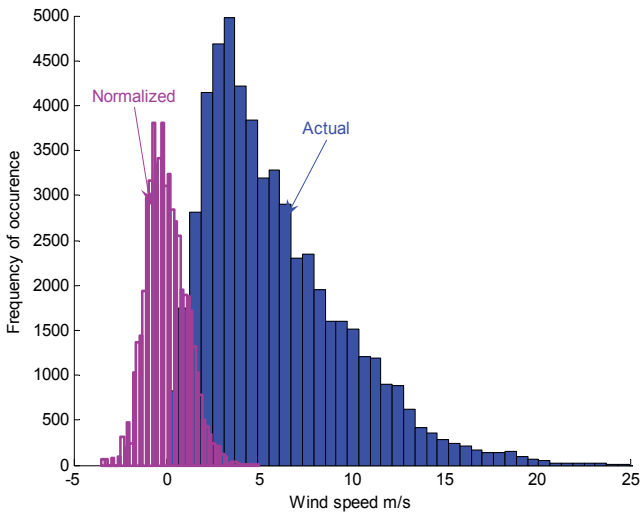

Fig. 2. Actual & normalized frequency occurrence of wind speed data.

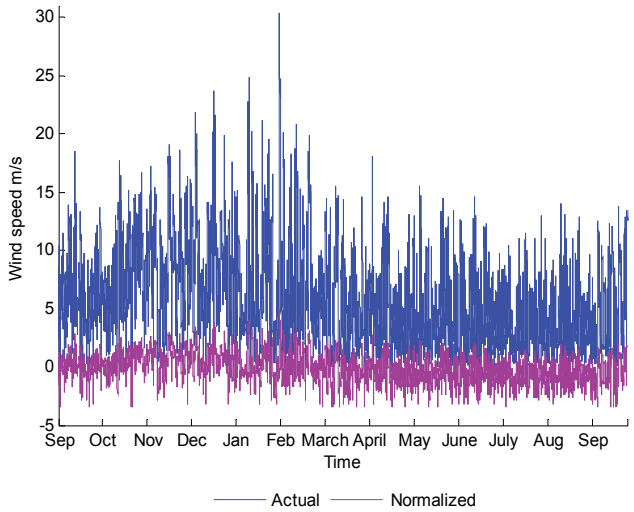

Fig. 3. Actual and normalized wind speed data.

2.2 Normalization of wind speed data

The initial step in the prediction process is data normalization. This step is done by transforming the actual wind speed data X into Normal wind speed data, Xn (i.e., Xn is a normalized Gaussian RV with zero mean and unit variance). This transformation is performed using the Normal CDF inversion as follows:

$$\left.\begin{aligned} F_X(x) &= 1 - e^{-\alpha x^{\beta}} \\ &= F_{X_n}(x_n) = G(0,1) \end{aligned}\right\} \quad \Leftrightarrow \quad x_n = F_{X_n}^{-1}\left(F_X(x)\right) \tag{6}$$

Normal transformation is performed for the sole purpose of prediction, for both the fitting and prediction processes. Figures 2 and 3 show the histograms and time series, respectively, for both the actual (Weibull) wind speed X and Normal wind speed *Xn*. The shape of the Normal signal Xn is shifted down with negative values (Figure 3) compared to the actual signal X due to the normalization process.

2.3 Linear prediction and filter design

This section presents finite impulse response (FIR) and infinite impulse response (IRR) filters. Both filters are being used to determine the prediction coefficients needed to process the normalized wind speed signal x_n, except that we drop the subscript "n" so as not to be confused with the discrete time index. In discrete time, the Z-transform of a signal has been used of a filter as follows:

$$g(n) = \sum_i g_i \delta(n-i) \;\Rightarrow G(z) = \sum_i g_i z^{-i} \qquad \text{(General signal/IIR filter)}$$

$$h(n) = \sum_i^N h_i \delta(n-1) \;\Rightarrow\; H(z) = \sum_{i=0}^N h_i z^{-i} \qquad \text{(FIR filter)}$$

Where δ(n) is the Kronecker delta function. The wind speed random process x(n) is characterized as wide sense stationary (WSS) Gaussian (Normal) process, and hence will remain Gaussian after any stage of linear filtering. However, the wind speed process is NOT white but can be closely modeled as Auto-Regressive (AR) process as will be shown next.

2.4 Linear Predictive Coding (LPC) and Finite Impulse Response Filter (FIR)

For prediction purposes of normalized wind speed data, we use Linear Predictive Coding (LPC) based on the autocorrelation method to determine the coefficients of a forward linear predictor. Prediction coefficients are calculated by minimizing the prediction error in the least squares sense (P. P. Vaidyanathan, 2008). The method provides the LPC predictor and its prediction error as follows:

$$\hat{x}_{LPC}(n) = -\sum_{i=1}^{N} b_i\, x(n-i)$$
$$e_N(n) = x(n) - \hat{x}_{LPC}(n) = x(n) + \sum_{i=1}^{N} b_i\, x(n-i) \tag{7}$$

Where N is defined as the prediction order (using N past data samples) and the coefficients {b1, .., bN} are the fitting coefficients which minimize the mean square (MS) prediction error signal. Yule-Walker (or normal) equations based on autocorrelation matrix have been used to compute those prediction coefficients (P. P. Vaidyanathan, 2008). The LPC predictor has a direct equivalent implementation as an FIR filter if we observe that the error Z-transform is obtained as:

$$\mathrm{E}_N(z) = \mathrm{X}(z) \times \mathrm{B}_N(z) \;\Rightarrow\; \mathrm{X}(z) = \mathrm{B}_N^{-1}(z) \times \mathrm{E}_N(z)$$
$$\mathrm{B}_N(z) = 1 + \sum_{i=1}^{N} b_i\, z^{-i} \tag{8}$$

Where BN(z) is the FIR filter transfer function used to compute the output error signal. In other terms, it is also called the prediction polynomial (P. P. Vaidyanathan, 2008). Figure 4 shows how to obtain the output error signal using two equivalent forms: a) LPC prediction and subtraction, and, b) direct FIR filter design, (Noha Abdel-Karim at el., 2009).

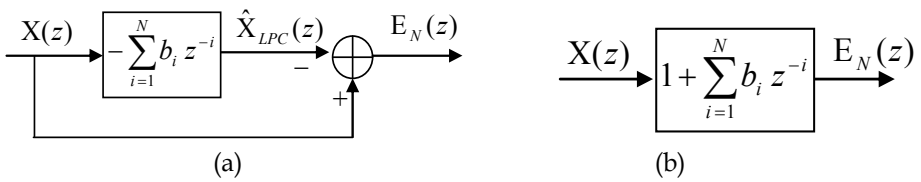

Fig. 4. Output prediction error signal using: a) LPC prediction and subtraction. b) Direct FIR filter design.

To predict the normalized wind speed data, a forward LPC predictor $\hat{x}_{LPC}(n)$ can certainly be used, but its accuracy is rather poor. However, the main advantage of LPC is that, as the prediction order N increases sufficiently, the prediction error $e_N(n)$ tends to be closely approximated as white noise (P. P. Vaidyanathan, 2008). This helps in modeling the Normal

wind speed as AR signal as will be shown next. Thus, forward LPC is considered an important initial pre-coding step, (Noha Abdel-Karim at el., 2009).

2.5 Auto-Regressive (AR) model prediction and Infinite Impulse Response Filter (IIR) filtering

The true wind speed can be obtained by multiplying the error signal $E_N(z)$ – if it is known – by the inverse of the FIR filter $B_N^{-1}(z)$, (Equation 8), which is now an *all-pole* IIR filter. If the error signal is equivalent to white noise for large prediction order N, then the *z*-multiplication (i.e., convolution or filtering in discrete time) now yields a signal that is modeled as Gaussian Auto-Regressive (AR) process. Figure 5 shows the AR model block diagram, while the reproduced AR signal is obtained by rewriting equation (7) in terms of error as:

$$x(n) = -\sum_{i=1}^{N} b_{i,N}\, x(n-i) + e_N(n) \tag{9}$$

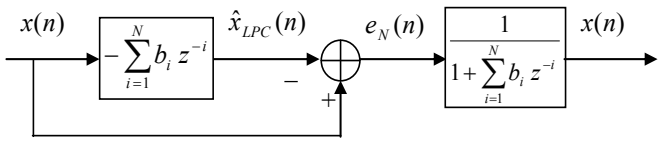

Fig. 5. Auto-regression generation process using LPC estimation method

Equation (9) seems to be an ideal reproduction of $x(n)$ by inversion and it assumes the following:

1. The error signal is exactly updated in real time at the prediction time "n". This is a *genie assisted* condition, as $\hat{x}(n)$ is not available yet!
2. All the true N past data samples are available or exactly estimated (measured) by the wind turbine speed meter and reported on time to the prediction algorithm.
3. The prediction coefficients $\{b_1, \ldots, b_N\}$ are computed using the true past data samples and updated for each new prediction.

In a practical prediction algorithm, these genie conditions do not hold. As for the prediction error, different computation models can be used such as:

1. Prediction error is *estimated* as a random generation of white noise of zero mean & unit variance (P. P. Vaidyanathan, 2008).
2. For initial or limited time intervals, the error can be *exactly computed* using true available data samples to investigate the tracking of the algorithm, but not for long term prediction.
3. The prediction error can be *estimated* from exact measurements but up to a delay of one or more samples, i.e., measurement at time (n – L) applies at time "n". For example, if the prediction update interval is 10 minutes and the measurement delay is 1 hour, then the sample count delay is L = 60/10 = 6 samples. The minimum estimation delay is L = 1.

In our work we excluded the white noise generation alternative and considered the two other alternatives for wind speed forecasting.

2.6 The prediction algorithm for wind speed

2.6.1 Linear prediction phases

More than 50,000 data samples collected in a 10-minute intervals have been used in this short term prediction. A time reference $n = N_S$ has been used which sets the end of known data and start of prediction, where $N_S \leq 50{,}000$ and the remaining samples can be used for tracking the algorithm.

A measurement reporting interval of L samples has been assumed and that there is no error in the measurement or the reporting process. At time epochs $n = N_S + m\,L$, where m is integer, the L measurements $x(n - L + 1)$, $x(n - L + 2)$, …, $x(n)$ are reported and will be available to use at the next epoch, $(N_S + m\,L + 1)$. Depending on L, we have the following extreme cases:

$$L = 1: \rightarrow \text{Point estimator case.}$$

$$L = \infty: \rightarrow \text{Time series case, i.e., no estimation at all.}$$

The following signals and associated time epochs have been defined for prediction purposes as follows:

$x(n)$: True Normal signal known within $0 \leq n \leq N_S$ or whenever measurement is available as above.

$\hat{x}(n)$: Predicted signal using IIR filter or AR recursion.

$x_{REF}(n)$: Reference signal used to produce $\hat{x}(n)$.

$x_{REF}(n) = x(n)$ within $0 \leq n \leq N_S$ or whenever measurement is available

$e_N(n) = x(n) - \hat{x}(n)$: True prediction error, only known if $x(n)$ & $\hat{x}(n)$ are known.

$\hat{e}_N(n)$: Prediction error estimate, either white noise or delayed measurement.

The prediction algorithm can be summarized as follows:

a. ***Training phase*** within $0 \leq n \leq N_S$: Apply the LPC algorithm on the true samples $x(0)$, … , $x(N_S)$ to obtain the prediction coefficients $\{1, b_1, \ldots, b_N\}$. Then we filter the same samples using the FIR coefficients $\{-b_1, \ldots, -b_N\}$ to compute the predictor $\hat{x}(n)$ and true prediction error $e_N(n) = x(n) - \hat{x}(n)$ within $0 \leq n \leq N_S$. Further, we pre-load the reference signal $x_{REF}(n) = x(n)$ within $0 \leq n \leq N_S$.

Prediction phase for $n \geq N_S + 1$: We apply the AR model of equation (9) after computing the error estimate $\hat{e}_N(n)$. We use the same prediction coefficients obtained in the training phase if we plan short-term prediction, which is our case. Otherwise, we have to update the coefficients for long-term prediction. The steps for prediction at epoch "n" are given by:

1. Compute the prediction error estimate using:

$$\begin{aligned} \hat{e}_N(n) &= x_{REF}(n-1) - \hat{x}(n-1) \quad \text{if } x_{REF}(n-1) = x(n-1) \\ &= \hat{x}(n-2) - \hat{x}(n-1) \quad , \text{ if } x_{REF}(n-1) = \hat{x}(n-1) \end{aligned} \tag{10}$$

   We can set $\hat{e}_N(n)$ as randomly generated white noise or also import a snapshot from the past true prediction error series obtained in the training phase.

2. By inspecting equation (9), we compute the predicted signal via the AR recursion:

$$\hat{x}_{AR}(n) = -\sum_{i=1}^{N} b_{i,N}\, x_{REF}(n-i) + \hat{e}_N(n) \tag{11}$$

3. Update the reference signal entries as follows:

$$\text{If n} \neq N_S + m\,L \rightarrow \qquad x_{REF}(n) = \hat{x}_{AR}(n)$$

$$\text{If n} = N_S + m\,L \rightarrow \text{b} \qquad [x_{REF}(n - L + 1),$$

$$x_{REF}(n - L + 2), \ldots, x_{REF}(n)] = [x(n - L + 1), x(n - L + 2), \ldots, x(n)]$$

4. Update the prediction coefficients if needed by running the LPC on the reference signal. It is best to make such update at n = $N_S + m\,L$ because $x_{REF}(n)$ would be just updated by measurements.
5. Increment n and go back to step 1.

Figure 6 shows the two phases of the prediction process

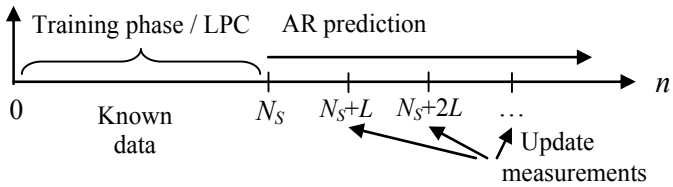

Fig. 6. The two phases of prediction process.

2.6.2 Wind speed prediction results

Wind speed data have been gathered from Dunkirk weather station in the west zone of New York State. Those data have been used for the stochastic prediction of wind speed (National Weather Station, Available online).

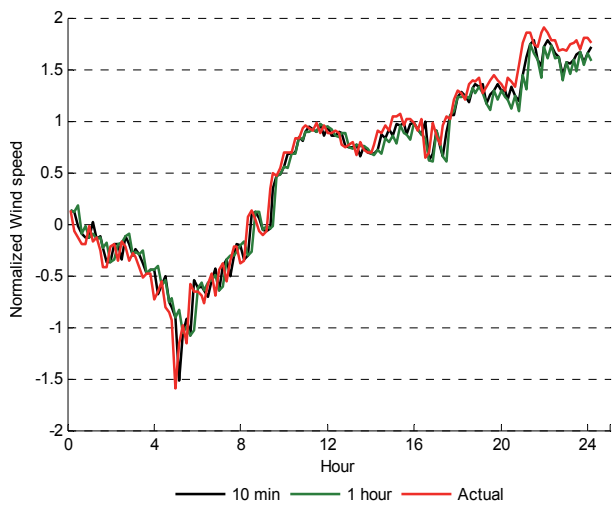

Fig. 7. Ten minutes and one hour prediction using 10 minute past value

Figures 7 and 8 assist remarkable observation that the prediction model insensitive to the prediction order which is defined as the number of observed data (history) used in the

prediction. The 10-minute wind speed prediction model shows persistence for all prediction orders used.

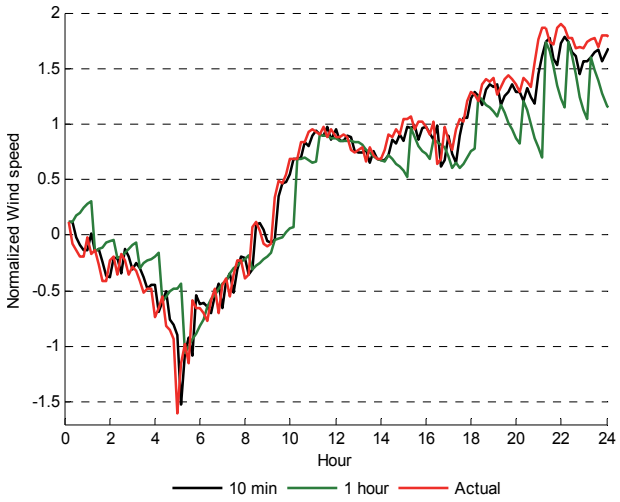

Fig. 8. Ten min and one hour prediction using 1 hour past values

The effect of how the increase in the number of present and past wind speed sample data does not significantly reduce the root mean square error (RMSE), (Figure 9). This led us to an interesting valuation of data structuring and modeling. If only can one recent sample random variable captures stochastic statistics of wind signal to predict future values, then time and memory reductions in presenting such signal can be modeled as a discrete Markov process; the process that stated generally the independencies between past and present values to present signal statistics and structure using state and transition probabilities that will be discussed in detail later.

3. Wind speed signal decomposition

In electricity markets, decisions of utility companies on power selling/buying, production levels, power plants scheduling and investment are made with risks and uncertainties due to volatility and unpredictability of renewable energy patterns. For that, coming up with reasonable modeling of wind speed in different patterns with different time scales, ranging from hours up to few years, are of most importance in many power grid applications. In doing so, different wind signal trends require different data analyses that capture different frequencies. Those frequencies are defined as:

1. Low frequency range: for economic development such as long term policies adaptation and generation investment, (time horizon: many years)
2. Medium frequency range: To detect seasonal weather variations, and therefore help in assigning mid-term generation capacities which influence electricity market prices and power grid generation planning for few weeks with no effect beyond a year.
3. High frequency range: for Intra-day and Intra-week variations for regular generation dispatches and forced generation outage, for fast variations of few hours but not beyond a week.

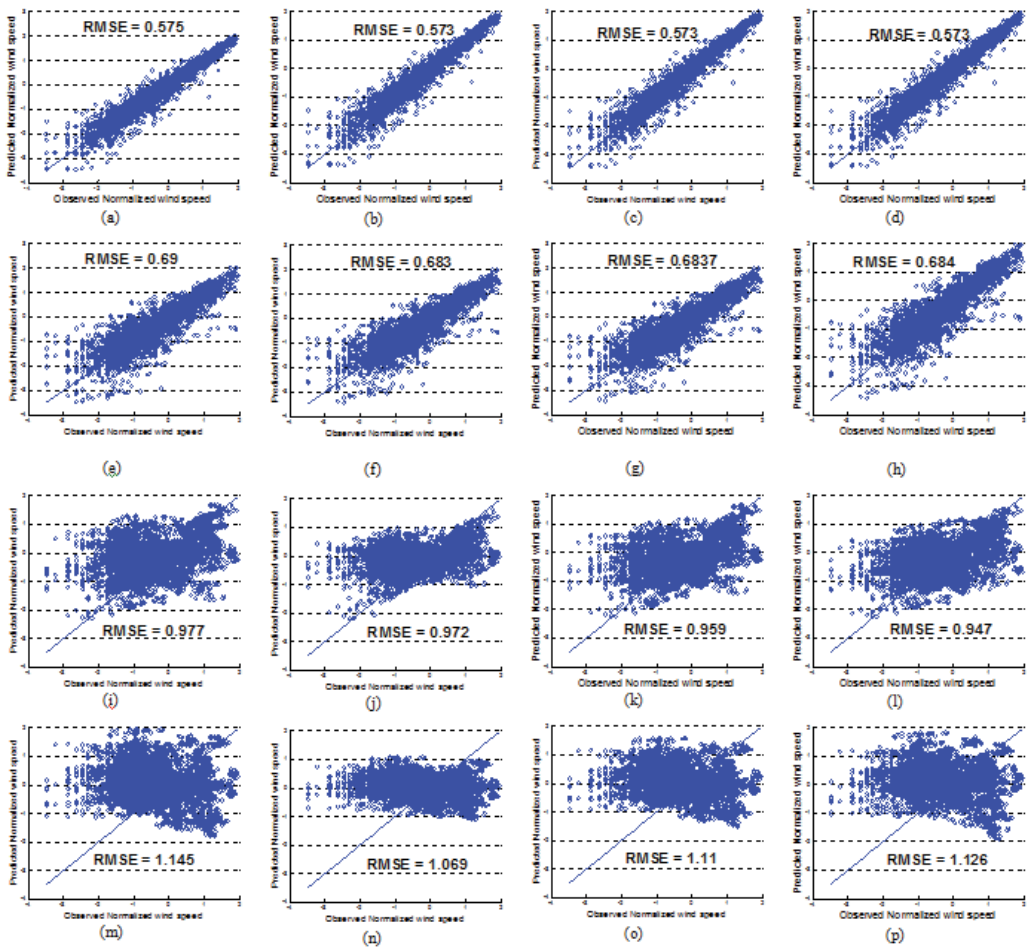

Fig. 9. Wind speed prediction using various past wind speed data in 10 minute resolution:
1st raw: 10 minute prediction using: (a) 10 min, (b) one hour, (c) 12 hours, and (d) 24 hours past data.
2nd raw: 1 hour prediction using: (e) 10 min. , (f) one hour, (g) 12 hours , and (h) 24 hours past data.
3rd raw: 12 hours prediction using: (i) 10 min. , (j) one hour, (k) 12 hours , and (l) 24 hours past data.
4th raw: 24 hours prediction using: (m) 10 min. , (n) one hour, (o) 12 hours , and (p) 24 hours past data.

In this section, short, medium and long-terms wind speed trends have been decomposed by applying Discrete Fourier transform (Yang HE, 2010).
A Discrete Fourier Transform (DFT) X[k], is computed for the natural logarithm of wind speed signal, x[n]. The DFT is then decomposed in frequency domain into low, medium and high frequency components, each of different frequency index range as:

$$X[k] = X_L[k] + X_M[k] + X_H[k] \tag{12}$$

Where $X_L[k]$, $X_M[k]$ and $X_H[k]$ are the low, medium and high frequency components, respectively. The DFT applies only to finite discrete signal (i.e., sequence of length "N").

$$x[n] \;\; for \;\; 0 \le n \le N-1$$

Where n is a discrete time index. The DFT, X[k], is also a discrete sequence of length "N" and k is a discrete frequency index. The main frequency coefficients for each component are given by:

$$\begin{aligned} X_L[k] &= \begin{cases} X[k] & , 0 \le k \le k_y \\ 0 & , k_y \le k \le N/2 \end{cases} \\ X_M[k] &= \begin{cases} X[k] & , k_y < k \le k_d \\ 0 & , otherwise \end{cases} \\ X_H[k] &= \begin{cases} X[k] & , k_d < k \le N/2 \\ 0 & , 0 \le k \le k_d \end{cases} \end{aligned} \tag{13}$$

It is noted that the DFT X[k] exhibits complex conjugate symmetry around $k = N/2$; hence all the decomposition components in (13) have conjugate symmetric coefficients within $N/2 < k \le N-1$. The thresholds k_y , k_w and k_d are the yearly, weekly and daily discrete frequency indices and are related to their analog frequency values by:

$$\begin{aligned} f_y &= \frac{f_s}{8760} = \frac{k_y f_s}{N} \\ f_w &= \frac{f_s}{168} = \frac{k_w f_s}{N} \\ f_d &= \frac{f_s}{24} = \frac{k_d f_s}{N} \end{aligned} \tag{14}$$

Where f_s = 1 sample/hr is the sampling frequency and N is the sample size covering 16 years from 1994 till 2009 in hourly resolution (National Weather Station, Available online).
Then we take the Inverse DFT (IDFT) of each component in (13), we obtain the aggregated IDFT of (12) in time domain:

$$x_t[n] = x_L[n] + x_M[n] + x_H[n] \tag{15}$$

Each IDFT signal component in (15) is modeled as a Gaussian time series. By taking the exponent of each signal in (15), we obtain the log-normal time domain signals that represent the low, medium and high frequency components of the original wind speed signal. Each pattern can be used to characterize the behavior of wind speed for different purposes. Figure 10 shows the aggregation of the three log-normal wind speed components in the time domain. Each decomposed wind speed signal is of important use in different applications in power systems, e.g., wind power predictions, scheduling and investment decisions.

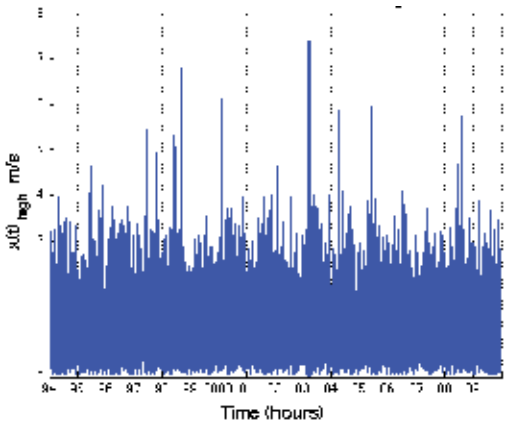

I. $x_H(t)$

$$x_t(t) = x_H(t) + x_M(t) + x_L(t)$$

II. $x_M(t)$

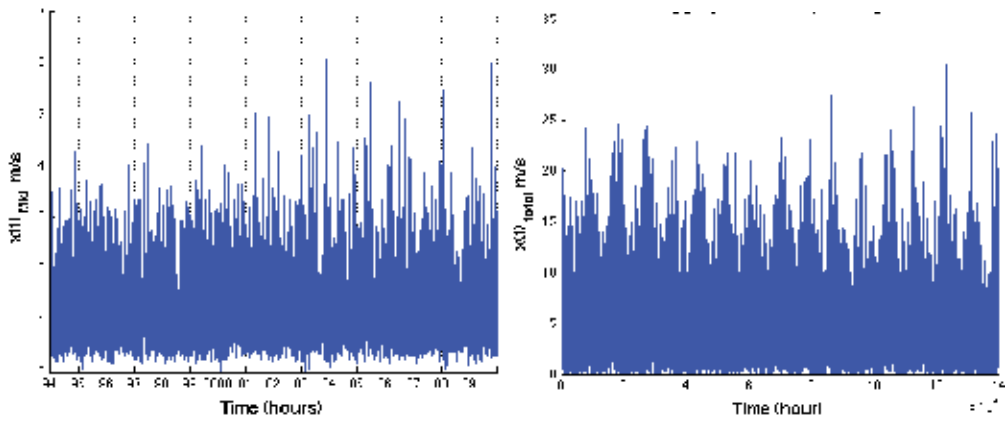

III. $x_L(t)$

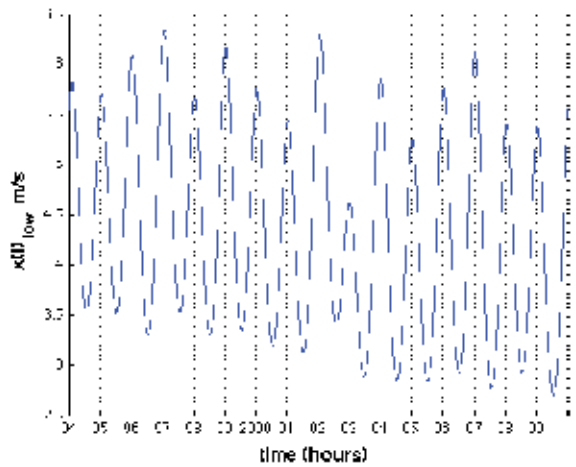

Fig. 10. Construction of wind speed signal using low, medium and high frequency components

4. Discrete Markov process

The interesting results obtained in section 2 (Figure 9) show Independencies from past observed data except for the nearest one. Model representation using Markov process is then valid, which is defined as the likelihood of next wind speed value in state *k* is conditioned on the most recent value of wind speed in state *m.* Equation (15) defines this likelihood – state relationship.

$$P(X_k = i \,|\, X_m = x_m, x_{m-1}, \ldots, X_1 = j) = P(X_k = i \,|\, X_m = x_m) \tag{15}$$

However, to identify state levels and state values, uniform midrise quantization process is carried out to discretize wind speed signal to state levels with optimum threshold or cutoffs values.

4.1 Design of optimum uniform quantizer

A midrise uniform Quantizer has been implemented that minimizes the mean square quantization error given a set of M states; we define $x = [x_1\, x_2 \cdots x_M]$ as a state value vector, and $x_t = [x_t(1) x_t(2) \cdots x_t(M-1)]$ as a quantized threshold levels or partitions vector. x is the original analog wind speed signal and x_q is the quantization signal. The quantization step Δ is defined as;

$$\Delta = x(m+1) - x(m) = x_t(m+1) - x_t(m) \tag{16}$$

The uniform Quantizer works as follows:

$$x_q = \begin{cases} x(1) & if \quad x \le x_t(1) \\ x(M) & if \quad x \succ x_t(M-1) \\ x(m)\ if\ x_t(m-1) \prec x \le x_t(m) \end{cases} \tag{17}$$

4.2 State and transition probabilities in discrete state space Markov model

Given the initial and final boundaries of each state; state probabilities can now be defined as:

$$\begin{aligned} P(m) &= P\left[x_i(m) \prec x \le x_f(m) \right] \\ &= P\left[x(m)\right] = \int_{x_i(m)}^{x_f(m)} f_X(x)\, dx \\ &= F_X(x_f(m) - F_X(x_i(m)) \end{aligned} \tag{18}$$

Where m is defined as any given state index and has the range from m= 1 to m=M. Equation (19) presents Markov linear state space model that takes prediction coefficients error signal modeled as disturbance *d,* and a regeneration time τ in which the signal updates itself, for example updates every 10 minutes (1 sample), or every one hour (6 samples) and so on.

$$x_\tau(n) = \sum_{j=1}^{N} a_j x(n-j) + d_j(n) \tag{19}$$

we define a processing time from $\tau_o \to \tau$ by a rectangular function. Equations (20) and (21) define subsequent use of state space representation.

$$x_{j,\tau}(n) = \sum_{j=1}^{N+1} a_{j+1} x(n-j) + d_j(n) \tag{20}$$

$$\overline{x_{j,\tau}}(n) = [A] \times \overline{x_{j-1,\tau}}(n) + d_j(n) \tag{21}$$

Where $[A]$ is the prediction coefficient matrix. Transition probabilities are calculated based on the counting method discussed in [11], in which we define :

$N_{trans}(k \mid m) \equiv$ The number of transitions from state m to state k in the time series,(m is the originating state, k is the next state)

$N_{state}(m) \equiv$ The number of occurrences of state m in the time series signal.

Both state and transition counters are related by (22) and the total size of the time series is defined in (23)

$$N_{state}(m) = \sum_{k=1}^{M} N_{trans}(k \mid m) \tag{22}$$

$$N = \sum_{m=1}^{M} N_{state}(m) = \sum_{m=1}^{M} \sum_{k=1}^{M} N_{trans}(k \mid m) \tag{23}$$

Using the statistical counter values of $N_{state}(m)$ and $N_{trans}(k \mid m)$, the transition and state probabilities can be statistically computed as:

$$P_{trans}(k \mid m) = \frac{N_{trans}(k \mid m)}{N_{state}(m)} \tag{24}$$

$$P_{state}(m) = \frac{N_{state}(m)}{N} \tag{25}$$

Where, *K = 1,…, M and, m= 1,…, M.* Note that (25) represent the statistical (actual) state probabilities of wind speed signal while (18) represent the theoretical state probabilities defined be either Weibull or Normal probability density functions. The probability state space representation is defined as:

$$P(\overline{x_{j,\tau}}(n)) = [P_{trans}] \times \overline{x_{j-1,\tau}}(n) \tag{26}$$

Where $[P]$ is the transition probability matrix.

In Figures 11, transition probability plots of normalized wind speed data are shown. The plots are generated from the same one-year sample size used in short term prediction (section 2). Those transition probabilities obviously appeared in cluster around the diagonal. This means smooth transitions between states and suggesting that the data does not exhibit frequent wind gusts. Moreover, we see the difference between theoretical and actual (statistical state probabilities (Figures 17 & 18). The reason is due to the use of the uniform quantization while we conjecture that a non-uniform quantizer will achieve a better match between the actual and theoretical probabilities.

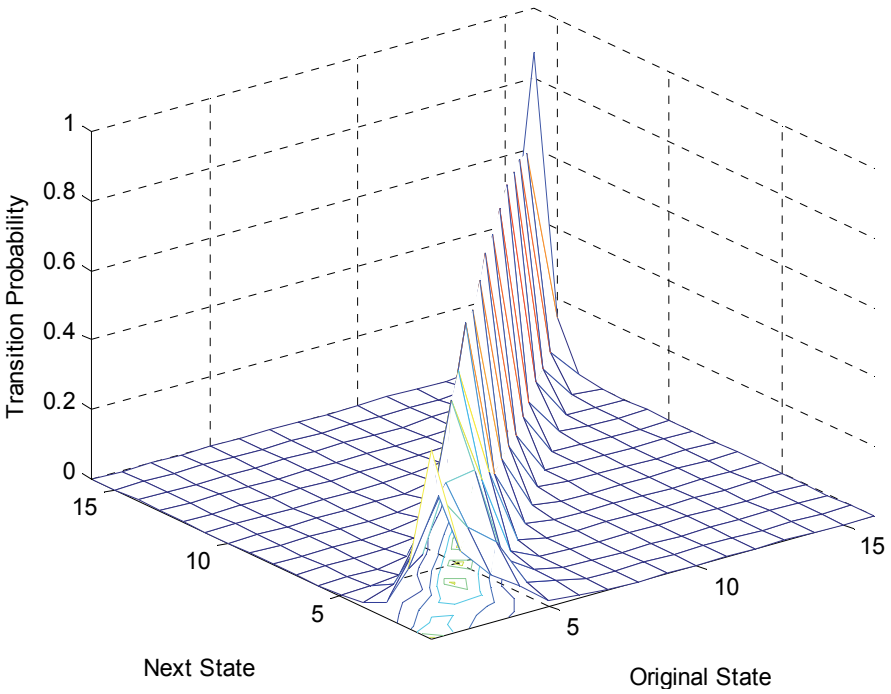

Fig. 11. Gaussian transition probabilities for M = 16 states

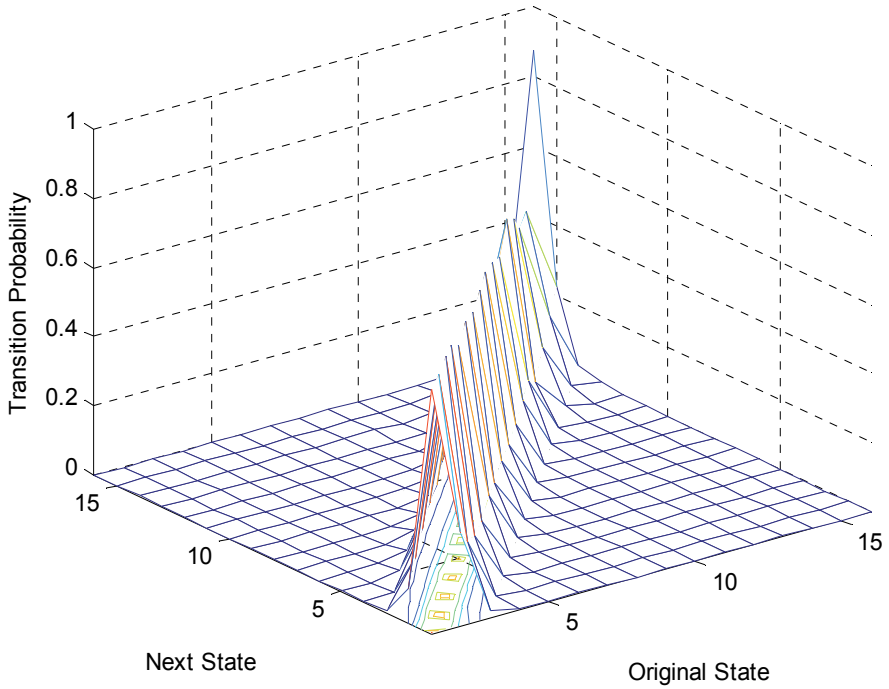

Fig. 12. Weibull transition probabilities for M = 16 states

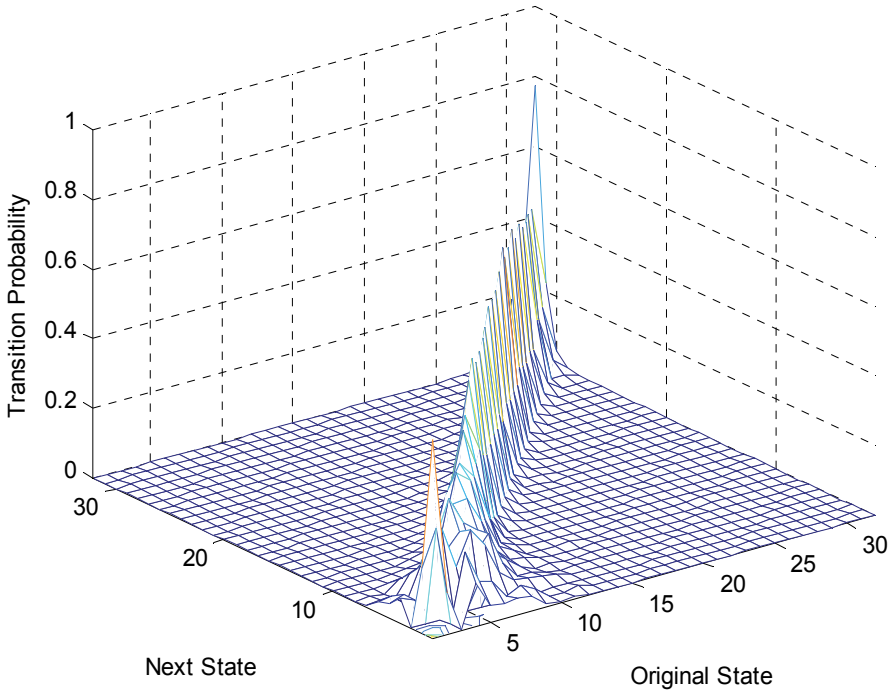

Fig. 13. Gaussian transition probabilities for M = 32 states

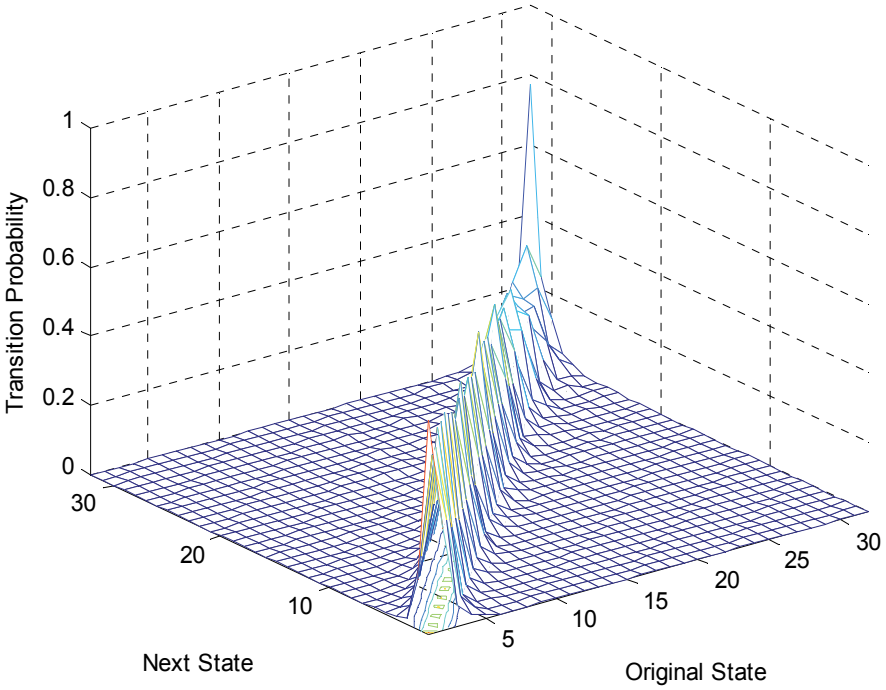

Fig. 14. Weibull transition probabilities for M = 32 states

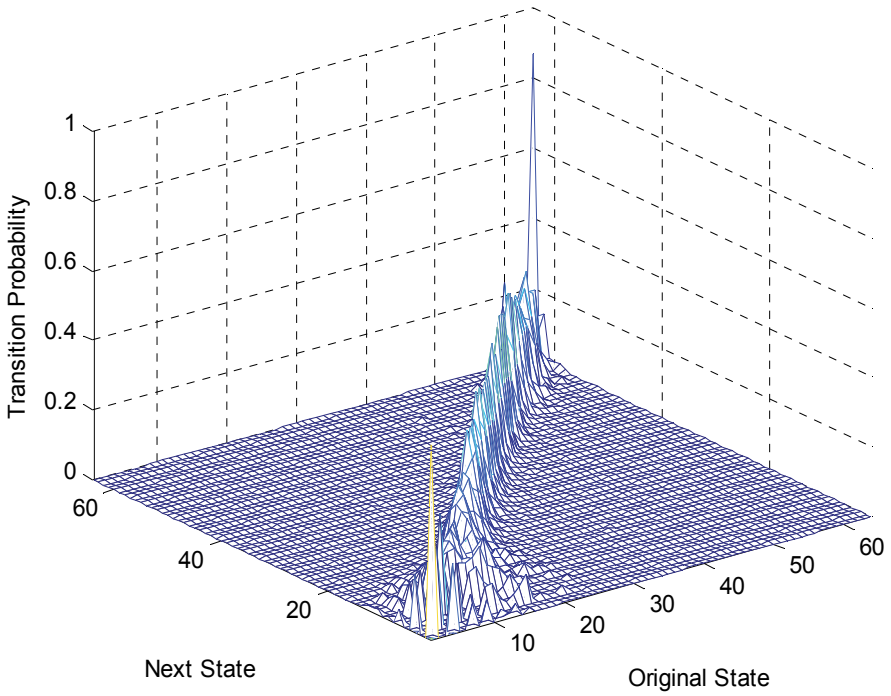

Fig. 15. Gaussian transition probabilities for M = 64 states

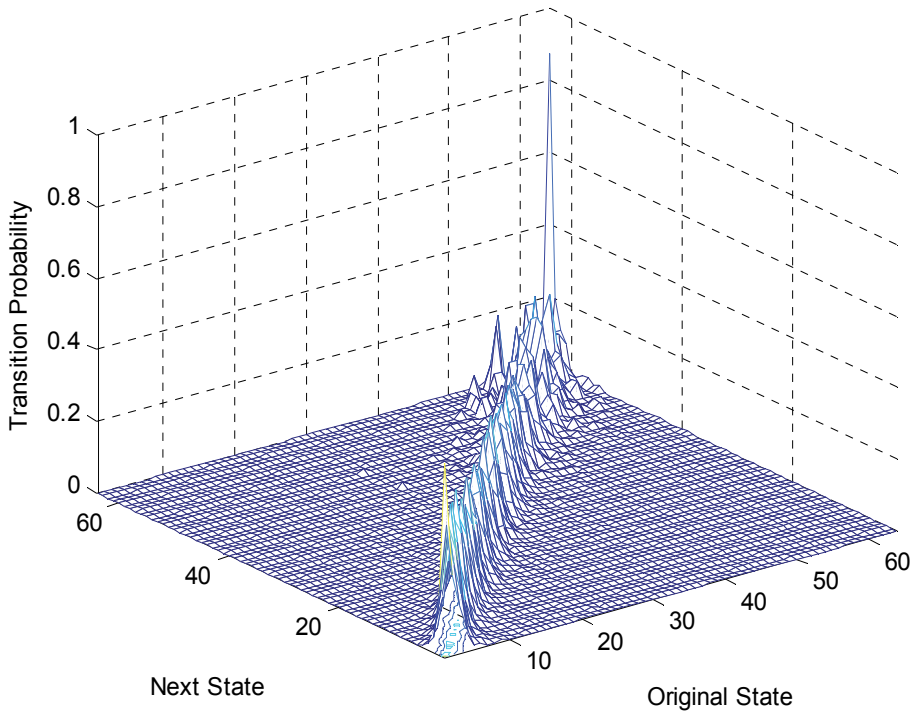

Fig. 16. Weibull transition probabilities for M = 64 states

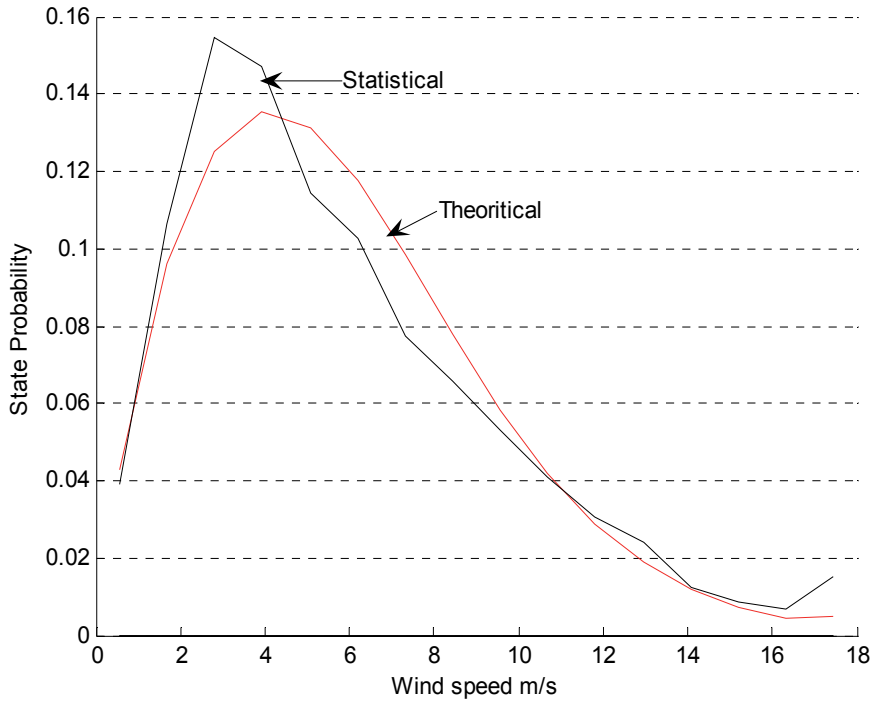

Fig. 17. Weibull state probabilities for M = 16 states

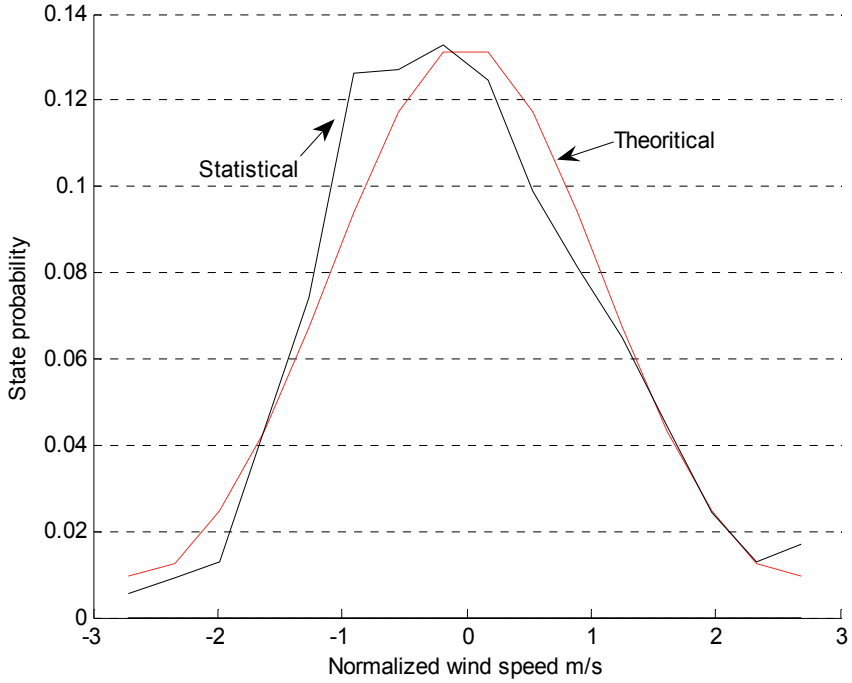

Fig. 18. Gaussian state probabilities for M = 16 states

Applying the quantization process and Markov state model to the decomposed wind speed signals presented in Figure 10 (16-year time series in hourly resolution) results in log normal distribution of wind speed state probabilities. The final results of the state probabilities are shown in Figures 19 - 21. Figures 22 – 24 show the transition probabilities for each decomposed wind speed signal. It is shown that smooth transitions appear in medium and low frequency component signals (i.e., centered around the diagonals), while high frequency component transition probabilities exhibit significant non-uniformities and disruptions due to fast changes and high frequencies variations driving the high frequency decomposed wind speed signal.

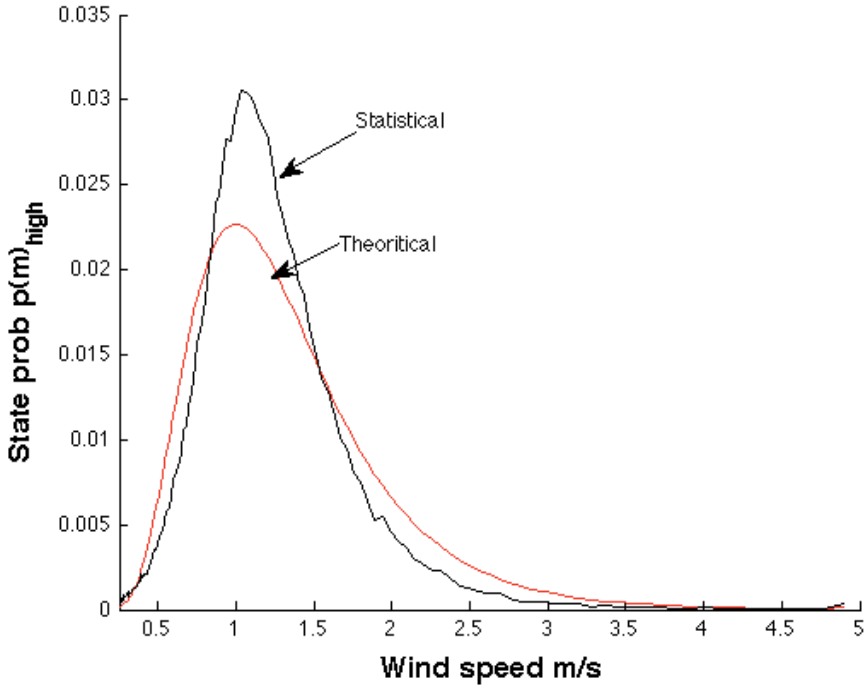

Fig. 19. Lognormal state probabilities (M = 128) for high frequency wind signal.

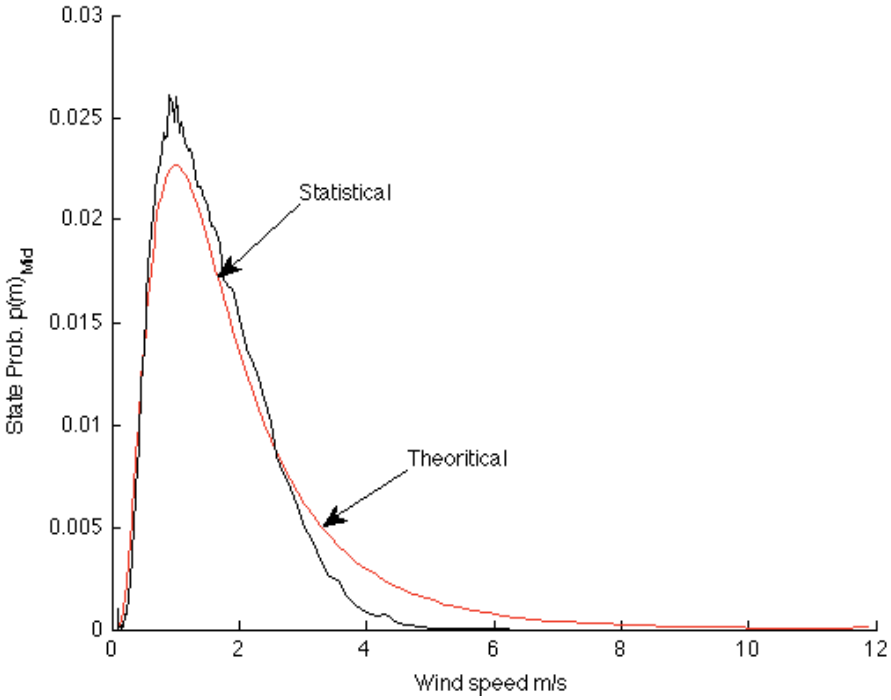

Fig. 20. Lognormal state probabilities (M = 128) for medium frequency wind signal.

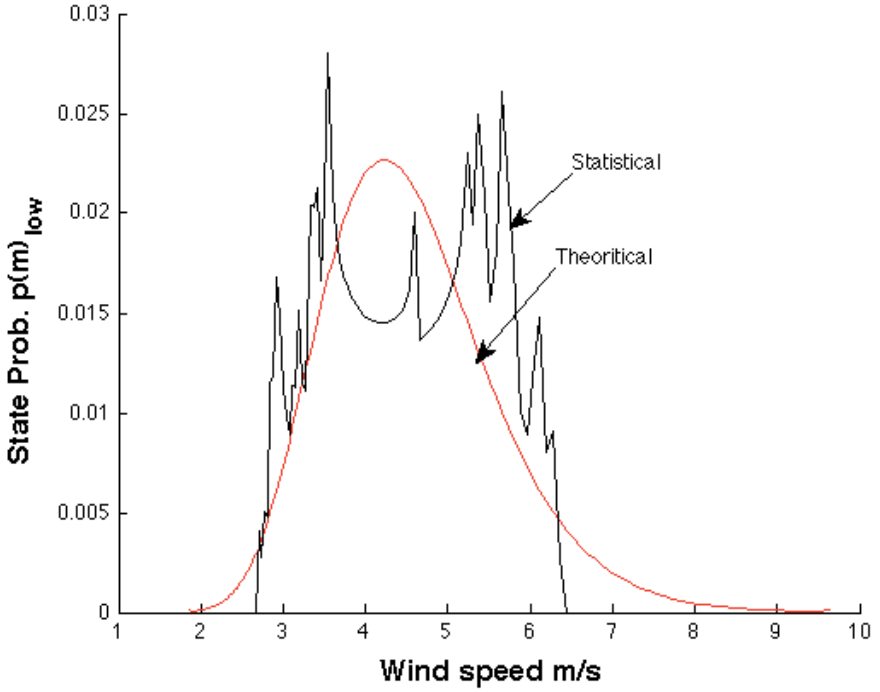

Fig. 21. Lognormal state probabilities (M = 128) for low frequency wind signal.

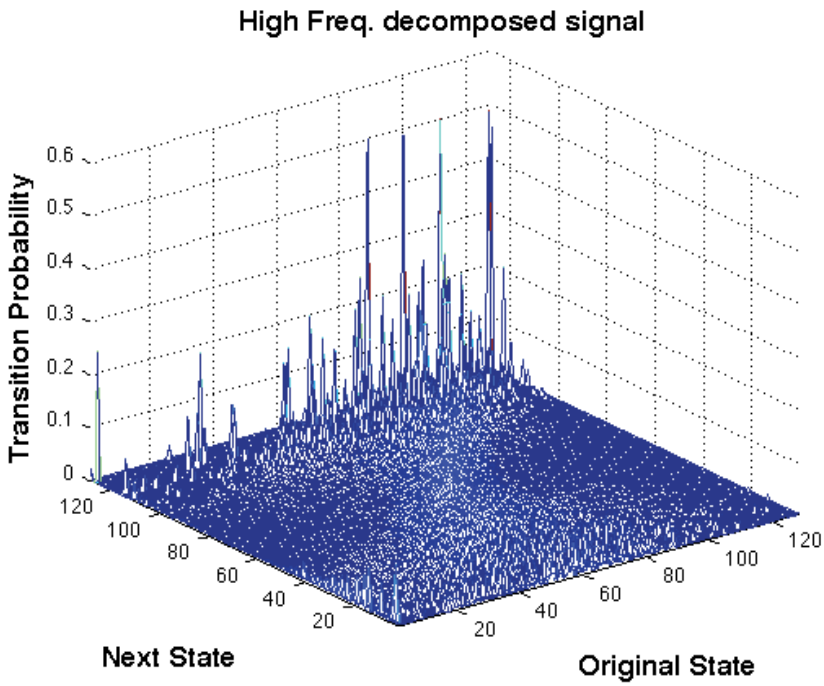

Fig. 22. Lognormal transition probabilities (M = 128) for high frequency wind signal.

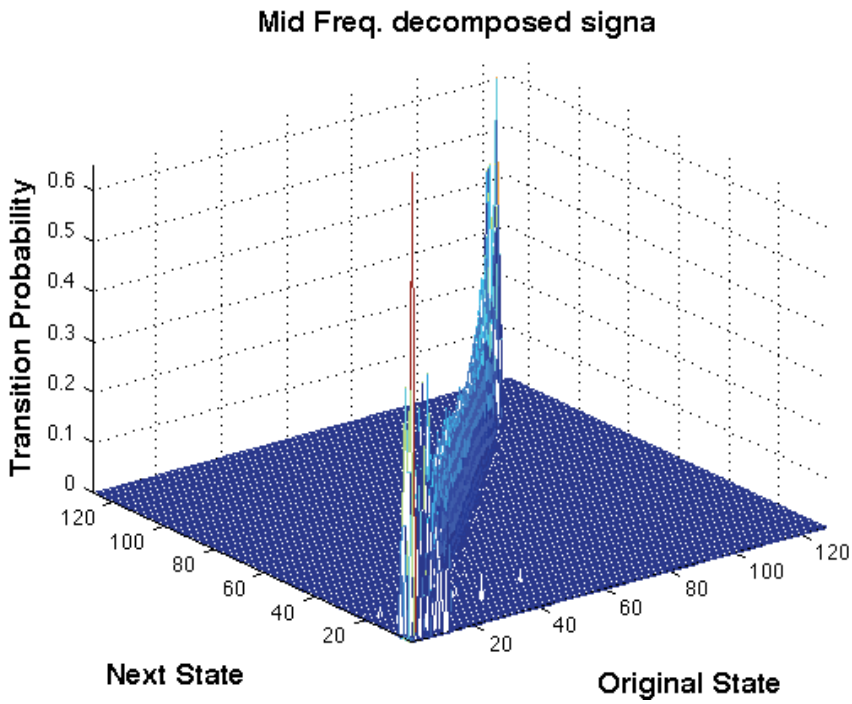

Fig. 23. Lognormal transition probabilities (M = 128) for medium frequency wind signal.

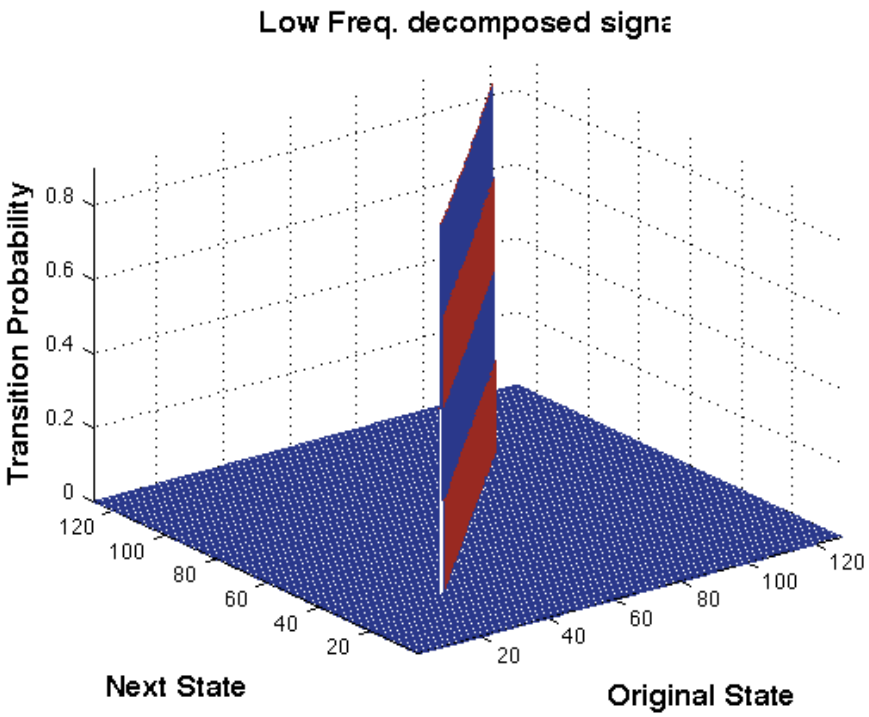

Fig. 24. Lognormal transition probabilities (M = 128) for low frequency wind signal.

5. Conclusion

This chapter characterizes wind speed signal using stochastic time series distribution models. It presents a short term wind speed prediction model using a linear prediction method by means of FIR and IIR filters. The prediction model was based on statistical signal representation by a Weibull distribution. Prediction accuracies are presented and they show independencies on past value expect for the most recent one. These in turn validate a Markov process presentation for stationary wind speed signals. The chapter also studies the integration of a complete wind speed pattern from a decomposition model using Fourier Transform for different wind time series models defined by different frequencies of each wind pattern.
Uniform quantization and discrete Markov process have been applied to the short, medium and long term wind speed time series signals. The actual state and transition probabilities have been computed statistically based on the counting method of the quantized time series signal itself. Theoretical state probabilities have been also computed mathematically using the fitted PDF model. A comparison of the statistical and theoretical state probabilities shows a good match. Both low and medium frequency signals exhibit smooth variation in state transition probabilities, while the high frequency component exhibit irregularity due to fast, short term variations.

6. References

[1] GE Energy, (March 2005), Report on "*The Effects of Integrating Wind Power on Transmission System Planning, Reliability, and Operations*" Prepared for:The New York State

Energy Research and Development Authority. Available online: http://www.nyserda.org/publications/wind_integration_report.pdf

[2] C. Lindsay Anderson, Judith B. Cardell, (2008), "Reducing the Variability of Wind Power Generation for Participation in Day Ahead Electricity Markets," *Proceedings of the 41st Hawaii Inter national Conference on System Sciences, IEEE*.

[3] Kittipong M., Shitra Y., Wei Lee, and James R., (Nov. 2007), "An Integration of ANN Wind Power Estimation Into Unit Commitment Considering the Forecasting Uncertainty," *IEEE Transactions On Industry Applications*, Vol., 43, No. 6,

[4] Marcos S. Miranda, Rod W. Dunn, (2006), "One-hour-ahead Wind Speed Prediction Using a Bayesian Methodology," *IEEE*.

[5] D. Hawkins, M. Rothleder, (2006), "Evolving Role of Wind Forecasting in Market Operation at the CAISO," *IEEE PSCE*, pp. 234 -238,

[6] Alberto F., Tomas G., Juan A., Victor Q., (Aug. 2005), "Assessment of the Cost Associated With Wind Generation Prediction Errors in a Liberalized Electricity Market," *IEEE Transactions on Power Systems*, Vol. 20, No. 3, pp. 1440-1446,.

[7] Dale L. Osborn, (2006), "Impact of Wind on LMP Market," *IEEE PSCE*, pp. 216-218.

[8] Cameron W. Potter, Micheal Negnevistsky,(2005) "Very Short-Term Wind Forecasting for Tasmanian Power Generation", IEEE, TPWRS Conference.

[9] National weather station, available online, http://www.ndbc.noaa.gov/data/5day2/DBLN6_5day.cwind

[10] B. A. Shenoi, (2006), "Introduction to Digital Signal Processing and Filter Design" John Wiley & Sons, Inc.

[11] F. Castellanos, (Aug. 2008), " Wind Resource Analysis and Characterization with Markov's Transition Maatrices," IEEE Transmission and Distribution Conf., Latin America,

[12] Noha Abdel-Karim, Mitch J. Small, Marija Ilic, (2009), "Short Term Wind Speed Prediction by Finite and Infinite Impulse

[13] Response Filters: A State Space Model Representation Using Discrete Markov Process", Powertech Conf. Bucharest, 2009.

[14] P. P. Vaidyanathan, (2008), *The Theory of Linear Prediction*, California Institute of Technology, 1st ed., Morgan & Claypool, 2008

[15] Yang HE, (2010), Modeling Electricity Prices for Generation Investment and Scheduling Analysis., Thesis proposal, University of Hong Kong.

12

Modelling and Simulation of a 12 MW Active-Stall Constant-Speed Wind Farm

Lucian Mihet-Popa[1] and Voicu Groza[2]
[1]*Politehnica University of Timisoara*
[2]*University of Ottowa*
[1]*Romania*
[2]*Canada*

1. Introduction

The conventional energy sources such as oil, natural gas, or nuclear are finite and generate pollution. Alternatively, the renewable energy sources like wind, solar, tidal, fuel cell, etc are clean and abundantly available in nature. Among those the wind energy has the huge potential of becoming a major source of renewable energy for this modern world. In 2008, 27 GW wind power has been installed all over the world, bringing world-wide install capacity to 120.8 GW (GWEC publication, 2009).
The wind energy industry has developed rapidly through the last 20-30 years. The development has been concentrated on grid connected wind turbines (wind farms) and their control strategies. Conventional stall wind turbines are equipped with cage rotor induction generators, in which the speed is almost constant, while the variable speed and variable pitch wind turbines use doubly-fed induction generators or synchronous generators in connection with a power converter (partial rate or full rate). The variable speed wind turbine has a more complicated electrical system than the fixed-speed wind turbine, but it is able to achieve maximum power coefficient over a wide range of wind speeds and about (5-10) % gain in the energy capture can be obtained (Hansen, A.D. et.al, 2001).
In this paper a complete simulation model of a 6 x 2 MW constant-speed wind turbines (wind farm) using cage-rotor induction generators is presented using data from a wind farm installed in Denmark. The purpose of the model is to simulate the dynamical behaviour and the electrical properties of a wind turbine existing in a wind farm. The wind farm model has also been built to simulate the influence on the transient stability of power systems. The model of each wind turbine includes the wind fluctuation model, which will make the model useful also to simulate the power quality and to study control strategies of a wind turbine.

2. Wind turbine modelling

In order to simulate the wind turbine as a part of a distribution system, models have been developed for each element and implemented in the dedicated power system simulation tool DIgSILENT Power Factory.
The purpose of the model is to simulate the dynamical behaviour and the electrical properties of a wind turbine. The modelling of the wind turbine should create a model as

simple as possible from a mechanical point of view, but capable of providing a good description of the electrical characteristics of a wind turbine.
The wind turbine model consists of different component models: wind model, aerodynamic model, transmission model and of the electrical components such as induction generator, soft-starter, capacitor bank and transformer model (Mihet-Popa, 2004). Aerodynamics is normally integrated with models for different wind conditions and structural dynamics.
The wind turbine is characterized by the non-dimensional curves of the power coefficient C_p as a function of both tip speed ratio λ, and the blade pitch angle, θ_{pitch} . The tip speed ratio is the ratio of linear speed at the tip of blades to the speed of the wind.
As shown in Fig. 1, the wind model generates an equivalent wind speed u_{eq}, which, together with the blade pitch angle θ_{blade} and rotor speed ω_{rot}, are input to the aerodynamic block. The output of the aerodynamic model is the aerodynamic torque T_{rot}, which is the input for the transmission system together with the generator speed ω_{gen}. The transmission system has as output the mechanical torque T_{hss} on the high-speed shaft, which is used as an input to the generator model. Finally, the blade angle control block models the active control loop, based on the measured power and the set point.
A simplified block diagram of the wind turbine model is presented in Fig. 1.

2.1 The wind speed model

The wind models describe the fluctuations in the wind speed, which influence the power quality and control characteristics of the wind farm. Thus, the wind speed model simulates the wind speed fluctuations that influence the fluctuations in the power of the wind turbines. The wind acting on the rotor plane of a wind turbine is very complex and includes both deterministic effects (mean wind, tower shadow) and stochastic variations due to turbulence (Mihet-Popa, 2003).

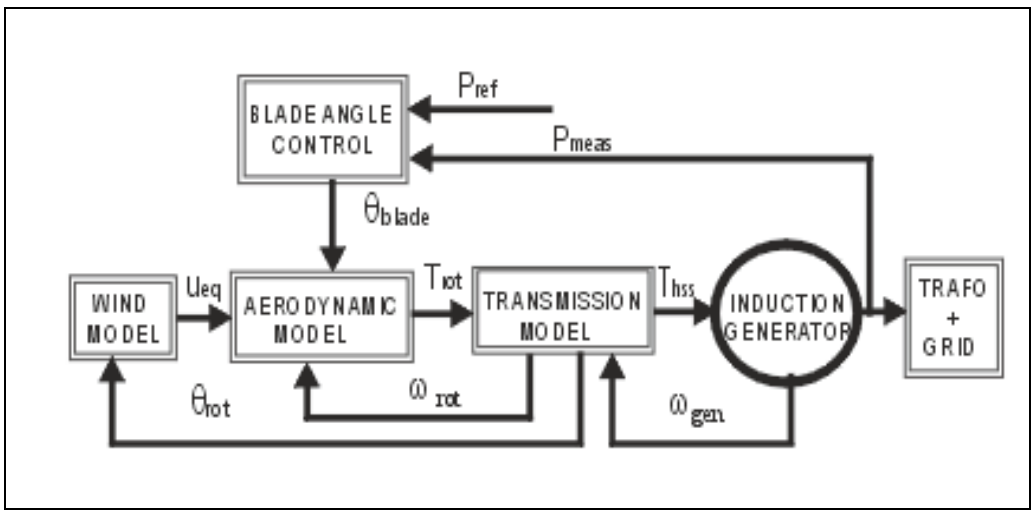

Fig. 1. The block diagram of a simplified model for a constant-speed wind turbine using induction generator.

The simulations shown in Fig. 2 illustrate the effect of the rotational sampling. This hub wind speed is used as input to the rotor wind model to produce an equivalent wind speed

(u_{eq}), which accounts for the rotational sampling on each of the blades. The wind speed (*wspoint*), which influences the power quality, should be filtered to generate a hub wind speed (*wsfic*).
Figure 2 shows a simulation result for one wind turbine, based on a look-up table, at an average wind speed of 10 m/s.
As expected, both wind speed models fluctuate with three times the rotational frequency (3p).

2.2 The aerodynamic model

A wind turbine is essentially a machine that converts the kinetic energy of the moving air (wind) first into mechanical energy at the turbine shaft and then into electrical energy (Heier S., 1998).
Fig. 3 describes the conversion of wind power (P_{WIND}) into mechanical (P_{MEC}) and thereafter into electrical power (P_{EL}).

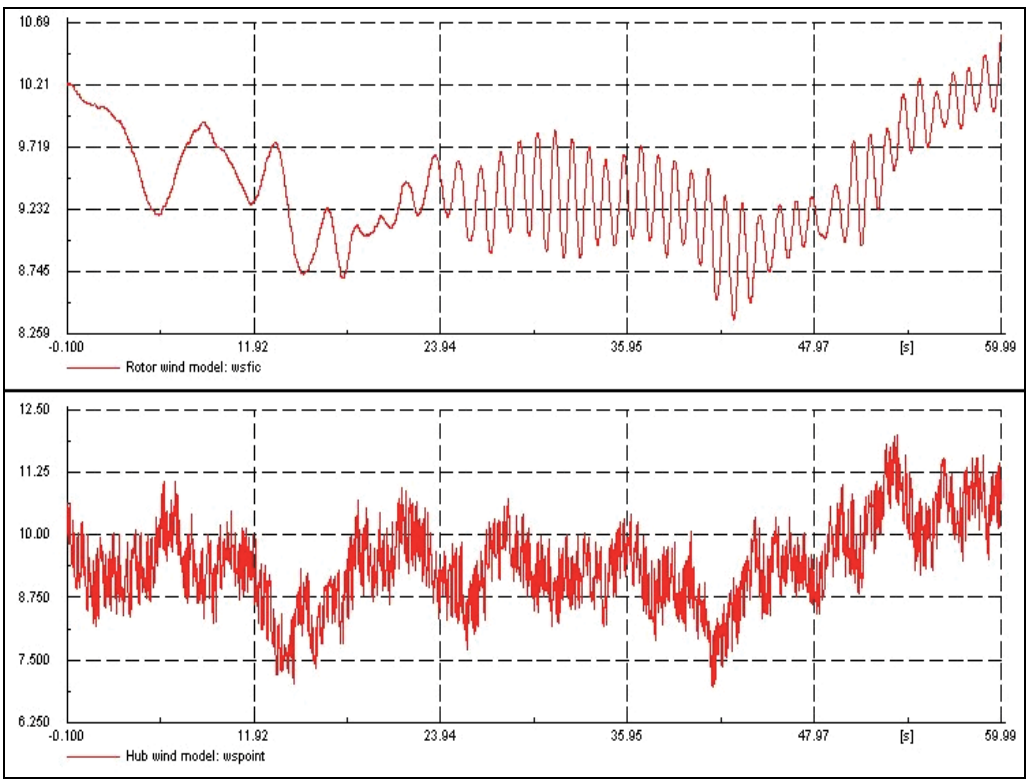

Fig. 2. Rotor wind speed and hub wind speed model.

The interaction of the turbine with the wind is complex but a reasonably simple representation is possible by modelling the aerodynamic torque or the aerodynamic power as described below. Aerodynamic modelling also concerns the design of specific parts of wind turbines, such as rotor-blade geometry and the performance prediction of wind farms.
The force of the wind creates aerodynamic lift and drag forces on the rotor blades, which in turn produce the torque on the wind turbine rotor (Hansen et. al, 2003).

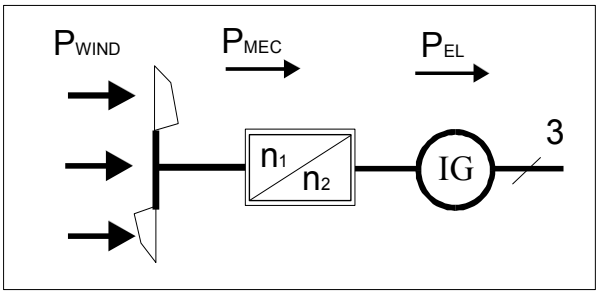

Fig. 3. A block diagram of the power conversion in a wind turbine.

The aerodynamic torque is given by:

$$T_{rot} = \frac{P_{aero}}{\omega_{rot}} = \frac{1}{2\lambda} \rho \pi R^3 C_p(\lambda, \theta_{pitch}) \tag{1}$$

Where P_{aero} is the aerodynamic power developed on the main shaft of a wind turbine with radius R at a wind speed u_{eq} and air density ρ. It is expressed by:

$$P_{aero} = \frac{1}{2} \rho \pi R^2 u_{eq}^3 C_p(\lambda, \theta_{pitch}) \tag{2}$$

The air density ρ is depending on the temperature and on the pressure of the air.
The dimensionless power coefficient $C_p(\lambda, \theta_{pitch})$ represents the rotor efficiency of the turbine. It is taken from a look-up table, which contains the specific aerodynamic characteristics for the turbine.
This coefficient depends on the tip speed ratio $\lambda = \omega_{rot} \cdot R / u_{eq}$ and on the blade angle θ_{pitch}, ω_{rot} denotes the rotor speed. For a constant speed turbine, the power coefficient decreases when the wind speed increases (λ small). This fact is used in the passive stall control wind turbine.
The efficiency coefficient (C_p) changes with different negative values of the pitch angle (0^0, -1^0, -2^0, -3^0) but the best efficiency is obtained for $\theta_{pitch}=0^0$.
The aerodynamic model is based on C_p curves for the given rotor blades.

2.3 Transmission system model

To describe the impact of the dynamic behaviour of the wind turbine, a simple model is considered, where the tower bending mode and the flap-bending mode of the wind turbine are neglected.
It is assumed that all the torsion movements are concentrated in the low speed shaft, as T_{lss}. Emphasis is placed on the parts of the dynamic structure of the wind turbine, which contributes to the interaction with the grid, i.e. which influence the power. Therefore only the drive train is considered in the first place because the other parts of the wind turbine structure have less influence on power.
The drive train model is illustrated in Fig. 4.
The rotor is modelled by inertia I_{rot}, low speed shaft only by a stiffness k_s (the torsion damping is neglected), while the high-speed shaft is assumed to be stiff. Thus the transmission is described by the following equations:

$$I_{rot} \cdot \frac{d\omega_{rot}}{dt} = T_{rot} - T_{lss} \tag{3}$$

$$\frac{dT_{lss}}{dt} = k_s \left(\omega_{rot} - \frac{\omega_{gen}}{n_{gear}} \right) \tag{4}$$

It is also assumed that the losses in the gearbox are zero, thus the gear transmits ideally from the low speed to high speed. The output of the model is:

$$T_{hss} = \frac{T_{lss}}{n_{gear}} \tag{5}$$

where n_{gear} is ratio of the gear box.

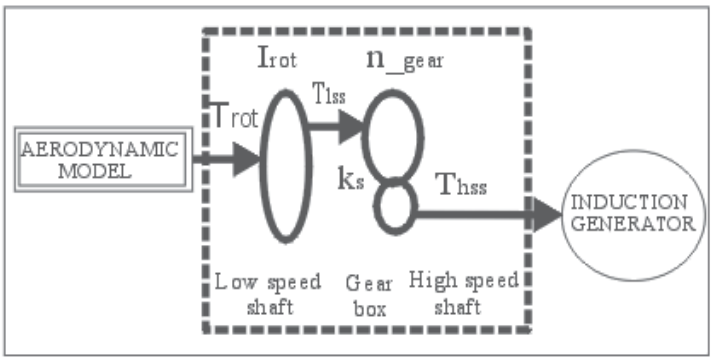

Fig. 4. Drive train model of the wind turbine.

2.4 The induction generator model

The induction machine model is a combined mechanical and electro-magnetic model. The mechanical model includes the inertia of the generator rotor in the generator model.
Induction generators are 4/6 pole single cage machines (2MW/500kW) implemented using their nominal nameplate parameters.
The torque–slip and short-circuit test curves are used as a definition in the built–in DigSILENT asynchronous machine model.
Electrical parameter variations and different cage rotors with rotor current displacement can also be considered (DIgSILENT Power Factory user manual, 2010).
In the simulations presented in the following the induction generator is a single cage machines implemented using their nominal nameplate parameters, as can be seen in Fig. 5.
To wider the range of the output electrical power the generators are with double stator windings (2/0.5MW).
The switching between 4/6 pole operation is made as a function of output power.

2.5 The soft-starter model

In order to reduce the transient current during connection of the induction generator to the grid a soft starter is used. The soft-starter could minimize the impact of machine starting on the electrical network and also could helps to prolong the life of mechanical components.

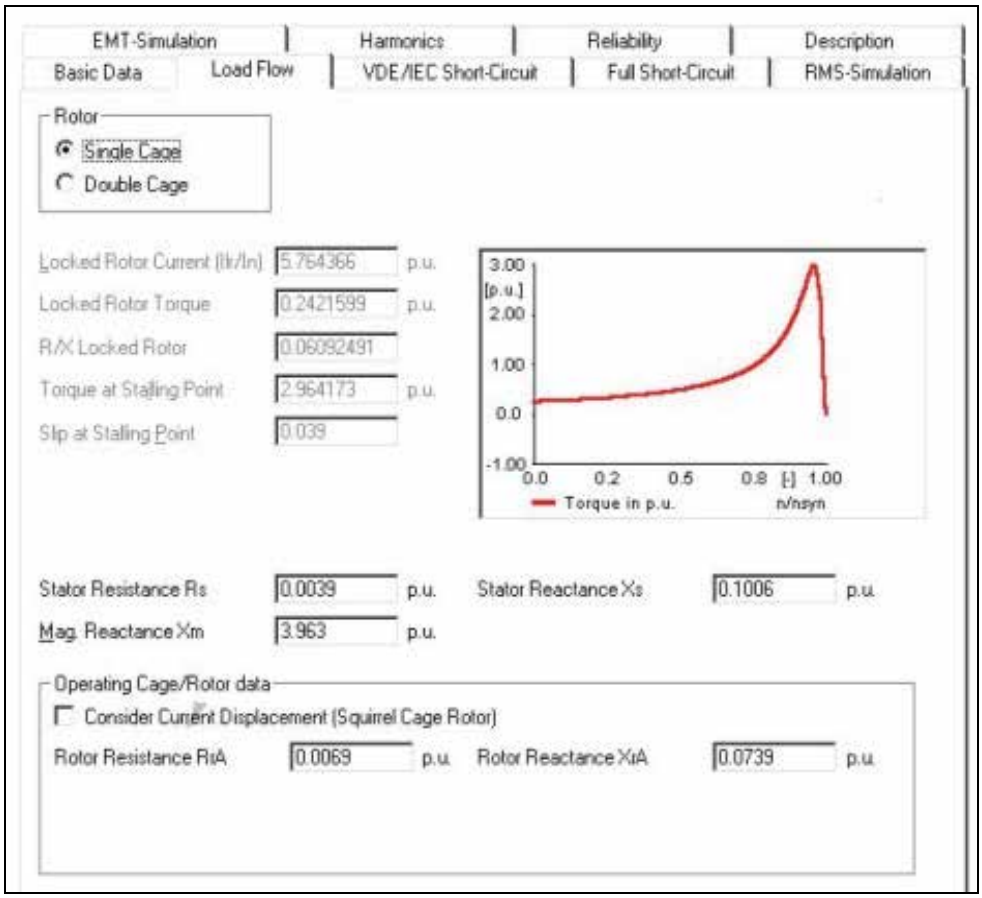

Fig. 5. Induction generator of 2 MW rating power implemented in DIgSILENT simulation tool based on its torque-slip curve and name plate values.

A soft-starter is an ac voltage controller in which the voltage is adjusted through the setting of the thyristors firing angle (Deleroi & Woudstra, 1991).

The soft-starter is designed to meet the industrial requirements of wind generator applications. In DIgSILENT Power Factory the soft starter is a stand-alone element. The commutation devices are 2 thyristors connected in anti-parallel for each phase.

The soft-starter modelling and its control implementation are described in details and a set of simulations are performed using DIgSILENT software simulation tool.

When the wind generator is driven to just bellow synchronous speed (approximately 93 %), under the action of its aerodynamic rotor, the soft starter is connected and using the firing angle control the machine is connected over the grid.

The connection diagram of soft starter fed a 4/6 poles double stator windings induction machine is presented in Fig. 6 a). Figure 6 b) shows the fully controlled topology with a delta-connected load. If thyristors are delta-connected, their control is simplified and their ratings considerably reduced. The delta arrangements generate, in the load, all the odd harmonics, but no triple harmonics. Harmonics of order 5, 7, 11, 13 … remain.

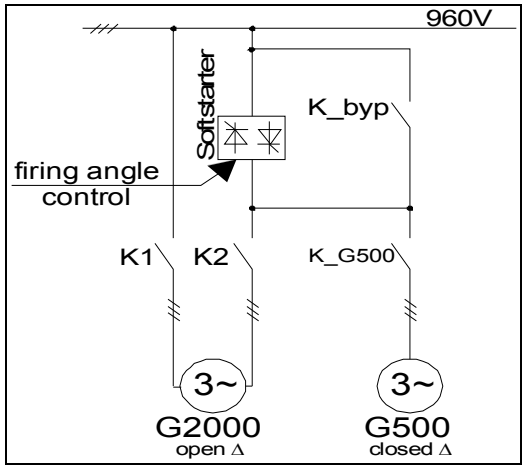

a)

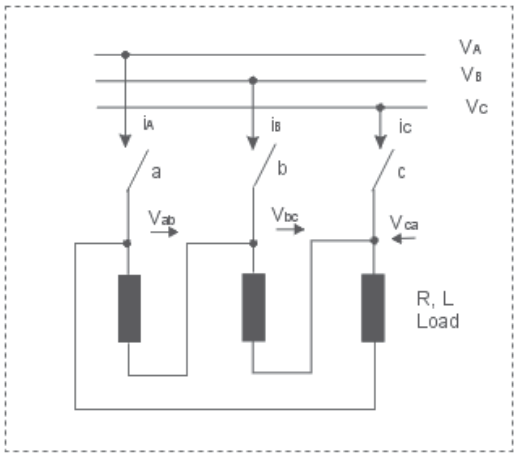

b)

Fig. 6. a) Connection diagram of the soft-starter with induction generators and schematic diagram of the soft-starter with delta connected load, b).

To get the controller started, two or three switches must be fired simultaneously to provide the path for current necessary to maintain the on-state. Switching variables may be introduced for 2 thyristors connected in anti-parallel for each phase and defined as equal to 1 when a given thyristor is conducting and equal to 0 otherwise. It can easily be demonstrated that the output voltages of the controller (soft-starter) are given by (6):

$$\begin{bmatrix} V_{ab} \\ V_{bc} \\ V_{ca} \end{bmatrix} = \begin{bmatrix} ab & -\frac{1}{2}a & -\frac{1}{2}b \\ -\frac{1}{2}c & bc & -\frac{1}{2}b \\ -\frac{1}{2}c & -\frac{1}{2}a & ca \end{bmatrix} \times \begin{bmatrix} V_{AB} \\ V_{BC} \\ V_{CA} \end{bmatrix} \tag{6}$$

Depending on the firing angle, three modes of operation of the soft-starter can be distinguished, with a purely resistive load (Rombaut, et. al, 1987):

1. $0^\circ \le \alpha < 60^\circ$: 2 or 3 switches conducting (in either direction);
2. $60^\circ \le \alpha < 90^\circ$: 2 switches conducting;
3. $90^\circ \le \alpha < 150^\circ$: none or two switches conducting.

Analysis of operation of the controller with RL load is difficult since the extension angle and the so-called limit angle must be known. Mode 2, characterized by rapid changes of the output currents is impossible due to the load inductance. The ranges of the two remaining operation modes are $\varphi \le \alpha < \alpha_{lim}$ for mode 1 and $\alpha_{lim} \le \alpha < 150°$ for mode 3. The limit angle can be determined numerically from (7):

$$\frac{\sin(\alpha_{\lim} - \varphi - \frac{4}{3}\pi)}{\sin(\alpha_{\lim} - \varphi)} = \frac{2e^{-\frac{\pi}{3tg(\varphi)}} - 1}{2 - e^{-\frac{\pi}{3tg(\varphi)}}} \tag{7}$$

The equations for the RMS output voltage, of the fully controlled soft-starter with purely resistive and inductive loads are provided bellow:
Resistive load:

$$V_{out} = V_{in} \cdot \sqrt{\frac{1}{\pi} \cdot \left[\pi - \frac{3}{2} \cdot \alpha + \frac{3}{4} \sin(2\alpha) \right]} \tag{8}$$

for $0^\circ \le \alpha < 60^\circ$

$$V_{out} = V_{in} \cdot \sqrt{\frac{1}{\pi} \cdot \left[\frac{\pi}{2} + \frac{3\sqrt{3}}{4} \cdot \sin(2\alpha + \frac{\pi}{6}) \right]} \tag{9}$$

for $60^\circ \le \alpha < 90^\circ$

$$V_{out} = V_{in} \cdot \sqrt{\frac{1}{\pi} \cdot \left[\frac{5\pi}{4} - \frac{3}{2} \cdot \alpha + \frac{3}{4} \cdot \sin(2\alpha + \frac{\pi}{3}) \right]} \tag{10}$$

for $90^\circ \le \alpha < 150^\circ$
Inductive load

$$V_{out} = V_{in} \cdot \sqrt{\frac{1}{\pi} \cdot \left[\frac{5\pi}{2} - 3\alpha + \frac{3}{2} \cdot \sin(2\alpha) \right]} \tag{11}$$

for $90° \le \alpha < 120°$

$$V_{out} = V_{in} \cdot \sqrt{\frac{1}{\pi} \cdot \left[\frac{5\pi}{2} - 3\alpha + \frac{3}{2} \cdot \sin(2\alpha + \frac{\pi}{3}) \right]} \tag{12}$$

for $120° \le \alpha < 150°$
The envelope of control characteristics given by (8) through (12) is shown in Fig. 7. The relationship between the firing angle and the resulting amplification of the soft starter is

highly non-linear and depends additionally on the power factor of the connected element. In the case of a resistive load α can vary between 0 (full on) and 90 (full off) degrees. While in the case of a purely inductive load α varies between 90 (full on) and 180 (full off) degrees. For any power factor in between, it will be somewhere between these limits, as can also be seen in Fig. 7.

In DIgSILENT the control parts (electrical controllers) of the wind turbine system, as the soft-starter control implementation, are written in the dynamic simulation language DSL. DSL implementation includes a complete mathematical description of (time-) continuous linear and nonlinear systems. A DSL model can also be converted into a graphical representation.

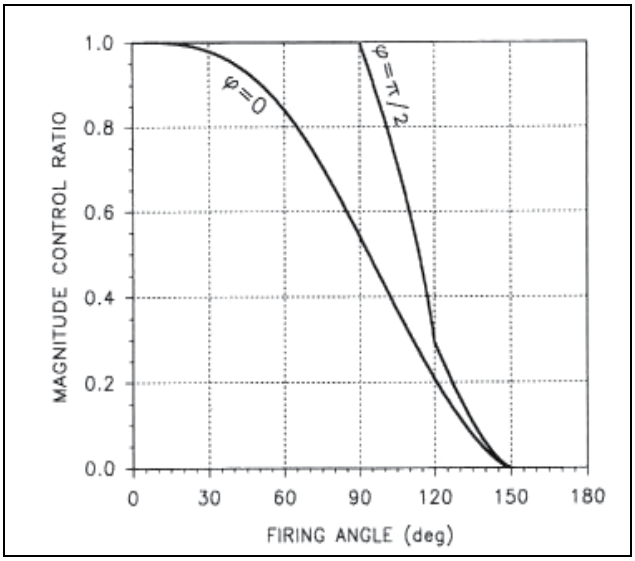

Fig. 7. Control characteristic, Vout=f(α), for a fully controlled soft-starter (Rombaut, 1987).

Fig. 8 shows the soft-starter composite model implemented in DIgSILENT, in which "Control slot" represents the soft-starter controller while "Soft starter slot" is a block for checking the soft-starter state (working / bypassed).

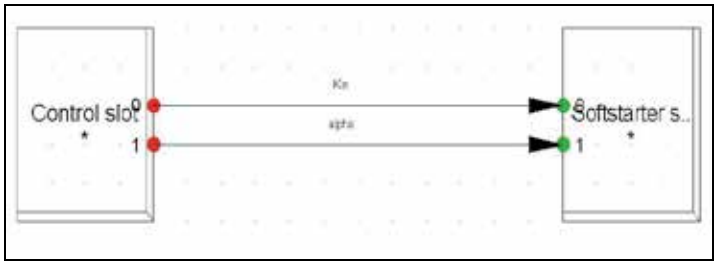

Fig. 8. Soft-starter composite model implemented in DIgSILENT.

The firing angle (α) is calculated according to the amplification factor (K_{in}) so that if Kin varies from 0 to 1, α will take values starting from a1 down to a2, (Mihet-Popa, L. et.al, 2008).

$$\alpha = \frac{\pi}{180^0} \cdot \left[a_2 + \left(a_2 - a_1 \right) \cdot \left(K_{in} - 1 \right) \right] \tag{13}$$

In witch a1, a2-maximum and minimum angles in degrees and a, b, c-switching variables for thyristors;

3. Control strategies for wind turbines

Wind turbines are designed to produce electrical energy as cheaply as possible. Therefore there are generally designed so that they yield maximum output power at wind speeds around (12-15) meters per second (Hansen, 2001).
In case of stronger winds it is necessary to waste a part of the excess energy of the wind in order to avoid damaging the wind turbine. All wind turbines are therefore designed with some sort of power control.
There are two different ways of doing this safely on modern wind turbines: pitch control and active stall control, as will be described as follows.

3.1 Pitch controlled wind turbines

On a pitch controlled wind turbine the electronic controller checks the output power of the turbine several times per second. When the output power becomes too high, it sends an order to the blade pitch mechanism which immediately pitches (turns) the rotor blades slightly out of the wind. Conversely, the blades are turned back into the wind whenever the wind drops again. The rotor blades thus have to be able to turn around their longitudinal axis (to pitch). During normal operation the blades will pitch a fraction of a degree at a time - and the rotor will be turning at the same time. Designing a pitch-controlled wind turbine requires some clever engineering to make sure that the rotor blades pitch exactly the amount required. The pitch mechanism is usually operated using hydraulics or electric stepper motors (Heier, 1998 & Muljadi, 1999).
As with pitch control it is largely an economic question whether it is worthwhile to pay for the added complexity of the machine, when the blade pitch mechanism is added.

3.2 Stall controlled wind turbines

Stall controlled (passive stall controlled) wind turbines have the rotor blades bolted onto the hub at a fixed angle. The geometry of the rotor blade profile however has been aerodynamically designed to ensure that the moment when the wind speed becomes too high ; it creates turbulence on the side of the rotor blade which is not facing the wind. This stall prevents the lifting force of the rotor blade from acting on the rotor. As the actual wind speed in the area increases, the angle of attack of the rotor blade will increase, until at some point it starts to stall. If you look closely at a rotor blade for a stall controlled wind turbine you will notice that the blade is twisted slightly as you move along its longitudinal axis. This is partly done in order to ensure that the rotor blade stalls gradually rather than abruptly when the wind speed reaches its critical value. The basic advantage of stall control is that one avoids moving parts in the rotor itself, and a complex control system (Mihet-Popa, L., 2003).
A normal passive-stall controlled wind turbine will usually have a drop in the electrical power output for higher wind speeds, as the rotor blades go into deeper stall. On the other hand, stall control represents a very complex aerodynamic design problem, and related

design challenges in the structural dynamics of the whole wind turbine, e.g. to avoid stall-induced vibrations.

3.3 Active stall controlled wind turbines

An increasing number of larger wind turbines (1 MW and more) are developed with an active stall power control mechanism. Technically the active stall turbines resemble pitch-controlled turbines, since they have pitch able blades. In order to get a reasonably large torque (turning force) at low wind speeds, the wind turbines will usually be programmed to pitch their blades much like a pitch controlled wind turbine at low wind speeds. Often they use only a few fixed steps depending upon the wind speed.

When the turbine reaches its rated power, however, it will notice an important difference from the pitch controlled wind turbines: If the generator is about to be overloaded, the turbine will pitch its blades in the opposite direction from what a pitch-controlled wind turbine does. In other words, it will increase the angle of attack of the rotor blades in order to make the blades go into a deeper stall, thus wasting the excess energy in the wind.

One of the advantages of active stall is that one can control the active power more accurately than with passive stall, so as to avoid overshooting the rated power of the turbine at the beginning of a gust of wind. Another advantage is that the wind generator can be run almost exactly at the rated power of the machine at all high wind speeds.

3.4 Rotor efficiency under stall and pitch controlled wind turbines

The output power of wind turbines varies with wind speed, but is not proportional to it, as the energy that the wind contains increases with the cube of the wind speed. At low wind speeds (1-3 m/s), wind turbines are shut down, as they would be able to generate little or no power (Fig. 9).

Wind turbines only start-up at wind speeds between 2.5 and 5 m/s, known as the "cut-in" wind speed. "Nominal" or "rated" wind speed, at which nominal output power is reached, is normally between 12 and 15 m/s. The precise value depends on the ratio of generator capacity to rotor surface area, and is a design variable. Finally, any wind turbine has a "cut-out wind speed": this is the wind speed at which the turbine is shut down to avoid structural overload. Its value is around 25 m/s for IEC Wind class I and II turbines. For IEC Wind Class III turbines, which generate maximum output power at lower wind speeds, the cut-out value is in the range of 17-20 m/s. Wind turbines are shut down if the 10-minute average of the wind speed is above this design value. Below nominal wind speed, the aim is to maximize rotor efficiency (Fig. 9).

The rotor efficiency depends on the ratio of the rotor blade tip speed and wind speed, known as the "tip speed ratio" (λ), described by:

$$\lambda = \omega_{rot} \cdot R / u_{eq} \tag{14}$$

The tip speed ratio of a fixed speed wind turbine cannot be controlled, as the rotor speed (and thus the blade tip speed) is fixed. Nevertheless, the tip speed ratio varies with wind speed, and thus reaches the optimum value at one wind speed only in case of fixed speed designs (or at two speeds if the wind turbine can operate at two different, but constant, rotor speeds).

With a variable speed wind turbine, the tip speed ratio varies, and depends both on wind speed and rotor speed. For maximum rotor efficiency, the tip speed ratio must be

maintained at the value that corresponds to optimum rotor efficiency (usually 6-9) at all times. This is achieved by controlling the rotor speed accordingly. The higher aerodynamic efficiency that is thus achieved explains why a variable speed turbine generates more energy for the same wind speed regime.
At wind speeds below nominal, the aim is to extract energy from the wind as efficiently as possible; however, this ceases to apply above nominal wind speed, as this would overload the generator and/or the converter system. Above nominal wind speed, therefore, the mechanical power extracted from the wind must remain constant. To achieve this, the aerodynamic rotor efficiency must be reduced when the wind speed increases, as can also be seen in Fig. 9.

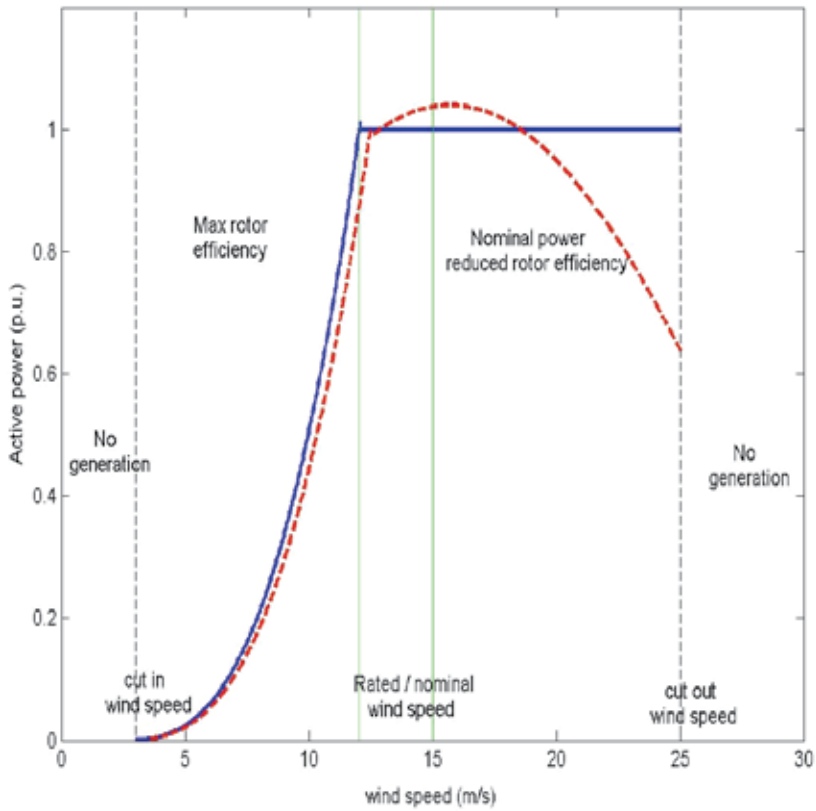

Fig. 9. Typical power curves and operation areas of a stall (dashed line) and pitch controlled (solid line) wind turbines.

In a stall controlled wind turbine, the blades are designed such that the rotor efficiency "collapses" at high wind speeds. Due to the blade design, this behaviour is intrinsic, and no active control systems are required to achieve the aerodynamic efficiency reduction. In a pitch controlled wind turbine, the blades are gradually turned out of the wind, so the wind impact angle changes and the aerodynamic efficiency is reduced. In this case active stall control is applied, by means of hydraulics or an electric drive system. The input variable for the pitch controller is the rotor speed, as it is depicted in Fig. 10.

The higher the rotor speed, the more the blades are turned out of the wind. The blades are turned back into the wind when the rotor speed falls. In general, fixed speed turbines use stall control for technical reasons, while variable speed turbines are usually equipped with pitch control.

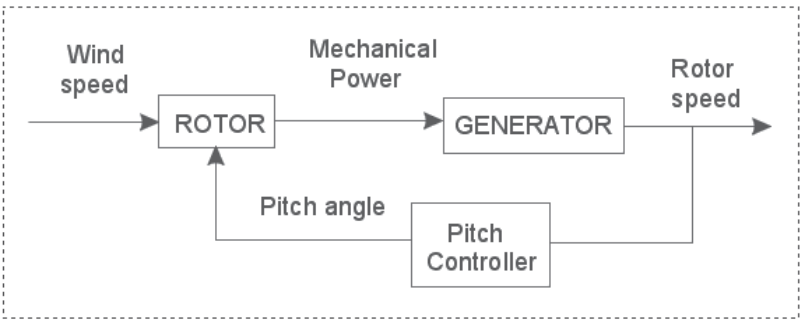

Fig. 10. Rotor speed control principle for wind speeds above nominal.

The active-stall concept is similar to normal stall power limitation, except that the whole blade can be rotated backwards (in the opposite direction as is the case with pitch control) by a few (3-5) degrees at the nominal speed range in order to give better rotor control. The application of this concept is more or less restricted to fixed speed turbines.
Typical active-stall representatives are the Danish manufacturers Bonus (1 MW and over) and NEG Micon (now Vestas) (1.5, 2 MW and over).
The difference from active pitch control is not only that the range of blade angle variation is less, but also that the direction of the variation is opposite.

3.5 Control design for an active-stall constant speed wind turbine

A common control concept for megawatt-size wind turbines/wind farms without power electronic converters is the active stall regulation. An active stall wind turbine is a stall controlled turbine with variable pitch angle. At high wind speeds, the pitch angle is adjusted to obtain the desired rated power level. When connecting the wind generator to the grid, the pitch angle is also adjusted in order to obtain a smooth connection. The use of active stall control also facilitates the emergency stopping of the turbine.
The control strategy called active-stall constant-speed involves the combined interaction between wind model, pitch control and the aerodynamics of the wind turbine, as can be seen in Fig. 11.
The blade angle control block models the active-stall control of the wind turbine based on the measured power and the reference one (Sorensen, P. et.al, 2001).
The most used electrical generator of an active-stall constant-speed turbine is a cage rotor induction generator connected to the grid through a soft-starter, as it is shown in Fig. 11.
A clear difference between stall and active stall controlled wind turbines is a pitch actuator system for variable pitch angles, as can be seen in Fig. 12, which allows the stall effect to be controlled.
The model of the pitch control system is based on the measured generator power (P_m) and the aerodynamic power (P_{aero}) of wind turbine as a function of measured wind speed (v_{wind}) at different pitch angles (θ).

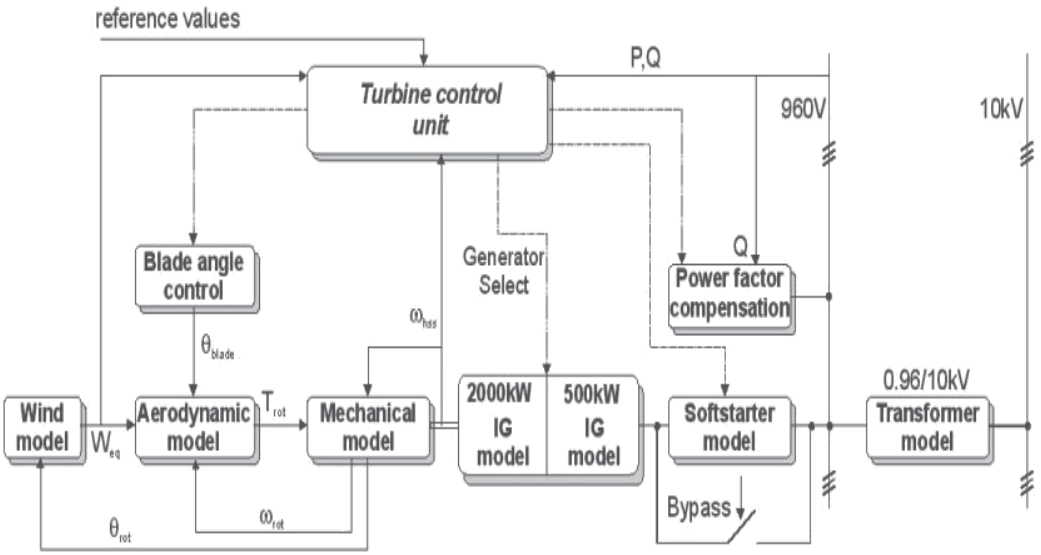

Fig. 11. Block diagram of an active-stall controlled wind turbine with constant speed using a cage-rotor induction generator

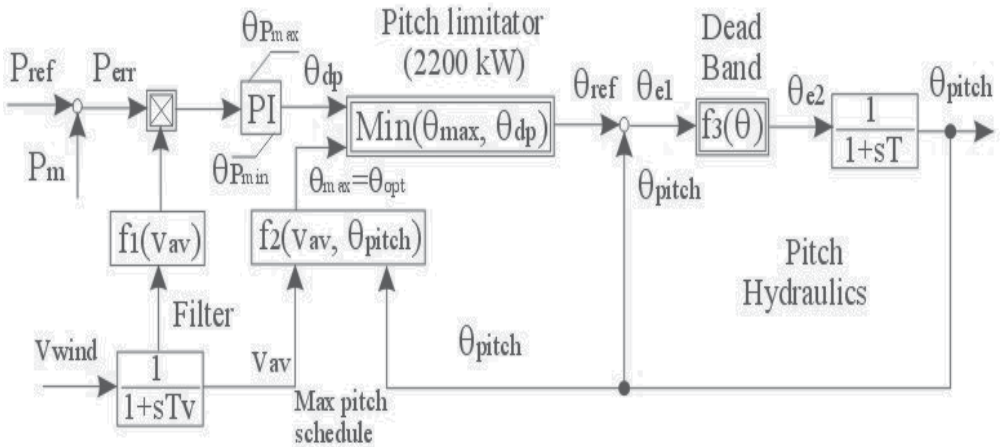

Fig. 12. The block diagram of blade pitch angle control system.

The measured power is compared with its reference (P_{ref}) and the error signal (P_{err}) multiplied by pitch angle of power control ($f_1(v_{av})$) is sent to the PI-controller producing the pitch angle demand (θ_{dp}), which together with maximum pitch angle-upper limit (θ_{max}) are sent to the pitch limitation non-linear block producing the reference value of the pitch angle (θ_{ref}). The reference value is in the range between the optimised pitch (θ_{dp}) and the maximal pitch angle (θ_{max}=90^0). The maximum value is defined as a function of average wind speed

($f_2(v_{av})$). The reference value is, further, compared to the actual pitch angle (θ_{pitch}) and the error signal (θ_{e2}) is corrected by the pitch hydraulics.

This control strategy takes its origin in the power coefficient curves $C_p(\theta, u)$, typical for a 2 MW constant speed wind turbine, as it is depicted in Fig. 13.

C_p represents the rotor (aerodynamic) efficiency of the wind turbine and depends on the pitch angle θ and on the tip speed ratio λ. In order to achieve maximum power yield for each wind speed the maximal C_p and the corresponding θ has to be found.

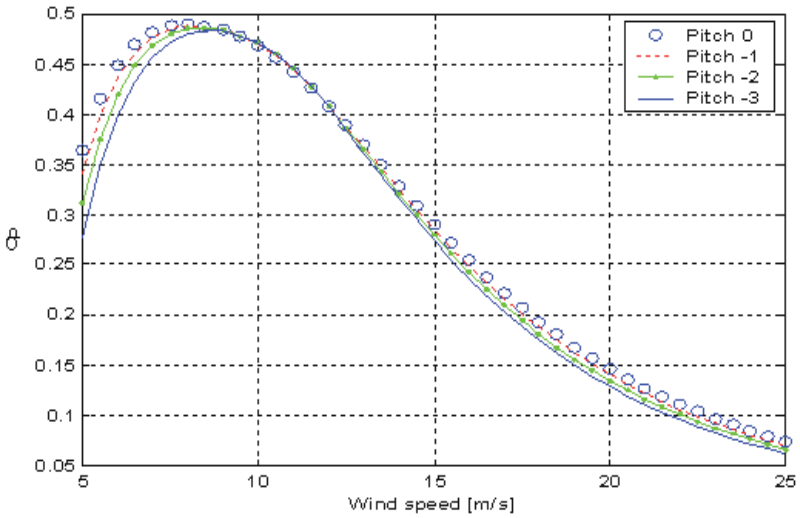

a)

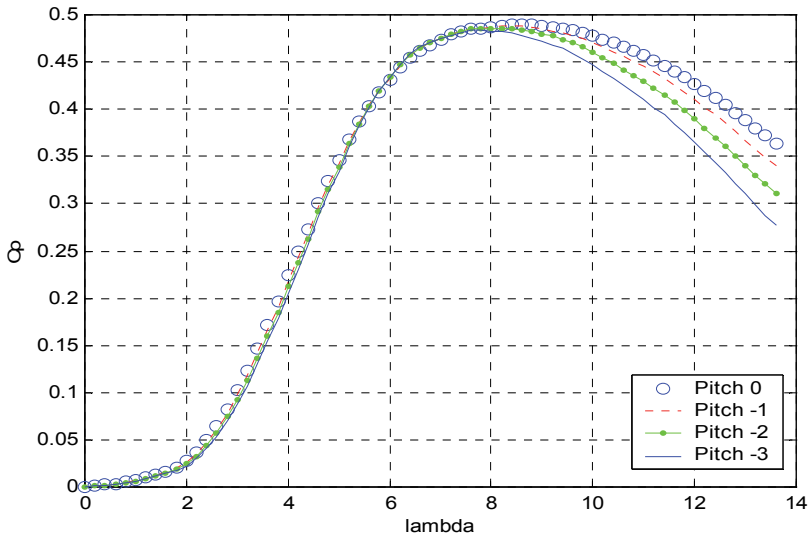

b)

Fig. 13. Power coefficient (Cp) of a 2MW wind turbine versus wind speed (a), and the tip speed ration (λ), (b) at different pitch angles.

In order to achieve maximum power yield for each wind speed the maximal C_p and the corresponding θ has to be found. In fact, the control strategy is characterised by two terms: the optimal region and the power limiting region. In the optimal region (between start-up wind speed and nominal wind speed), the output power is designed to fulfil the criterion of maximal C_p, which corresponds to the optimal energy capture, by keeping the tip speed ration (λ) constant. In the power limiting region (between nominal wind speed and cut-out wind speed), the output power is kept constant, while the wind turbine will pitch the blades a few degrees every time when the wind changes in order to keep the rotor blades at the optimum angle. When the wind turbine reaches its rated power, and the generator is about to be overloaded, the turbine will pitch its blades in the opposite direction. In this way, it will increase the angle of attack of the rotor blades in order to make the blades go into a deeper stall, thus wasting the excess energy in the wind.

4. Wind farm modelling

The wind farm contains 6 wind turbines of 2 MW each of them. The model of wind turbine, presented before, was implemented for each wind turbine.
The layout of the active-stall wind farm is shown in Fig. 14 and a load flow simulation for one wind turbine in Fig. 15. Each wind turbine is connected to a 10 kV bus bar. The induction generators, soft-starters, capacitor banks for reactive power compensation and the step-up transformers are all palaces in nacelle and thus the transformer is considered part of the wind turbine.
The control of active and reactive power is based on measured reactive power at the point of common coupling. The wind turbine controller must be able to adjust the wind turbine production to the power reference computed in the wind farm control system, according to the demands imposed by the system operator. In case of normal operation conditions the wind turbine has to produce maximum power. In power limitation operation mode the wind turbine has to limit its production to the power reference received from the wind farm controller.

4.1 Electrical diagram

The Fig. 14 contains the grid representation from 50 kV double bus-bar systems down to the wind turbines. Two 16 MVA 50/10kV transformers are included, one is connected to the wind farm and one supplies some custom loads.
10 kV cables make the connection between the 10 kV substation and the wind turbines.
As the turbines are placed in groups of 3, a backup cable is also represented on the scheme. The wind turbine contains also the tower cable making the connection between the 0.96 kV/10 kV transformer and the 10 kV cable at the bottom of the tower. The 10 kV cables are modelled using the existing DIgSILENT model toolbox.
The power factor compensation units are represented by a capacitor bank on this scheme and a Static VAR System (SVS) unit. The switching of capacitors is done as a function of average value of measured reactive power. In order to limit the starting current transients during the 2 MW generator connections to the grid, a soft starter start-up is used. The generators are connected when the generator speed is higher than the synchronous speed. The generators are full load compensated.

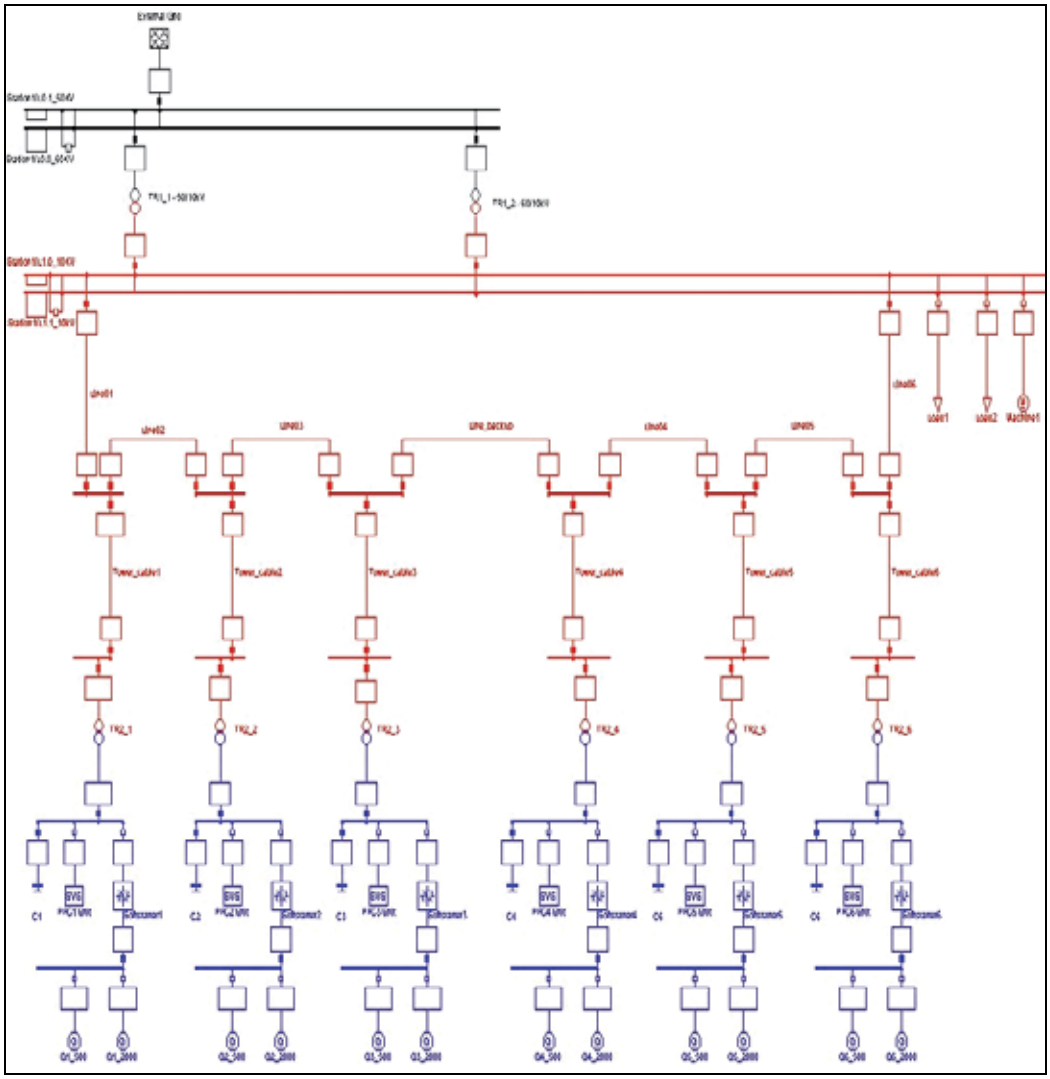

Fig. 14. 12 MW wind farm diagram implemented in Digsilent.

4.2 Load flow simulation

In Fig. 15 is depicted a case of load flow simulation when the wind turbines are work at nominal conditions (2MW) and full power factor compensation is used.

5. Simulation results

To evaluate the performance of wind turbine control system a set of simulations are performed using a power system analysis software-DIgSILENT Power Factory, which provides the ability to simulate load flow, RMS fluctuations and transient events in the same software environment. This makes the developed models useful for the power quality studies as well as for the grid fault studies. The RMS simulations are based on

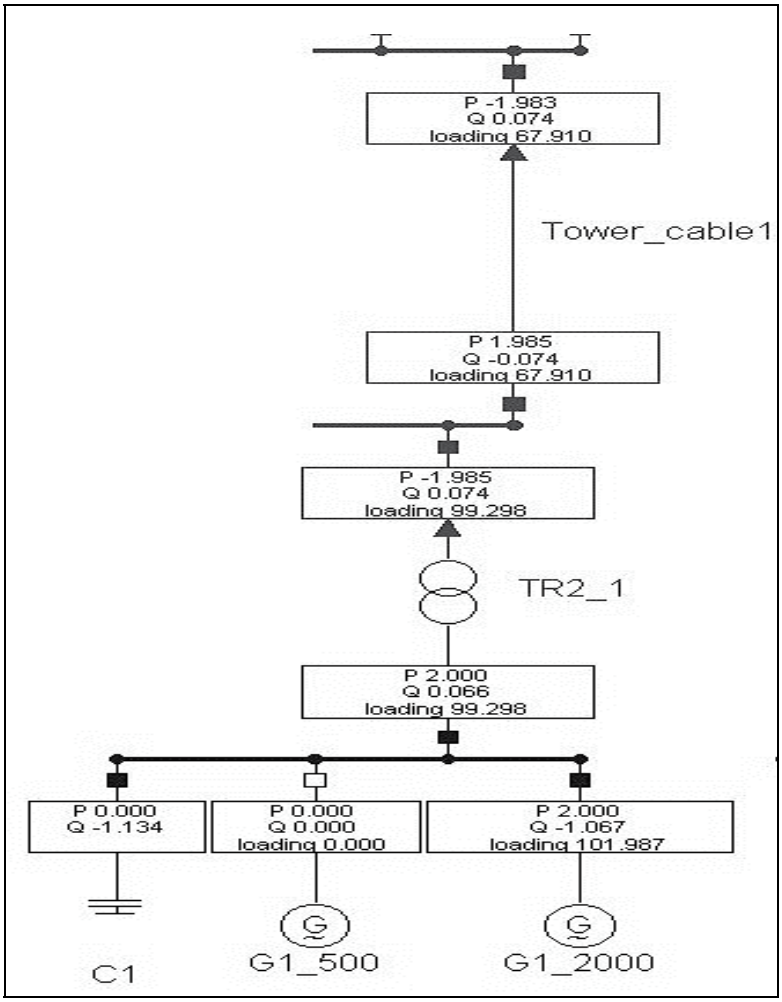

Fig. 15. Power-flow simulation for a wind turbine working at nominal conditions.

electro-mechanical transient models, which are simplified models than those used in EMT simulations. They are more appropriate for the most studies of power quality and control issues. They are much faster than the instantaneous value simulation compared to the period, which is simulated. The EMT simulations, as they are based on detailed electromagnetic transient models, are appropriate for studies of the behaviour during grid faults.

5.1 DIgSILENT power factory software tool

To simulate the wind turbines, models have been developed for each element and implemented in the dedicated power system simulation tool DIgSILENT (DIgSILENT Power Factory user manual, 2010). The DIgSILENT simulation tool has a dedicated model for many components, such as induction generators, which take into account the current displacements in the rotor, the torque–slip and short circuit test curves. Also models of synchronous machines, transformers, bus bars, grid models, static converters etc are provided.

5.2 Transmission model simulation during start-up

The aerodynamic torque (torque_rot-T_{rot}) accelerates the wind turbine rotor, with the generator disconnected from the grid, until the rotor speed (omega_rot-ω_{rot}) is close to its nominal value. Then the generator is connected to the grid as seen in Fig. 16. The basic idea is to control the rotational speed using only measurement of the power (or torque), as it is depicted in Fig. 1 and by equations (1) and (2) as well.

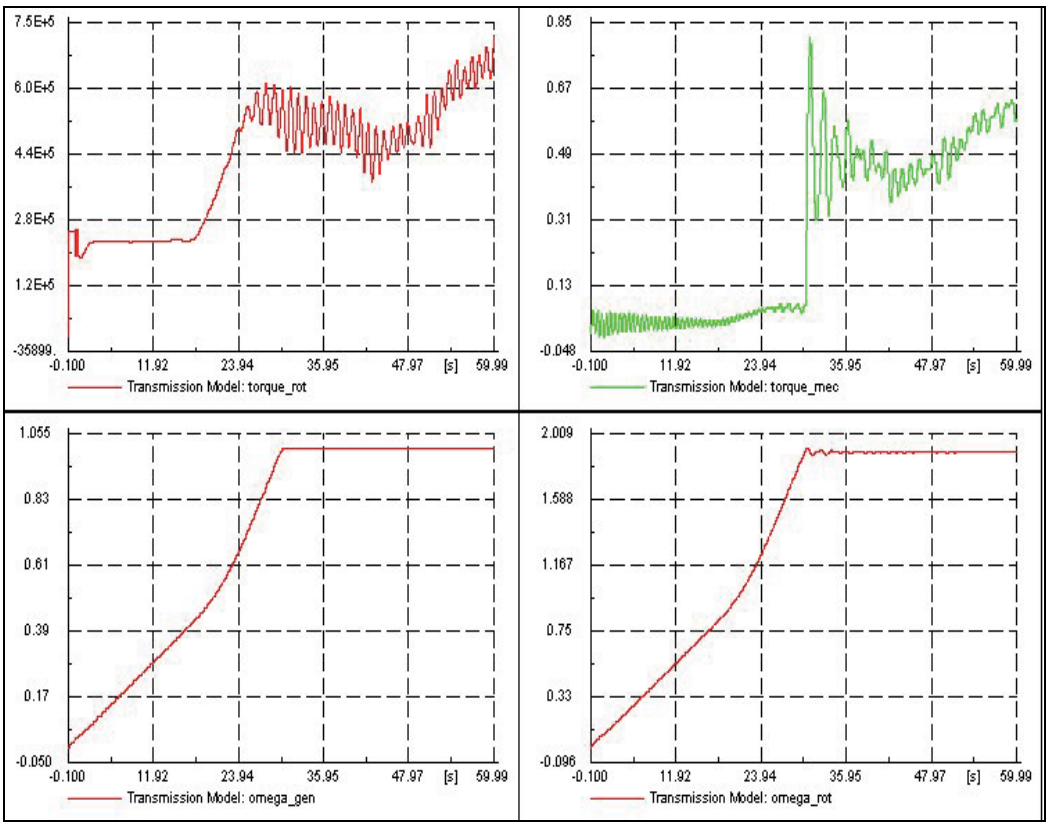

Fig. 16. Transmission model during start-up. Aerodynamic torque (torque_rot), mechanical torque (torque_mec), generator speed (omega_gen) and rotor speed (omega_rot) of wind turbine system.

5.3 Simulation results during start-up, normal operation and heavy transients

The control strategy of active stall constant speed wind turbine contains three modes of operation: acceleration control (speed control), power control (power limiting region) and direct pitch control (blade angle control).

The acceleration and pitch control modes are used during start-up, shut down and emergency conditions, while the power control mode is only used during normal operations.

Figure 17 shows how a 2 MW wind turbine with constant speed works during different operation conditions, such as sudden changes in wind speed (wind gusts) with a turbulence intensity of 12 %, at high wind speed.

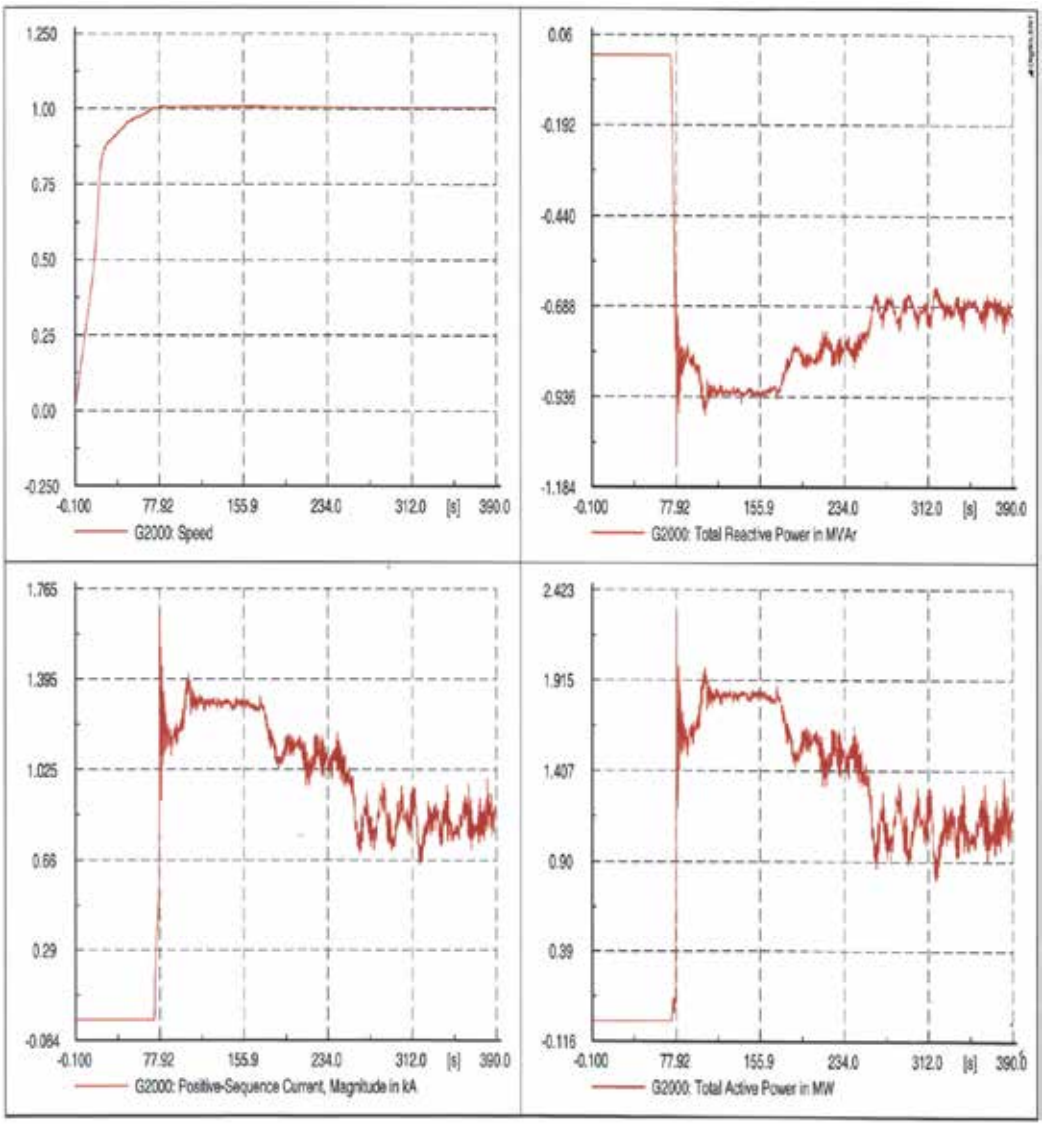

Fig. 17. Simulation results during sudden changes in wind speed for a 2MW active stall constant-speed wind turbine using CRIG.

In Fig. 18 the 2 MW induction generator was connected to the grid through a soft-starter (in order to reduce the transient current), at t=73 seconds and then the soft-starter was by-passed at t=77 seconds.
In the same time the power factor compensation unit started to work using capacitor switching, as a function of average value of measured reactive power.
The mean wind speed was 12 m/s. At t=100 seconds the mean wind speed was modified to 18 (m/s) and at t=170 seconds mean wind speed was modified again at 11 (m/s) to simulate sudden changes in wind speed and to test the system performance and implemented control strategy, as it is also shown in Fig. 17.

The active and reactive powers have been able to follow these changes in all situations. It is concluded that the wind turbine absorbed the transients very fast and the control strategy offers a good stability of the system during transition of dynamic changes.

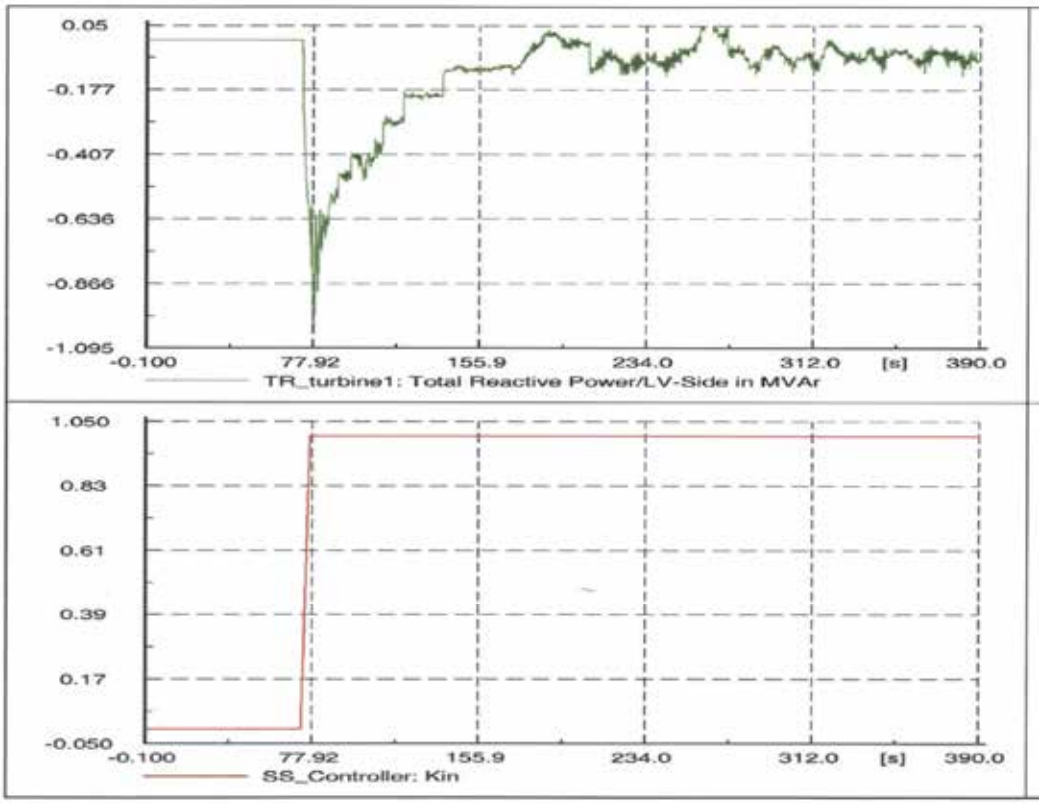

Fig. 18. Reactive power compensation with capacitors connected in steps (on top) and the soft-starter by-passed controller (SS_controller: K_{IN}).

6. Comparison between measurements and simulation results

The comparison between simulations and measurements will be done to validate the developed model. It is performed for the case of continuous operation, and is based on power quality measurements for a 2 MW wind turbine from an existing wind farm in Denmark. The wind speed measurement was provided by the anemometer of the control system placed on the top of the nacelle and the power quality measurements were performed as sampling of instantaneous values of three-phase currents and voltages with a sampling frequency of 3.2 kHz, as shown in Fig. 19a).

Fig. 19 presents a comparison between measured (Fig. 19a) and simulated (Fig. 19b) of wind speed, pitch angle and active power of a 2 MW WT under power control mode. The power control mode is used during normal operations. It is clear that at high wind speed (around 18 m/s), using the active stall regulation, the pitch angle is continuously adjusted to obtain the desired rated power level (2 MW).

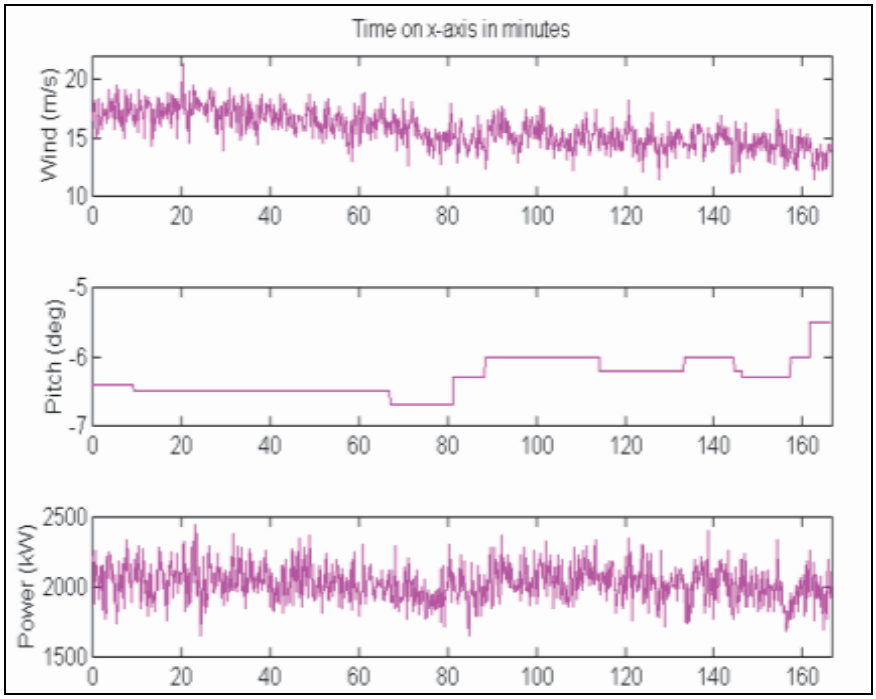

a)

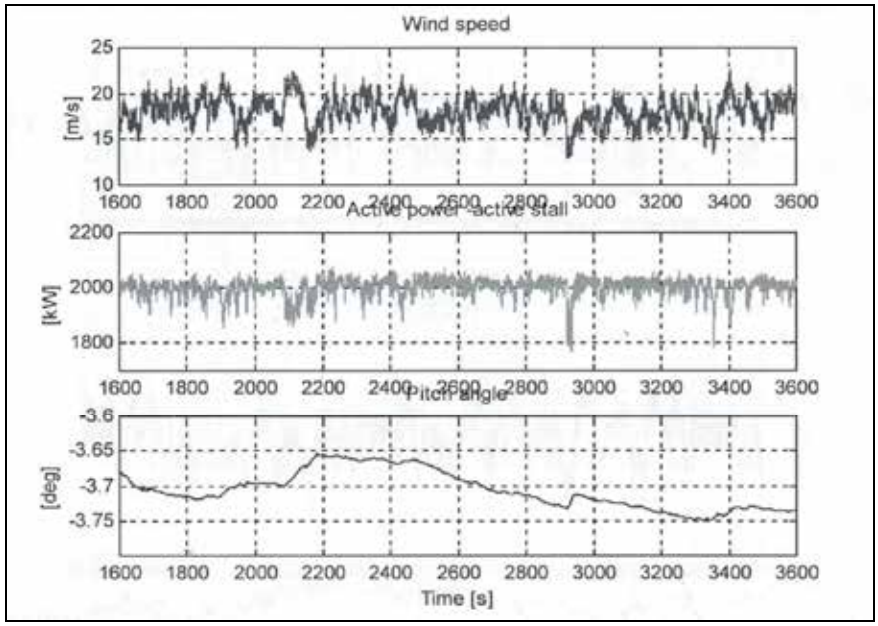

b)

Fig. 19. Power control mode of a 2 MW active-stall constant speed WT. Measured wind speed and active power under pitch control regulated during 170 minutes (a) and simulation of wind speed, active power and pitch angle versus time (b).

7. Discussion and conclusion

In this paper simulation of a 6 x 2 MW wind turbine plant (wind farm) has been presented.
A wind farm model has been built to simulate the influence on the transient stability of power systems. The model of each wind turbine includes the wind fluctuation model, which will make the model useful also to simulate the power quality and to study control strategies of a wind turbine.
The control scheme has been developed for each wind turbine control including soft starter start-up, and power factor compensation.
The above presented model can be a useful tool for wind power industry to study the behaviour and influence of big wind turbines (wind farm) in the distribution network.
The computer simulations prove to be a valuable tool in predicting the system behaviour. Especially in wind power applications, DIgSILENT Power Factory has become the de-facto standard tool, as all required models and simulation algorithms are providing unmet accuracy and performance.
One future research step is to investigate and enhance the controller's capabilities to handle grid faults. Another interesting issue is to explore the present controllers in the design of a whole wind farm and the connection of the wind farm at different types of grid and storage systems.

8. Acknowledgment

This work was carried out with the support of Aalborg University-Denmark. I would like to thanks Professor Frede Blaabjerg for his suggestions and useful discussions.

9. References

Deleroi W.and Woudstra J.B. (1991), Connecting an asynchronous generator on the grid using a thyristor switch, *IEEE Transactions on Industry Applications*, Vol. 2, pp. 55-60.

http://www.digsilent.de DiGSILENT Power Factory user manuals (2010), DiGSILENT GmbH, Germany. http://www.gwec.com. Gary-Williams Energy Corporation (GWEC, 2009).

Hansen A.D., Sorensen P., Janosi L. & Bech J. (2001). *Proceedings of IECON,* Vol.3, No.4, pp. 1959-1964, ISSN 1729-8806;

Hansen A.D., Jauch C., Sorensen P., Iov F. & Blaabjerg F. Dynamic Wind Turbine Models in Power System Simulation Tool DIgSILENT, *Research Report of Riso-R-1400(EN) National Laboratory*, Roskilde, December 2003, ISBN 87-550-3198-6;

Hansen L.H., Helle L., Blaabjerg F., Ritchie E., Munk-Nielsen S., Bidner H., Sorensen P. and Bak-Jensen B. (2001), *Conceptual survey of generators and power electronics for wind turbines*, Riso-R-1205 (EN);

Heier S. (1998). *Wind Energy Conversion Systems,* John Wiley & Sons Inc., ISBN 0-471-971-43, New York, USA ;

Mihet-Popa L. (2003). *Wind Turbines using Induction Generators connected to the Grid*, Ph. D. Thesis, POLITEHNICA University of Timisoara-Romania, October 2003, ISBN 978-973-625-533-5;

Mihet-Popa L., Blaabjerg F. and Boldea I. (2004), Wind Turbine Generator Modeling and Simulation where Rotational Speed is the Controlled Variable, *IEEE-IAS*

Transactions on Energy Conversion, January / February 2004, Vol. 40, No. 1, pp. 3-10, ISSN: 0093-9994;

Mihet-Popa L. and Boldea I. (2006), Dynamics of control strategies for wind turbine applications, *the 10th International Conference on Optimisation of Electrical and Electronic Equipment, OPTIM 2006*, May 18-19, Poiana Brasov, Vol. 2, pp. 199-206;

Mihet-Popa L., Proştean O. and Szeidert I. (2008), The soft-starters modeling, simulations and control implementation for 2 MW constant-speed wind turbines, *The International Review of Electrical Engineering – IREE*, Vol. 3, No. 1, January-February 2008, pp. 129-135, ISSN: 1827-6660;

Mihet-Popa L. and Groza V. (2010), Modeling and simulations of a 12 MW wind farm, *Journal of Advances in Electrical and Computer Engineering*, Vol. 10, No. 2, 2010, pp. 141-144, ISSN 1582-7445;

Mihet-Popa L. and Pacas J.M. (2005), Active stall constant speed wind turbine during transient grid fault events and sudden changes in wind speed, *Proceedings of International Exhibition & Conference for Power Electronics Inteligent Motion Power Quality, 26th International PCIM Conference*, Nuremberg, 7-9 June, pp. 646-65;

Muljadi, E.; Butterfield, Pitch-controlled variable-speed wind turbine generation, *Industry Applications Conference, 1999. IAS Annual Meeting*. Conference Record, Vol. 1, pp 323 –330.

Petru, T. & Thiringer T. (2002), Modeling of Wind Turbines for Power System Studies, *IEEE Trans. On Power Systems*, Vol. 17, No. 4, Nov. 2002, pp. 1132 – 1139.

Rombaut, C; Seguier, G. and Bausiere, R.; *Power Electronic Converters-AC/AC Conversion* (New York; McGraw-Hill, 1987).

Slootweg, J.G. & Kling, W.L. (2002). Modeling and Analysing Impacts of Wind Power on Transient Stability of Power Systems, *International Journal of Wind Engineering*, Vol. 26, No. 1, pp. 3-20;

Sorensen P., Hansen A.D., Thomsen K., Buhl T., Morthorst P.E., Nielsen L.H., Iov F., Blaabjerg F., Nielsen H.A., Madsen H. and Donovan M.H. (2005), *Operation and Control of Large Wind Turbines and Wind Farms*, Riso Research Report-R-1532 (EN), Riso National Laboratory of Denmark-Roskilde;

13

Wind Integrated Bulk Electric System Planning

Yi Gao
State Power Economic Research Institution
P.R.China

1. Introduction

The utilization of the wind to generate electrical energy is increasing rapidly throughout the world. By the end of 2009, the worldwide installed wind capacity reached 159,213 MW (World Wind Energy Report 2009). Wind turbine generators can be added and are being added in large grid connected electric power systems. Wind power, however, behaves quite differently than conventional electric power generating facilities due to its intermittent and diffuse nature. The incorporation of wind energy conversion system (WECS) in bulk electric system (BES) planning, therefore, requires distinctive and applicable modeling, data and method considerations to ensure BES reliability levels as wind power penetration levels increase.

The objective of power system planning is to select the most economical and reliable plan in order to meet the expected future load growth at minimum cost and optimum reliability subject to economic and technical constraints. Reliability assessment, which consists of adequacy and security, is an important aspect of power system planning. A BES security assessment normally utilizes the traditional deterministic criterion known as the N-1 security criterion (North American Electric Reliability Council Planning Standards, 2007) in which the loss of any BES component (a contingency) will not result in system failure. The deterministic N-1 (D) planning criterion for BES has been used for many years and will continue to be a benchmark criterion (Li, 2005). The D planning criterion has attractive characteristics such as, simple implementation, straightforward understanding, assessment and judgment. The N-1 criterion has generally resulted in acceptable security levels, but in its basic simplest form does not provide an assessment of the actual system reliability as it does not incorporate the probabilistic nature of system behaviour and component failures.

Probabilistic (P) approaches to BES reliability evaluation can respond to the significant factors that affect the reliability of a system. There is, however, considerable reluctance to use probabilistic techniques in many areas due to the difficulty in interpreting the resulting numerical indices. A survey conducted as part of an EPRI project indicated that many utilities had difficulty in interpreting the expected load curtailment indices as the existing models were based on adequacy analysis and in many cases did not consider realistic operating conditions. These concerns were expressed in response to the survey and are summarized in the project report (EPRI report, 1987).

This difficulty can be alleviated by combining deterministic considerations with probabilistic assessment in order to evaluate the quantitative system risk and conduct

system development planning. A relatively new approach that incorporates deterministic and probabilistic considerations in a single risk assessment framework has been designated as the joint deterministic-probabilistic (D-P) approach (Billinton et al., 2008). This chapter extends this approach and the concepts presented in (Billinton et al., 2010; Billinton & Gao, 2008) to include some of the recent work on wind integrated BES planning.

2. Study methods and system

2.1 Study methods

The D planning criterion for transmission systems has been used for many years and will continue to be a benchmark criterion. In a basic D approach, using the N-1 criterion, the system should be able to withstand the loss of any single element at the peak load condition. An N-2 criterion is used in some systems. The likelihood of the designated single element failing is not included in an analysis using the D approach.

The P method is used in transmission planning (Fang R. & Hill, 2003; Chowdhury & Koval, 2001) as it provides quantitative indices which can be used to decide if the system performance is acceptable or if changes need to be made, and can be used for performing economic analyses. In the P approach, the system risk should not exceed a designated criterion value (Rc).

The D-P approach includes both deterministic and probabilistic criteria and is defined as follows: The system is required to satisfy a deterministic criterion (N-1) and also meet an acceptable risk criterion (Pc) under the designated (N-1) outage condition (Billinton et al., 2008). The D-P technique provides a bridge between the accepted deterministic and probabilistic methods. The basic deterministic N-1 technique results in a variable risk level under each critical outage condition. This is particularly true when the critical outage switches from a transmission element to a generating unit or vice versa. In the D-P approach the system must first satisfy the D criterion. The system risk given that the critical element has failed must then be equal to or less than a specified probabilistic risk criterion (Pc). If this risk is less than or equal to the criterion value, the D and D-P approaches provide the same result. If the risk exceeds this value then the load must be reduced to meet the acceptable risk level (Pc). The D-P technique provides valuable information on what the system risk level might be under the critical element outage condition using a quantitative assessment.

The MECORE (Li, 1998) software package which utilizes the state sampling Monte Carlo simulation method (Billinton & Allan, 1996) is used to conduct the reliability studies described in this chapter.

2.2 Study system

The well known reliability test system IEEE-RTS (IEEE Task Force, 1979) has a very strong transmission network and a relatively weak generation system. The total installed capacity in the RTS is 3405 MW in 32 generating units and the peak load is 2850 MW. It was modified in this chapter to create a system with a relatively strong generation system and a weak transmission network. The modified RTS is designated as the MRTS.

Three steps were used to modify the IEEE-RTS to create the MRTS:

Step 1. Generating unit modifications: The FOR of the four 20 MW units were changed from 0.1 to 0.015 and the mean time to repair (MTTR) modified from 50 to 55 hrs.

The FOR of the two 400 MW units were changed from 0.12 to 0.08 and the MTTR modified from 150 to 100 hrs.

Step 2. Transmission line modifications: The lengths of all the 138 KV lines were doubled except for Line 10 which is a 25.6 km cable. The 230 KV lines were extended as follows: the lengths of lines L21, L22, L31, L38 were increased by a factor of three; the lengths of lines L18 to L20, L23, L25 to L27 were increased by a factor of four; the lengths of lines L24, L28 to L30, and L32 to L37 were increased by a factor of six. The transmission line unavailabilities were modified based on Canadian Electricity Association data (CEA, 2004).

Step 3. The numbers of generating units were doubled at Buses 16, 18 and 21, and 2×50 MW and 1×155 MW generating units were added at Bus 22 and Bus 23 respectively. The rating of Line 10 was increased to 1.1 p.u. of the original rating.

The total number of generating units in the MRTS is now 38 units. The total system capacity is 4615 MW. The load value at each load points was increased by a factor of 1.28. The reference peak load of the MRTS is 3650 MW.

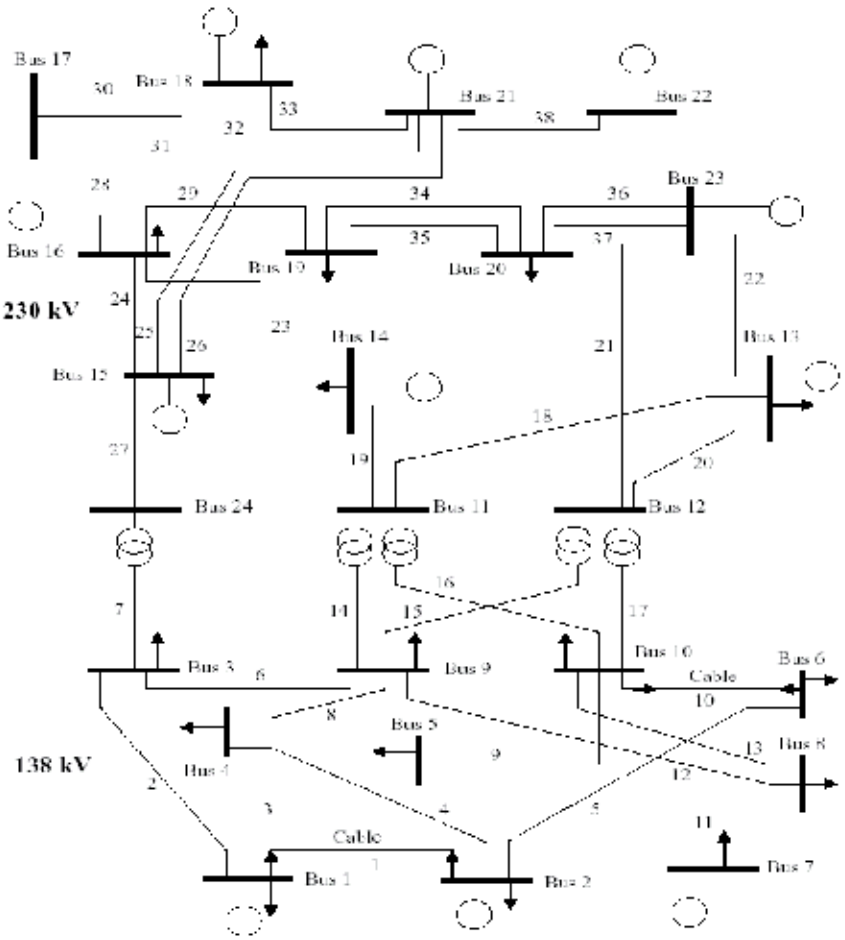

Fig. 1. Single line diagram of the MRTS

3. Wind energy conversion system model

3.1 Modeling and simulating wind speeds

One of the first steps for a utility company to consider when developing wind as an energy source is to survey the available wind resource. Unfortunately, reliable wind speed data suitable for wind resource assessment are difficult to obtain, and many records that have been collected are not available to the general public. Many utilities and private organizations, however, are now engaged in collecting comprehensive wind speed data. These data can be used to create site specific wind speed models.

A time series model has been developed (Billinton et al., 1996) to incorporate the chronological nature of the actual wind speed. Historical wind speeds are obtained for a specific site, based on which, future hourly data are predicted using the time series model. This time series model is used in the research described in this chapter to generate synthetic wind speeds based on measured wind data at a specific location.

The wind speed model and data for the Swift Current and Regina sites located in the province of Saskatchewan, Canada have been used in the studies described in this chapter. Table 1 shows the hourly mean wind speed and standard deviation at the Regina and Swift Current sites.

Sites	Regina	Swift Current
Mean wind speed (km/h) , μ	19.52	19.46
Standard deviation (km/h), σ	10.99	9.70

Table 1. Wind speed data for the two sites

The Swift Current and Regina wind models were developed and published in (Billinton et al., 1996) and (Wangdee & Billinton, 2006) respectively. The ARMA models for the two sites are given in (1) and (2) respectively.

Regina: ARMA (4, 3):

$$\begin{aligned} y_t = {} & 0.9336y_{t-1} + 0.4506y_{t-2} - 0.5545y_{t-3} + 0.1110y_{t-4} \\ & + \alpha_t - 0.2033\alpha_{t-1} - 0.4684\alpha_{t-2} + 0.2301\alpha_{t-3} \end{aligned} \tag{1}$$

where $\alpha_t \in$NID(0,0.4094232) is a normal white noise process with zero mean and the variance 0.4094232.

Swift Current: ARMA (4, 3):

$$\begin{aligned} y_t = {} & 1.1772y_{t-1} + 0.1001y_{t-2} - 0.3572y_{t-3} + 0.0379y_{t-4} \\ & + \alpha_t - 0.5030\alpha_{t-1} - 0.2924\alpha_{t-2} + 0.1317\alpha_{t-3} \end{aligned} \tag{2}$$

where $\alpha_t \in$NID(0,0.5247602) is a normal white noise process with zero mean and the variance 0.5247602.

The wind speed time series model can be used to calculate the simulated time dependent wind speed SW_t using (3):

$$SW_t = \mu_t + \sigma_t \times y_t \tag{3}$$

where μ_t is the mean observed wind speed at hour t; σ_t is the standard deviation of the observed wind speed at hour t.

Figure 2 shows a comparison of the observed wind speed probability distributions for the original 20 years of Swift Current wind speed data and the simulated wind speed probability distribution obtained using the ARMA (4, 3) model shown in Equation 2 and a large number (8,000) of simulated years. The observed average wind speed is 19.46 km/h, and the simulated value is 19.52 km/h. The observed wind speed probability distribution is not as continuous as the simulated distribution, as it is based on only 20 years of data.

Figure 2 shows that the ARMA (4, 3) model provides a reasonable representation of the actual wind regime. The observation is often made that wind speed can be represented by a Weibull distribution. Simulation results are used to generate the wind speed probability distributions in the studies described later in this chapter.

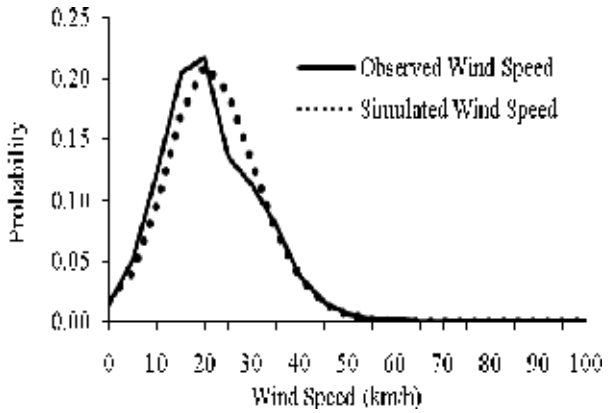

Fig. 2. Observed and simulated wind speed distributions for the Swift Current site

In practice, wind farms are neither completely dependent nor independent but are correlated to some degree if the distances between sites are not very large. The wind speed correlation between two wind farms can be calculated using cross correlation. The cross-correlation coefficient equation is shown in (4).

$$R_{xy} = \frac{\frac{1}{n}\sum_{i=1}^{n}(x_i - \mu_x)(y_i - \mu_y)}{\sigma_x \sigma_y} \tag{4}$$

where x_i and y_i are elements of the first and second time series respectively, μ_x and μ_y are the mean values of the first and second time series, σ_x and σ_y are the standard deviations of the first and second time series, and n is the number of points in each time series.

The ARMA time series model has two parts, one part is the autoregressive (AR) model involving lagged terms in the time series itself, the other one is the moving average (MA) model involving lagged terms in the noise or residuals. It is possible to adjust the wind speed correlation level between two or more different wind locations by selecting the

random number seeds (initial numbers) for a random number generator process used in the MA model. Reference (Wangdee & Billinton, 2006) uses a trial and error process to generate appropriate random number seeds by selecting a factor K between the dependent wind locations. This is a relatively straightforward method, but can require considerable time and effort and is not very flexible. Reference (Gao & Billinton, 2009) extends this application by describing a Generic Algorithm used to select the optimum random number seeds in the ARMA model to adjust the degree of wind speed correlation for two wind sites. A genetic algorithm can quickly scan a vast solution set. It is a very useful method coupled with ARMA models to adjust the simulated wind speed correlation levels for different wind sites (Gao & Billinton, 2009).

The simulated wind speed time series during a selected period for the Regina and Swift Current sites with high correlation level (Rxy=0.8), middle correlation level (Rxy=0.5) and low correlation level (Rxy=0.2) are shown in Figure 3. The simulated average wind speeds for the Regina and Swift Current sites are 19.58 km/h and 19.52 km/h respectively.

3.2 Modeling wind turbine generators

The power output characteristics of a Wind Turbine Generator (WTG) are quite different from those of a conventional generating unit. The output of a WTG depends strongly on the wind regime as well as on the performance characteristics (power curve) of the generator. Figure 4 shows a typical power curve for a WTG.

The hourly wind speed data are used to determine the time dependent power output of the WTG using the operational parameters of the WTG. The parameters commonly used are the cut-in wind speed Vci (at which the WTG starts to generate power), the rated wind speed Vr (at which the WTG generates its rated power) and the cut-out wind speed Vco (at which the WTG is shut down for safety reasons). Equation 5 can be used to obtain the hourly power output of a WTG from the simulated hourly wind speed.

$$P(SW_t) = \begin{cases} 0 & 0 \le SW_t < V_{ci} \\ (A + B \times SW_t + C \times SW_t^2) \times P_r & V_{ci} \le SW_t < V_r \\ P_r & V_r \le SW_t < V_{co} \\ 0 & SW_t \ge V_{co} \end{cases} \quad (5)$$

where P_r, V_{ci}, V_r and V_{co} are the rated power output, the cut-in wind speed, the rated wind speed and the cut-out wind speed of the WTG respectively. The constants A, B, and C depend on V_{ci}, V_r and V_{co} are presented in (Giorsetto P, 1983). The WTG units used in the studies in this chapter are considered to have a rated capacity of 2 MW, and cut-in, rated, and cut-out speeds of 14.4, 36 and 80 km/h, respectively.

3.3 The capacity outage probability table of the WTG

The hourly mean wind speeds and output power for a WTG unit without considering its unavailability or forced outage rate (FOR) are generated using the ARMA time series model and the power curve respectively. The capacity outage probability table (COPT) of a WTG unit can be created by applying the hourly wind speed to the power curve. The procedure is briefly described by the following steps (Billinton & Gao, 2008):

1. Define the output states for a WTG unit as segments of the rated power.

2. Determine the total number of times that the wind speed results in a power output falling within one of the output states.
3. Divide the total number of occurrences for each output state by the total number of data points to estimate the probability of each state.
4. The WTG COPT can be formed using this approach.

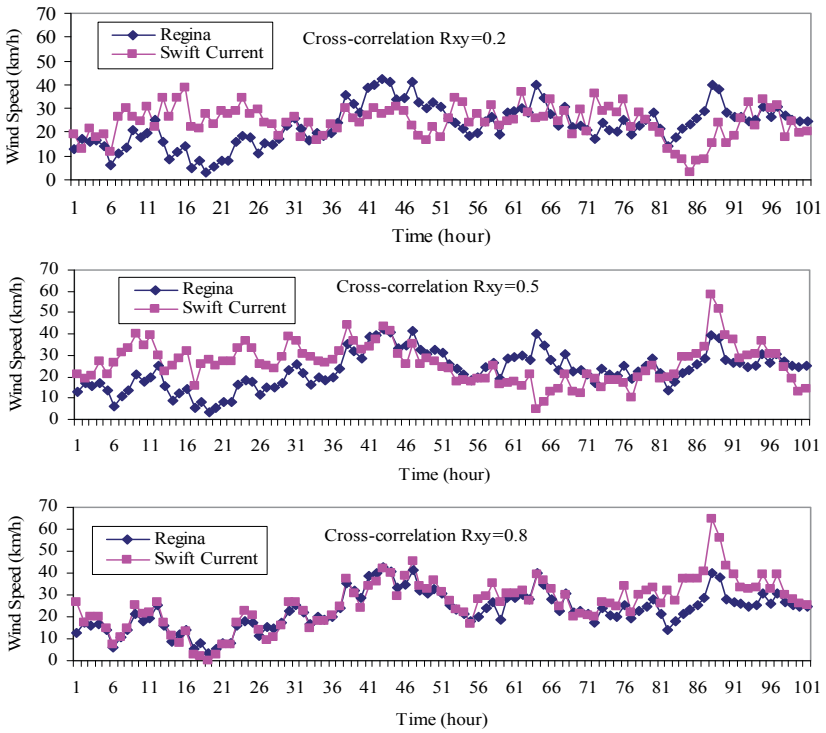

Fig. 3. Different simulated wind speed correlation levels between the Regina and Swift Current sites

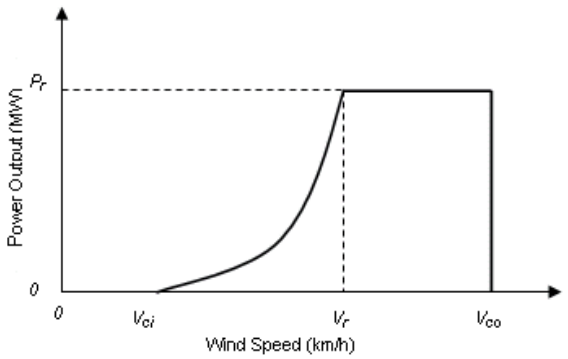

Fig. 4. Wind turbine generating unit power curve

Two cases are illustrated in this example. The first case utilizes the actual observed 20 years of Swift Current data. The second case uses the 8,000 simulated years of data. Figure 5 shows the two capacity outage probability distributions. The class interval width is 5% in this figure and the indicated capacity outage level is the midpoint of the class.

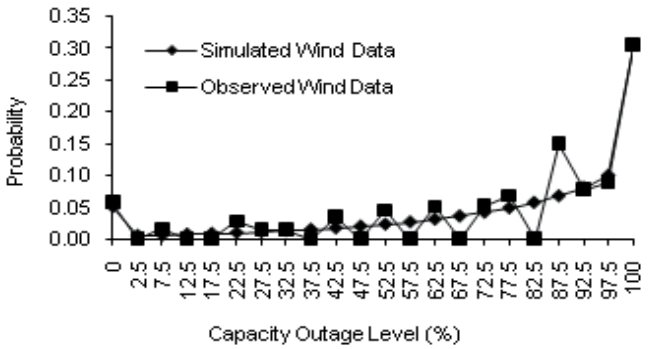

Fig. 5. Capacity outage probability profile for the WTG unit

Figure 5 shows that the observed data probability profile is discontinuous due to the limited wind data collection and that the simulated wind data provides a reasonable representation for adequacy assessment. The power output characteristics of a WTG are very different from those of conventional generating units. The WTG can be considered as a generating unit with many derated states (Billinton & Allan, 1996). Figure 5 shows that the probability of having full WTG output (0% capacity outage) is relatively low for this wind regime. There are many derated states in which the output of a WTG can reside in over the course of its operating history. A basic requirement in practical adequacy assessment is to represent the WTG by an acceptable reduced number of derated states.

3.4 Multi-state WECS model

There are many derated states in which the output of WECS can reside in the course of its operating history. The apportioning method (Billinton & Allan, 1996) can be used to create selected multi-state models for a WTG and the WECS. In this approach, the residence times of the actual derated states are apportioned between the completely up, selected derated and completely down states. A detailed analytical procedure that incorporates the WTG FOR is presented and used to build a series of multi-state WECS models in (Billinton & Gao, 2008). The probability of being in the full outage state is known as the Equivalent Forced Outage Rate (EFOR) in the NERC Generation Availability Data System and the Derated Adjusted Forced Outage Rate (DAFOR) (Billinton & Allan, 1996) in the CEA Equipment Reliability Information System. A wind energy conversion system can contain one or more WTG. A WECS has two basic parts: one is the wind resource and the other is the actual WTG units. If the WECS consists of identical WTG units with zero FOR, the WECS multi-state model is basically the same as that of the single WTG unit. If the FOR of the WTG units is not zero, the WECS derated state capacity outage probability table is not the same as that of a single WTG unit (Billinton & Gao, 2008).

Studies have shown that a five state capacity outage probability table can be used to reasonably represent a WTG in a capacity adequacy assessment (Billinton & Gao, 2008)

using the state sampling method. This model can also be used to represent a wind farm containing a number of WTG. Table 2 shows the capacity and probability values in a five state model for a 20 MW wind energy conversion system (WECS) containing identical 2 MW WTG.

	Regina Site	Swift Current Site
Capacity Outage (%)	Probability	Probability
0	0.07585	0.07021
25	0.06287	0.05944
50	0.11967	0.11688
75	0.23822	0.24450
100	0.50340	0.50897
DAFORW	0.75761	0.76564

Table 2. The independent WECS five-state models

Reference (Gao & Billinton, 2009) shows that the multi-state WECS models created for independent wind sites can be used in the state sampling simulation method to represent WECS considering wind speed correlation between the wind farms. The WECS models shown in Table 2 will be used in the following studies.

4. MRTS analysis with WECS

Two 400 MW WECS with Regina and Swift Current site data are added in the MRTS through transmission lines. The wind penetration level is about 15%. The length of each transmission line is 88 km. The admittance, unavailability and repair time of the facility connection line is 4.73485 (p.u.), 0.00058, 10 hrs respectively. The assumed carrying capacity of the circuit is the installed capacity of the WECS. The series of 400 MW WECS multi-state models for the Regina and Swift Current wind sites are very similar to the 20 MW WECS multi-state models shown in Table 2. The WECS model shown in Table 2, therefore, are used in the MECORE program applications described in this chapter. The annual wind speeds between the Regina and Swift Current wind sites are moderately correlated based on hourly wind speed time data from 1996-2003 found from the National Climate Data and Information Archive on the Environment Canada web site (Gao et al., 2009).

In the state-sampling technique, the states of all components are sampled and a non-chronological system state is obtained. The basic state sampling procedure is conducted assuming that the behaviour of each component can be categorized by a uniform distribution under {0, 1} and component outages are independent events. Detailed descriptions of a state sampling simulation procedure are provided in (Gao & Billinton, 2009). Conventional unit and independent WECS outages are assumed to be independent events in the basic state sampling simulation procedure. This assumption, however, is not applicable to partially dependent WECS. It is therefore necessary to generate correlated random numbers, which have a uniform distribution and specified correlations, in the simulation process.

Random numbers distributed uniformly under {0, 1} are divided into two clusters in this approach. Random numbers in the first cluster represent conventional units or independent WECS. Random numbers X1, X2 between 0 and 1 in the second cluster represent correlated WECS. If the second variable vectors X2 are generated from the first independent random number set with probability P and generated from the second independent random number set with probability (1-P), the cross-correlation coefficient Rxy between X1 and X2 in the second cluster is equal to the probability P. This approach was used in the state sampling simulation method to generate correlated random numbers to represent the correlated WECS. A detailed development of this approach is given in (Gao & Billinton, 2009).

4.1 Wind capacity credit analysis using the ELCC method

The Effective Load Carrying Capacity (ELCC) reliability measure was developed in order to measure the adequacy impacts of generating unit additions (Garver, 1966). The ELCC method is also a popular reliability-based approach to assess wind capacity credit (Milligan, 2007; Billinton et al., 2010). The basic concept in this approach is to gradually increase the system peak load until the level of system reliability in the wind assisted system is the same as that of the original system without WECS and therefore determine the increase in load carrying capability. The most commonly used reliability index in the ELCC approach is the Loss of Load Expectation (LOLE) (Billinton & Allan, 1996).

The wind capacity credit of the 400 MW WECS with the two site data shown in Table 2 was calculated using this method. The system LOLE for the MRTS is 0.75 hrs/yr utilizing a chronological load profile. The MRTS can carry a peak load of 3770 MW at a LOLE of 0.75 hrs/yr after the two 400 MW WECS are added. The increase in peak load carrying capability is 120 MW. Reference (Billinton et al., 2010) shows that it is a reasonable to evenly divide the total wind capacity credit between the two farms when the two WECS have identical installed capacities. The wind capacity credit for each 400 MW WECS is therefore 60 MW and is used in the following studies described in this chapter.

4.2 Effects of the WECS location

In this section, the effects of the WECS location on the system adequacy are analyzed using the D, P and D-P methods. The WECS locations in the MRTS are considered in two cases:

Case 1: the WECS are added at Buses 1 and 3.

Case 2: the WECS are added at Buses 1 and 6.

4.2.1 Application of the D method

A contingency list for the two cases were obtained by applying the D criterion, involving single generating unit or single transmission elements. The purpose of a contingency selection process is to reduce and limit the set of outage components to be considered. In the case of generation facilities, the largest generating units at different locations in the system are considered. In the case of transmission facilities, the transmission line selections can be done through power flow analyses. The most severe single contingency can be determined from the contingency analysis list. The rank contingency order and the corresponding system peak load carrying capacity (PLCC) for the two cases are shown in Table 3. In Table 3, the designation G18-400/ G21-400 indicates the removal of a 400 MW unit at Bus 1 or Bus 21 and L10 means Line 10 is removed from service.

	Case 1		Case 2	
Rank Order	Outage	PLCC (MW)	Outage	PLCC (MW)
1	L10	3670	L23	3910
2	L23	3940	L7/L27	3958
3	L7/L27	3958	L19	4275
4	L5	4046	L21	4286
5	L21	4286	G18_400/G21_400	4334
6	L19	4305	G23_350	4378
7	G18_400/G21_400	4334	L10	4487

Table 3. The rank orders for the two cases using the D method

Table 3 shows that the line outages tend to have a higher rank than generating unit outages in the two cases. L10 and L23 outages are the most severe contingency for Cases 1 and 2 respectively. The MRTS associated with the WECS have obvious transmission deficiencies, especially in the southeast part of the system. Table 3 shows that the system PLCC values using the D approach for Cases 1 and 2 are 3670 MW and 3910 MW respectively. The system PLCC improves to 3910 MW in Case 2 due to the fact that the transmission stress on Line 10 is reduced by adding a WECS at Bus 6.

4.2.2 The P method

Probabilistic analyses for the two cases were conducted using the state sampling technique. The variations in the system severity index (SI) (SM/yr) (Billinton & Allan, 1996) as a function of the peak load are shown in Table 4 obtained using the P method. Table 4 shows that there is relatively little difference in the system SI between Case 1 and Case 2 using the P method.

Peak load (MW)	Case 1	Case 2
3650	1.740	1.506
3750	2.765	2.617
3850	4.715	4.52
3950	8.472	8.153
4050	14.678	14.364
4150	25.774	25.29
4250	43.613	42.793
4350	72.314	71.074
4450	119.155	117.135
4550	187.834	184.529

Table 4. The system SI (SM/yr) obtained using the P method

4.2.3 The D-P method

The procedure for D-P analysis of Case 1 is briefly illustrated as follows:

Step 1. Apply the deterministic N-1 criterion to the system. The largest generating unit in the MRTS with the WECS installed at Buses 1 and 3 has a capacity of 400 MW. The outage of a WECS with 60MW capacity credit does not therefore constitute the most severe contingency under the D criterion.

Step 2. Probabilistic analysis is then conducted using the MECORE program. The analysis is conducted on the MRTS with the WECS installed at Buses 1 and 3 with L10 removed from the system. The analysis results for Case 1 are shown in Table 5.

Case 1 (L10)	Peak load (MW)	3650	3670
	SI (SM/yr)	33.68	33.89
Case 2 (L23)	Peak load (MW)	3650	3910
	SI (SM/yr)	86.48	157.78

Table 5. The system SI obtained using the D-P method

It can be seen from Table 5 that the system PLCC for Case 1 is 3670 MW and the corresponding system SI is 33.89 SM/yr under the condition of L10 outage. The procedure for D-P analysis of Case 2 is same as that of Case 1. When Line 23 (L23) is removed from service, the system PLCC is 3910 MW and the corresponding system SI is 157.78 SM/yr. The PLCC for Case 2 is larger than that of Case 1.

The studies in this section show the effect of connecting two correlated WECS at different locations in the MRTS. The WECS locations have obviously impact on the system PLCC using the D and D-P methods. The effects of WECS location on the system SI differ when using the P and D-P methods. The MRTS associated with WECS located at Bus 1 and Bus 6 (Case 2) is considered as the base system in the following planning studies described in this chapter.

5. Wind integrated MRTS reinforcement planning using the D, P and D-P methods

As noted earlier, the MRTS with the two 400 MW WECS located in Bus 1 and Bus 6 is designated as the base system in these studies. The total installed generation capacity includes 4615 MW of conventional capacity and 900 MW of wind power. The system peak load is 3650 MW.

The analysis results for the base system obtained using the three methods are given in Tables 3 to 5. Table 3 shows that the most critical element contingency for the base system is a L23 outage. The variation in the system SI as a function of the peak load is shown in Table 4 obtained using the P method. Table 5 indicates that under the most critical contingency, the base system PLCC is 3910 MW using the D-P method and a Pc of 157.78 SM/yr. Table 6 shows the yearly peak loads in a next ten year planning time frame assuming that the peak load in Year 0 is 3900 MW and each year has a 2% peak load growth.

Year	*0*	*1*	*2*	*3*	*4*	*5*
Peak Load	3900	3980	4060	4140	4220	4300
Year	*5*	*6*	*7*	*8*	*9*	*10*
Peak Load	4300	4390	4480	4570	4660	4760

Table 6. Annual peak load (MW)

The base system PLCC of 3910 MW obtained using the D-P method and shown in Table 5 cannot meet the system peak load growth over the next ten years. The selection of the Pc and Rc values impact the system acceptable risk level using the D-P and P approaches. The particular Pc value used in the D-P method and Rc value used in the P approach are very dependent on the utility management philosophy and what constitute an acceptable risk level. A Pc of 50 SM/yr and a Rc of 10 SM/yr are applied as the base system risk criteria respectively in the following studies.
The planning time frame is an eleven year period and is considered to include two stages: Stage 1 is from the 0th to 4th year to meet the system peak load of 4220 MW. Stage 2 is from the 5th to 10th year to meet the system peak load of 4760 MW.

5.1 The system planning using the D approach

The intent of this study is not to cover all the aspects of the planning process. The focus is on transmission reinforcement planning. It is assumed that generation expansion has determined that 6x50 MW conventional generating units will be installed at Bus 22, 1x350 MW and 3x155 MW units will be added at Bus 23. The total installed conventional generating capacity therefore increases to 5730 MW in the eleven year planning time frame.
The selection of planning alternatives to meet the N-1 criterion over a planning time frame is examined. Six expansion planning alternatives are proposed based on practical planning considerations. In the case of a large-scale transmission system, it is reasonable to limit the study to an area or subsystem. Doing so can provide more realistic results than evaluating the whole system (Li, 2005). These alternatives are listed in Table 7.

5.2 System planning using the P approach

The probabilistic evaluation for the six alternatives over the planning time frame was conducted using MECORE. The system SI values for the peak loads of 4220 MW and 4760 MW are shown in Table 8.
It can be seen from Table 8 that although the six alternatives meet the system load requirement in the second planning time period based on the Rc of 10 SM/yr, the system SI values for Alternatives 1 and 3 exceed the designated Rc in Stage 1. Alternatives 1 and 3 are unacceptable schemes using the P method.

5.3 The system planning using the D-P approach

In applying the D-P method, the D analysis described above is followed by probabilistic analysis to determine the system risk under each critical outage condition. A probabilistic evaluation for each alternative is conducted with the most severe contingency to determine the system risk for the alternative in the planning time period. The system load requirement at the end of Stage 1 and Stage 2 are 4220 MW and 4760 MW respectively. The system SI values for the peak load of 4220 MW and 4760 MW under the D criterion are shown in Table 9.

Alternative 1		Most severe outage condition	PLCC (MW)
Stage 1	Step 1: Double Lines 23 and 19	L7	4080
	Step 2: Double Line 6	G23_350	4250
Stage 2	Step 3: Add 6×50 MW units at Bus 22, a 350 MW and 3×155 MW units at Bus 23	L12/L13	4575
	Step 4: Double Line 12	L21	4835
Alternative 2		Most severe outage condition	PLCC (MW)
Stage 1	Step 1: Add a line between Buses 11 and 15	L7	4060
	Step 2: Double Line 6	G18_400	4330
Stage 2	Step 3: Add 6×50 MW units at Bus 22, a 350 MW and 3×155 MW units at Bus 23	L12/L13	4575
	Step 4: Double Line 12	L21	4800
Alternative 3		Most severe outage condition	PLCC (MW)
Stage 1	Step 1: Double Line 23	L7	4080
	Step 2: Double Lines 7 and 27	G23_350	4250
Stage 2	Step 3: Add 6×50 MW units at Bus 22, a 350 MW and 3×155 MW units at Bus 23	L12/L13	4575
	Step 4: Double Line 12	L12	4880
Alternative 4		Most severe outage condition	PLCC (MW)
Stage 1	Step 1: Double Lines 23 and 19, add 6×50 MW units at Bus 22 and a 350 MW at Bus 23	L7	4080
	Step 2: Double Line 6	L12/L13	4575
Stage 2	Step 3: Double Line 12	G23_350	4680
	Step 4: Add 3×155 MW units at Bus 23	L21	4835
Alternative 5		Most severe outage condition	PLCC (MW)
Stage 1	Step 1: Add a line between Buses 11 and 15, add 6×50 MW units at Bus 22 and a 350 MW at Bus 23	L7	4080
	Step 2: Double Line 6	L12/L13	4575
Stage 2	Step 3: Double Line 12	L7	4760
	Step 4: Add 3×155 MW units at Bus 23	L21	4800
Alternative 6		Most severe outage condition	PLCC (MW)
Stage 1	Step 1: Double Line 23, add 6×50 MW units at Bus 22 and a 350 MW at Bus 23	L7	4080
	Step 2: Double Lines 7 and 27	L12/L13	4575
Stage 2	Step 3: Add a line between Buses 6 and 8	G23_350	4720
	Step 4: Add 3×155 MW units at Bus 23	L21	4880

Table 7. The system PLCC value for the six alternatives using the D method

	Alt. 1	Alt. 2	Alt. 3	Alt. 4	Alt. 5	Alt. 6
Stage 1	39.8	2.72	31.5	2.95	2.04	1.64
Stage 2	8	9.8	5.5	7.2	9.8	5.4

Table 8. The system SI (SM/yr) for the alternatives obtained using the P method

	Alt. 1	Alt. 2	Alt. 3	Alt. 4	Alt. 5	Alt. 6
Stage 1	175	184	168	38.4	39	37.5
Stage 2	36	41	40	36	41	40

Table 9. The system SI values (SM/yr) for the alternatives at the end of two stages obtained using the D- P method

As noted earlier, a Pc of 50 SM/yr and a Rc of 10 SM/yr were selected as system criteria in this study. Table 9 shows that the system SI for Alternatives 1, 2 and 3 exceed 50 SM/yr in Stage 1. Alternatives 1, 2 and 3 were, therefore, eliminated from the candidate planning list due to their inability to meet the designated Pc value in the first planning time period and Alternatives 4, 5 and 6 are therefore acceptable planning alternatives using the D-P method. The selected planning schemes for the D, D-P and P techniques are shown in Table 10. It can be seen from this table that the planning alternatives selected are different for the different criteria. All six alternatives are satisfied under the D criterion. Alternatives 4, 5 and 6 are acceptable using the D-P method. Alternatives 2, 4, 5 and 6 are candidate planning schemes using the P method.

Method	D	P	D-P
Selected Alternatives	1, 2, 3, 4, 5, 6	2, 4, 5, 6	4, 5, 6

Table 10. The selected planning schemes for the different techniques

Analysis results shown in Table 10 indicate that the application of the D-P method provides more stringent results for a system with wind energy than the D method. The D-P approach introduces an element of consistency in the assessment by introducing the concept of an acceptable risk level under the critical element outage condition. The D-P technique is driven by the deterministic N-1 criterion with an added probabilistic perspective which recognizes the power output characteristics of a WECS.

6. Conclusions

The research described in this chapter is focused on the utilization of state sampling Monte Carlo simulation in wind integrated bulk electric system reliability analysis and the application of these concepts in system planning and decision making. The techniques and multi-state models developed to permit dependent wind energy facilities to be incorporated in bulk electric system adequacy evaluation using the state sampling Monte Carlo

simulation technique are presented. The wind capacity credit of a WECS is examined using the Effective Load Carrying Capacity (ELCC) method.

The increasing use of wind power as an important electrical energy source clearly indicates the importance of considering the impacts of wind power in power system planning and design, and developing appropriate evaluation techniques. Most electric power utilities use deterministic techniques such as the traditional N-1 security criterion to assess system reliability in transmission system planning. These deterministic (D) approaches are not consistent and do not provide an accurate basis for comparing alternate equipment configurations and performing economic analyses as they do not incorporate the probabilistic or stochastic nature of system behavior and component failures. There is therefore growing interest in combining deterministic considerations with probabilistic (P) assessment in order to evaluate the quantitative system risk and conduct bulk power system planning. A relatively new approach that incorporates deterministic and probabilistic considerations in a single risk assessment framework has been designated as the joint deterministic-probabilistic (D-P) approach.

The MRTS was created in order to conduct planning analysis in a transmission weak system using the D, P and D-P techniques. The studies in this chapter show the effects of connecting two correlated WECS at different locations in the MRTS have obviously impact on the system peaking load carrying capacity using the D and D-P methods. The effects of WECS location on the system SI differ when using the P and D-P methods. The MRTS with WECS located at Bus 1 and Bus 6 was used as the base system in the planning studies described in this chapter.

Six planning alternatives are proposed as candidate development options in this chapter. Although the six planning schemes meet the deterministic N-1 planning criterion, three of the six alternatives are selected as the candidate planning alternatives based on the D-P method. The reason is that the SI values for Alternatives 1, 2, 3 do not meet the specified Pc requirement at the end of Stage 1. The six designated alternatives in the planning time period are also examined using the P method. Alternatives 1 and 3 are eliminated from the candidate list due to their inability to meet the specified Rc value. The research work illustrates that the joint deterministic-probabilistic approach can be effectively used as a planning tool in bulk power systems containing wind energy.

It is believed that the models, methodologies, and results presented in this chapter should assist system planners to conduct wind integrated bulk electric system planning.

7. Acknowledgement

The author would like to express her deepest gratitude and appreciation to Dr. Roy Billinton for his invaluable guidance and support all the time during research at the University of Saskatchewan in Canada.

8. References

World Wind Energy Reprot (2009), Available from:
http://www.wwindea.org/home/images/stories/
worldwindenergyreport2009_s.pdf

North American Electric Reliability Council Planning Standards (2007), Available from:
http://www.nerc.com

Li W. (2005), *Risk Assessment of Power Systems: Models, Methods, and Applications,* John Wiley &Sons, Hoboken, NJ, USA.

EPRI Final Report, Composite-System reliability Evaluation: Phase 1 – Scoping Study (1987), Tech. Report EPRI EL-5290.

Billinton R., Bao H. and Karki R. (2008), A Joint Deterministic- Probabilistic Approach To Bulk System Reliability Assessment, *Proceedings of Probability Method Applied to Power System Symposium*, Puerto Rico, USA, June, 2008.

Billinton R., Gao Y. and Karki R. (2010), Application of a Joint Deterministic- Probabilistic Criterion to Wind Integrated Bulk Power System Planning, *IEEE Trans. on Power Systems*, Vol. 25, No. 3, Aug. 2010, pp. 1384-1392.

Billinton R., and Gao Y. (2008), Multi-state Wind Energy Conversion System Models for Adequacy Assessment of Generating Systems Incorporating Wind Energy, *IEEE Trans. on Energy Conversion*, Vol.23, No.1, Mar. 2008, pp.163-170.

Billinton R., and Gao Y. (2008), Adequacy Assessment of Composite Power Generation and Transmission Systems with Wind Energy, *International Journal of Reliability and Safety*, Vol. 2, No. 1/2, 2008, pp. 79-98.

Fang R. and Hill D. J. (2003), A New Strategy for Transmission Expansion in Competitive Electricity Markets, *IEEE Trans. on Power Systems*, Vol. 18, No. 1, Feb. 2003, pp. 374-380.

Chowdhury A. A. and Koval D. O. (2001), Application of Customer Interruption Costs in Transmission Network Reliability Planning, *IEEE Trans. on Industry Applications,* Vol. 37, No. 6, Nov./Dec. 2001, pp. 1590-1596.

Li W., *Installation Guide and User's Manual for the MECORE Program*, July 1998.

Billinton R. and Allan R. (1996), *Reliability Evaluation of Power Systems*, 2nd Edition, Plenum Press, New York, 1996.

IEEE Task Force (1979), IEEE Reliability Test System, *IEEE Transactions on Power Apparatus and Systems,* Vol. PAS-98, Nov/Dec. 1979, pp. 2047-2054.

2004 Forced Outage Performance of Transmission Equipment, Canadian Electricity Association.

Billinton R., Chen H. and Ghajar R. (1996) , Time-series Models for Reliability Evaluation of Power Systems Including Wind Energy, *Microelectronics Reliability*, Vol. 36, No. 9, 1996, pp. 1253-1261.

Wangdee W. and Billinton R. (2006), Considering Load-carrying Capability and Wind Speed Correlation of WECS in Generation Adequacy Assessment, *IEEE Transactions on Energy Conversion*, Vol. 21, No. 3, September 2006, pp. 734-741.

Gao Y. and Billinton R. (2009), Adequacy Assessment of Generating Systems Containing Wind Power Considering Wind Speed Correlation, *IET Renewable Power Generation*, Vol. 3, Issue 2, June 2009, pp. 217-226.

Giorsetto P and Utsurogi KF (1983), Development of a New Procedure for Reliability Modeling of Wind Turbine Generators. *IEEE Transactions on Power Apparatus and Systems*, Vol. PAS-102, No. 1, pp.134-143.

Billinton R., Gao Y. And Karki R. (2009), Composite System Adequacy Assessment Incorporating Large-Scale Wind Energy Conversion Systems Considering Wind Speed Correlation, *IEEE Transactions on Power Systems*, Vol. 24, Issue 3, Aug. 2009, pp. 1375-1382.

Gao Y., Billinton R. and Karki R. (2009), Composite Generation and Transmission System Adequacy Assessment Considering Wind Energy Seasonal Characteristics, *Proceeding of the IEEE General Meeting 2009*, July 2009, Calgary, Alberta, Canada.

Garver L. (1966), Effective Load-Carrying Capability of Generating Units, *IEEE Trans. Power Apparatus & Sys.* V. PAS-85, No. 8 (1966), pp. 910 – 919.

Milligan M. (2007), Capacity Credit for Wind, Consultant National Renewable Energy Laboratory, USA, April 26, 2007.

14

Agent-Based Simulation of Wind Farm Generation at Multiple Time Scales

Enrique Kremers[1], Norbert Lewald[1], Pablo Viejo[1], José María González De Durana[2] and Oscar Barambones[2]
[1]*EIFER - European Institute for Energy Research (EDF and KIT), Karlsruhe*
[2]*E. U. de Ingeniería de Vitoria-Gasteiz - University of the Basque Country*
[1]*Germany*
[2]*Spain*

1. Introduction

Since the past decade, energy systems are undergoing a deep paradigm shift, caused by the liberalisation of energy markets, the introduction of renewable energies, and the emergence of new, distributed producers that feed into the grid at almost every level of the system.
The general trend towards the introduction of renewable energy sources in the industrialised countries implies one of the greatest changes in the structure of energy systems. These systems are moving away from a centralised and hierarchical energy system, where the production follows a top-down principle under the strict control of the electricity supply companies towards a new system where diverse actors influence the energy supply. The production is no longer limited to large energy providers, as small decentralised producers now exist and inject energy at much lower voltage levels than before. These energy systems are suffering the consequences of such a paradigm change. This change basically consists in new regulations and the introduction of new energy production technologies that transform traditional centralised systems into decentralised ones. This whole process is part of the framework of the fight against the causes of climate change, which is mostly due to CO_2 emissions. This paradigm change encompasses new tools and methods that can deal with decentralised decision-making, planning and self-organisation. The large amount of new actors and technologies in the energy production chain requires a shift from a top-down to a more bottom-up approach.
Multi-scale simulation systems offer several advantages over classical models. The ability to run simulations on different time scales using the same model is an important issue for the upcoming modelling of energy systems. The main advantages are that there are fewer models and no need to port data between platforms. This leads to a more efficient simulation run and decision-making support. The challenges of these kind of simulations are that a multi-scale model for the moment will not be as accurate as a purpose made model. So, the modelling method, the parameters, etc. included must be carefully chosen to ensure both flexibility and accuracy.
The work presented in this chapter concerns the wind generation module of an agent-based model for integral energy systems (developed at the European Institute for Energy Research

(EIFER) in cooperation with the EUI de Vitoria-Gasteiz). It is based on earlier works where the model is already partially presented Kremers et al. (2009).
The proposed model aims to represent the wind power production by modelling wind farms consisting of wind turbine units on different time scales, ranging from short (minutes) to long-term simulations (months), taking into account fluctuating wind speeds and technical reliability. The model is able to compute the aggregated output power of the wind farm influenced by different random factors and can thus recreate a realistic power unit to be used in integral energy system simulations. The simulation of this data is performed in real time, so that the power output at a specific time can be reproduced and injected into the energy system simulation.

2. Agent based modelling for energy system simulation

Agent-based modelling (ABM) is a technique that is gaining more and more importance during the past two decades. An agent-based model combines the use of small, reproducible entities called agents, that interact among themselves and with an environment and lead to complex system behaviour, like emergence. These models possess several characteristic, as they can create a wide solution space and allow the appearance of distributed intelligence. They are commonly used to obtain decentralised solutions where a central controlled solution method is not applicable. These include open or at least very dynamic environments, systems constituted naturally by agents and systems that have to be easily extendible or scalable. A detailed introduction to the subject is given by (Wooldridge, 2009).
Basically, ABM focuses on the modeling of systems at the local level through the definition of their elementary units (called agents) and their interactions. These units are intended to be modeled in a simple way, while the complexity of the system is an emergent property of their interactions. There are three main groups of actions that must be modeled:

1. Sensing the environment: Agents are capable to acquire information of the local environment through sensors.
2. Taking decisions: Each agent can autonomously decide what action should be taken regarding its local information to fulfill his objectives.
3. Reaction to the environment: Through actuators, the decisions made by the agents have a response on the environment. Therefore a feedback loop exists between the environment and the agents.

It has to be noted that the decision making process can be of complex nature, but does not have to. In the case of the wind turbine modelled in this paper, we will see that this process is quite simple. It is basically reduced to checking the status (failure or not) and produce electricity if there is enough wind.
The agent-based modeling approach has been applied successfully to a large number of fields (e.g. biology, sociology) during the last decades. Nevertheless their application in energy systems is nowadays still marginal. There exist some approaches related to management and control of power grids , demand modelling and electricity markets . In the field of production though, few applications can be found (e.g. Chappin & Dijkema (2007), which is though closely related to markets and CO_2 emissions).
Agent-based modelling can be easily combined with other approaches, because of its nature. So, an agent can include a decision algorithm which is based on a completely different approach, as for example, System Dynamics or Discrete Event models. This possibility to use agents in an multi-method environment is an additional benefit.

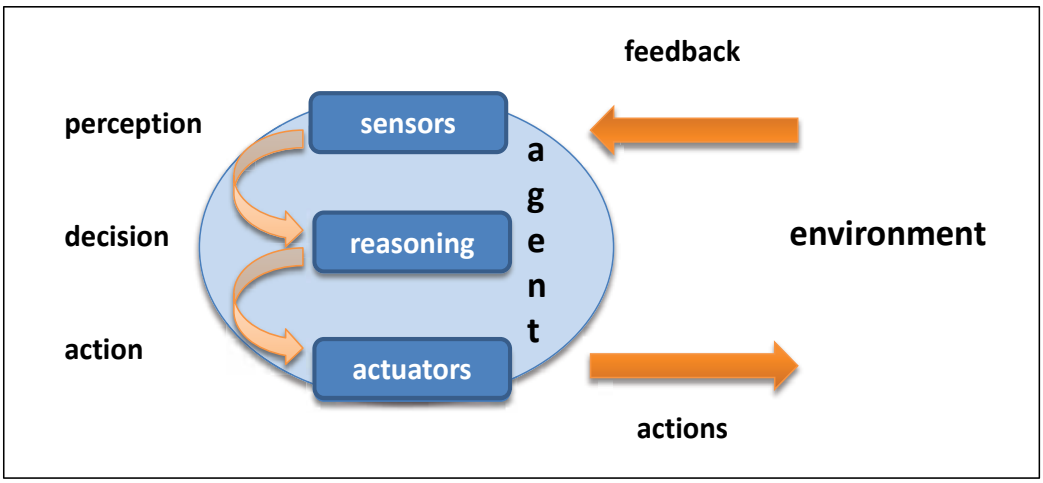

Fig. 1. Structure of a generic agent (adapted from Wooldridge (2009))

In order to integrate the wind power production into an integral energy systems simulator, an simplified but still enough accurate simulator for wind speeds and generation was necessary. The agent based approach was chosen because of several reasons:

- the facility to integrate heterogeneity among the agents
- the possibility to create a modular structure which is interoperable with other platforms (using JAVA)
- the ability to represent different time scales with the same model
- the possibility to use more than one approach and combine them in the model
- the easy scalability of the model (allowing to add and remove agents dynamically, e.g. failures, scenarios of enlargement of the farm, etc.)

3. Stochastic wind speed simulation

Generating realistic wind speeds is an important task when the effects of wind production in an electricity system have to be analysed. The fluctuating wind speed is the origin of the temporal variation of the power injected by this production type and thus has direct effects on the production-demand balance and the grid stability. One of the challenges of wind speed simulators is mainly to reproduce the different scale term fluctuations, as described in (Nichita et al., 2002). To this end, different models have been developed during the past decades. The model chosen here is built up in two steps, comprising two components, a slow and a fast called and is the same as in (Bayem et al., 2008) with some minor modifications. More accurate wind models (that take into consideration e.g. long-term (Billinton et al., 1996) or cross-correlations (Allerton, 2008)) are available, but this one should be sufficient for the purposes of this work. An overview of some more approaches can be found in (Aksoy et al., 2004). It is important to add that to get a realistic simulation of a specific site, records of historical data are needed to obtain the parameters of the model, as even the best model is useless if not accurately fitted.

3.1 The slow component

The first part, which was already used in a previous work of the author (Kremers et al., 2009; Viejo & Kremers, 2009) is a generator of hourly mean wind speeds. This time series model is based on an ARMA (Auto-Regressive Moving-Average) model which is given by

$$\begin{aligned} y_t = {} & \phi_1 y_{t-1} + \phi_2 y_{t-2} + \ldots + \phi_n y_{t-n} \\ & + \alpha_t + \theta_1 \alpha_{t-1} + \theta_2 \alpha_{t-2} + \ldots + \theta_m \alpha_{t-m} \end{aligned} \tag{1}$$

The data series y_t is used to build the model, i.e. to calculate the auto-regressive ϕ_i; $i = 1, 2, \ldots, n$ and the moving average parameters θ_j; $j = 1, 2, \ldots, m$. $\{\alpha_t\}$ is a Gaussian white noise process with zero mean and standard deviation of σ_α which is part of the moving average (MA) part of the model. Considering the orders, the process is referred to as ARMA(n, m). The parameters used in this work were chosen from an ARMA(3,2) approach, but the model was developed up to ARMA(4,3) and can be easily adapted to other orders. For example, a pure AR(2) model (Aksoy et al., 2004) which was also implemented before can be seen as a as an ARMA model with $n = 2$ and $m = 0$. The order of the model depends on the quantity of historical data available, since, if there is only a little data, an accurate model cannot be reached even with higher orders. There is a range of literature available regarding parameter estimation. Fitting models are normally based on the least squares regression methods that try to minimise the error value. For AR parameter estimation, the Yule-Walker equations are widely used.
The simulated hourly mean wind speed (Billinton et al., 1996) can be obtained by

$$\overline{v}_1(t) = \mu + y_t \tag{2}$$

where μ is the mean wind speed of all the observed data. If observed hourly mean speeds μ_h and standard deviations σ_h are available, a more realistic simulated wind speed can be calculated as:

$$\overline{v}_2(t) = \mu_h + \sigma_h \cdot y_t \tag{3}$$

The method is explained in detail in (Billinton et al., 1996).

3.2 The fast component

Being able to compute hourly mean wind speeds might be enough for several applications of the energy systems model, but as temporal scalability was a requirement for the latter, a more detailed model was needed. The ability to reproduce realistic wind speeds in real time can be gained by adding a so called fast component to the previously described slowly varying signal. For this purpose turbulent phenomena are modelled by a highly fluctuating signal given in (Bayem et al., 2008) by the following differential equation:

$$\frac{dw}{dt}(t) = -\frac{w(t)}{T} + \kappa v_h(t) \sqrt{\frac{2}{T}} \xi(t) \tag{4}$$

where $T = L/\overline{v}$, being L the turbulence length scale, κ a factor that depends on the geographical location of the wind turbine site (Welfonder et al., 1997), $\xi(t)$ a Gaussian white noise and $v_h(t)$ the hourly mean wind speed. The equation describes a stationary Gaussian process. This component allows us to generate a time continuous signal that represents a real time wind speed.

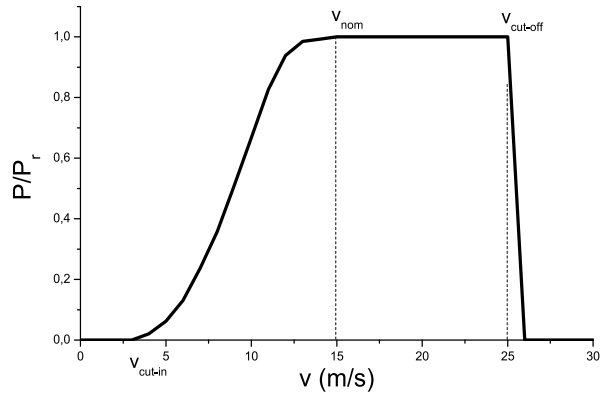

Fig. 2. A sample power curve. P_r is the rated power

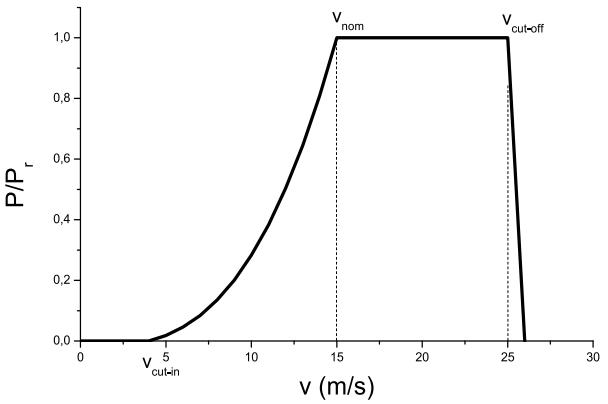

Fig. 3. Polynomial approximated power curve

4. Turbine model

There are plenty of technical models for wind turbines. The model used here is a generic approach, which takes into consideration the agent-based approach of the framework. As the wind turbine has to be able to be replicated (in order to create wind farms with tens or even more turbines), a simple model was chosen to ensure fluid simulations. The basis of this model is the relation between the power output of the turbine, which is a function of the wind speed actuating on its rotor blades. Three different models that are commonly used have been identified in the course of this work. The *real model* is not a mathematical model itself. It just shows the $P(v)$ curve of a specific turbine - based on the manufacturer's data. In general, the curve has a shape similar to the one shown in Figure 2.

The curve shows the typical profile of a wind turbine. The cut-in speed is the minimum wind speed at which the turbine can start working, the nominal wind speed is the point at which rated power of the turbine is achieved. This power is normally almost constant up until the cut off wind speed is reached, at this point the turbine must be shut down to avoid damage caused by too strong winds. So, four principal working states can be defined as:

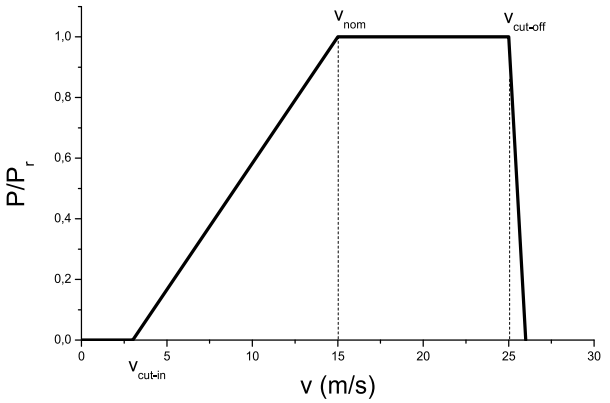

Fig. 4. Linear simplified power curve

- Stopped: for $v < v_{cut-in}$
- Partial load: for $v_{cut-in} < v < v_{nom}$
- Rated load: for $v_{nom} < v < v_{cut-off}$
- Cut-off: for $v > v_{cut-off}$

The transitions between the states are smooth because of the technical characteristics of the rotor and generator in the real curve. The most interesting state to be observed is the partially loaded state, where the turbine shows a non-linear $P(v)$ dependence. Here it can observed the start dynamics of the turbine as well as the adaptation to the fully loaded capacity at rated speed. This phase can be approximated by a polynomial term as shown in Figure 3. The polynomial model assures the curved shape of the curve, but the trace just before achieving the nominal wind speed is idealised. The linear approximation of the curve, which is used in more simplified models, can be defined by linearly interpolating the values for v_{cut-in} and v_{nom}. It can be seen in Figure 4. The last model might have use when only the characteristic wind speeds of the turbine (and no power curve) are available. Though, the polynomial approach can be also be used as approximation by using a polynomial of degree three as described in (Chedid et al., 1998).
The cut-off state is reached when the turbine gets shut-down because of exceeding $v_{cut-off}$. Further, a $v_{cut-back-in}$ parameter can be defined for the model. Its value denotes the wind speed, at which the turbine gets back to work after having entered the cut-off state. This value adds the restart behaviour of the machines after strong wind periods.
Being MTBF the Mean Time Between Failures of a unit defined by

$$MTBF = \frac{1}{\lambda} = \frac{operational\ time}{number\ of\ failures} \tag{5}$$

where λ is the failure rate. Using $MTBF$ allows modelling the availability of a wind turbine over time. The equation describing the Mean Time To Recover

$$MTTR = \frac{down\ time}{number\ of\ failures} \tag{6}$$

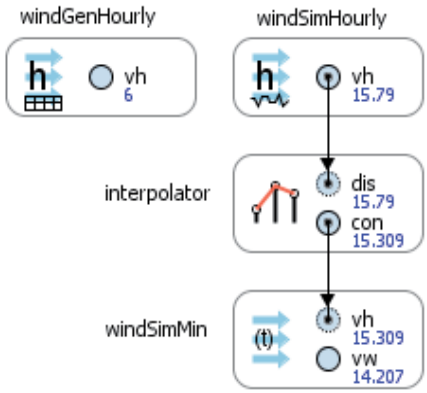

Fig. 5. Modules of the wind simulator

is also included, where *down time* is the time when the turbine is inactive because of a failure, maintenance or reparations. The MTTR is so an indicator for the average time until the unit gets started up again after an incident. Considering these two parameters, a failure model is integrated into the turbine model. The rates (inverse values of them) are used to determine failure probability used in the transition among states.

5. Implementation

5.1 Wind simulator implementation

To build the wind simulator, different modules were developed in Anylogic, a software package from XJ Technologies (XJ Technologies, 2010). Each module was encapsulated to work independently and has well defined interfaces. This allows for different releases for the same module which can be easily replaced.
The wind simulator modules are the following:

- **Hourly speed module:** The hourly speed module has to provide the hourly wind speeds. In the current model, there are two possible implementations:
  1. The hourly wind speed generator is a module that allows using a given dataset for the speed generation. Normally it uses historical as input, which gives hourly mean wind speeds. It can also be used to test extreme situations by simulating extreme conditions. Further, it allows for replicable simulation runs, by using the same time series as input for multiple simulations.
  2. The hourly simulator implements the slow component ARMA model described in section 3.1. The parameters of the model are the hourly mean wind speed μ_h, the hourly standard deviation σ_h, the standard deviation σ_α of the $\{\alpha_t\}$ process and the AR and MA coefficients $\phi_1 \dots \phi_4$ and $\theta_1 \dots \theta_4$, respectively. The output generated is the hourly mean wind speed $v_h(t) = \overline{v}_2(t)$ by implementing the method described in Equation (3).
- **Detailed module:** The detailed module is needed for short time-scale wind simulations. The present release is a simulator. It is the implementation of the fast component using an average hourly wind speed as input. The input signal $v_h(t)$ is superposed with some

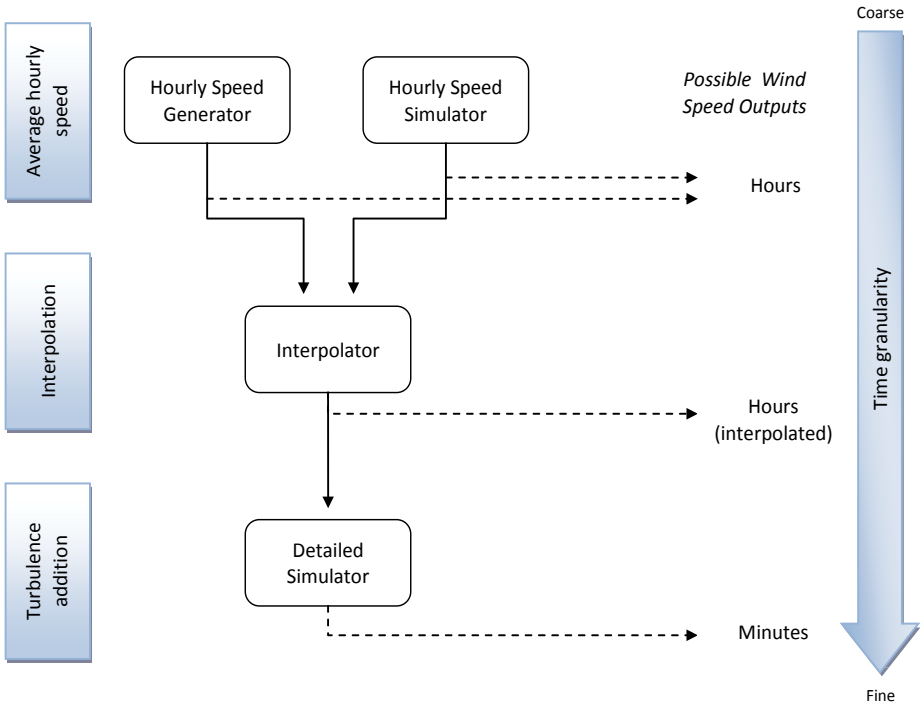

Fig. 6. Time granularity of the model

turbulences. This can be fitted to real turbulence data by the parameters κ and L described in Section 3.2. The solution to the differential equation is computed by Anylogic's engine using the Euler method.

- **Interpolator module:** The interpolator is necessary to generate smoothed final wind speeds. As the hourly mean wind speed is calculated or given in discrete values for each step, the change of the mean would cause a non continuous piecewise function with abrupt jumps in the final wind speed signal. Thus, a linear interpolation for the hourly wind speed was implemented. The module owns a parameter to determine the interpolation interval t_i measured in time steps of the current model time. It is interconnected between the hourly simulator and the detailed simulator, as shown in Figure 5.

The interoperability of the modules allows several combinations. For example, when historical data of hourly mean wind speeds are available, and continuos values are needed, the wind speed generator and the detailed module can be used. However, if only statistical data on the site are given, the hourly wind speeds can simulated through the hourly simulator based upon that data.

5.2 Turbine implementation

The wind turbine is the core of wind power production. The requirements of the turbine were to convert the wind speed to a suitable magnitude for the power system, i.e. the injected power. This reflects the process of the wind turbine converting the kinetic energy of the wind into electric energy by means of the generator. The wind turbine is modelled as an agent,

because it will be replicated several times to create wind farms and each entity has similar but not exactly identical characteristics. The agent can be customised through its parameters, which are shown in Table 1.
Making use of Anylogic's features to create hybrid models (Borshchev et al., 2002; Denault, n.d.; Helal, 2008), the turbine was modelled using the power curve model of the $P(v)$ relation described in Section 4 in combination with UML state charts. The power curve model was chosen to ensure flexibility in the application of the model. It is assumed that when modelling a wind farm, detailed information about the used turbines is available. This way, it is possible to customise each turbine with its correspondent power curve. The model of the wind turbine agent remains the same in any case.
The state chart elaborated here is classified in states dependent on the output power and failure state. The three working states of the turbine are as follows:

- Off: this state is active when the turbine is not producing any output power, regardless of the cause (no wind, too strong wind speeds, etc.) except in the case of a failure
- Failure: this state is achieved when there is a failure or a shutdown of the turbine due to maintenance.
- On: the turbine is in this state when producing output power, regardless if the rated power is gained or the turbine is only partial loaded.

The transition conditions between the states are defined by the wind speed for the transitions between the *On* and *Off* states, and by the corresponding rates of the MTBF and MTTR in the case of transitions to and from the *Failure* state, respectively. The MTBF is used for both transitions from the *On* and *Off* states. The rates are always adapted to the current timescale by a factor that is proportional to it and set automatically by the model in function of the scale chosen.

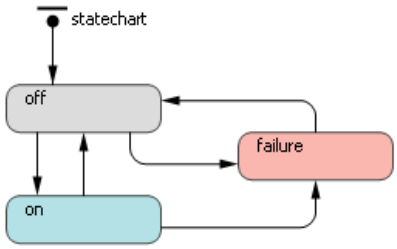

Fig. 7. State chart of the wind turbine including failure behaviour

Parameter	Description	Value
P_{nom}	Nominal power	275 kW
v_{cut-in}	Cut-in wind speed	3 m/s
$v_{cut-off}$	Cut-off wind speed	20 m/s
$v_{cut-back-in}$	Cut-back-in wind speed	18 m/s
$MTBF$	Mean Time Between Failures	1900 h
$MTTR$	Mean Time To Recover	80 h

Table 1. Wind turbine parameters

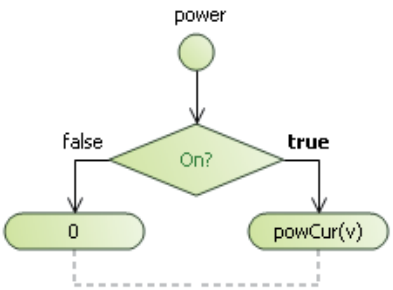

Fig. 8. Action chart of the wind turbine

For the computation of the output power, the so-called action chart of Anylogic is used to link both the discrete state chart approach with the continuous power curve. The output power is only taken from the power curve, if the current state is set to *On*. The state chart and the action chart are shown in Figure 7 and 8.

6. Integral multi-scale wind power simulation

After implementing the basic elements of our simulation, the wind turbine agents are grouped into an environment that defines common values for all agents within it and creates a framework among them that allows us to extract common statistical data. For instance, the aggregated output power of the wind farm, or the mean power by turbine is computed.
A wind farm with 25 wind turbines is generated in the current sample, being this is a typical number for medium size onshore wind farms. The power curve of the generators is the same for all, since it is assumed that the same type of turbines are installed. The power curve used here is inspired by the turbine type GEV MP 275 from the manufacturer Vergnet Eolien. It has a 32m diameter rotor and a rated power of 275kW and is specially designed to be used in remote locations and can sustain hurricane winds when secured to the ground.
The wind parameters for the wind simulator were taken from models developed previously. The ARMA coefficients used for the hourly simulations were taken from (Karki et al., 2006) for the "North Battleford" site. The parameters L and κ were taken from (Welfonder et al., 1997).

6.1 Simulating wind speeds at different time scales

In the following, three case studies were performed in order to show the abilities of the model, to the analyse the results and asses the performance of the simulations. The first two studies were both simulated for a period of 24h. The difference between them is that in the first case, a day with low wind speeds is simulated, whereas in the second case high wind speeds are recreated. The third case is a simulation for a whole week, where (due to the duration) both high and lower speeds can be observed. The first two simulations allow us to analyse the reactions of the turbine park to low speed effects such as the cut-in process when the wind is starting to blow. They also allow for analysing the effects on high speeds where cut-off phenomena can be observed. In the third simulation over a week, effects over a longer simulation period can be observed. In all cases, hourly and continuous simulations were run to compare the accuracy and performance of the models.

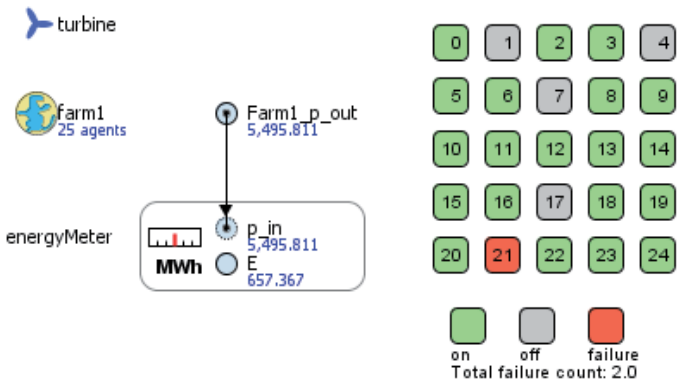

Fig. 9. Representation of the states of the turbines composing a wind farm

It has to be noted in both cases, that the hourly values are computed from a simulation taking as input for the wind turbine directly the hourly output of the wind speed generator, and they are not averaged values from the continuous wind speed time series. For the hourly simulations, the interpolated hourly wind speed is taken as input for the wind farm (turbines) model.

6.1.1 Low wind speed day

In Figure 10 two plots are shown. In the upper plot, the wind speed as a comparison between hourly mean and continuous simulation is represented. The hourly mean wind speed, the interpolated hourly values and the simulated real-time speed (fast term) are shown in the first plot. The piecewise function of the not interpolated hourly wind speed is the output of the slow term module. The interpolated hourly mean values are taken from the linear interpolator. These are again used as input for the fast term module. The outputs of the wind farms is plotted below. Two outputs are shown, one using the interpolated hourly mean speeds as inputs, and the second using the real-time, continuous wind speed output.
This first simulation shows a period of 24h where the wind speeds are relatively low, not exceeding 18 m/s. In particular there are periods with low speeds below 10 m/s where a significant decrease of the output power of the turbines can be observed. Falling under the cut-in speed, they even can stop completely. The simulated wind farms are identical. The difference between them is the wind speed input data. The first farm takes the interpolated hourly mean wind speeds, the second one the real time speeds.
In Figure 10 we can see that the hourly computed power output of the farm follows more or less what could be a hourly mean of the continuous values. There are no great deviations, except a small one around 21h, due to a drop of the continuous wind speed caused by a turbulence in the fast term.
Due to the random failure behavior, some differences caused by turbines in failure status can be observed (e.g. less total power at the last 2 hours of the day in the continuous simulation). It can be seen that the hourly power output follows approximately the continuous simulation, and only short term peaks are neglected (e.g. drop down of the wind speed at 21h that leads to a power drop is not visible in the case of the hourly simulation).

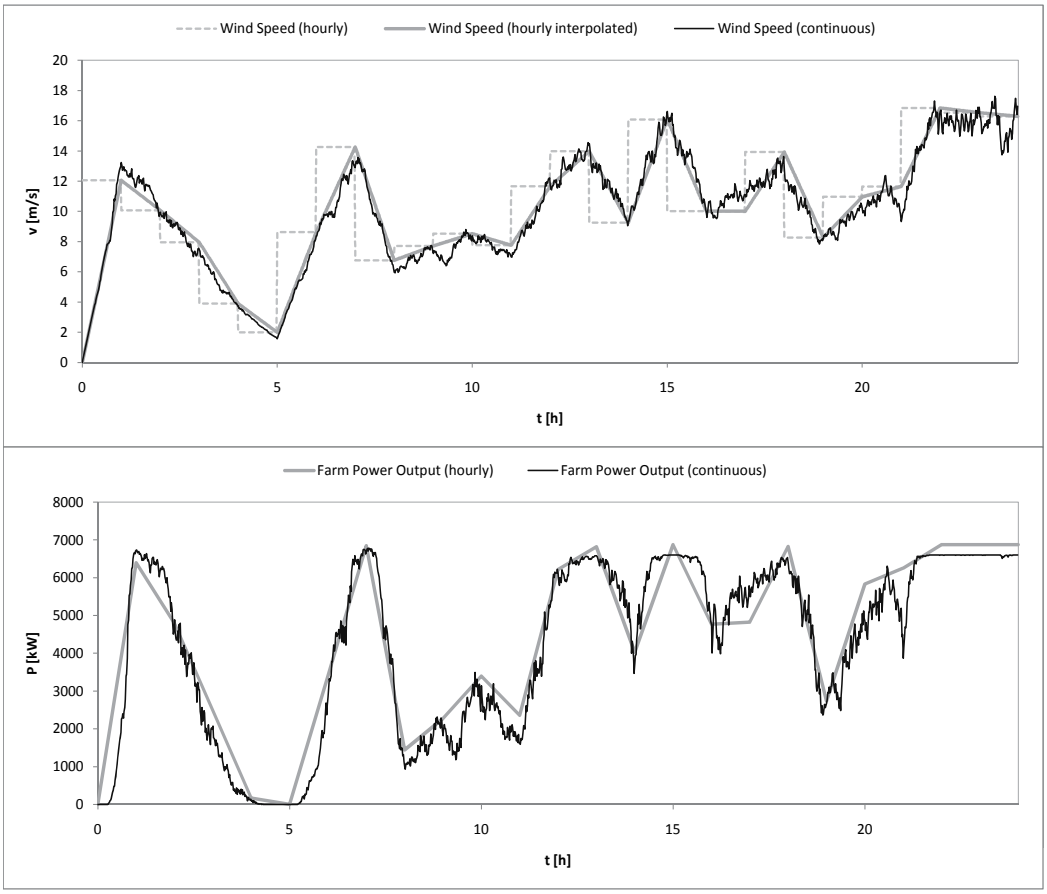

Fig. 10. Comparison hourly and continuous power outputs (bottom) and corresponding wind speeds (top) for a day with low wind speeds.

6.1.2 High wind speed day

In Figure 11 there can be again two plots seen. On top, the hourly and continuous wind speeds are represented, below the aggregated electrical power outputs of the farm can be seen. In this case, a day with high wind speeds was chosen. The speeds (once stabilised) are in the range of 12-25 m/s, being $v_{cut-off}$ = 20 m/s, so inside that range. Where the continuous wind speed is $v_w(t) > v_{cut-off}$, a cut-off for some or all (see Section 6.3) is achieved and they shut down, which leads in a complete power drop at individual turbine scale, and important drops at the aggregated farm output. When $v_w(t) < v_{cut-back-in}$, the turbine starts again which causes a power increase. These effects explain the strong fluctuations that can be observed for the continuous power output in the lower plot of Figure 11. It is interesting to observe the hourly output, too. There, such strong fluctuations are not present, which can be clearly seen in the period between 8-20h. Furthermore, in the continuous output cut-offs can occur (due to a surpass of the cut-off speed by some turbulences caused in the fast term module) which are not considered in the hourly output, as the hourly mean remains $v_{h(t)} < v_{cut-off}$. This can be seen in the power drop between 4-5h, while the hourly output stays at the nominal

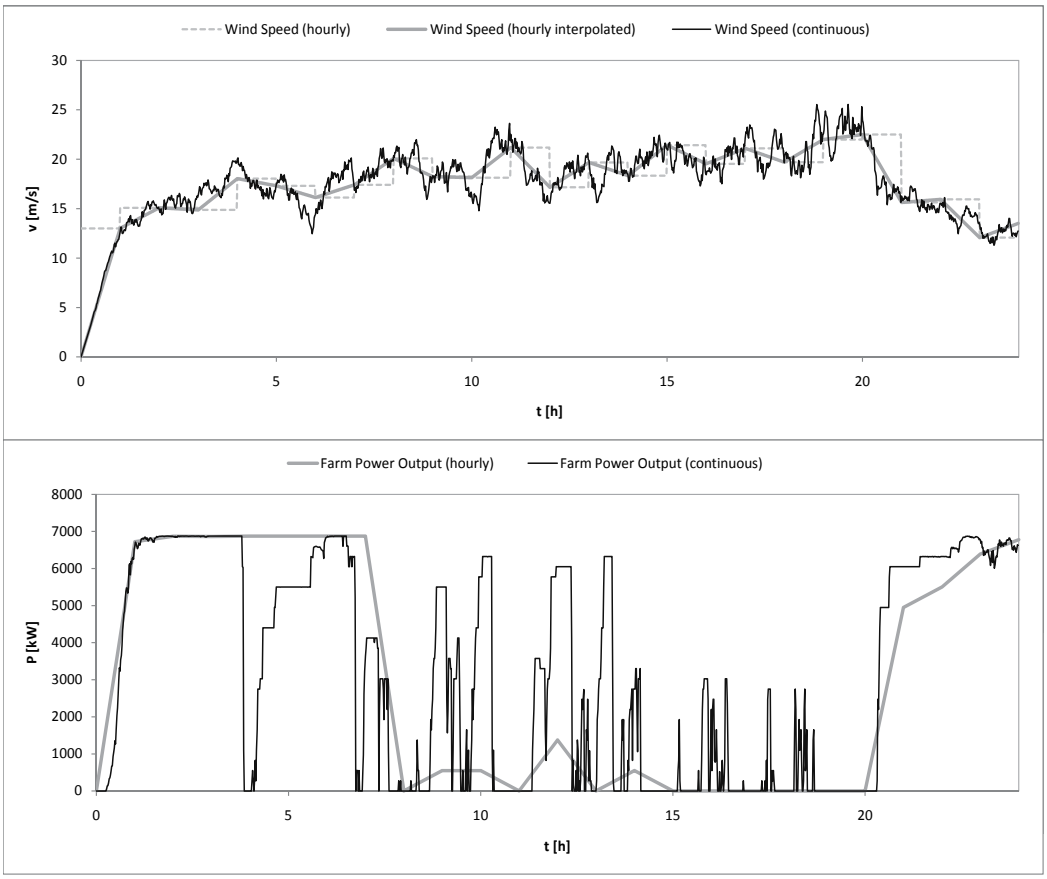

Fig. 11. Comparison hourly and continuous power outputs (bottom) and corresponding wind speeds (top) for a day with high wind speeds. The cut-offs of the turbines can be clearly observed, especially for the continuous simulation.

farm output. Thus, when dealing with fast speeds, the continuous model reflects much better strong fluctuations, which are neglected in the hourly simulation.

6.1.3 Simulation over a week

In this case, a complete week was simulated. Figure 12 shows two plots of the power output for a 25 turbine wind farm (the same as in the examples before), for the hourly and continuous outputs, at top and bottom, respectively. As can be seen on the plots, over 7 days the output of each method differs strongly only in some cases. There are some points where $v_w(t) > v_{cut-off}$. The turbines shut down because of over speed reasons in this case, but looking at the same point in the hourly mean simulation, there is not such a power drop. This is because $v_w(t)$ surpasses the hourly mean $v_h(t)$ punctually. To reach a power drop in the hourly simulation, $v_h(t) > v_{cut-off}$ is needed. These drops are a problem for the grid stability, as they are very significant and occur in a short time. Indeed, control mechanisms of the wind farms that shut down turbines proactively depending on wind speed forecasts or similar to prevent such abrupt drops have not been considered yet. Furthermore, the rapidly fluctuating

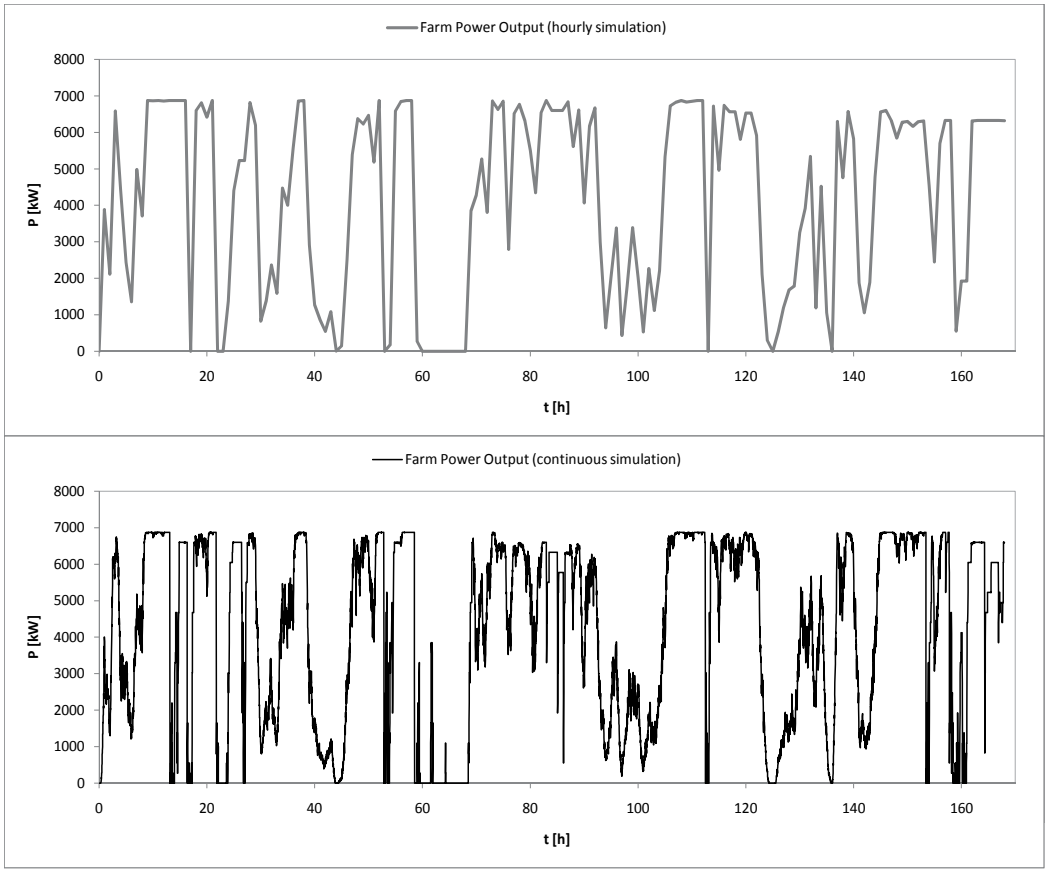

Fig. 12. Comparison hourly (top) and continuous (bottom) simulation for one week

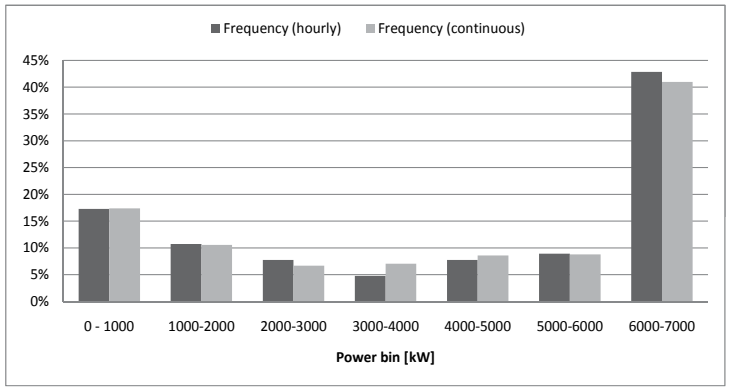

Fig. 13. Histogram for the hourly and continuous simulations of the output power for one week

wind speed component is transmitted to the power output of the plot below, while the curve of the hourly one is much smoother.

In Figure 13, the histogram of both the continuous simulation (10.080 points) and the hourly average simulation (168 points) are compared. It can be seen that no large differences exist and the distribution is only slightly affected by one method or the other. For example, the high power values (6-7 MW) are more frequent in the hourly simulation, as some cut-offs are not considered in this model.
This is an example of how the model can be adapted to different of energy system simulation requirements. If short term data is needed, a real-time simulation can be run in order to get data that is continuous in time. If the simulation takes place over the medium term, i.e. some weeks or months, hourly mean speeds are used and the fast term component module is deactivated, giving a more efficient computation. For long-term simulations, the statistical data provided for the simulation can be used to compute monthly energy output of wind farms.

6.1.4 Comparison of the simulations

The simulations run above can be also compared regarding computational performance. In Table 2 a comparison of different features is shown. The use of only hourly mean value allows for avoiding the use of the fast term component. This component is computationally slower, as it is based on a differential equation solver. By waiving this component, simulation performance can be importantly increased, (around factor 50). However, it has to be taken into account that this increase is only affordable when accuracy and short term fluctuation do not have to be considered (e.g. for longer term simulation). For simulating at higher temporary resolutions though, the model including the fast term can be very interesting. Memory use is not considerably affected by the choice of the time resolution of the model.

Simulation period	24h		168h (1 week)	
Resolution	Continuous	Hourly	Continuous	Hourly
Number of turbines	25		25	
Execution time	122,0s	2,3s	753,8s	14,5s
Memory used	16MB	16MB	21MB	15MB

Table 2. Simulation run comparison

6.2 Failure behaviour of the turbine units

As explained previously, the turbine model is provided with a failure function that allows us to simulate technical failures using specific parameters that can be obtained empirically. In this way, failures of individual units are randomly simulated over time. The average time to restart the turbines after such a failure is also considered.
Randomly driven timeouts are used to represent the transition to the failure state, which is triggered according to a rate. This rate is the inverse vale of the MTBF. In order to get back to the working state, the rate corresponding to the MTTR is used. To trigger the transitions, exponentially distributed random numbers are used. The distribution is parametrised by the rate.
In Figure 9 the representation of the turbines and their current state is shown. The model can easily show the state of each turbine and the aggregated current output and energy production. Also the state of an individual generator and its production values can be observed. The inclusion of the failure behaviour in real-time allows us to consider its direct influence on the power output of the farm within the same model.

6.3 Distributed parameters

All turbine manufacturers provide technical specifications that document their characteristics in detail. The values shown in these documentation normally are not specified for each unit individually, as they are obtained using average values for all units of the same type. Although the units are supposed to be identical in construction, small differences cannot be avoided.
To model this heterogeneity among the same units, the parameters of the turbines were slightly varied among themselves, by distributing them normally with a mean $\mu_{[value]}$ corresponding to the indicated value and a small standard deviation of $\sigma_{[value]} = 0.1\mu_{[value]}$. Further studies could get exact values for the variation of parameters among different units. This leads to small variations in the behaviour of each unit, that can result in aggregated effects on the wind farm output, and which are usually not considered in classical models. One of the strengths of the model is that it relies on the heterogeneous modelling of the individual agents.
Figure 14 shows the breakdown of the power production of the wind farm by individual turbines. Their heterogenous behaviour can be observed in the Figure. Having different characteristics as well as a slight variation of the local wind speed lead to unsynchronised operation of the turbines. This makes the model more realistic.

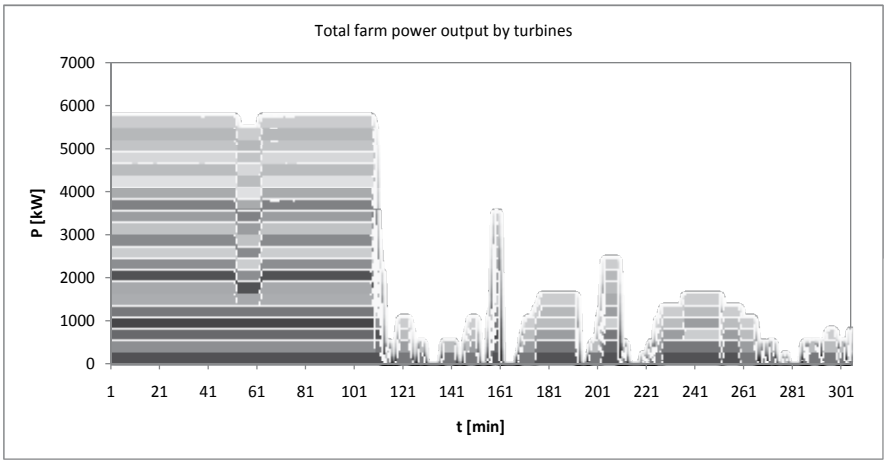

Fig. 14. Total power output for a wind farm (continuous simulation) broken down by individual turbines

7. Conclusion

Modelling the power output of wind farms at different time scales can be a quite complex activity. In this chapter, a model for simulating wind power system on multiple time scales was presented. The multi-method approach was chosen in order to satisfy the various needs of the model, where not only the pure generator but also failure related and the consideration of a wind farm as a whole is integrated. Furthermore, the model was conceived to allow for the simulation at different time scales, looking for the best computational efficiency in each case. The scalability included in this model allows to integrate different time scale simulations into the same module and reduce the number of total modules.
The model allows us to simulate wind power generation at different scales using the same model, only switching between the different modules. The characteristics of the model are

maintained at the different scales. So, for example, failure behaviour is modelled and can affect also short term simulations, if needed. The following scope was made:

- The primary aim of the model is not to estimate the accumulated energy productions over a period (used for example for the dimensioning of wind farms) but rather to simulate real time power outputs for energy system simulations.
- At high speeds, cut-off effects are better reflected in a high resolution (continuous simulation) model.
- The hourly model though seems to approximate the hourly mean well in low speed periods.
- The model is flexible enough to cover different needs arising from different time scales in integrated energy systems simulation.

This model brings together different modelling approaches, unifying continuous models, (differential equations, e.g. Equation 4) with discrete events (hourly changing mean speeds, state chart modelling within the turbines) and agent-based modelling (e.g. of the failure behaviour and for the integration of the turbines into the wind farm). The use of different paradigms allows us to create more realistic models that can take advantage of the different strengths of each approach. Due to the agent based approach, it is possible to set distributed parameters to the individual turbines, creating a heterogeneous park which recreates a more realistic behavior not only at individual, but also at aggregated scale. Further, each turbine can be customised with real data (e.g. power curves, etc.). In this way it is possible to simulate realistic behaviour of wind farms in contrast to static, homogeneous multiplication of identical objects.

A compromise between accuracy of the output powers and performance of the model can be found in dependance of the application scope of the model. In large scale energy systems simulations (over several months or years), the estimation of the low term is enough, profiting from the performance and this lightweight model. For medium term, interpolated values can be used. For short term simulations (up to some days), the fast term providing a model which simulates high resolution turbulences can give better results.

Even though, some drawbacks of the model were identified, among them wind direction, which is not taken into account for the moment, so the turbines are supposed to follow it fairly well. The model is also only valid for active power injections, as reactive effects are not considered yet. In order to optimise the continuous simulation it could be replaced by a minute by minute one, as the power output is not as directly coupled to wind speed as represented in the model, because of inertia of the rotor and modern automatic turbine regulation of the output.

Even taking into consideration these limitations (or especially because of them), a simplified model that does not need large number of parameters was created, allowing for integration to energy systems simulation as a light weighted and optimised model for different time scales.

8. Acknowledgements

The work concerning this multi-scale wind generation model was possible through the cooperation of the European Institute for Energy Research (EIFER) and the University College of Engineering from the University of the Basque Country.

9. References

Aksoy, H., Fuat Toprak, Z., Aytek, A. & Erdem Ünal, N. (2004). Stochastic generation of hourly mean wind speed data, *Renewable Energy* 29(14): 2111–2131.

Allerton, T. (2008). Simulating the distribution and cross-correlation of wind farm output, *Technical report*, EON and Heriott-Watt University.

Bayem, H., Phulpin, Y., Dessante, P. & Bect, J. (2008). Probabilistic computation of wind farm power generation based on wind turbine dynamic modeling, *10th International Conference on Probabilistic Methods Applied to Power Systems - PMAPS 2008*, Porto Rico, pp. 1–6.

Billinton, R., Chen, H. & Ghajar, R. (1996). Time-series models for reliability evaluation of power systems including wind energy, *Microelectronics and Reliability* 36(9): 1253–1261.

Borshchev, A. V., Kolesov, Y. B. & Senichenkov, Y. B. (2002). Java engine for uml based hybrid state machines, Vol. 2, IEEE, pp. 1888–1894.

Chappin, E. J. L. & Dijkema, G. P. J. (2007). An agent based model of the system of electricity production systems: Exploring the impact of co2 emission-trading, *System of Systems Engineering, 2007. SoSE '07. IEEE International Conference on*, pp. 1–5.

Chedid, R., Akiki, H. & Rahman, S. (1998). A decision support technique for the design of hybrid solar-wind power systems, *Energy conversion, ieee transactions on* **13**(1): 76–83.

Denault, A. (n.d.). Hybrid (differential equations-statecharts) modeling in anylogic-reading report, *Technical report*, McGill University, Montreal.

Helal, M. (2008). *A hybrid system dynamics-discrete event simulation approach to simulating the manufacturing enterprise*, PhD thesis.

Karki, R., Po, H. & Billinton, R. (2006). A simplified wind power generation model for reliability evaluation, *Energy conversion, IEEE Transactions on* 21(2): 533–540.

Kremers, E., Lewald, N., Barambones, O. & González de Durana, J. (2009). An agent-based multi-scale wind generation model, *The Ninth IASTED European Conference on Power and Engineering Systems, EuroPES 2009*, Vol. 681, Acta Press, Palma de Mallorca, Spain, pp. 064–166.

Nichita, C., Luca, D., Dakyo, B. & Ceanga, E. (2002). Large band simulation of the wind speed for real-time wind turbine simulators, *Power Engineering Review, IEEE* 22(8): 63–63. 0272-1724.

Viejo, P. & Kremers, E. (2009). Simulation of energy system scenarios for regional planning decision-making using agent-based modeling, *11th International Conference on Computers in Urban Planning and Urban Management CUPUM*, Hong Kong.

Welfonder, E., Neifer, R. & Spanner, M. (1997). Development and experimental identification of dynamic models for wind turbines, *Control Engineering Practice* 5(1): 63–73.

Wooldridge, M. J. (2009). *An introduction to multiagent systems*, Wiley, Chichester, West Sussex, United Kingdom.

XJ Technologies (2010). Anylogic simulation software tool, `www.xjtek.com`.

Edited by Gastón Orlando Suvire

During the last two decades, increase in electricity demand and environmental concern resulted in fast growth of power production from renewable sources. Wind power is one of the most efficient alternatives. Due to rapid development of wind turbine technology and increasing size of wind farms, wind power plays a significant part in the power production in some countries. However, fundamental differences exist between conventional thermal, hydro, and nuclear generation and wind power, such as different generation systems and the difficulty in controlling the primary movement of a wind turbine, due to the wind and its random fluctuations. These differences are reflected in the specific interaction of wind turbines with the power system. This book addresses a wide variety of issues regarding the integration of wind farms in power systems. The book contains 14 chapters divided into three parts. The first part outlines aspects related to the impact of the wind power generation on the electric system. In the second part, alternatives to mitigate problems of the wind farm integration are presented. Finally, the third part covers issues of modeling and simulation of wind power system.

ISBN 978-953-51-6025-0

Photo by MR1805 / iStock

IntechOpen